Properties of
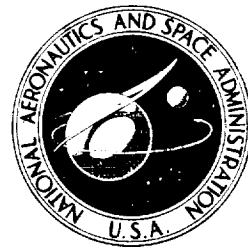
Magnetic Materials

for Use in

High-Temperature

Space Power

Systems

NATIONAL AERONAUTICS

AND SPACE ADMINISTRATION

PROPERTIES OF MAGNETIC MATERIALS

FOR USE IN HIGH-TEMPERATURE

SPACE POWER SYSTEMS

by

P. E. KUESER, D. M. PAVLOVIC, D. H. LANE,

J. J. CLARK, and M. SPEWOCK

Westinghouse Electric Corporation

Lima, Ohio

●

PREFACE

This publication is a collection of information on the properties of eight selected materials found suitable for use in high-temperature advanced electric power systems. A literature search was conducted to determine the available information, and the remaining information not available from the literature was obtained in experimental studies. These studies were conducted under NASA Contract NAS 3-4162 by the Westinghouse Electric Corporation, Aerospace Electrical Division, for the NASA Lewis Research Center. The Technical Manager was Mr. Russell A. Lindberg of the Lewis Space Power Systems Division.

The discussion herein is limited to eight materials. It is recognized, however, that other materials equally suitable for the application may either exist or be developed, although this was not indicated by the literature search. Information contained in this volume has been presented in a way to make it useful as a handbook of engineering properties of the magnetic materials studied.

CONTENTS

PROPERTIES OF MAGNETIC MATERIALS FOR USE IN

HIGH-TEMPERATURE SPACE POWER SYSTEMS

by P. E. Kueser, D. M. Pavlovic, D. H. Lane, J. J. Clark, and M. Spewock

SUMMARY

Test data are given and evaluated for eight magnetic materials that were found suitable for use in high-temperature liquid alkali-metal system applications. Each material is discussed with respect to its use in equipment parts operating at two different temperature levels.

In general, the magnetic materials tested can be grouped in three temperature ranges, together with their fields of application:

(1) 600° to 800° F: Most materials qualify for this temperature range. However, Cubex alloy ($3\frac{1}{4}\%$ Si-Fe, doubly oriented) is preferred for use in stators at inductions up to 18 kilogauss. H-11 steel (5% Cr, 1% Mo, Fe) and maraging steel (15-18% Ni, 8-9% Co, Fe) are recommended for rotors, and Supermendur (2% V, 49% Co, 49% Fe) in controls using high quality, saturable-core reactors.

(2) 800° to 1100° F: Hiperco 27 alloy (27% Co, Fe) is suggested for high inductions and Cubex alloy for inductions up to 15 to 18 kilogauss in stators. In rotors, H-11 steel qualifies for lower temperatures and Nivco alloy (approximately 72% Co, 23% Ni) for the higher temperatures in this range. Supermendur and Cubex alloys can be used for controls with Cubex preferred for the higher temperatures.

(3) 1100° to 1400° F: Hiperco 27 alloy is recommended for stators and Nivco alloy for rotors in this temperature range.

INTRODUCTION

Electric power systems for use in space require better performance and reli-

1

ability than most terrestrial applications. The success in fabrication and design analysis of these space power systems is dependent on reliable material properties. Very little design information was available prior to this study. This lack of information became evident during a search which was made of the world's literature in an attempt to minimize the amount of testing to be conducted. This report presents the magnetic, mechanical, and thermophysical properties of magnetic materials suitable for application to advanced space electric power systems.

In general, little information was found in the literature which could be used. In a few cases, desirable data were found, but because test conditions, test atmospheres, and sample geometry and history were not listed, these data were not always considered of sufficient reliability to warrant their reporting. Therefore, almost all data presented represent testing accomplished during the program.

This report is divided into three discussion areas. The first area describes the applications of electrical materials to advanced space electric power systems and is followed by a discussion of the selected materials and the observations made during the test program. A second area, Materials, Preparation, and Test Procedures, defines the material specifications, specimen configurations, and test procedures followed during the program, while the third area presents the data. This last section, MAGNETIC MATERIALS PROPERTIES, does not contain a discussion, so that it can be used as a design manual. It includes a master index for all properties, and data for each material are preceded by a summary that can be used as a guide in material selection. This summary is extracted from the data presented in tabular and graphic form for each material, which are quite extensive.

APPLICATION OF MATERIALS TO ELECTRIC POWER SYSTEMS

General Requirements

The desired properties of magnetic materials for high-temperature space power system components should approach those of the magnetic materials used in conventional power systems. Because high-temperature designs are influenced by the material properties, the mechanical and magnetic properties must be well documented to make any design study meaningful.

Laminated and forged materials used in rotating parts must have high-strength capabilities, particularly in resisting creep, to be suitable for high-temperature operation. Good magnetic properties are desirable but are secondary to the physical properties necessary for a long-life dimensionally stable rotor. Stator lami-

nations are not normally subjected to high mechanical stresses, so the magnetic properties such as high magnetic flux density can predominate with reasonably low magnetizing forces and low losses. The same magnetic parameters apply to transformers, which are static devices.

The magnetic amplifier (magamp) requires a magnetic material which has a square hysteresis loop. This material, as tape, is wound into a toroidal core. Although materials for this application are limited, a few are available that show promise at high temperatures. These materials possess little physical strength, but since the magamp is a static device, this characteristic is less important.

The solenoid considered in this report has only dc flux in its magnetic circuit. Therefore, magnetic losses are not important and the primary requirement is that the magnetic circuit be able to carry a substantial amount of flux with low magnetizing forces.

Specific Applications to Electric Apparatus

The component designs discussed herein are the most likely designs for use in a liquid alkali-metal system at the present state of development. Component drawings in this section illustrate the manner in which the materials under consideration probably can be used. Part temperatures are based on (1) coolant temperature, (2) calculations from previous design, and (3) test results from an experimental model. The purpose of these part temperatures is to indicate the probable temperature with respect to the coolant and to provide a base against which material properties can be evaluated. Two coolant temperatures were chosen, 600° and 1000° F, except for the solenoid and magamp, where temperatures of 300° and 1000° F were chosen. The lower temperature is representative of control apparatus where other components such as semiconductors limit the temperature capability.

Motor. - The ac motor is a dynamic device consisting of a rotor and stator with their associated windings, bore seal, insulation, bearings and seals, a cooling system and encapsulation as required.

The rotor must be able to withstand the thermal and mechanical stresses which will be encountered and must be mechanically stable so that it will retain its balance under all operating conditions. The rotor must also be capable of carrying magnetic flux at high temperatures.

The coils of the stator are wound with magnet wire clad to prevent oxidation resulting from the high-temperature and alkali-metal contamination of the conductor.

1. Motor frame
2. Stator coolant passage
3. Stator lamination
4. Stator winding
5. Metal end piece bore seal
6. Ceramic cylinder bore seal
7. Rotor lamination
8. Rotor end ring
9. Rotor can
10. Rotor shaft
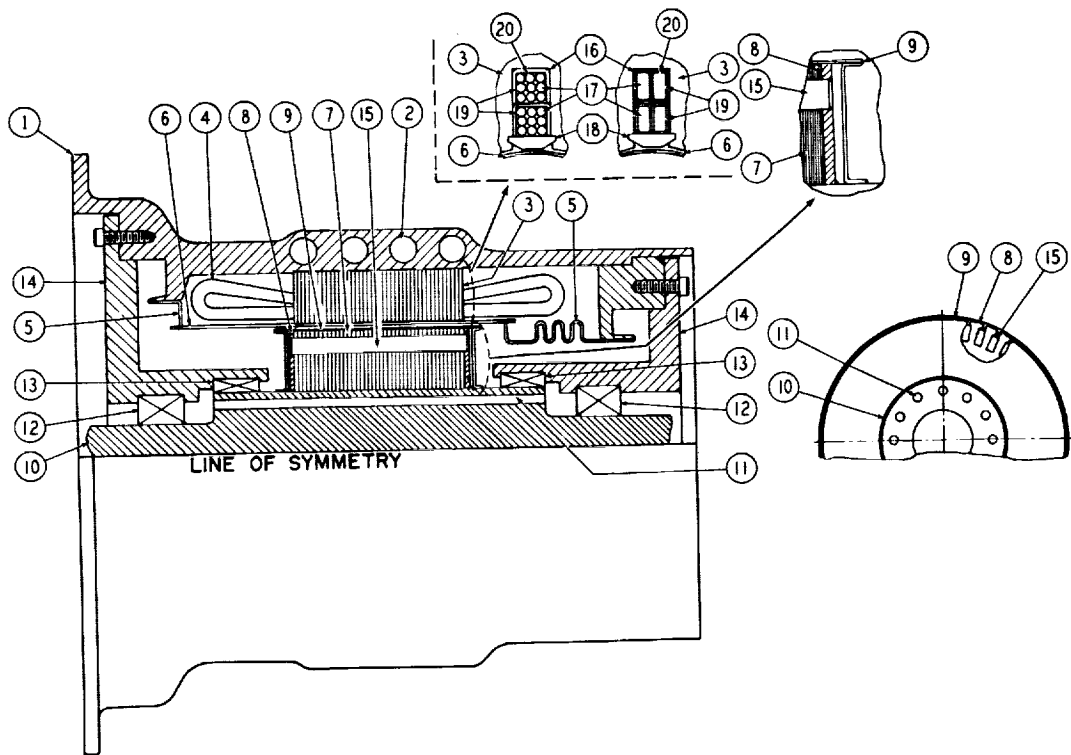
11. Rotor coolant passage
12. Support shaft bearing
13. Shaft seal
14. Bearing and seal retainer
15. Rotor conductor
16. Stator winding insulation slot
17. Stator conductor
18. Winding retainer slot
19. Conductor cladding
20. Conductor insulation

Figure 1. - AC motor, general assembly.

TABLE 1. - MAGNETIC MATERIAL USAGE, AC MOTOR

Material	Maximum useful material temperature, °F		Rotor magnetic and mechanical suitability (a)				Stator laminations magnetic suitability (a)	
			Magnetic		Typical creep values (0.4% at 10 000 hr)			
	Sealed	Open to vacuum	$^b950°$ F	$^c1350°$ F		$^b900°$ F	$^c1300°$ F
Cubex alloy								
0.006-in. laminations	1100	1100	1	2	3	1	2
0.011-in. laminations	↓	↓	↓	↓	↓	↓	↓
Hiperco 50 alloy								
0.004-in. laminations								
0.008-in. laminations								
Supermendur								
0.006-in. laminations	↓	↓	↓	↓	↓	↓	↓
Hiperco 27 alloy								
0.004-in. laminations	1400	1400		3	11 500 psi at 950° F		1
0.008-in. laminations	1400	1400		3	11 500 psi at 950° F		1
Maraging steel, 15%								
0.014-in. laminations	750	750	2	2	160 000 psi at 750° F	2	2
0.025-in. laminations	750	750	2	↓	160 000 psi at 750° F	2	↓
H-11 steel, R_c 45								
0.014-in. laminations	1100	1100	1		23 000 psi at 950° F	1	
0.025-in. laminations	1100	1100	↓		23 000 psi at 950° F	↓	
Nivco alloy								
0.014-in. laminations	1250	1250	↓	↓	90 000 psi at 950° F	↓	↓
0.025-in. laminations	1250	1250	↓	↓	90 000 psi at 950° F	↓	↓

[a]Legend: 1, satisfactory; 2, unsatisfactory; 3, material is unsuitable at this temperature for use in parts subjected to high rotational stresses.

[b]Anticipated part temperature with coolant temperature of 600° F.

[c]Anticipated part temperature with coolant temperature of 1000° F.

Insulation required for the stator winding is in the form of a coating on the conductor and in rigid or flexible form as a ground insulation. Impregnants may be used to add rigidity and protection to the coil structure, and potting material may be used for mechanical strength and to aid in heat transfer.

Rotor conductors are made of clad material, but insulation is not required either for the conductors in the slots or for the end ring because the electrical potential is low and the lamination insulation will provide sufficient dielectric strength.

Figure 1 shows a typical design of a motor suitable for operation in a high-temperature, liquid alkali-metal system and identifies the major parts and features of the motor. The rotor laminations and conductors are protected from alkali-metal vapors by a hermetically sealed sheet-metal can. The stator laminations and windings are protected by a ceramic bore seal and associated end pieces that form a chamber sealed from alkali-metal vapors. This chamber may either be hermetically sealed or be open to the vacuum of space. Heat generated in the motor is removed by a liquid metal coolant flowing through coolant flow passages in the rotor shaft and stator housing. Bearings and seals shown in the motor are not covered in this discussion.

Rotational stress must be considered in selecting a satisfactory material. Since rotational stresses are considered more critical in the generator application, typical rotational stress are shown in the discussion of the generator.

Magnetic materials are used in the motor stator and rotor laminations. Table 1 lists magnetic materials and the suitability of each material for use in the rotor or stator.

Generator. - The ac generator is a dynamic device consisting of a rotor without windings, stator, ac windings, dc excitation coil, insulation, encapsulation as required, bore seal, bearings and seals, and a cooling system.

The rotor must be able to withstand the thermal and mechanical stresses that will be encountered and must be mechanically stable to retain its balance under all operating conditions. The rotor must also be able to carry flux at high temperature without requiring excessive excitation. Pole face losses must be kept low, either by using a laminated pole face or by cutting circumferential slots in the pole face.

The coils of the stator are wound with magnet wire clad to prevent oxidation because of the high-temperature and alkali-metal contamination of the conductor.

Insulation is required as a coating on the conductor and in sheet or molded form as a ground insulation. Impregnants may be used to add rigidity and protection to the coil structure, and potting material may be used for mechanical strength and to aid in heat transfer.
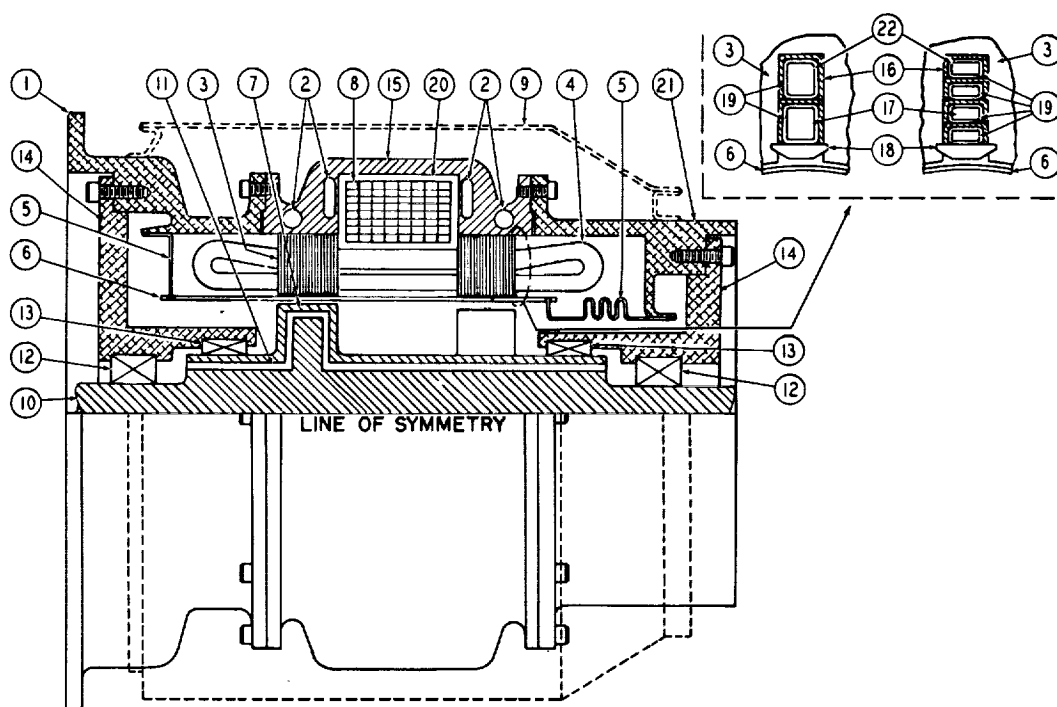
1.	Bracket	12.	Rotor shaft bearing
2.	Stator coolant passage	13.	Shaft seal
3.	Stator ac laminations	14.	Bearing and seal carrier
4.	Stator ac winding	15.	Magnetic frame
5.	Metal end piece bore seal	16.	Stator winding Insulation slot
6.	Ceramic cylinder bore seal	17.	Stator conductor
7.	Rotor pole	18.	Winding retainer slot
8.	Field dc coil	19.	Conductor cladding
9.	Shield (if inert gas cover is used)	20.	Insulation for dc coil
10.	Rotor	21.	Bracket
11.	Rotor coolant passage	22.	Stator conductor Insulation

Figure 2. - AC generator, general assembly.

Figure 2 shows a typical design of a radial-gap inductor generator capable of operation in a high-temperature liquid alkali-metal system.

The rotor shown is made from a solid forged magnetic material that does not require any special protection against the corrosive effects of alkali vapors. The stator magnetic material consists of laminations having interlaminar insulation, and a cast magnetic housing to complete the magnetic circuit. The stator laminations and conductors are protected from alkali-metal vapors by a ceramic bore seal and associated end pieces, which form a hermetically sealed chamber.

Heat generated in the rotor, stator, and windings is removed by using liquid metal as a coolant. Coolant flow passages are provided in the rotor and stator housing. Bearings and seals indicated in the drawing are not covered in this discussion.

Magnetic materials are used in the stator laminations, rotor pole, and magnetic frame. The rotor pole is an integral part of the shaft and is of solid construction. Table 2 lists the magnetic materials and material forms and the suitability of each material for use in the generator rotor and stator. Creep and fatigue are the limiting mechanical properties in choosing a rotor material. Creep increments of 0.2 and 0.4 percent were used as baselines in the material study described herein. Allowable creep must be traded off against other mechanical and electrical properties for each specific application.

The following shows typical rotor stresses in terms of rotor diameter and rotational speed. These stresses were calculated for a solid drum rotor rather than for a specific generator rotor design. The formulas used (ref. 1) were:

$$S_t = \frac{3 - 2\mu}{8(1 - \mu)} \rho\omega^2 \left(b^2 - \frac{1 + 2\mu}{3 - 2\mu} r^2\right)\frac{1}{144} \quad \text{(tangential stress)}$$

$$S_r = \frac{3 - 2\mu}{8(1 - \mu)} \rho\omega^2 \left(b^2 - r^2\right)\frac{1}{144} \quad \text{(radial stress)}$$

where

μ Poisson's ratio

ω rotational speed, rad/sec

ρ density, slugs/cu ft

b   outer radius, ft

r   radius at which stress is being calculated, ft

When $r = 0$, $S_t = S_r$. Typical stress levels are given in table 3. Additional information on generator rotor stresses can be found in reference 2.

TABLE 2. - MAGNETIC MATERIAL USAGE, AC GENERATOR

Material	Maximum useful material temperature, °F		Rotor magnetic and mechanical suitability (a)			Stator magnetic suitability (a)			
	Sealed	Open to vacuum	Magnetic		Typical creep values (0.4% at 10 000 hr)	Frame		Laminations	
			b_{950}°F	c_{1350}°F		a_{750}°F	b_{1150}°F	a_{900}°F	b_{1300}°F
Cubex alloy									
0.006-in. laminations	1100	1100	1	2	3	2	2	1	2
0.011-in. laminations	↓	↓	↓	2	↓	↓	↓	↓	2
Hiperco 50 alloy									
0.004-in. laminations				3					1
0.008-in. laminations				3					1
Supermendur									
0.006-in. laminations	↓	↓	↓	2	↓				2
Hiperco 27 alloy									
0.004-in. laminations	1400	1400	2	2	11 500 psi at 950° F				1
0.008-in. laminations	↓	↓	2	2	11 500 psi at 950° F	↓	↓	↓	1
Forging, annealed, vacuum melted			1	3	11 500 psi at 950° F	1	1	2	2
Castings, annealed, air melted	↓	↓	1	3	11 500 psi at 950° F	1	1		
1% Si-Fe, AMS 5210									
Casting	1300	1300	1	2	3	1	1		
Maraging steel, 15%									
Forging	750	750	2	2	160 000 psi at 750° F	1	2		
0.014-in. laminations	750	750	2	↓	160 000 psi at 750° F	2	↓		
0.025-in. laminations	750	750	2		160 000 psi at 750° F	2			
H-11 steel, R_c 45									
Forging	1100	1100	1		23 000 psi at 950° F	1		1	
0.016-in. laminations	1100	1100	↓		23 000 psi at 950° F	2	↓	1	
0.025-in. laminations	1100	1100	↓		23 000 psi at 950° F	2		1	
Nivco alloy									
Forging	1250	1250			90 000 psi at 950° F	1	1	2	
0.014-in. laminations	1250	1250			90 000 psi at 950° F	2	2	1	
0.025-in. laminations	1250	1250	↓	↓	90 000 psi at 950° F	2	2	1	↓

[a]Legend: 1, satisfactory; 2, unsatisfactory; 3, material is unsuitable at this temperature for use in parts subjected to high rotational stresses.

[b]Anticipated part temperature with coolant temperature of 600° F.

[c]Anticipated part temperature with coolant temperature of 1000° F.

TABLE 3. - TYPICAL STRESS LEVELS

Rotor diameter, in.	Rotor speed, rpm	Stress level, psi
10	5 000	2 300
	10 000	9 180
	15 000	20 600
15	5 000	5 190
	10 000	20 700
	15 000	46 500
20	5 000	9 260
	10 000	37 000
	15 000	83 000

Exciter-regulator and magnetic amplifier (magamp). - The exciter-regulator is a static device that provides regulation and control for the electrical output of the ac generator. In the present state of the art, the rectifier and diodes or the exciter-regulator are essentially low temperature devices. Because of its intimate relation to other parts, the exciter-regulator becomes a low temperature device that requires a coolant temperature of 120° F or less.

The usual exciter-regulator contains a power transformer to provide power for the field of the ac generator. The power transformer occupies a substantial portion of the exciter-regulator package and also contributes significantly to the losses. Further, available materials permit building a transformer which can operate with a coolant temperature of 600° to 1000° F. The power transformer is, therefore, considered as a component separate from the exciter-regulator and is described later. Figure 3 shows the components of the exciter-regulator.

Another component that is intimately associated physically with the exciter-regulator is the magnetic amplifier (magamp). When used in conjunction with sensitive components, such as semiconductors, a 300° F coolant temperature may be required. If the magamp is separated from the sensitive components a higher coolant temperature is possible.

The magamp is a static device that consists of a magnetic toroid core, an insulating core box and damping fluid, insulated control and gate (output) windings, insulation between windings, an encapsulant or potting material, and a container which restricts mechanical strain on the magnetic material. For high-temperature operation, cooling must be supplied by the mount that supports the entire assembly.

1. Cover
2. Capacitor
3. Filter choke
4. Three-phase magamp
   supply transformer
5. Three-phase sensing
   transformer
6. Diodes

7. Aluminum printed circuit
   board
8. Voltage adjustment
9. Magamp
10. Cold plate
11. Coolant
12. Cooling tubes
13. Insulator
14. Silicon control rectifier
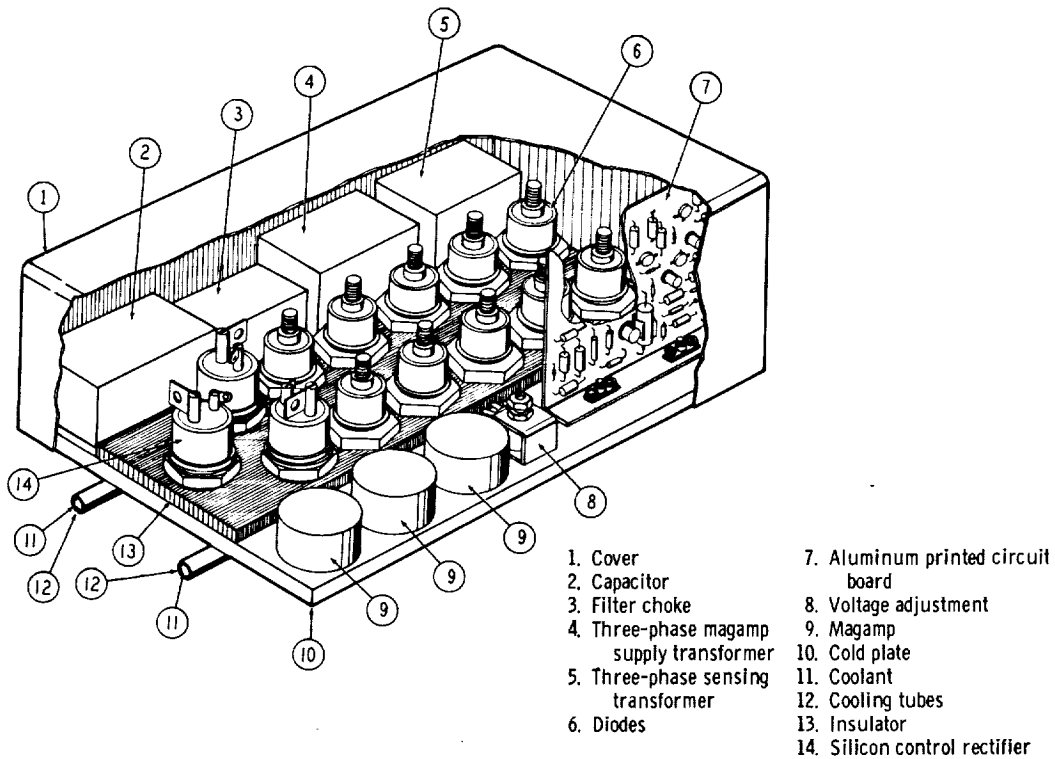
Figure 3. - Exciter-regulator, general assembly.

SECTION A-A

1. Control coil
2. Core box
3. Damping media
4. Interwinding insulation
5. Gate coil
6. Core
7. Hermetic container
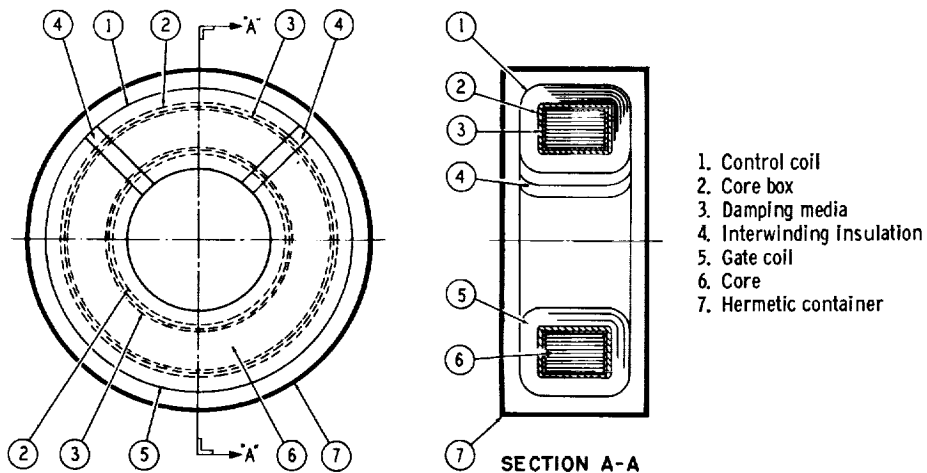
Figure 4. - Magnetic amplifier, general assembly and cross section.

The magamp core must be made from a saturable magnetic material so that an overriding input signal can cause saturation and control the output signal. The core may be assembled from tape or from punched laminations.

Insulation is required on the windings as an insulation coating on the conductor, between adjacent turns, as rigid insulation between adjacent windings, and as a molded box between the core and windings. Potting material is used to anchor the magamp in its container.

Figure 4 shows the various parts and features of a typical magamp design. The construction shown is based on the use of magnetic tape for the core. The core is installed in a core box with a suitable damping media, and the control and gate windings are wrapped around the box. Figure 4 includes a cross-sectional drawing showing the magnetic tape laminations and some details of the windings.

TABLE 4. - MAGNETIC MATERIAL USAGE, MAGAMP

Material	Maximum useful material temperature, °F		Core tape and laminations magnetic suitability (a)	
	Sealed	Open to vacuum	[b]565° F	[c]1350° F
Cubex				
0.002-in. tape	1100	1100	1	2
0.006-in. tape				
0.006-in. laminations				
0.011-in. laminations				
0.002-in. tape magnetic anneal, toroid				
0.006-in. tape magnetic anneal, toroid	↓	↓		
Supermendur				
0.002-in. tape, toroid, small	800	800		
0.002-in. tape, toroid, large	800	800		
0.006-in. laminations	800	800	↓	↓

[a]Legend: 1, satisfactory; 2, unsatisfactory.
[b]Anticipated part temperature with coolant temperature of 300° F.
[c]Anticipated part temperature with coolant temperature of 1000° F.

Table 4 is a tabulation of magnetic materials and material forms showing the suitability of each material for use in the magamp core. Since it is possible that these devices may operate either in a vacuum or a hermetically sealed chamber, the suitability of each material for both conditions is shown in table 4.

Solenoid. - The solenoid is a semistatic dc device that is always in one of two possible positions, actuated or not actuated. It consists of a magnetic plunger, actuator rod, close and trip coils and associated magnetic cores, permanent magnet, magnet-latch circuit, conductor and ground insulation, actuator return spring, suitable actuator rod stops, and a hermetically sealed container. Actuation and deactuation is accomplished by very short current applications and the solenoid is latched closed magnetically. Two environmental temperatures of 300° and 1000° F were chosen. The first is characteristic of applications where the solenoid is used with sensitive components such as semiconductors. The 1000° F is characteristic of the temperature expected if the solenoid were removed from the area of the sensitive components. No internal cooling provisions are required because the heat generated is small.

The solenoid application is such that the magnetic materials are all solid rather than laminated. Since the magnetic circuits carry only dc flux, magnetic flux losses are relatively unimportant. It is important that the magnetic circuits be able to carry a substantial amount of flux with low-magnetizing forces. The coils of the close and trip windings are wound with magnetic wire that is clad for high-temperature application. Insulation is required as a coating on the conductor and in sheet or molded form as a ground insulation. Figure 5 shows the major parts and features of a typical dc solenoid capable of operation in a high-temperature liquid alkali-metal system.

When current is passed through the close coil (fig. 5), the magnetic plunger and actuator rod are pulled in a downward direction (as drawn). A magnetic latch plate serves as a stop and also completes a magnetic circuit with the permanent magnet, which holds the actuator rod in the downward position when current through the close coil is stopped. The solenoid is deactuated by energizing the trip coil, which diverts the permanent magnet flux from the latch plate and allows the spring to return the actuator rod to its original position.

Magnetic materials are used in the actuator plunger, close core and trip coil cores, latch plate, and the trip and hold circuit core. Since dc magnetic properties are the main requirement for this application, only one material covered by this study (1%, Si-Fe AMS 5210) is satisfactory. Table 5 shows the temperature capability for this material. Although this design shows only a hermetically
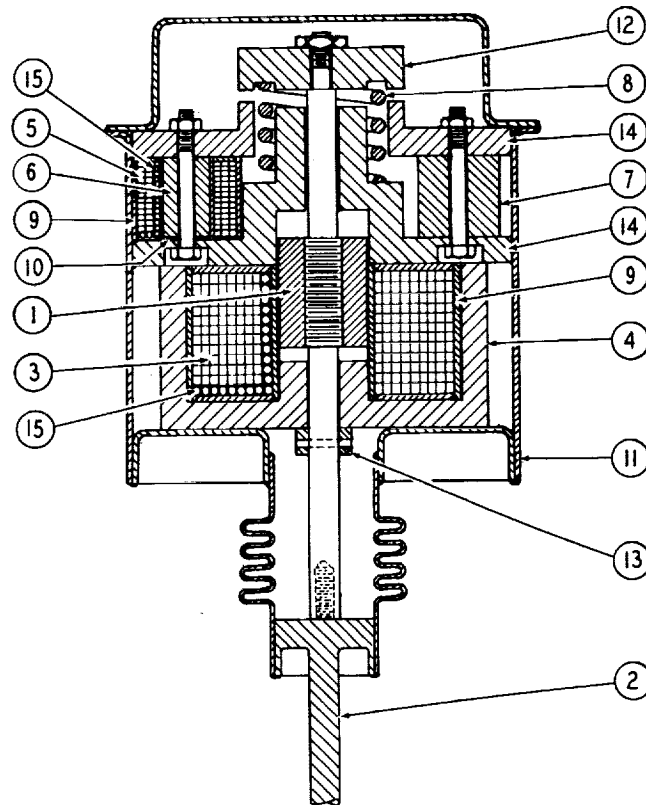
1. Actuator plunger   6. Trip coil core   11. Hermetically sealed container
2. Actual rod   7. Permanent magnet   12. Latch plate
3. Close coil   8. Return spring   13. Rod and plunger stop
4. Close coil core   9. Ground insulation   14. Trip and hold circuit core
5. Trip coils   10. Nonmagnetic washer   15. Conductor

Figure 5. – Solenoid, general assembly.

TABLE 5. - MAGNETIC MATERIAL USAGE, DC SOLENOID

Material	Maximum useful material temperature, ^{O}F		Plunger, core, and latch magnetic and mechanical suitability (a)	
	Sealed	Open to vacuum	[b]300° F	[c]1000° F
1% silicon iron AMS 5210	1300	1300	1	1

[a]Legend: 1, satisfactory.
[b]Anticipated part temperature with solenoid in a 300° F environ-
    ment with no internal cooling.
[c]Anticipated part temperature with solenoid in a 1000° F environ-
    ment with no internal cooling.

sealed application, the possibility of this material being exposed to a space vac-
uum is recognized and suitability of the material for this condition is also shown
in table 5.

Transformer. - The power transformer is a static device consisting of two or
more coils of wire, a magnetic core, insulation, a cooling system and means of
holding the parts in place. The coils of the transformer are wound with magnet
wire. A clad coil material is used to meet system temperature requirements.

The transformer core may be assembled from tape or from punched lamina-
tions. Since low losses and exciting volt-amperes per pound are very important
in transformers, special consideration must be given to these properties in the
material. Insulation is required as a coating on the conductor between adjacent
turns, as sheet insulation between layers of coils, and as sheet or some other
form between coils and core. Impregnants may be used to add rigidity and protec-
tion to the coil structure, and potting material may be used for mechanical
strength and to aid in heat transfer.

Figure 6(a) shows the various parts and features of a typical three-phase
transformer design. The construction shown is based on the use of magnetic tape
for the core. Each leg is then encased by primary and secondary coils and coolant
passages. If the core were constructed of laminations rather than tape, the only
major change required would be to relocate the core coolant passages so that they
draw heat from the edges of the laminations. In either case, manifolding will be
required to tie together the coolant-in and coolant-out passages, respectively, in
proper sequence.

1. Core laminations
2. Strap
3. Cooling duct
4. Primary coil
5. Secondary coil
6. Coil conductor
7. Ground insulation
8. Coolant inlet manifold
9. Coolant outlet manifold
10. Coolant inlet (manifolded) tubes
11. Coolant outlet (manifolded) tubes
12. Heat conduction plates
13. Core leg parting line
14. Hermetic housing

(a) General assembly.

LINE OF SYMMETRY

SECTION A-A

(b) Cross section.

Figure 6. - Transformer.

TABLE 6. - MAGNETIC MATERIAL USAGE, TRANSFORMER

Material	Maximum useful material temperature, $^\circ$F		Core tape and laminations magnetic suitability (a)	
	Sealed	Open to vacuum	[b]750° F	[c]1150° F
Cubex alloy				
0.002-in. tape	1100	1100	1	2
0.006-in. tape				
0.006-in. laminations				
0.011-in. laminations				
0.002-in. tape, magnetic-field annealed				
0.006-in. tape, magnetic-field annealed				
Hiperco 50 alloy				
0.004-in. laminations				
0.008-in. laminations				
Supermendur				
0.002-in. laminations				
0.006-in. laminations				
Hiperco 27 alloy				
0.004-in. tape	1400	1400		1
0.008-in. laminations	1400	1400	1	1

[a]Legend: 1, satisfactory; 2, unsatisfactory.
[b]Anticipated part temperature with coolant temperature of 600° F.
[c]Anticipated part temperature with coolant temperature of 1000° F.

Figure 6(b) includes a cross-sectional drawing showing the magnetic core and some details of the coils and coolant passages. Table 6 is a tabulation of magnetic materials and forms showing the suitability of each material for use in the transformer core. This table shows suitability of the materials used in the transformer either hermetically sealed in a chamber or exposed to space vacuum.

Electromagnetic pump. - The electromagnetic pump described herein is a static device consisting of two magnetic core sections, a series of insulated coils in each section, a cooling system, a duct to carry the liquid metal, and insulation between the liquid metal duct and the magnetic core.

Figure 7(a) shows the various parts and features of a typical linear-type electromagnetic pump design. The function of the rotor in a motor is fulfilled by the

(b) Cross section.

(c) Stator slot and magnetic core detail.

(a) General assembly.

1. Hermetically sealed housing
2. Combined coolant tube through-bolt
3. Through-bolt insulation
4. Stator laminations
5. Stator end lamination
6. Cooling fluid manifold
7. Insulation sheet
8. Fluid metal pumping duct
9. Pumping duct end conductor
10. Stator winding
11. Pumping duct inlet and outlet passage
12. Through-bolt nut
13. Conductor cladding
14. Stator winding slot insulation
15. Stator winding insulation retaining
16. Conductor
17. Conductor insulation

Figure 7. - Electromagnetic pump.

TABLE 7. - MAGNETIC MATERIAL USAGE,

ELECTROMAGNETIC PUMP

Material	Maximum useful material temper- ature, ^{O}F		Stator laminations (a)	
	Sealed	Open to vacuum	[b]900° F	[c]1100° F
Cubex alloy				
0.006-in. laminations	1100	1100	1	1
0.011-in. laminations				
Hiperco 50 alloy				
0.004-in. laminations				
0.008-in. laminations				
Supermendur				
0.006-in. laminations	↓	↓		
Hiperco 27 alloy				
0.004-in. laminations	1400	1400	↓	↓
0.008-in. laminations	1400	1400		

[a]Legend: 1, satisfactory.

[b]Anticipated part temperature with coolant temperature of 600° F.

[c]Anticipated part temperature with coolant temperature of 1000° F.

liquid metal as it is pumped through the duct.

The pump is of sandwich construction with an insulating sheet between the pumping duct and each stator. Heat generated in the laminations and windings is carried away by a coolant that flows through passages at the outer periphery of each stator. The cooling passage tubes also serve to hold the assembly together.

Figures 7(b) and (c) include cross-sectional drawings showing the magnetic laminations and some details of the cooling tubes. Table 7 shows the suitability of various magnetic materials for this application.

Additional discussion on various types of electromagnetic pumps and the power conditioning requirement is contained in reference 3.

DISCUSSION OF MATERIAL PROPERTIES

General Discussion of Magnetic Material Properties

Efficient operation of space power systems requires unusual combinations of properties in magnetic materials, including satisfactory behavior at temperatures to 1400° F and above and at frequencies up to 3200 cps. To improve design knowledge on the potential capabilities of those existing magnetic materials that are suitable for space power systems, additional information was needed about their behavior at various temperatures and frequencies. The following major groups of magnetic materials were considered in this study to fulfill the specific requirements of different system components.

(1) Materials for the stator core: Ring laminations of Hiperco 27 alloy (27% Co-Fe) and Hiperco 50 alloy (2% V, 49% Co, 49% Fe) as well as of Cubex, a doubly oriented $3\frac{1}{4}$-percent silicon-iron alloy, are suitable for advanced applications. Major magnetic requirements include a high flux carrying capacity and low core losses at high temperatures; only serviceable mechanical properties are required for these low-stressed parts.

(2) Materials for the rotor core: Forgings and ring laminations of H-11 Steel (5% Cr, 1% Mo, Fe), 15- and 18-percent nickel maraging steels, and Nivco alloy (approximately 72% Co, 23% Ni, and certain other elements), represent characteristic rotor materials. A solid or laminated rotor for a generator or motor is subjected to high rotational speeds that place high strength as the primary material requirement at elevated temperature. A generator rotor material, for example, is expected to possess a high creep strength at operating temperatures, preferably under 0.4 percent strain in 10 000 hours at stresses in excess of 40 000 psi. Although magnetic requirements are secondary for the solid rotor core, an induction exceeding 8 to 10 kilogauss at operating temperature under normal excitation conditions is expected. Because the rotor pole pieces are subject to losses, they might be either "slotted" or built from laminations, since their magnetic performance requirements are more critical than their mechanical needs.

(3) Materials for controls and electronic applications, including magnetic amplifiers: Supermendur (domain-oriented 2% V, 49% Co, 49% Fe) and Cubex alloy are suitable materials for tape and ring laminations. High saturation, high permeability, combined with a square hysteresis loop are desirable in these specific applications.

(4) Pole material for standard control apparatus: AMS 5210 (1% Si-Fe) casting was considered over iron primarily because of its lower losses, better casting characteristics, and higher resistivity.

The detailed data obtained in this study are presented in the section, MAGNETIC MATERIALS PROPERTIES. The following are some general comments, together with a discussion of the materials considered in the study with respect to their magnetic and mechanical stability and capability in different temperature ranges.

The magnetic properties of the single-phase materials, such as Cubex and Hiperco 27, followed the patterns expected at high temperatures. As the temperature increased, the magnetization curves rose more quickly at lower fields, and then flattened out and saturated at lower inductions. In addition, coercive force, residual induction, and core loss decreased with increasing temperature. The excitation (volt-amperes per pound) curves at high inductions followed the opposite trend. The steep drop in high-field induction begins in Cubex alloy above 1100° F. At this temperature, however, Hiperco 27 alloy still has an induction of 21 kilogauss.

As shown in figures 192 (p. 176), 209 (p. 184), and 218 (p. 189) and 53 (p. 86), 120 (p. 119), and 121 (p. 120), respectively, Hiperco 27 and Cubex alloy were not affected by the 1000-hour stability test at 1000° F. The dc and ac magnetic properties of both alloys, which were measured at room temperature after the stability test, showed no significant change from those measured before testing. A decrease in the magnetic properties measured at 1000° F agrees with an expected short-time reversible change with temperature. The tensile properties of these two materials followed the general pattern for solid solution alloys. At an elevated temperature below $1/2$ T_m (the midpoint temperature, in $^{\circ}$K, between absolute zero and the melting point), there is a considerable change in slope and the decrease in strength with increasing temperature becomes more rapid. It is important to observe that Hiperco 27 alloy displayed a relatively high-creep strength at 900° F, surpassing that of maraging steel at the temperature as shown in figure 8.

The materials in which a phase change takes place at test temperatures showed some deviations from the above pattern. These materials differ from Cubex and Hiperco 27 alloys, in which the Curie point and the limitations in solid solution strength determine the limits of their magnetic and mechanical capabilities at high temperatures. The capabilities of alloys with phase changes are controlled primarily by the phase changes and the temperatures at which they occur. These materials include Hiperco 50 alloy and Supermendur, which undergo an atomic ordering (and probably a phase addition due to the presence of vanadium) at elevated

temperatures, as well as all three high-strength materials, Nivco alloy, H-11 steel, and maraging steels, in which precipitation of one or several new phases makes a major contribution to high-temperature strength. In maraging steels, the temperature capability of magnetic and mechanical properties is controlled by the reversion to austenite.

The primary deviations from initial magnetic properties were measured as an increase in coercive force with a corresponding effect on core loss, both at the temperature where structural change takes place and at room temperature, after exposure to a critical high temperature. In mechanical properties, the high-temperature phase change brought about either a decrease in strength (e.g., in the high strength alloys) or an increase in strength in the lower strength alloys (e.g., Hiperco 50). This latter effect caused an increase in tensile strength over a certain temperature region (e.g., Supermendur). These phase changes were also reflected in the thermophysical properties that caused a peak in the specific heat of Hiperco 50 alloy and Supermendur.

As expected, stability testing at 1000° F for 1000 hours resulted in major changes in the magnetic properties of H-11 steel and 15 percent nickel maraging steel (figs. 278, p. 246, and 254, p. 226, respectively).

The coercive force of H-11 steel decreased steadily during stability testing. After test the room temperature value was lower than that originally measured. However, maraging steel exhibited a considerable increase in coercive force and a decrease in high-field induction at both 1000° F and room temperature after testing. The continuous decrease in the coercive force of H-11 steel is a sign of overaging of the complex carbide precipitates and continued tempering of the martensite. This overaging and tempering results in an overall relaxation of internal stresses. In addition, the overaging also removed many of the obstacles to domain wall movement. While the above changes are generally beneficial to the magnetic properties, the creep strength decreases accordingly.

The structural change in maraging steel at 1000° F is based primarily on partial reversion of the ferrite matrix to austenite. Since austenite is nonmagnetic, it dilutes the magnetic matrix and, as can be seen from the stability results, lowers the high-field induction value. In certain crystallographic positions with respect to the matrix and in certain particle sizes, reverted austenite apparently creates enough stress to increase the coercive force considerably. Data obtained in this study, particularly the magnetization curves for 1100° F, show that a decrease in nickel content from 18 to 15 percent raises the temperature capability of maraging steels. The results from the 1000-hour stability test indicate that the temperature limit of the 15-percent nickel material lies below 1000° F, probably

between 750° and 850° F.

Nivco alloy (fig. 310, p. 277) was included in the group of materials tested for magnetic stability at 1000° F. No magnetic aging was observed for Nivco at 1000° F, primarily because the precipitation hardening reaction of this material takes place at considerably above the stability test temperature. However, annealing Nivco at 1100° and 1400° F (fig. 309, p. 276) resulted in a structural change, probably overaging, and brought about a considerable decrease in the coercive force both at temperature and at room temperature after exposure. It also increased the room temperature value of the high-field induction.

No stability tests were conducted on Hiperco 50 alloy and Supermendur. However, literature review and short-time tests in this program indicate that structural changes take place in these materials at elevated temperature. For instance, Hiperco 50 shows a considerable increase in the room temperature coercive force after exposure to 1400° F. This may be associated with strain or with rearrangements in atom positions brought about by an atomic ordering reaction, which (for 50% Co-Fe) occurs at temperatures up to 1350° F. Tests on Supermendur, both in this study and in previous Westinghouse programs, indicate that the effects of the ordering reaction and the associated changes in magnetic properties may occur at temperatures as low as 700° F. This lowers the temperature capability of these materials considerably below those of Hiperco 27 and Cubex alloys (refs. 4 and 5).

Graphical information on mechanical properties is displayed in the Larson-Miller creep curves for each material in the section, MAGNETIC MATERIALS PROPERTIES. Creep data as a function of temperature at 0.4 percent creep strain for rotor materials and Hiperco 27 alloy at temperatures up to 1100° F are shown in figure 8.

Nivco alloy required a stress of 70 000 psi to produce 0.4 percent creep strain at 1100° F in 10 000 hours. This surpasses the temperature capability of all other materials tested. The 15-percent nickel maraging steel has outstanding creep strength at 700° F, but a temperature increase to 900° F brings about a rapid decrease in its creep strength. The H-11 steel has very useful creep strength of about 90 000 psi at 800° F, but loses it rapidly as the temperature increases.

Figure 9 displays the high field induction of all the materials tested as a function of temperature. At 1400° F, both Hiperco alloys reached an induction of 18 to 18.5 kilogauss and Nivco an induction of about 10 kilogauss.

Core loss data of the high-saturation materials are shown in figures 10 and 11. At 1100° F and inductions below 18 kilogauss the Cubex alloy competes successfully with both Hiperco alloys. However, above 1100° F Hiperco 27 appears to be the best choice for stator core material. Hiperco 50 should not be considered for
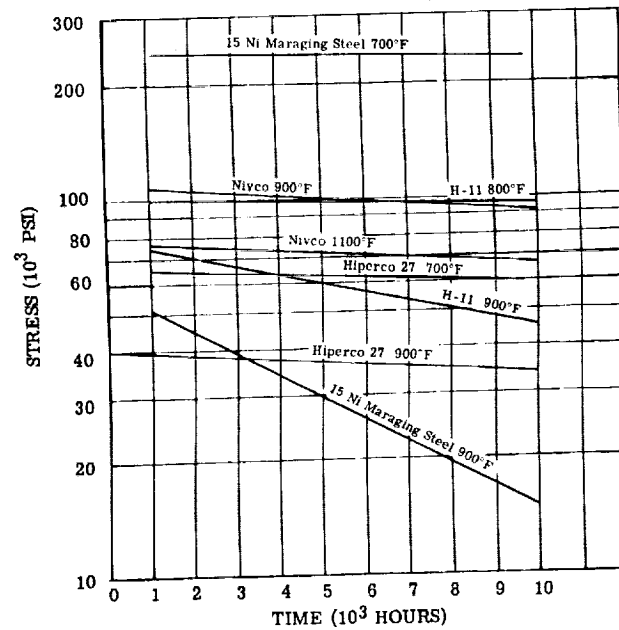
Figure 8. - Comparison of stresses required to produce 0. 4 per-
cent creep strain at indicated temperature. Data extrapolated
from Larson-Miller presentations.
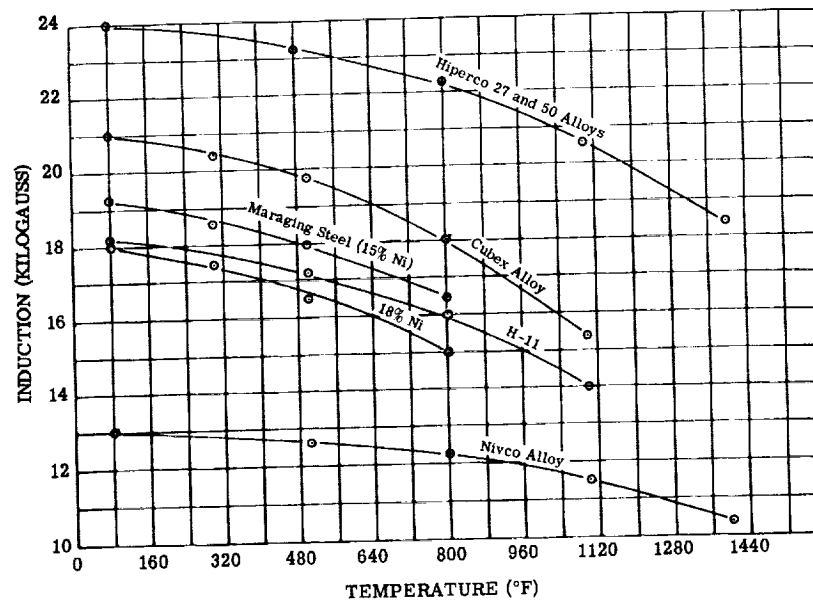
Figure 9. - Summary of induction for materials tested at magnetization of 250 to 300
oersteds as function of temperature.
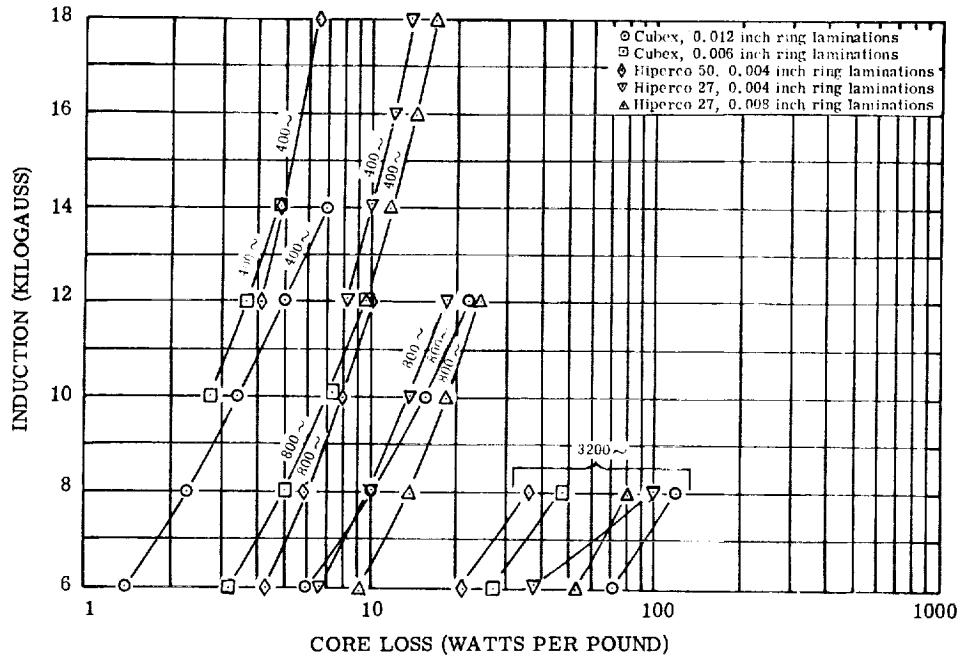
Figure 10. - Summary of core loss at 400 to 3200 cps. Alloys as indicated; tested in argon at 1100° F
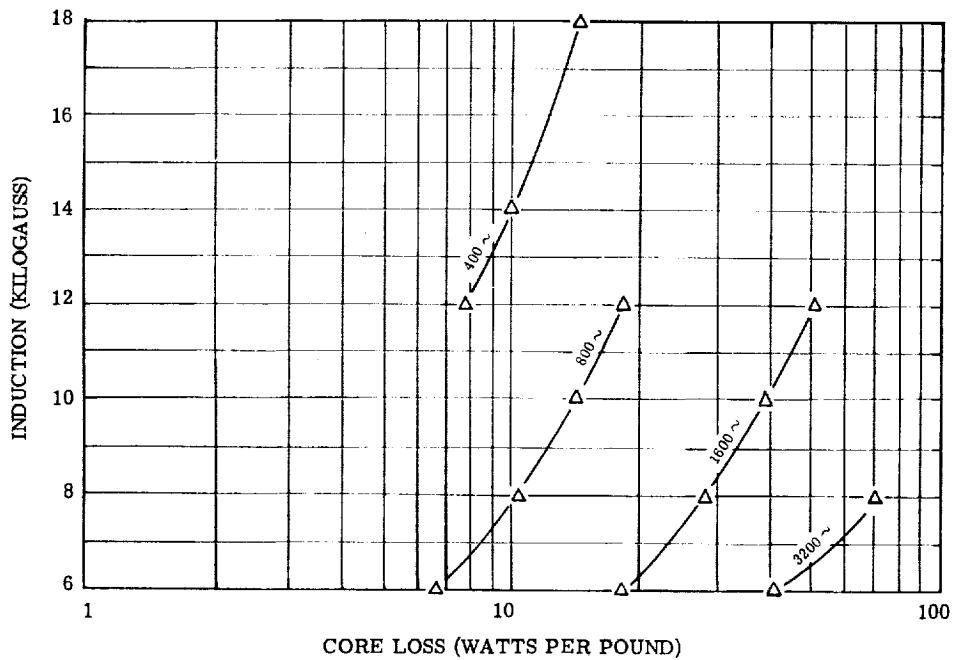
Figure 11. - Core loss at 400 to 3200 cps for Hiperco 27 alloy. Laminations, 0.008 inch; test atmosphere, argon at 1400° F.

high temperatures because of magnetic stability problems.

In considering the preceding data, the following grouping of the materials may be made with respect to three temperature ranges:

(1) 600° to 800° F: Most of the materials tested qualify for this temperature range. However, Cubex alloy is preferred for use in stators at inductions up to 18 kilogauss. H-11 steel and maraging steel are recommended for rotors, and Supermendur for control devices.

(2) 800° to 1100° F: Hiperco 27 alloy is suggested for high inductions and Cubex alloy for inductions up to 15 to 18 kilogauss in stators. H-11 steel qualifies for the lower temperatures and Nivco alloy for the higher temperatures in this range. Supermendur and Cubex alloys can be used for controls with Cubex being preferred for the higher temperatures.

(3) 1100° to 1400° F: Hiperco 27 alloy is recommended for stators and Nivco alloy for rotors in this temperature range.

Radiation Effects on Magnetic Materials

The combined effects of nuclear radiation and a high-temperature environment are an important factor in determining the overall capability of a space power system. Limited information available on these combined environments shows that grain-oriented silicon-iron performs satisfactorily under these conditions. Temperature was the predominant factor influencing performance. These are also indications that the effect of nuclear radiation decreases as the temperature is raised.

Published information on radiation levels of 10^{17} nvt (time integrated flux) on metals and alloys indicates that structural changes are primarily responsible for changes in structure-sensitive magnetic properties. These include coercive force and permeability. Among the structural changes induced by irradiation are the disordering effect on an originally ordered material, introduction of imperfections in the lattice, and acceleration of precipitation reactions. Gordon (ref. 6) observed that only the softest magnetic materials, with a coercive force of less than 0.5 oersted, were significantly affected by irradiation, which causes an increase in the coercive force and a decrease in squareness in the hysteresis loop. Most of the alloys evaluated in this manner came from those regions of the nickel-iron systems where atomic ordering takes place. Gordon also observed that radiation-induced changes in magnetic properties were not affected by time, but that reheat treatment of irradiated cores restored the original preirradiation properties.

As a result of these observations, it is assumed that both silicon-iron alloys covered in this study should not be seriously affected by nuclear radiation. The same should be true of Hiperco 27 alloy, even though cobalt-containing materials are expected to be subject to secondary beta and gamma radiation caused by the radioactive decay of cobalt 60. Hiperco 50 alloy and Supermendur are expected to be radiation sensitive because of the ordering reaction which takes place in 50-percent cobalt iron.

High-strength materials may experience an acceleration of overaging due to nuclear radiation, but this effect may be counteracted by high-temperature exposure. From the meager data available of the effects on the creep or fatigue behavior of metals, irradiation does not appreciably increase the creep rate of most metals.

Detailed Discussion of Materials

Cubex alloy. - A summary of Cubex alloy properties is included in the MAGNETIC MATERIALS PROPERTIES section. Cubex alloy is a high-purity $3\frac{1}{4}$ percent silicon-iron that is processed to achieve cube-on-face orientation. The material responds to annealing in a magnetic field, which imparts further improved magnetic properties to the alloy. The stress-relief-annealed condition is commonly used in rotating machinery and the field-annealed material is reserved for high-performance transformers and magnetic amplifiers.

Specific heat: Between 72° and 572° F, the specific heat of Cubex alloy is nearly constant as shown in figure 42 (p. 78). Above 572° F, the specific heat increases exponentially to a value of 0.222 Btu per pound per $^{\circ}$F at 1112° F.

Thermal conductivity: The thermal conductivity of Cubex alloy was measured over the range of 72° to 1320° F and was found nearly constant as shown in figure 43 (p. 79).

Electrical resistivity: The resistivity of Cubex alloy was measured over the range of 77° to 1100° F. A plot of resistivity as a function of temperature is shown in figure 44 (p. 79).

Magnetic properties: The magnetic properties of different forms of Cubex alloy were measured at temperatures to 1100° F and at frequencies of 60, 400, 800, 1600, and 3200 cps. A sample from each tape-wound configuration was magnetic-field annealed (MFA) and the balance were stress-relief annealed (SRA). Plots of the magnetic test data for Rowland ring and toroid tape-wound samples are shown in figures 45 to 121 (pp. 82 to 120).

Coercive force, residual induction, and core loss decreased with increasing test temperature for all samples. Room temperature inductions of 16 and 17 kilogauss were obtained on 0.006-inch-thick and 0.011-inch-thick stack Rowland ring samples of Cubex alloy at a field of 10 oersteds (figs. 51, p. 85, and 52, p. 85). Increasing the field to 300 oersteds raised the induction for the ring samples to 21 kilogauss. At 1100° F, the induction of both Rowland ring samples had decreased to 12.8 kilogauss at 10 oersteds and 15.5 kilogauss at 300 oersteds. The coercive force of both lamination thicknesses decreased from room temperature values of 0.1 oersted (0.011 in.) and 0.18 oersted (0.006 in.) to 0.06 oersted at 1100° F. The 72° F dc magnetic properties were not changed by exposure to 1100° F in argon for short times or for times up to 1000 hours at 1000° F in argon (fig. 53, p. 86). The ac properties were unchanged after a 1000-hour stability test (figs. 120, p. 119, and 121, p. 120).

Cubex core-loss data are summarized in table 12 (p. 80). These data are shown for 70° and 1100° F at all the test frequencies. Test samples were both stress-relief and magnetic-field annealed. Core loss decreases with increasing temperature and increases with frequency. Core loss is also decreased by decreasing the alloy stock thickness. The decrease, which is attributed to increasing temperature, amounts to 60 percent of the initial room-temperature 400-cps value at 15 kilogauss. The amount of decrease in low induction core loss is less at the higher frequencies. The core loss values obtained on ring laminations were somewhat higher than those obtained for the tape-wound toroids because of grain orientation effects discussed earlier. The 72° F losses measured on field-annealed 0.002-inch-thick tape-wound toroids were slightly lower than losses measured on stress-relief annealed toroids. The effect of magnetic field annealing gradually disappeared as the test temperature neared 1100° F.

The effect of increasing temperature on exciting volt-amperes was opposite the effect of temperature on core loss at all test frequencies.

Constant-current flux-reset (CCFR) properties (400-cps sine wave) were measured at room temperature, 500° and 1100° F for tape thicknesses of 0.002 and 0.006 inch thick, for two different annealing treatments (stress-relief anneal and magnetic-field anneal), and for two toroid sizes. The results indicate that: magnetic field annealing slightly improves the properties of 0.002-inch-thick tape but the amount of improvement decreases with temperature; and the 0.002-inch-thick tape has better CCFR properties than does the 0.006-inch-thick tape. The CCFR properties of Cubex tapes decrease with temperature in a pattern which is similar to that observed for other Cubex magnetic properties. The room temperature CCFR properties, after exposure to 1100° F, show practically no adverse effect of

the heating cycle for either tape gage, except for a slight decrease in the loop squareness for a few samples. Table 13 (p. 81) is a summary of CCFR properties.

Poisson's ratio: Poisson's ratio data for 0.011-inch-thick Cubex alloy are presented in table 14 (p. 121). Considerable scatter in the data had been expected because of normal, large-grain size of the alloy. The summary of data presented in table 14 shows that the measured values of Poisson's ratio are influenced by the location of the strain gages. Strains measured in a single grain differ from strains measured across the grain boundaries between adjacent grains. Published information on the measurement of Poisson's ratio for some materials notes an effect of applied stress on the measured value. No such effect was noted in the Cubex alloy data.

Tensile and compressive properties: A tabulation of longitudinal and transverse tensile and compressive properties for Cubex alloy is presented in tables 15 (p. 121) and 16 (p. 122) and plotted in figures 122 to 126 (pp. 123 to 125). These data are typical of soft high-purity materials except for the unexplainably low modulus of elasticity at all test temperatures. Both the tensile and compressive strength properties of Cubex alloy are isotropic and the tensile ductility is anisotropic. However, at no temperature does the elongation of Cubex alloy fall below 10 percent.

Supermendur and Hiperco 50 alloys. - The properties for these materials are located in the section MAGNETIC MATERIALS PROPERTIES.

Specific heat: Specific heat data for Supermendur rolling stock are plotted in figure 127 (p. 131). Supermendur exhibits a constant specific heat up to about 700° F and then shows a rapid increase. The inflection point on this curve is indicative of changes occurring within the alloy. In the case of Supermendur, 750° F corresponds to the order-disorder temperature of the alloy. The specific heat of Hiperco 50 alloy was not measured for this program since it was expected that the specific heat of both Supermendur and Hiperco 50 alloy would be equivalent. This assumption may not be valid since the vanadium content of the Hiperco 50 alloy was double that of Supermendur.

Electrical resistivity: Electrical resistivity data for 0.002-inch-thick Supermendur tape (magnetic field annealed) are given in table 17 (p. 132). Because room-temperature measurements had shown that the resistivity of the ribbon might vary as much as 3 percent from the end of a wound toroid to the center, complete tests were made on specimens from both locations. The change in resistivity with temperature was found to be essentially the same in both.

Magnetic properties: Hiperco 50 alloy was tested as ring laminations in two

thicknesses, 0.004 and 0.008 inch (figs. 129 to 146, pp. 135 to 143). Although both samples were annealed at the same time, the measured dc properties were quite different. Room-temperature properties for the 0.004-inch-thick sample were a coercive force of 0.616 oersted, residual induction of 10.9 kilogauss, and an induction of 18.8 kilogauss at a magnetizing force of 10 oersteds. For the 0.008-inch-thick sample, the properties were a coercive force of 2.74 oersteds, residual induction of 6.6 kilogauss, and induction of 9.6 kilogauss at 10 oersteds. It is not known why the annealing cycle did not develop the correct magnetic properties in the 0.008-inch-thick material. Up to 1400° F, both the magnetization curves and coercive forces for 0.004-inch-thick ring laminations are characteristic of the alloy. At 1100° F, the coercive force decreased to 0.31 oersted. Also at 1100° F the induction decreased to 18 and 21.5 kilogauss at magnetization intensities of 10 and 300 oersteds, respectively. However, the coercive force increased at both 1400° F and at room temperature after exposure to 1400° F. This increase indicated that some permanent structural change had taken place in the material during exposure to elevated temperature. The induction values at 1400° F were 16 and 18.4 kilogauss for field intensities of 10 and 250 oersteds, respectively. The core-loss data as a function of temperature follow the same temperature-dependent trend as the coercive force data. At a frequency of 400 cps, room-temperature core losses of 11.5 and 8.6 watts per pound were observed at inductions of 18 and 15 kilogauss, respectively. Core loss decreased to 6.5 and 5.3 watts per pound at 1100° F but subsequently increased to 17 and 12 watts per pound at 1400° F. This pattern was reversed at temperatures up to 1100° F for exciting volt-amperes. These data illustrate the competing mechanisms of core loss and permeability. At 3200 cps, the core loss at 8 kilogauss was 55 and 37 watts per pound at 72° and 1100° F, respectively. The corresponding exciting volt-ampere values were 185 and 109 volt-amperes per pound.

Supermendur magnetic properties were measured at temperatures to 800° F and at frequencies to 3200 cps on 0.002-inch-thick tape-wound toroids and on 1/2-inch-high stacks of 0.006-inch-thick ring laminations. Two different size tape-wound toroids were tested. Properties at elevated temperature were measured in argon. At 500° F (fig. 146, p. 143) the coercive force of the large 0.002-inch-thick tape-wound toroid decreased from its room-temperature value of 0.33 to 0.2 oersted; the residual induction increased from 18.2 to 20.3 kilogauss, which resulted in increased loop squareness. When the temperature was increased to 800° F, the coercive force increased and the remanent induction decreased. The decrease in magnetic properties was evident in the room-temperature measurements made after exposure to 800° F. An increase in coercive force to 0.4 oer-

sted and a 40-percent decrease in residual induction to 7.5 kilogauss was observed after Supermendur was heated to 800° F. The core loss and exciting volt-ampere data were affected similarly, particularly over the frequency range of 800 to 3200 cps. Both core loss and exciting volt-amperes increased gradually with increasing temperature while the slope of their curves decreased as the test frequency increased, as shown on figures 150 to 173 (pp. 145 to 157).

Supermendur core loss data were obtained on the large (4-in.) 0.002-inch-thick tape-wound toroid. The small $1\frac{1}{4}$-inch toroid was tested at 72° F only. The dc properties of the smaller toroid were similar to those measured on the large toroid. However, the core loss and exciting volt-amperes of the small toroid were twice those measured on the 4-inch toroid. The 1/2-inch-high stack of 0.006-inch-thick ring laminations did not exhibit the increase in squareness noted in the data for the tape-wound toroids tested at 500° F. The coercive force measured on the Rowland ring sample gradually increased with temperature and was combined with a simultaneous decrease in residual induction. Magnetization curves obtained at temperature show less deviation from the room-temperature curve than do those for 0.002-inch-thick tape-wound toroids. The core loss and exciting volt-ampere curves obtained at different temperatures are close together.

Constant-current flux-reset (CCFR) tests (400 cps) were conducted in air at 72° F and in argon at 500° and 1100° F. All specimens were placed in nonmagnetic, stainless-steel core boxes where an argon atmosphere could be maintained. Silicate fiber insulation was wrapped around the specimens and the core boxes. CCFR test results are listed in table 18 (p. 134). The room-temperature peak induction values (B_m) were reached in a field of 5 oersteds (H_m) and ranged from 18.15 to 20.10 kilogauss for a 1/2-inch stack of 0.006-inch-ring laminations and from 21.7 to 22.8 kilogauss for 0.002-inch-thick tape-wound toroids. Induction values obtained on the small toroids were higher than those measured on the large toroids. Other CCFR properties measured on samples of both gages were similar, except for sample 1 of 0.002-inch-thick tape, where the H_o values (a property comparable to coercive force) ranged from 0.6 to 0.65 oersted. The loop-squareness ratio of all samples was from 0.825 to 0.925.

Loop squareness improved at 500° F for most specimens and decreased slightly at 1100° F. The loop width followed the general pattern discussed earlier, that is, the width decreases with increasing temperature, reaching an H_o value of 0.42 to 0.52 oersted at 1100° F. However, the room-temperature value of H_o for all CCFR properties was badly degraded by exposure at 1100° F. All samples showed a considerable increase in H_o, with its value raised to 1 oersted. A decrease in B_m and squareness was noted in most samples.

Significant changes occurred in Supermendur CCFR properties as the test temperature was increased. These changes were particularly pronounced at 500° F where both increases or decreases in B_m were observed. This change is the result of atomic ordering and phase changes which take place at elevated temperatures in the iron-cobalt alloy system. However, the inconsistency in the trend of the changes observed at 500° F appears to be associated with the heat treatment of the samples. Note that a change was observed in the slope of the 500° F dc magnetization curve obtained on the small tape-wound toroid and that there was an improvement in loop squareness. Therefore, use of Supermendur above 500° F is not recommended for critical applications where predictable performance is required.

Tensile properties: Supermendur and Hiperco 50 alloy materials have been compiled together in this report to make a direct comparison of properties. Both Supermendur and Hiperco 50 alloy nominally contain 49 percent each of cobalt and iron with an addition of 2 percent vanadium for improved workability. The Supermendur tested, however, was analyzed and found to contain only 1 percent vanadium. The commercial specification and technical literature call for a vanadium content of 1.5 to 2.5 percent. While it was not known what the exact effect of the low vanadium content would be, no major differences were anticipated between the properties of Supermendur and Hiperco 50 alloy. It was surprising to note the unusually high ultimate tensile strength of the annealed 0.006-inch-thick Supermendur sheet obtained at all test temperatures except room temperature (see table 20, p. 161, and figs. 178 and 179, p. 162). The pseudobinary phase diagram of iron-cobalt plotted against vanadium calls for a two-phase field at vanadium contents above about 1.5 percent. If the second phase existed in the samples of 2 percent vanadium Hiperco 50 alloy, the strain-hardening coefficient for that material could easily have been much less than that of the single-phase Supermendur. Note that the tensile strength of both materials increases with temperature and that the Hiperco 50 alloy must be heated above 1100° F before the tensile strength falls below the 72° F strength. Neither material has much ductility, as shown in figures 176 (p. 160), 177 (p. 160), and 179 (p. 162).

Hiperco 27 alloy (vacuum-melted forged bar and investment cast bar). - A summary of the properties of these materials is located in the section, MAGNETIC MATERIALS PROPERTIES.

Specific heat: Specific-heat data for both the vacuum melted and investment cast alloy are plotted in figure 180 (p. 167). Differences between the two curves are probably caused by differences in grain size and impurity content.

Electrical resistivity: The electrical resistivity as a function of temperature

for vacuum-melted forged Hiperco 27 alloy is presented in table 21 (p. 168) and is plotted in figure 181 (p. 169). These data are uniform and have negligible hysteresis.

Magnetic properties: Hiperco 27 alloy was tested in three basic forms, an investment cast ring, vacuum-melted forged bar, and two lamination thicknesses (4 and 8 mil). The magnetic properties of all three forms changed with increasing test temperature in a manner typical of single-phase alloys.

The dc properties of Hiperco 27 alloy samples conformed to properties information in the supplier's published product literature with the exception of relatively high 72° F coercive force values of 5.12 and 3.40 oersteds for both the forged and cast rings. A larger grain size may be responsible for the lower coercive force of the casting as compared with the forging. Both solid rings approach an induction of 24 kilogauss in a field of 300 oersteds at 72° F (figs. 182 and 183, p. 171).

The 72° F coercive force values for the laminated ring samples were between 1.4 and 1.7 oersteds (figs. 184 to 192, pp. 172 to 176). The corresponding induction value for the sheet material approached 24 kilogauss in a field of 300 oersteds. Hiperco 27 alloy loss decreased at all test frequencies with increasing temperature to 1400° F. The core-loss values for the two lamination thicknesses were relatively close at a frequency of 400 cps but diverged slowly as the test frequency increased. At 400 cps and 18 kilogauss, the 0.008-inch-thick ring laminations had a core loss of 16.2 and 14.3 watts per pound at 1100° and 1400° F, respectively (fig. 214, p. 187).

One problem observed with Hiperco 27 alloy laminations in 1400° F tests was the apparent deterioration of the interlaminar insulation that, in turn, caused a considerable increase in core loss at inductions above 12 kilogauss. Testing of additional samples after improvement and reapplication of the interlaminar insulation was necessary. Table 22 (p. 170) gives test program details and results. An analysis of these data shows that interlaminar insulation of the original (sample 1) Hiperco 27 alloy sample was inadequate. The high core-loss condition was improved, particularly at high induction, by recoating, as observed in sample 2. However, after again improving the insulation application methods, there was still a slight increase in room-temperature core loss after exposure to 1400° F at inductions above 12 kilogauss for samples 3, 4, and 5. This change in core loss is probably the result of changes in grain size and orientation and resulted in a decrease of the coercive force and a leveling off of the magnetization curve at high inductions. The dc properties of the Hiperco 27 alloy samples listed in table 22 show no appreciable change in the room-temperature data after exposure to 1400° F. The coer-

cive force, which is considered a sensitive indicator of structural changes, showed even lower temperature values for all samples after exposure to 1400° F. Electrical resistivity measurements conducted after test displayed no appreciable changes in the material after exposure to 1400° F or after insulation recoating. Photomicrographs showed only slight oxidation of the sample surface with minor penetration of oxygen along grain boundaries. Only data on 0.008-inch-thick laminations for samples 3 and 4 are given, since these data are the most characteristic when adequate interlaminar insulation is present. The magnetic properties of Hiperco 27 alloy are presented on figures 182 to 218 (pp. 171 to 189).

Poisson's ratio: The Poisson's ratio data for vacuum-melted forged Hiperco 27 alloy are presented in table 23 (p. 190). Six average values were obtained on two separate specimens. Individual values were obtained for every 250 pounds of specimen load up to a stress of 48 450 psi. Two longitudinal and two transverse strain gages were cemented to each side of the sample. Hiperco 27 alloy is a fine-grained material and was not expected to cause difficulties in the measurement of Poisson's ratio. The data for several test runs are plotted on figures 219 to 224 (pp. 191 to 193).

Tensile properties: The tensile properties, including the modulus of elasticity for the Hiperco 27 alloy materials, are shown in data form in tables 24 (p. 194) and 25 (p. 196) and are plotted in figures 225 to 229 (pp. 195 to 197). Duplicate tension tests were made on both forms of the alloy at room temperature, 500°, 700°, 1000°, and 1400° F. The room temperature, 500° and 700° F tests were run in air; one of the 1000° F tests on vacuum-melted material was run in a flooded-argon atmosphere and the others in air to determine the effect of oxidation at 1000° F. No significant differences in tensile properties were observed. The 1400° F tests were run in a chamber flooded with argon. A low indicated yield strength was noted on one room temperature test on vacuum-melted Hiperco 27 alloy. The yield strength of this sample was a yield point rather than 0.20 percent offset yield strength. No explanation of the appearance of the yield point can be offered. The short-time elevated temperature tensile data appear to show no effect of test atmosphere on the properties of Hiperco 27 alloy.

An expected drop in the elevated temperature ductility for Hiperco 27 alloy (figs. 226, p. 195, and 229, p. 197) occurs in the temperature range between 700° and 1400° F. This drop is observed in nearly all materials (ref. 7) and marks the temperature range at which vacancies are generated and move to grain boundaries but are not subsequently annihilated by recrystallization. The mode of fracture changes from transgranular to intergranular and back to transgranular over this temperature range. Only the low room temperature ductility of the cast material

deserves mention, since it is a condition common to as-cast and annealed Hiperco 27 alloy. The elevated temperature ductility of cast Hiperco 27 alloy was a minimum at 1000° F.

The compressive strength properties of the vacuum-melted material are presented in table 26 (p. 198) and are plotted in figures 230 (p. 199) and 231 (p. 199). Elevated temperature compressive modulus data for Hiperco 27 alloy are higher than for the tensile modulus.

Creep: Creep data for air-, argon-, and vacuum-tested Hiperco 27 alloy material (vacuum-melted and investment-cast materials) are presented as Larson-Miller plots in figures 232 (p. 200) and 234 (p. 201) for 0.2 and 0.4 creep strain. It is apparent from these plots that the vacuum-melted material (fig. 232) was not affected by the test atmosphere. The investment-cast material was, however, improved by testing in a vacuum (fig. 234). No effects of the vacuum tests were noted on the before and after test gas analysis performed on any of the materials studied. The greater creep resistance of the vacuum-tested Hiperco 27 alloy casting was considered due to the absence of surface oxygen that apparently contributed to lower strength for the air-tested investment-cast material. The creep of the vacuum-melted alloy was not affected by the testing atmosphere.

On the basis of tests completed, Hiperco 27 alloy lacks the strength required to determine 10 000-hour strength at and above 1400° F. Creep data are presented as log-log plots of stress against time and are shown in figures 233 (p. 200) and 235 (p. 201). The stress was raised on some of the test specimens when little or no creep could be measured or recorded during the test. These data are considered valid for the strains involved.

Tables 27 to 32 (pp. 202 to 214) and figures 236 to 247 (pp. 203 to 213) show tabulations and plots of creep data at various temperature and stress levels. These plots show the stage of creep for each specimen at each time data points were obtained.

1-Percent silicon-iron investment cast material. - A summary of the properties for this material is located in the section, MAGNETIC MATERIALS PROPERTIES.

Specific heat: The specific heat of AMS 5210 is presented in figure 248 (p. 217). This property remains fairly constant to 572° to 662° F and then increases exponentially to a value of 0.155 Btu per foot per °F at 932° F.

Magnetic properties: Only dc properties were measured on this material. The change in properties with temperature followed the pattern observed for other silicon-irons. Residual induction, coercive force, and induction at 250 oersteds decreased with increasing temperature while permeability at 2 kilogauss first de-

creased and then increased with increasing temperature. There was little change in the magnetization curve after temperature cycling to 1100° F, though coercive force increased by 15 percent. At 1100° F the coercive force decreased from 1.05 oersteds at room temperature to 0.58 oersted and the induction for 250 oersteds from 19.2 to 16.7 kilogauss. Data for dc tests are presented in figures 249 (p. 217) and 250 (p. 218).

Tensile properties: The tensile properties of AMS 5210 are presented in table 33 (p. 219) and figures 252 (p. 220) and 253 (p. 226). The cast bars were annealed in accordance with AMS 5210 before testing. No clarification of the tensile data is required for this material. The expected ductility minimum of AMS 5210 occurs at 500° F. This material, like several of the other soft magnetic materials, is not intended for use under high stresses.

Maraging steels (15% and 18% nickel grades). - Summaries of the properties of the maraging steels are located in the section, MAGNETIC MATERIALS PROPERTIES. Until recently, the maraging steels have been available in three basic grades containing 25, 20, and 18 percent nickel. The 18-percent-nickel grade is available in three subgrades referred to by nominal yield strengths as 200, 250, and 280 ksi as determined by the titanium, cobalt, and molybdenum content. (Grade 280 is commercially known as the 300 grade.) Now, a fourth basic grade has been introduced, the 15-percent-nickel grade. This steel possesses better stability and higher strength at elevated temperature. The improved stability is attributed to the lower nickel and higher molybdenum content.

At the time work under this contract was initiated, no elevated temperature ac or dc magnetic properties were available for the 18-percent-nickel grade, but the elevated-temperature mechanical properties were well documented. Properties of the 15-percent-nickel grade were not documented, so tests were planned to determine the elevated temperature magnetic properties of the 18-percent-nickel, 250 grade, and the magnetic properties and 1000° F magnetic stability of the 15-percent-nickel grade. The discussion of the properties found in the literature, as well as those obtained in this investigation, follows.

Magnetic properties: In this program magnetic tests were conducted at temperatures up to 800° F on 0.014-inch-thick laminations of 18-percent-nickel and 0.016-inch-thick laminations of 15-percent-nickel maraging steels (figs. 255 to 257, pp. 227 and 228, and 259 to 261, pp. 229 and 230, respectively). In addition, a 1000-hour stability test at 1000° F was performed on a solid ring of 15-percent-nickel maraging steel. These data are plotted in figure 254 (p. 226). On another program, magnetic tests were performed on 15- and 18-percent maraging steel forgings at temperatures up to 1100° F (figs. 253, p. 226, and 258, p. 228).

The data obtained on forgings, particularly the magnetization curves for 1100° F, show that a decrease in nickel content from 18 to 15 percent nickel raises the temperature capability of maraging steels. The results from the 1000-hour stability test (fig. 254, p. 226) indicate that the temperature limit of the 15-percent-nickel maraging steel lies below 1000° F, probably between 750° and 850° F. At 700° F, both the 15- and 18-percent-nickel maraging steel forgings reach an induction of 16 kilogauss in a field of 300 oersteds and display a coercive force of 16 to 18.6 oersteds.

Test data on sheet material (figs. 257, p. 228, and 261, p. 230) show little difference in core loss for different grades. Respective core-loss values for 0.016- and 0.014-inch-thick laminations, respectively, of 15- and 18-percent-nickel maraging steels are 218 and 195 watts per pound at room temperature; 200 and 208 watts per pound at 500° F; 195 and 190 watts per pound at 800° F; and 213 and 243 watts per pound at room temperature after 800° F. No significant changes in room-temperature values of the coercive force and high-field induction occur in 15-percent-nickel maraging steel laminations after exposure to 800° F. However, changes did occur in the 18-percent-nickel maraging steels at 800° F; the values for this material are 22.6 and 19.6 oersteds and 19.3 and 16.6 kilogauss for room temperature and 800° F, respectively.

Tensile properties: The tensile properties of both grades of maraging steel are shown in tables 34 (p. 231) and 35 (p. 231) and are plotted in figure 262 (p. 232). The elastic modulus of the 18-percent 250 grade is shown in figure 263 (p. 233). Selection of the 18-percent 250 grade rather than the 300 grade was based on the superior ductility, impact strength, and overall mechanical similarity of the 18-percent 250 grade to the 15-percent 280 grade even though the 15-percent material is basically a higher strength alloy. The extremely high 800° and 1000° F strength data of the 15-percent grade, are higher than those obtained on any other maraging steel.

Creep: Larson-Miller plots for creep of the 15- and 18-percent-nickel grades are shown in figures 264 (p. 233) and 266 (p. 234), respectively. The creep data for the 15 percent nickel are shown in table 36 (p. 235) and are plotted as stress-time curves in figure 265 (p. 234) and figures 267 to 275 (pp. 238 to 242). Creep data for both grades were obtained on material solution heat-treated at 1500° F and aged at 900° F. It should be noted that the creep properties of the 15-percent-nickel grade may be improved when the material is solution-annealed at 1800° F and then aged at 900° F (ref. 8). The lower-temperature solution treatment was selected for this program because it was the commonly accepted heat treatment suggested by the supplier. The maraging steel creep data have allowed the follow-

ing conclusions to be made: (1) The 15-percent-nickel grade is not adversely affected by air contamination during testing to 900° F since vacuum test data fell on the curves generated with air test data; (2) the start of reversion from martensite to austenite in the 15-percent grade appears to start between 700° and 800° F and is apparently well underway at 900° F; and (3) the creep rate of the 18-percent grade is well above that of the 15-percent grade, especially at 800° and 900° F.

The vacuum creep data are also presented on the Larson-Miller plot (fig. 264, p. 233) for the 15-percent grade. The plots of creep-time data included in figures 267 to 275 (pp. 238 to 242) will be useful to those who wish to know the stage of creep for each specimen at the time the data points were obtained.

Fatigue: A room-temperature fatigue curve on 18-percent nickel material is shown in figure 276 (p. 242). The melting technique is an important variable influencing the fatigue properties of the maraging steels and it is therefore important to consider this factor when selecting maraging steel for any given application.

AISI Grade H-11 steel AMS 6487 (bar and forgings) and AMS 6437 (sheet). - When H-11 was first studied as a candidate material for high-stress applications at moderately elevated (800° F) temperatures, it was selected because of its strength and strength-retention characteristics at elevated temperatures. The magnetic properties of this alloy at high hardness (Rockwell C52) levels were at best marginal. Subsequent work by Westinghouse under an Air Force Program (Contract AF33(615)-1551) on the heat treatment and mechanical properties of H-11 achieved acceptable magnetic properties and managed to maintain the strength at a high level. Actually, the elevated-temperature creep strength of the H-11 at the lower hardness (Rockwell C45) was better than the creep strength of the material heat-treated to the most commercially used hardness (Rockwell C52). This improvement in creep characteristics is probably the result of a finely dispersed carbide precipitate formed during high-temperature tempering, which increases the creep resistance of the martensitic matrix.

Magnetic properties: Figures 277 to 288 (pp. 246 to 251) present dc and ac magnetic properties of this material. The changes in coercive force and permeability with increasing temperature follow the same general pattern in both forged and sheet materials. At 250 oersteds, an induction value of over 18 kilogauss is reached at room temperature. The coercive force decreases to 15 oersteds at 1100° F. As discussed previously in this report, on stability testing at 1000° F for 1000 hours, there was a progressive increase in permeability (fig. 278). In general, the dc magnetic properties improved with time at a given temperature.

As the gage thickness decreased, there was no change in coercive force. There was little difference in losses between the 0.014- and the 0.025-inch-thick

sheet materials at either room or elevated temperature. Surprisingly, the 0.025-inch-thick sheet displayed somewhat lower losses than those measured for the 0.014-inch-thick sheet. (Refer to figs. 283, p. 249, 287, p. 251, and 288, p. 251, for comparative data.)

Tensile properties: Tensile properties of AMS 6487 are listed in table 39 (p. 252) and are plotted in figure 289 (p. 253). These data were taken from reference 10 and represent typical values obtained for material from different heats at a nominal hardness of Rockwell C45.

Creep: As pointed out in the introduction to the H-11 section, a large amount of tensile and creep data were obtained from another Westinghouse program. These creep data are presented and discussed here since a specific creep program was not planned for this investigation in anticipation of the availability of data from that program. A sheet-material creep program was included in these studies, however, since no data on H-11 sheet were available on material thinner than 0.050 inch. The technology required to produce 0.014- and 0.025-inch AMS 6437 was also needed and subsequently developed as indicated in the section, MATERIALS, PREPARATION, AND TEST PROCEDURES. Creep data on sheet material were obtained on samples taken transverse to the rolling direction, since the transverse creep properties were expected to be most affected by processing 0.050-inch material into thinner gage sheet. In addition, creep test checks were made using selected longitudinal samples. The sheet specimens were hardened to Rockwell C45. Creep data for bar and sheet material are shown in tables 40 to 43 (pp. 256 to 262). The sheet and vacuum creep on forged-material data were obtained in these studies and the bar data in air were obtained from studies performed by Westinghouse for the SNAP-50 SPUR-Power System (Contract AF33(615)-1551). All air and vacuum creep data so obtained on different lots of AMS 6487, heat treated to Rockwell C45, are shown in the Larson-Miller plot (fig. 290, p. 253).

Creep data obtained on H-11 sheet are shown in similar Larson-Miller plots in figures 292 (p. 254) and 293 (p. 255). The strain-time curves for tests in air are presented in figures 295 to 299 (pp. 258 to 260). These curves are useful in determining the transition from first- to second-stage creep. A comparison of air and vacuum creep data for bar material, as compared with sheet material in air, is plotted in figure 291 (p. 254).

From the creep data, the following conclusions are made: (1) the creep properties of AMS 6437 (H-11 sheet) are isotropic at a hardness level of Rockwell C44.5 to 45.5 and are equivalent to those obtained on bar; (2) bar material (AMS 6487) is not adversely affected by testing in air or vacuum atmosphere up to 1000° F and a vacuum of 10^{-6} torr; and (3) at 900° F and 10 000 hours, a charac-

teristic stress of 45 000 psi for 0.4 percent extension is realized from Larson-Miller extrapolations.

A tabulation of the 800° and 1000° F fatigue data obtained in these studies is presented in tables 44 to 46 (pp. 262 to 265). These data are plotted on figures 302 to 305 (pp. 266 and 267). Fatigue data were obtained at stress ratios A of 0.25 and 2.00. The stress ratio A is defined as the ratio of alternating stress to mean stress. Modified Goodman diagrams of these fatigue data are shown in figures 300 (p. 263) and 301 (p. 263). No points are located on the X-axis of these plots since no known material property measurement (yield, tensile, creep, or stress rupture strength) would be meaningful. The shapes of these modified Goodman plots do not always follow the usual trends, and no explanation for their shape can be offered. H-11 was notch-sensitive under all conditions of test, although the degree of sensitivity was noticeably lessened by the application of a superimposed static stress. In heat treating H-11, this alloy was found to be extremely sensitive to decarburization. Several lots of fatigue specimens were lost because of decarburization during heat treatment. As little as 0.001 inch of decarburization can adversely affect the quality-test data. H-11 should be heat-treated only in atmospheres that will cause neither carburization nor decarburization.

Nivco alloy. - A summary of Nivco alloy properties is given in the section, MAGNETIC MATERIALS PROPERTIES.

Specific heat: The specific heat data for forged Nivco alloy are presented graphically in figure 306 (p. 272). A constant value for specific heat of 0.102 calorie per gram per °C (or Btu/(lb)(°F)) was measured at temperatures to 300° C (572° F). Above 300° C, the curve behaves exponentially and reaches a specific heat of 0.156 calorie per gram per ° C at 700° C (0.156 Btu/(lb)(°F) at 1292° F).

Electrical resistivity: Test results for Nivco alloy sheet are listed in tables 47 (p. 273) and 48 (p. 275). Resistivity measurements were made during both heating and cooling to and from 1600° F, respectively. The first test showed a degree of hysteresis as shown in figure 307 (p. 274). The second test plot (fig. 308, p. 276) shows the electrical-resistivity results for forged Nivco alloy in the equilibrium condition, in which the cooling curve followed the heating curve exactly.

Magnetic properties: Tests on forged stock show that coercive force and residual induction as well as permeability at high inductions decrease with increasing temperature; however, permeability at low inductions increases with increasing temperature. After the test at 1400° F, the room temperature coercive force was 8.9 oersteds, a reduction from the 11.5 oersteds measured initially. After stability testing (fig. 310, p. 277) for 1000 hours at 1000° F, the magnetic properties

of the Nivco alloy forging were virtually unchanged. This indicated that the mate-
rial is stable at this temperature.

Changes in the dc properties of 0.014- and 0.025-inch-thick laminations follow
the same trend with increasing temperature as those measured for the forging.
However, coercive force of sheet materials is considerably higher (40.3 and
35.5 Oe at room temperature for 0.014- and 0.025-in.-thick laminations, respec-
tively) at both room and elevated temperatures. There is little difference in core-
loss values for both sheet thicknesses in spite of different gages. At 400 cps and
8 kilogauss, the core-loss values for 0.014- and 0.025-inch-thick laminations, re-
spectively, are 158 and 135 watts per pound at room temperature and 46 and
44 watts per pound at 1400° F. Upon return to room temperature, the losses are
84 and 88 watts per pound after exposure to 1400° F (figs. 314, p. 279, and 316,
p. 280). A considerable decrease in coercive force appears to be primarily re-
sponsible for the decrease in losses at room temperature. This phenomenon was
previously mentioned.

Tensile properties: The short-time-elevated-temperature tensile properties
for forged Nivco alloy are tabulated in table 49 (p. 281) and are graphically shown
by figures 317 (p. 280) and 318 (p. 282). The room-temperature tensile properties
for forged Nivco alloy show the 0.2-percent offset yield strength to be approxi-
mately 68 percent of the ultimate strength. The 0.2-percent yield strength and
ultimate strength do not dip appreciably up to 1100° F. Nivco alloy overages
rapidly at 1400° and 1600° F.

The short-time-elevated-temperature properties of 0.025-inch-thick trans-
verse Nivco sheet are shown in table 50 (p. 283) and figures 319 (p. 284) and 320
(p. 284). The room-temperature 0.2-percent offset yield strength is 95 percent
of the ultimate strength for sheet, as compared with 68 percent of tensile strength
for bar. This ratio is reduced continuously with temperature to a value of 78 per-
cent at 1100° F.

Creep tests: Test results for forged Nivco alloy are tabulated in tables 51
to 54 (pp. 287 to 297) and are plotted in figures 321 to 328 (pp. 285 to 289). The
900° and 1100° F tests required stresses above the yield strength of the alloy to
produce 0.2- and 0.4-percent creep strain in 1000 hours or less. Creep testing
above the yield strength of a material introduces scatter not normally encountered
in creep data. However, the data obtained in this manner could be easily fitted to
smooth curves in both Larson-Miller and stress-time data plots. Nivco alloy did
not initially appear to be adversely affected by the test atmosphere, whether the
atmosphere was air or argon (fig. 322, p. 285). However, creep resistance was
affected when the alloy was tested in air above 1400° F or in vacuum above 900° F,

as shown in the Larson-Miller plots of figure 321 (p. 285), which were prepared after a parameter constant of 30 had been calculated for Nivco alloy. The Larson-Miller plot shows that it requires an apparent stress of 80 000 psi to produce 0.4-percent creep strain in 10 000 hours at 1000° F.

Table 55 (p. 297) and figures 339 to 341 (p. 298) are for 0.025-inch-thick transverse Nivco sheet. The 0.2- and 0.4-percent creep strains were produced at stresses which are lower than required to produce equivalent deformations in forged Nivco bar. These data were obtained on samples which had been reheat-treated for improved creep strength. A large amount of initial creep data were obtained on samples which had been simply cold-finished and then aged after solution heat treatment. These samples possessed extremely low creep strength. Data on the low-strength materials are included for reference only and should not be used except for comparison purposes. Creep strength for the sheet Nivco samples was improved after the remaining test specimens were again solution-heat-treated at 1900° F, 175° F above the nominal solution treatment temperature of the material (1725° F), and subsequently aged for 25 hours at 1225° F to produce maximum hardness. It was assumed that the initial low creep strength of the Nivco sheet was connected with the cold-finishing operation used on Nivco sheet after solution annealing.

Shop practice for making magnetic alloy sheet usually requires cold-finishing of the materials. The Nivco used for this program was bought in the solution-heat-treated and cold-finished condition. A controlled research program is required to completely restore the creep properties of Nivco sheet to the level achieved with bar stock. Creep test results on the reheat-treated material are shown in the summary in the section, MAGNETIC MATERIALS PROPERTIES. The creep-time curves of figures 329 to 341 (pp. 290 to 298) show the stage of creep for each specimen at the time the data points were obtained.

Fatigue tests: Fatigue data for forged Nivco alloy bar are listed in tables 56 to 58 (pp. 299 to 302). The fatigue tests were conducted on smooth and notched bar specimens at temperatures of 900°, 1000°, and 1100° F with the use of stress ratios A of infinity and 0.25. Figures 343 to 348 (pp. 303 to 305) are curves representing smooth- and notched-bar fatigue lives at different stresses. The notched-bar properties are 30 000 to 40 000 psi below the smooth-bar stresses at a stress ratio of infinity. These data show the expected notch sensitivity of forged Nivco alloy. At a stress ratio of 0.25, the notched and unnotched fatigue properties for forged Nivco alloy are improved. The notched sensitivity is almost eliminated, and an increase of 50 000 to 60 000 psi in maximum stress is obtained. The only deviation in the improved fatigue properties occurs after 10^6 cycles at 1100° F. At this

test condition, the forged Nivco alloy gives indications of becoming notch-sensitive.

Table 58 (p. 302) contains the tabulated data used to construct the modified Goodman diagram (fig. 342, p. 300). This figure shows the deviation between smooth- and notched-bar fatigue properties at 1100° F for 10^7 cycles for a stress ratio of 0.25.

MATERIALS, PREPARATION, AND TEST PROCEDURES

Material Specifications and Preparation

The magnetic materials tested, their sources, and purchasing specifications were as follows:

Material and form	Source	Product specification
Westinghouse Cubex alloy; 6- and 12-mil sheet and 2- and 6-mil tape-wound cores (3Si-Fe)	Westinghouse Research and Development Center, Pittsburgh 35, Pa., and Westinghouse Specialty Transformer Division, Beaver, Pa.	No commercial specification available
Supermendur; 2-mil tape, 6-mil sheet, and 2V-Permendur bar (49Fe-49Co-2V)	Arnold Engineering Corp., Marengo, Ill.	Arnold Engineering Product Specification for Supermendur with Westinghouse core-loss requirement
Hiperco 50 alloy; 4- and 8-mil sheet (49Fe-49Co-2V) Hiperco 27 alloy; 4- and 8-mil sheet bar and casting (27Co-Fe)	Westinghouse Materials Manufacturing Dept., Blairsville, Pa.	Westinghouse Product Specification
Iron 1-percent silicon investment casting	Hitchener Manufacturing Co., Milford, N. H.	AMS 5210
Nivco alloy sheet and bar (23Ni-1.1Zr-1.8Ti-Co)	Westinghouse Research and Development Center, Pittsburgh 35, Pa., and Westinghouse Materials Manufacturing Dept., Blairsville, Pa.	No commercial specification available
Maraging steel bar and sheet (15-18Ni-Co-Mo-Fe)	Allegheny Ludlum Steel Corp.	Allegheny Ludlum Product Specification Almar 15 and Almar 18
AISI Grade H-11 sheet; 0.050-in.-thick premium quality material (5Cr-1Mo-1V-Fe)	Universal Cyclops Steel Corp. Rerolled to 0.014- and 0.025-inch and heat-treated by Westinghouse Research and Development Center, Pittsburgh 35, Pa.	AMS 6437
AISI Grade H-11; bar and forgings premium quality material (5Cr-1Mo-1V-Fe)	Universal Cyclops Steel Corp.	AMS 6487

Three of these materials, Nivco alloy, H-11, and 15-percent maraging steel in thin-gage sheet, were not commercially available at the time this program was started. Consequently, sheet rolling technology was developed to produce limited quantities of both alloys for this program. A detailed account of the rolling procedures is given in subsequent paragraphs.

Nivco alloy sheet preparation. - Starting material for the Nivco strip consisted of a 5- by 5- by 10-inch-long forged bar which was subsequently hot-forged at 1850° to 2100° F to a 5/8- by 5-inch slab. The slabs were then hot-rolled to a 0.125-inch strip. A heavy, tenacious oxide which formed on the alloy during the hot-rolling operation was removed by grit blasting and pickling in a mixture of 35 percent hydrochloric acid, 50 percent nitric acid, and 15 percent water.

After pickling, the 0.125-inch strip was cold-rolled in an 8- by 8-inch, two-high mill to 0.062 inch thick and annealed at 1825° F in dry hydrogen. The cold rolling proceeded in the two-high mill to 0.025 inch thick where half the strip was again annealed and finished in a four-high mill to 0.015 inch. The 0.015-inch strip was skin-passed in a two-high mill to achieve a flat product.

H-11 (AMS 6437) sheet preparation. - The as-received, 0.050-inch thick, annealed H-11 certified to meet AMS 6437 was cold-rolled in a two-high mill directly to 0.025 inch. Half the material was finished to 0.015 inch on the four-high mill and flattened by a final pass through the two-high mill. No intermediate annealing was required on the H-11 material.

15- and 18-percent-nickel maraging steel sheet preparation. - The starting material was a 10-pound 1-inch-diameter bar of 15-percent-nickel maraging steel that was hot-rolled after heating in hydrogen at 1850° F. No difficulty was experienced in preparing the 0.100-inch strip. The strip material was cooled to 1500° F, held for 15 minutes, then water-quenched to 72° F. After hot rolling, the as-quenched strip was cold-rolled to 0.022-inch thickness and was then again solution-annealed at 1500° F, quenched, pickled, and cold-rolled to 0.016 inch. The rolling was done in a two-high mill. After punching and deburring, the laminations were aged in hydrogen for 3 hours at 900° F and then were coated with aluminum orthophosphate. The 18-percent-nickel maraging steel sheet was supplied in the punched and fully heat-treated condition.

Test Specimen Preparation

A series of drawings showing typical examples of mechanical and thermophysical test specimens are presented in figures 12 to 41 (pp. 57 to 69). Unless

otherwise specified, all dimensions shown on the drawings are in inches.

Solid dc test ring. - All the heat-treatable alloys were machined to 0.020-inch oversize, heat-treated, finish-machined, and ground to size. The heat treatments used on the different alloys are listed later in this section.   *

Rowland-ring test samples. - The sheet materials were blanked and pierced by precision dies to hold deburring to a minimum. After blanking, all laminations (except those of Supermendur, which were returned to the supplier for further processing) were degreased and insulated with one coat of aluminum orthophosphate to prevent sticking during magnetic-field or stress-relief annealing. Unless otherwise specified, all samples were stress-relief annealed (SRA). After annealing, a second coat of aluminum orthophosphate was applied as an interlaminar insulation. When deburring was necessary, the rings were passed through an automatic belt sander.

All the finished cores were wound with insulated wire and tested. Wire selection depended on the test temperature and the driving voltages. Nickel-coated copper wire insulated with refractory-oxide composite insulation was used for tests to 1100° F and 100 volts. Above these limits wire insulated with fiber glass and refractory oxide was used.

Mechanical and thermophysical test specimens. - The mechanical and thermophysical test specimens were the following types:

Smooth-bar specimens: The smooth-bar specimens were rough-machined to 0.020 inch oversize and heat-treated when required. They were then rough-ground to 0.008 inch oversize, and then finish-ground in 0.0002-inch increments to 0.001 inch oversize with coolant and polished with 180-, 400-, and 600-grit abrasive as necessary to achieve the specified finish and size. When specified, they were lapped to the indicated finish.

Notched-bar specimens: After heat treatment, the notch was rough machined in the notched-bar specimens to 0.010 inch oversize then finish machined to size with a carbide-tipped cutting tool that was exactly ground to the notch contour. Finishing and polishing with an appropriate string impregnated with abrasive for finishing the notch was then performed. Care was taken not to alter the notch contour by lingering in the notch. All fatigue specimens were required to be longitudinally polished.

Specimen heat treatment: H-11 test bars were preheated to 1200° to 1300° F, transferred to a hydrogen-atmosphere furnace, heated to $1850^{\circ} \pm 25^{\circ}$ F, held at temperature for 1 hour, and air-quenched to room temperature. Parts were tempered three times in air at 1120° to 1140° F for three $1\frac{1}{2}$-hour periods to achieve a final hardness of Rockwell C44 to C45.5.

The annealing of 1-percent silicon-iron was in accordance with AMS 5210.

Nivco alloy bar and sheet magnetic test specimens were heated to $1725^\circ \pm 15^\circ$ F in an air atmosphere, held at temperature 1 hour, water-quenched, then age-hardened at $1225^\circ \pm 5^\circ$ F for 25 hours in air to a minimum hardness of Rockwell C36.

Hiperco 27 alloy (sheet, bar, forgings, and castings) was ordered in the fully annealed condition.

H-11 sheet (Rowland rings and mechanical test specimens) was obtained as 0.014- and 0.025-inch sheet in the annealed and cold-rolled condition. The as-rolled sheet was punched and blanked, deburred, degreased and coated on both sides with aluminum orthophosphate to prevent sticking during heat treatment. The heat treatment was conducted in a hydrogen-atmosphere furnace in which the dewpoint was maintained at a maximum of -40° F. The punched laminations were held between two plates and preheated to 1200° to 1300° F and then transferred to a hydrogen-atmosphere furnace held at $1850^\circ \pm 25^\circ$ F. Time at temperature was 1 hour, followed by an air-blast quench. As quenched, the sheet had a hardness of Rockwell C60 (converted from Rockwell 15N). Hardness gas also acted as the protective gas during tempering at 1050° to 1125° F. Three $1\frac{1}{2}$-hour tempering cycles were required to bring the hardness to nominal Rockwell C45 and to effect complete transformation of austenite to martensite. After heat treatment, the rings were recoated on both sides with aluminum orthophosphate and wound for magnetic test. Mechanical test sheet specimens were heat-treated as mentioned previously. However, the aluminum orthophosphate treatments were omitted and the samples were dusted with high-purity alumina to prevent sticking.

Nivco alloy sheet (mechanical test specimens only) as 0.014- and 0.025-inch-thick sheet was initially solution-heat-treated in air, water-quenched, pickled, and cold-finished (76% reduction of area). Nivco sheet in the solution-annealed condition requires a 25-hour air age at $1225^\circ \pm 5^\circ$ F to achieve a minimum hardness of Rockwell C38. Actual hardness achieved on trial samples approached Rockwell C43 (converted from Rockwell 15N). However, these samples exhibited extremely poor creep resistance and were subsequently again solution-heat-treated at 1900° F in hydrogen, water-quenched, and aged as mentioned previously in dry hydrogen.

Test Procedures

A summary tabulation of the magnetic materials tested, type of test, drawing reference number, and test method or specification is found in table 8. Different size specimens were frequently run for the same general type test because of the

TABLE 8. - TEST PROCEDURES

(a) Thermophysical and mechanical tests

Material	Type of test	Figure	Test method
H-11			
Forging	Axial fatigue	35	ASTM STP 91
Forging	Axial fatigue	36	ASTM STP 91
Forging	Creep	12	ASTM 139
Forging	Creep	28	ASTM E139
Sheet	Creep	27	ASTM E139
Sheet	Creep	39	ASTM E139
Nivco alloy			
Forging	Axial fatigue	37	ASTM STP 91
Forging	Axial fatigue	36	ASTM STP 91
Forging	Specific heat	22	Drop-water calorimeter
Forging	Electrical resistivity	21	ASTM B70 Kelvin bridge
Forging	Tensile	23	ASTM E21
Forging	Creep	24	ASTM E139
Forging	Creep	31	ASTM E139
Forging	Creep	20	ASTM E139
Sheet	Creep	27	ASTM E139
Sheet	Creep	39	ASTM E139
Sheet	Tensile	27	ASTM E21
15% maraging steel	Creep	13	ASTM E139
15% maraging steel	Creep	14	ASTM E139
15% maraging steel	Creep	28	ASTM E139
Hiperco 27 alloy			
Cast	Creep	20	ASTM E139
Cast	Specific heat	22	Drop-water calorimeter
Forging	Creep	33	ASTM E139
Forging	Creep	28	ASTM E139
Forging	Creep	32	ASTM E139
Forging	Tensile	23	ASTM E21
Forging	Compression	37	ASTM E9
Forging	Specific heat	22	Drop-water calorimeter
Forging	Electrical resistivity	21	ASTM B70 Kelvin bridge
Sheet	Poisson's ratio	25	ASTM E132
Hiperco 50 alloy sheet	Tensile	26	ASTM E21
Cubex alloy			
Sheet	Specific heat	30	Drop-water calorimeter
Sheet	Thermal conductivity	29	Comparison bar
Sheet	Tensile	26	ASTM E21
Sheet	Compression	38	ASTM E21
Sheet	Poisson's ratio	25	ASTM E132
1% silicon-iron	Tensile	20	ASTM E21
1% silicon-iron	Specific heat	22	Drop-water calorimeter
Supermendur	Specific heat	22	Drop-water calorimeter
Supermendur	Electrical resistivity	34	ASTM B70 Kelvin bridge
Supermendur	Tensile	26	ASTM E21

(b) Magnetic tests

All materials	Normal induction and	18	ASTM A341
	hysteresis of mag-	15	ASTM A341
	netic materials	17	ASTM A341
		16	ASTM A341
		19	ASTM A341
All materials	Magnetic properties	15	ASTM A343
	(ac)	17	ASTM A343
		16	ASTM A343
		19	ASTM A343
Supermendur and cubex alloy	Constant-current flux-	15	AIEE 430, 431, 432
	reset properties	19	AIEE 430, 431, 432

materials high strength or because of size limitations such as imposed by sheet materials. A discussion of the many different tests and procedures follows.

Thermophysical properties. - The following thermophysical properties were determined:

Specific heat: Precise measurements of specific heat were made in a drop-water calorimeter (according to a method described by J. Valentich of Westinghouse Research Laboratories in Materials Engineering Report 5973-3031). The only specimen requirement for measurement of specific heat is that a compact mass of approximately 30 grams be available for test. Oxidation was prevented by sealing the specific-heat specimens in evacuated quartz capsules. During normal testing, the specimen temperature was measured with a platinum-rhodium thermocouple mounted in a quartz well inserted halfway down the center of the specimen. Since quartz is not as good a heat conductor as the metal, it was necessary to determine the difference in temperature between the quartz well and the specimens. To do this, a 1/16-inch-diameter hole was drilled in a standard copper specimen to within 3/16 inch of the quartz well, and thermocouples were positioned in both the specimen and the quartz well. Temperatures were recorded at both locations as the specimen was taken through a complete test. The quartz cover on the bottom of the specimen was left out in the test to facilitate the placement of the thermocouple in the specimen. The results show that the temperatures in the quartz well and in the specimen were within 1 percent except at 1500° F where they differed by about 1.5 percent. This means that the thermocouple in the quartz well measures the specimen temperature with good accuracy over the entire testing temperature range. No difficulties were encountered during any of the measurements of specific heat.

Electrical resistivity: The standard Kelvin bridge method of ASTM B-70 was used for all measurements of electrical resistivity. A refinement added to ensure accurate data was use of a vacuum of 10^{-4} torr as the test atmosphere. Strip and wire materials were wound on a 5/8-inch-diameter quartz mandrel and the balance of the materials were simply supported in the furnace hot zone.

A Kelvin bridge was used to measure the resistance. Short pieces of Alumel wire were used in the furnace hot zone and silver wire in the room temperature zone as lead wires. Resistance welding was used to fix the Alumel leads to the specimens. The elevated-temperature tests were conducted in a vacuum of 5×10^{-5} torr, and the average temperature variation over the 2-inch coil length was less than ±1 percent. All the samples were heated at a rate of 10 F° per minute and the resistance of each specimen was measured at 100° F increments with increasing and decreasing temperatures. Preliminary tests on a sample of thoria-dispersion strengthened nickel wire showed that the resistance measured at this heating rate

duplicated the results obtained by soaking at each temperature increment for 20 minutes. For this reason, all other specimens were tested at a constant heating rate of 10 F^o per minute. In all tests the integrity of the elevated temperature leads was checked at room temperature by comparing the resistance measured with the special high-temperature leads and the resistance measured using the standard room-temperature clamps.

The Kelvin bridge used to measure the resistivity of the specimens had a resolution of 10^{-8} ohm. Resistivity was computed and reported in ohm-centimeters.

Thermal expansion: The thermal expansion measurements were made in a quartz-tube dilatometer in which the specimen is heated within a resistance wound furnace. In this apparatus, the furnace and tube are oriented in a horizontal position. The furnace is stationary while the tube and associated measuring apparatus can be moved in and out of the furnace on a rail. The quartz tube is slotted at the closed end so that a 2-inch long specimen can be placed in it with one end contacting the bottom. A quartz rod attached to a linear-displacement transducer is in contact with the other end of the specimen. As the specimen expands, the quartz rod moves, and the transducer measures the amount of the movement. The transducer is an unbonded Wheatstone bridge circuit whose sensitivity can be varied by regulating the voltage input. Length changes as small as 1 microinch can be measured. The output of the transducer was recorded on one axis of a recorder; the output of a Chromel-Alumel thermocouple wired to the specimen was recorded on the other axis of the recorder. The resultant curve was then corrected for the expansion of quartz. The temperature rise of the specimen was preprogramed at 3 C^o per minute using a program controller. Argon gas was continuously flooded over the specimen to prevent oxidation at the higher temperatures.

Thermal conductivity: This property was only measured on one material with the use of the comparison bar technique. In this method, the specimen (1/2 in. in diam by $4\frac{1}{2}$ in. long) is fixed to a heater block through a snug tapered fit. The other end of the specimen is fixed through a threaded connection to a comparison bar of nickel (1/2 in. in diam by 4 in. long), whose thermal conductivity is known. A heat sink, cooled by circulating water, is fixed to the free end of the nickel rod. The nickel and specimen rod assembly is held in a vertical position with the heater at the bottom. The rod system is surrounded with alumina insulation that is enclosed with a $2\frac{1}{2}$-inch-diameter shield. The shield is made from 302 stainless steel and nickel. The stainless-steel portion is as long as the specimen, and the nickel portion is as long as the comparison bar. The nickel and stainless-steel sections were butt-welded and the joints alined with the specimen nickel joint. A heater was fixed around the shield circumference at this joint. Three Chromel-

Alumel thermocouples were fixed to the specimen, the first 1/2 inch down from the nickel joint and the remaining two at 1-inch intervals below the first. Four thermocouples were fixed to the comparison bar, the first 1/2 inch above the specimen joint and the other three at 1-inch intervals above the first. Seven thermocouples were similarly placed on the shield at the same height as those on the bars. The entire assembly was set on alumina insulation that was on a steel baseplate and surrounded with 5-inch-inside-diameter asbestos-cement composite tube. The area between the shield and the tube was filled with alumina insulation. A bell jar was placed around the asbestos-cement composite pipe and the system evacuated.

In the comparison bar technique, as the heater temperature rises the specimen temperature rises, and heat flows up the specimen through the joint and to the water sink at the end of the nickel bar. Unidirectional heat flow up the specimen is obtained by adjusting the heaters on the shield and the heater block and by adjusting the water flow. The thermocouples on the bar and shield at the same height are maintained at equal temperatures to prevent radial heat flow. After these conditions have been established for about four hours at a test temperature, all thermocouples on the comparison bar and the specimen are read and recorded. The thermal conductivity of the specimen is then computed.

Magnetic tests. - The test methods used in performance of this contract followed the general ASTM test methods. Since room-temperature techniques only were applicable to the basic test method, slight modifications were made in the details to adapt the methods to the geometry of the test specimens and/or to permit their use at high temperatures and high inductions.

dc tests: The dc tests were made according to ASTM A341 for both solid Rowland-ring and wound toroid-ring specimens.

ac tests: The ac tests were made in accordance with the standard ASTM A343 wattmeter method except that the samples were ring samples wound with primary and secondary windings rather than Epstein samples. High sensitivity reflecting-type wattmeters were used for all ac tests.

Power supplies: Tests at 400, 800, and 1600 cps were made utilizing a variable frequency motor generator set having a rated output of 7.5 kilovolt-amperes, three phase, at 120 volts. Frequency was measured with an electronic counter and was controlled ±1 cps. Tests at 3200 cps were made with a 25-kilowatt power amplifier driven by an oscillator. When necessary, feedback could be applied to the amplifier to maintain a sinusoidal waveform.

Elevated temperature atmosphere chambers: Oxidation protection for the specimens was afforded by a number of welded retorts that were constructed to fit

in available laboratory ovens and furnaces. Type 304 stainless steel was used for the 1100° F boxes and Inconel 600 for the 1400° F boxes. The lid joints of the atmosphere chambers were machined and ground for a close tight fit.

The many lead wires from each specimen were brought through an asbestos-cement composite plug located in the pipe leading from the atmosphere chambers. All joints were further sealed with a high-temperature Saureisen cement. A second tube was provided as a gas outlet and led to a bubbler to prevent back-diffusion. Specimen temperature was controlled or measured by a thermocouple placed on the actual test rings and wound into the maze of windings as an integral part of the specimen.

Special winding techniques: In order to use the same sample for both ac and dc tests to 1400° F at frequencies to 3200 cps, a series of unique winding techniques were devised. It was also desired to have a peak magnetizing force of at least 250 oersteds for the dc tests, and the selection of this force automatically set the minimum number of turns for the primary windings. To complicate matters, the voltage capability of the available ac power supplies dictated the maximum number of turns which could be used for the high-frequency tests. After a series of insulation failures at high temperature, a novel winding technique was devised which proved completely satisfactory. Where possible, sample area was reduced to reduce voltage requirements for high-frequency testing. The primary windings were sectionalized to reduce induced voltage during high-frequency testing. Anaconda Wire and Cable's Anadur-insulated nickel-clad copper wire was used. Silicate fiber mat insulation backed by glass tape for insulation between layers of the windings was used and ceramic tubes brought all lead wires through the winding.

Constant current flux reset testing: All constant current flux reset (CCFR) tests at room and elevated temperature followed the procedures described in AIEE test specifications 430, 431, and 432. Since relatively few turns were required, commercial high-temperature lead wires were used for conductors. An atmosphere box similar to that described for elevated temperature atmosphere chambers previously was used for the elevated-temperature tests.

Mechanical properties. - Tensile property measurements: All properties that are normally determined in tension and compression were determined in strict accordance with ASTM procedures. Strain rates were 0.005 inch per inch per minute to the yield strength and 0.05 inch per inch per minute above the yield strength.

Some difficulty was encountered in the measurement of Poisson's ratio and of the compressive strength of Cubex alloy. The Cubex alloy was only available in thin sheet gages, which made awkward specimens. Poisson's ratio measurements on Cubex alloy were further complicated by the extremely large grain size and the

anisotropy associated with large grain size in grain-oriented materials. Although these problems contributed materially to the observed scatter, the source and amount of the scatter were determined by placing eight strain gages on each of two Poisson's-ratio sheet specimens. Normally, only four strain gages are required for accurate strain measurements. The eight gages were arranged as shown in figures 40 and 41 (p. 69). The gages were placed in both the longitudinal and the transverse directions on a single grain as well as across the grain boundaries. The strain gages cemented onto the sample were chosen for their size, stability, and ease of mounting.

For accuracy, a Wiedeman-Baldwin Mark B-20 testing machine was used in conjunction with a Budd digital strain indicator. Strains were recorded at numerous load increments with each set of readings made at constant load.

Tests made on the tensile specimens revealed variations in Poisson's ratio within different grains in both directions as well as across different grain boundaries. No difficulties were encountered in the measurement of Poisson's ratio for materials other than Cubex alloy.

Creep testing: All creep testing performed exceeded the ASTM specifications for creep testing in air, inert atmosphere, or vacuum. The additional attention to detail was mandatory if reliable creep strains of 0.20 and 0.40 percent were to be obtained in the desired times. Both spring and lever machines were used, and specimens were thermocoupled and instrumented with an extensometer. A number of checks were performed during the program to verify the performance of the creep test equipment.

Two pieces of Billet No. 4C804T1 were obtained from the creep rupture specimen bank of the ASTM-ASME Joint Committee on Effect of Temperature on Properties of Metals. These pieces were sectioned and tested according to instructions. The mean rupture life in spring machines was 102 hours and the mean rupture life in lever machines was 116 hours. Both values fall within the 95-percent-confidence limits established by the committee for this material. The material used for these tests was 304 stainless steel and was tested in the following manner: The samples were placed in the machines, heated to 1300° F, and left unloaded overnight. The following morning the temperature was raised to 1350° F, held for 1 hour, and the specimens were then loaded to 13 500 psi and tested to rupture.

The vacuum creep test equipment was checked for pressure, leak rates, and gas analysis before testing was started. A record of pressure was kept during each test. An analysis of the gases in the chamber are listed in table 9 together with the blank-off leak rate. Actual measured gas transfer rates measured by a cryogenic pump and a mass spectrometer are an order of magnitude greater and

TABLE 9. - GAS TRANSFER (MOLE PERCENT)

[Blank-off leak rate, $1-2\times10^{-6}$ (cc)(atm)/sec.]

Temperature	H_2	CO	N_2	O_2	CO_2	Other hydro-carbons
	Gas transfer, mole percent					
Room	6.63	-----	30.39	8.23	31.35	23.40
1600° F	34.19	22.92	14.79	3.41	10.19	14.5

show that the chamber provided some of the pumping. The leak rates were checked at the beginning of each test both at ambient and test temperatures. All pressures were maintained well within the specified limits of 1×10^{-5} torr maximum pressure. A pressure of 1.5×10^{-7} torr was typical of normal pressures obtained at 1600° F within a chamber.

As a final precaution and in accordance with a recommended Materials Advisory Board procedure (NASA Research Advisory Committee on Materials), a piece of dead-soft columbium with a Vickers hardness (10 kg) of 42.1 was exposed at 2200° F for 1 hour in the creep machine under test vacuum. The final hardness was 43.1, confirming that the vacuum quality met existing Materials Advisory Board specifications.

After proving the quality of the vacuum test chambers, it was decided to check for possible change in the creep specimens which might affect the measured creep rates. To do this, the creep properties of air, argon, and vacuum creep specimens were compared, and a gas analysis of both the tested and the untested vacuum test specimens was made for oxygen and carbon. This analysis is presented in table 10. No changes in oxygen or carbon content were observed. The slight differences between the values listed in table 10 are due to standard experimental errors. Before the vacuum creep tests were started, baseline data were obtained first in air and argon using extensometers on the specimens. The stresses and test temperatures selected for vacuum testing were taken from Larson-Miller plots of the air-test data, since the vacuum tests were expected to check the air and argon data. Because of equipment limitations, the extensometer could not be fastened directly to the vacuum test specimens but was connected to the machine crosshead. The vacuum test extensometer data were then corrected for linkage

TABLE 10. - TOTAL OXYGEN ANALYSIS OF VACUUM CREEP TEST SPECIMENS

Material	Specimen	Test temperature, $^{\circ}$F	Test stress, psi	Test time, hr	Oxygen, percent	Carbon, percent
AMS 6487 (H-11) forging (bar)	As-received	----	-------	---	[a]0.0048 [b].0015	0.42 ------
	V1	1000	33 000	---	.0024	------
	V2	900	90 000	170	.0026	------
	V3	850	100 000	502	.0013	------
	V4	1000	37 000	650	.0019	.40
Nivco forging (bar)	As-received	----	-------	---	0.0008	0.0040
	V1	1400	16 000	5	.0012	------
	V2	1400	8 000	163	.0012	------
	V3	1100	85 000	496	.0007	.0048
	V4	1100	80 000	356	.0009	------
15% maraging steel (bar)	As-received	----	-------	---	0.0023	0.0062
	V1	900	60 000	502	.0007	------
	V2	900	90 000	192	.0010	------
	V3	800	107 500	283	.0007	.0064
Hiperco 27 forging (bar)	As-received	----	-------	---	0.0015	0.0054
	V1	1100	12 000	498	.0017	------
	V2	900	46 000	340	.0017	------
	V3	700	70 000	498	.0016	.0056
	V4	1100	7 000	211	.0015	------
Hiperco 27 investment castings	As-received	----	-------	---	0.0087	------
	V1	1100	8 000	405	.0060	------
	V2	700	36 800	212	.0075	------
	V3	900	32 000	308	.0079	------
	V4	1100	11 000	168	.0078	------

[a]Taken near surface.
[b]Taken near center.

errors. The creep strain rate obtained in this manner agreed with those obtained by the use of extensometers on the specimens.

The creep strain was also measured after test at room temperature as an additional check on all the air and vacuum test data. In all cases the creep strain observed by extensometer agreed with that measured at room temperature within experimental error. The vacuum creep strains found at the end of the test also verified this observation.

The test program on H-11 and Nivco alloy sheet was planned to check data already available for bar stock rather than to establish basic creep properties. Because there is often a difference between properties measured in the transverse and longitudinal directions of sheet, the majority of specimens were selected for test in that direction considered most likely to be affected, namely, the transverse.

The creep data for H-11 were obtained by means of measured elongation resulting from stressing test samples for given lengths of time at temperature. The current tests were made in the same manner with stress and temperature selected to duplicate tests already completed on the forged alloy on another Westinghouse program. Extensometers were used on the Nivco alloy sheet to check data obtained for forged bars.

Combination smooth- and notched-bar creep test specimens (stress concentration K_t, 3.0) were mixed in with smooth-bar test specimens for nearly all materials to determine possible notch sensitivity. Only two of the 150 creep samples suffered a notch failure. These two samples, both Nivco, appeared to be defective and were disregarded.

Fatigue testing: All fatigue tests run on this program were planned in an air atmosphere. The decision to air-test the H-11 and Nivco alloys was made when the literature failed to provide the required air-atmosphere fatigue data on either of these alloys. A large amount of inert-gas atmosphere fatigue data has been obtained for other alloys on another Westinghouse program. These data showed a modest effect of atmosphere purity on the fatigue life of various nickel and iron-base high-temperature alloys. However, both beneficial and adverse effects of the purified test atmosphere on the alloys studied were noted. In general, effects were a function of grain size, alloy composition, and test-atmosphere purity. A comprehensive study was beyond the scope and time limitations of this program. It was decided to obtain the best possible baseline air-atmosphere data from which a detailed atmosphere test program could be planned if such data became a necessity. Several high-purity argon-atmosphere tests were made to check the alloys of interest on this program for this sensitivity and to alert the designer to these
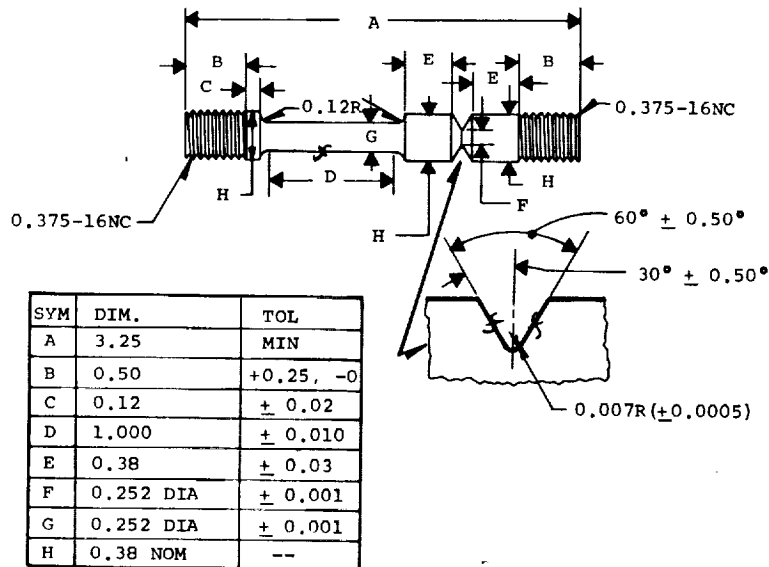
trends. A similar check had also been made early in the creep program with no significant differences in the measured property observed in either case except at temperatures over 1400° F. All fatigue specimen notch geometry was calculated to give a stress concentration K_t of 3.

The fatigue specimens were mounted into a 5:1 stress-multiplying fixture and assembled into a Sonntag Model SF-1U fatigue machine for test. Specimen eccentricity, with respect to the centerline of the grips, was held to less than 0.00025 inch. A specimen, previously calibrated in a tensile machine, was used with a recording oscillograph and amplifier to check the dynamic calibration of the fatigue machine.

Dynamic creep tests that combined the effects of static stress and alternating stress were conducted to permit the presentation of modified Goodman diagrams.

Inert gas purity. - Argon gas used for all tests requiring inert gas protection was certified to the following analysis by the supplier:

Oxygen, ppm . . . . 10 Max.

Hydrogen, ppm . . . . 5 Max.

Nitrogen, ppm . . . . 40 Max.

Carbonaceous gases, ppm . . . . 3 Max.

Dewpoint, °F . . . . -80

SYM	DIM.	TOL
A	3.25	MIN
B	0.50	+0.25, -0
C	0.12	± 0.02
D	1.000	± 0.010
E	0.38	± 0.03
F	0.252 DIA	± 0.001
G	0.252 DIA	± 0.001
H	0.38 NOM	--

NOTE - Finish specimen to $\overset{8}{\bigvee}$ or better on all "f" surfaces.

NOTE - The difference between Dims. "F" & "G" shall not exceed 0.001 inch.

NOTE - Taper gauge length "D" to center so that dia "G" at ends of gauge length exceeds dia "G" at center of gauge length by not less than 0.0005 inch nor more than 0.001 inch.

Figure 12 - Combination creep-rupture specimen bar for high-strength materials.
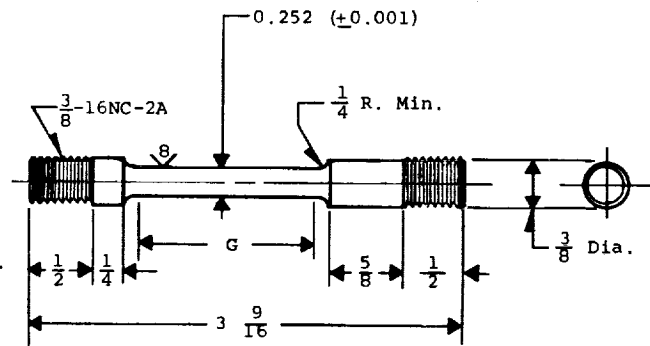
NOTE: Taper gauge length "G" to center so that the diameter at the ends of the gauge length exceeds the diameter at the center of the gauge length by not less than 0.0005 inch nor more than 0.001 inch.

Figure 13. - Tensile-creep specimen for high-strength materials.

Figure 15. - Tape-wound toroid for magnetic tests.

NOTE: The difference between the 0.252 inch ($\pm$0.001)
        dimensions shall not exceed 0.001 inch.

NOTE: Taper gauge length "G" to center so that the diameter
        at the ends of the gauge length exceeds the diameter
        at the center of the gauge length by not less than
        0.0005 inch nor more than 0.001 inch.

Figure 14. - Combination creep-rupture specimen bar for high-strength materials.

ITEM	T
1	0.004
2	0.006
3	0.008
4	0.012
5	0.014
6	0.025

3.501
(±0.002)

4.016
(±0.002)

T (Stock Thickness)

Diameters to be concentric
within 0.005 inch Total
Indicator Reading.

Figure 17. – Rowland ring lamination.

$3\frac{1}{2}$

4

$\frac{1}{2}$

Figure 16. – Stacked Rowland ring sample for magnetic testing of laminated material.

Figure 19. - Tape-wound toroid for magnetic tests.

NOTE: Taper gauge length "G" to center so that the diameter at the ends of the gauge length exceeds the diameter at the center of the gauge length by not less than 0.0005 inch nor more than 0.002 inch.

Figure 20. - Tensile-creep specimen for investment cast materials.

Figure 18. - Solid ring for direct current magnetic testing.

Figure 22. - Specific heat specimen.

Figure 24. - Creep specimen for moderate strength materials.

Figure 21. - Electrical resistivity specimen.
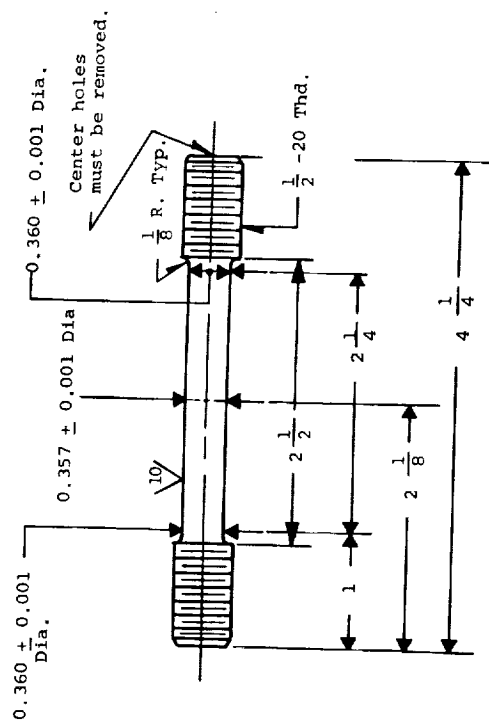
Figure 23. - Tensile-creep specimen for moderate strength materials.
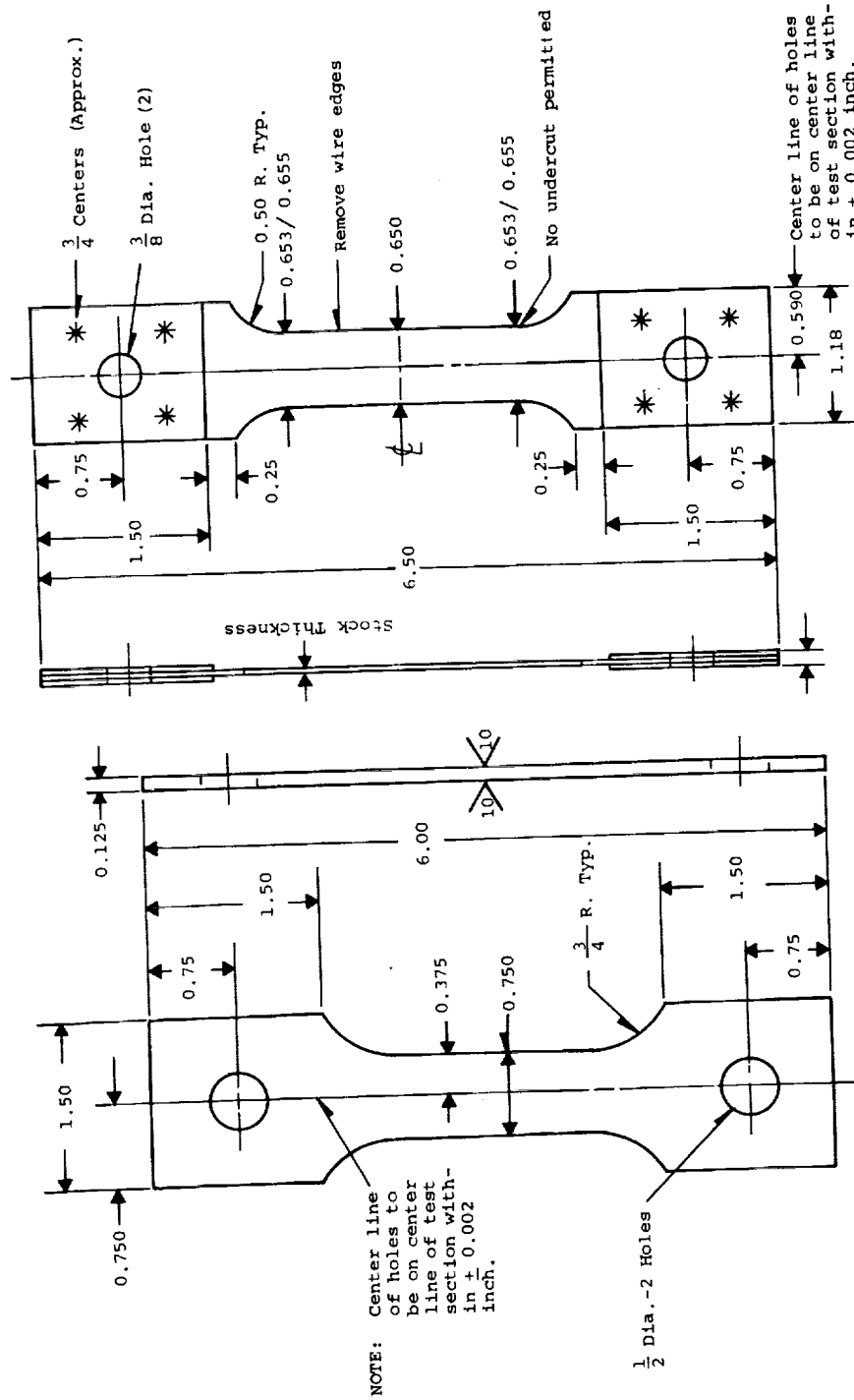
Figure 26. – Tensile-creep specimen for sheet materials.

Figure 25. – Poisson's ratio specimen.

Center line of holes
to be on center line
of test section with-
in ± 0.002 inch

$\frac{3}{8}$ Dia. 2 Holes

$\frac{3}{4}$ Centers
(Approx.)

$\frac{1}{8}$ R. Typ. (No under
cut permitted)

0.590

1.18

0.75

0.650

0.75

1.38

1.38

5.00

Stock Thickness

0.125*
*Welded pads
must be same
thickness on
each side.
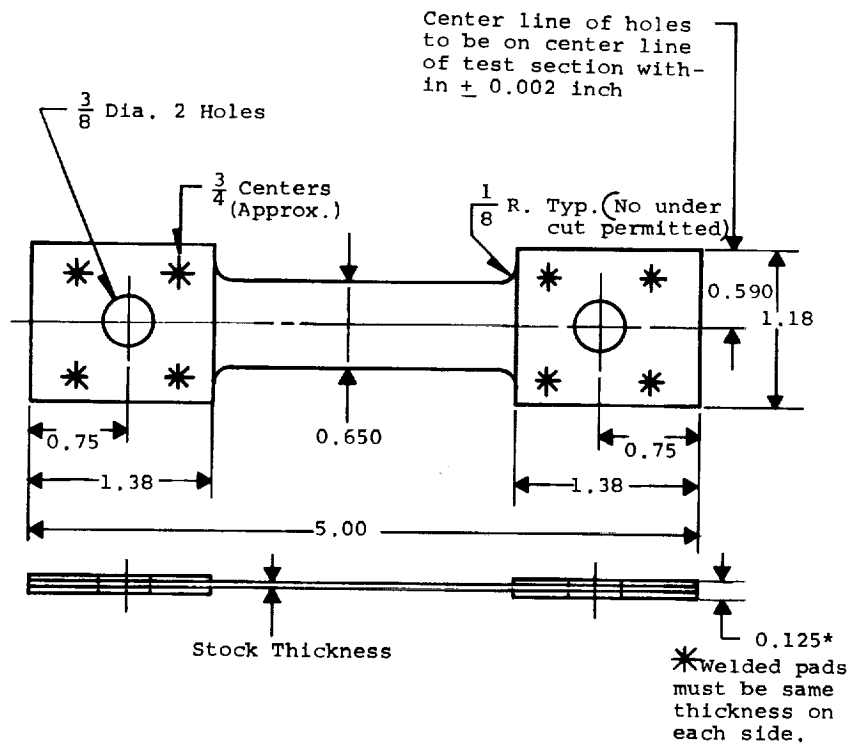
Figure 27. - Tensile-creep specimen with sheet materials for transverse specimens taken from narrow sheet.

$\frac{0.178}{0.179}$ Dia.

0.235 $^{+0.000}_{-0.001}$ Dia.

$\frac{3}{8}$ Dia.

0.031 ±
0.003R. Typ

8

0.063 ±
0.003R. Typ.

$\frac{1}{16}$

$\frac{1}{4}$

$\frac{5}{16}$

1.500 ±0.005

$\frac{1}{16}$

$\frac{5}{16}$

$\frac{1}{4}$

2 $\frac{3}{4}$
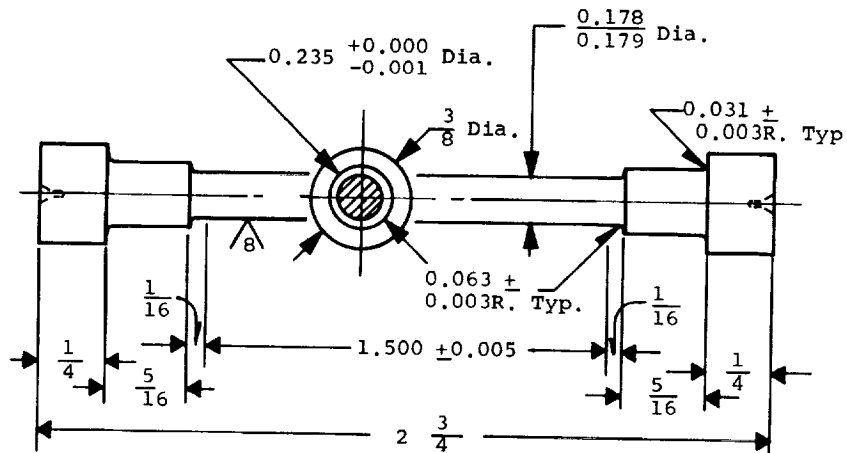
NOTE: Eccentricity on end centers must not exceed 0.0005 inch.

Figure 28. - Vacuum creep specimen for all bar materials.
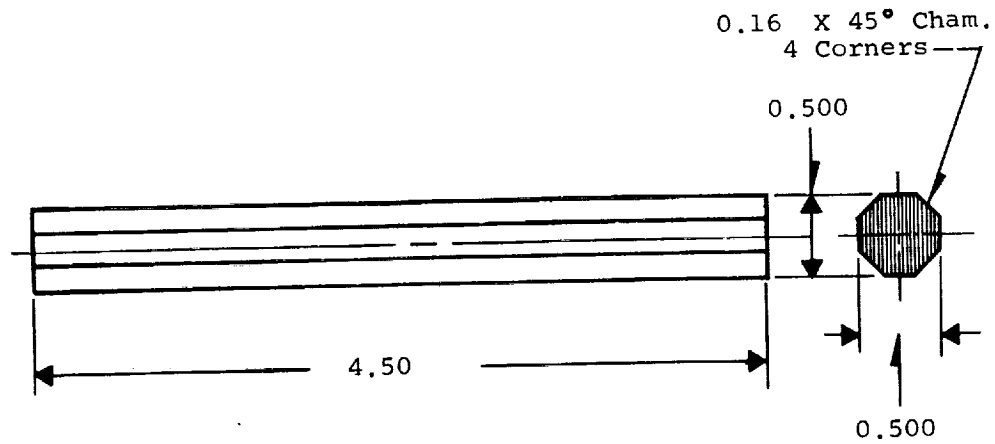
Laminations heliarc welded before grinding to finish
dimensions.

Figure 29. - Thermal conductivity specimen for sheet materials only.
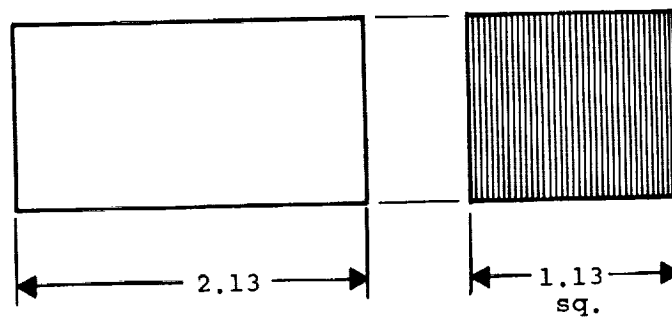
Laminations heliarc welded before grinding to finish dimensions

Figure 30. - Specific heat specimen for sheet materials only.
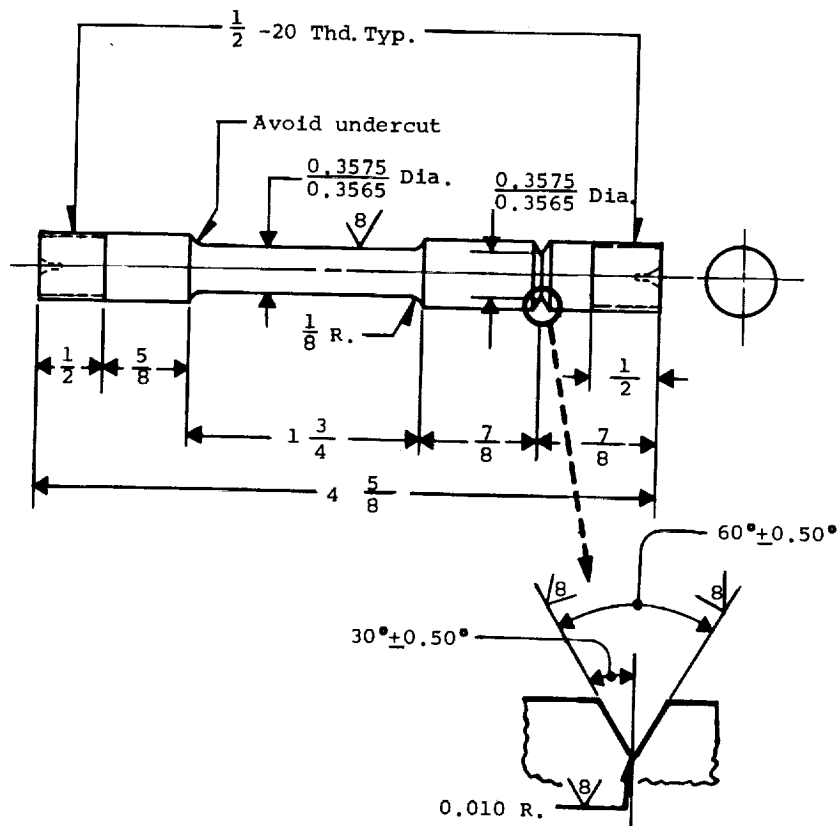
Figure 31. - Combination creep-rupture specimen bar for moderate-strength materials.
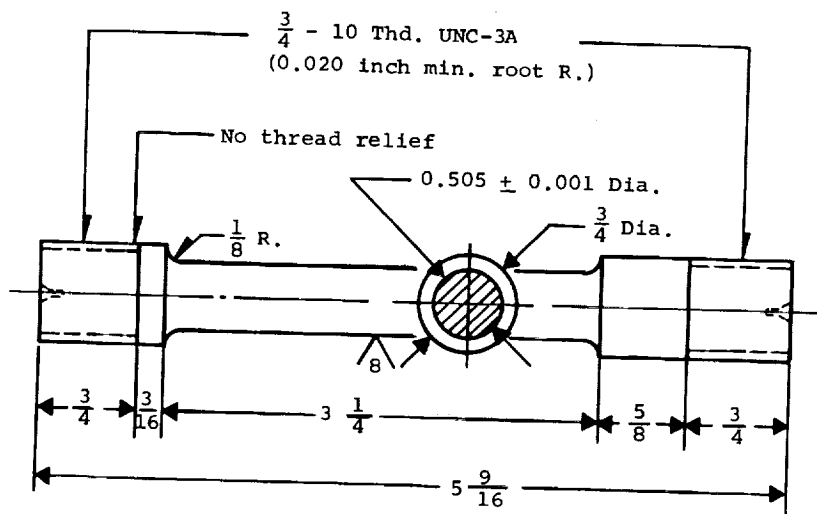
Figure 32. - Tensile-creep specimen for low-strength materials.
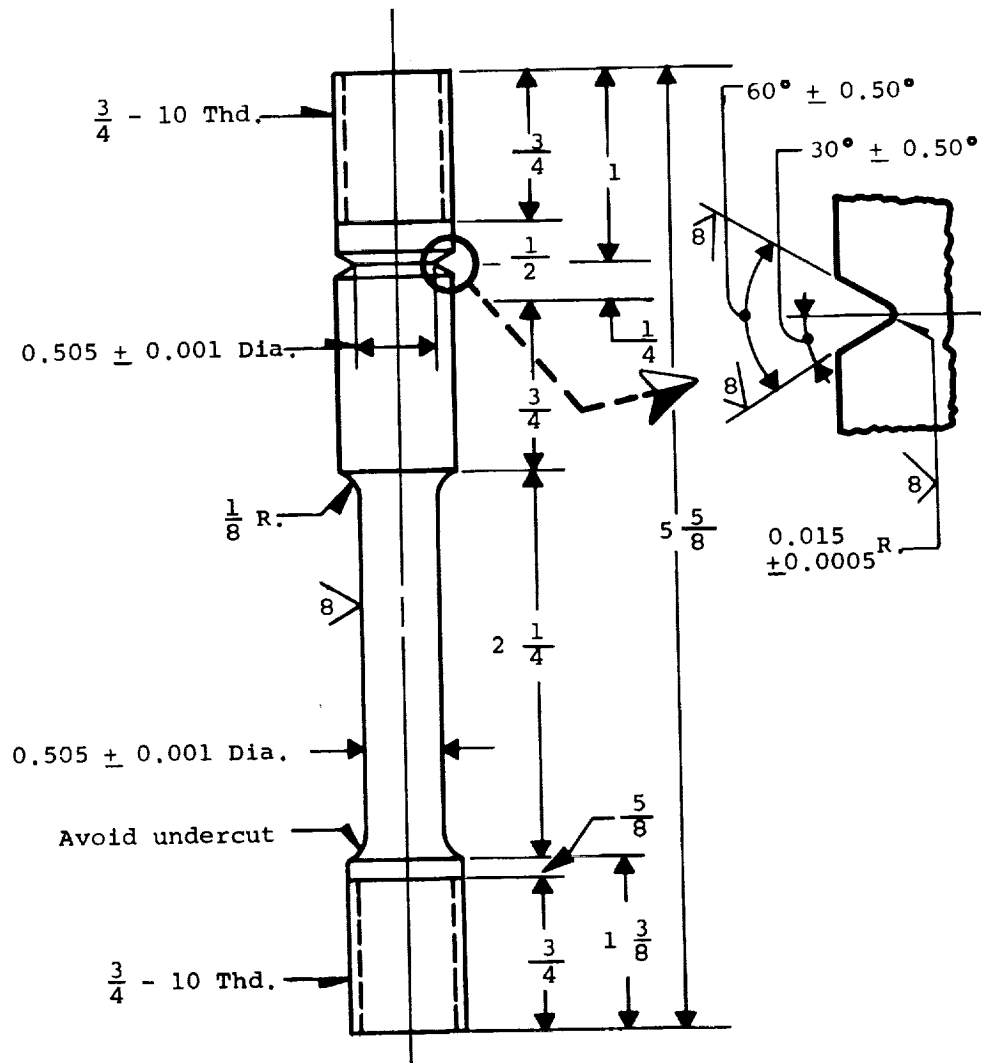
Figure 33. - Combination creep-rupture specimen bar for low-strength materials.
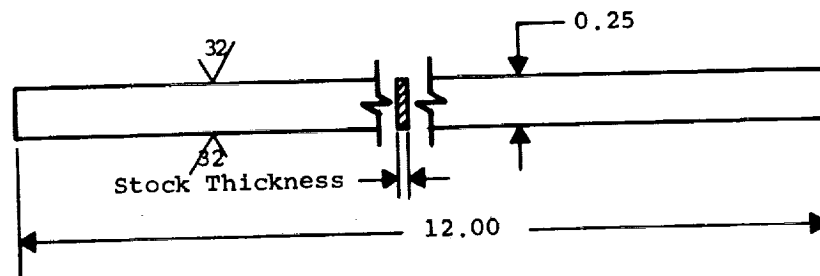
Figure 34. - Electrical resistivity specimen for sheet only.
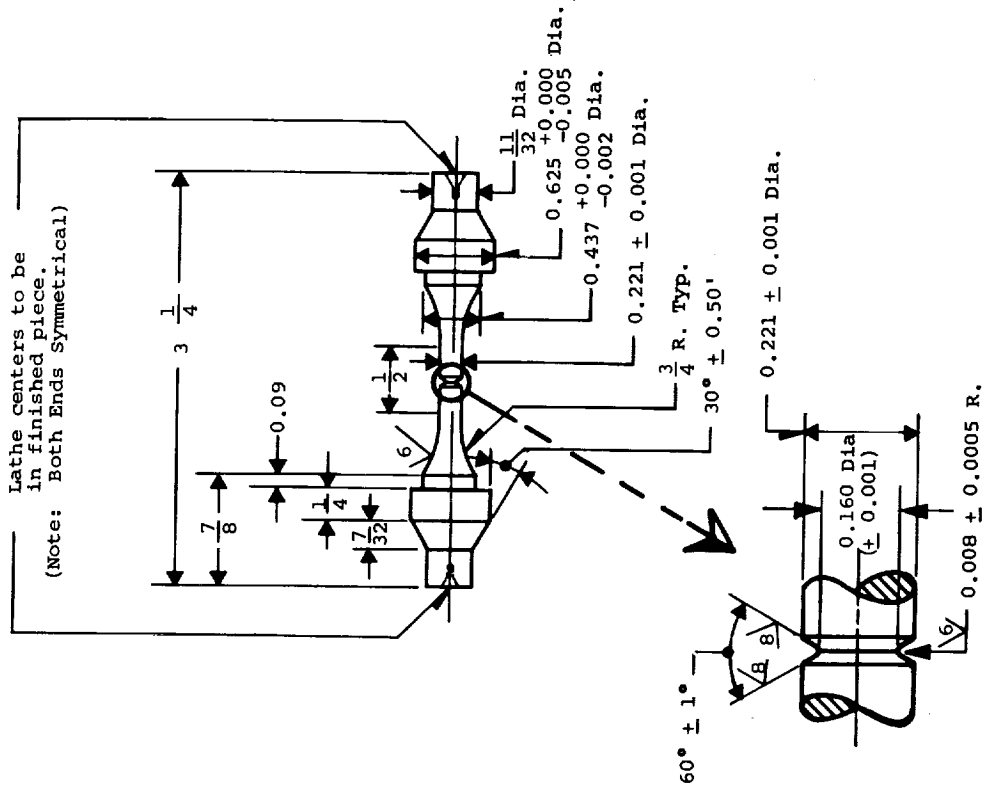
Figure 36. - Axial fatigue specimen for notched bar.
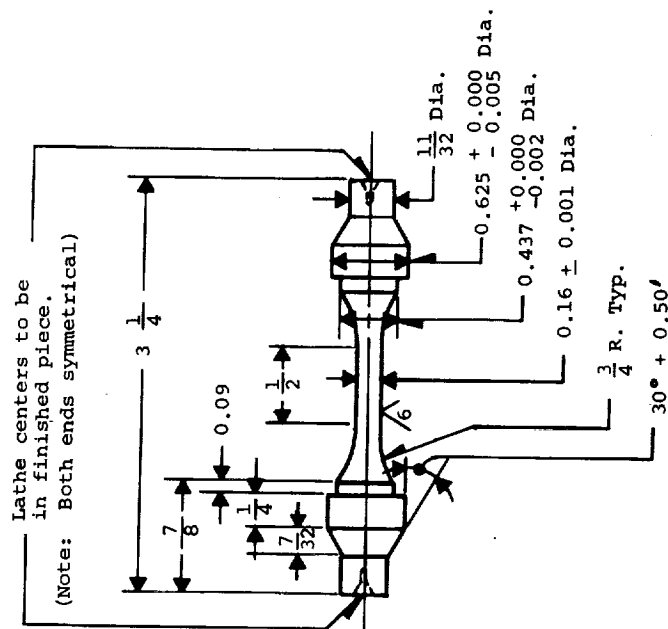
Figure 35. - Axial fatigue specimen for smooth bar.
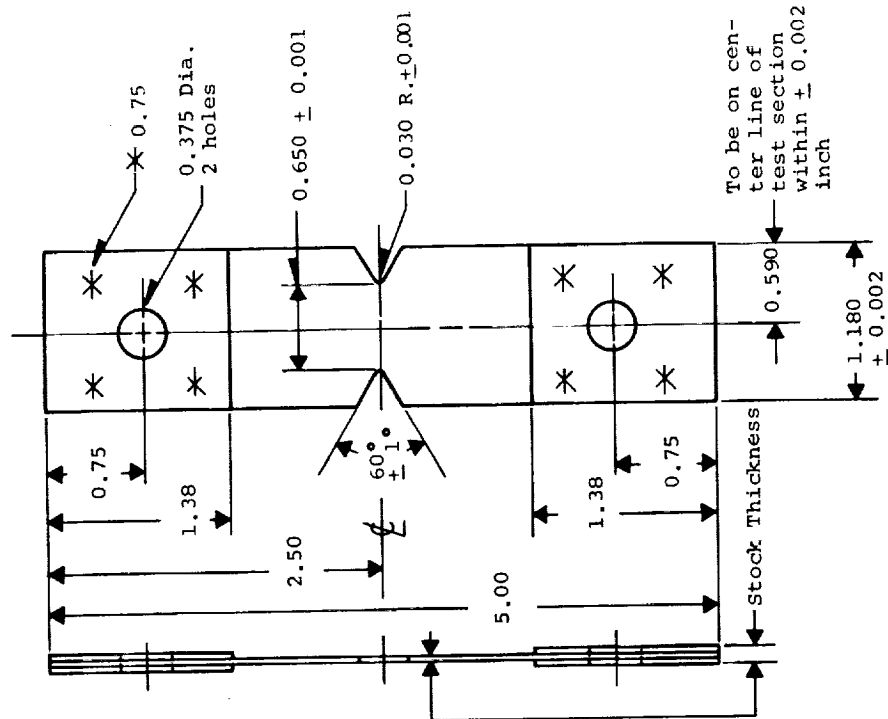
Figure 39. – Notched creep specimen for sheet materials.

0.75

0.375 Dia.
2 holes

0.650 + 0.001

0.030 R. +0.001

To be on cen-
ter line of
test section
within + 0.002
inch

0.590

1.180
+ 0.002

0.75

1.38

60° +1°

2.50

5.00

Stock Thickness

Finish surface
all over

0.50

1.50

Ends must be parallel within
+ 0.0001 inch and must be
perpendicular to longitudinal
axis.
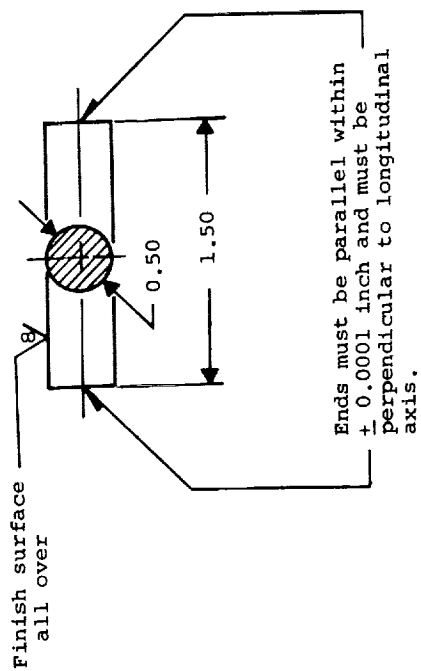
Figure 37. – Compressive test specimen for bar stock.

0.50

t

2.25

Ends must be
parallel within
+ 0.0001 inch and
must be perpendicular
to longitudinal axis.
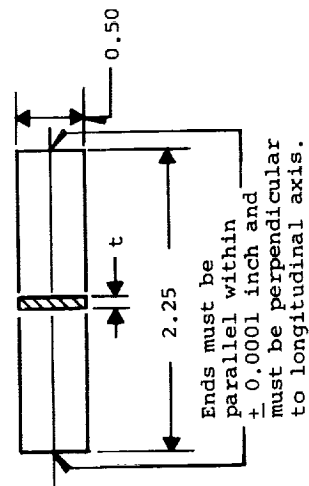
Figure 38. – Compressive test specimen for sheet materials.
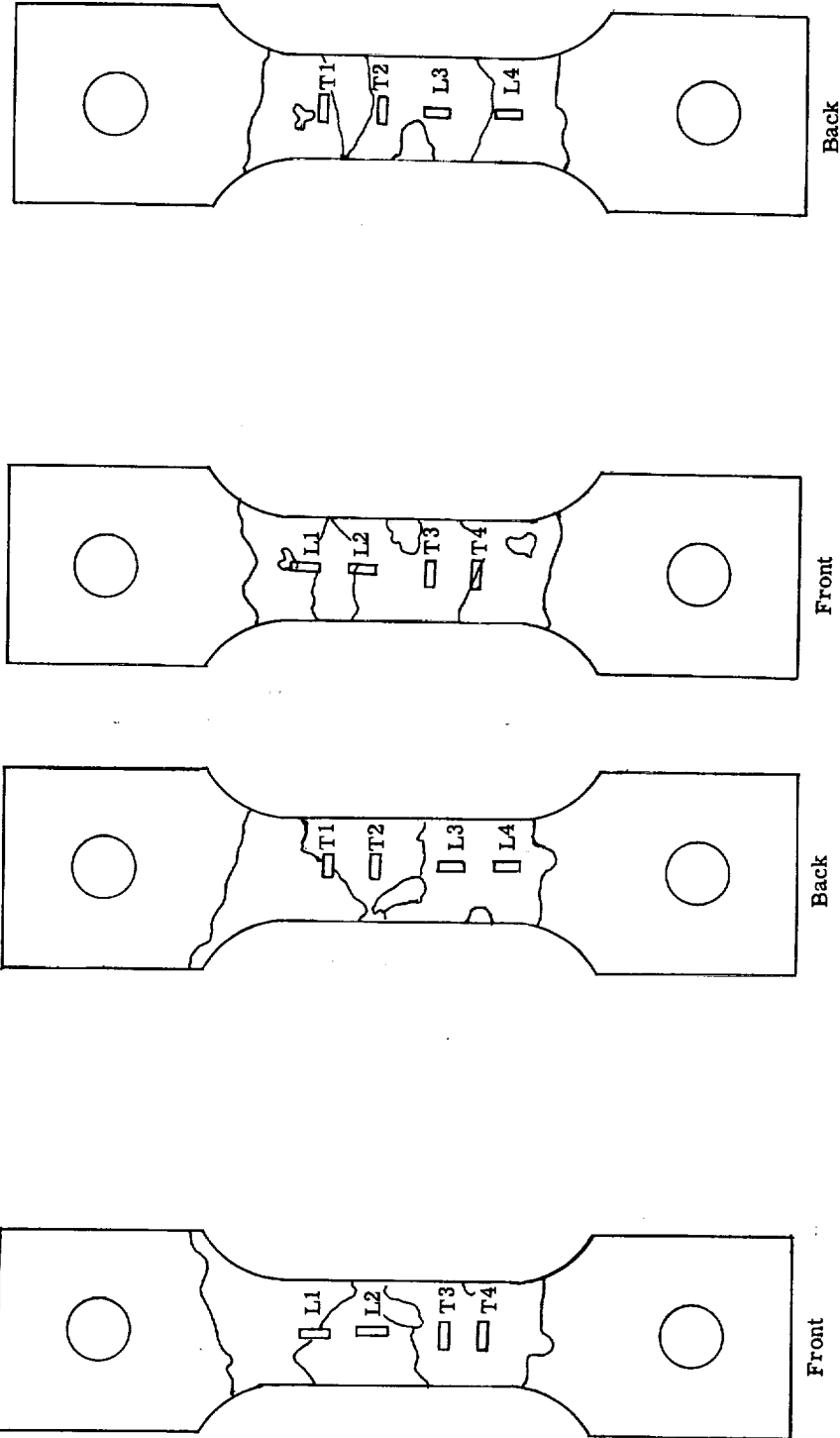
Figure 41. - Cubex Specimen 1, showing orientation of gages with reference to cube structure. Specimens etched with Diversey 914.

Figure 40. - Cubex Specimen 2, showing orientation of gages with reference to cube structure. Specimens etched with Diversey 914.

MAGNETIC MATERIALS PROPERTIES

This section presents the properties of the high-temperature magnetic materials studied in this program. The properties are arranged as thermophysical, magnetic, and mechanical in table 11, which is a master index of all properties listed. Each material is headed by a summary of the material properties containing a synopsis of important parameters to aid in screening and selecting those materials warranting further detailed analysis. This summary is important because the data presented in tabular and graphic form on each material are extensive.

No text is included in this section so that it can be used as a design manual. The technical discussion on each material is given in preceding sections.

References are given on each curve or table crediting the source of data not obtained in this program.

In preparing for the experiments, an analysis was made of the tests to be conducted. All equipment calibrations were checked to ensure they were traceable to Bureau of Standards or other accepted procedures. Test procedures were evaluated so that systematic errors could be minimized. Test points were selected to provide the best statistical inference. Since the broad scope of the program required an exceedingly large number of tests, it was not possible to minimize all the random errors. In general, sufficient replication was undertaken in those areas where additional confidence was needed. It is expected that all systematic errors should fall within 2 percent of the reported data. Additional controls instigated to ensure useful data included Creep-Bank specimens, leak-rate tests, and vacuum-fusion analysis of selected specimens. These precautions are discussed in the section MATÉRIALS, PREPARATION, AND TEST PROCEDURES.

A least-squares curve-fit program for the IBM 7040 computer was applied to fatigue, tensile, electrical-resistivity, thermal-expansion, and specific-heat test data. In addition, the computer calculated polynomial equations from first to fifth order. From this information the equation which best fitted the test data was selected, that is, the equation of lowest order which would yield an error of 5 percent or less.

The results of the analysis of the computer runs are as follows:

(1) Fatigue test: Out of 22 curves examined, four curves had over 6-percent error, with the worst being 11 percent; most others were well under 6 percent. Most polynomial equations were of third order or less.

(2) Tensile test: A total of 39 sets of test data were run; of these sets, only two had an error of approximately 6 percent, all others had errors of 5 percent or less, with the bulk of the errors being effectively zero. The most prevalent polynomial equation selected to fit the data was of the fourth order.

(3) Electrical resistivity: The worst error in this case was 7 percent for one case. All other cases had errors of 5 percent or less.

(4) Specific heat: Only one case was run when this text was prepared with an error of 4.4 percent. There are insufficient test data to make any general statement, but it is anticipated that this error will be fairly representative.

(5) Thermal expansion: All fits were within 4 percent.

Selected polynomial expressions are printed on their respective curves for ease in using the data in computer programs or in rigorous hand calculations. No attempt was made to fit the magnetic data, as smooth curves were observed in all the data analysis, and polynomial expressions that can be derived do not have as broad an area of application as the other properties. Creep data are presented in the Larson-Miller form to facilitate long-term extrapolations. In most cases, a new Larson-Miller constant was found which represents a better fit for the data than the commonly used value of 20.

Stability tests on magnetic properties are presented for times up to 1000 hours. Because of the sensitivity of these tests, analytical extrapolations must be tempered with a technical understanding of the material. One interpretation of this property can be found in the section, General Discussion of Magnetic Material Properties.

TABLE 11. - INDEX TO MAGNETIC

Material properties summary	Composition, material name, and form (a)	Specific heat	Thermal conductivity	Electrical resistivity	dc magnetization	ac magnetization
				Page		
74	$3\frac{1}{4}$ Si-Fe (Cubex Alloy)	78	79	79		
	0.002-in. tape (SRA)				82	86-88
	0.002-in. tape (MFA)				82	90-92
	0.006-in. tape (SRA)				83-84	98-100
						102-104
						106-108
	0.006-in. tape (MFA)				83	94-96
	0.006-in. sheet (SRA)				85	111-113
	0.011-in. sheet (SRA)				85	115-117
126	49Co-49Fe-2V (Hiperco 50 Alloy)	126, 131	126, 128	126		
	0.004-in. sheet (SRA)				135	136-137
	0.008-in. sheet (SRA)				135	140-142
128	49Co-49Fe-2V (Supermendur)	131	128	132-133		
	0.002-in. tape (MFA)				144	145-147
						149-151
	0.006-in. sheet (MFA)				145	153-155
163	27Co-Fe (Hiperco 27 Alloy)	163, 167	163			
	0.004-in. sheet (SRA)				172	176-178
	0.008-in. sheet (SRA)				170, 172-175	180-184
	Forging (SRA)			168-169	171	
	Casting (SRA)				171	
215	1SiFe		215	215		215
	AMS 5210, casting (SRA)	217			217-218	
221	15Ni-9Co-5Mo-0.70Al-0.70Ti-Fe (15% Nickel maraging steel)			221		
	Bar (SRA)				226	
	0.016-in. laminations (SRA)				227	227
223	18Ni-8Co-4Mo-0.4Ti-Fe (18% Nickel maraging steel)	223				
	Steel bar (SRA)		250	250	258	
	0.014-in. laminations (SRA)				259	260
243	5Cr-1Mo-0.5V-Fe (AISI Grade H-11)	243	243	243		
	AMS 6487, forging (SRA)				246	
	AMS 6437, 0.014-in. sheet (SRA)				247	248
	AMS 6437, 0.025-in. sheet (SRA)				247	250
268	23Ni-2Ti-1Zr-Co-Fe (Nivco Alloy)		268			
	Forging (SRA)	272			276	
	0.014-in. sheet (SRA)				277	278
	0.025-in. sheet (SRA)			273-276	278	279

[a] SRA, stress relief annealed; MFA, magnetic field annealed.

MATERIALS PROPERTIES - TABLES AND FIGURES

Core loss	Constant current flux reset	Magnetic stability	Poisson's ratio	Tensile and compressive strength	Creep	Larson-Miller plot	Fatigue	Goodman diagram
				Page				
80, 88-90	81				77		77	
80, 92-94	81							
80, 100-102	81							
104-106								
109-111								
80, 96-98								
80, 113-115								
80, 117-119		86, 119-120	121	121-125				
138-139	127				127		127	
142-143				158-160				
147-149	134				130		130	
151-153								
155-157				161-162				
178-180	164		191-193				165	
170, 185-188		176, 184, 189						
				194-195	194-200	200		
				198-199	202-209	201		
				196-197	201, 210-214			
215	215				216		216	
				219-220				
	221	226	222					
				231, 232	233-234	233	222	
228					235-242			
	223		224					
				231-233	224, 234	266	276	
261								
	243		244	252-253	256, 262			
		246						
					253-254	253-254	262, 264-267	263
					261			
249								
251					254-255	254-255		
					257-260			
	268		269					
		277		281-282	285-286	285	299, 301-305	300
					287-297			
279								
280				283-284	286, 297-298			

Cubex Alloy

Cubex alloy is a doubly grain-oriented $3\frac{1}{4}$-percent silicon-iron alloy that is available in limited quantities only from Westinghouse Electric Corporation, Pittsburgh, Pennsylvania. The nominal composition is $3\frac{1}{4}$ percent silicon-iron, but the tested composition was not analyzed for exact composition. When this material is used as a magnetic material, it should be purchased to a performance requirement rather than to a chemical analysis.

<u>Thermophysical properties</u>. -

Density, g/cu cm 7. 65

Solidus temperature, ^{O}F 2672

Curie temperature, ^{O}F 1400

Thermal conductivity (at 72°, 500°, and 800° F),
  (Btu)(ft)/(sq ft)(hr)(^{O}F) 17. 05

Coefficient of thermal expansion (from 72° to 1200°F),
  in./(in.)(^{O}F) (ref. 9). . . . . .7. 07×10^{-6}

Specific heat, Btu/(lb)(^{O}F), at –
  72° F 0. 109
  700° F 0. 115
  900° F 0. 136
  1100° F 0. 204

Electrical resistivity, ohm-cm, at –
  77° F . . . . 44. 53×10^{-6}
  511° F . . . . 57. 98×10^{-6}
  700° F . . . . 66. 36×10^{-6}
  900° F . . . . 79. 66×10^{-6}
  1100° F . . . . 89. 94×10^{-6}

Magnetic properties. -

Direct current:

Annealing	Temperature, °F	Tape-wound toroid thickness, in.		Lamination thickness, in.	
		0.002	0.006	0.006	0.011
		Induction,[a] B_{tip}, kG			
Stress relief	72	20.4	20.5	20.3	19.9
	500	19.2	19.5	19.1	19.1
	700	----	----	----	18.3
	800	17.6	17.8	18.0	----
	1100	14.9	15.0	15.3	14.3
Magnetic field	72	20.8	20.6	----	----
	500	----	19.5	----	----
	800	17.9	17.6	----	----
	1100	14.9	14.5	----	----

[a]H, 250 Oe.

Alternating current (400 cps):

| Annealing | Temperature, °F | B, kG | Exciting volt-amperes per pound | | | | Core loss, W/lb | | | |
| | | | Tape-wound toroid thickness, in. | | Lamination thickness, in. | | Tape-wound toroid thickness, in. | | Lamination thickness, in. | |
			0.002	0.006	0.006	0.011	0.002	0.006	0.006	0.011
Stress relief	72	15	9.1	18.5	46.5	46	6.8	9.5	11.5	13.0
	500	15	9.8	----	-----	---	5.6	---	----	----
	800	15	14.3	55.8	133	120	4.4	7.0	7.8	9.8
	1100	13	22.1	45.8	75	[a]250	2.8	3.9	4.2	[b]7.0
Magnetic field	72	15	7.3	19.3	-----	----	6.1	10.2	---	----
	800	15	17.8	69.8	-----	----	4.7	7.0	---	----
	1100	13	19.5	58.4	-----	----	2.9	3.8	---	----

[a]B, 14 kG.

[b]B, 15 kG.

Constant current flux reset (CCFR) properties for 0.002-inch-thick tape-wound toroid (magnetic-field annealed):

| Property | Temperature, °F | | |
	72	500	1100
B_m, kG, at 10 Oe (SAT/2)	19.20	18.25	13.85
$B_m - B_r$, kG	1.10	2.0	4.2
H_1, Oe (AT)	0.42	0.28	0.12
H_2, Oe (AT + DAT)	0.49	0.34	0.165
H_0, Oe (AT + DAT/2)	0.45	0.31	0.14

Mechanical properties. -

Tensile and compressive properties:

Temperature, $^\circ$F	0.02-Percent offset yield strength, psi	Tensile strength, psi	Elongation in 2 in., percent	Modulus of elasticity, psi	Compressive yield strength, psi
Longitudinal					
72	37 150	40 200	22.0	22 $\times 10^6$	37 120
500	27 300	40 800	21.0	13.5	32 950
800	25 300	32 250	11.9	9	29 200
1100	14 750	16 650	26.0	6	[a]11 100
Transverse					
72	39 050	46 400	14.5	--------	40 600
500	29 800	41 200	38.0	--------	30 800
800	25 200	34 350	10.0	--------	27 500
1100	[b]12 900	13 350	11.5	--------	[a]11 325

[a]0.02 Percent offset.

[b]Upper yield point.

Poisson's ratio at 72° F (average of six variable readings): 0.335

Creep: Material is not used in highly stressed applications.

Fatigue: Material is not used in cyclic stressed applications.

Normal stress-relief heat treatment: Material is heated to 800°±10° C in an atmosphere of purified dry hydrogen, held 2 hours at temperature, and furnace-cooled to below 150° C.
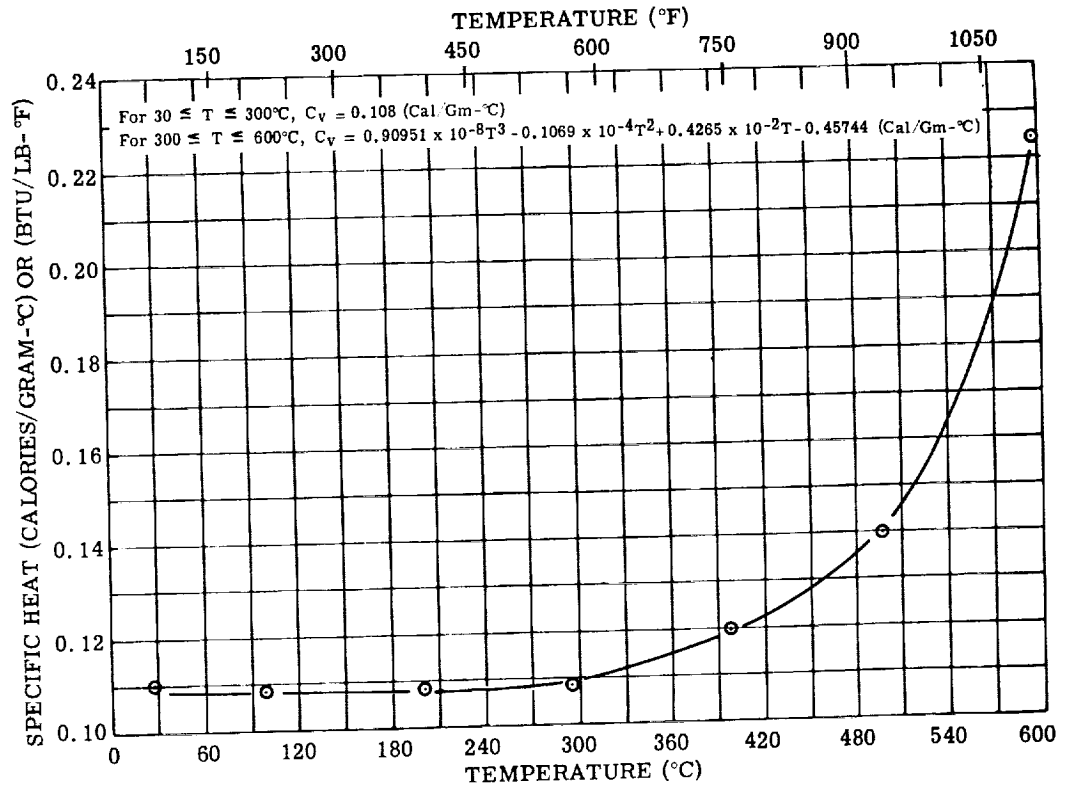
Figure 42. - Specific heat of Cubex alloy measured in 10^{-5} torr vacuum.
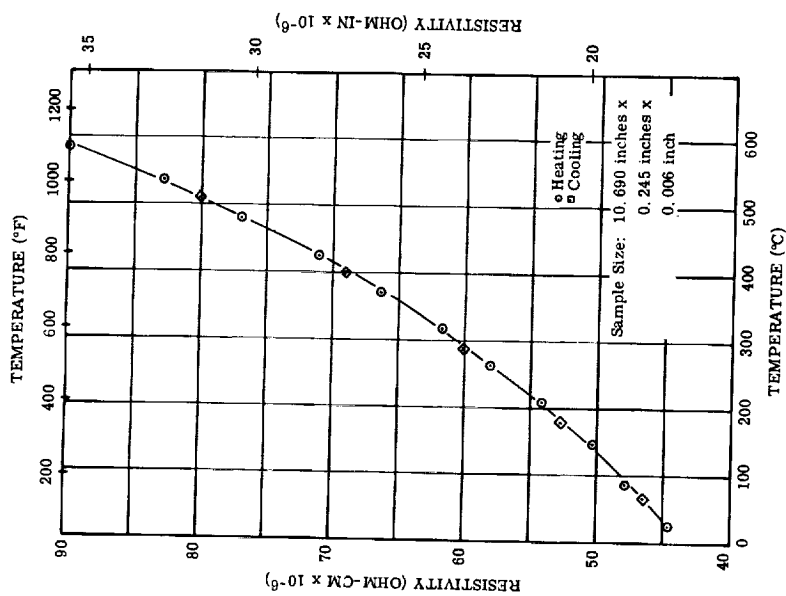
Figure 44. – Electrical resistivity of 0.006-inch Cubex alloy sheet, stress-relief annealed and tested in 1×10^{-4} torr vacuum.
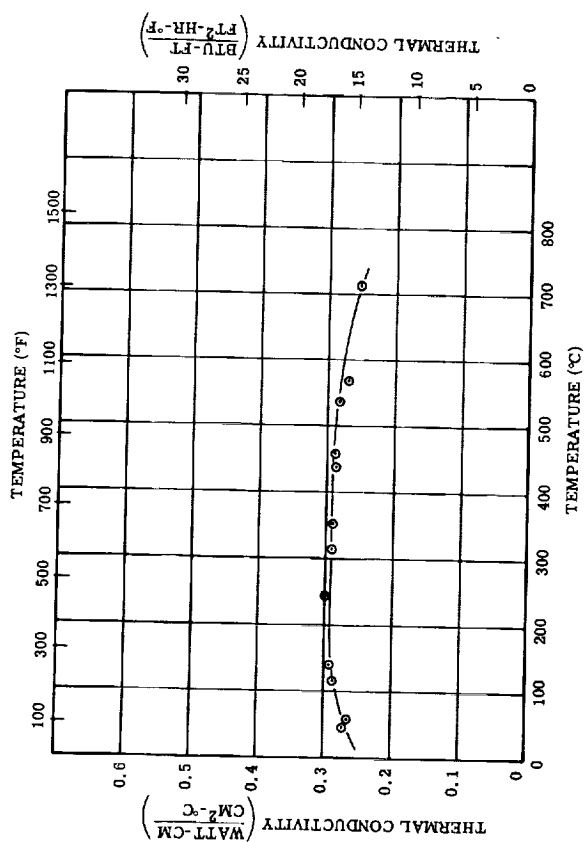
Figure 43. – Thermal conductivity of Cubex alloy in vacuum.

TABLE 12. - SUMMARY OF CORE LOSSES OF CUBEX ALLOY

Material	400 cps, 15 kG		800 cps, 12 kG		1600 cps, 12 kG		3200 cps, 8 kG	
	Temperature, °F							
(a)	72	1100	72	1100	72	1100	72	1100
	Core losses, W/lb							
Toroid, sample 1 0.006-in.-thick tape, SRA	9.4	----	17.5	8.8	49.0	26.5	68.0	38.0
Toroid, sample 2 0.006-in.-thick tape, SRA	9.8	----	17.5	8.9	50.8	26.5	70.0	39.5
Toroid, sample 3 0.006-in.-thick tape, SRA	9.2	----	16.0	8.8	44.4	26.1	62.5	43.5
Ring laminations 0.006-in. thick, SRA	11.5	----	28.0	10.0	55.0	31.0	100.0	47.0
Toroid 0.002-in.-thick tape, SRA	6.8	----	11.0	5.5	27.0	13.7	38.0	19.5
Toroid 0.002-in.-thick tape, MFA	6.0	----	9.7	6.0	24.5	16.0	37.5	23.5
Ring laminations 0.011-in. thick, SRA	19.2	----	39.0	22.0	28.5	----	170.0	122.0

aSRA, stress relief annealed; MFA, magnetic field annealed.

TABLE 13. - CONSTANT CURRENT FLUX RESET PROPERTIES[a] OF CUBEX ALLOY

[400 cps - sine wave; H_m, 10 Oe.]

Core	Material thickness, in.	Core size	Treatment (d)	Temperature, °F	Test environment	B_m, kG	$B_m - B_r$, kG	$\dfrac{B_r}{B_m}$	H_0, Oe	H_1, Oe	H_2, Oe
1	0.002	(b)	SRA	72	Air	16.15	4.52	0.720	0.570	0.474	0.696
				500	Air	15.33	6.98	.545	.363	.252	.554
				1100	Argon	11.75	6.15	.477	.128	.083	.212
				e72	Air	16.42	5.15	.686	.582	.514	.680
2	0.002	(b)	MFA	72	Air	19.00	1.18	0.938	0.453	0.418	0.484
				500	Argon	17.76	2.32	.869	.305	.277	.340
				1100	Argon	13.68	4.18	.694	.126	.108	.148
				e72	Air	18.96	2.80	.852	.509	.448	.567
3	0.002	(c)	SRA	72	Air	18.08	7.02	0.612	0.618	0.530	0.733
				500	Air	16.42	8.07	.509	.400	.288	.568
				1100	Argon	12.91	8.23	.363	.216	.053	.384
				e72	Air	17.56	6.02	.657	.705	.574	.850
4	0.002	(c)	SRA	72	Air	17.74	6.34	0.643	0.660	0.548	0.785
				500	Air	16.49	8.24	.500	.535	.296	.565
				1100	Argon	12.67	8.11	.360	.207	.050	.353
				e72	Air	17.59	6.27	.644	.618	.532	.720
7	0.006	(b)	SRA	72	Air	16.46	3.83	0.768	0.526	0.436	0.604
				500	Air	15.84	4.44	.720	.393	.318	.469
				1100	Argon	12.62	5.35	.580	.156	.116	.206
11	0.006	(c)	SRA	72	Air	16.52	2.66	0.839	0.473	0.272	0.669
				500	Air	15.02	8.62	.426	.305	.123	.512
				1100	Argon	12.37	7.46	.397	.179	.078	.339
				e72	Air	16.88	7.58	.551	.493	.294	.658
12	0.006	(c)	SRA	72	Air	16.60	7.75	0.533	0.473	0.269	0.655
				500	Air	15.49	8.53	.449	.358	.160	.571
				1100	Argon	12.63	7.62	.397	.193	.070	.515
				e72	Air	16.54	7.62	.539	.479	.283	.655

[a]Test procedure for Toroidal Magnetic Amplifier Cores, AIEE No. 432, January 1959.

[b]Toroid, $3\frac{1}{2}$ by 4 by 1/2 in.

[c]Toroid, 1 by $1\frac{1}{4}$ by 1/4 in.

[d]MFA, magnetic field anneal; SRA, stress relief anneal.

[e]Room-temperature test after 1100° F exposure.

MAGNETIZING FORCE (AMPERE TURNS/INCH)

	H_c	B_r	From
	(Oersteds)	(Gauss)	(Oersteds)
✗ Initial RT	0.376	13,500	100
⊙ 300°F	0.344	12,600	100
△ 500°F	0.291	11,100	100
□ 800°F	0.175	7,500	100
✳ 1100°F	0.117	3,300	100
◇ RT After 1100°F	0.376	12,700	100

MAGNETIZING FORCE (OERSTEDS)
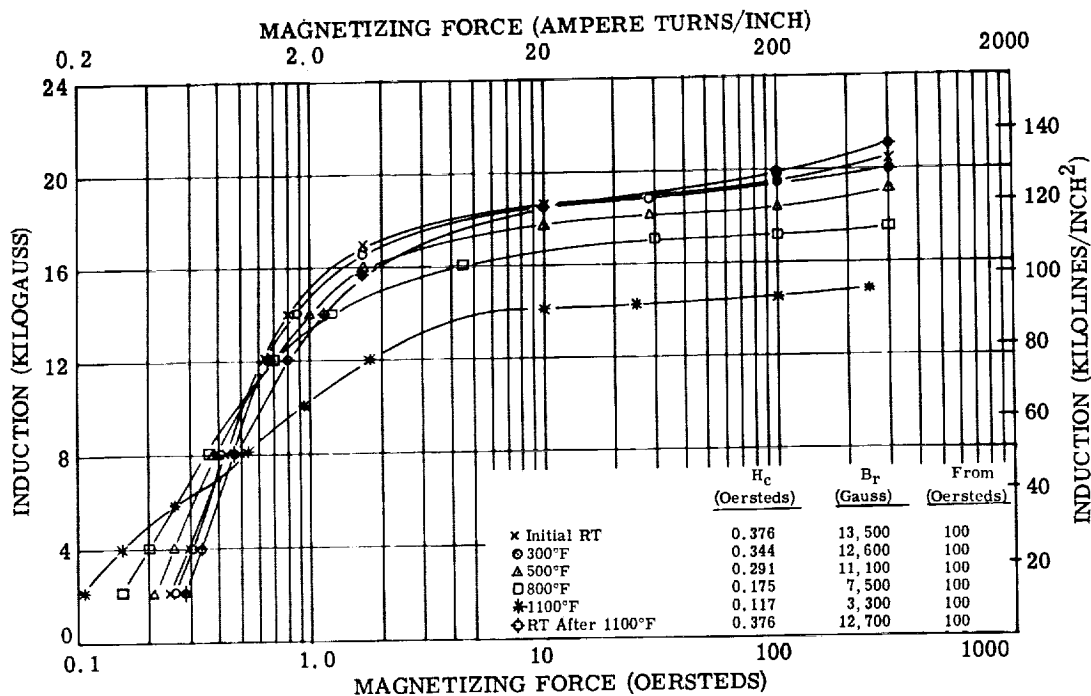
Figure 45. - Direct-current magnetization curves for 0.002-inch Cubex alloy tape toroid $3\frac{1}{2}$ by 4 by 1/2 inch.
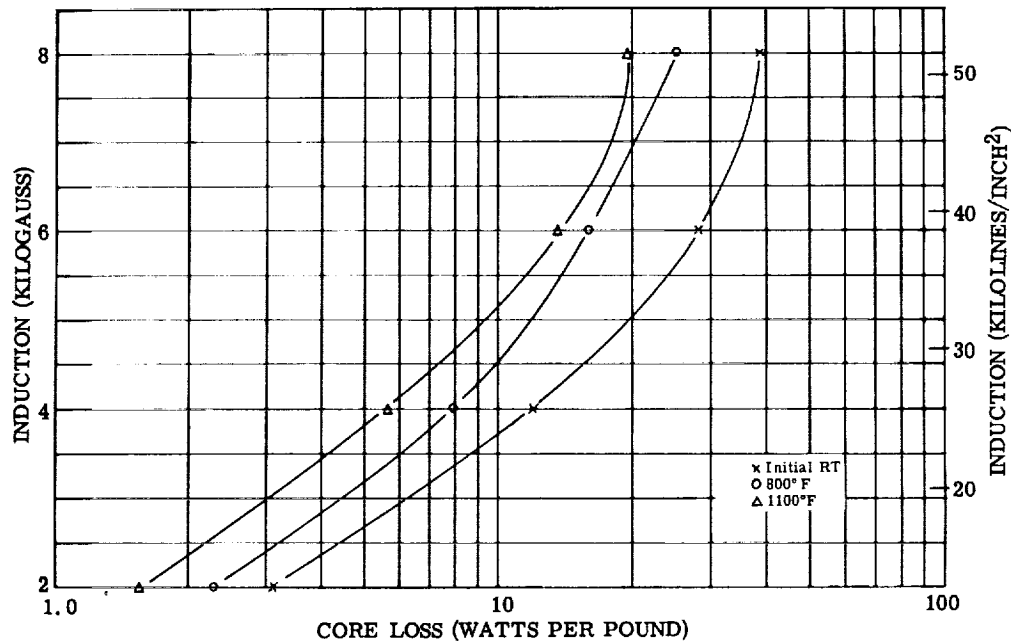Test atmosphere, air to 300° F and argon above 300° F; interlaminar insulation, aluminum orthophosphate.

MAGNETIZING FORCE (AMPERE TURNS/INCH)

	H_c	B_r	From
	(Oersteds)	(Gauss)	(Oersteds)
✗ Initial RT	0.306	16,500	100
⊙ 800°F	0.155	8,400	100
△ 1100°F	0.093	3,300	100
□ RT After 1100°F	0.330	14,100	100

MAGNETIZING FORCE (OERSTEDS)
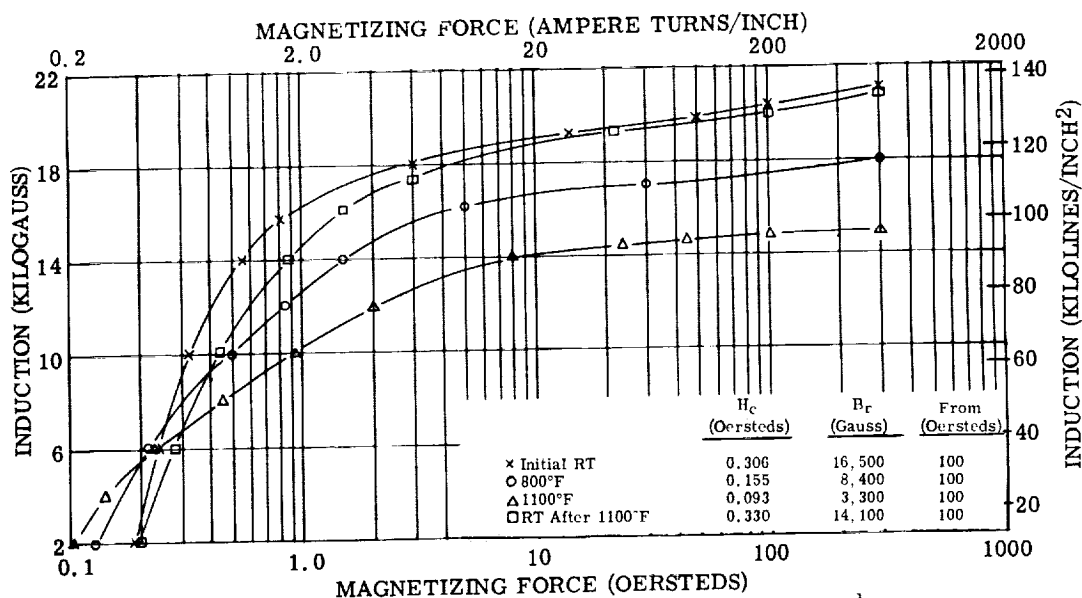
Figure 46. - Direct-current magnetization curves for 0.002-inch Cubex alloy tape toroid $1\frac{1}{4}$ by 1 by 1/4 inch.
Magnetic-field annealed; test atmosphere, air to 800° F and argon above 800° F; interlaminar insulation,
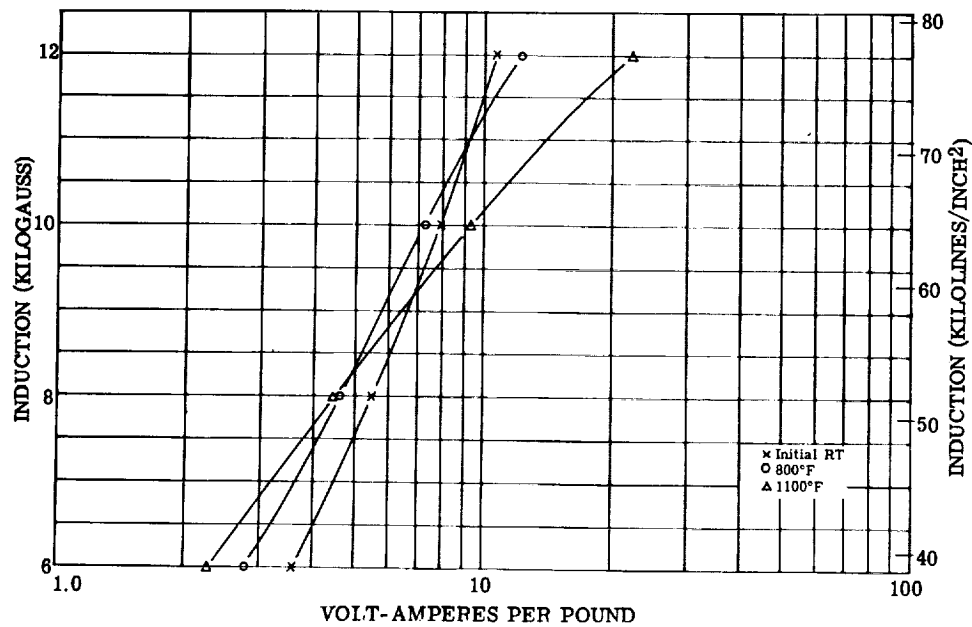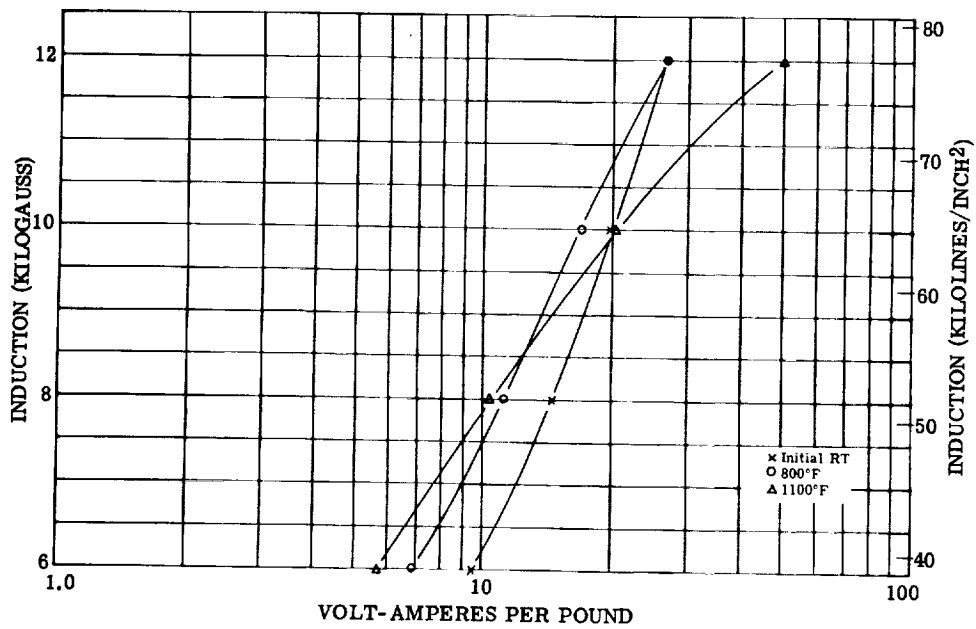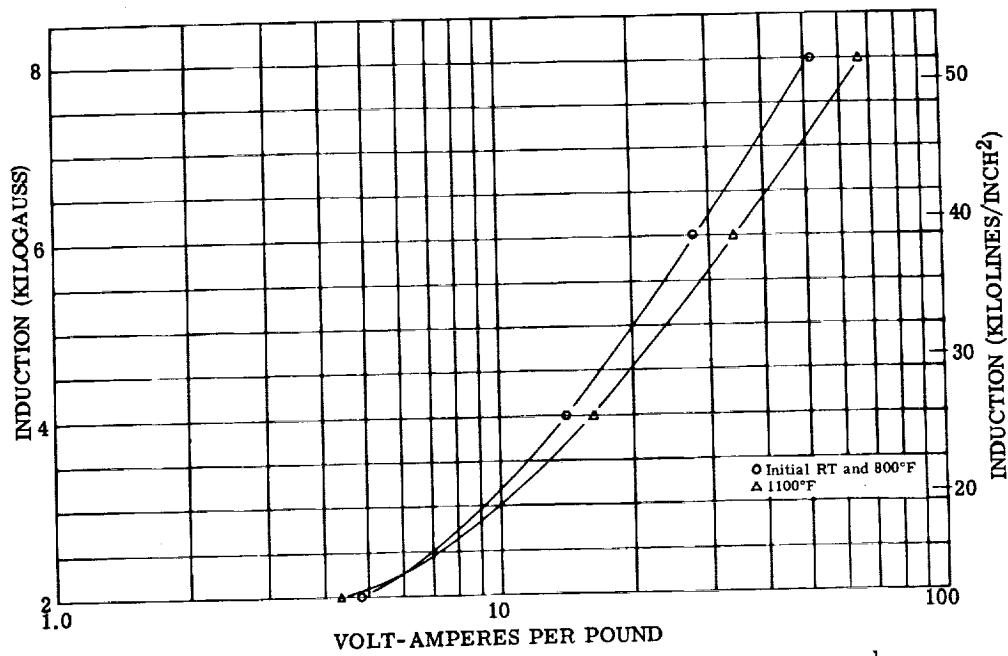aluminum orthophosphate.
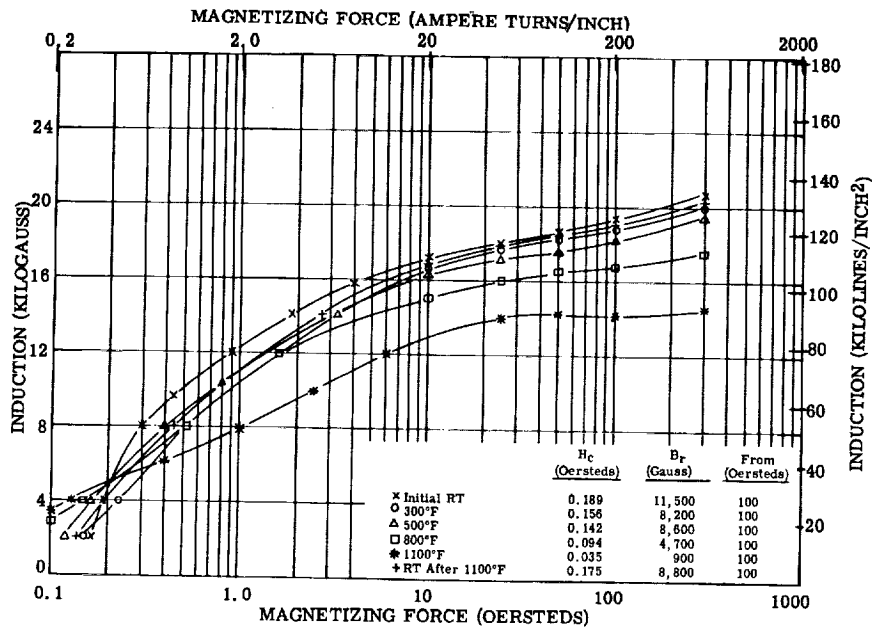
Figure 47. - Direct-current magnetization curves for 0.006-inch Cubex alloy tape. Magnetic-field annealed. Test atmosphere, air to 500° F and argon above 500° F; interlaminar insulation, mica aluminum orthophosphate.
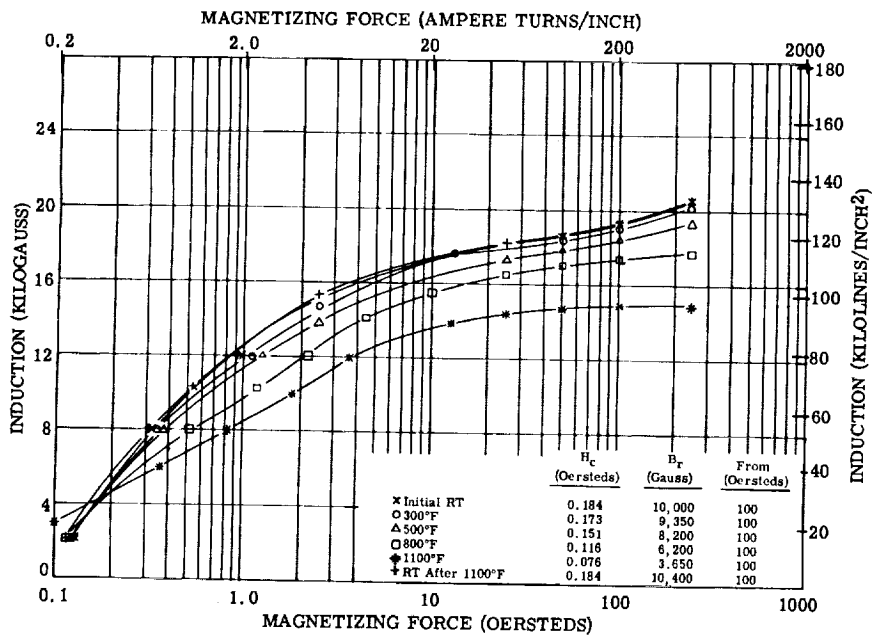
Figure 48. - Direct-current magnetization curves for 0.006-inch Cubex alloy tape, sample 1. Test atmosphere, argon; interlaminar insulation, mica aluminum orthophosphate.

MAGNETIZING FORCE (AMPERE TURNS/INCH)

INDUCTION (KILOGAUSS)

INDUCTION (KILOLINES/INCH^2)

	H_c (Oersteds)	B_r (Gauss)	From (Oersteds)
x Initial RT	0.179	9,100	100
O 300°F	0.164	8,200	100
△ 500°F	0.136	7,050	100
▢ 800°F	0.093	4,900	100
✱ 1100°F	0.056	1,250	100
+ RT After 1100°F	0.179	9,500	100

MAGNETIZING FORCE (OERSTEDS)
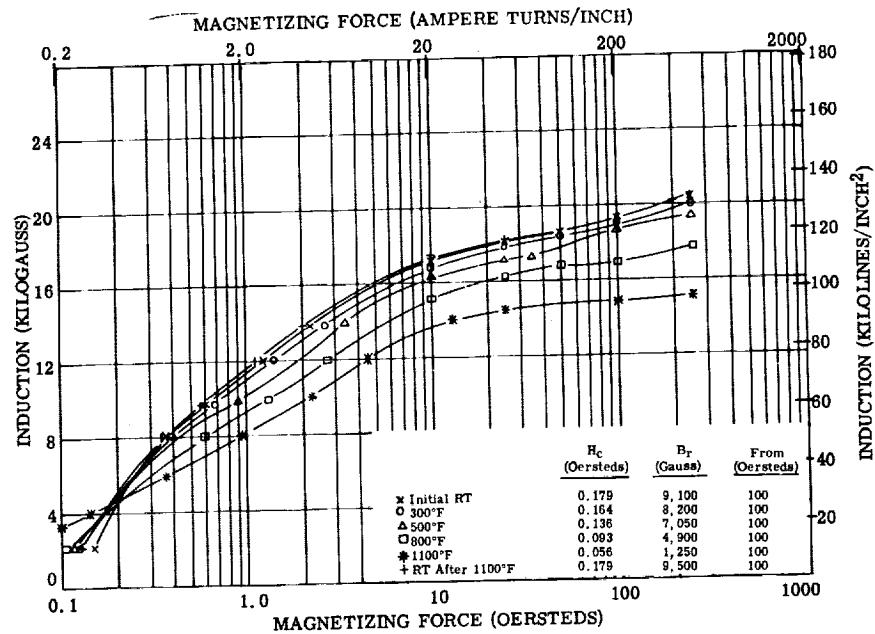
Figure 49. - Direct-current magnetization curves for 0.006-inch Cubex alloy tape, sample 2. Test atmosphere, argon; interlaminar insulation, mica aluminum orthophosphate.

MAGNETIZING FORCE (AMPERE TURNS/INCH)

INDUCTION (KILOGAUSS)

INDUCTION (KILOLINES/INCH^2)

	H_c (Oersteds)	B_r (Gauss)	From (Oersteds)
x Initial RT	0.218	11,100	100
O 300°F	0.199	10,700	100
△ 500°F	0.169	9,600	100
▢ 800°F	0.129	6,600	100
+ 1100°F	0.065	1,600	100
✦ RT After 1100°F	0.203	11,100	100

MAGNETIZING FORCE (OERSTEDS)
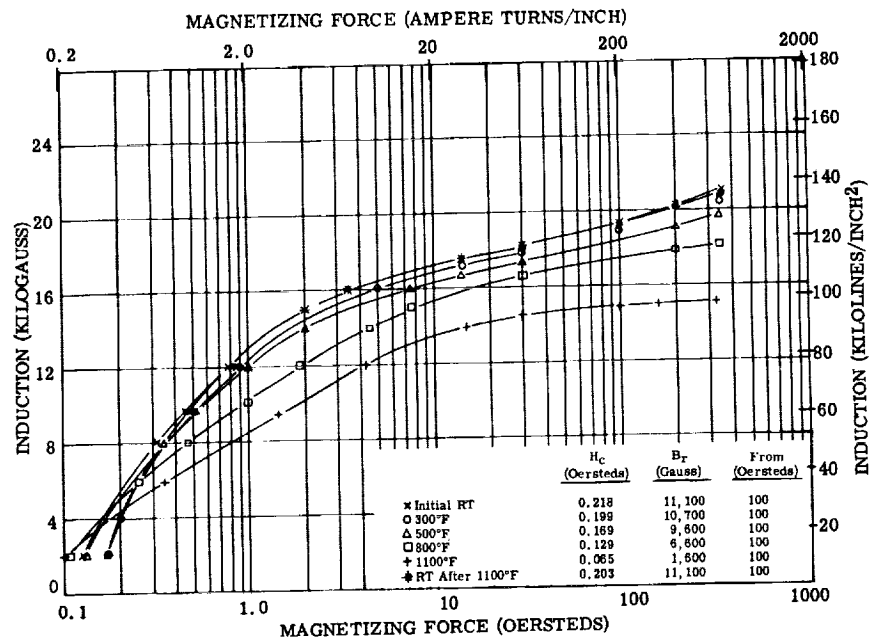
Figure 50. - Direct-current magnetization curves for 0.006-inch Cubex alloy tape, sample 3. Test atmosphere, air to 500° F and argon above 500° F; interlaminar insulation, mica aluminum orthophosphate.

MAGNETIZING FORCE (AMPERE TURNS/INCH)

	Hc (Oersteds)	Br (Gauss)	From (Oersteds)
✕ Initial RT	0.186	6,500	100
○ 300°F	0.168	5,600	100
△ 500°F	0.151	4,300	100
☐ 800°F	0.087	2,600	100
✦ 1100°F	0.061	1,500	100
✚ RT After 1100°F	0.186	7,500	100

MAGNETIZING FORCE (OERSTEDS)
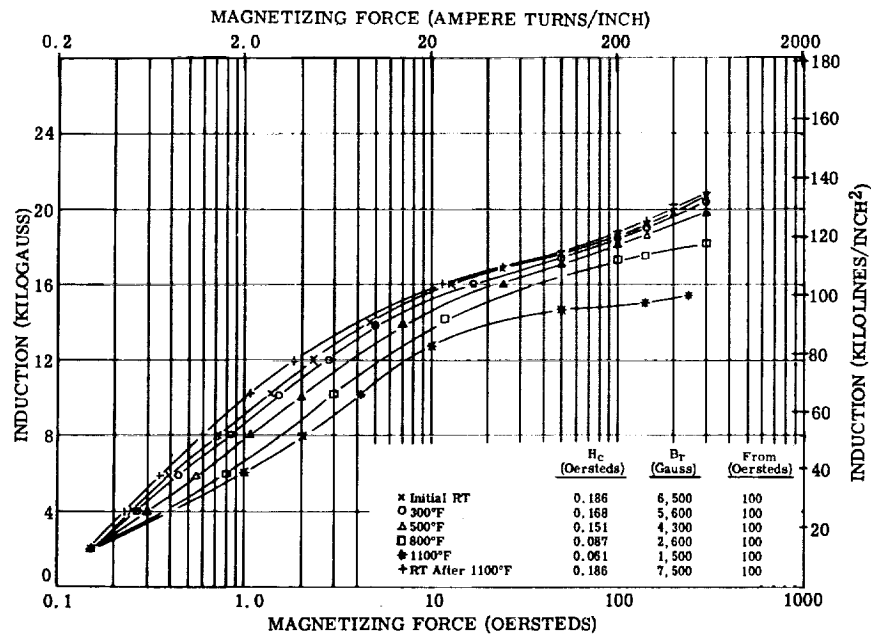
Figure 51. - Direct-current magnetization curves for 0.006-inch Cubex alloy laminations. Test atmosphere, air to 500° F and argon above 500° F; interlaminar insulation, mica aluminum orthophosphate.

MAGNETIZING FORCE (AMPERE TURNS/INCH)

✕ Initial RT
⊙ 300°F (Est)
△ 500°F (Est)
⊡ 800°F (Est)
✦ 1100°F (Est)

MAGNETIZING FORCE (OERSTEDS)
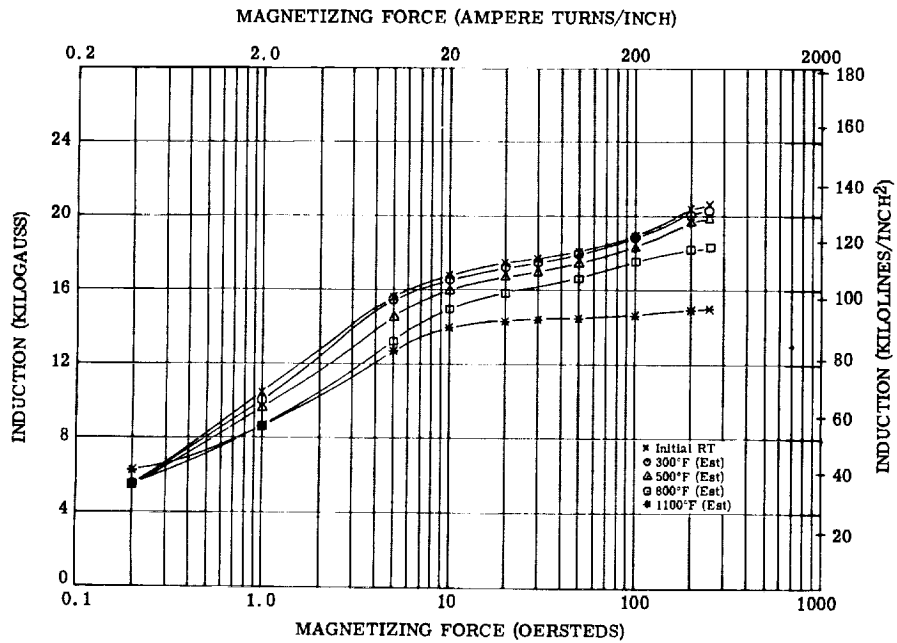
Figure 52. - Direct-current magnetization curves for 0.011-inch Cubex laminations. Test atmosphere, air; interlaminar insulation, mica aluminum orthophosphate.
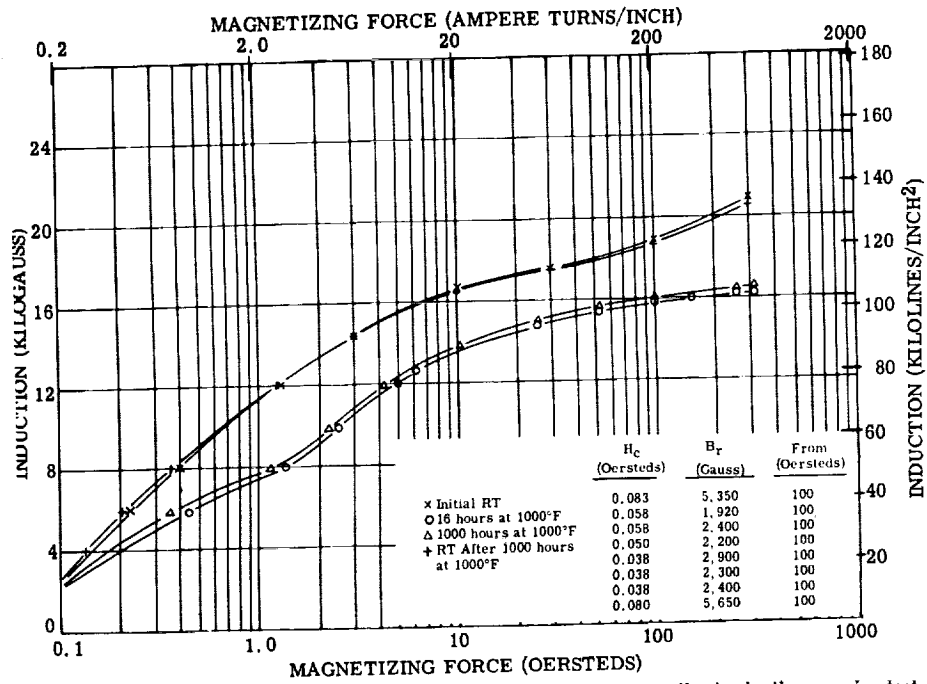
Figure 53. - Direct-current magnetization curves for 0.011-inch Cubex alloy laminations - aging test. Test atmosphere, argon; interlaminar insulation, mica aluminum orthophosphate.
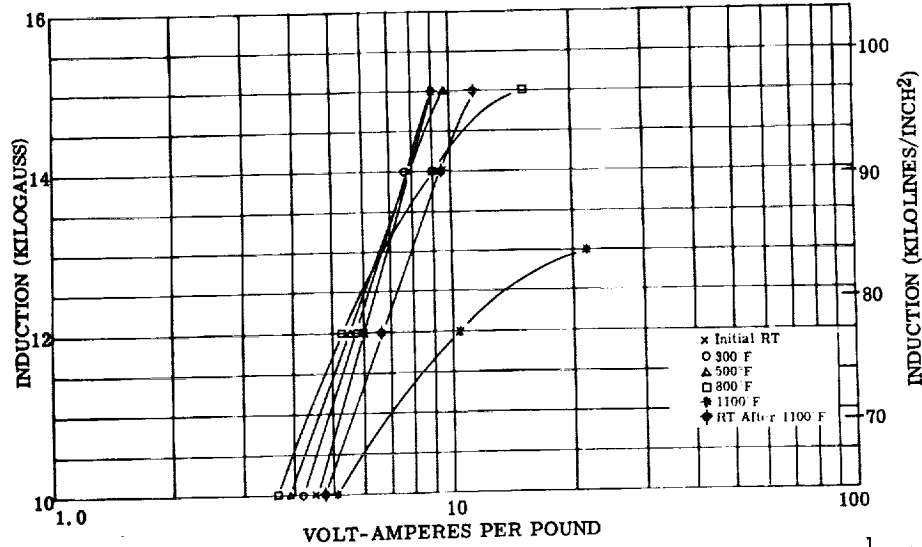
Figure 54. - Exciting volt-amperes per pound at 400 cps for 0.002-inch Cubex alloy tape toroid $3\frac{1}{2}$ by 4 by 1/2 inch. Test atmosphere, air to 300° F and argon above 300° F; interlaminar insulation, aluminum orthophosphate.
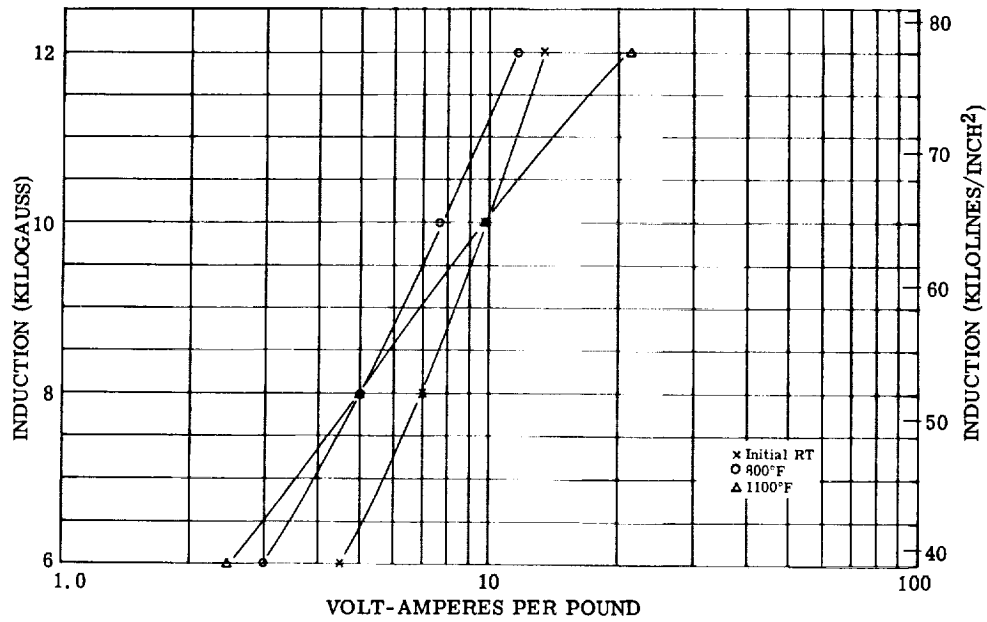
Figure 55. - Exciting volt-amperes per pound at 800 cps 0.002-inch Cubex alloy tape toroid $3\frac{1}{2}$ by 4 by 1/2-inch. Test atmosphere, air to 300° F and argon above 300° F; interlaminar insulation, aluminum orthophosphate.
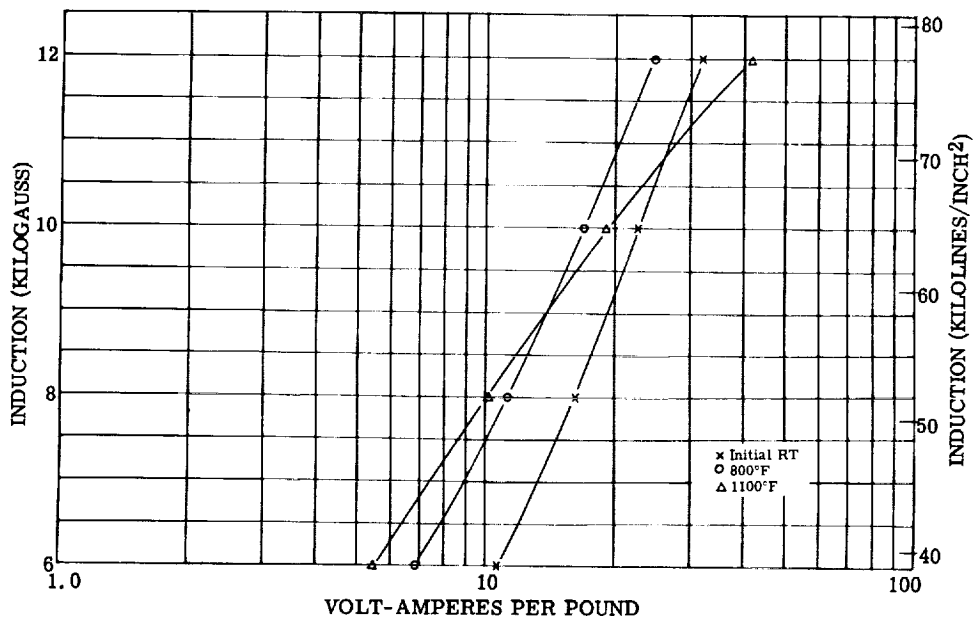
Figure 56. - Exciting volt-amperes per pound at 1600 cps 0.002-inch Cubex alloy tape toroid $3\frac{1}{2}$ by 4 by 1/2-inch. Test atmosphere, air to 300° F and argon above 300° F; interlaminar insulation, aluminum orthophosphate.
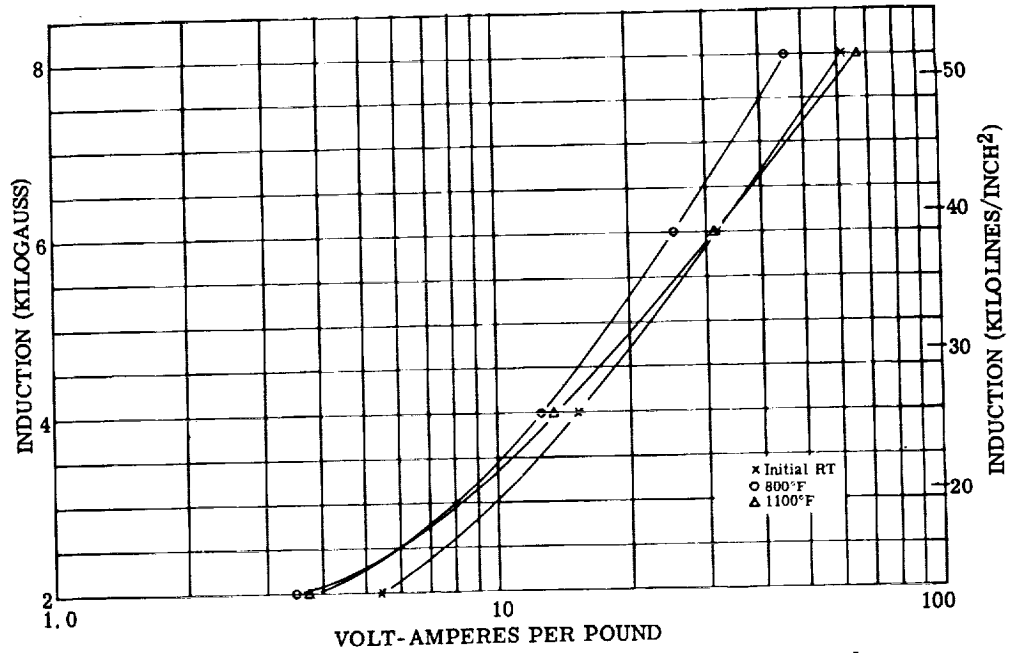
Figure 57. - Exciting volt-amperes per pound at 3200 cps 0.002-inch Cubex alloy tape toroid $3\frac{1}{2}$ by 4 by 1/2 inch.
Test atmosphere, air to 300° F and argon above 300° F; interlaminar insulation, aluminum orthophosphate.
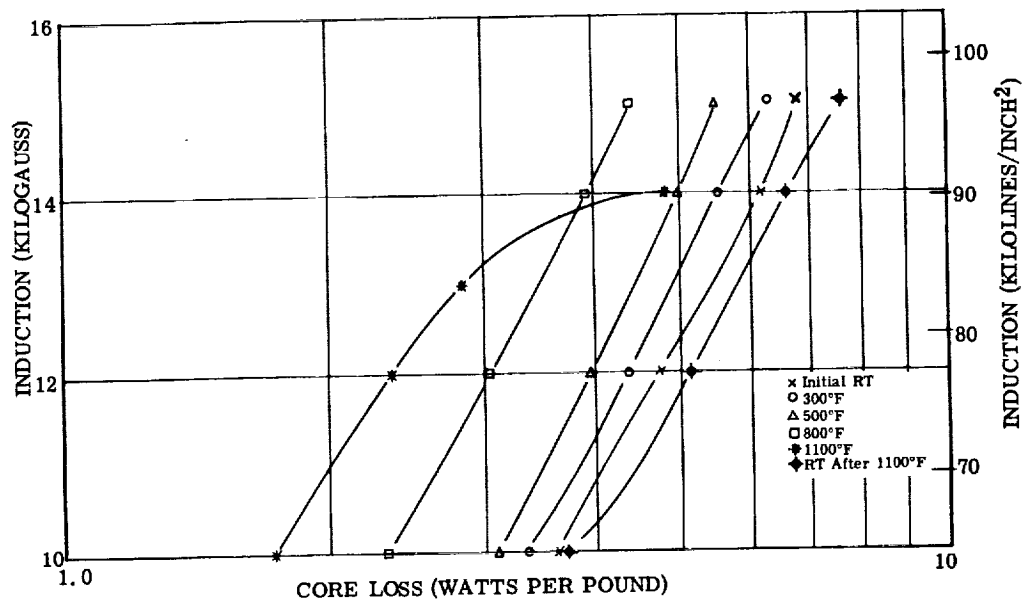
Figure 58. - Core loss at 400 cps for 0.002-inch Cubex alloy tape toroid $3\frac{1}{2}$ by 4 by 1/2 inch. Test atmosphere, air
to 300° F and argon above 300° F; interlaminar insulation, aluminum orthophosphate.
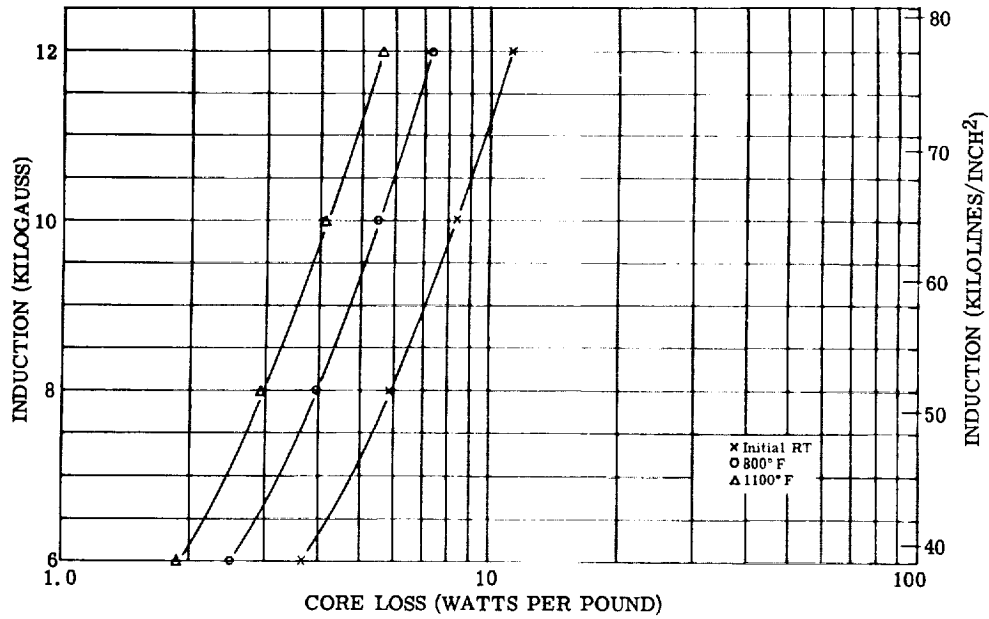
Figure 59. - Core loss at 800 cps for 0.002-inch Cubex alloy tape toroid $3\frac{1}{2}$ by 4 by 1/2 inch. Test atmosphere, air to 300° F and argon above 300° F; interlaminar insulation, aluminum orthophosphate.
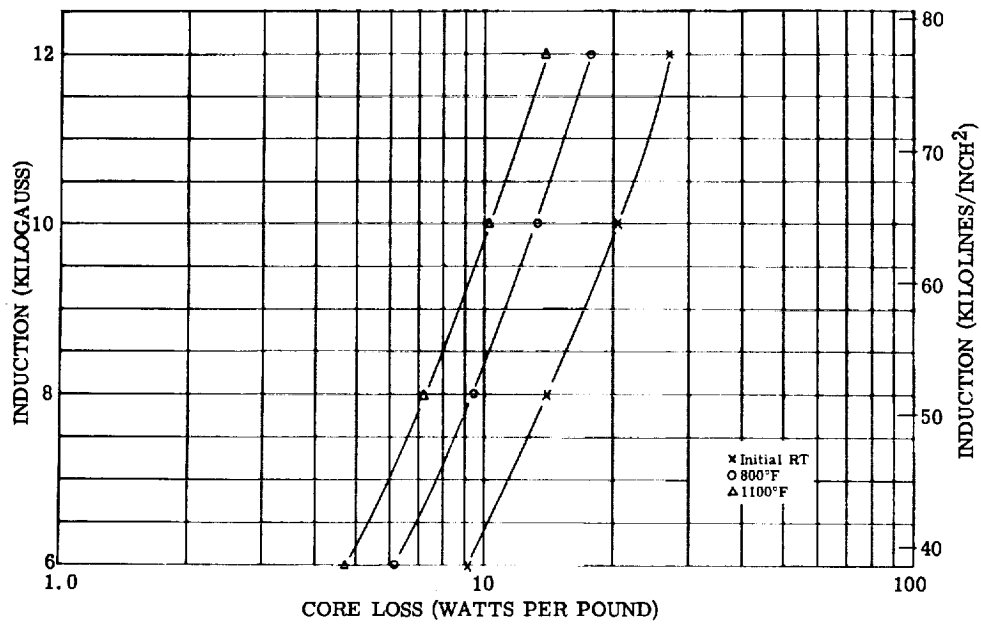
Figure 60. - Core loss at 1600 cps for 0.002-inch Cubex alloy tape toroid $3\frac{1}{2}$ by 4 by 1/2 inch. Test atmosphere, air to 300° F and argon above 300° F; interlaminar insulation, aluminum orthophosphate.
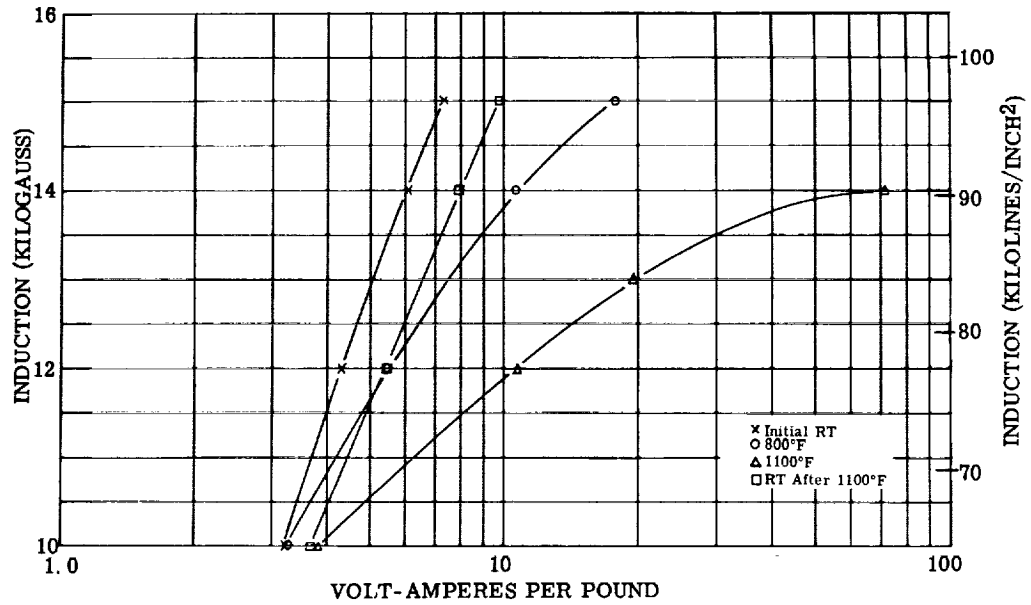
Figure 61. - Core loss at 3200 cps for 0.002-inch Cubex alloy tape toroid $3\frac{1}{2}$ by 4 by 1/2 inch. Test atmosphere, air to 300° F and argon above 300° F; interlaminar insulation, aluminum orthophosphate.

Figure 62. - Exciting volt-amperes per pound at 400 cps for 0.002-inch Cubex alloy tape toroid $1\frac{1}{4}$ by 1 by 1/4 inch, magnetic-field annealed. Test atmosphere, air to 800° F and argon above 800° F; interlaminar insulation, aluminum orthophosphate.
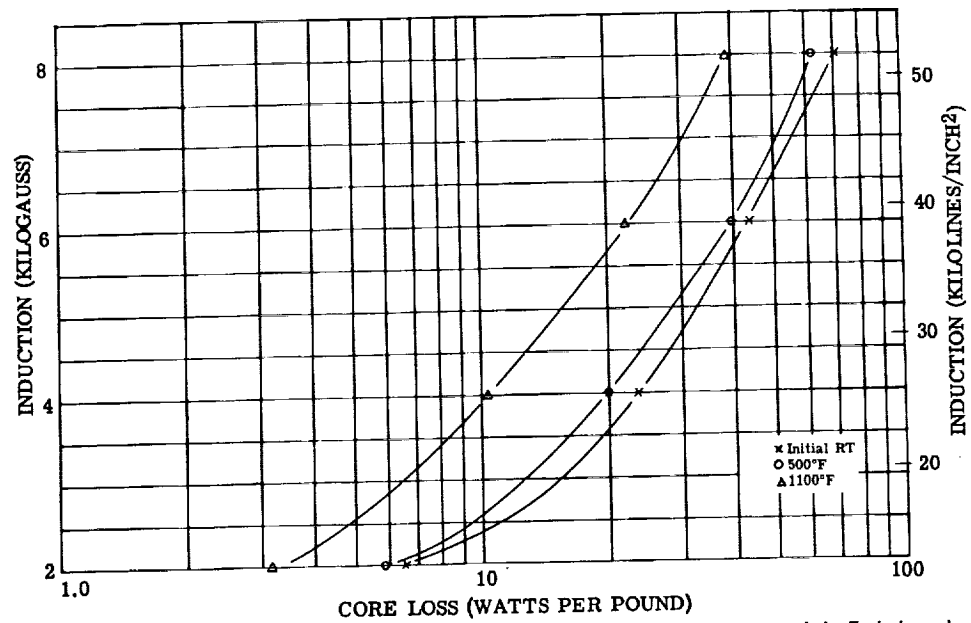
Figure 63. - Exciting volt-amperes per pound at 800 cps for 0.002-inch Cubex alloy tape toroid $1\frac{1}{4}$ by 1 by 1/4 inch, magnetic-field annealed. Test atmosphere, air to 800° F and argon above 800° F; interlaminar insulation, aluminum orthophosphate.
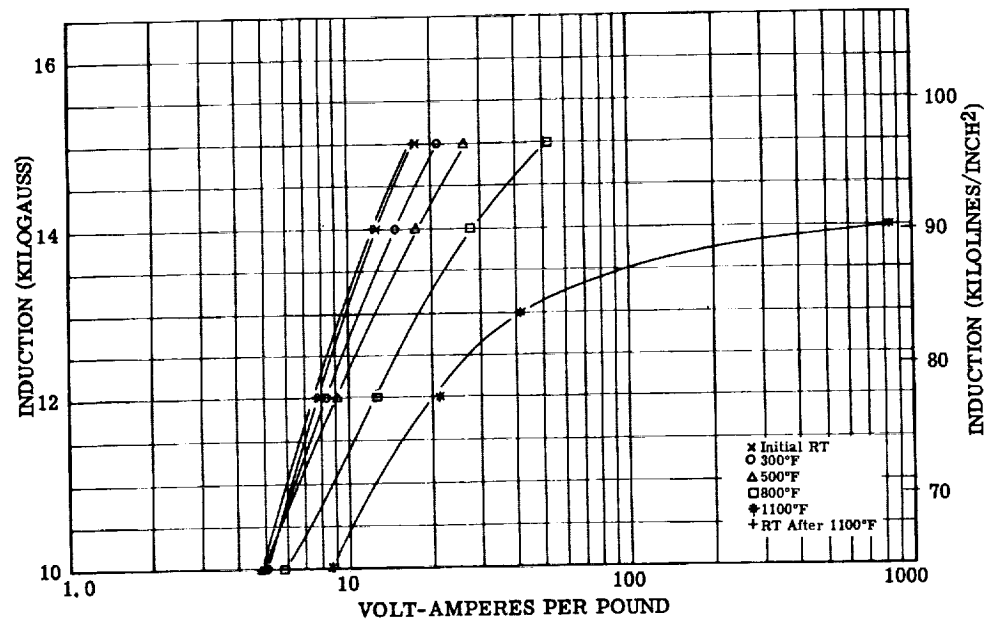

Figure 64. - Exciting volt-amperes per pound at 1600 cps for 0.002-inch Cubex alloy tape toroid $1\frac{1}{4}$ by 1 by 1/4 inch, magnetic-field annealed. Test atmosphere, air to 800° F and argon above 800° F; interlaminar insulation, aluminum orthophosphate.

Figure 65. - Exciting volt-amperes per pound at 3200 cps for 0.002-inch Cubex alloy tape toroid $1\frac{1}{4}$ by 1 by 1/4 inch, magnetic-field annealed. Test atmosphere, air to 800° F and argon above 800° F; interlaminar insulation, aluminum orthophosphate.
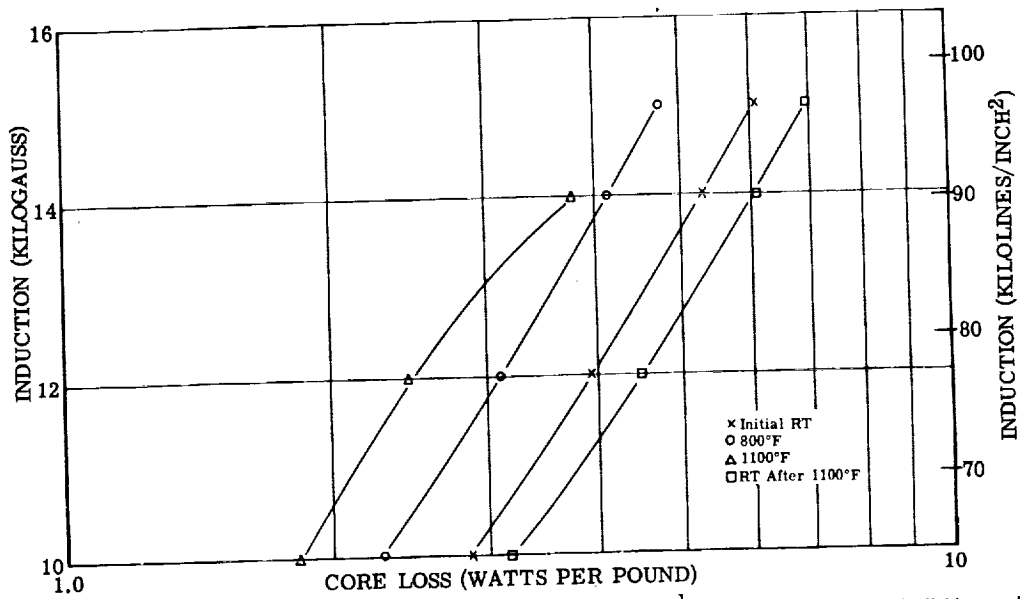
Figure 66. - Core loss at 400 cps for 0.002-inch Cubex alloy tape toroid $1\frac{1}{4}$ by 1 by 1/4 inch, magnetic-field annealed. Test atmosphere, air to 800° F and argon above 800° F; interlaminar insulation, aluminum orthophosphate.
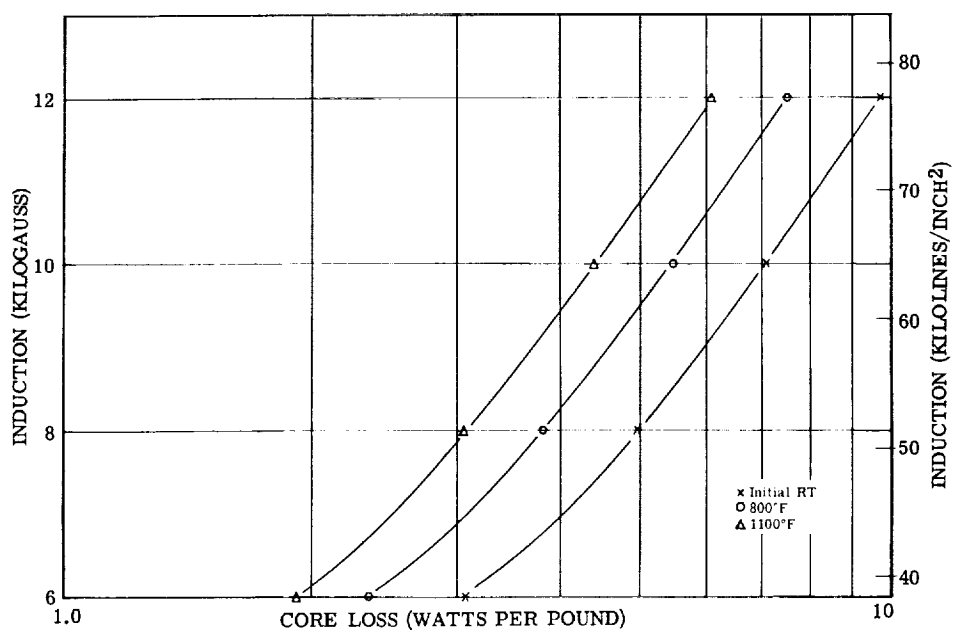
Figure 67. - Core loss at 800 cps for 0.002-inch Cubex alloy tape toroid $1\frac{1}{4}$ by 1 by 1/4 inch, magnetic-field annealed. Test atmosphere, air to 800° F and argon above 800° F; interlaminar insulation, aluminum orthophosphate.
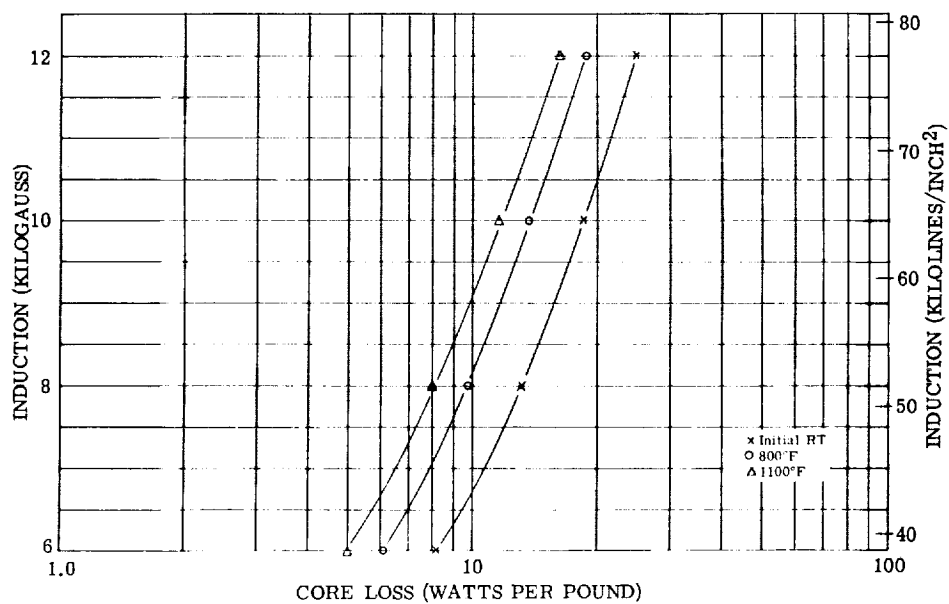
Figure 68. - Core loss at 1600 cps for 0.002-inch Cubex alloy tape toroid $1\frac{1}{4}$ by 1 by 1/4 inch, magnetic-field annealed. Test atmosphere, air to 800° F and argon above 800° F; interlaminar insulation, aluminum orthophosphate.
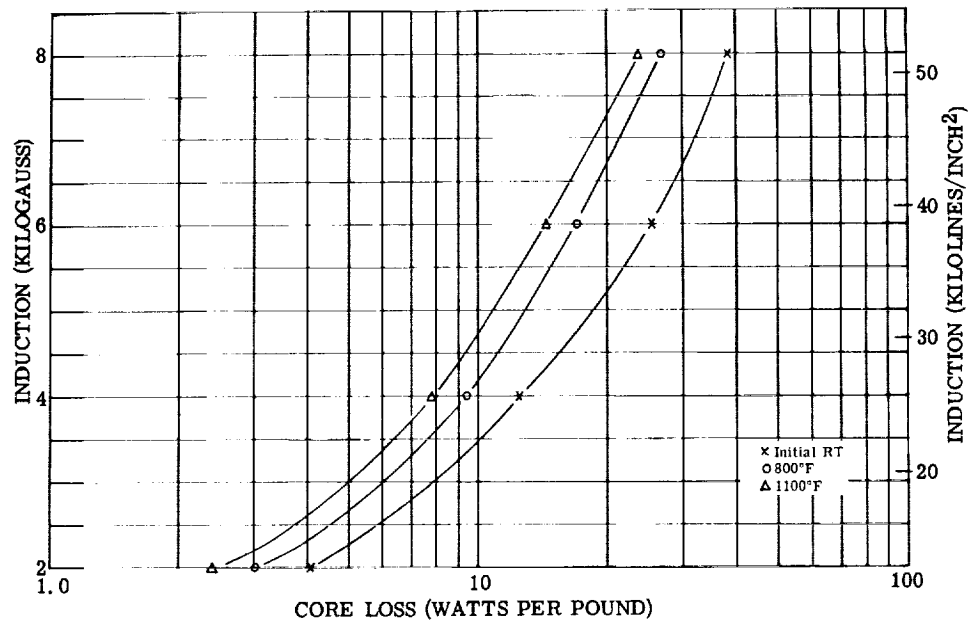
Figure 69. - Core loss at 3200 cps for 0.002-inch Cubex alloy tape toroid $1\frac{1}{4}$ by 1 by 1/4 inch, magnetic-field annealed. Test atmosphere, air to 800° F and argon above 800° F; interlaminar insulation, aluminum orthophosphate.
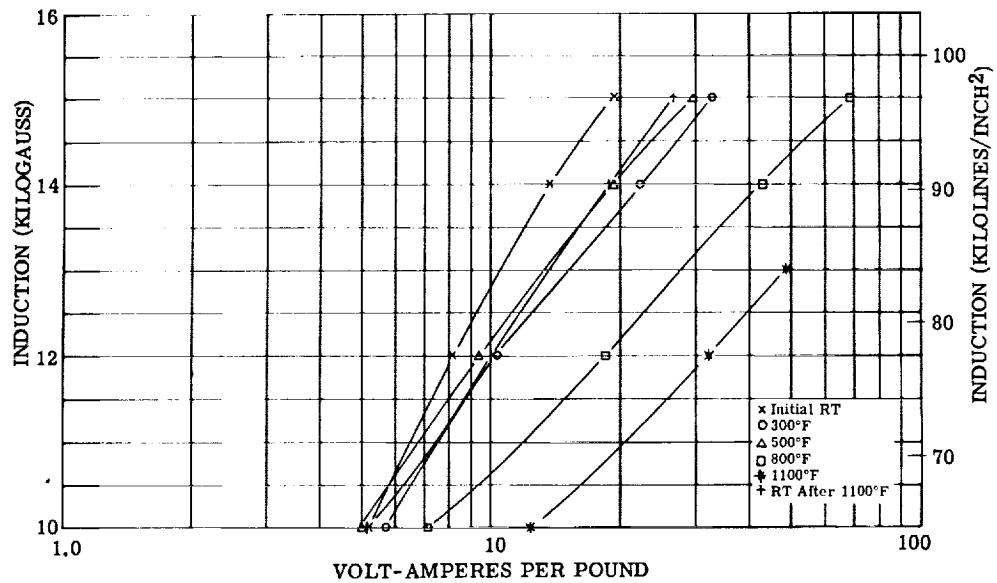
Figure 70. - Exciting volt-amperes per pound at 400 cps for 0.006-inch Cubex alloy tape, magnetic-field annealed. Test atmosphere, air to 500° F and argon above 500° F; interlaminar insulation, mica aluminum orthophosphate.
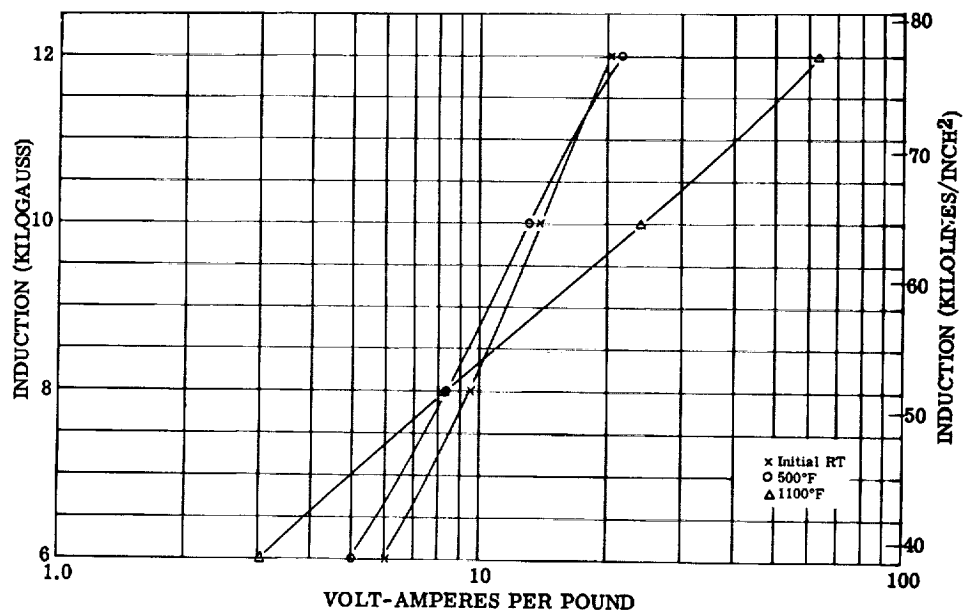
Figure 71. – Exciting volt-amperes per pound at 800 cps for 0.006-inch Cubex alloy tape, magnetic-field annealed. Test atmosphere, air to 500° F and argon above 500° F; interlaminar insulation, mica aluminum orthophosphate.
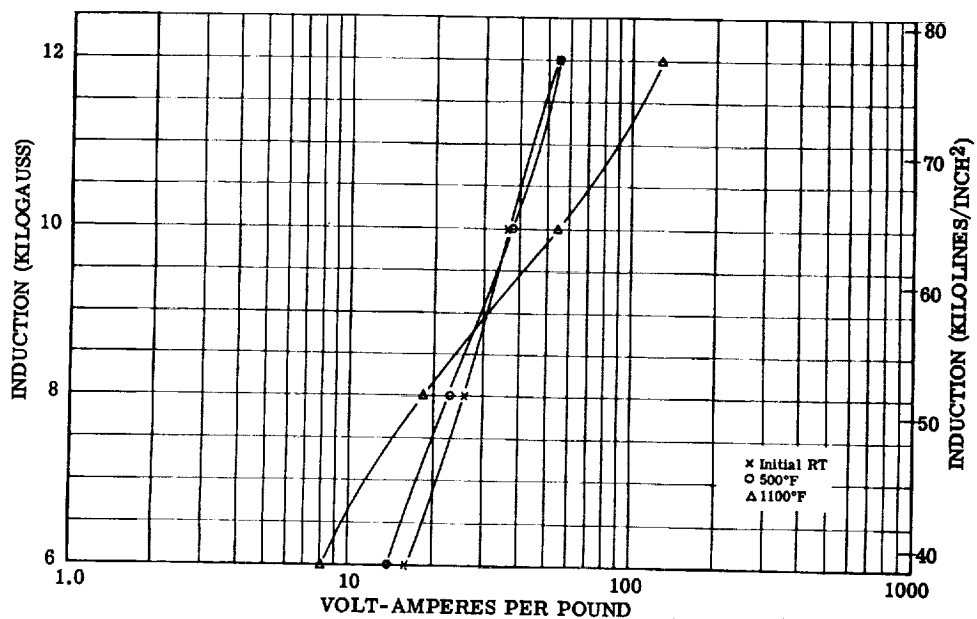
Figure 72. – Exciting volt-amperes per pound at 1600 cps for 0.006-inch Cubex alloy tape, magnetic-field annealed. Test atmosphere, air to 500° F and argon above 500° F; interlaminar insulation, mica aluminum orthophosphate.
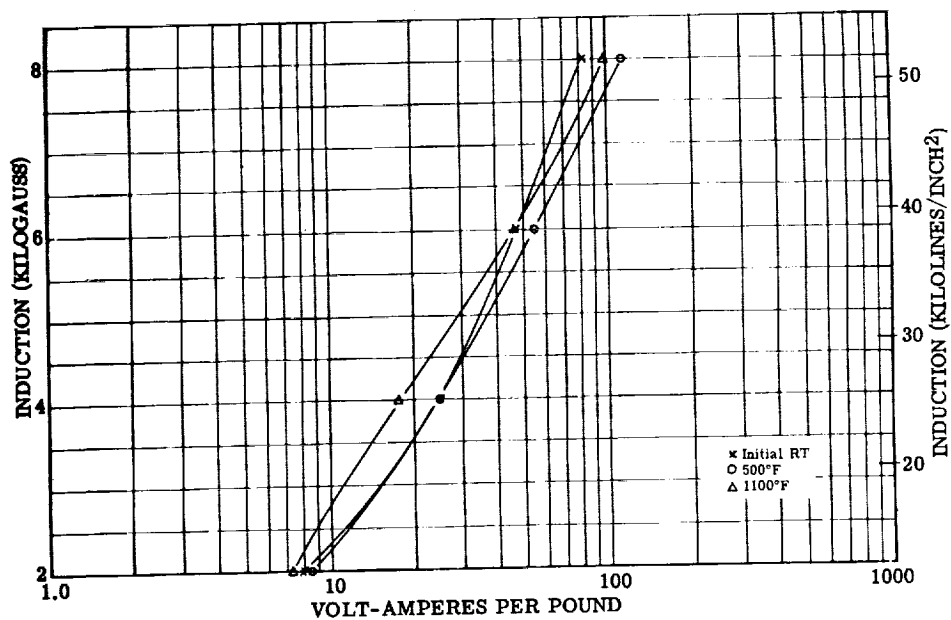
Figure 73. - Exciting volt-amperes per pound at 3200 cps for 0.006-inch Cubex alloy tape, magnetic-field annealed. Test atmosphere, air to 500° F and argon above 500° F; interlaminar insulation, mica aluminum orthophosphate.
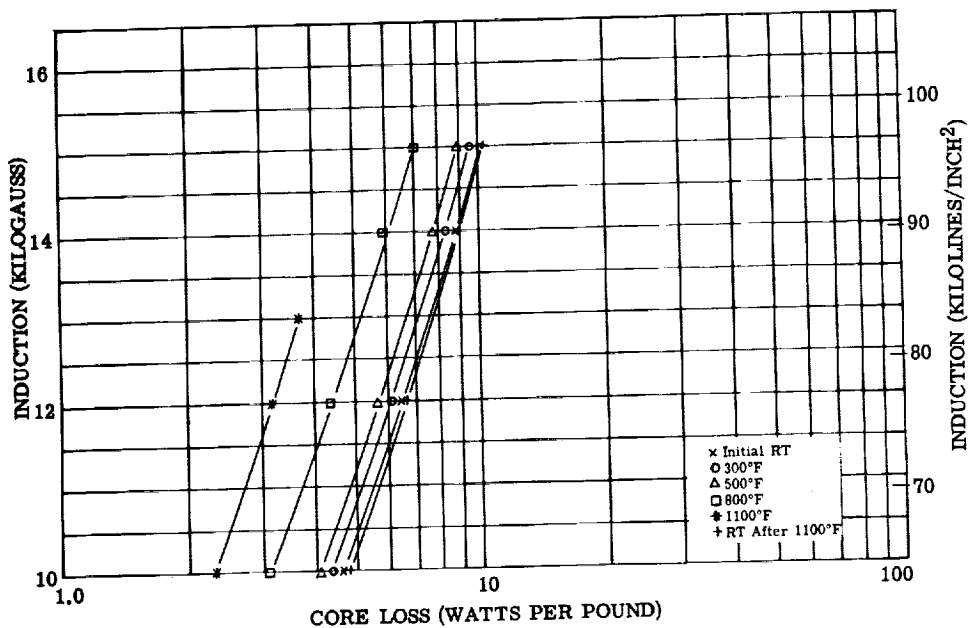
Figure 74. - Core loss at 400 cps 0.006-inch Cubex alloy tape, magnetic-field annealed. Test atmosphere, air to 500° F and argon above 500° F; interlaminar insulation, mica aluminum orthophosphate.
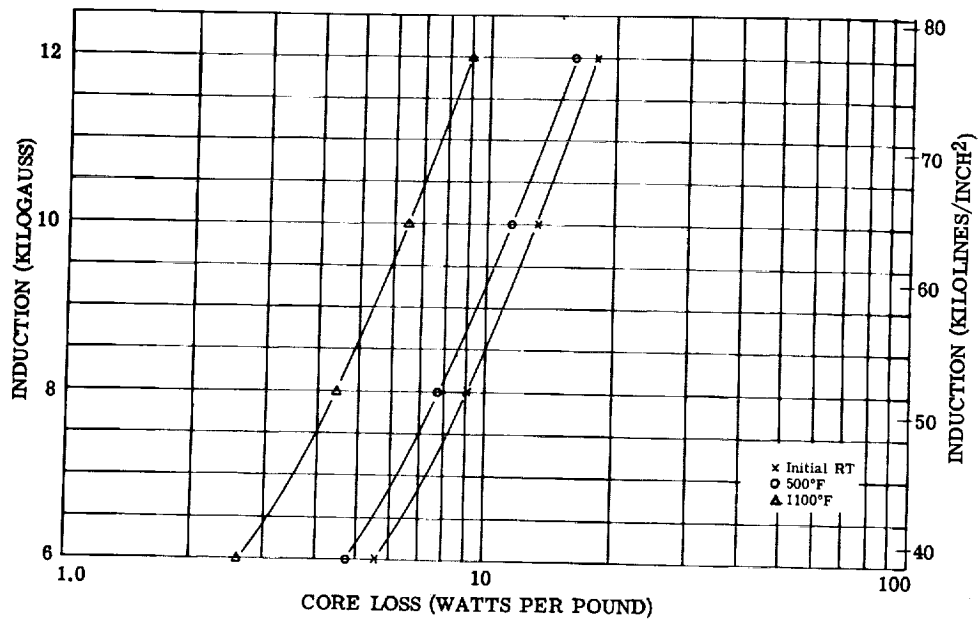
Figure 75. - Core loss at 800 cps for 0.006-inch Cubex alloy tape, magnetic-field annealed. Test atmosphere, air to 500° F and argon above 500° F; interlaminar insulation, mica aluminum orthophosphate.
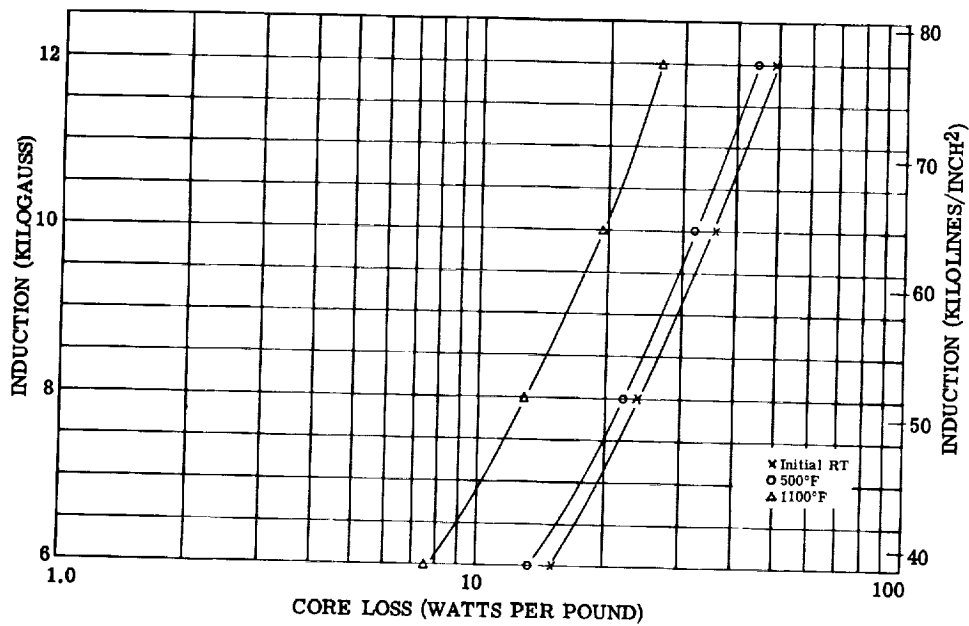
Figure 76. - Core loss at 1600 cps for 0.006-inch Cubex alloy tape, magnetic-field annealed. Test atmosphere, air to 500° F and argon above 500° F; interlaminar insulation, mica aluminum orthophosphate.

Figure 77. - Core loss at 3200 cps for 0.006-inch Cubex alloy tape, magnetic-field annealed. Test atmosphere, air to 500° F and argon above 500° F; interlaminar insulation, mica aluminum orthophosphate.
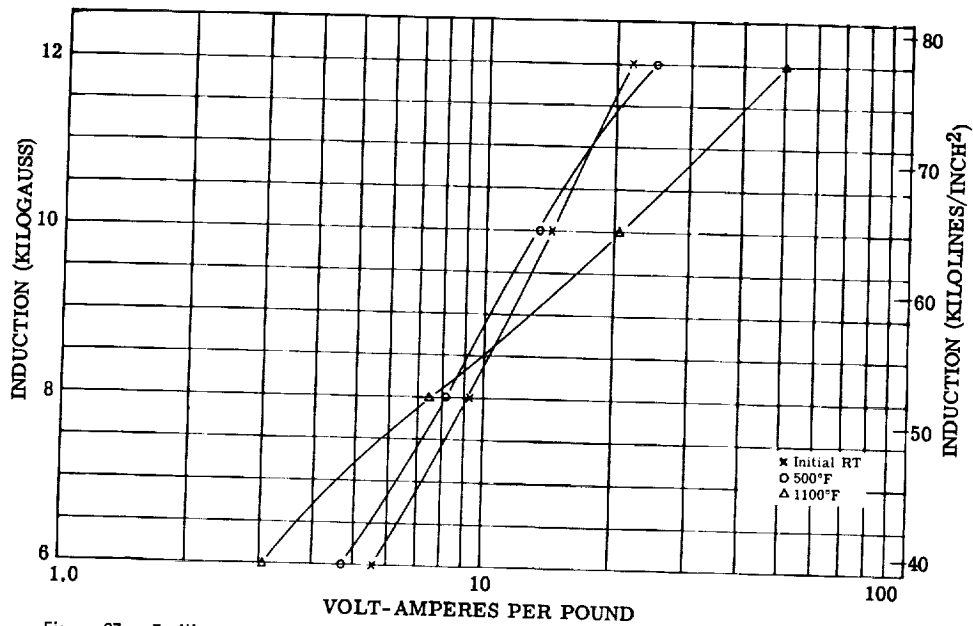

Figure 78. - Exciting volt-amperes per pound at 400 cps for 0.006-inch Cubex alloy tape, sample 1. Test atmosphere, argon; interlaminar insulation, mica aluminum orthophosphate.
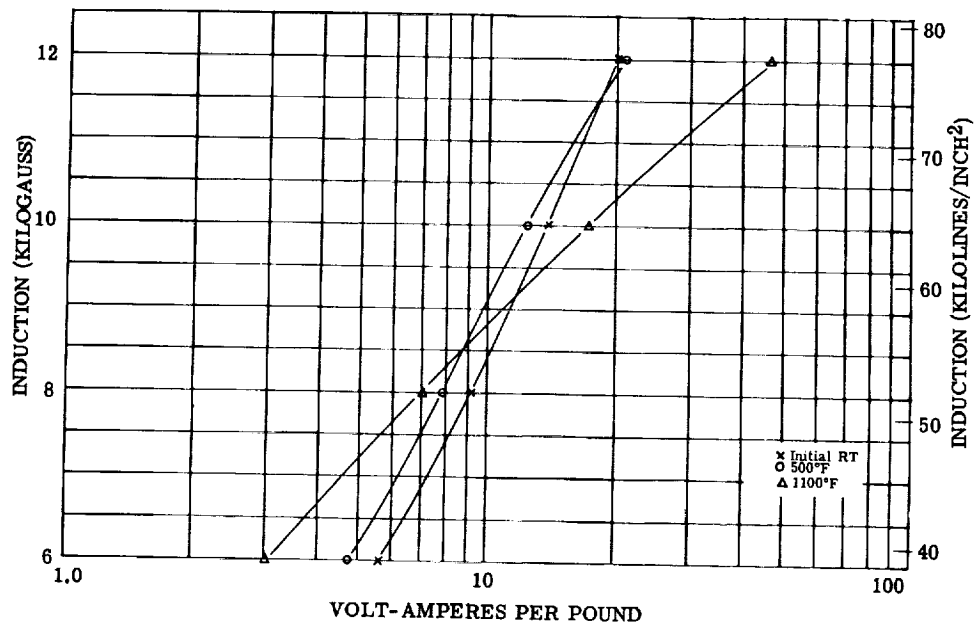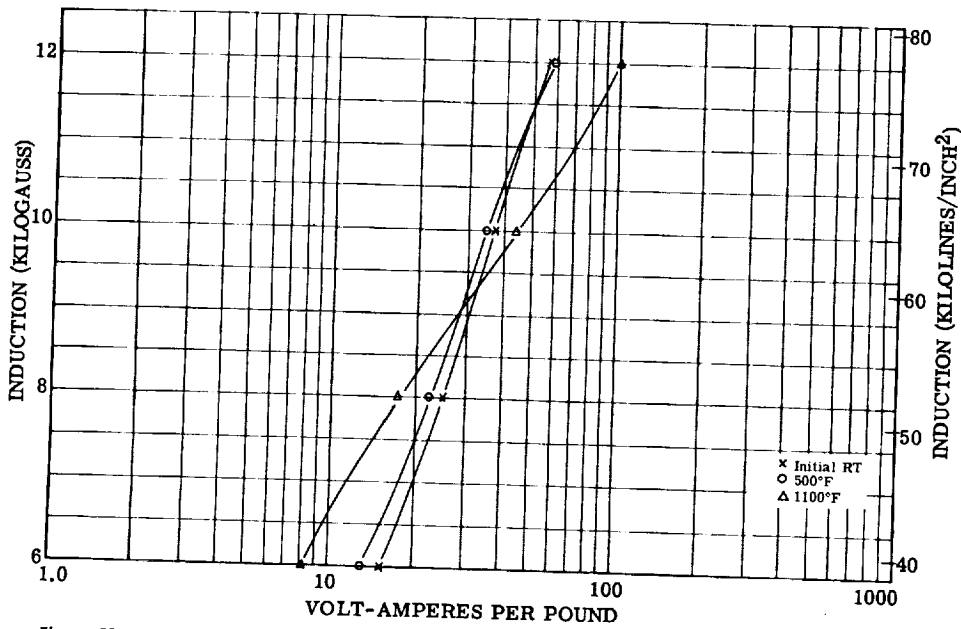
Figure 79. - Exciting volt-amperes per pound at 800 cps for 0. 006-inch Cubex alloy tape, sample 1. Test atmosphere, argon; interlaminar insulation, mica aluminum orthophosphate.
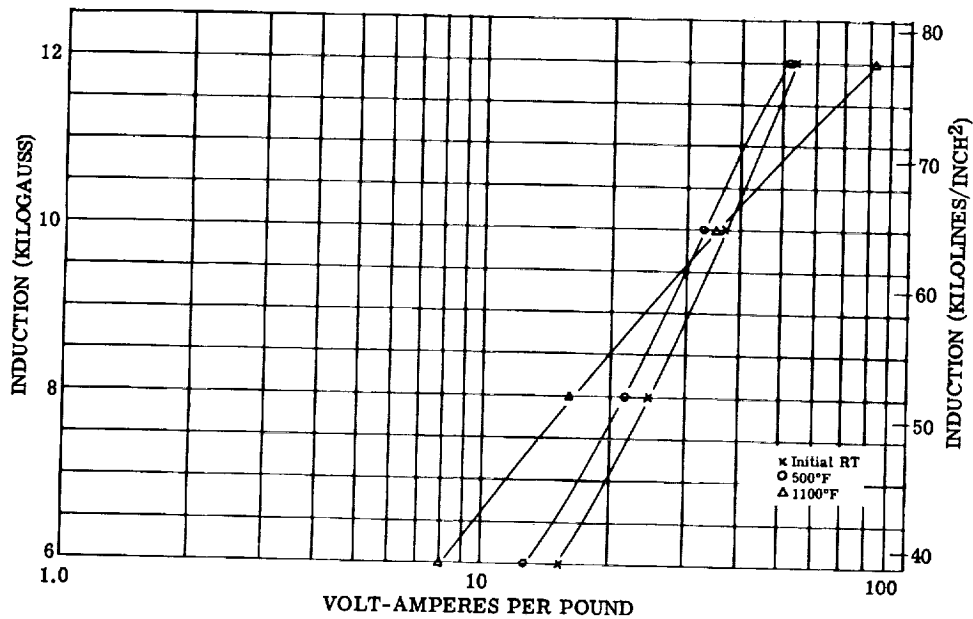
Figure 80. - Exciting volt-amperes per pound at 1600 cps for 0. 006-inch Cubex alloy tape, sample 1. Test atmosphere, argon; interlaminar insulation, mica aluminum orthophosphate.
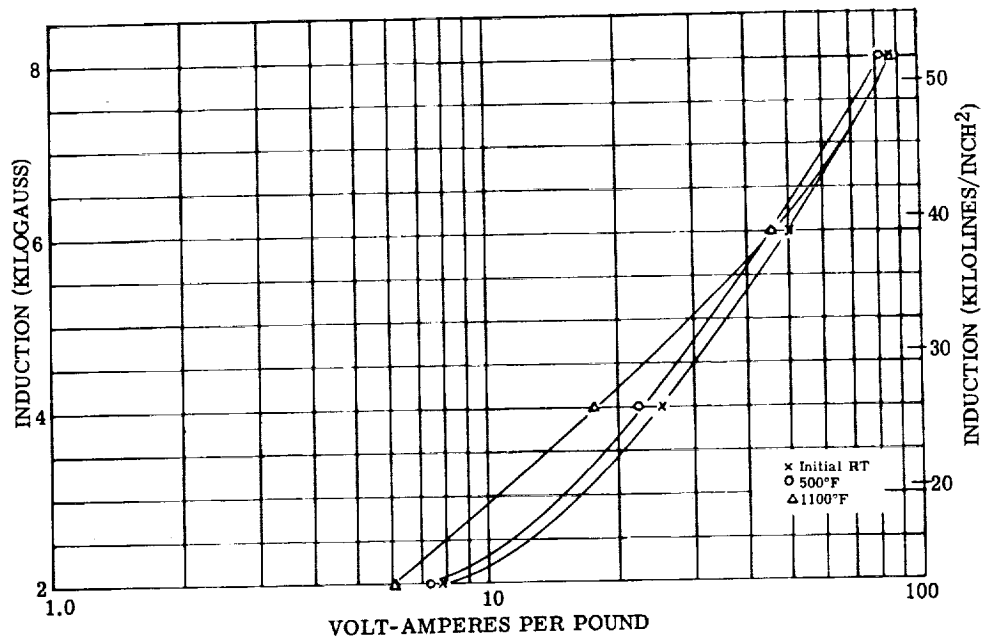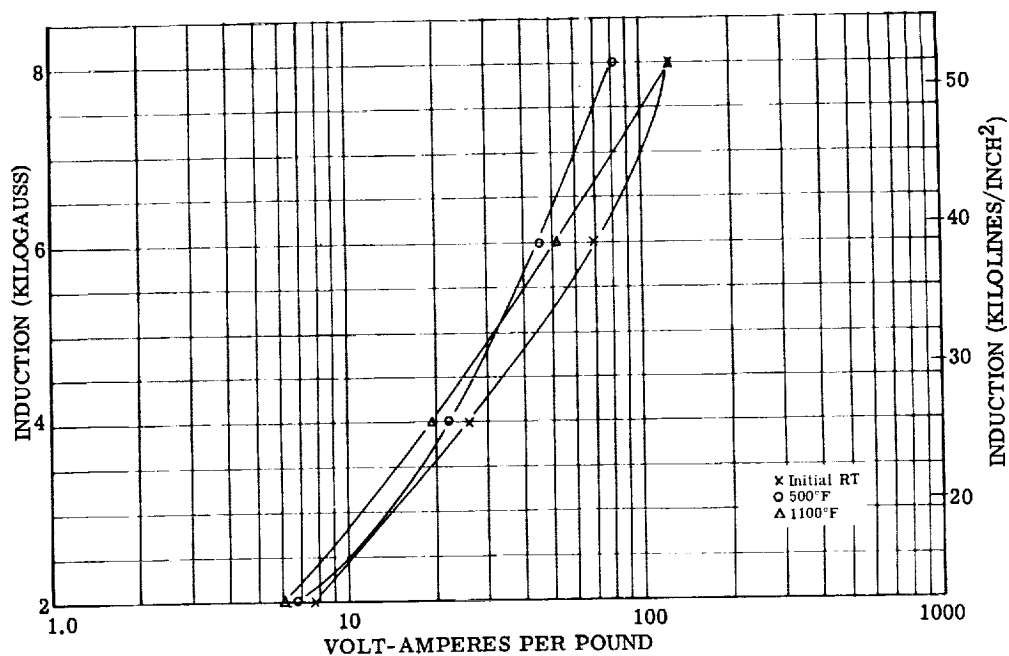
Figure 81. - Exciting volt-amperes per pound at 3200 cps for 0.006-inch Cubex alloy tape, sample 1. Test atmosphere, argon; interlaminar insulation, mica aluminum orthophosphate.
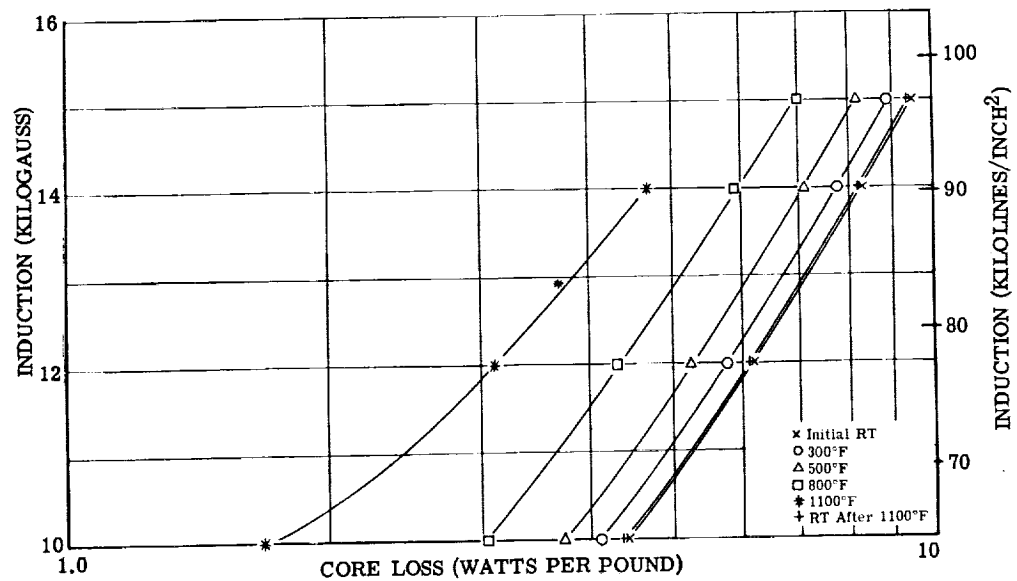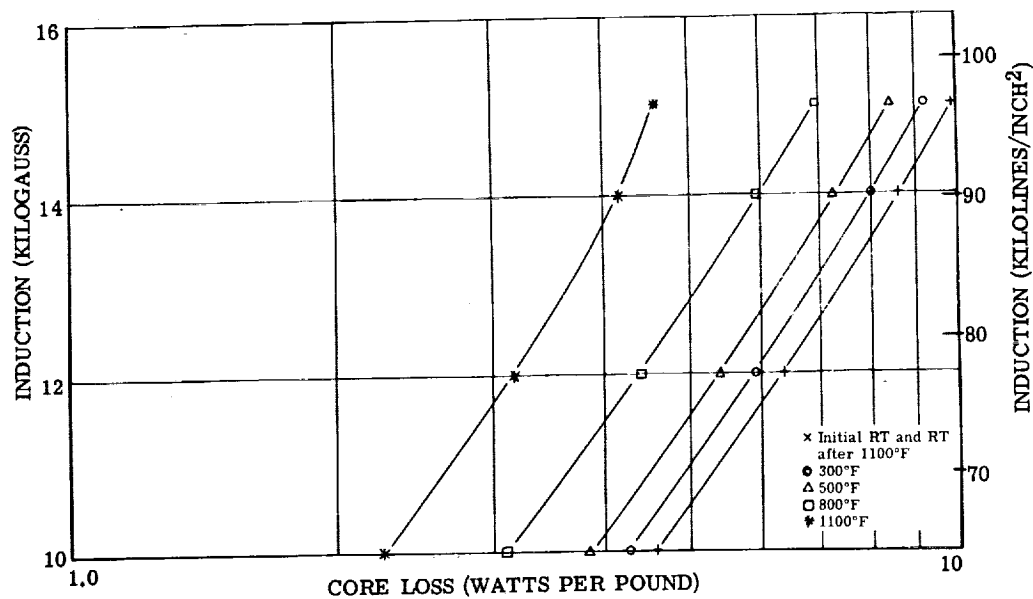

Figure 82. - Core loss at 400 cps for 0.006-inch Cubex alloy tape, sample 1. Test atmosphere, argon; interlaminar insulation, mica aluminum orthophosphate.
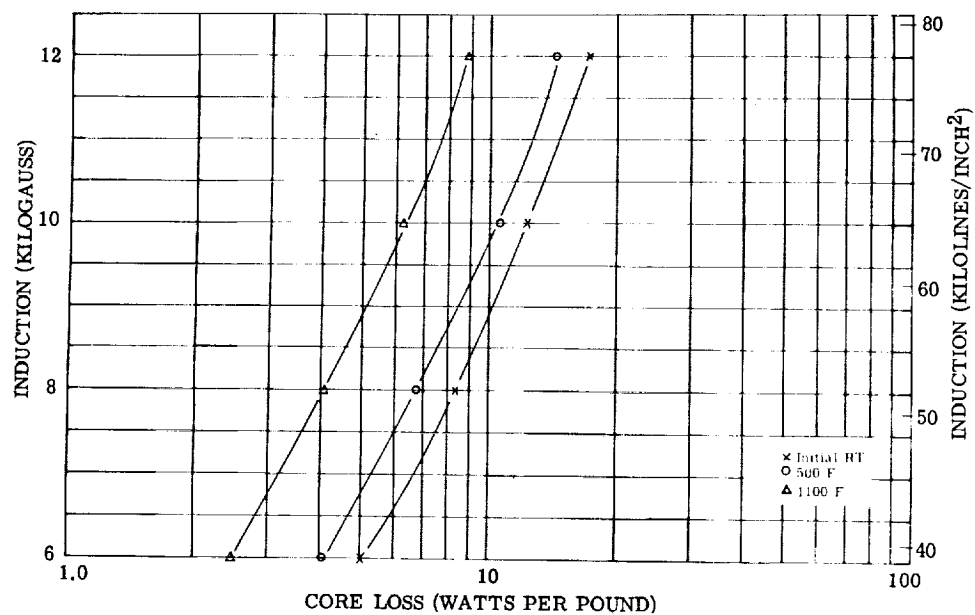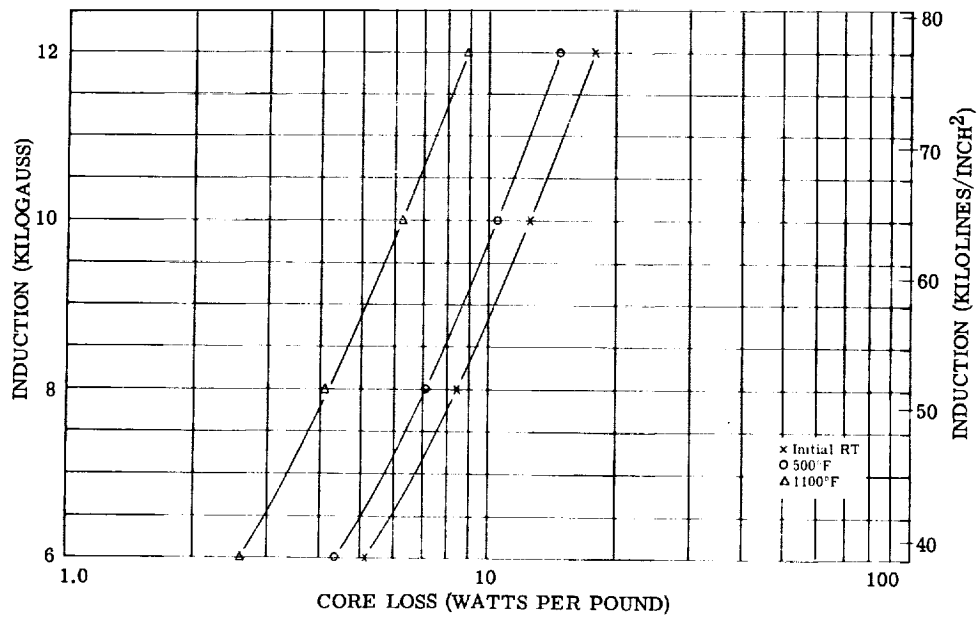
Figure 83. - Core loss at 800 cps for 0.006-inch Cubex alloy tape, sample 1. Test atmosphere, argon; inter-laminar insulation, mica aluminum orthophosphate.
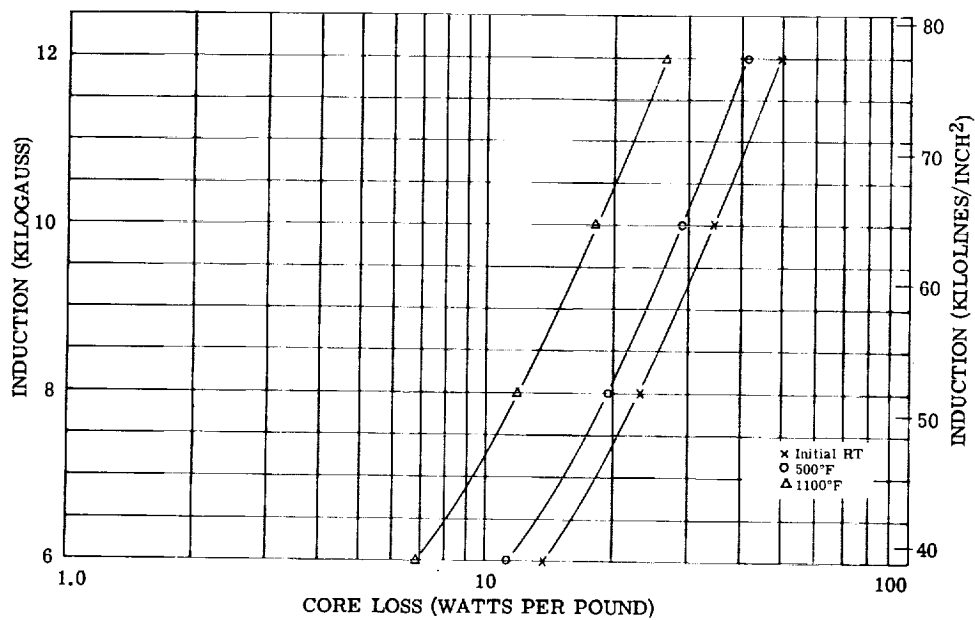
Figure 84. - Core loss at 1600 cps for 0.006-inch Cubex alloy tape, sample 1. Test atmosphere, argon; inter-laminar insulation, mica aluminum orthophosphate.
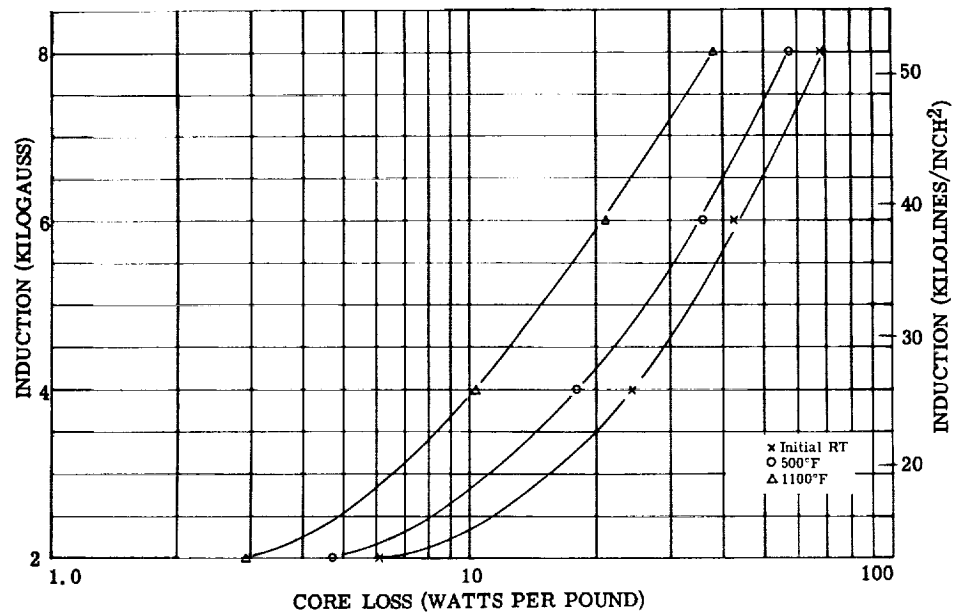
Figure 85. - Core loss at 3200 cps for 0.006-inch Cubex alloy tape, sample 1. Test atmosphere, argon; inter-laminar insulation, mica aluminum orthophosphate.
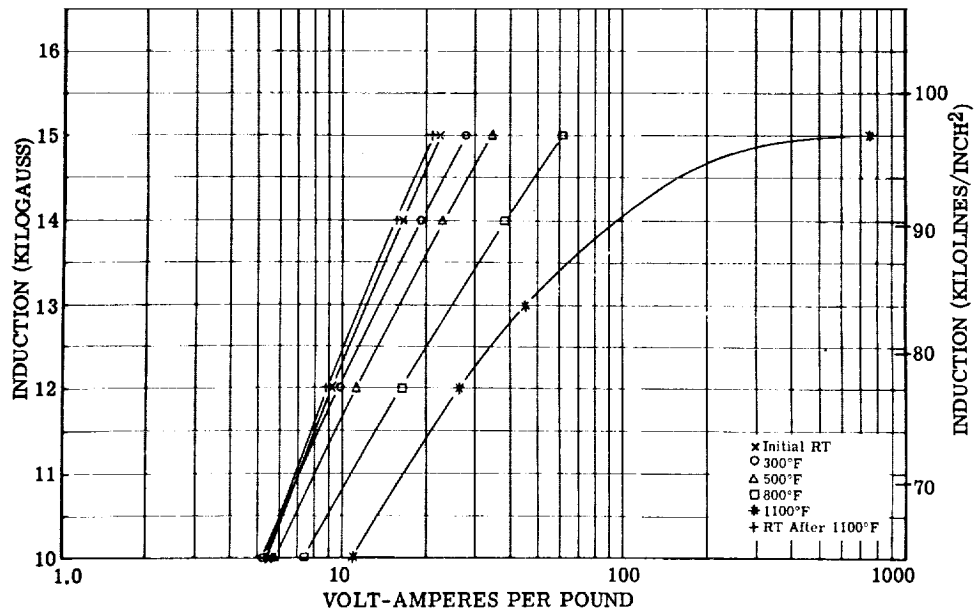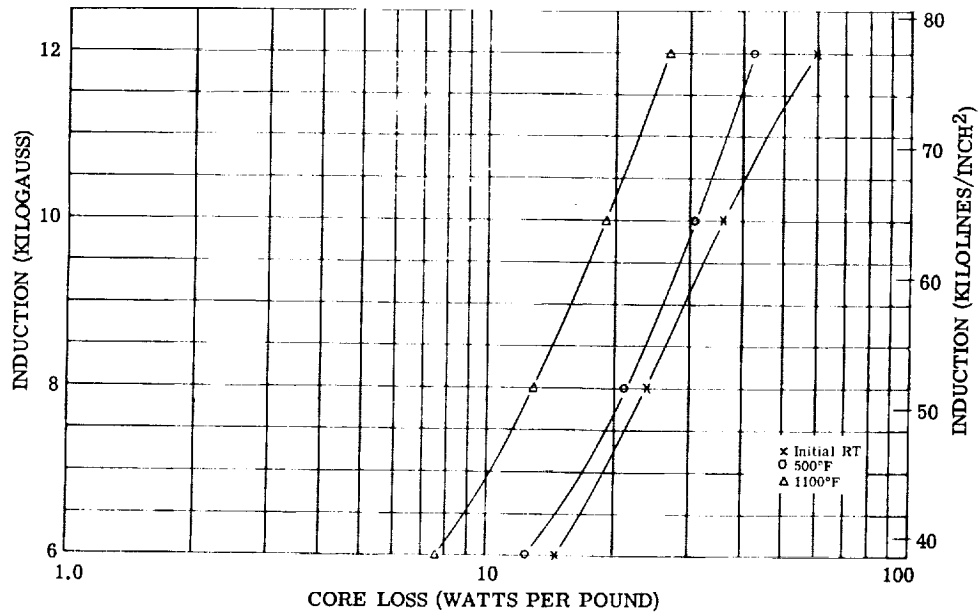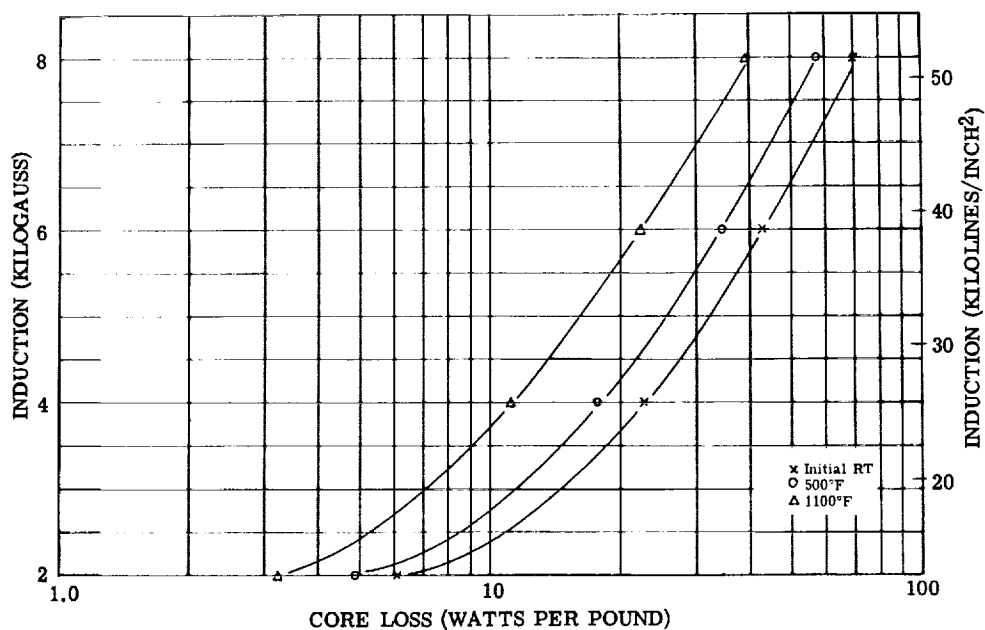

Figure 86. - Exciting volt-amperes per pound at 400 cps 0.006-inch Cubex alloy tape, sample 2. Test atmos-phere, argon; interlaminar insulation, mica aluminum orthophosphate.

Figure 87. - Exciting volt-amperes per pound at 800 cps for 0.006-inch Cubex alloy tape, sample 2. Test atmosphere, argon; interlaminar insulation, mica aluminum orthophosphate.

Figure 88. - Exciting volt-amperes per pound at 1600 cps for 0.006-inch Cubex alloy tape, sample 2. Test atmosphere, argon; interlaminar insulation, mica aluminum orthophosphate.

Figure 89. - Exciting volt-amperes per pound at 3200 cps for 0.006-inch Cubex alloy tape, sample 2. Test atmosphere, argon; interlaminar insulation, mica aluminum orthophosphate.

Figure 90. - Core loss of 400 cps for 0.006-inch Cubex alloy tape, sample 2. Test atmosphere, argon; interlaminar insulation, mica aluminum orthophosphate.
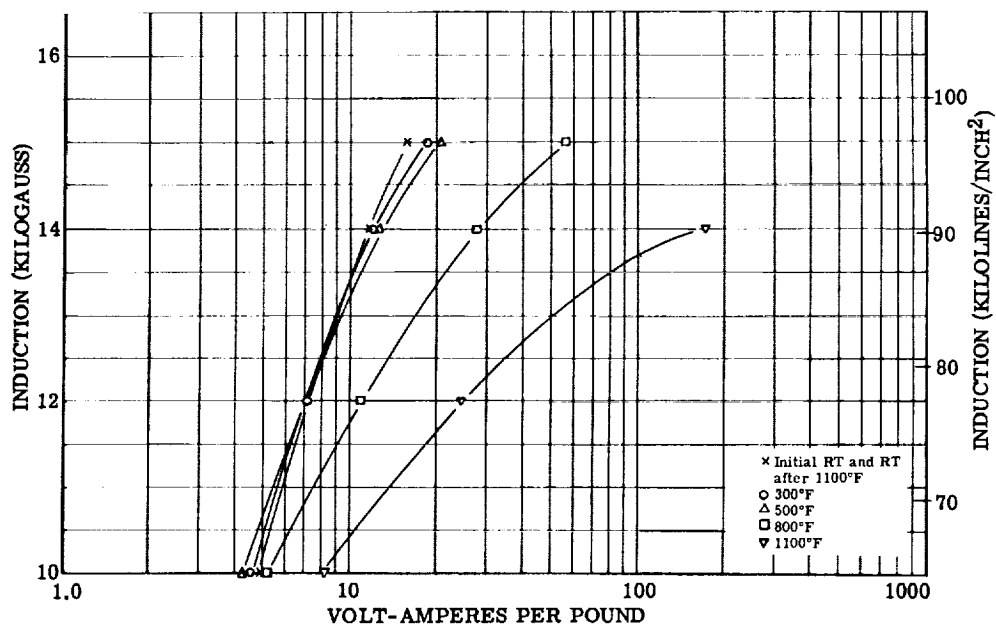
Figure 91. - Core loss at 800 cps for 0.006-inch Cubex alloy tape, sample 2. Test atmosphere, argon; inter-laminar insulation, mica aluminum orthophosphate.
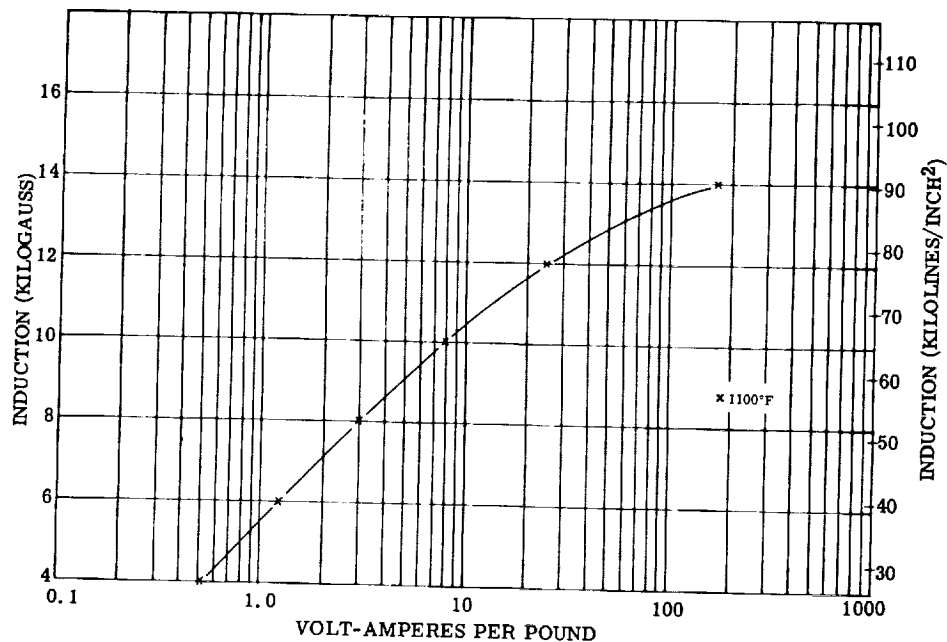

Figure 92. - Core loss at 1600 cps for 0.006-inch Cubex alloy tape, sample 2. Test atmosphere, argon; inter-laminar insulation, mica aluminum orthophosphate.

Figure 93. - Core loss at 3200 cps for 0.006-inch Cubex alloy tape, sample 2. Test atmosphere, argon; interlaminar insulation, mica aluminum orthophosphate.

Figure 94. - Exciting volt-amperes per pound at 400 cps for 0.006-inch Cubex alloy tape, sample 3. Test atmosphere, air to 500° F and argon above 500° F; interlaminar insulation, mica aluminum orthophosphate.
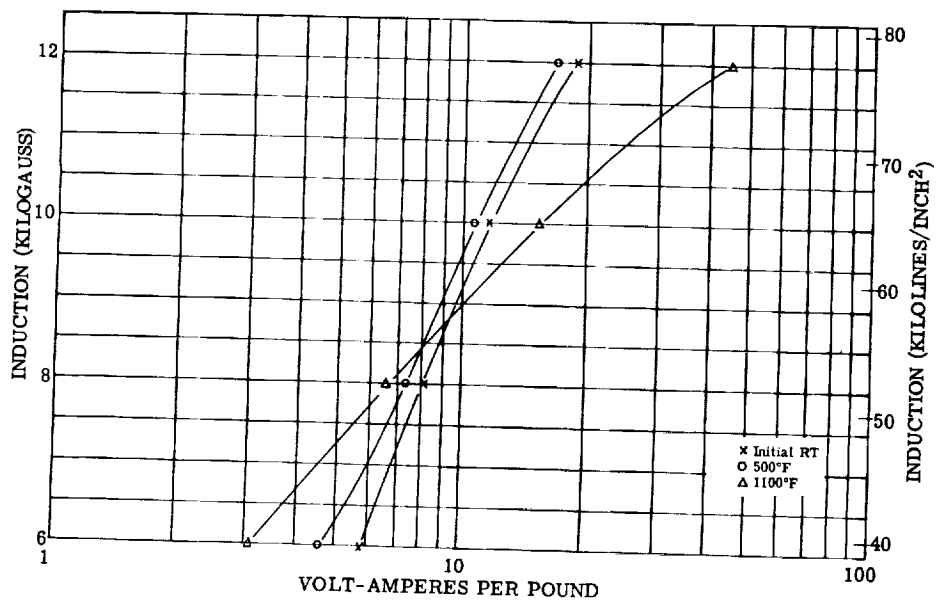
Figure 95. - Exciting volt-amperes per pound at 400 cps for 0.006-inch Cubex alloy tape, sample 3. Test atmosphere, air to 500° F and argon above 500° F; interlaminar insulation, mica aluminum orthophosphate.
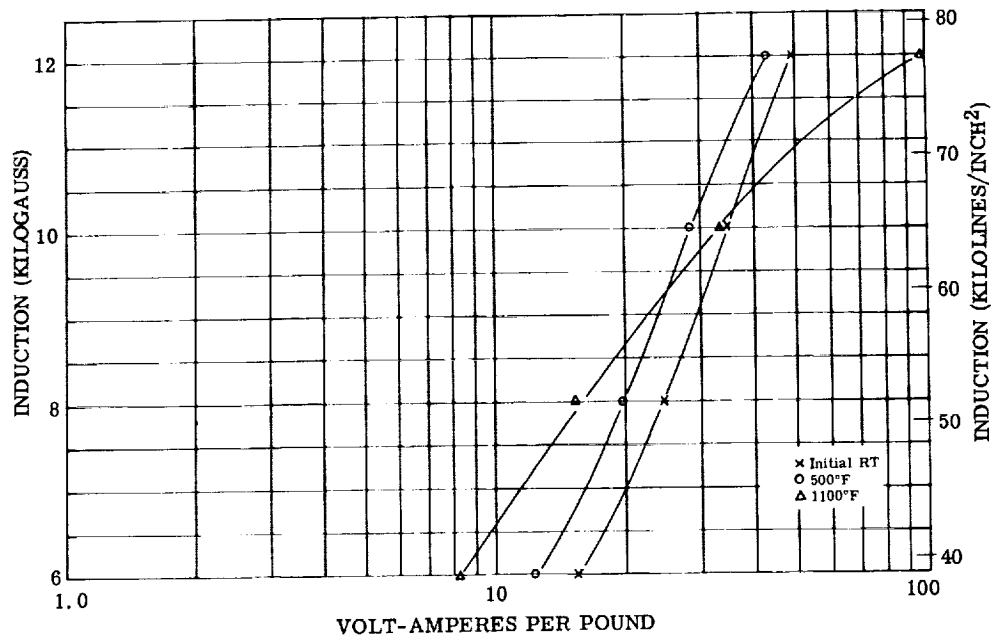

Figure 96. - Exciting volt-amperes per pound at 800 cps for 0.006-inch Cubex alloy tape, sample 3. Test atmosphere, air to 500° F and argon above 500° F; interlaminar insulation, mica aluminum orthophosphate.
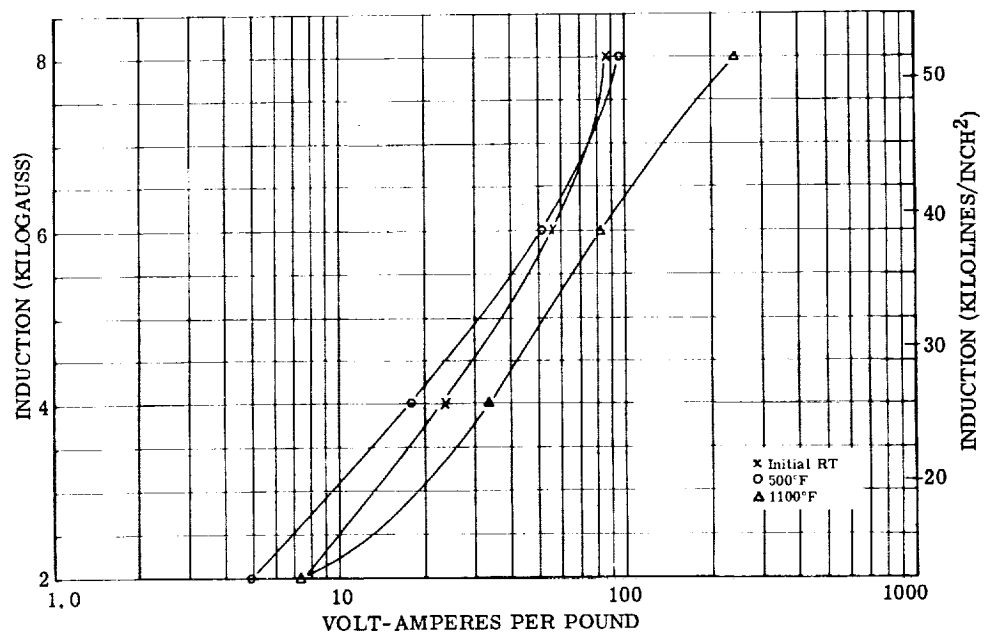
Figure 97. - Exciting volt-amperes per pound at 1600 cps for 0.006-inch Cubex alloy tape, sample 3. Test atmosphere, air to 500° F and argon above 500° F; interlaminar insulation, mica aluminum orthophosphate.

Figure 98. - Exciting volt-amperes per pound at 3200 cps for 0.006-inch Cubex alloy tape, sample 3. Test atmosphere, air to 500° F and argon above 500° F; interlaminar insulation, mica aluminum orthophosphate.
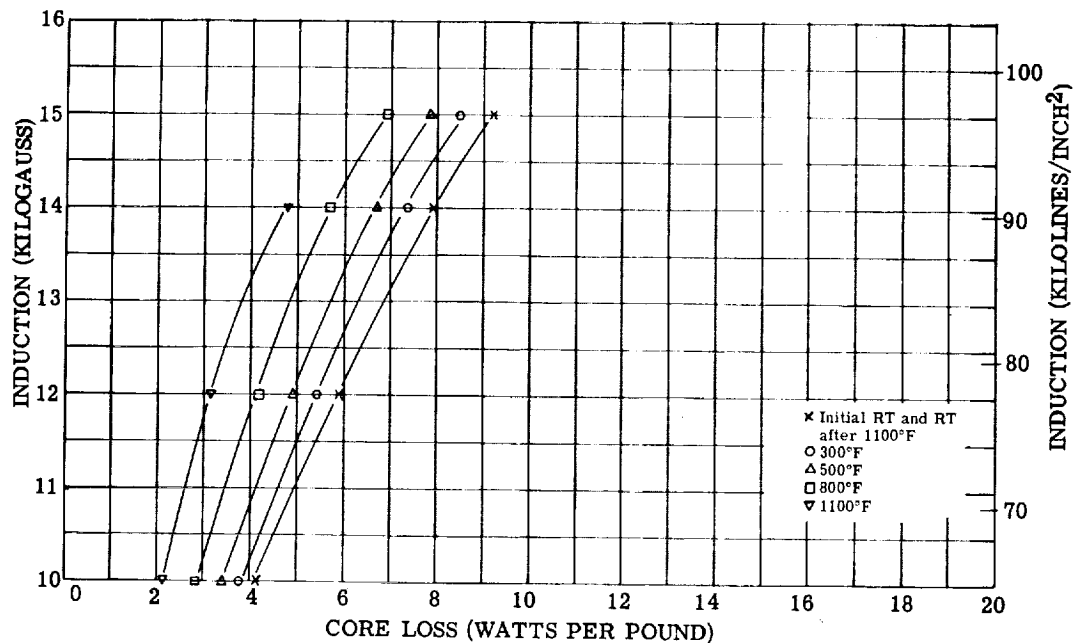
Figure 99. - Core loss at 400 cps for 0.006-inch Cubex alloy tape, sample 3. Test atmosphere, air to 500° F and argon above 500° F; interlaminar insulation, mica aluminum orthophosphate.
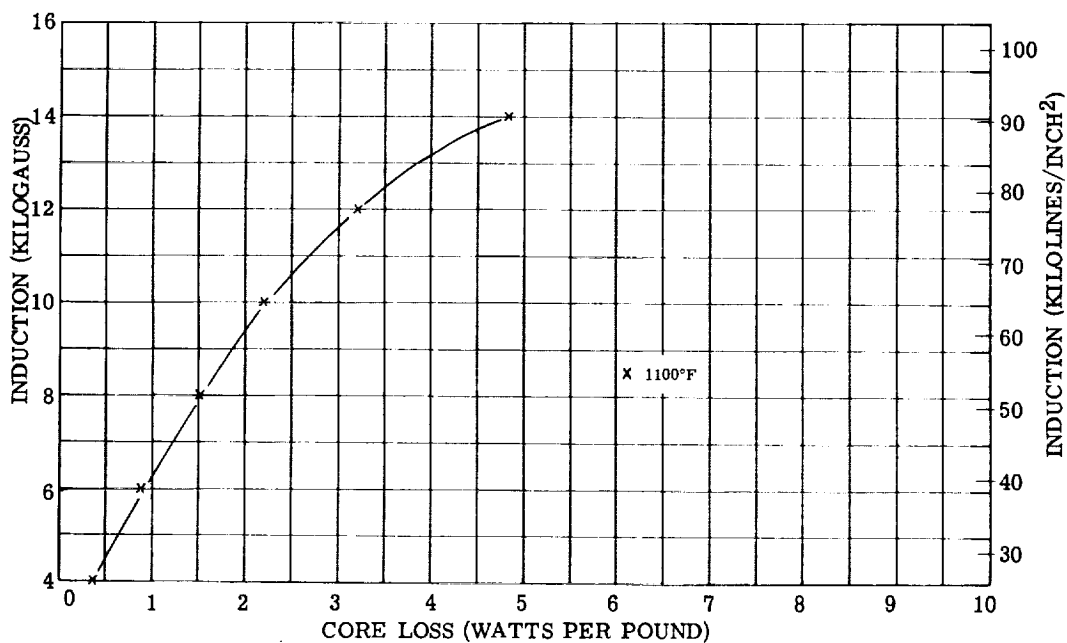

Figure 100. - Core loss at 400 cps for 0.006-inch Cubex alloy tape, sample 3. Test atmosphere, air to 500° F and argon above 500° F; interlaminar insulation, mica aluminum orthophosphate.

Figure 101. - Core loss at 800 cps for 0.006-inch Cubex alloy tape, sample 3. Test atmosphere, air to 500° F and argon above 500° F; interlaminar insulation, mica aluminum orthophosphate.
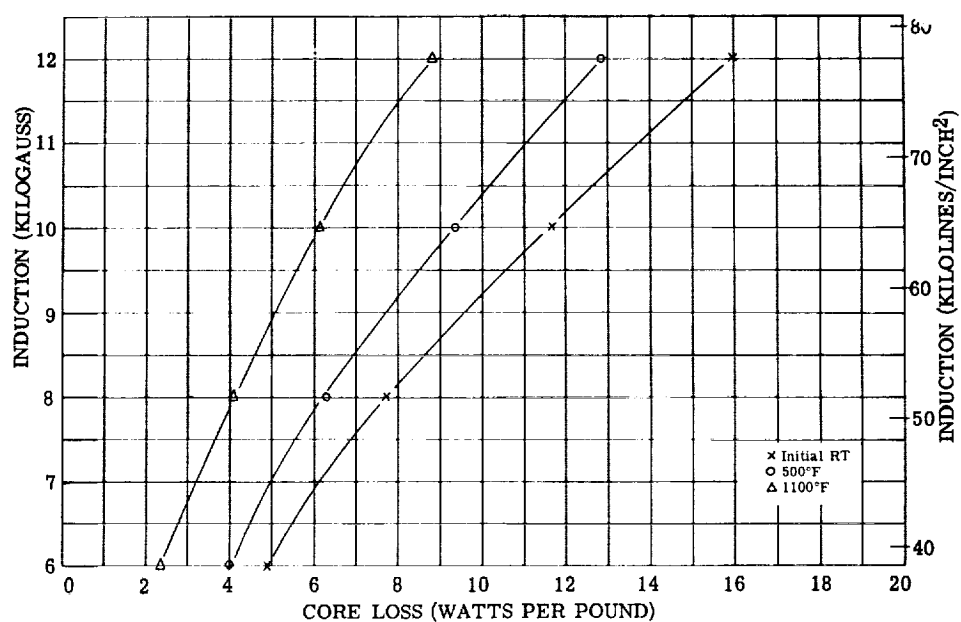

Figure 102. - Core loss at 1600 cps for 0.006-inch Cubex alloy tape, sample 3. Test atmosphere, air to 500° F and argon above 500° F; interlaminar insulation, mica aluminum orthophosphate.

Figure 103. - Core loss at 3200 cps for 0.006-inch Cubex alloy tape, sample 3. Test atmosphere, air to 500° F and argon above 500° F; interlaminar insulation, mica aluminum orthophosphate.
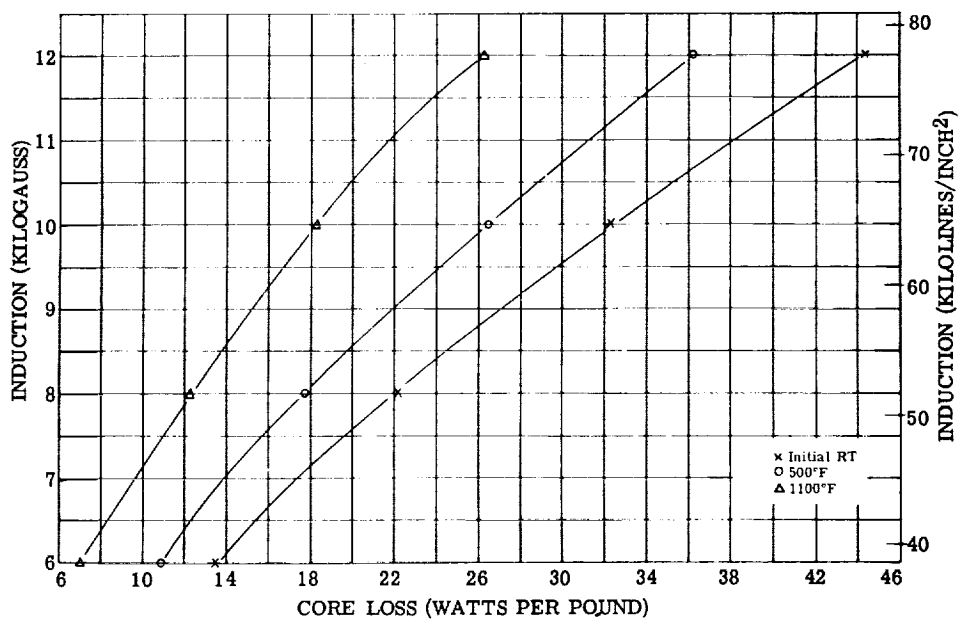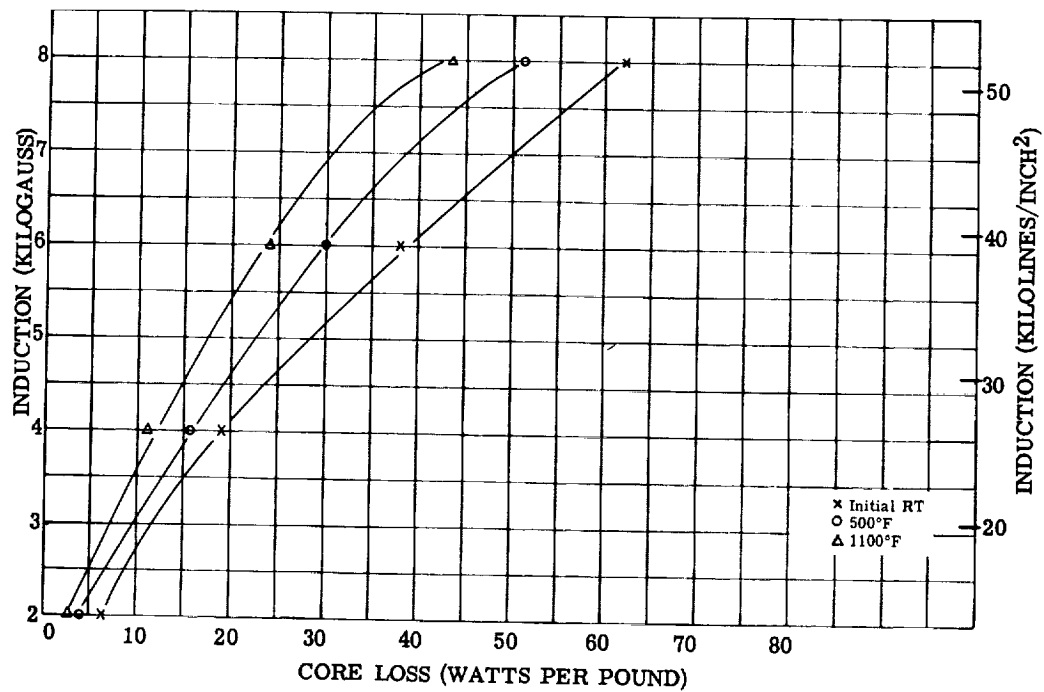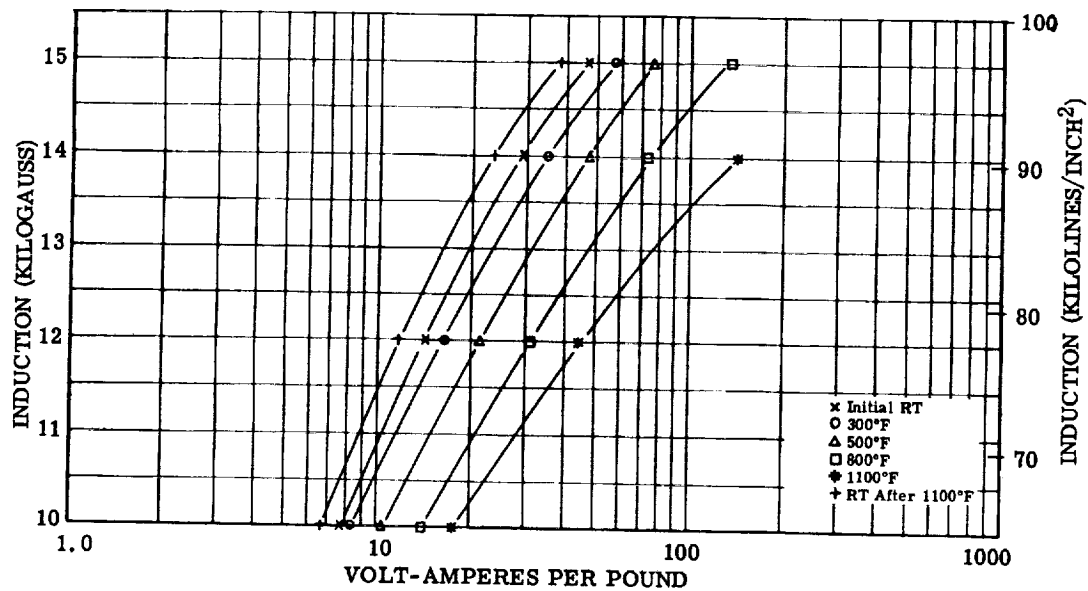

Figure 104. - Exciting volt-amperes per pound at 400 cps for 0.006-inch Cubex alloy laminations. Test atmosphere, air to 500° F and argon above 500° F; interlaminar insulation, mica aluminum orthophosphate.

Figure 105. - Exciting volt-amperes per pound at 800 cps for 0.006-inch Cubex alloy laminations. Test atmosphere, air to 500° F and argon above 500° F; interlaminar insulation, mica aluminum orthophosphate.

Figure 106. - Exciting volt-amperes per pound at 1600 cps for 0.006-inch Cubex alloy laminations. Test atmosphere, air to 500° F and argon above 500° F; interlaminar insulation, mica aluminum orthophosphate.

Figure 107. - Exciting volt-amperes per pound at 3200 cps for 0. 006 inch Cubex alloy laminations. Test atmosphere, air to 500° F and argon above 500° F, interlaminar insulation, mica aluminum orthophosphate.

Figure 108. - Core loss at 400 cps for 0. 006-inch Cubex alloy laminations. Test atmosphere, air to 500° F and argon above 500° F; interlaminar insulation, mica aluminum orthophosphate.

Figure 109. - Core loss at 800 cps for 0.006-Inch Cubex alloy laminations. Test atmosphere, air to 500° F and argon above 500° F; interlaminar insulation, mica aluminum orthophosphate.
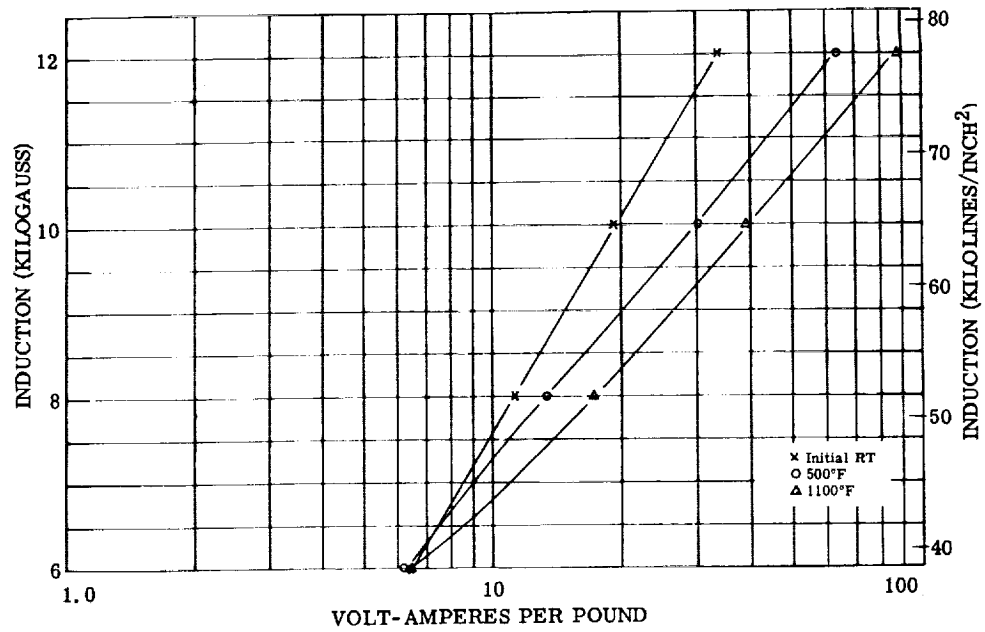
Figure 110. - Core loss at 1600 cps for 0.006-inch Cubex alloy laminations. Test atmosphere, air to 500° F and argon above 500° F; interlaminar insulation, mica aluminum orthophosphate.
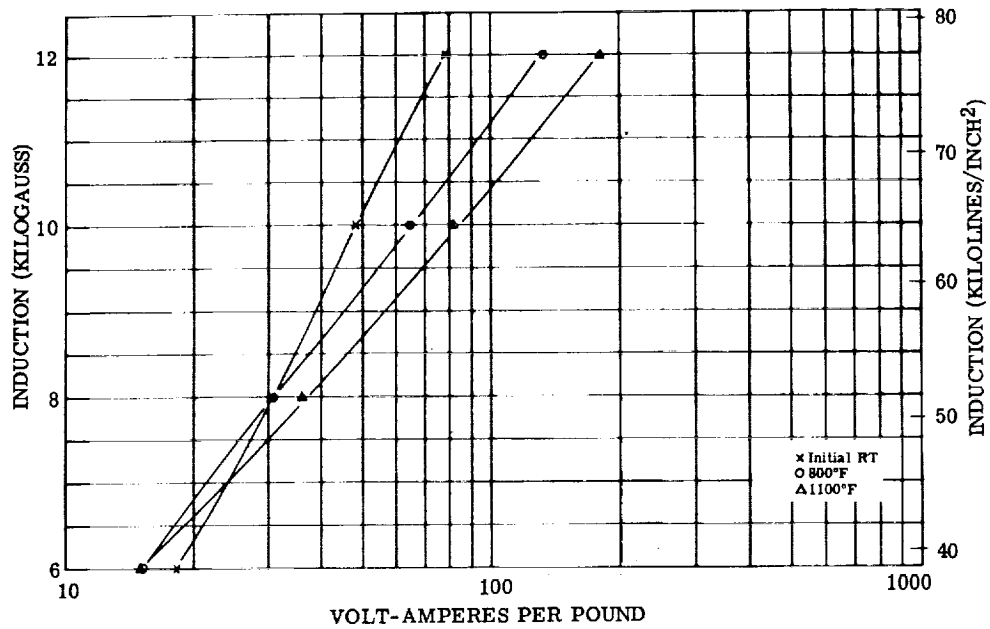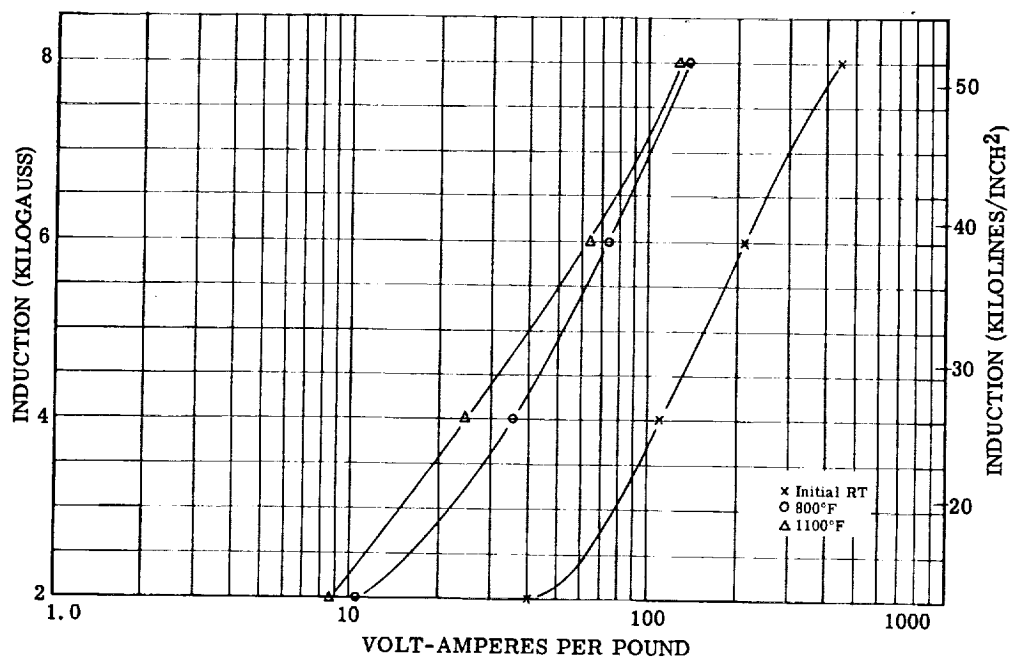
Figure 111. - Core loss at 3200 cps for 0.006-inch Cubex alloy laminations. Test atmosphere, air to 500° F and argon above 500° F; interlaminar insulation, mica aluminum orthophosphate.
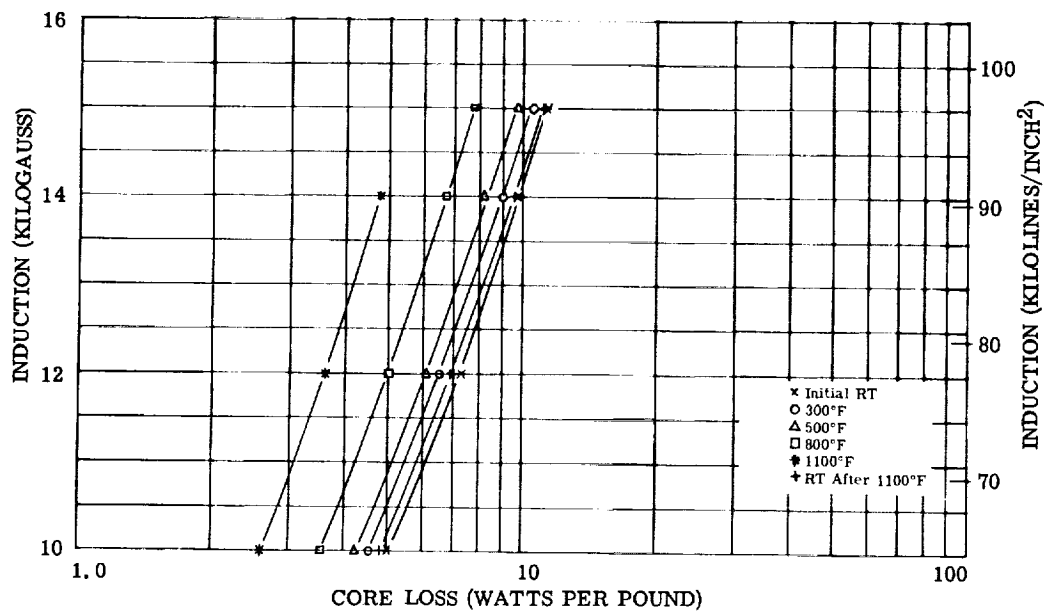

Figure 112. - Exciting volt-amperes per pound at 400 cps for 0.011-inch Cubex alloy laminations. Test atmosphere, air; interlaminar insulation, mica aluminum orthophosphate.

Figure 113. - Exciting volt-amperes per pound at 800 cps for 0. 011-inch Cubex alloy laminations. Test atmosphere, air; interlaminar insulation, mica aluminum orthophosphate.

Figure 114. - Exciting volt-amperes per pound at 1600 cps for 0. 011-inch Cubex alloy laminations. Test atmosphere, air; interlaminar insulation, mica aluminum orthophosphate.

Figure 115. - Exciting volt-amperes per pound at 3200 cps for 0. 011-inch Cubex alloy laminations. Test atmosphere, air; interlaminar insulation, mica aluminum orthophosphate.
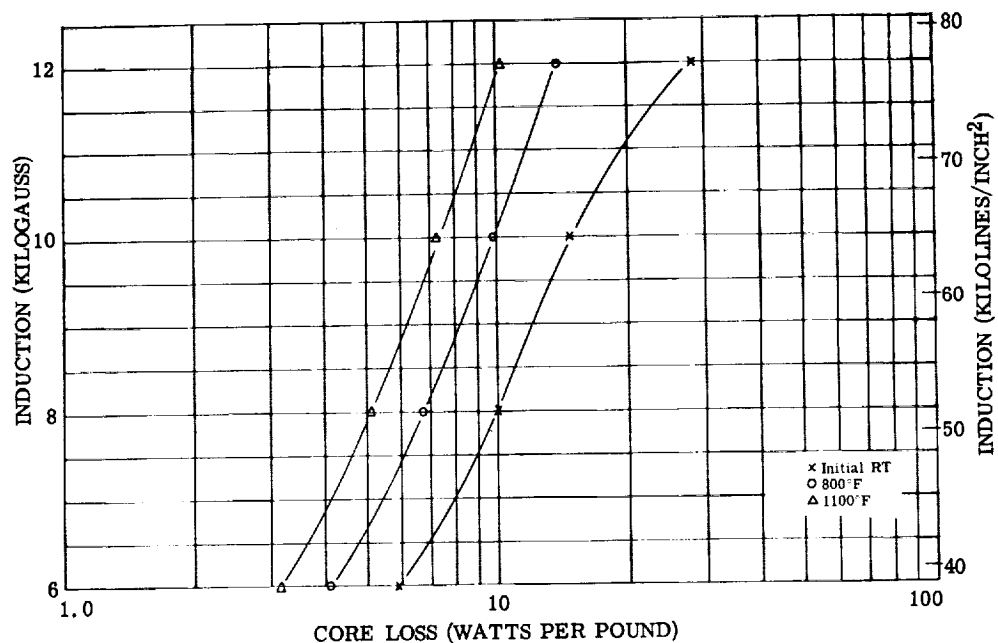

Figure 116. - Core loss at 400 cps for 0. 011-inch Cubex alloy laminations. Test atmosphere, air; interlaminar insulation, mica aluminum orthophosphate.
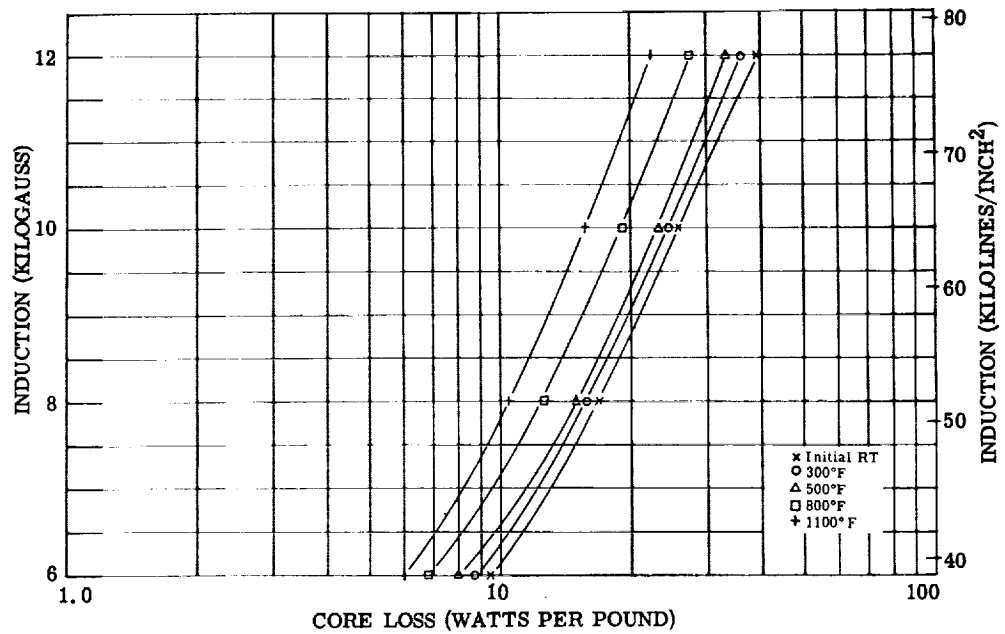
Figure 117. - Core loss at 800 cps for 0.011-inch Cubex alloy laminations. Test atmosphere, air; interlaminar insulation, mica aluminum orthophosphate.
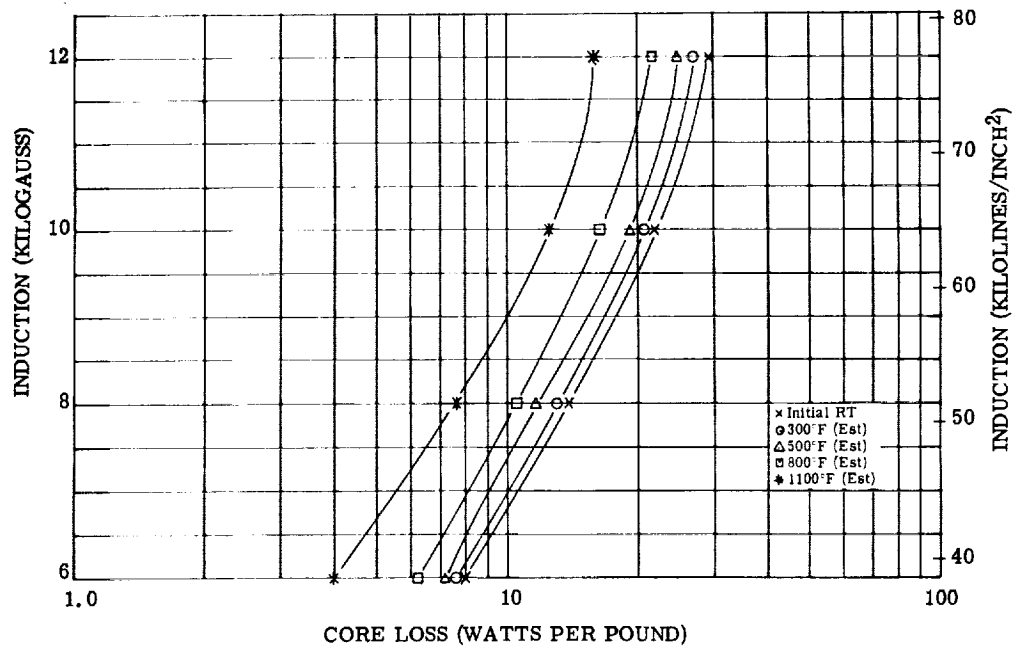
Figure 118. - Core loss at 1600 cps for 0.011-inch Cubex alloy laminations. Test atmosphere, air; interlaminar insulation, mica aluminum orthophosphate.
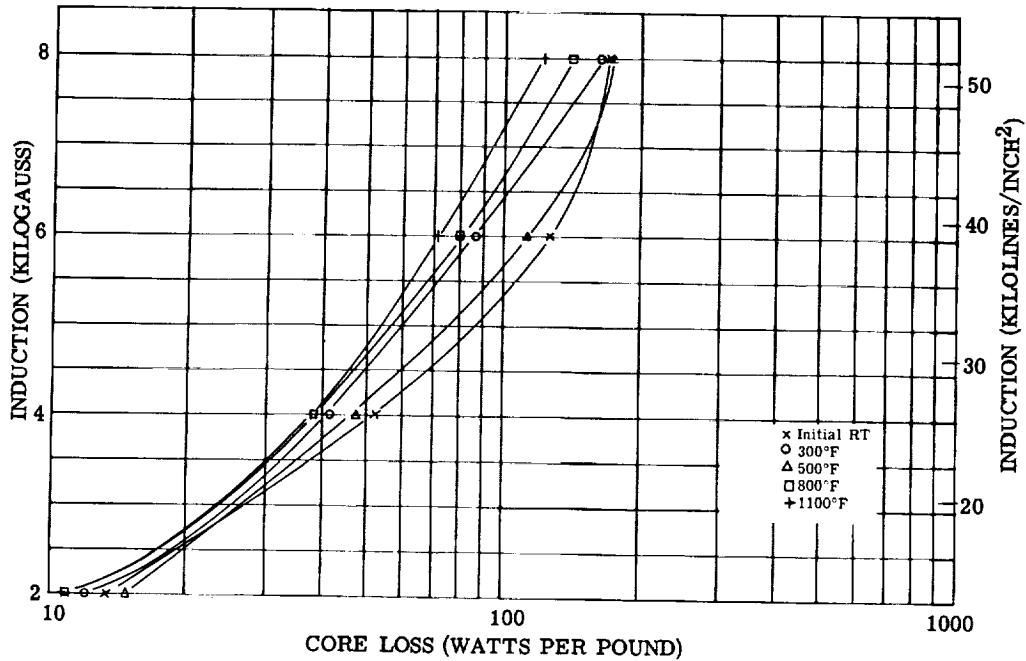
Figure 119. - Core loss at 3200 cps for 0.011-inch Cubex alloy laminations. Test atmosphere, air; interlaminar insulation, mica aluminum orthophosphate.
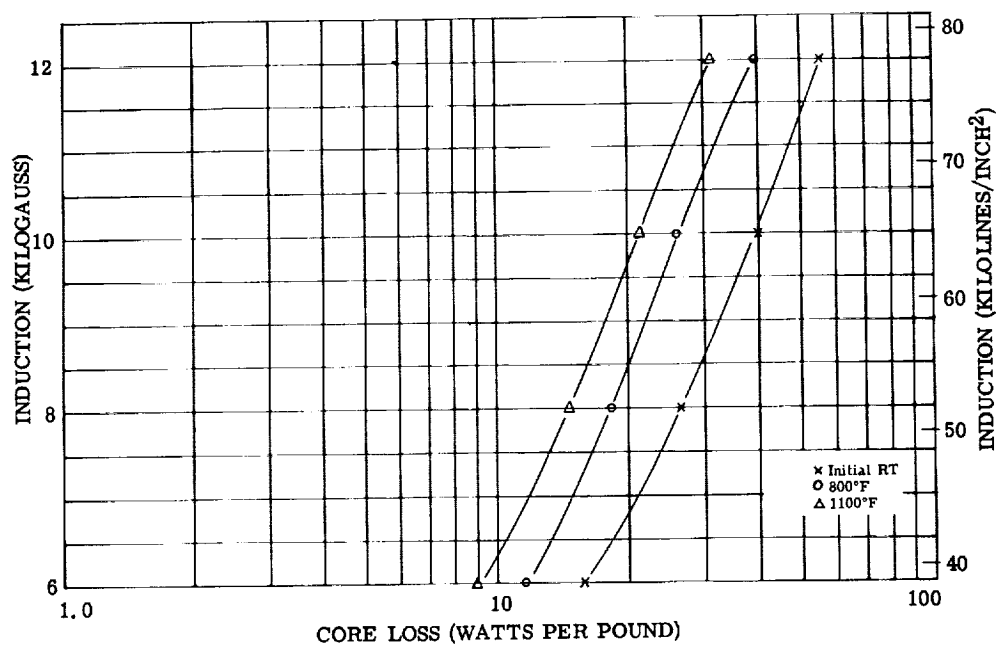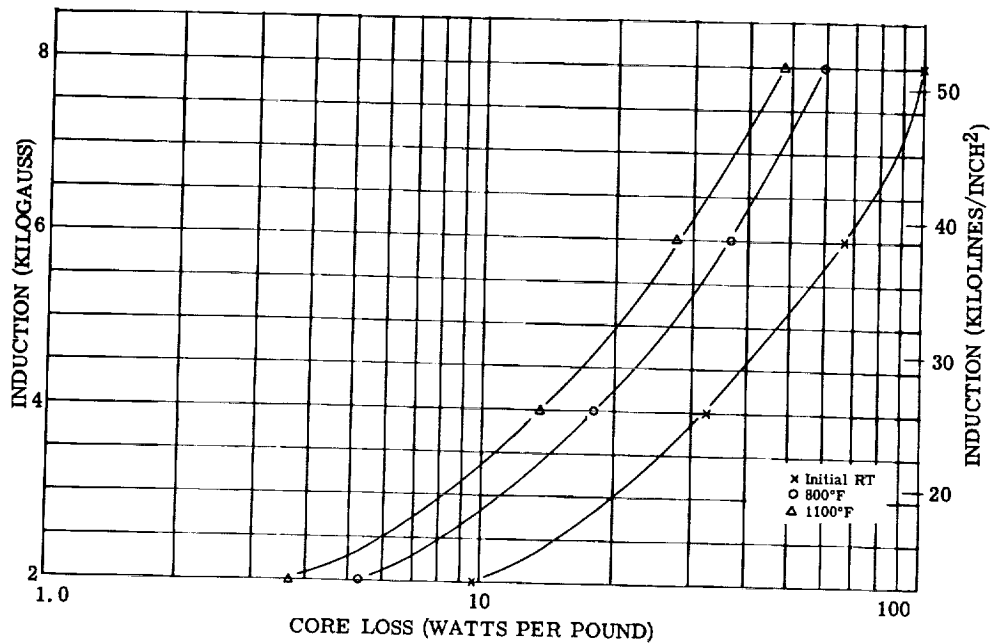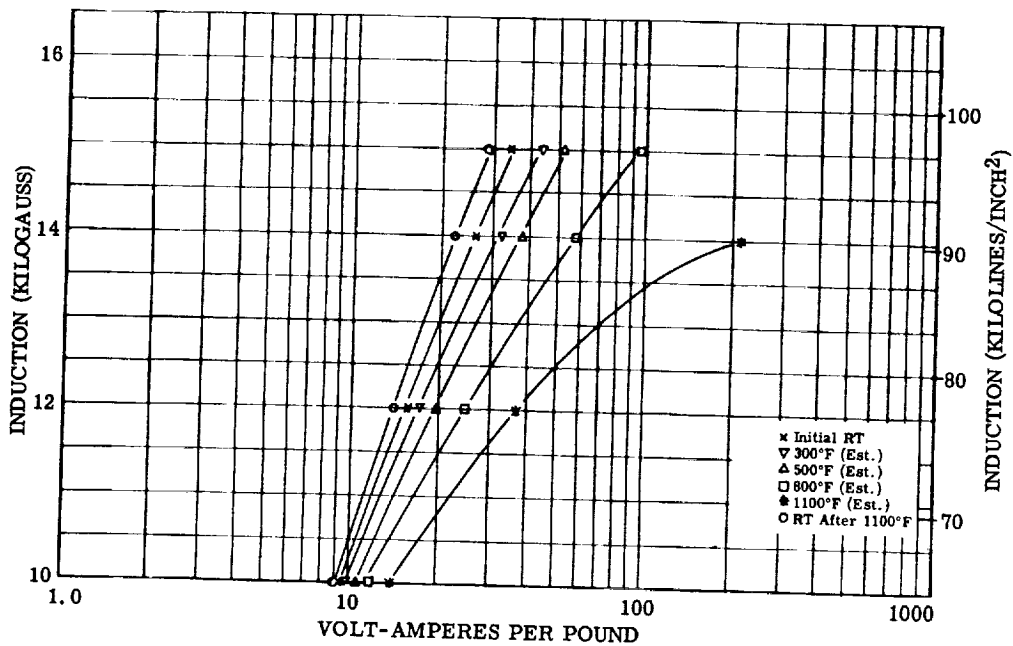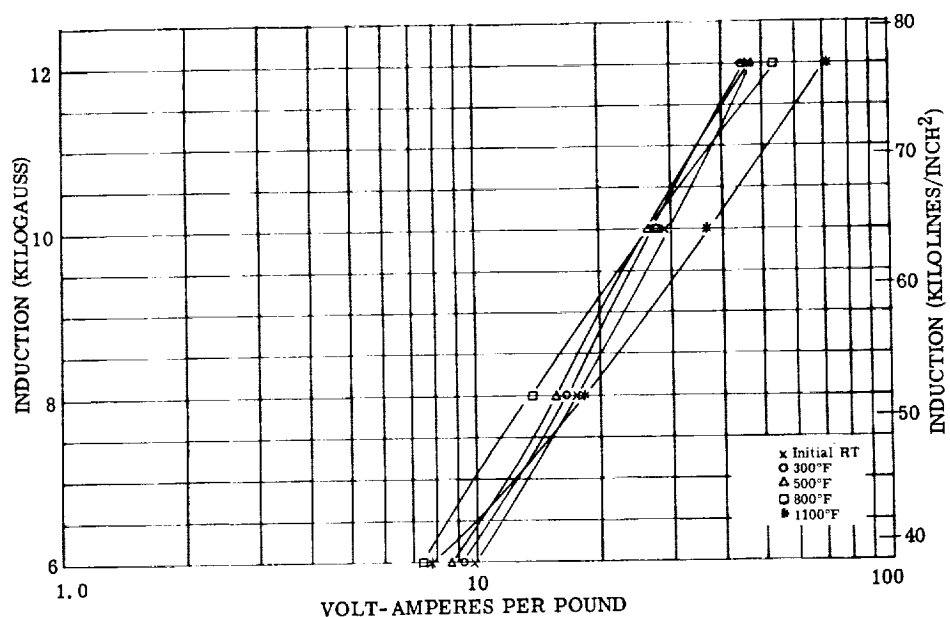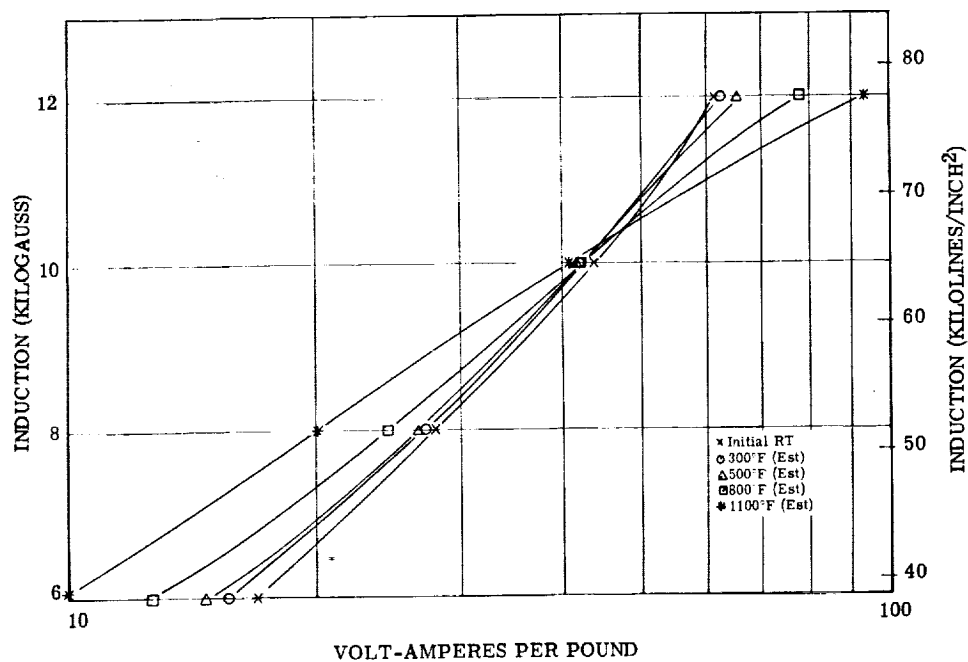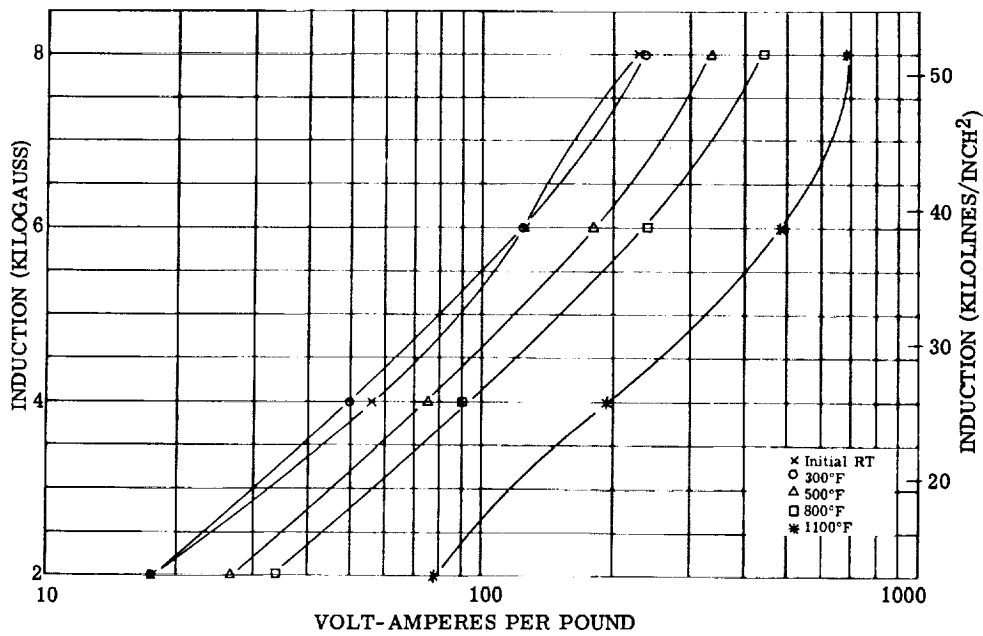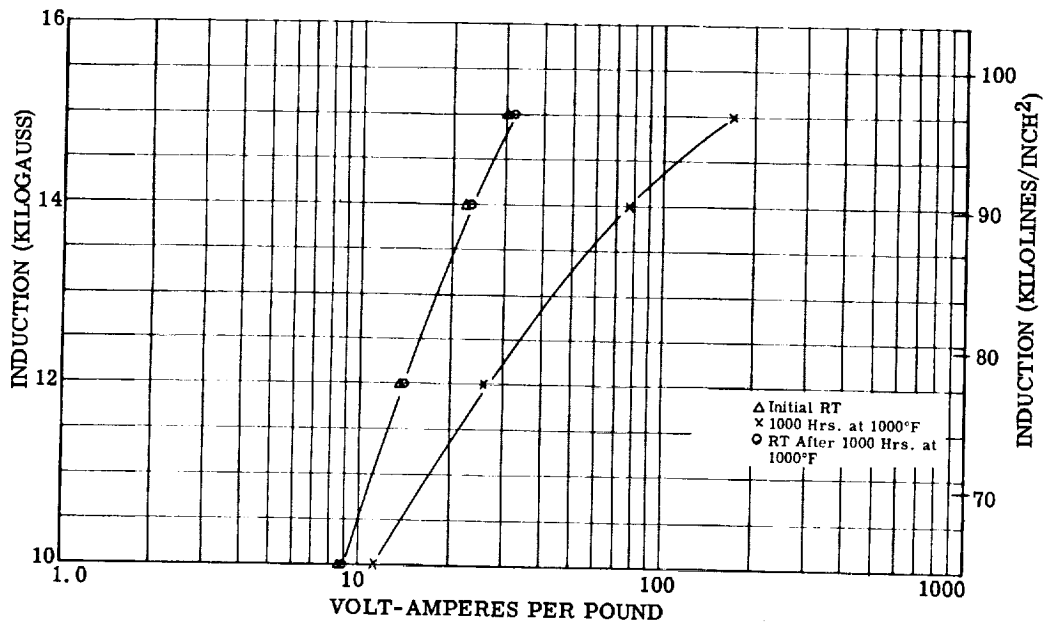

Figure 120. - Exciting volt-amperes per pound at 400 cps for 0.011-inch Cubex alloy laminations, aging test. Test atmosphere, argon; interlaminar insulation, mica aluminum orthophosphate.
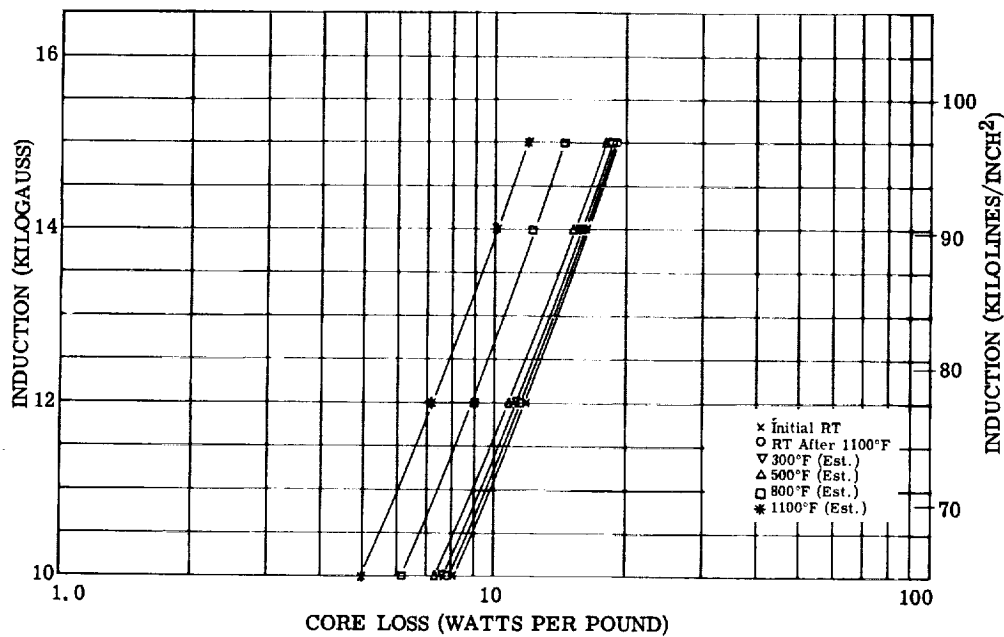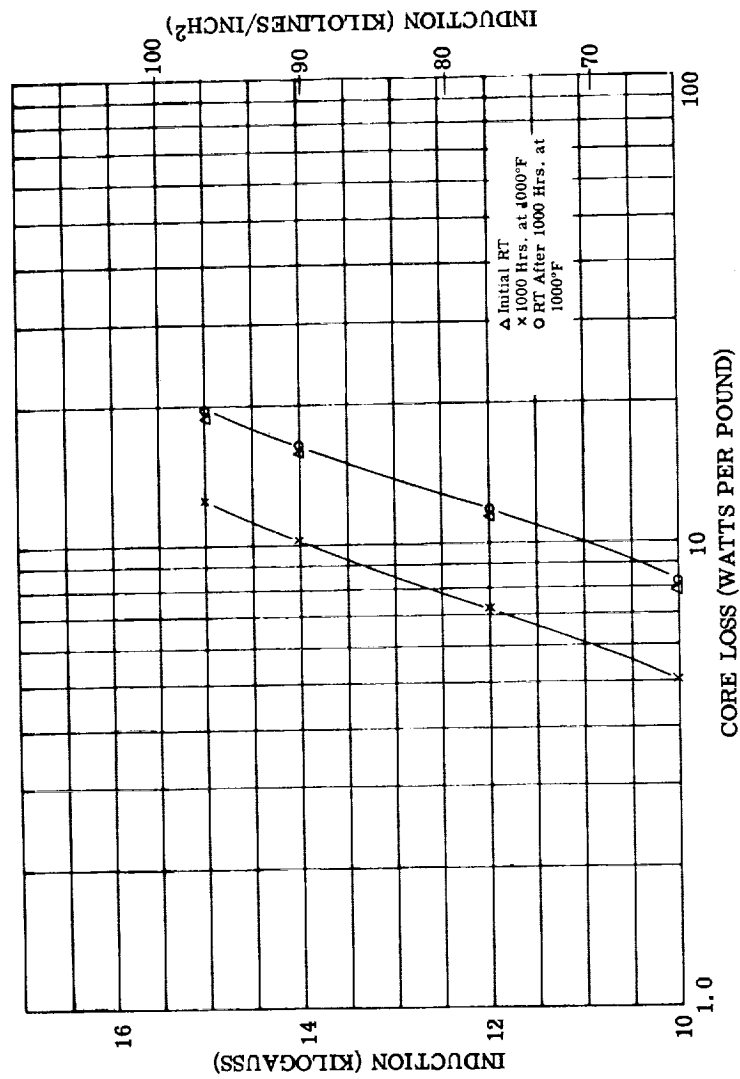
Figure 12L. - Core loss at 400 cps for 0.011-inch Cubex alloy laminations, aging test. Test atmosphere, argon; interlaminar insulation, mica aluminum orthophosphate.

TABLE 14. - POISSON'S RATIO OF 0.011 INCH THICK

CUBEX ALLOY AT ROOM TEMPERATURE

Specimen	Both gages on one grain	Both gages across grain boundary	Maximum (a)	Minimum (a)
1	0.325	0.362	0.419	0.325
2	.310	.345	.433	.303

[a]Values calculated without regard to the location of the strain gages.

TABLE 15. - TENSILE PROPERTIES OF 0.011-INCH-THICK CUBEX

SHEET TESTED IN AIR

Mark (a)	Test temperature, °F	0.02 Percent offset yield strength, psi	0.2 Percent offset yield strength, psi	Upper yield point, psi	Ultimate strength, psi	Elongation in 2 in., percent (a)	Modulus of elasticity, psi
L-1	70	37 150	------	37 800	40 200	22.0 Q	22.0×10^6
T-1	70	39 050	------	41 650	46 400	14.5 Q	--------
T	70	41 850	------	42 150	47 650	13.7	--------
L-2	500	24 200	27 300	------	40 800	21.0	13.5
T-2	500	29 250	29 800	------	41 200	38.0 Q	--------
L-3	800	23 900	25 300	------	32 250	11.9	9.0
T-3	800	23 500	25 200	------	34 350	10.0 Q	--------
L-4	1100	14 750	------	15 400	16 650	26.0	6.0
T-4	1100	12 900	------	13 350	13 350	11.5	--------
L-5	1400	700	2 150	------	3 500	7.0 Q	--------
L	1400	3 200	3 400	------	4 050	24.6 Q	--------

[a]Legend: Q, quarter break; L, longitudinal; T, transverse.

TABLE 16. - COMPRESSION DATA FOR 0.011-INCH-THICK

CUBEX SHEET

[Test, ASTM E-9; all tests made in air.]

	Specimen	Test temperature, °F	0.02 Percent offset yield strength, psi	0.2 Percent offset yield strength, psi	Yield point, psi
Longitudinal specimens	1	Room	29 600	36 000	------
	2	Room	30 400	38 250	------
	3	500	25 000	31 350	------
	4	500	21 450	34 550	------
	5	800	27 550	31 550	------
	6	800	21 100	26 900	------
	7	1100	13 600	------	13 800
	8	1100	8 600	------	9 400
	9	1400	2 700	3 700	------
Transverse specimens	1	Room	33 450	37 900	------
	2	Room	37 100	43 200	------
	3	500	28 700	34 200	------
	4	500	24 300	27 350	------
	5	800	20 700	25 400	------
	6	800	25 750	29 600	------
	7	1100	9 200	10 500	------
	8	1100	13 450	------	13 500
	9	1400	3 300	3 450	------
	10	1400	3 800	4 400	------

For 70 ≤ T ≤ 1400° F, (0.02%) Tensile Stress = 1000[0.69452x10⁻¹⁰T⁴
        − 0.23411x10⁻⁶T³ + 0.25088x10⁻³T² − 0.11458 T + 46.22] (Psi)
For 500 ≤ T ≤ 1400° F, (0.20%) Tensile Stress = 1000[−0.2966x10⁻⁴T²
        +0.02756 T + 22.186] (Psi)
For 70 ≤ T ≤ 1400° F, Ultimate Strength = 1000[0.107x10⁻⁹T⁴
        − 0.29891x10⁻⁶T³ + 0.23799x10⁻³T² − 0.07327 T + 48.81] (Psi)

□   0.02 Percent Offset Yield Strength
⊙   0.2 Percent Offset Yield Strength
○   Ultimate Strength
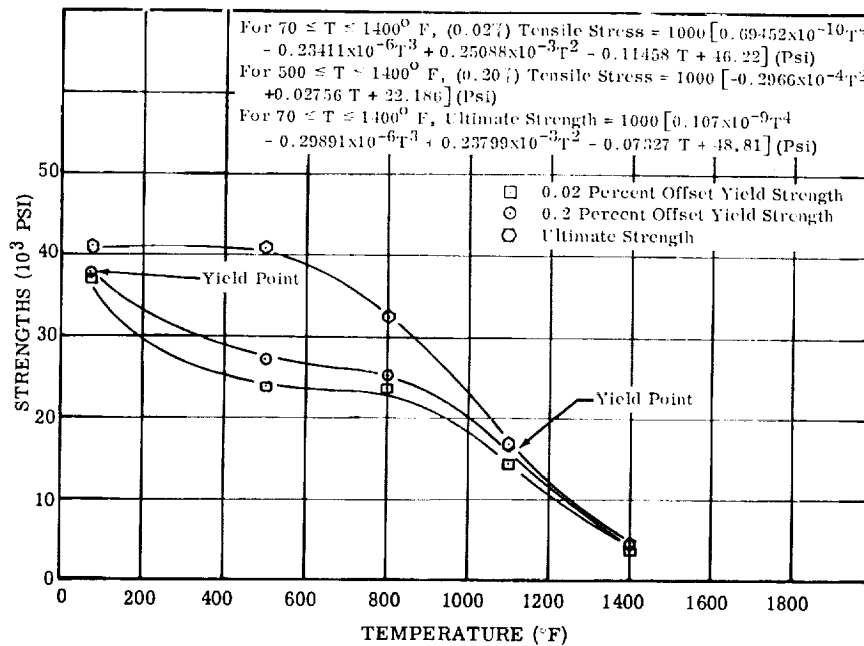
Figure 122. – Tensile strength of 0.011-inch-thick Cubex sheet tested in air (longitudinal). (See table 15.)

□ 0.02 Percent Offset Yield Strength
⊙ 0.2 Percent Offset Yield Strength
○ Ultimate Strength
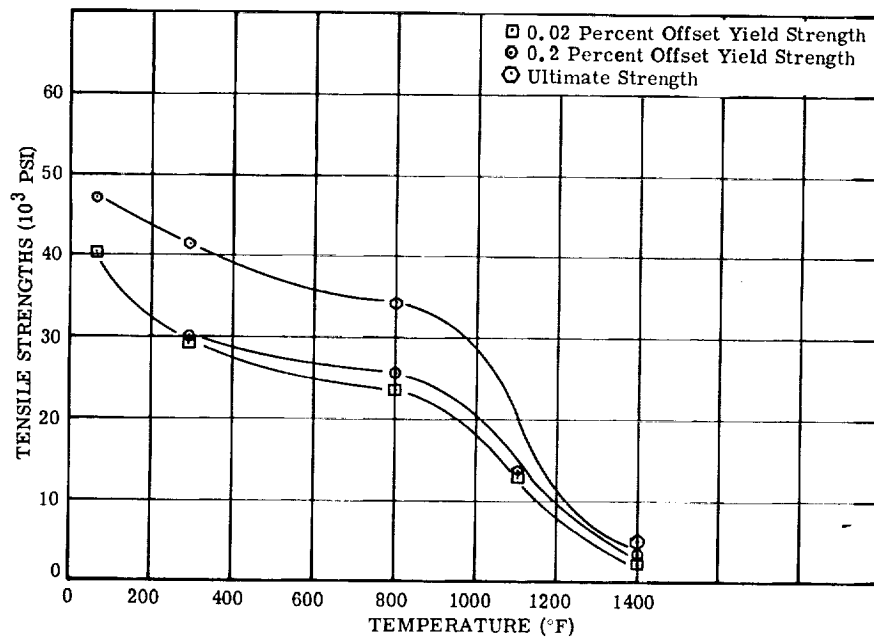
Figure 123. – Tensile strength of 0.011-inch-thick Cubex sheet tested in air (transverse). (See table 15.)
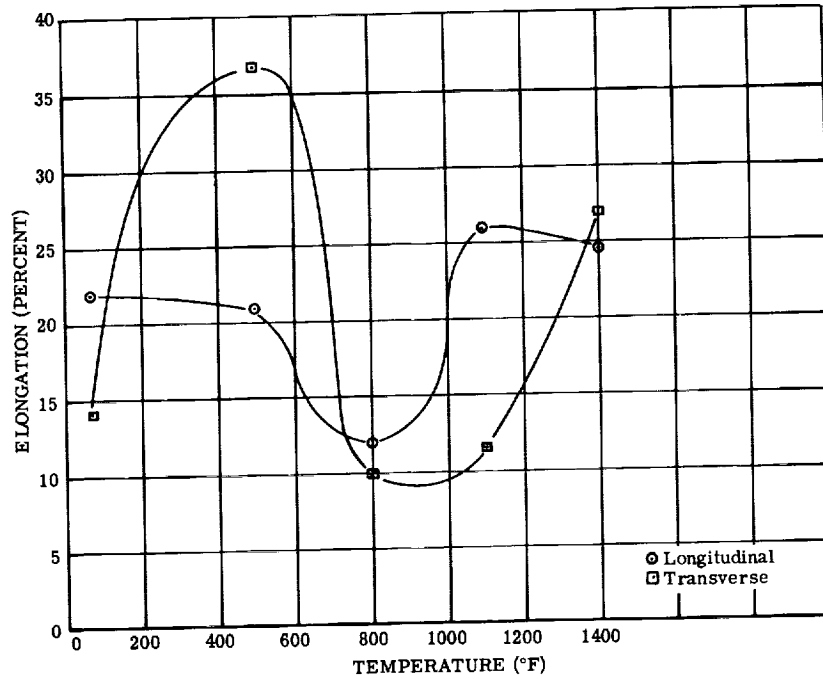
Figure 124. - Tensile ductility of 0.011-inch-thick Cubex sheet tested in air (longitudinal and transverse). (See table 15.)
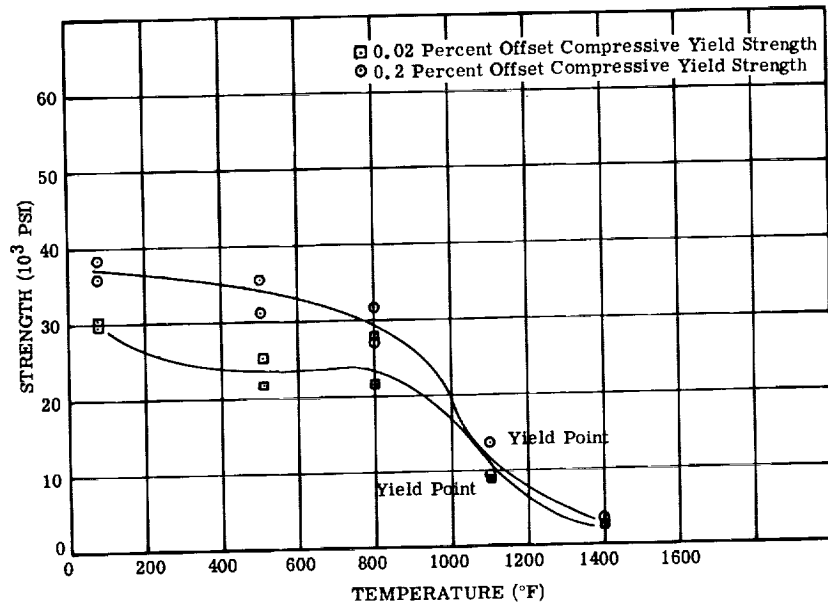
Figure 125. - Compressive strength of 0.011-inch-thick Cubex sheet tested in air (longitudinal). (See table 16.)
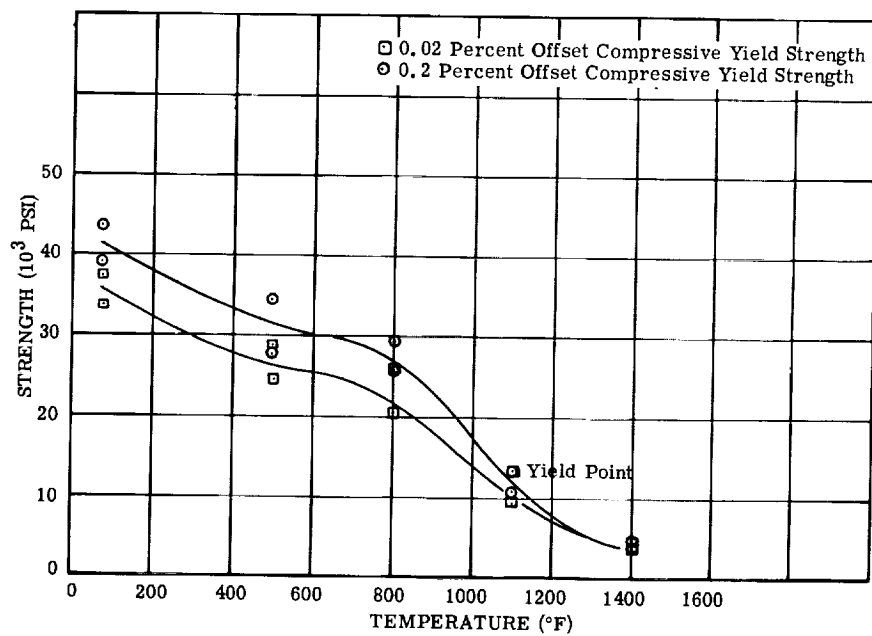
Figure 126. - Compressive strength of 0. 011-inch-thick Cubex sheet tested in air (transverse).
(See table 16.)

Hiperco 50 Alloy

Hiperco 50 alloy is a high-permeability cobalt-iron-vanadium alloy available commercially and having a nominal composition of 49 percent cobalt, 49 percent iron, and 2 percent vanadium. The tested composition was 48.8 percent cobalt, 49.6 percent iron, 1.91 percent vanadium, 0.003 percent carbon, 0.007 percent sulfur, and less than 0.002 percent phosphorus.

Thermophysical properties. - The thermophysical properties of Hiperco 50 alloy are the same as those of Supermendur except for electrical resistivity, which is from 35 to 40×10^6 ohm-centimeters for Hiperco 50.

Magnetic properties. - All magnetic materials are stress-relief annealed unless otherwise specified.

Direct-current:

Temperature, °F	Lamination thickness, in.	
	0.004	0.008
	Induction,[a] B_{tip}, kG	
72	24.1	23.5
500	23.4	22.7
800	21.9	22.4
1100	21.5	20.8

[a]H, 300 Oe.

Alternating current (400 cps) (B = 18 kG):

Temperature, °F	Lamination thickness, in.			
	0.004	0.008	0.004	0.008
	Exciting volt-amperes per pound		Core loss, W/lb	
72	55.4	472	11.5	37.8
500	60.6	498	10.4	37.0
800	74.7	524	8.9	35.1
1100	78.0	492	6.5	32.4

Constant current flux reset (CCFR) properties: CCFR properties are not applicable to Hiperco 50. They are measured only on materials used in magnetic amplifiers.

Mechanical properties (0.008-in.-thick sheet).

Tensile properties:

Temperature, $^{\circ}$F	0.20-Percent offset yield strength, psi	Tensile strength, psi	Elongation in 2 in., percent	Modulus of elasticity, psi
Longitudinal				
72	41 650	41 650	0.5	28.9×10^6
500	37 950	71 250	5.5	27.1
800	36 750	67 900	7.0	27.0
1100	33 750	62 600	6.0	20.0
Transverse				
72	------	37 700	---	38.0×10^6
500	38 950	55 250	1.5	33.2
800	38 050	60 150	4.9	29.7
1100	34 700	55 250	12.0	28.9

Creep: Material is not used in highly stressed applications.

Fatigue: Material is not used in cyclic stressed applications where a fatigue failure could occur.

Normal heat treatment: Material is heated to $1400^{\circ} \pm 20^{\circ}$ F in pure dry hydrogen, held at temperature for 1 to 4 hours, depending on furnace load, and fast-cooled in the hydrogen atmosphere to below 400° F.

Supermendur

Supermendur is a high-purity high-permeability cobalt-iron-vanadium alloy (obtained from Arnold Engineering Co. for testing) that responds to magnetic-field annealing and is commercially available in the nominal composition of 49 percent cobalt, 49 percent iron, and 2 percent vanadium. The tested composition was 49.5 percent cobalt, 49.5 percent iron, and 1.0 percent vanadium.

Thermophysical properties. -

Density, lb/cu in. (g/cu cm) 0.295 (8.20)
Solidus temperature, $^{\circ}$F 2700
Curie temperature, $^{\circ}$F 1724
Thermal conductivity, (Btu)(ft)/(sq ft)(hr)($^{\circ}$F), at -
185° F. 17.2
500° F. 21.7
Coefficient of thermal expansion, in./(in.)($^{\circ}$F) . . . . 5.28$\times10^{-6}$
Specific heat, Btu/(lb)($^{\circ}$F), at -
72° F 0.098
500° F 0.098
800° F 0.103
Electrical resistivity, ohm-cm, at -
72° F . . . . 45.73$\times10^{-6}$
500° F . . . . 50.75$\times10^{-6}$
800° F . . . . 57.25$\times10^{-6}$

Magnetic properties.

Direct current:

Temperature, $^{\circ}$F	0.002-in.-thick tape-wound toroid (a)	0.006-in.-thick laminations (b)
	Induction, B_{tip}, kG	
72	24.1	24.1
300	22.7	24.1
500	24.0	23.7
800	23.3	23.0

[a]H, 300 Oe.
[b]H, 250 Oe.

Alternating current (B = 18 kG):

Temper- ature, °F	0.002-in.-thick tape-wound toroid	0.006-in.-thick laminations	0.002-in.-thick tape-wound toroid	0.006-in.-thick laminations
	Exciting volt-amperes per pound		Core loss, W/lb	
72	8.2	15.0	7.0	10.0
300	6.8	22.1	6.2	10.6
500	7.5	23.5	7.0	10.6
800	24.8	31.1	10.8	9.7

Constant current flux reset (CCFR) properties for 0.002-inch-thick tape-wound toroid:

Property	Test temperature, °F		
	72	500	1100
B_m, kG, at 5 Oe (SAT/2)	23.15	24.70	21.95
$B_m - B_r$, kG	3.20	1.65	2.50
H_1, Oe (AT)	0.57	0.55	0.45
H_2, Oe (AT + DAT)	0.65	0.63	0.55
H_0, Oe (AT + DAT/2)	0.61	0.60	0.515

Mechanical properties (0.006-in.-thick sheet).

Tensile properties:

Temper- ature, °F	Yield point, psi	0.02-Percent offset yield strength, psi	Tensile strength, psi	Elongation in 2 in., percent	Modulus of elasticity, psi
72	38 500	------	43 300	2.1	34.7×10^6
500	------	32 800	99 450	9.8	32.8
800	------	33 250	96 250	10.9	29.8
1100	------	31 150	55 100	11.5	28.5

Creep: Material is not used in highly stressed applications.

Fatigue: Material is not used in cyclic stressed applications or where fatigue failure could occur.

Normal heat treatment: Material is heat-treated in dry hydrogen under the influence of a magnetic field. This process was performed by the supplier and specific details are not available. The material should be purchased to a performance requirement.

TEMPERATURE (°F)
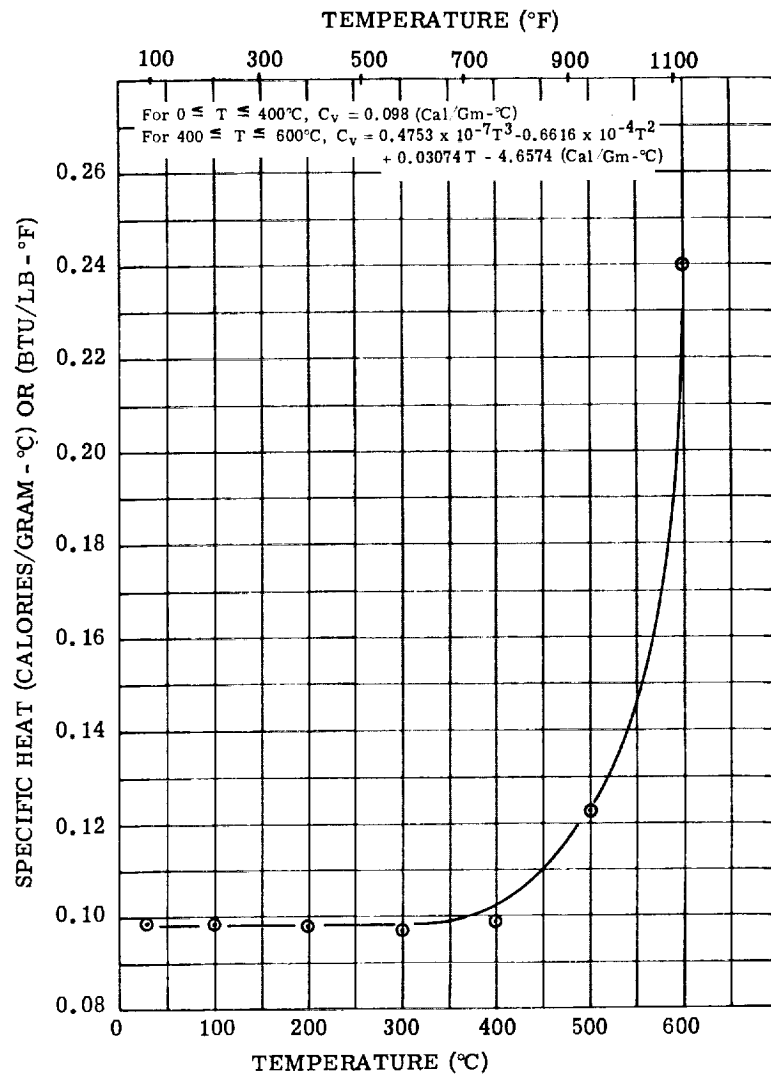
Figure 127. - Specific heat of Supermendur rolling stock tested in vacuum
(10^-5 torr).

TABLE 17. - ELECTRICAL RESISTIVITY OF

SUPERMENDUR (FIELD-ANNEALED) 2 MIL BY

0.250-INCH-WIDE RIBBON WITH CONTINUOUS

HEATING IN VACUUM (10^{-5} TORR)

[Specimen 1, 12.96 in. long; specimen 2,
11.39 in. long; test, ASTM A344.]

Temperature, $^\circ$F		Microhm-cm	
Specimen 1	Specimen 2	Specimen 1	Specimen 2
79	77	45.79	46.818
200	200	46.46	47.59
300	300	47.28	48.63
400	400	48.44	49.95
500	500	50.01	51.49
600	600	51.94	53.30
710	703	54.34	55.44
810	803	56.80	58.03
907	900	59.39	60.77
1000	1000	62.09	63.63
1100	1100	65.56	67.08
950	946	61.05	62.22
750	746	55.61	56.81
550	550	51.40	52.43
350	350	48.32	49.31
150	150	46.18	47.16

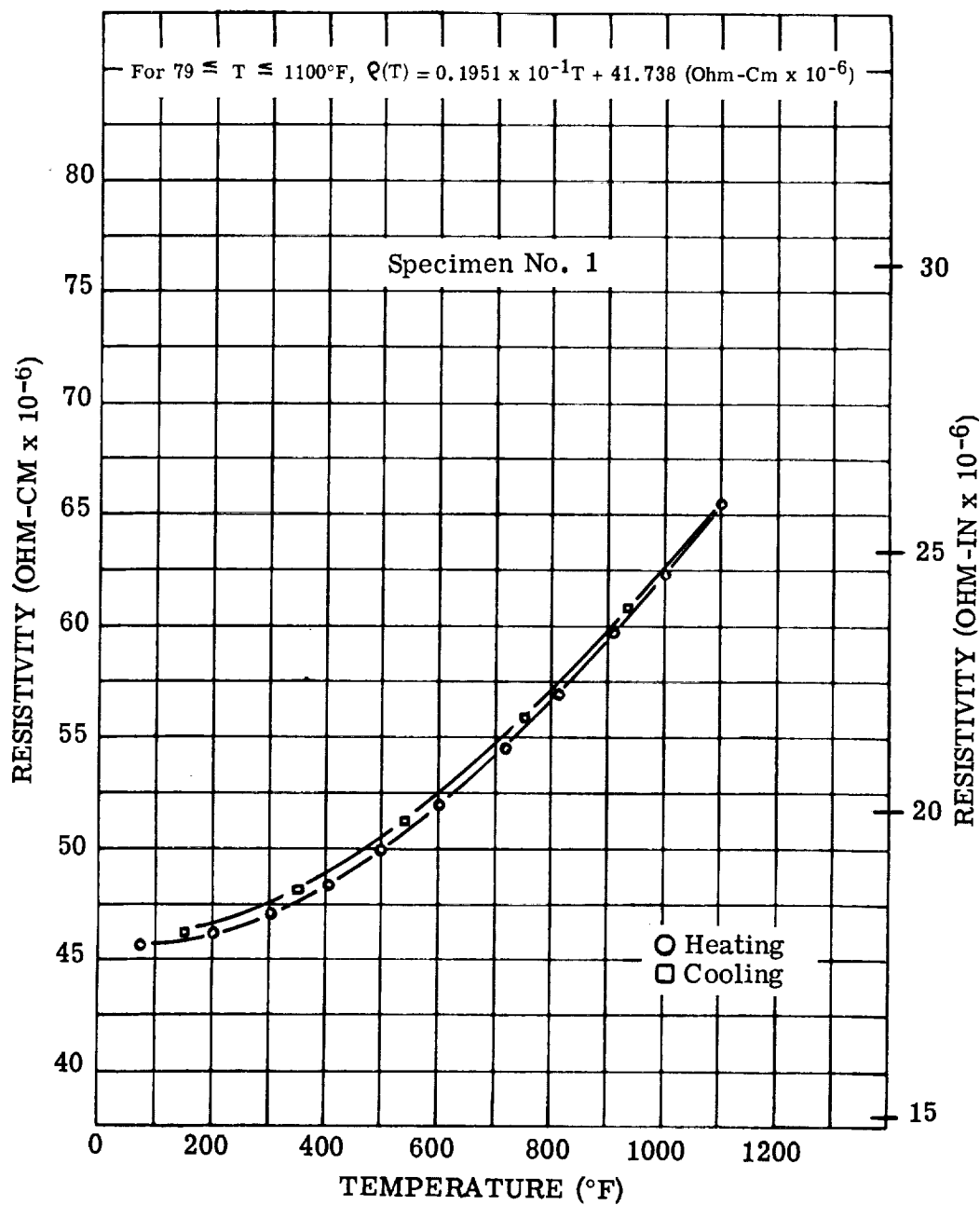Figure 128. - Electrical resistivity of Supermendur 2-mil ribbon tested in vacuum (10^{-5} torr). (See table 17.)

TABLE 18. – CONSTANT CURRENT FLUX RESET (CCFR) PROPERTIES OF SUPERMENDUR

[400 cps sine wave; test procedure for Toroidal Magnetic Amplifier Cores, AIEE No. 432, Jan. 1959; H_m, 5.0 Oe.]

Core	Material thickness, in.	Core size (a)	Temperature, °F	Test environment	B_m, kG	$B_m - B_r$, kG	$\dfrac{B_r}{B_m}$	H_0, Oe	H_1, Oe	H_2, Oe
1	0.002	A	72	Air	21.71	2.73	0.874	0.58	0.544	0.604
			500	Argon	24.10	1.99	.917	.466	.428	.504
			1100	Argon	21.16	2.15	.898	.418	.36	.481
			b72	Air	21.16	4.63	.781	.917	.85	.975
2	0.002	A	72	Air	22.77	2.09	0.910	0.64	0.62	0.665
			500	Argon	10.80	.66	.939	1.01	.806	-----
			1100	Argon	10.09	1.47	.854	-----	-----	-----
			b72	Air	20.84	2.77	.867	.906	.88	.941
3	0.002	B	72	Air	23.01	3.48	0.849	0.619	0.574	0.661
			500	Argon	24.18	2.52	.896	.49	.443	.51
			1100	Argon	22.05	2.88	.879	.526	.462	.641
			b72	Air	21.58	4.69	.783	1.078	1.022	1.162
4	0.002	B	72	Air	23.21	2.89	0.875	0.602	0.573	0.627
			500	Argon	24.56	.78	.969	.716	.661	.758
			1100	Argon	21.85	2.16	.901	.495	.442	.53
			b72	Air	20.94	3.96	.811	1.078	1.019	1.126
5	0.006	C	72	Air	20.10	2.15	0.893	0.643	0.594	0.687
			500	Argon	19.98	1.97	.901	.549	.506	.587
			1100	Argon	17.87	2.03	.886	.466	.416	.526

[a]Legend: A, toroid $3\frac{1}{2}$ by 4 by 1/2 in.; B, toroid 1 by $1\frac{1}{4}$ by 1/4 in.; C, ring lamination stack $3\frac{1}{2}$ by 4 by 1/2 in.

[b]Room temperature test after 1100° F exposure.

MAGNETIZING FORCE (AMPERE TURNS/INCH)

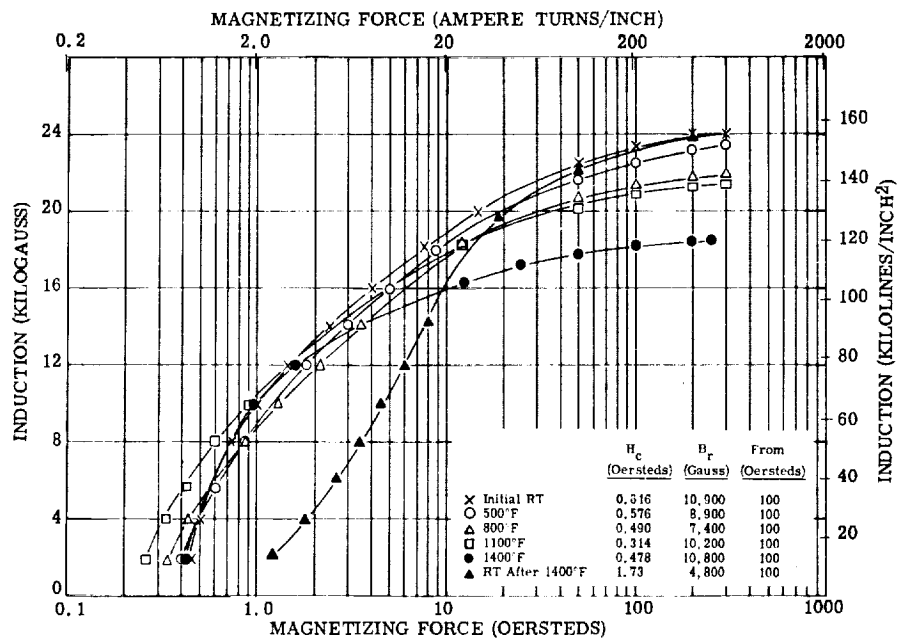| X | Initial RT | 0.316 | 10,900 | 100 |
O	500°F	0.576	8,900	100
△	800°F	0.490	7,400	100
□	1100°F	0.314	10,200	100
●	1400°F	0.478	10,800	100
▲	RT After 1400°F	1.73	4,800	100

MAGNETIZING FORCE (OERSTEDS)

Figure 129. - Direct-current magnetization curves for Hiperco 50 alloy 0.004-inch laminations. Test atmosphere, air to 800° F and argon above 800° F; interlaminar insulation, aluminum orthophosphate.

MAGNETIZING FORCE (AMPERE TURNS/INCH)

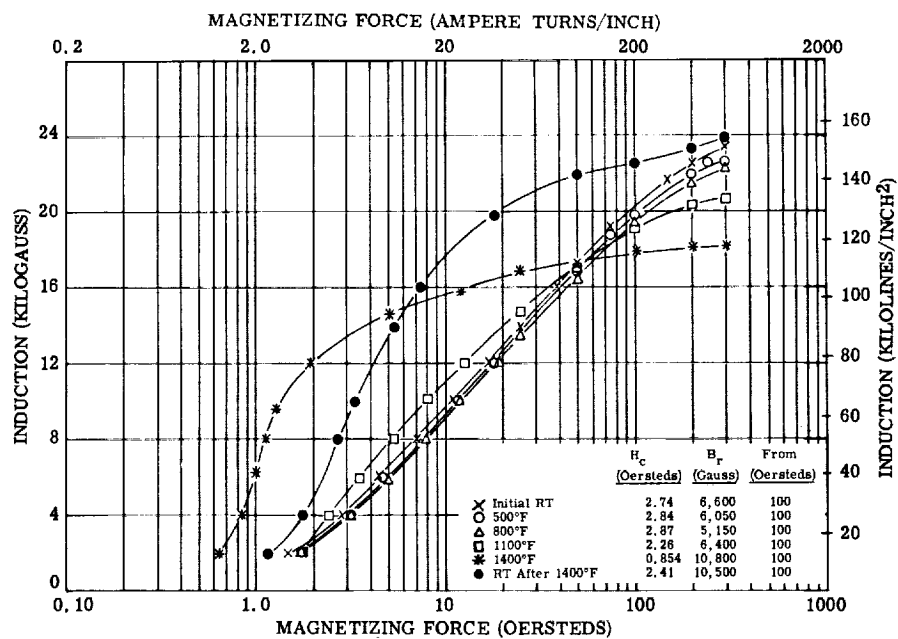| X | Initial RT | 2.74 | 6,600 | 100 |
O	500°F	2.84	6,050	100
△	800°F	2.87	5,150	100
□	1100°F	2.26	6,400	100
✳	1400°F	0.854	10,800	100
●	RT After 1400°F	2.41	10,500	100

MAGNETIZING FORCE (OERSTEDS)

Figure 130. - Direct-current magnetization curves for Hiperco 50 alloy 0.008-inch laminations. Test atmosphere, air to 800° F and argon above 800° F; interlaminar insulation, aluminum orthosphosphate.

Figure 131. - Exciting volt-amperes per pound at 400 cps for Hiperco 50 alloy 0.004-inch laminations. Test atmosphere, air to 800° F and argon above 800° F; interlaminar insulation, aluminum ortho-phosphate.
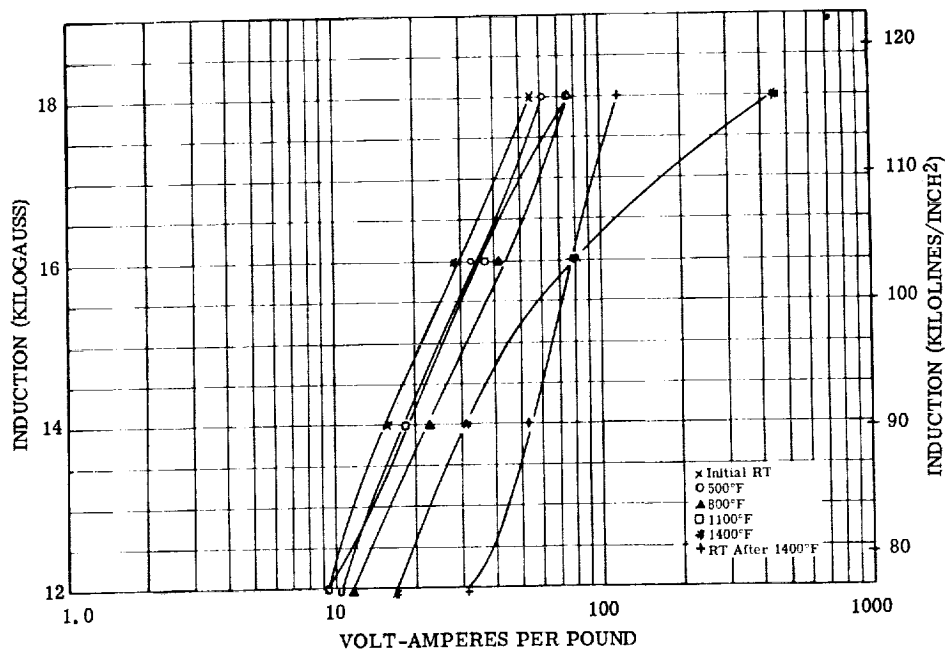

Figure 132. - Exciting volt-amperes per pound at 800 cps for Hiperco 50 alloy 0.004-inch laminations. Test atmosphere, air to 800° F and argon above 800° F; interlaminar insulation, aluminum ortho-phosphate.

Figure 133. - Exciting volt-amperes per pound at 1600 cps for Hiperco 50 alloy 0.004-inch laminations. Test atmosphere, air to 800° F and argon above 800° F; interlaminar insulation, aluminum ortho-phosphate.
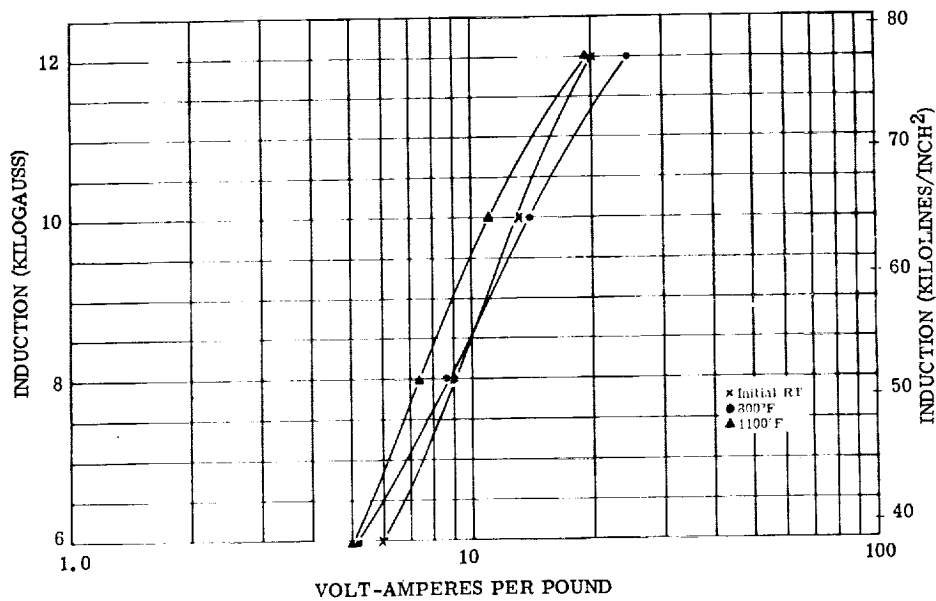

Figure 134. - Exciting volt-amperes per pound at 3200 cps for Hiperco 50 alloy 0.004-inch laminations. Test atmosphere, air to 800° F and argon above 800° F; interlaminar insulation, aluminum ortho-phosphate.

Figure 135. - Core loss at 400 cps for Hiperco 50 alloy 0.004-inch laminations. Test atmosphere, air to 800° F and argon above 800° F; interlaminar insulation, aluminum orthophosphate.
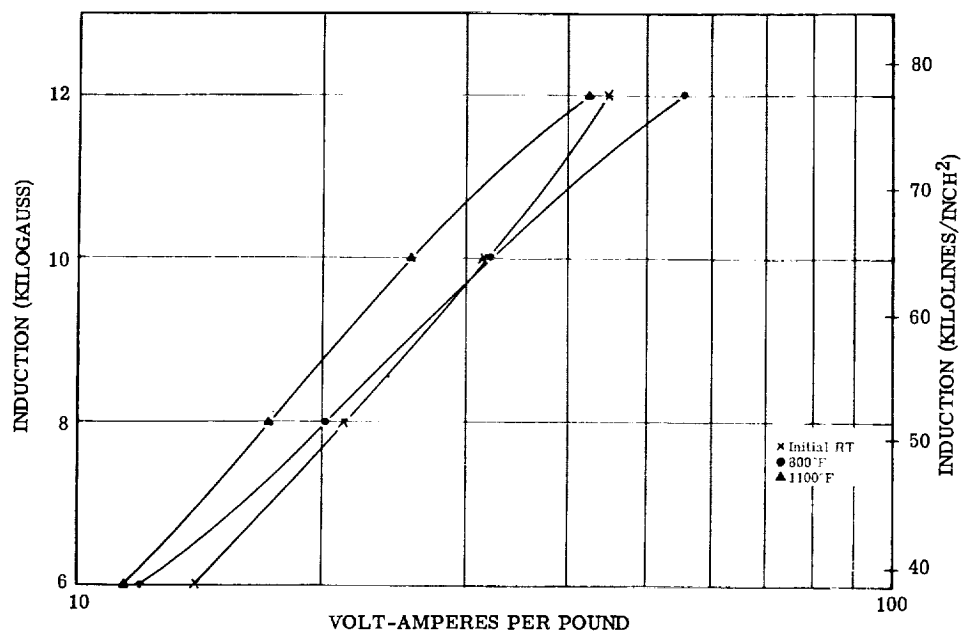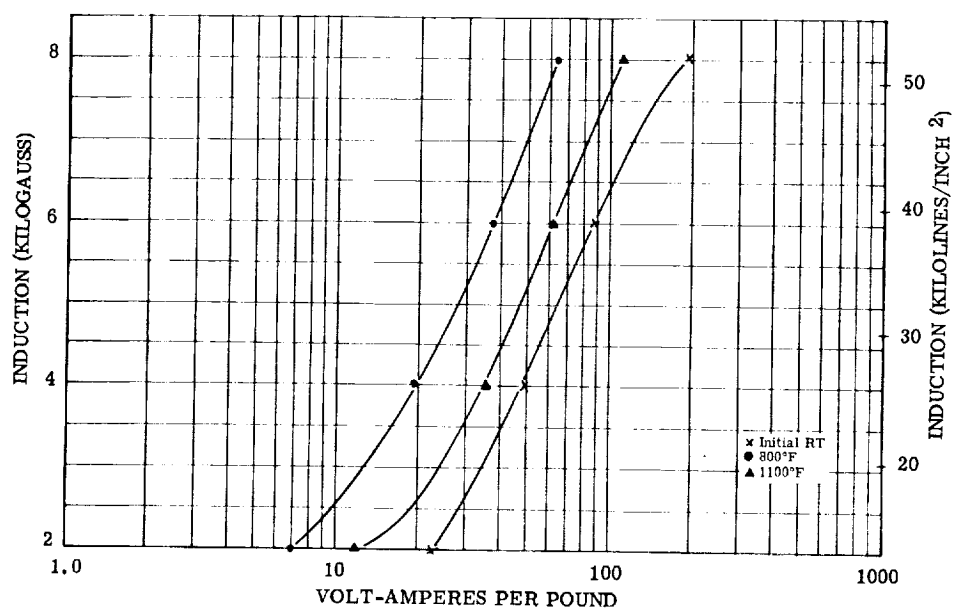

Figure 136. - Core loss at 800 cps for Hiperco 50 alloy 0.004-inch laminations. Test atmosphere, air to 800° F and argon above 800° F; interlaminar insulation, aluminum orthophosphate.

Figure 137. - Core loss at 1600 cps for Hiperco 50 alloy 0.004 inch-laminations. Test atmosphere, air to 800° F and argon above 800° F; interlaminar insulation, aluminum orthophosphate.

Figure 138. - Core loss at 3200 cps for Hiperco 50 alloy 0.004-inch laminations. Test atmosphere, air to 800° F and argon above 800° F; interlaminar insulation, aluminum orthophosphate.

Figure 139. - Exciting volt-amperes per pound at 400 cps for Hiperco 50 alloy 0.008-inch laminations. Test atmosphere, air to 800° F and argon above 800° F; interlaminar insulation, aluminum orthophosphate.
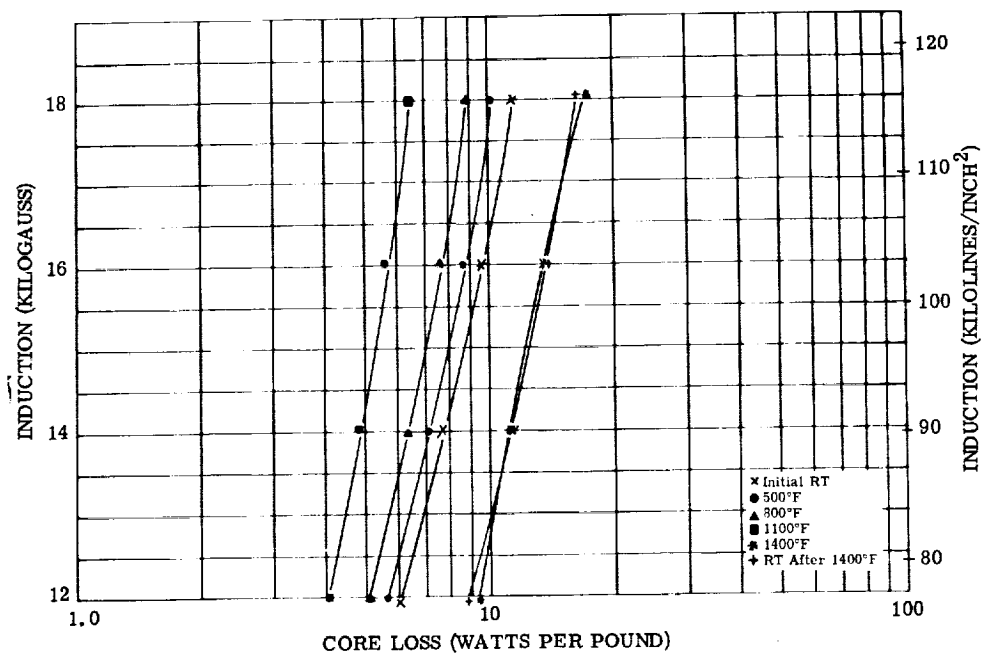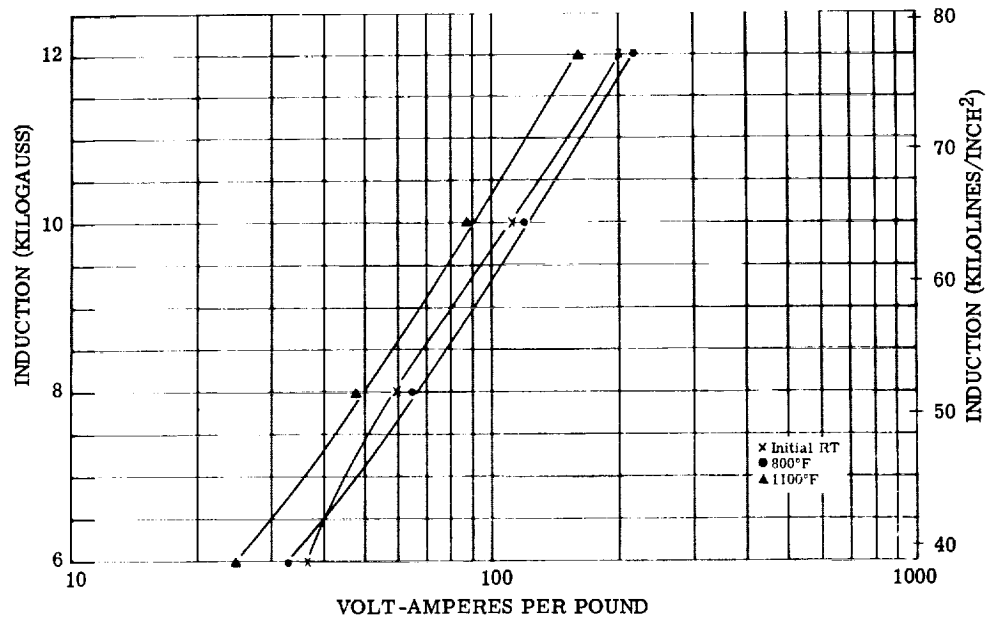

Figure 140. - Exciting volt-amperes per pound at 800 cps for Hiperco 50 alloy 0.008-inch laminations. Test atmosphere, air to 800° F and argon above 800° F; interlaminar insulation, aluminum orthophosphate.
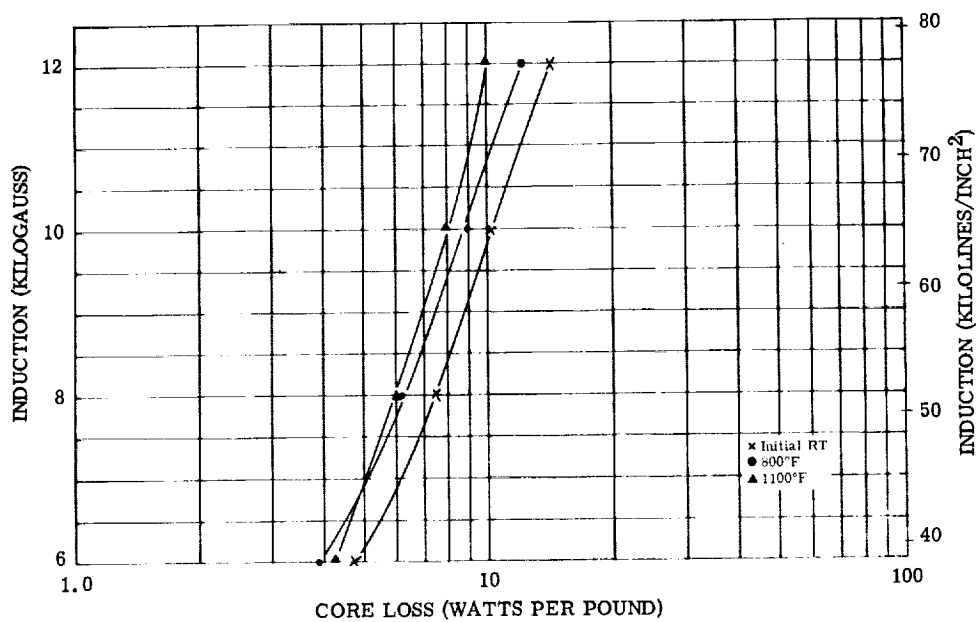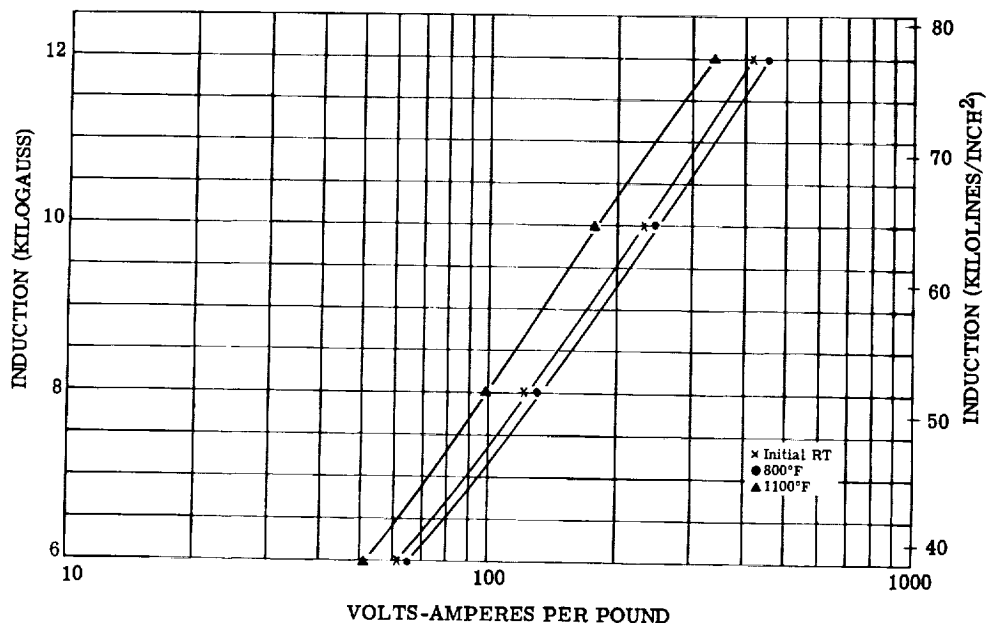
Figure 141. - Exciting volt-amperes per pound at 1600 cps for Hiperco 50 alloy 0.008-inch laminations. Test atmosphere, air to 800° F and argon above 800° F; interlaminar insulation, aluminum orthophosphate.
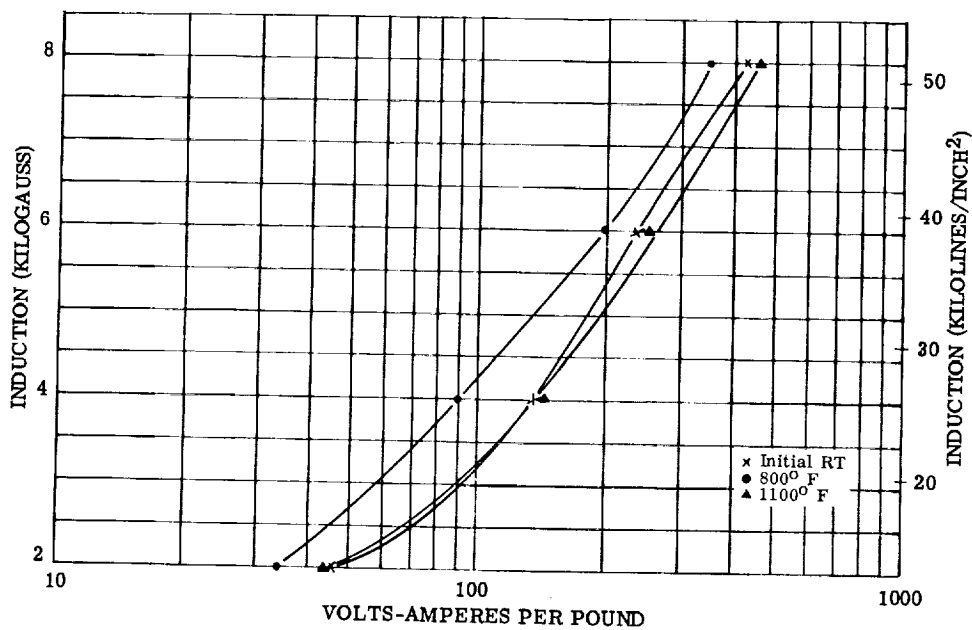
Figure 142. - Exciting volt-amperes per pound at 3200 cps for Hiperco 50 alloy 0.008-inch laminations. Test atmosphere, air to 800° F and argon above 800° F; interlaminar insulation, aluminum orthophosphate.
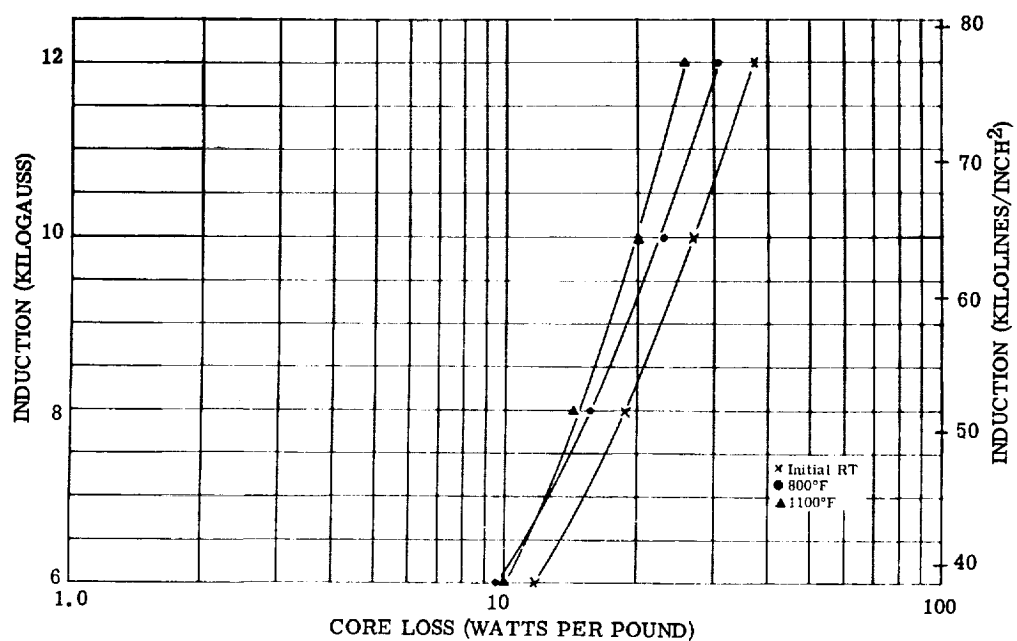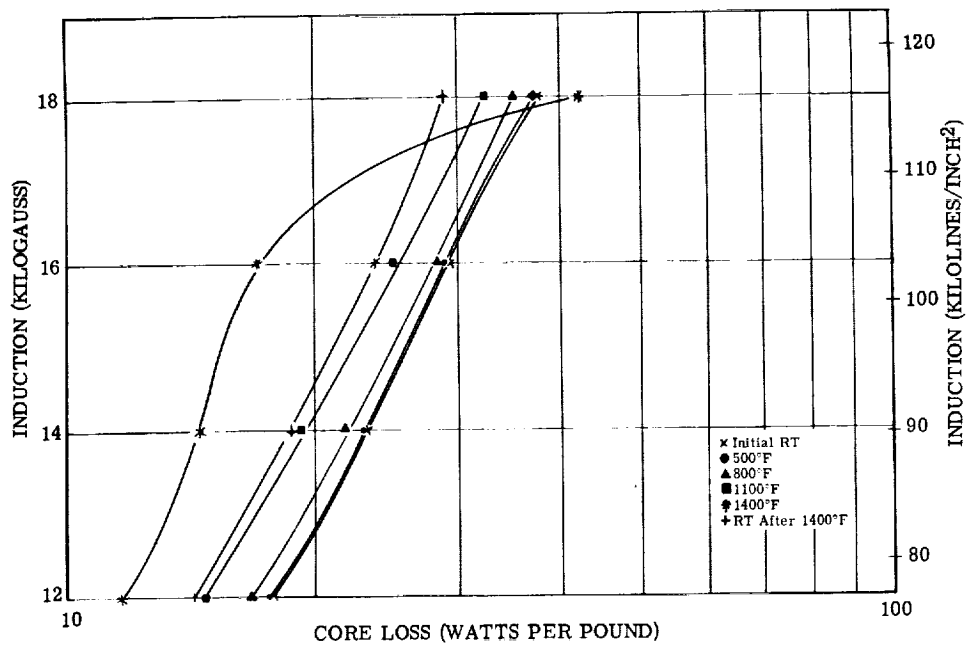
Figure 143. - Core loss at 400 cps for Hiperco 50 alloy 0.008-inch laminations. Test atmosphere, air to 800° F and argon above 800° F; interlaminar insulation, aluminum orthophosphate.
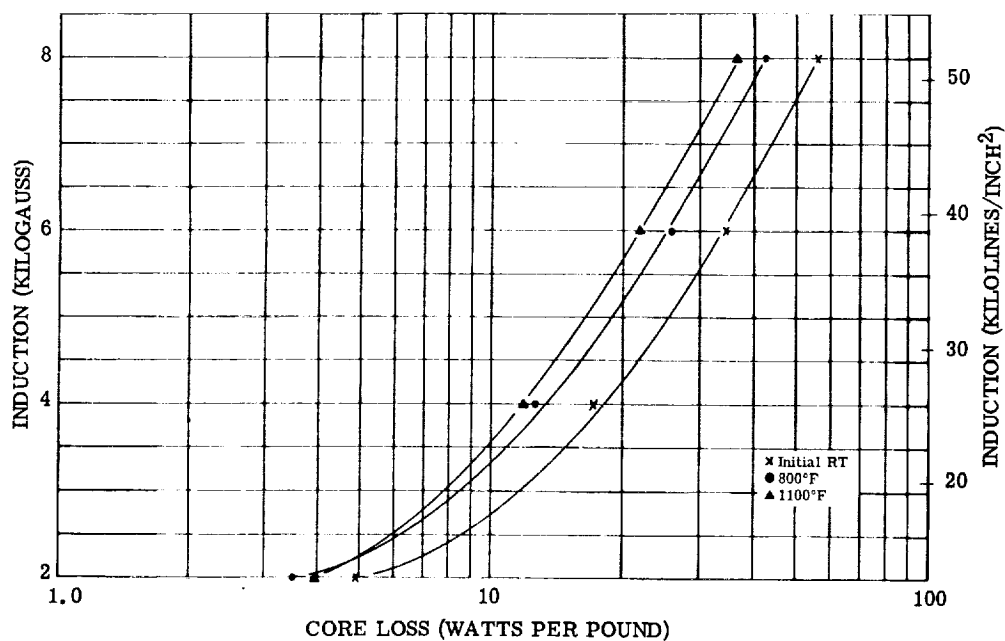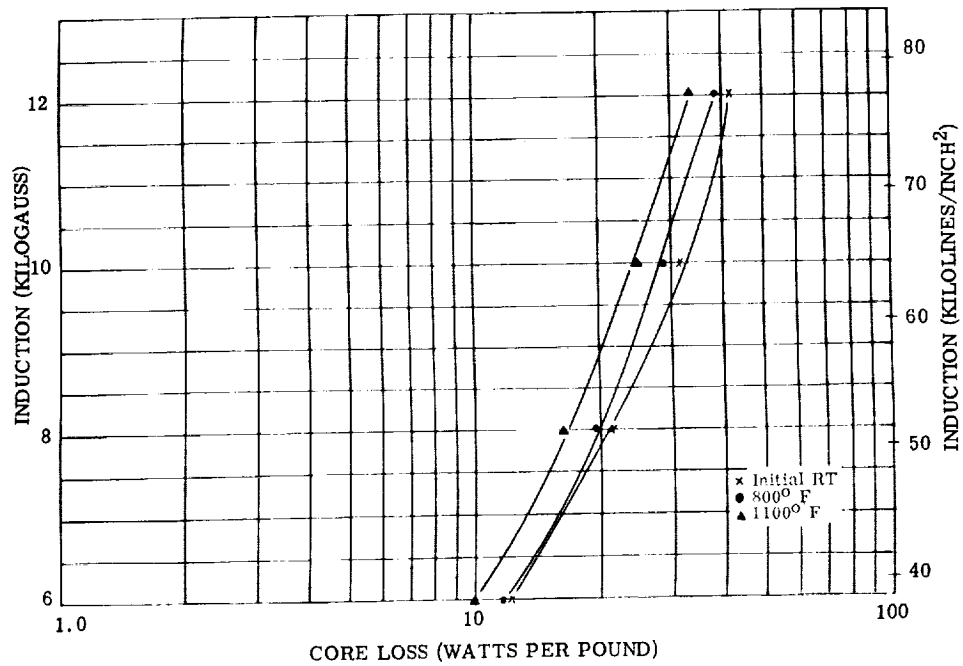

Figure 144. - Core loss at 800 cps for Hiperco 50 alloy 0.008-inch laminations. Test atmosphere, air to 800° F and argon above 800° F; interlaminar insulation, aluminum orthophosphate.
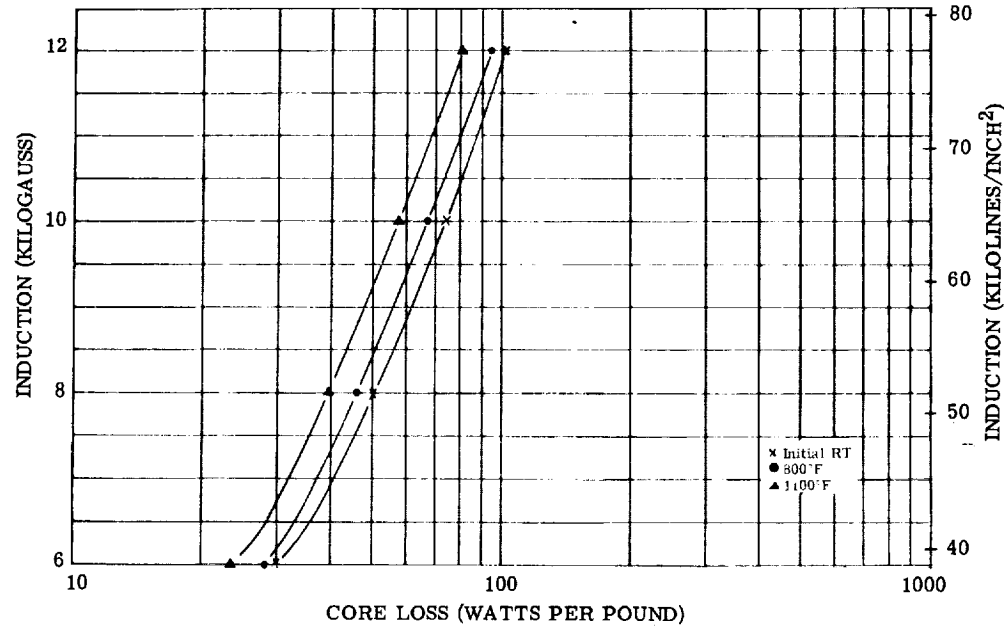
Figure 145. - Core loss at 1600 cps for Hiperco 50 alloy 0.008-inch laminations. Test atmosphere, air to 800° F and argon above 800° F; interlaminar insulation, aluminum orthophosphate.
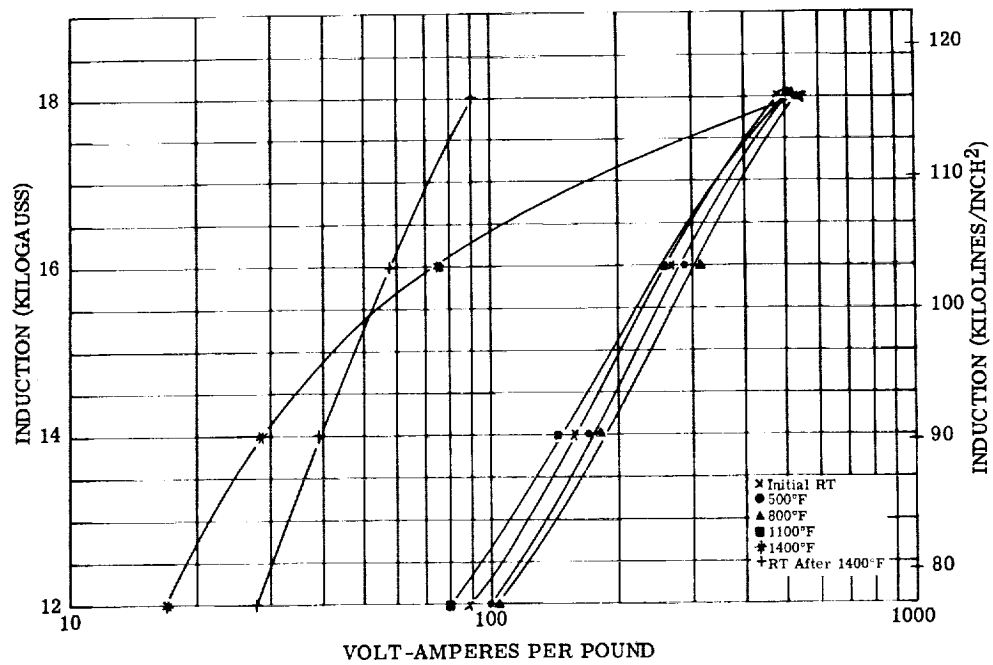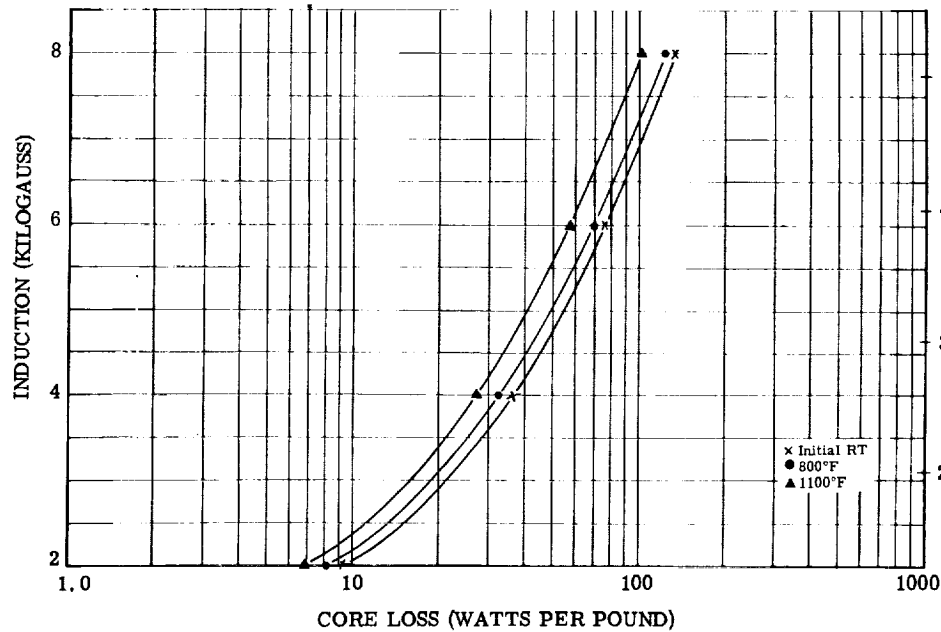

Figure 146. - Core loss at 3200 cps for Hiperco 50 alloy 0.008-inch laminations. Test atmosphere, air to 800° F and argon above 800° F; interlaminar insulation, aluminum orthophosphate.

MAGNETIZING FORCE (AMPERE TURNS/INCH)
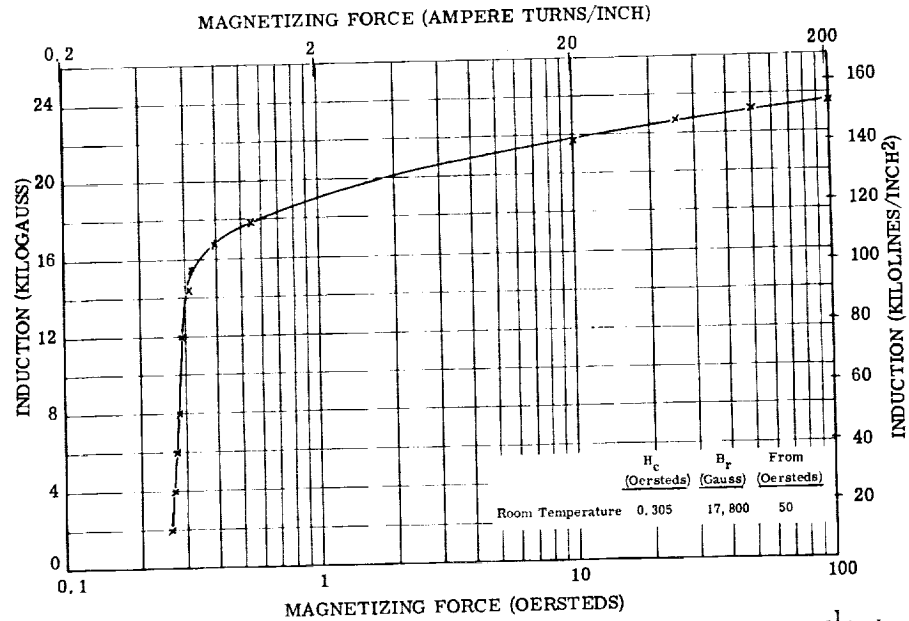
Figure 147. - Direct-current magnetization curves for Supermendur 0.002-inch tape toroid $3\frac{1}{2}$ by 4 by 1/2 inch. Test atmosphere, argon; interlaminar insulation, magnesium oxide.

MAGNETIZING FORCE (AMPERE TURNS/INCH)

Figure 148. - Direct-current magnetization curves for Supermendur 0.002-inch tape toroid $1\frac{1}{2}$ by 1 by 1/4 inch. Test atmosphere, air; interlaminar insulation, magnesium oxide.

MAGNETIZING FORCE (AMPERE TURNS/INCH)

	H_c (Oersteds)	B_r (Gauss)	From (Oersteds)
x Initial RT	0.309	16,200	100
O 300°F	0.347	14,000	100
△ 500°F	0.347	13,800	100
□ 800°F	0.359	12,000	100
◆ RT After 800°F	0.417	12,200	100

MAGNETIZING FORCE (OERSTEDS)

Figure 149. - Direct-current magnetization curves for Supermendur 0.006-inch laminations. Test atmosphere, argon; interlaminar insulation, aluminum orthophosphate.

VOLT-AMPERES PER POUND

Figure 150. - Exciting volt-amperes per pound at 400 cps for Supermendur 0.002-inch tape toroid $3\frac{1}{2}$ by 4 by 1/2 inch. Test atmosphere, argon; interlaminar insulation, magnesium oxide.

Figure 151. - Exciting volt-amperes per pound at 800 cps for Supermendur 0.002-inch tape toroid $3\frac{1}{2}$ by 4 by 1/2 inch. Test atmosphere, argon; interlaminar insulation, magnesium oxide.

Figure 152. - Exciting volt-amperes per pound at 1600 cps for Supermendur 0.002-inch tape toroid $3\frac{1}{2}$ by 4 by 1/2 inch. Test atmosphere, argon; interlaminar insulation, magnesium oxide.
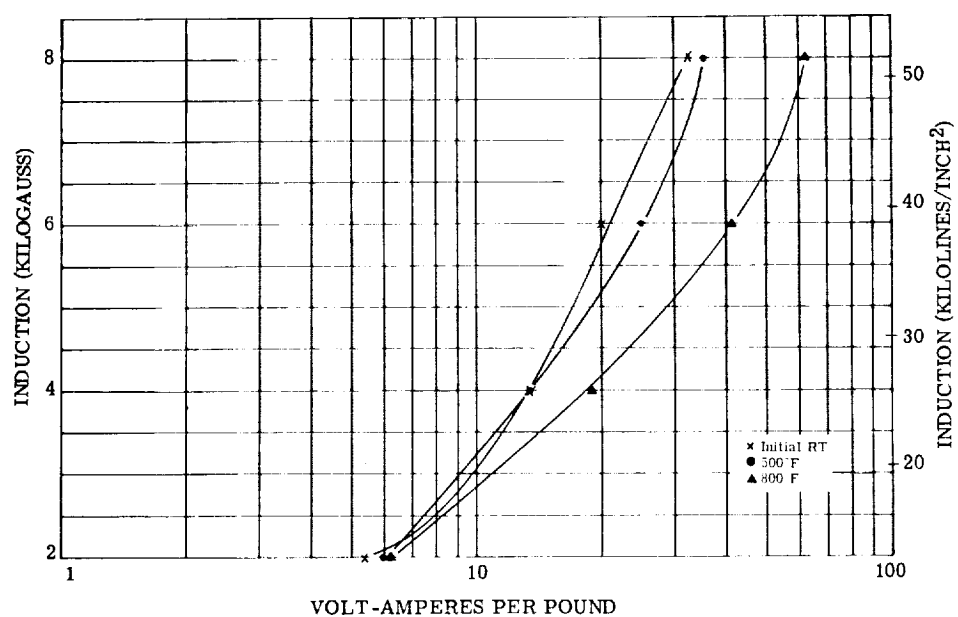
Figure 153. - Exciting volt-amperes per pound at 3200 cps for Supermendur 0.002-inch tape toroid $3\frac{1}{2}$ by 4 by 1/2 inch. Test atmosphere, argon; interlaminar insulation, magnesium oxide.
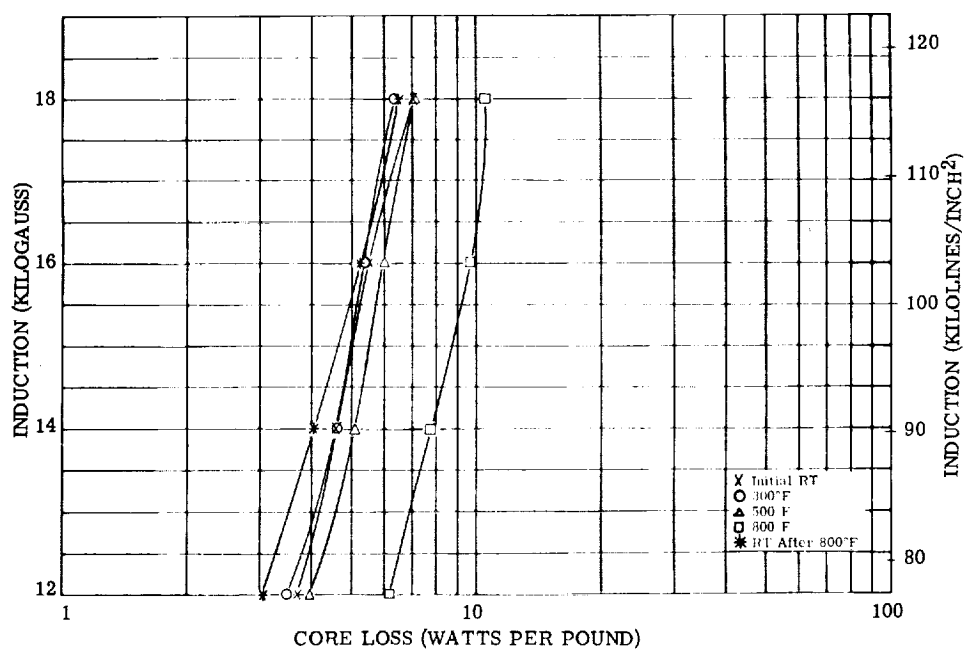
Figure 154. - Core loss at 400 cps for Supermendur 0.002-inch tape toroid $3\frac{1}{2}$ by 4 by 1/2 inch. Test atmosphere, argon; interlaminar insulation, magnesium oxide.
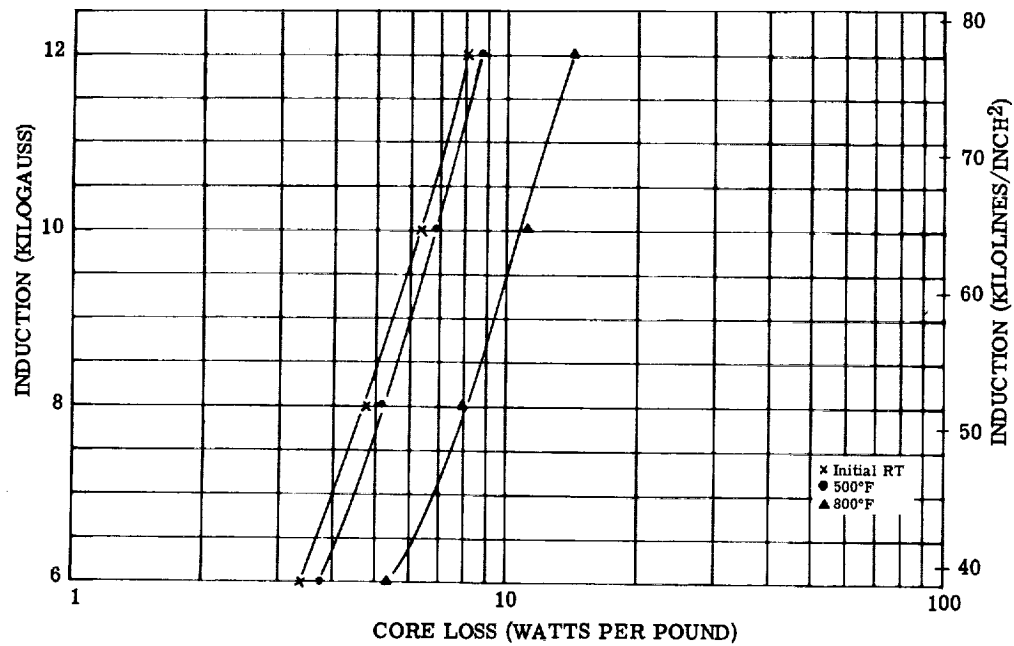
Figure 155. - Core loss at 800 cps for Supermendur 0.002-inch tape toroid $3\frac{1}{2}$ by 4 by 1/2 inch. Test atmosphere, argon; interlaminar insulation, magnesium oxide.
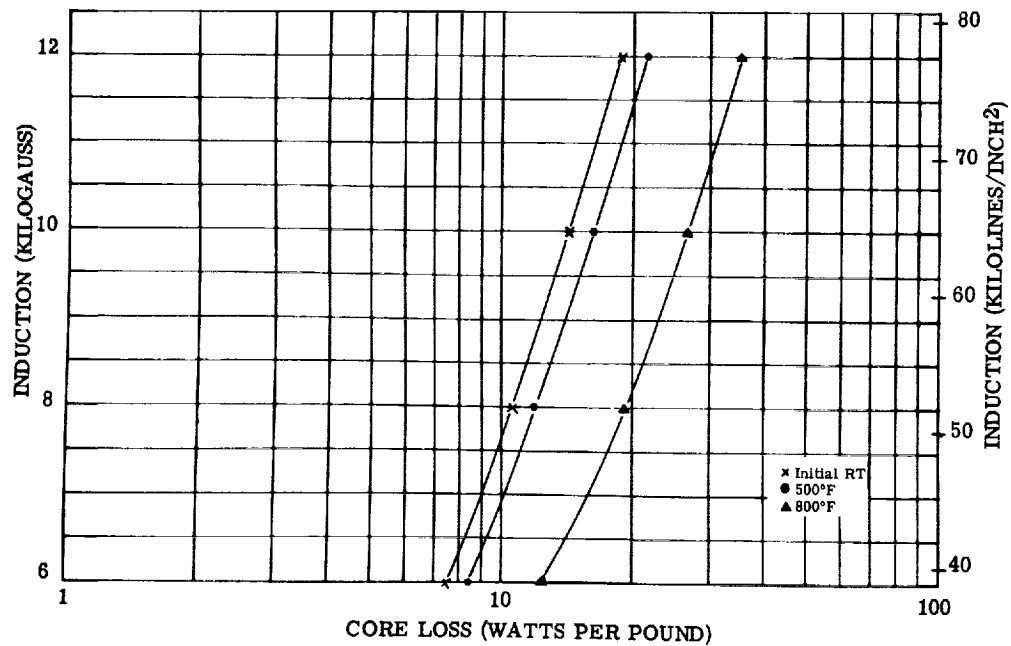
Figure 156. - Core loss at 1600 cps for Supermendur 0.002-inch tape toroid $3\frac{1}{2}$ by 4 by 1/2 inch. Test atmosphere, argon; interlaminar insulation, magnesium oxide.
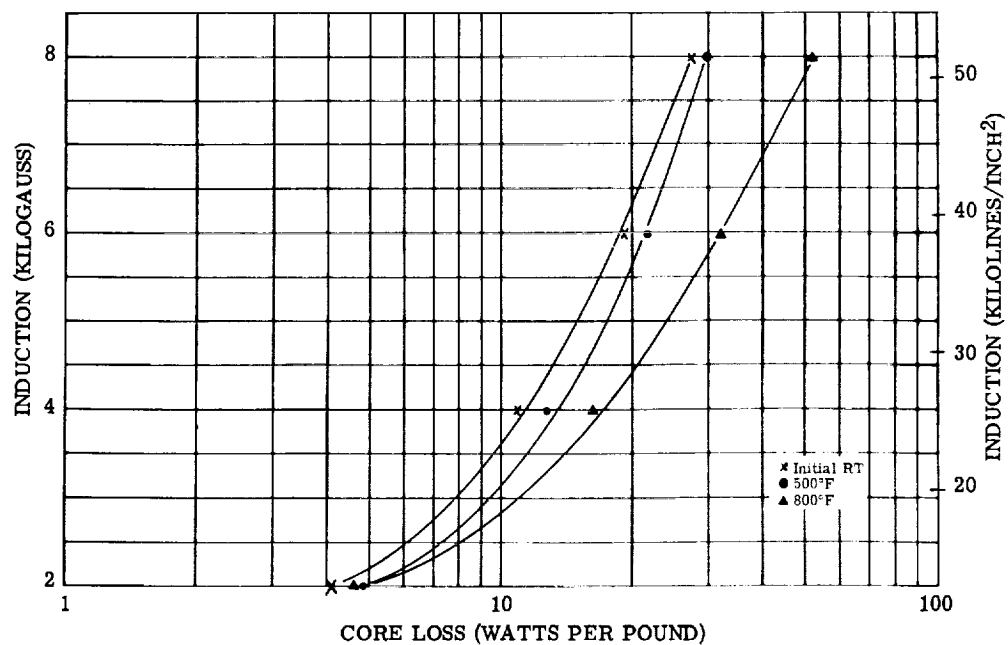
Figure 157. - Core loss at 3200 cps for Supermendur 0. 002-inch tape toroid $3\frac{1}{2}$ by 4 by 1/2 inch. Test atmosphere, argon; interlaminar insulation, magnesium oxide.
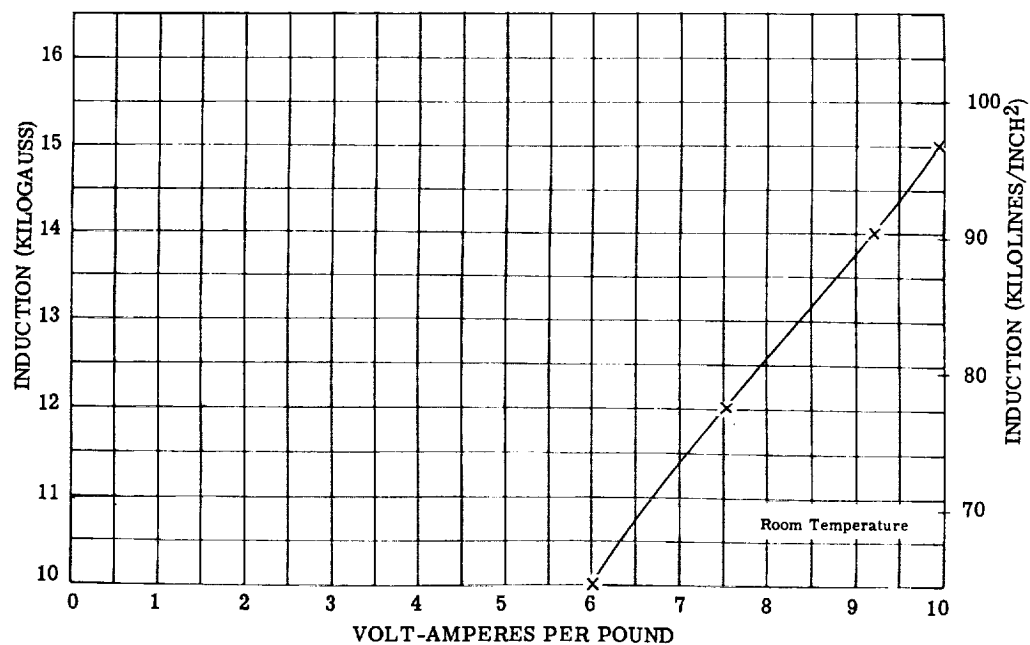
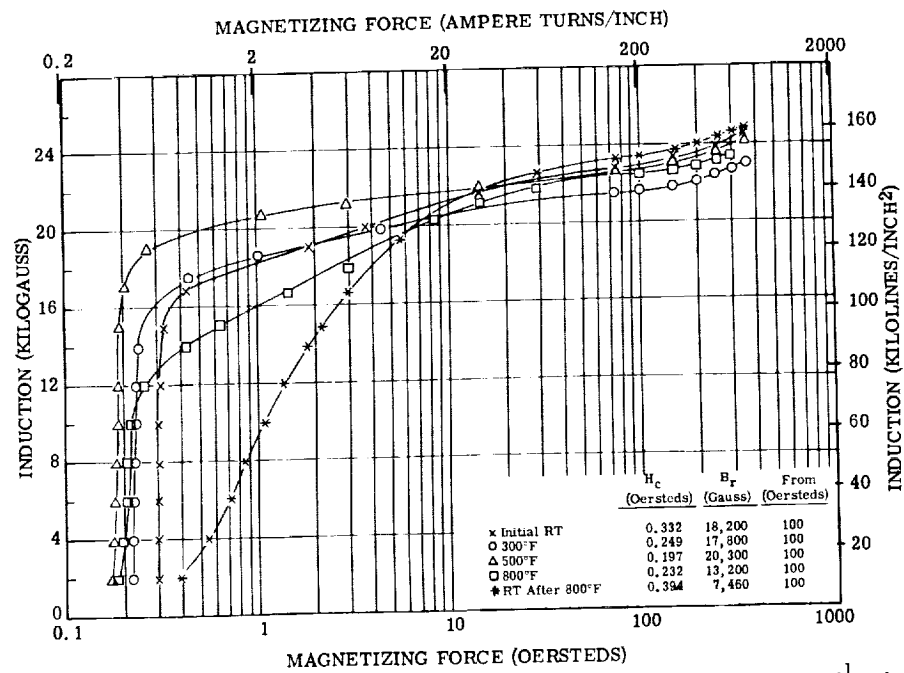Figure 158. - Exciting volt-amperes per pound at 400 cps for Supermendur 0. 002-inch tape toroid $1\frac{1}{4}$ by 1 by 1/4 inch. Test atmosphere, air; interlaminar insulation, magnesium oxide.
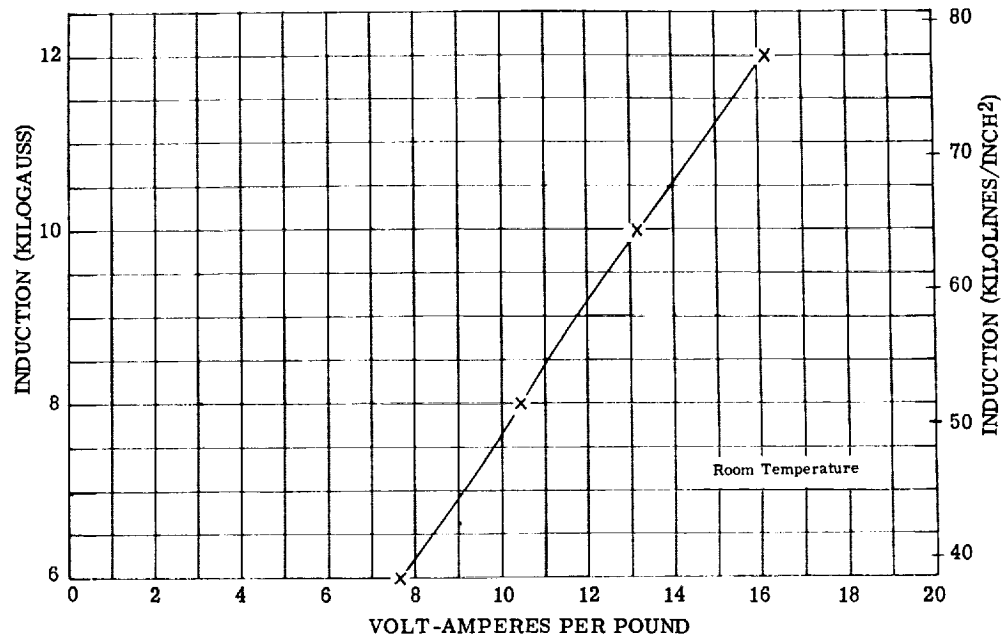
Figure 159. - Exciting volt-amperes per pound at 800 cps for Supermendur 0.002-inch tape toroid $1\frac{1}{4}$ by 1 by 1/4 inch. Test atmosphere, air; interlaminar insulation, magnesium oxide.
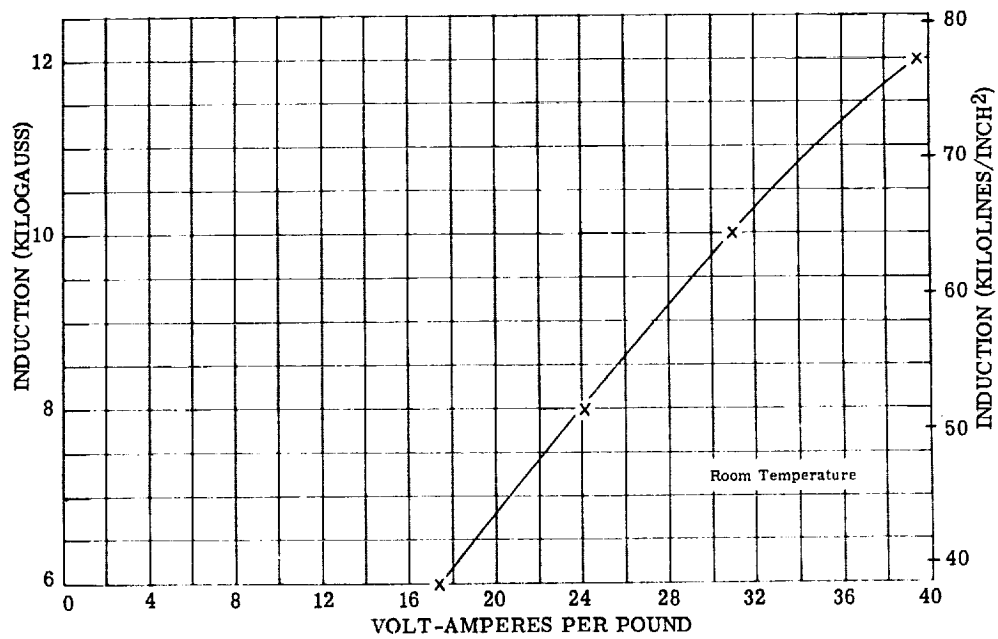
Figure 160. - Exciting volt-amperes per pound at 1600 cps for Supermendur 0.002-inch tape toroid $1\frac{1}{4}$ by 1 by 1/4 inch. Test atmosphere, air; interlaminar insulation, magnesium oxide.
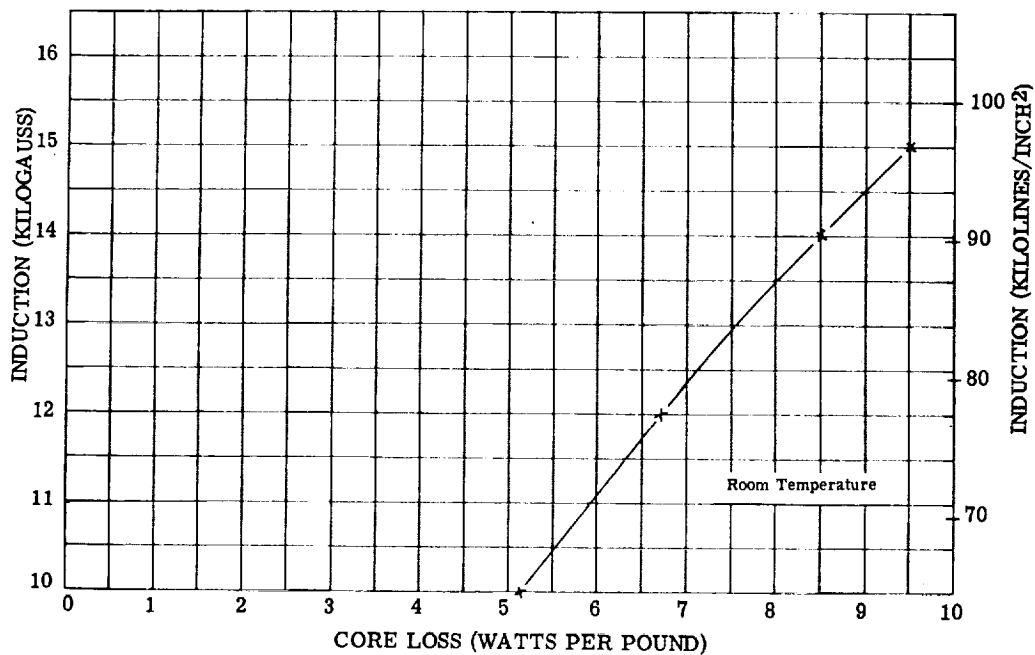
Figure 161. - Exciting volt-amperes per pound at 3200 cps for Supermendur 0.002-inch tape toroid $1\frac{1}{4}$ by 1 by 1/4 inch. Test atmosphere, air; interlaminar insulation, magnesium oxide.
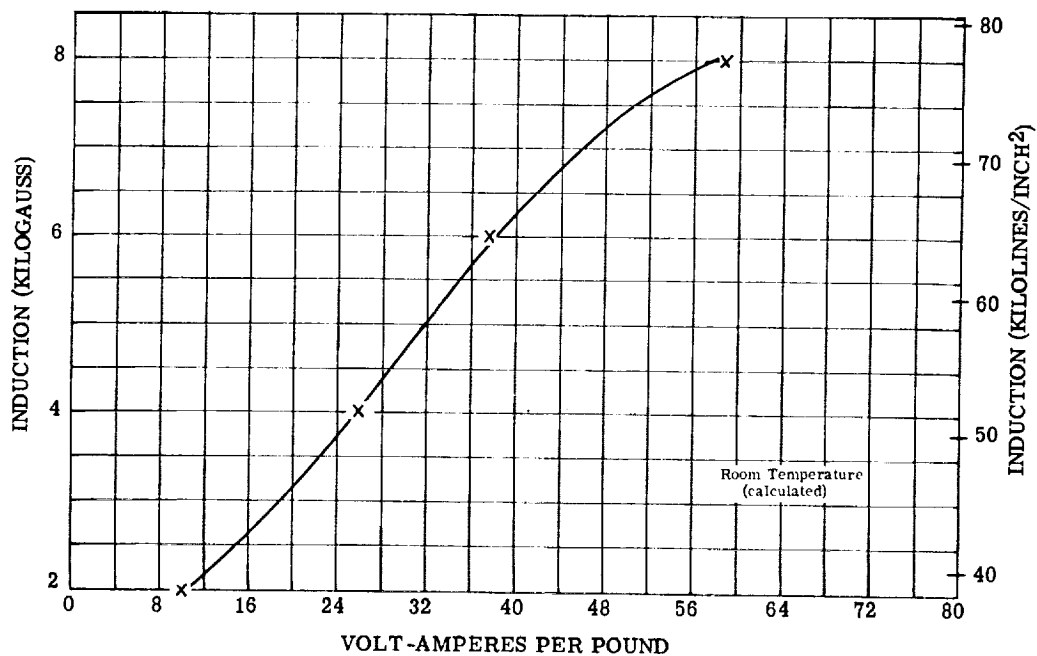
Figure 162. - Core loss at 400 cps for Supermendur 0.002-inch tape toroid $1\frac{1}{4}$ by 1 by 1/4 inch. Test atmosphere, air; interlaminar insulation, magnesium oxide.
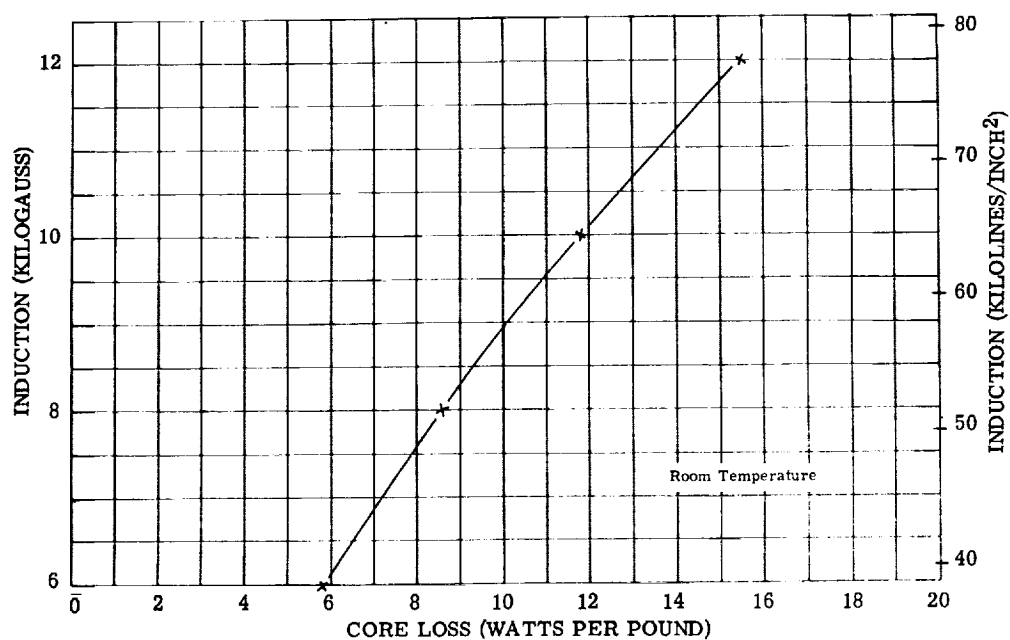
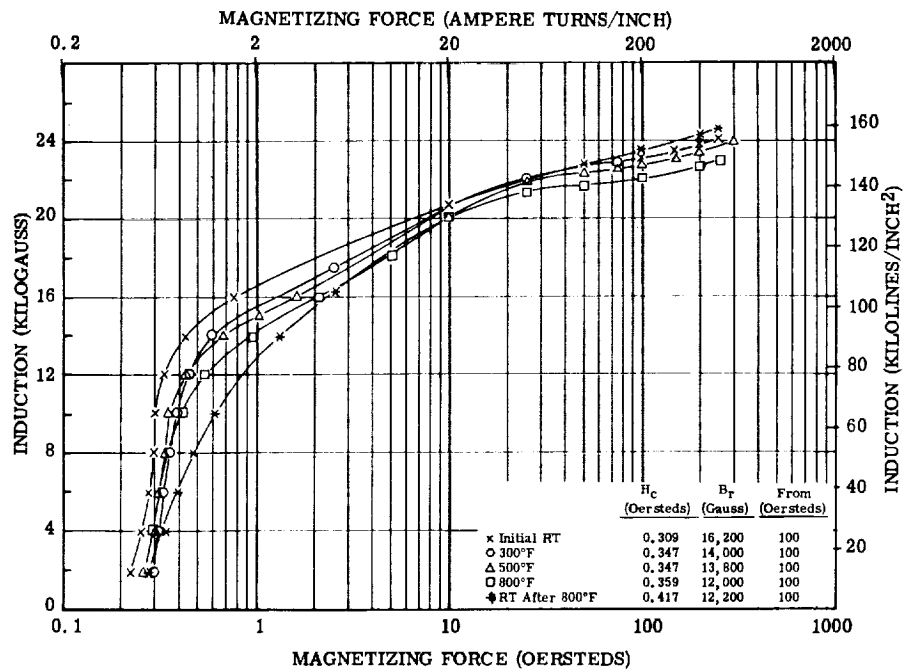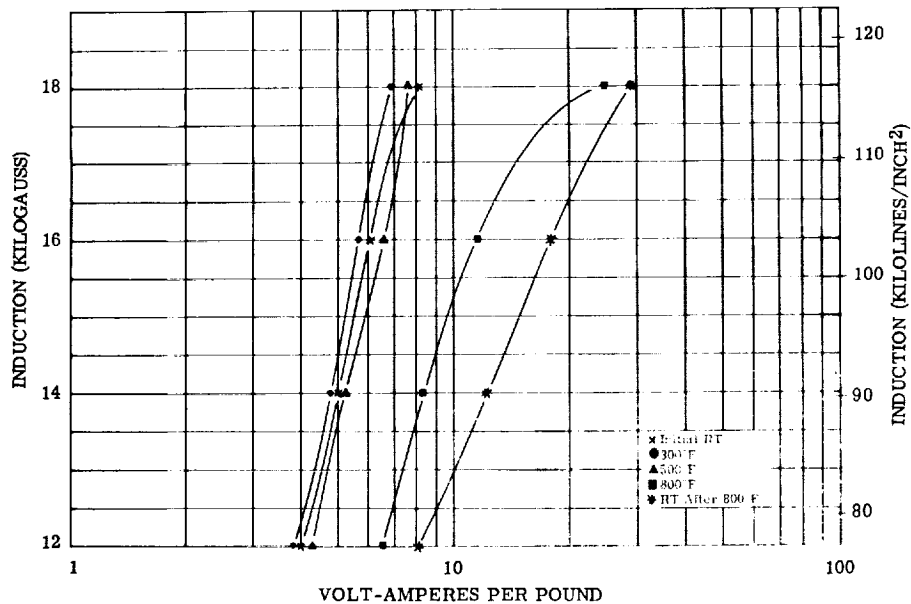Figure 163. – Core loss at 800 cps for Supermendur 0.002-inch tape toroid $1\frac{1}{4}$ by 1 by 1/4 inch. Test atmosphere air; interlaminar insulation, magnesium oxide.
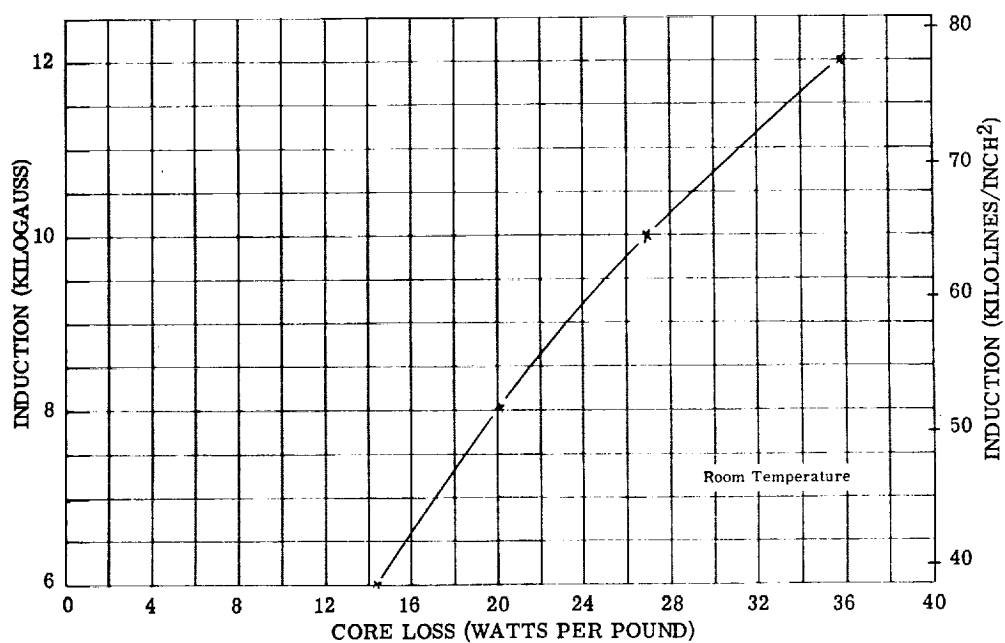
Figure 164. – Core loss at 1600 cps for Supermendur 0.002-inch tape toroid $1\frac{1}{4}$ by 1 by 1/4 inch. Test atmosphere, air; interlaminar insulation, magnesium oxide.
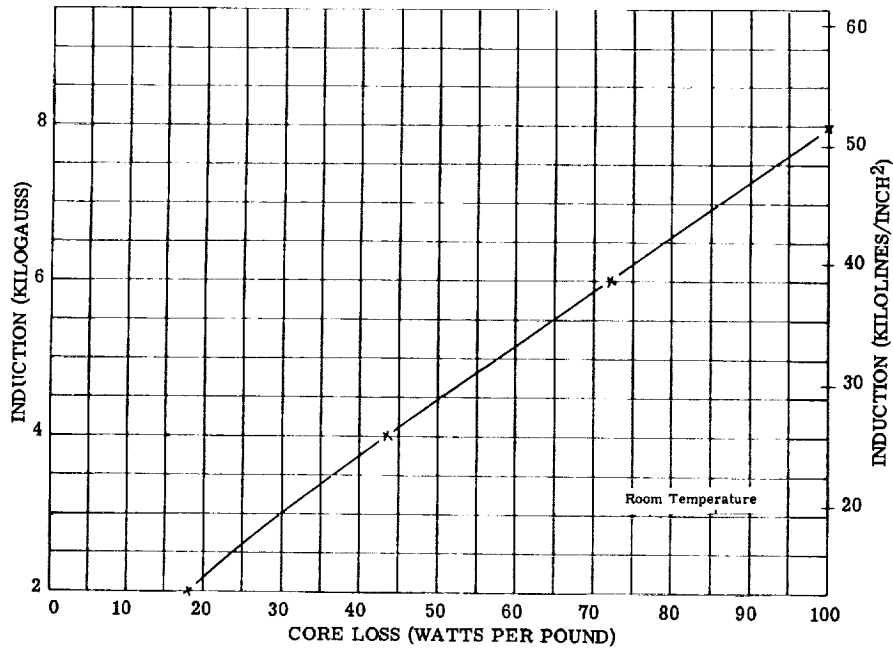
Figure 165. - Core loss at 3200 cps for Supermendur 0.002-inch tape toroid $1\frac{1}{4}$ by 1 by 1/4 inch. Test atmosphere, air; interlaminar insulation, magnesium oxide.
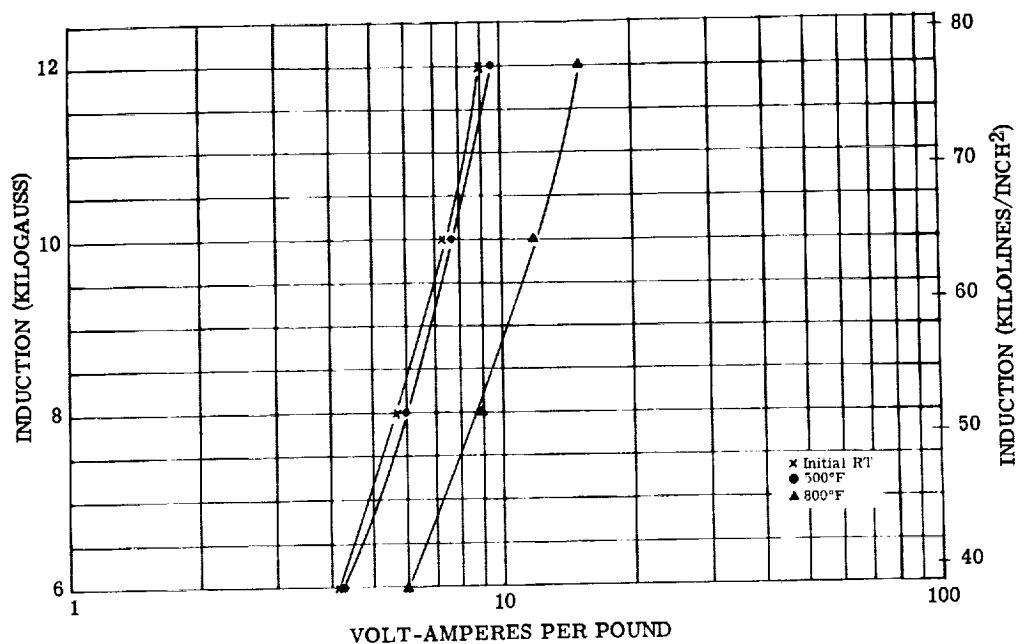

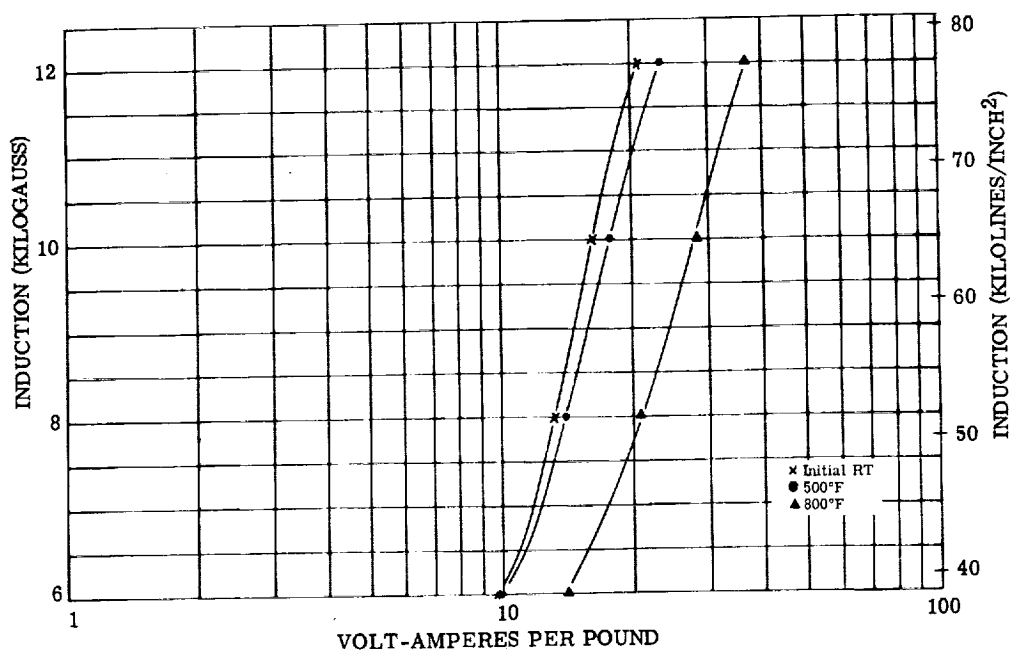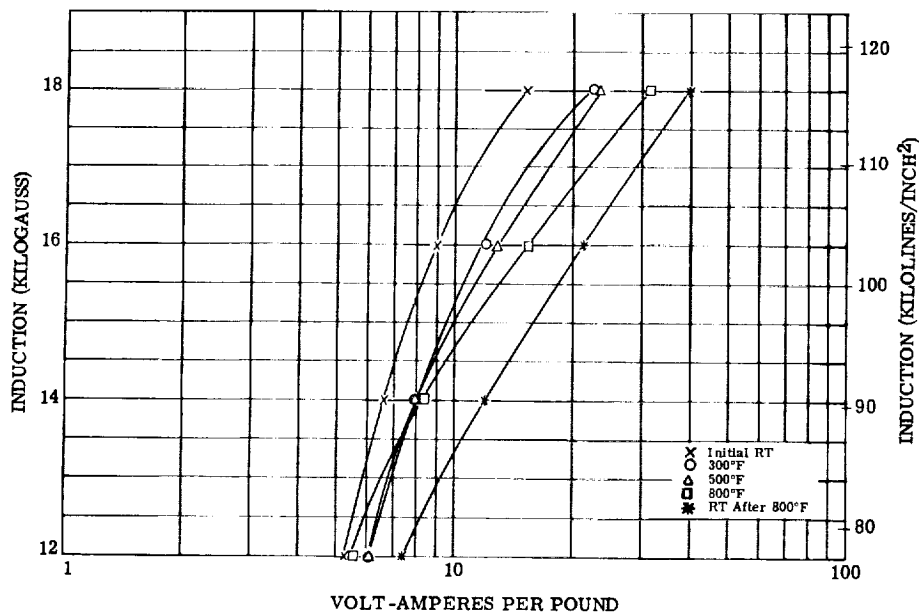Figure 166. - Exciting volt-amperes per pound at 400 cps for Supermendur 0.006-inch laminations. Test atmosphere, argon; interlaminar insulation, aluminum orthophosphate.
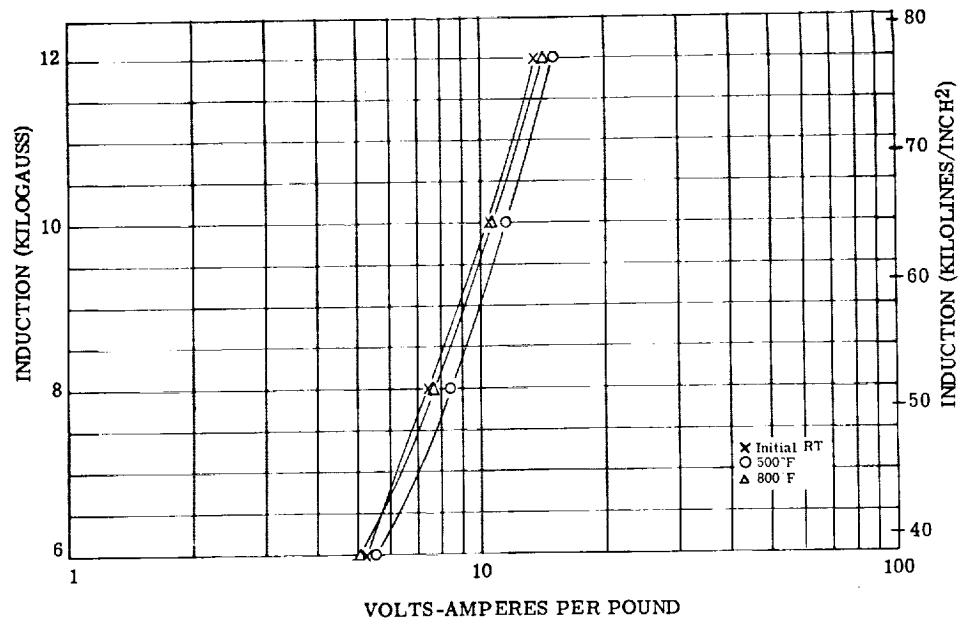
Figure 167. – Exciting volt-amperes per pound at 800 cps for Supermendur 0.006-inch laminations. Test atmosphere, argon; interlaminar insulation, aluminum orthophosphate.
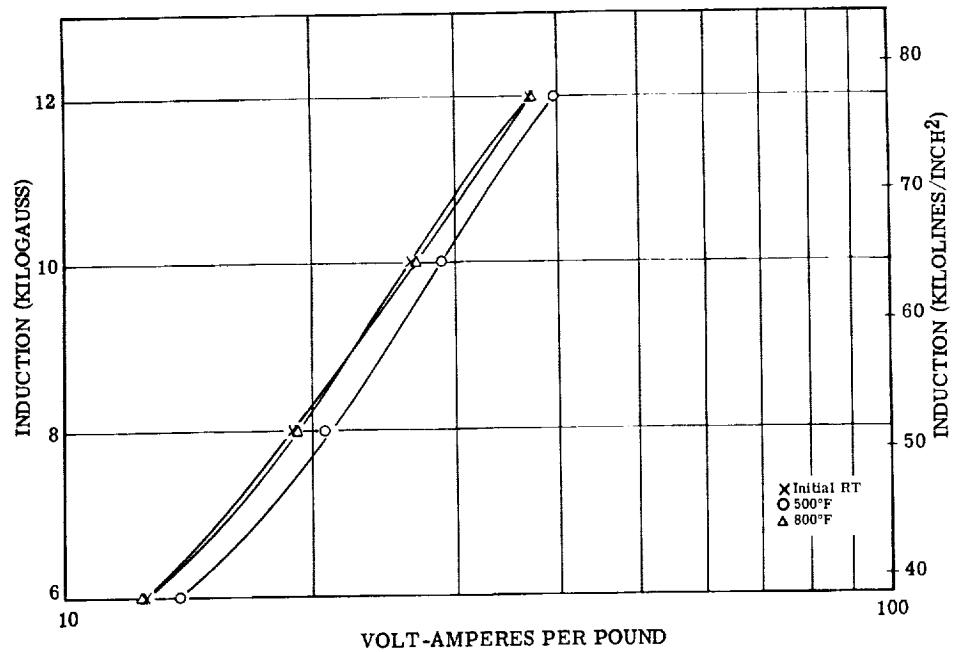
Figure 168. – Exciting volt-amperes per pound at 1600 cps for Supermendur 0.006-inch laminations. Test atmosphere, argon; interlaminar insulation, aluminum orthophosphate.
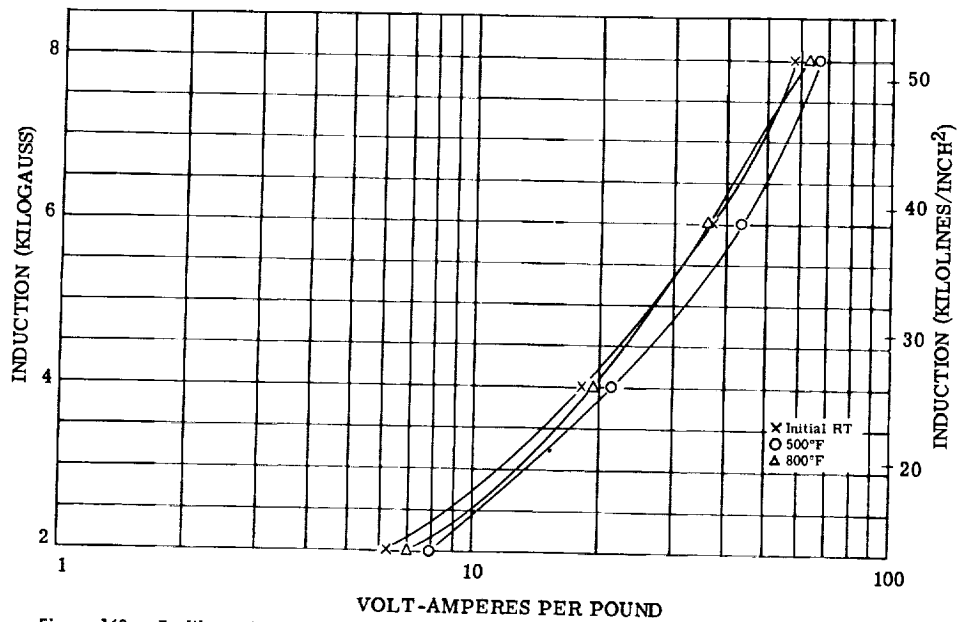
Figure 169. - Exciting volt-amperes per pound at 3200 cps for Supermendur 0.006-inch laminations. Test atmosphere, argon; interlaminar insulation, aluminum orthophosphate.
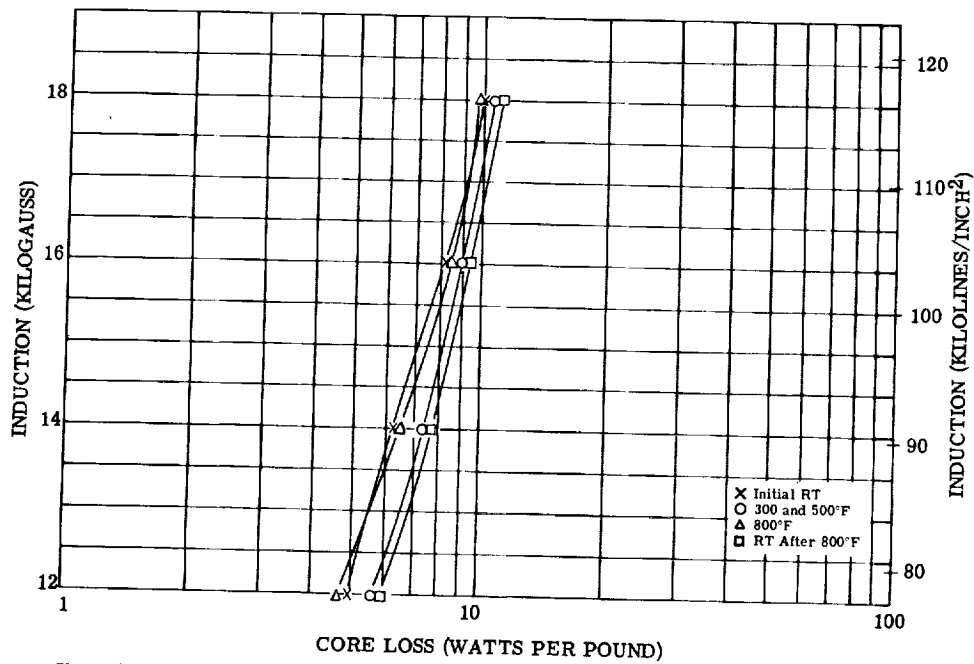
Figure 170. - Core loss at 400 cps for Supermendur 0.006-inch laminations. Test atmosphere, argon; interlamination insulation, aluminum orthophosphate.
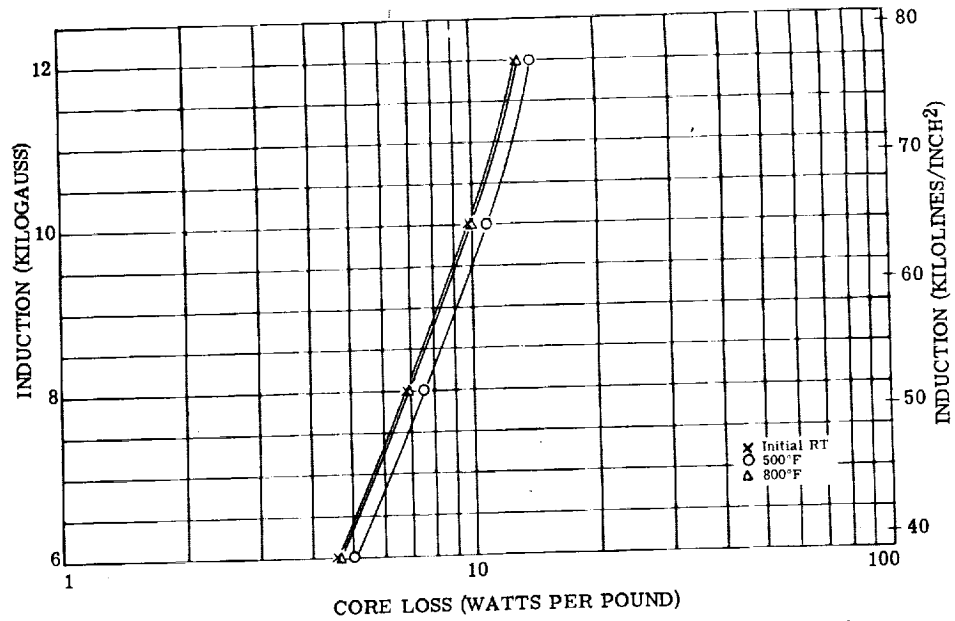
Figure 171. - Core loss at 800 cps for Supermendur 0.006-inch laminations. Test atmosphere, argon; interlaminar insulation, aluminum orthophosphate.
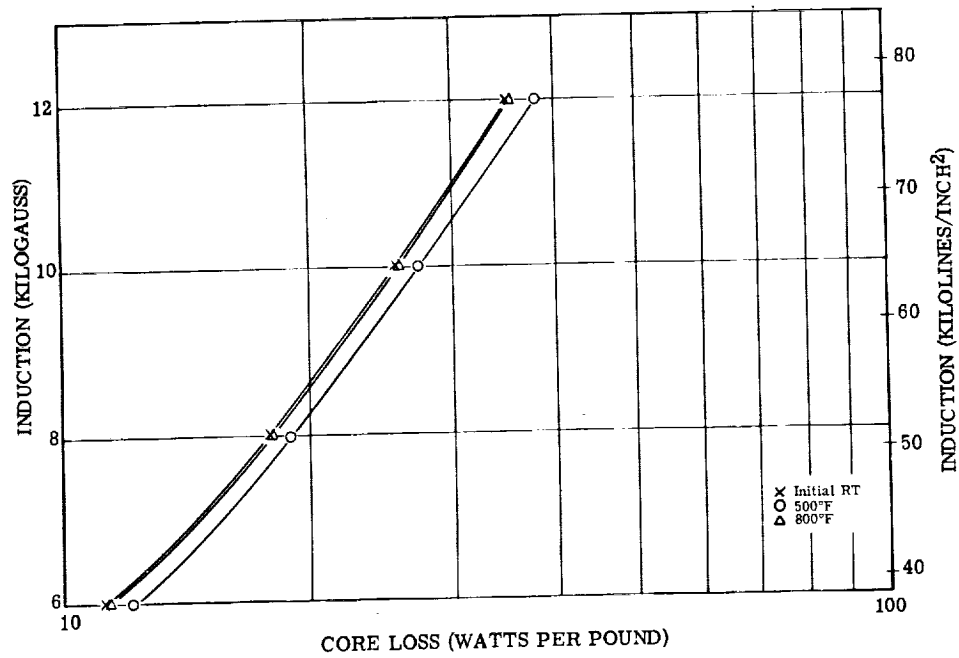
Figure 172. - Core loss at 1600 cps for Supermendur 0.006-inch laminations. Test atmosphere, argon; interlaminar insulation, aluminum orthophosphate.
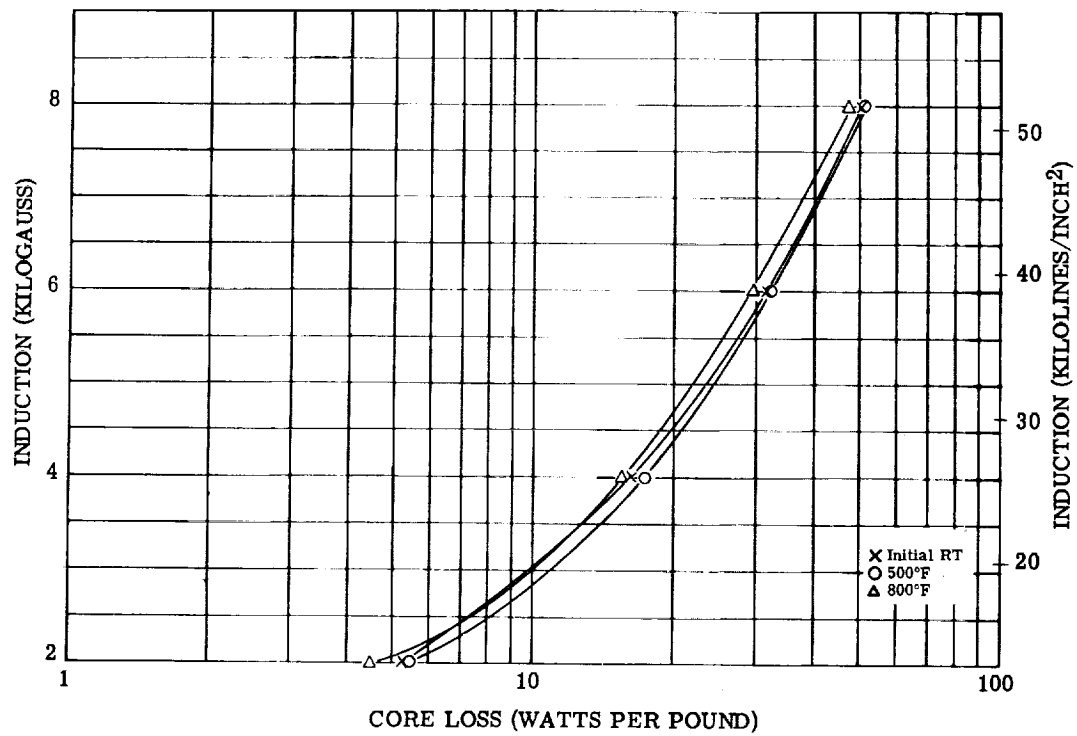
Figure 173. - Core loss at 3200 cps for Supermendur 0.006-inch laminations. Test atmosphere, argon; inter-
laminar insulation, aluminum orthophosphate.

TABLE 19. - TENSILE PROPERTIES OF ANNEALED HIPERCO 50 ALLOY

0.008-INCH-THICK SHEET TESTED IN AIR

[Test, ASTM E21; samples annealed at 875° C in dry hydrogen; see figs. 174 to 177.]

Mark (a)	Test temperature, °F	0.02 Percent offset yield strength, psi	0.2 Percent offset yield strength, psi	Ultimate strength, psi	Elongation in 2 in., percent (a)	Modulus of elasticity, psi
L-1	72	41 100	41 650	41 650	0.5 Q	28.9×10^6
T-1	72	36 800	(b)	37 700	Q	38.0
L-2	500	36 350	37 950	71 250	5.5 U	27.1
T-2	500	35 700	38 950	55 250	1.5 Q	33.2
L	800	30 250	36 750	67 900	7.0	27.0
T-5	800	30 600	38 050	60 150	4.9	29.7
L-4	1100	28 300	33 750	62 600	6.0 Q	20.1
T-4	1100	30 600	34 700	55 250	12.0	28.9
L-5	1400	5 450	6 400	8 400	27.0	--------
T-5	1400	9 750	------	10 850	9.0 Q	--------

[a]Legend: Q, quarter break; L, longitudinal; T, transverse; U, broke inside of end pads.

[b]Broke before 0.2 percent offset was reached.

$70 \leq T \leq 1400^\circ$ F, (0.02%) Tensile Stress = 1000 $[-0.14894 \times 10^{-9} T^4 + 0.4086 \times 10^{-6} T^3$
$- 0.3696 \times 10^{-3} T^2 + 0.1071$ T + 33.13] (Psi)
$70 \leq T \leq 1400^\circ$ F, (0.20%) Tensile Stress = 1000 $[-0.91975 \times 10^{-10} T^4 + 0.2105 \times 10^{-6} T^3$
$- 0.15547 \times 10^{-3} T^2 + 0.03353$ T + 39.995] (Psi)
$70 \leq T \leq 1400^\circ$ F, Ultimate Strength = 1000 $[-0.20623 \times 10^{-9} T^3 + 0.54715 \times 10^{-6} T^3$
$- 0.5353 \times 10^{-3} T^2 + 0.23131$ T + 25.924] (Psi)
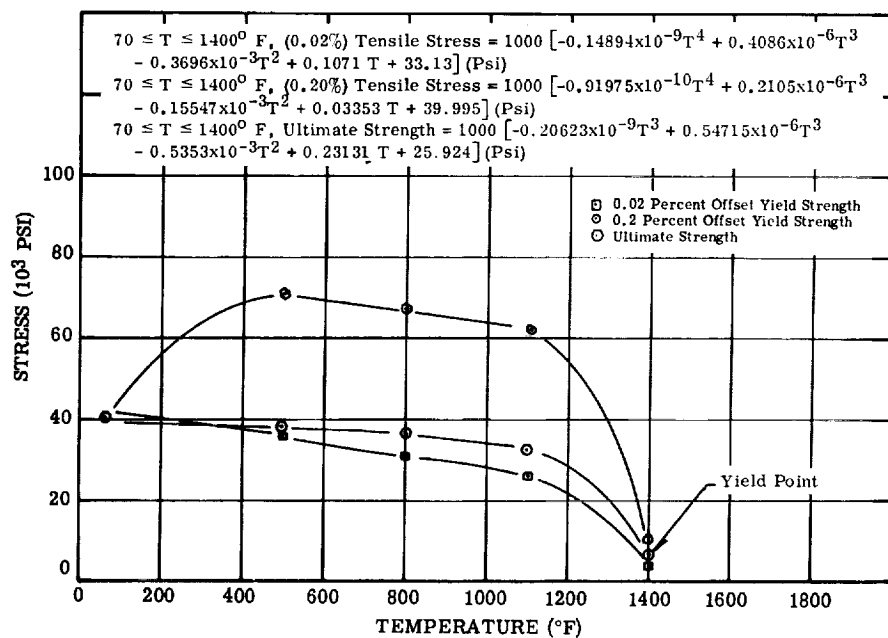
Figure 174. – Longitudinal tensile properties of 0.008-inch-thick annealed Hiperco 50 alloy sheet tested in air. (See table 19.)
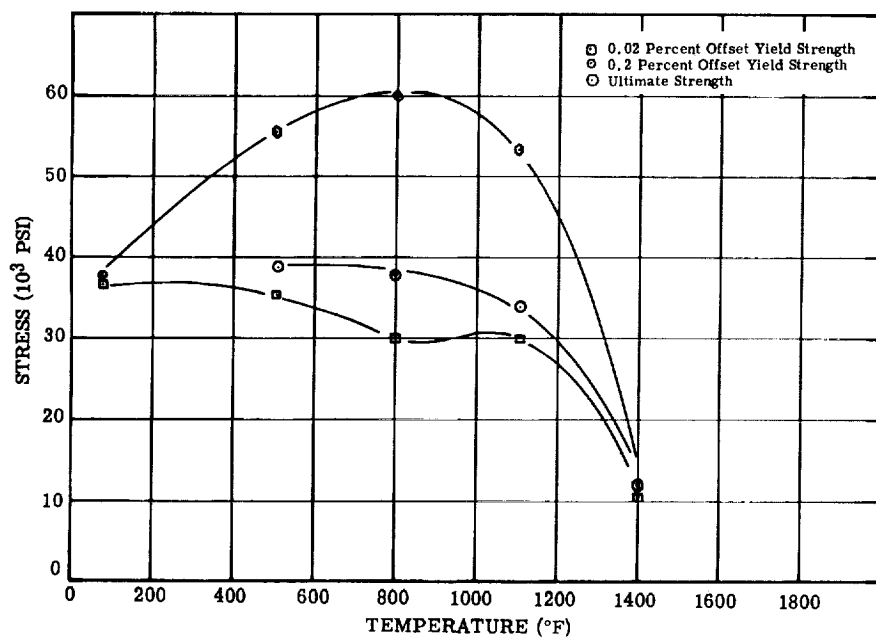
Figure 175. – Transverse tensile strengths of 0.008-inch-thick annealed Hiperco 50 alloy sheet tested in air. (See table 19.)
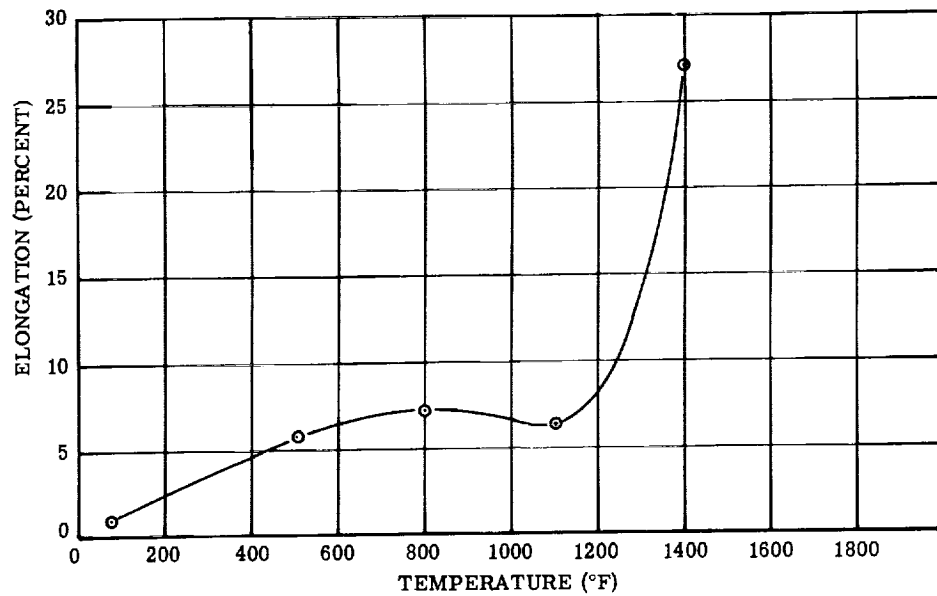
Figure 176. - Longitudinal tensile elongation of 0.008-inch-thick annealed Hiperco 50 alloy sheet tested in air. (See table 19.)
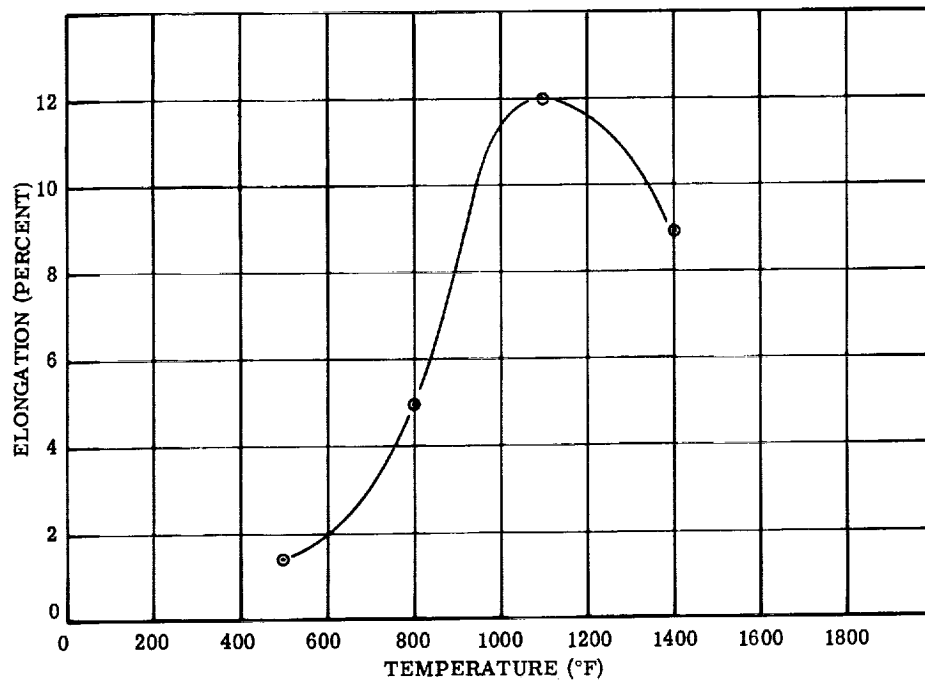
Figure 177. - Transverse tensile elongation of 0.008-inch-thick annealed Hiperco 50 alloy sheet tested in air. (See table 19.)

TABLE 20. - TENSILE TEST DATA FOR 0.006-INCH-THICK SUPERMENDUR SHEET

[Test, ASTM E21; samples annealed at 900° C in dry hydrogen; all tests made in air; see figs. 178 and 179.]

Specimen	Test temper- ature, °F	0.02 percent offset yield strength, psi	0.2 percent offset yield strength, psi	Yield point, psi	Ultimate strength, psi	Elongation in 2 in., percent	Modulus of elasticity, psi
1	72	33 800	(a)	------	35 500	0.4	34.7×10^6
2	72	37 350	------	38 000	51 150	3.3	--------
3	500	28 850	32 800	------	102 800	b10.9	32.8
4	500	30 000	32 700	------	96 150	8.7	--------
5	800	32 100	32 750	------	102 800	12.7	29.8
6	800	32 300	33 950	------	89 750	c9.2	--------
7	1100	27 600	31 150	------	54 100	11.5	28.5
8	1100	29 550	31 150	------	56 150	11.5	--------

aBroke before 0.2 percent offset was reached.
bBroke in fillet.
cBroke outside of punch marks.
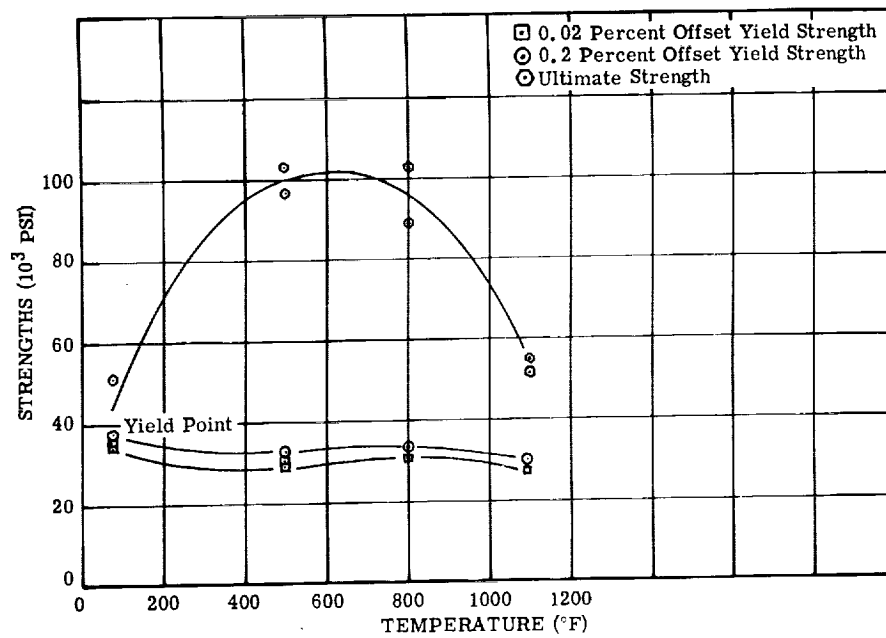
Figure 178. – Tensile properties of 0.006-inch-thick Supermendur sheet tested in air (samples cut longitudinally to rolling direction). (See table 20.)
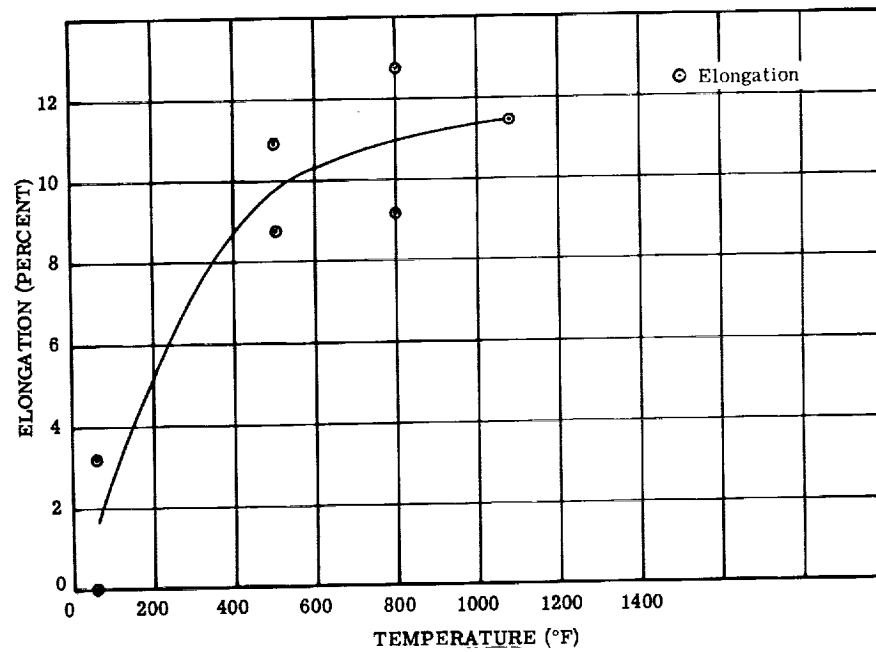
Figure 179. – Tensile elongation of 0.006-inch-thick Supermendur sheet tested in air (samples cut longitudinally to rolling direction). (See table 20.)

Hiperco 27 Alloy

Hiperco 27 alloy is a high permeability soft magnetic alloy manufactured only by the Westinghouse Electric Corporation, Blairsville, Pennsylvania. Available as sheet, bar, forgings, or castings, Hiperco 27 has a nominal composition of 27 percent cobalt-iron. Its tested composition was as follows:

	Ni	S	Mn	C	Co	P	Cr	Fe
	Composition, percent							
Bar	0.15	0.011	0.28	0.009	27.6	0.006	0.41	Bal.
Sheet	.14	.016	.39	.02	26.8	.009	.69	Bal.

Thermophysical properties. -

Density, lb/cu in. (g/cu cm) 0.285 (7.95)
Solidus temperature, ^{O}F 2732
Curie temperature, ^{O}F 1697
Thermal conductivity (ref. 10), (Btu)(ft)/(sq ft)(hr)(^{O}F), at -
72° F 31.7
1100° F 25.2
Coefficient of thermal expansion (from 72° to 1100° F) (ref. 10),
in./(in.)(^{O}F), at -
72° to 800° F . . . . 5.96×10^{-6}
72° to 1100° F . . . . 6.14×10^{-6}
Specific heat of vacuum melted forging, Btu/(lb)(^{O}F), at -
72° F 0.067
700° F 0.105
900° F 0.112
1100° F 0.119
Specific heat of investment casting, Btu/(lb)(^{O}F), at -
72° F 0.102
700° F 0.103
900° F 0.130
Electrical resistivity of vacuum melted forging, ohm-cm, at -
72° F . . . . 17.50×10^{-6}
900° F . . . . 39.56×10^{-6}
1100° F . . . . 50.33×10^{-6}

Magnetic properties. - All materials tested herein were stress-relief annealed unless otherwise specified. Constant current flux reset properties are not included for Hiperco 27 alloy, since they were measured only for materials used in magnetic amplifiers.

Direct current:

Temperature, ^oF	Annealed solid ring		Annealed lamination thickness, in.	
	Vacuum melted, forged	Investment cast	0.004	0.008
	Induction, B_{tip}, kG			
72	[a]24.9	[a]23.4	[b]24.2	[a]23.1
500	[a]24.6	[a]23.2	[b]23.4	[a]23.0
800	[a]24.0	[a]22.0	[b]22.3	[a]22.3
1100	[c]22.2	[c]20.5	[b]20.6	[a]20.8
1400	[c]19.0	[c]18.2	[a]17.6	[a]18.3

[a]H, 250 Oe.
[b]H, 300 Oe.
[c]H, 200 Oe.

Alternating current (400 cps) (B = 18 kG):

Temperature, ^oF	Lamination thickness, in.			
	0.004	0.008	0.004	0.008
	Exciting volt-amperes per pound		Core loss, W/lb	
72	270	275	27.6	34.7
500	290	294	----	----
700	---	---	23.1	27.8
800	325	308	----	----
900	---	---	18.2	23.6
1100	351	321	13.9	16.2
1400	315	524	----	14.3

Mechanical properties. - These properties were measured for Hiperco 27 bar stock and castings. Poisson's ratio at 72° F was 0.328. Fatigue was not measured, since Hiperco 27 alloy is not used in cyclically loaded operations. The normal heat treatment for material used in electromagnetic generators is to heat to 1472° to 1552° F in pure dry hydrogen and then to cool rapidly in the same atmosphere.

Tensile properties:

Temperature $^\circ$F	0.20-Percent offset yield strength, psi	Tensile strength, psi	Reduction in area, percent	Elongation, percent, in -		Modulus of elasticity, psi	Compressive modulus of elasticity, psi	0.20-Percent offset compressive yield strength, psi
				1 in.	2 in.			
Vacuum-melted bar stock								
72	82 450	95 000	75.2	----	28.2	33.9×10^6	31.4×10^6	97 600
700	53 500	86 400	75.5	----	25.2	26.8	$^a 27.3 \times 10^6$	$^a 80\ 950$
1000	50 050	64 600	41.2	----	12.4	23.6	$^b 25$	$^b 62\ 200$
Investment-cast bars								
72	43 900	64 200	0.80	2.0	----	--------	---------	-------
700	37 000	69 800	33.8	18	----	--------	---------	-------
1000	33 900	61 300	21.8	9.0	----	--------	---------	-------

[a]Obtained at 800° F.

[b]Obtained at 1100° F.

Creep for vacuum-melted bar stock tested in air: (Argon and vacuum test data are equivalent to air test data at 700° and 900° F. For creep testing of vacuum-melted bar stock tested in argon and vacuum above 900° F, refer to actual test data in figures and tables. For investment-cast bar stock tested in air and vacuum, see fig. 234, p. 201.)

Temper-ature, °F	Time, hr	Stress, psi, to produce plastic strain of -	
		0.20 Percent	0.40 Percent
700	1 000	62 000	66 500
700	10 000	53 000	60 000
900	1 000	33 700 to 36 500	39 800 to 41 800
900	10 000	26 800 to 29 200	33 800 to 35 600
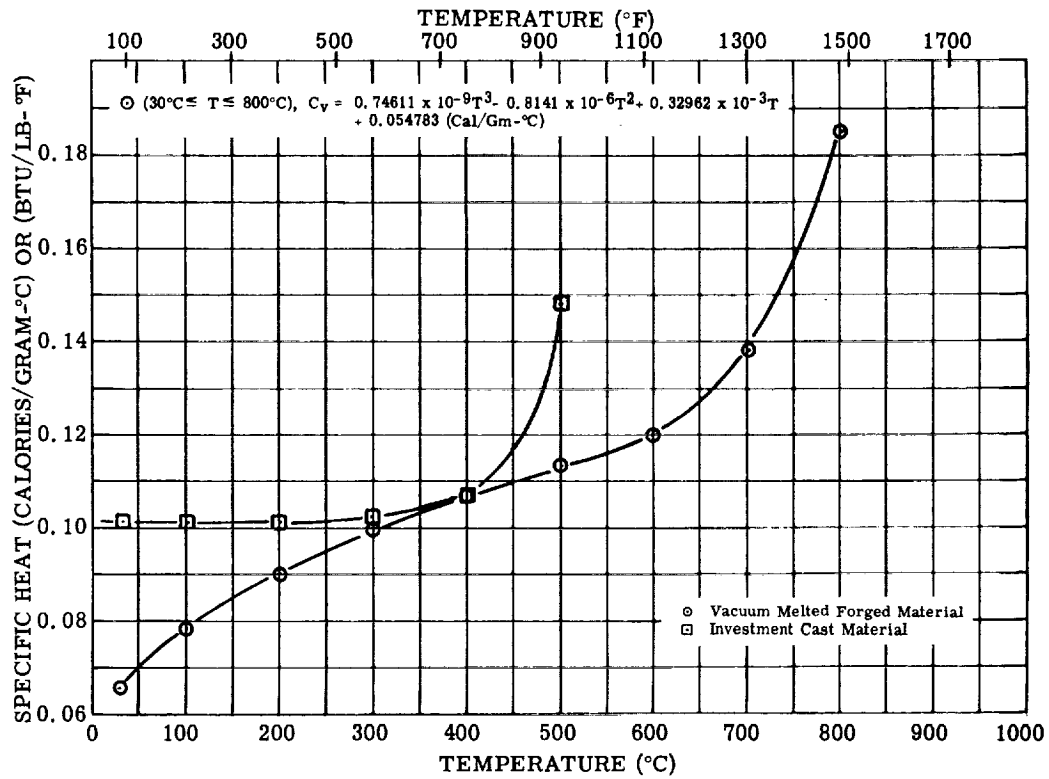
Figure 180. - Specific heat of vacuum-melted forged and investment cast Hiperco 27 alloy tested in vacuum (10^{-5} torr).

TABLE 21. - ELECTRICAL RESISTIVITY

OF VACUUM-MELTED FORGED

HIPERCO 27 ALLOY[a]

[Specimen 1 with continuous heating in
vacuum; wire diameter, 0.1253 in.; test
length, 11.32 in.; test, ASTM B193.]

Temperature, °F	Resistance, ohms	Resistivity, microhm-cm
77	0.006300	17.43
200	.006770	18.73
300	.007345	20.32
437	.008369	23.15
500	.008969	24.81
619	.01020	28.22
705	.01134	31.37
800	.01265	35.00
900	.01430	39.56
1000	.01616	44.71
1100	.01819	50.33
1200	.02050	56.72
1300	.02304	63.75
1400	.02578	71.33
1245	.02190	60.59
1050	.01745	48.28
850	.01384	38.29
650	.01102	30.49
445	.009010	24.93
250	.007445	20.60
150	.006689	18.51
79	.006180	17.10

[a]These data are plotted on fig. 181.
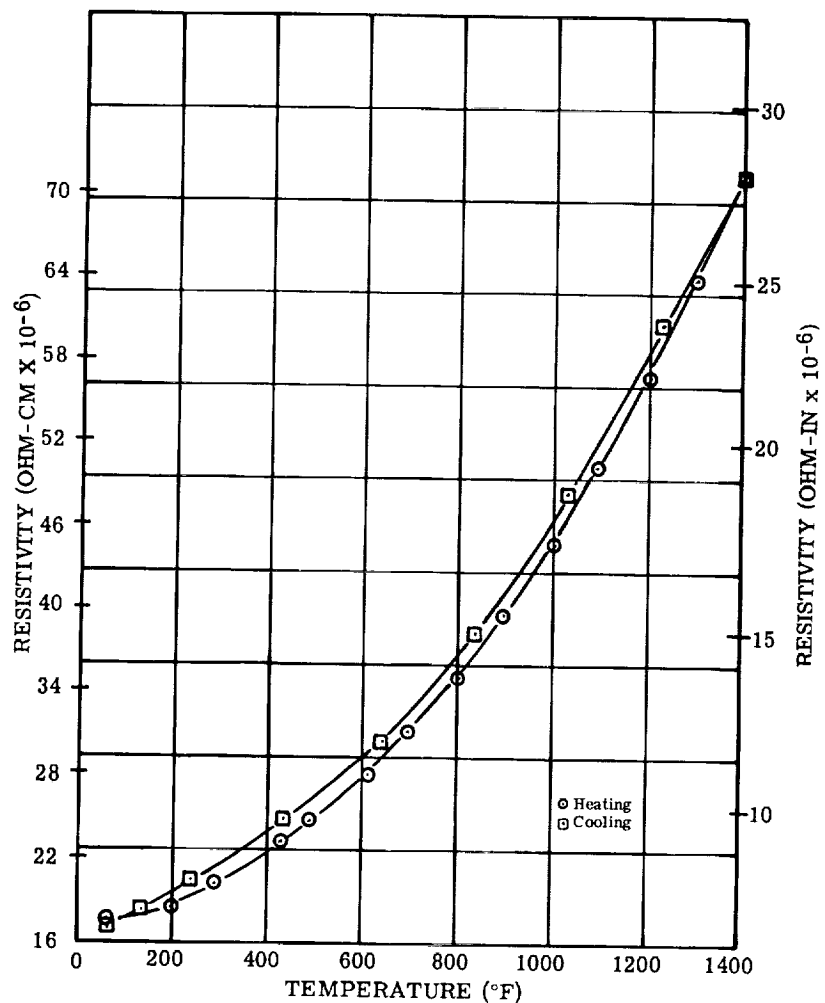
Figure 181. - Electrical resistivity of vacuum-melted forged Hiperco 27 alloy
tested in vacuum (10⁻⁴ torr). (See table 21.)

TABLE 22. - MAGNETIC PROPERTIES OF HIPERCO 27 ALLOY RING LAMINATIONS 0.008-INCH THICK AFTER

HIGH-TEMPERATURE ANNEALING AND RECOATING WITH ALUMINUM ORTHOPHOSPHATE

[Test, ASTM A343 in air at 72° F; heat treatment of samples 1, 2, and 3 conducted in vacuum; heat treatment of samples 4 and 5 conducted in hydrogen.]

	Sample 1		Sample 2			Sample 3		Sample 4		Sample 5	
	72° F	72° F After 1400° F	72° F	72° F After 1400° F	72° F After 1400° F; recoated	72° F	72° F After 1400° F; recoated	72° F	72° F After 1400° F	72° F	72° F; 1000 hr at 1000° F
dc tests											
B, kG, at -											
H, Oe											
250	23.15	23.1	23.3	23.0	22.6	23.2	23.1	23.1	23.1	23.4	23.0
100	20.8	20.6	20.9	20.25	19.85	20.75	20.4	20.45	20.5	21.0	20.45
H, Oe, for B = 10 kG	2.67	1.12	3.29	2.01	3.99	3.43	1.81	5.16	3.52	5.24	5.19
$^a H_c$, Oe	1.69	1.35	1.60	1.17	1.12	1.53	0.85	1.36	1.30	1.41	1.37
$^a B_r$, kG	10.1	12.3	9.3	10.85	9.45	8.9	10.7	6.65	9.5	7.1	7.45
400-cps tests											
Core loss, W/lb, for -											
B, kG											
12	18.37	17.10	17.29	22.64	20.9	16.46	16.42	18.32	15.36	^{b}18.32	18.96
14	22.72	22.45	21.93	29.04	27.0	20.58	21.34	23.4	25.9	23.4	24.44
16	27.76	56.50	25.72	37.10	31.88	25.27	27.55	28.7	32.4	28.7	31.06
18	33.47	70.62	30.88	46.12	42.60	30.82	33.88	34.7	40.28	34.7	39.09

^{a}Taken from induction corresponding to a field of 100 Oe.
^{b}Core loss properties were not measured originally on this sample. For comparison, core loss data in this column were taken from sample 4.

MAGNETIZING FORCE (AMPERE TURNS/INCH)

		H$_c$	B$_r$	From
		(Oersteds)	(Gauss)	(Oersteds)
x	Initial R. T.	5.12	11,000	100
o	500°F	4.82	10,300	100
Δ	800°F	4.43	9,900	100
□	1100°F	3.54	10,950	100
*	1400°F	2.64	12,000	100
+	R. T. After 1400°F	5.12	17,100	100

MAGNETIZING FORCE (OERSTEDS)
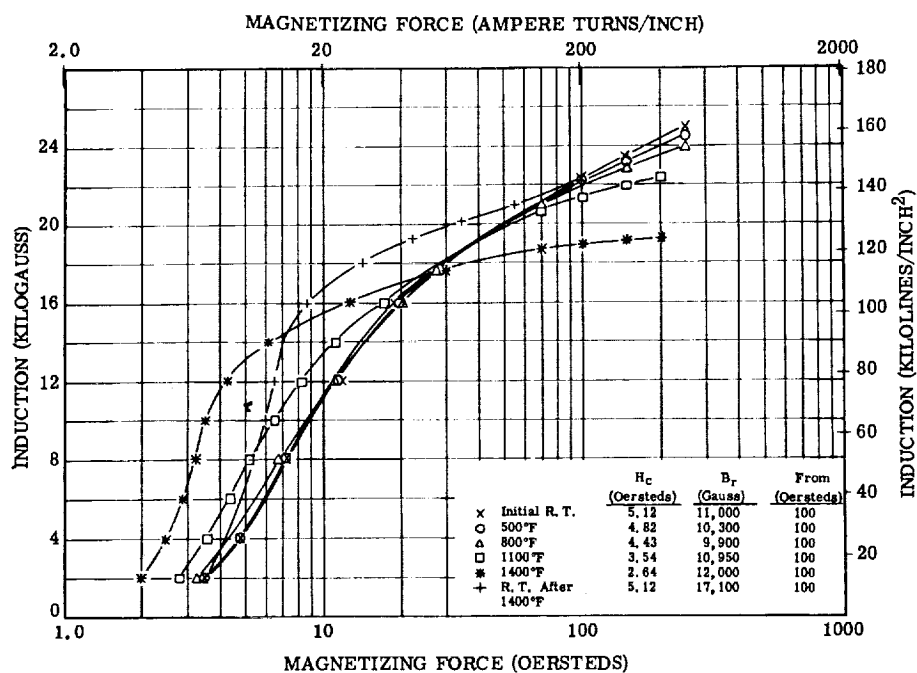
Figure 182. - Direct-current magnetization curves for Hiperco 27 alloy forging tested in argon.

MAGNETIZING FORCE (AMPERE TURNS/INCH)

		H$_c$	B$_r$	From
		(Oersteds)	(Gauss)	(Oersteds)
x	Initial R. T.	3.40	9,800	100
o	500°F	3.10	9,000	100
Δ	800°F	2.76	8,150	100
□	1100°F	2.32	8,000	100
*	1400°F	1.79	7,800	100
+	R.T. After 1400°F	3.21	10,700	100

MAGNETIZING FORCE (OERSTEDS)
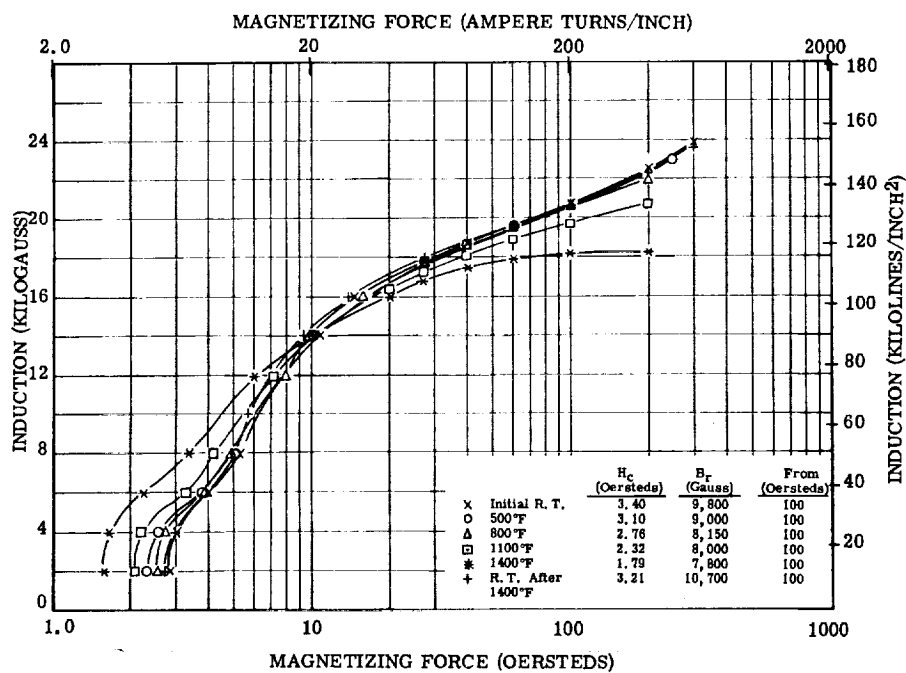
Figure 183. - Direct-current magnetization curves for Hiperco 27 alloy casting tested in air.

MAGNETIZING FORCE (AMPERE TURNS/INCH)

From (Oersteds)	B_r (Gauss)	From (Oersteds)

		From (Oersteds)	B_r (Gauss)	From (Oersteds)
●	Initial R.T.	1.71	6,000	100
○	500° F	1.50	5,100	100
△	800° F	1.29	2,900	100
□	1100° F	0.956	6,300	100
✳	1400° F	0.739	6,800	100
+	R.T. After 1400° F	1.89	9,100	100

MAGNETIZING FORCE (OERSTEDS)
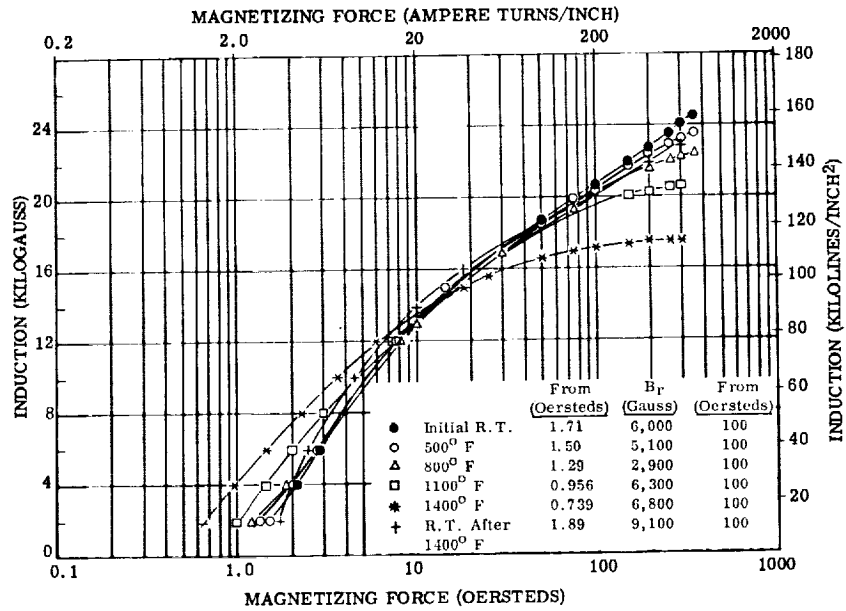
Figure 184. - Direct-current magnetization curves for Hiperco 27 alloy 0.004-inch laminations. Test atmosphere, air to 800° F and argon above 800° F; interlaminar insulation, mica aluminum orthophosphate bentonite.

MAGNETIZING FORCE (AMPERE TURNS/INCH)

		H_c (Oersteds)	B_r (Gauss)	From (Oersteds)
X	Initial R.T.	1.69	10,100	100
○	500° F	1.46	9,000	100
△	R.T. After 1400°	1.35	12,300	100

MAGNETIZING FORCE (OERSTEDS)

Figure 185. - Direct-current magnetization curves for Hiperco 27 alloy 0.008-inch laminations, sample 1. Test atmosphere, air to 800° F and argon above 800° F; interlaminar insulation, mica aluminum orthophosphate bentonite.

Figure 186. - Direct-current magnetization curves for Hiperco 27 alloy 0.008-inch laminations tested at 800°, 1100°, and 1400° F, sample 1. Test atmosphere, air to 800° F and argon above 800° F; interlaminar insulation, mica aluminum orthophosphate bentonite.

Figure 187. - Direct-current magnetization curves for Hiperco 27 alloy 0.008-inch laminations, sample 2. Test atmosphere, air to 800° F, and argon above 800° F; interlaminar insulation, aluminum orthophosphate.

Figure 188. - Direct-current magnetization curves for Hiperco 27 alloy 0.008-inch laminations tested at room temperature, 800°, and 1100° F, sample 2. Test atmosphere, air to 800° F and argon above 800° F; interlaminar insulation, aluminum orthophosphate.

Figure 189. - Direct-current magnetization curves for Hiperco 27 alloy 0.008-inch laminations, sample 3. Test atmosphere, air to 800° F and argon above 800° F; interlaminar insulation, aluminum orthophosphate.

MAGNETIZING FORCE (AMPERE TURNS/INCH)

Figure 190. - Direct-current magnetization curves for Hiperco 27 alloy 0.008-inch laminations tested at 800°, 1100°, and 1400° F, sample 3. Test atmosphere, air to 800° F and argon above 800° F; interlaminar insulation, aluminum orthophosphate.

MAGNETIZING FORCE (AMPERE TURNS/INCH)

Figure 191. - Direct-current magnetization curves for Hiperco 27 alloy 0.008-inch laminations, sample 4. Test atmosphere, argon; interlaminar insulation, mica aluminum orthophosphate bentonite.

Figure 192. - Direct-current magnetization curves for Hiperco 27 alloy 0.008-inch laminations, aging test, sample 5. Test atmosphere, argon; interlaminar insulation, mica aluminum orthophosphate bentonite.

Figure 193. - Exciting volt-amperes per pound at 400 cps for Hiperco 27 alloy 0.004-inch laminations. Test atmosphere, air to 800° F and argon above 800° F; interlaminar insulation, mica aluminum orthophosphate bentonite.

Figure 194. - Exciting volt-amperes per pound at 800 cps for Hiperco 27 alloy 0. 004-inch laminations. Test atmosphere, air to 800° F and argon above 800° F; interlaminar insulation, mica aluminum orthophosphate bentonite.

Figure 195. - Exciting volt-amperes per pound at 1600 cps for Hiperco 27 alloy 0. 004-inch laminations. Test atmosphere, air to 800° F and argon above 800° F; interlaminar insulation, mica aluminum orthophosphate bentonite.
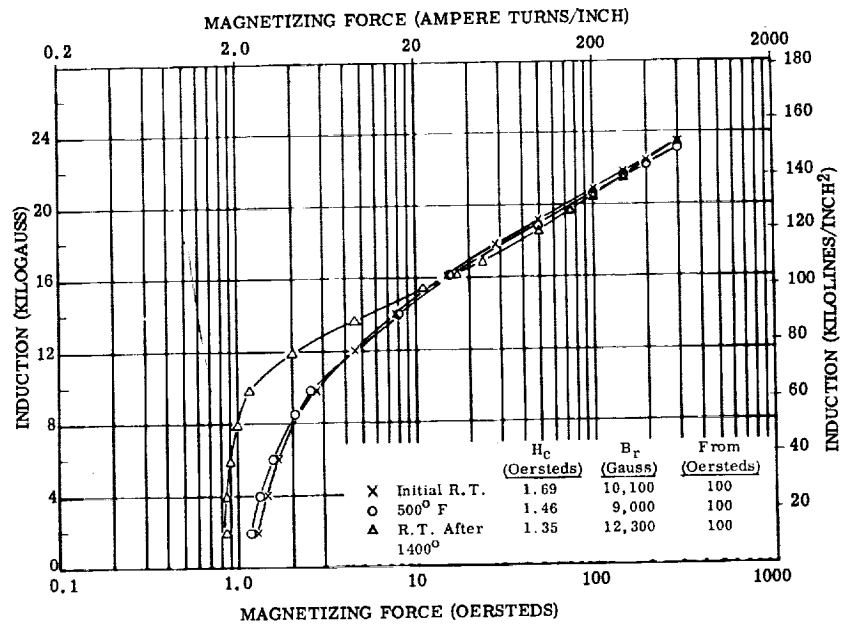
Figure 196. - Exciting volt-amperes per pound at 3200 cps for Hiperco 27 alloy 0. 004-inch laminations. Test atmosphere, air to 800° F and argon above 800° F; interlaminar insulation, mica aluminum orthophosphate bentonite.
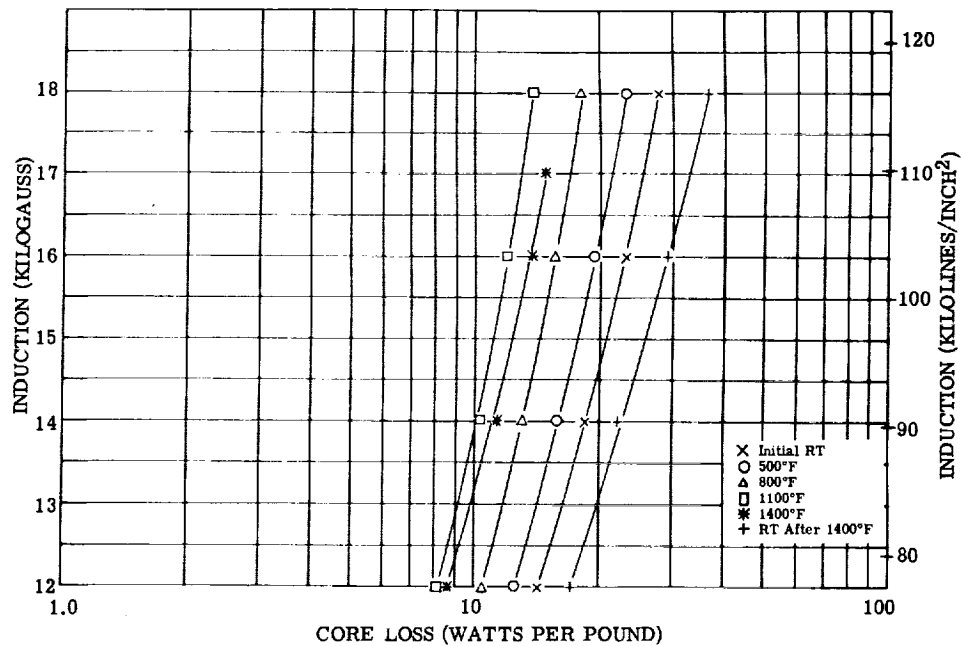
Figure 197. - Core loss at 400 cps for Hiperco 27 alloy 0. 004-inch laminations. Test atmosphere, air to 800° F and argon above 800° F; interlaminar insulation, mica aluminum orthophosphate bentonite.
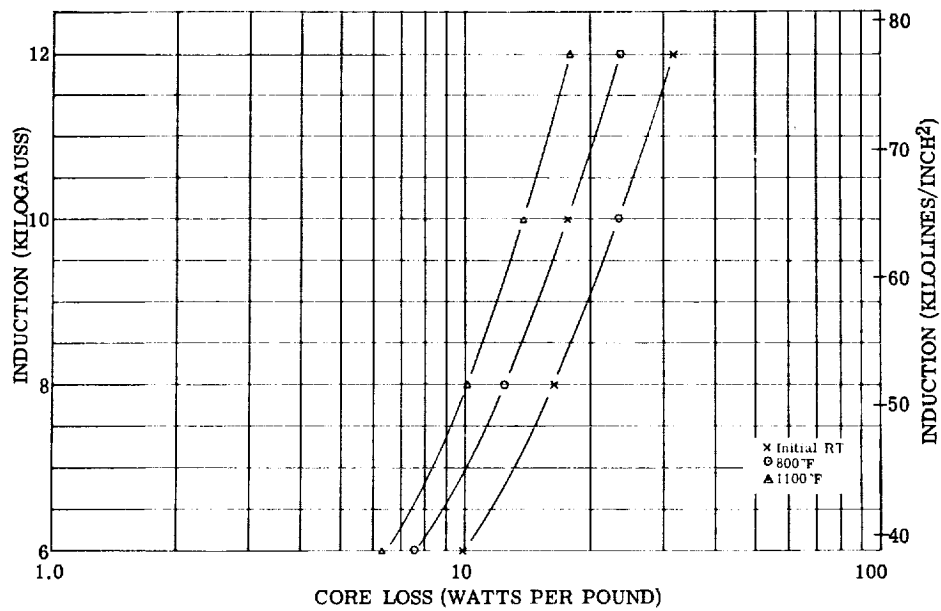
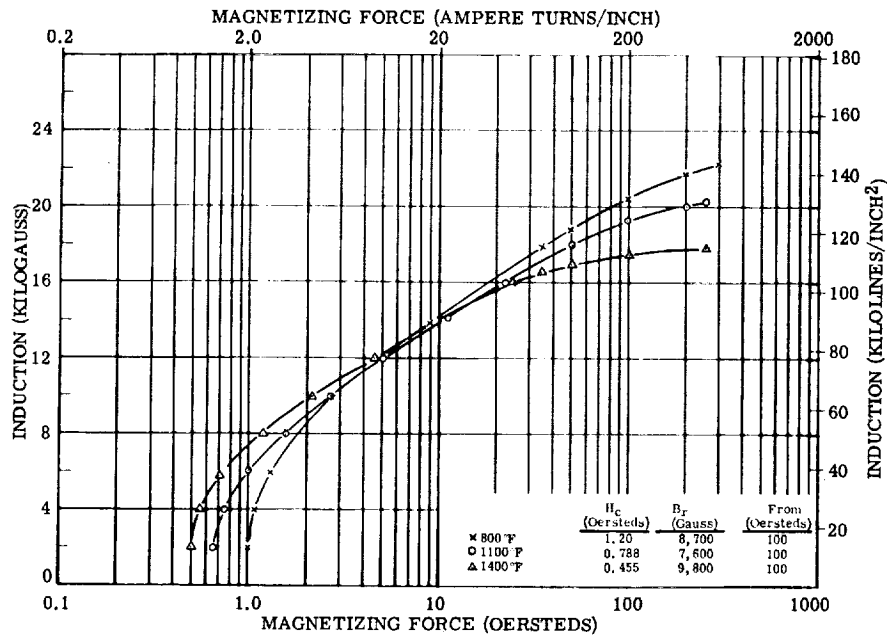Figure 198. - Core loss at 800 cps for Hiperco 27 alloy 0. 004-inch laminations. Test atmosphere, air to 800° F and argon above 800° F; interlaminar insulation, mica aluminum orthophosphate bentonite.
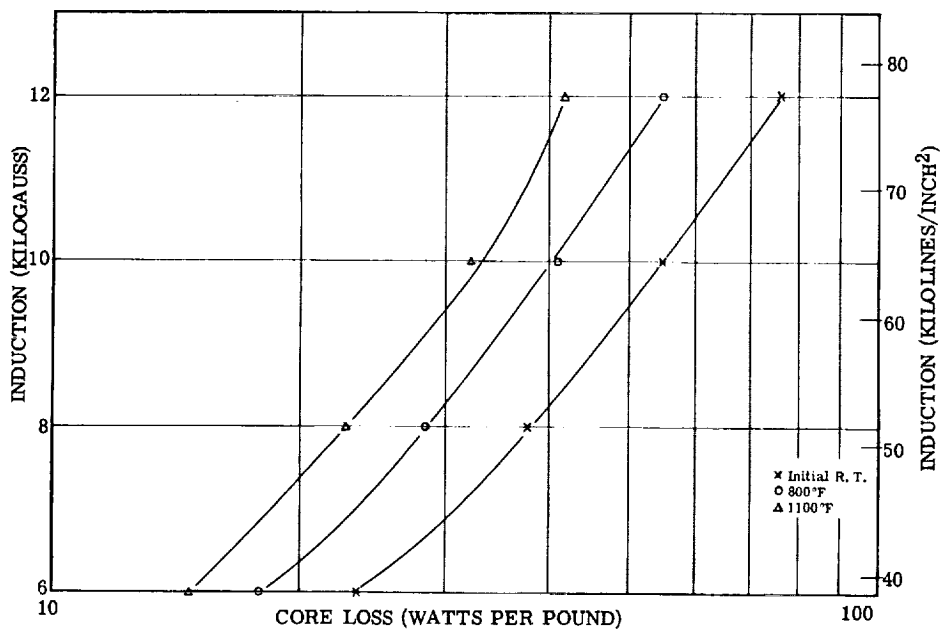
Figure 199. - Core loss at 1600 cps for Hiperco 27 alloy 0. 004-inch laminations. Test atmosphere, air to 800° F and argon above 800° F; interlaminar insulation, mica aluminum orthophosphate bentonite.
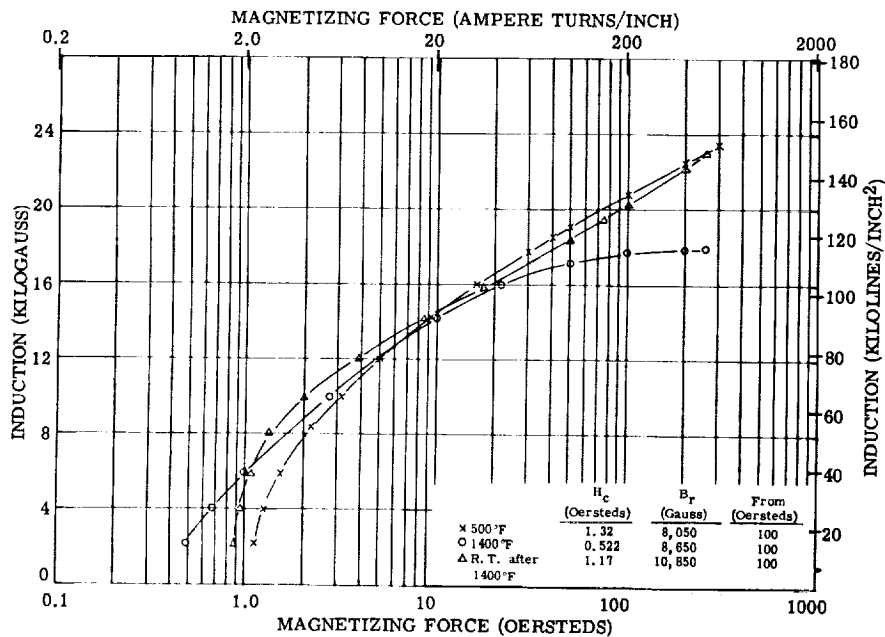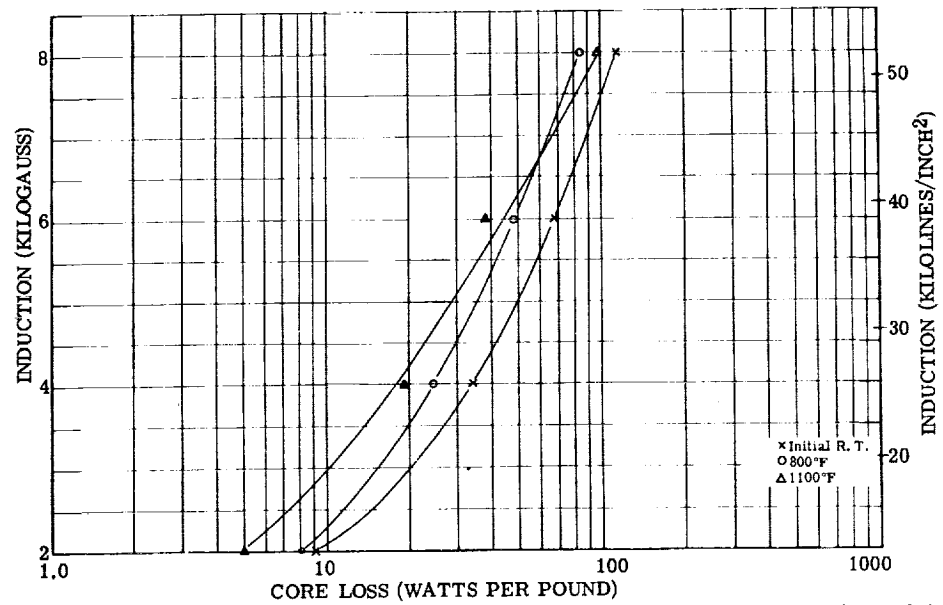
Figure 200. - Core loss at 3200 cps for Hiperco 27 alloy 0. 004-inch laminations. Test atmosphere, air to 800° F and argon above 800° F; interlaminar insulation, mica aluminum orthophosphate bentonite.
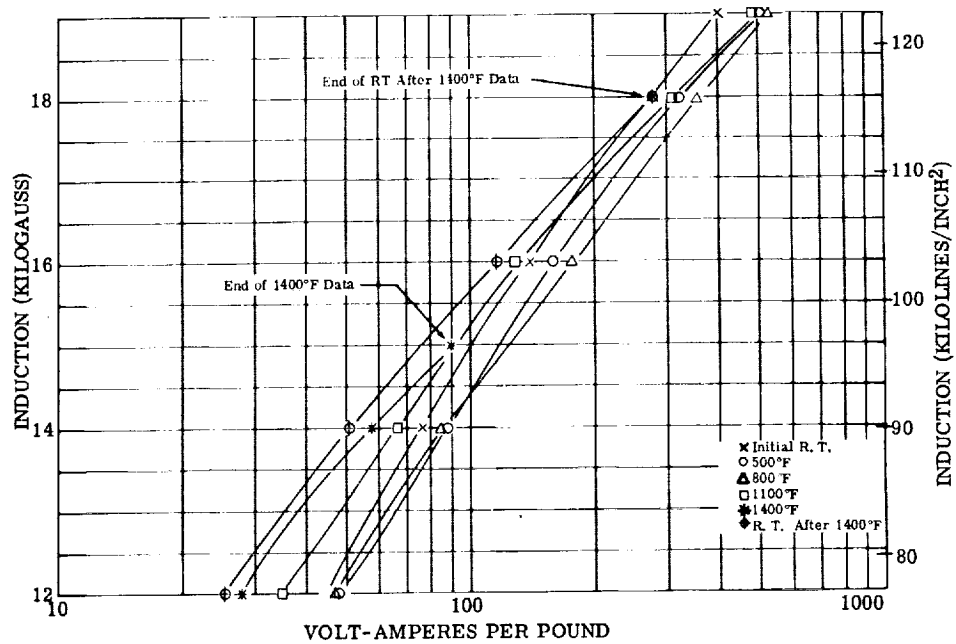
Figure 201. - Exciting volt-amperes per pound at 400 cps for Hiperco 27 alloy 0. 008-inch laminations, sample 3. Test atmosphere, air to 800° F and argon above 800° F; interlaminar insulation, aluminum orthophosphate bentonite.
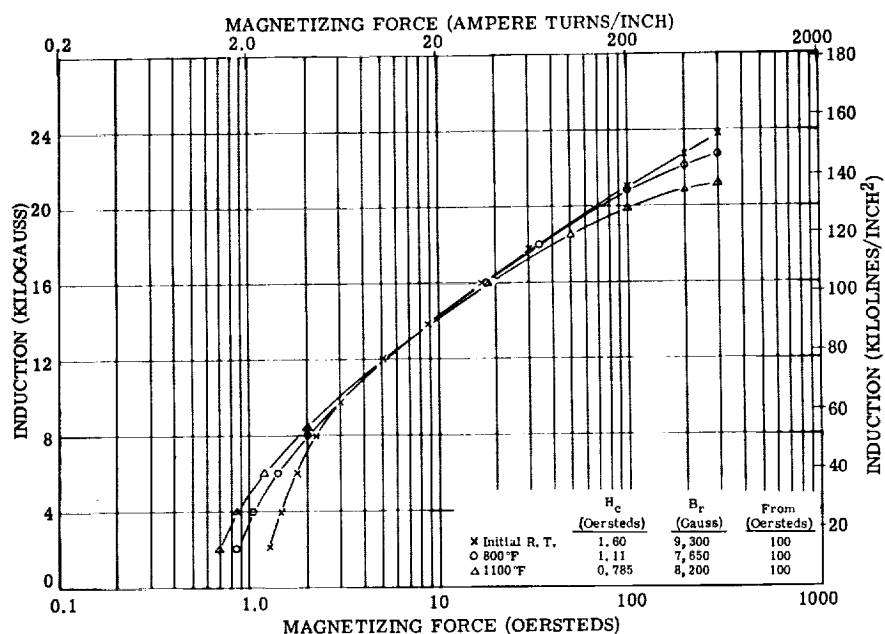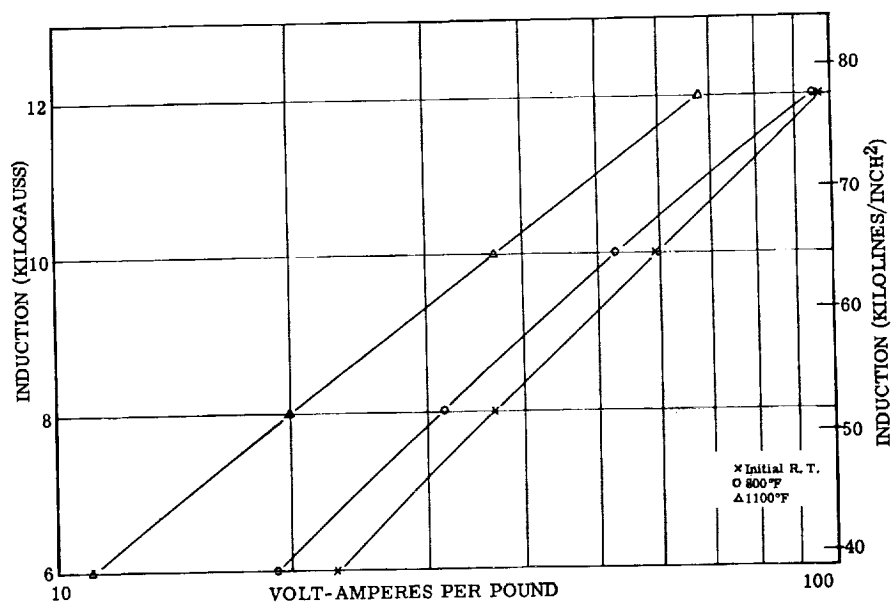
Figure 202. - Exciting volt-amperes per pound at 800 cps for Hiperco 27 alloy 0. 008-inch laminations, sample 3. Test atmosphere, air to 800° F and argon above 800° F; interlaminar insulation, aluminum orthophosphate.
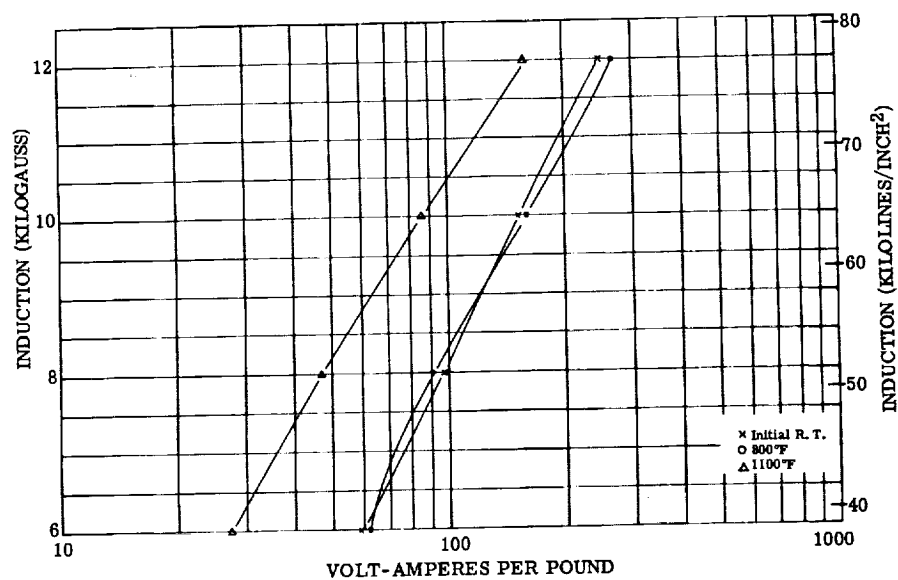
Figure 203. - Exciting volt-amperes per pound at 1600 cps for Hiperco 27 alloy 0. 008-inch laminations, sample 3. Test atmosphere, air to 800° F and argon above 800° F; interlaminar insulation, aluminum orthophosphate.
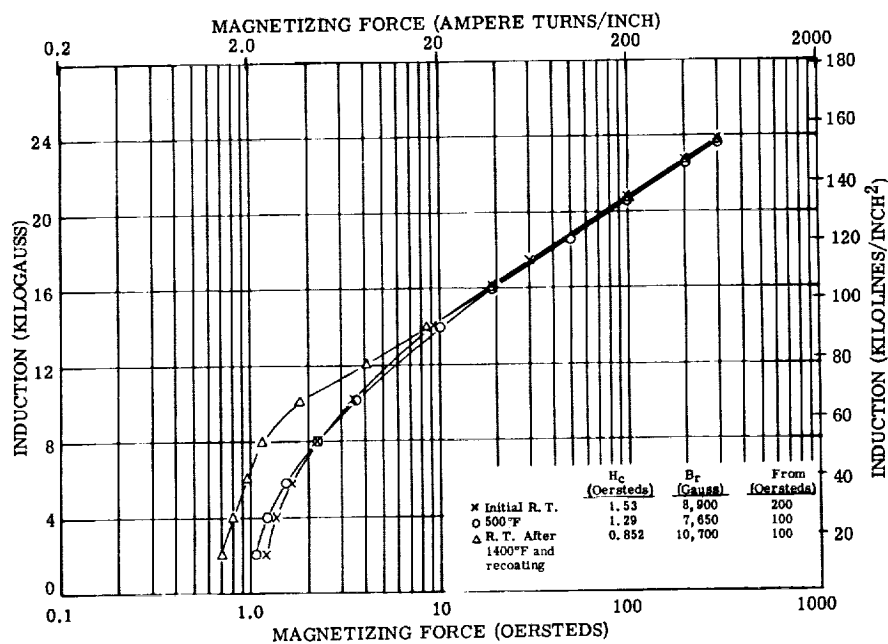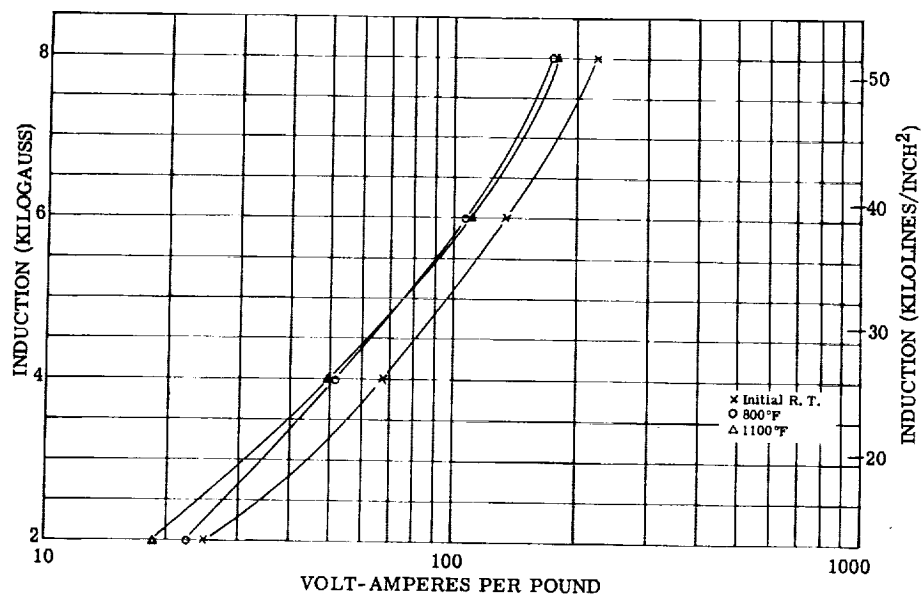
Figure 204. - Exciting volt-amperes per pound at 3200 cps for Hiperco 27 alloy 0.008-inch laminations, sample 3. Test atmosphere, air to 800° F and argon above 800° F; interlaminar insulation, aluminum orthophosphate.
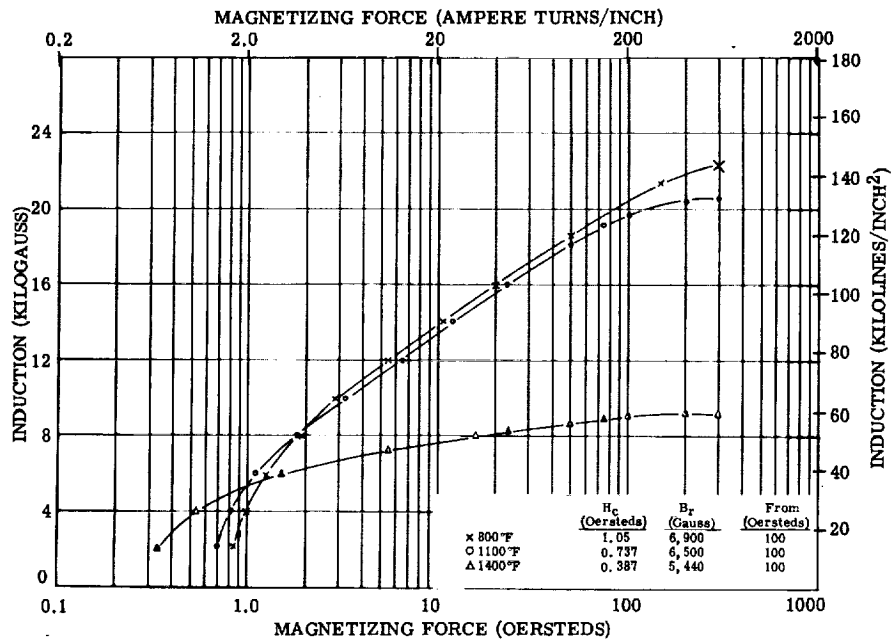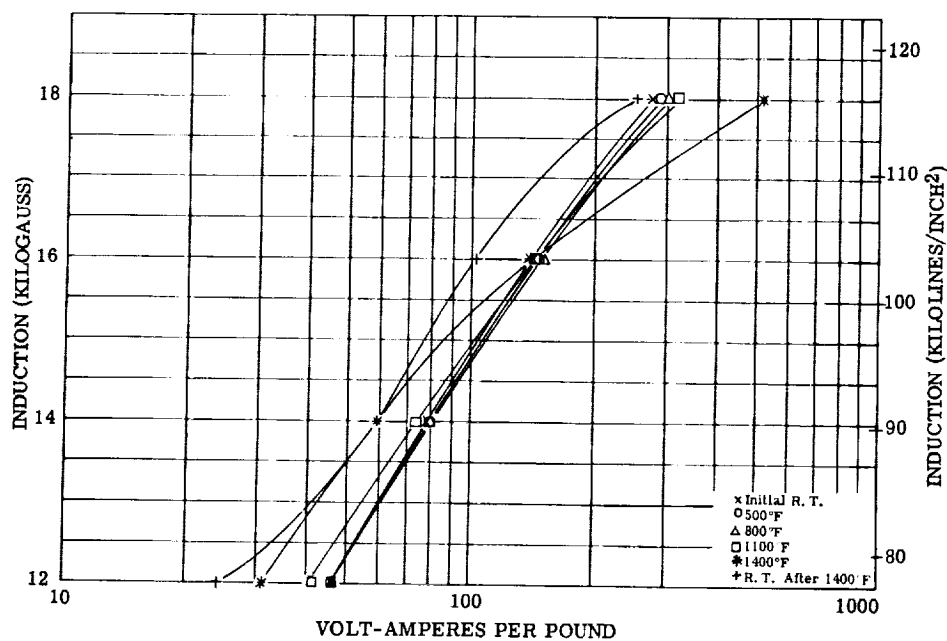

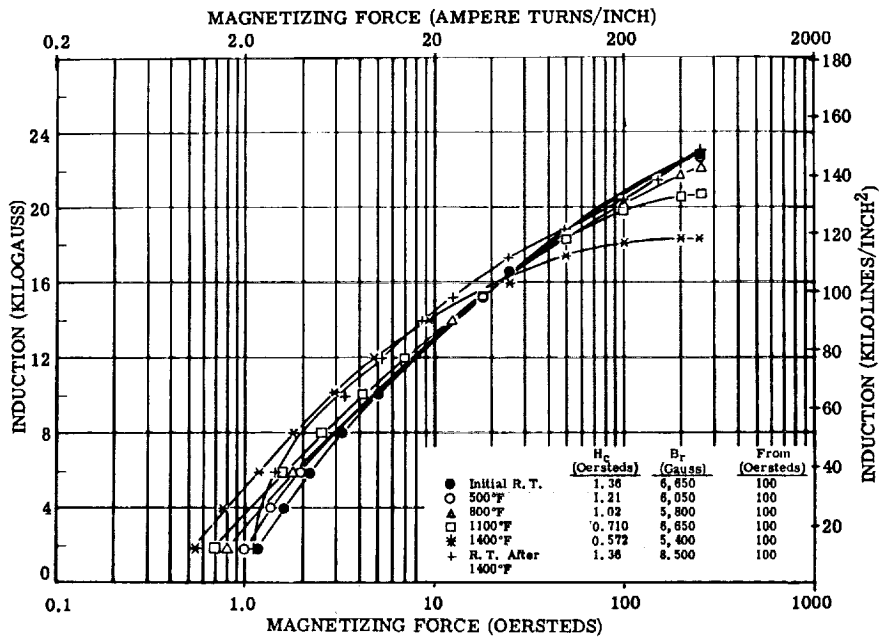Figure 205. - Exciting volt-amperes per pound at 400 cps for Hiperco 27 alloy 0.008-inch laminations, sample 4; test atmosphere, argon; interlaminar insulation, mica aluminum orthophosphate bentonite.
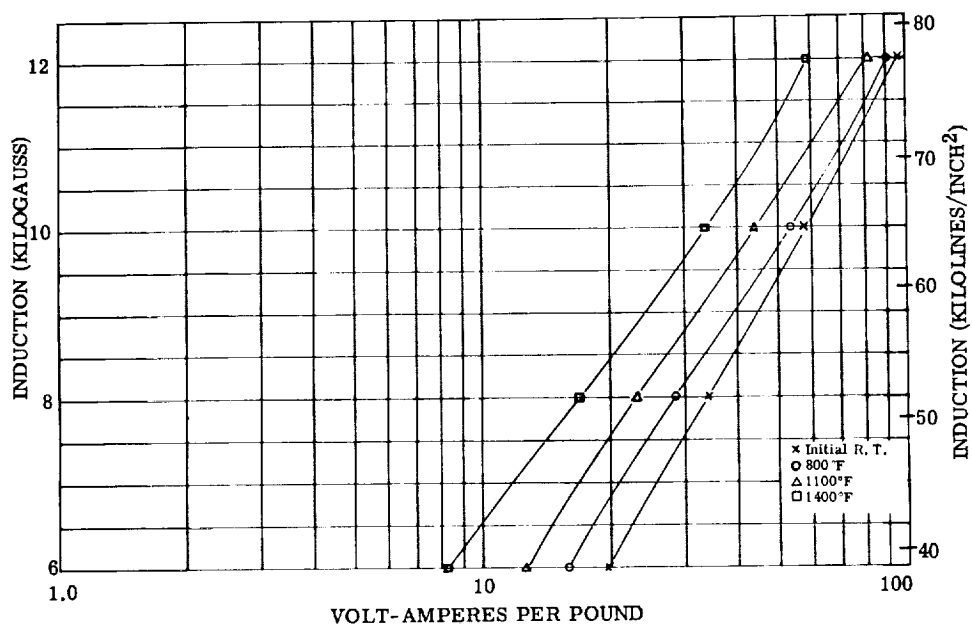
Figure 206. - Exciting volt-amperes per pound at 800 cps for Hiperco 27 alloy 0.008-inch laminations, sample 4. Test atmosphere, argon; interlaminar insulation, mica aluminum orthophosphate bentonite.
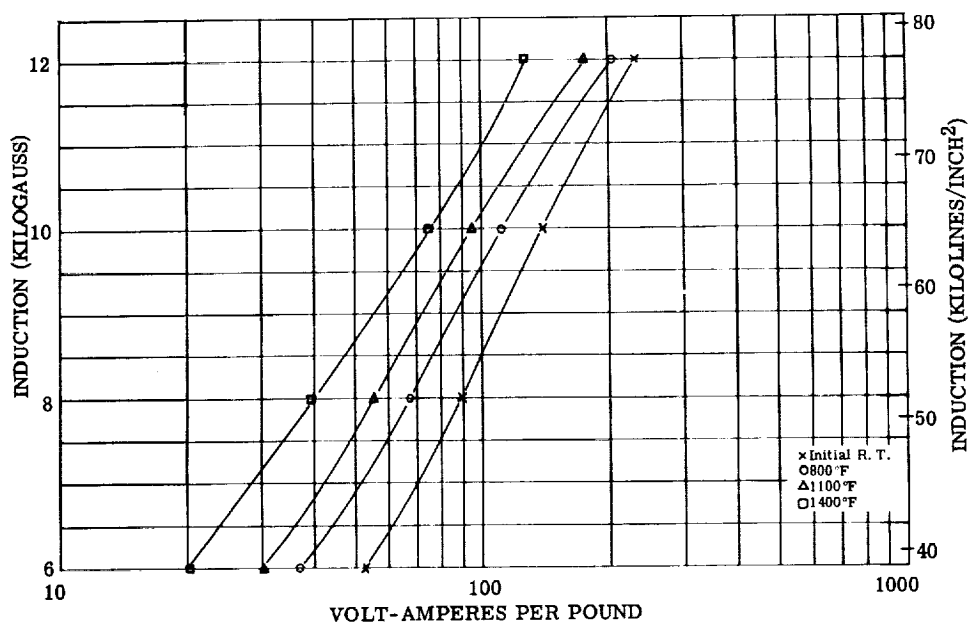
Figure 207. - Exciting volt-amperes per pound at 1600 cps for Hiperco 27 alloy 0.008-inch laminations, sample 4. Test atmosphere, argon; interlaminar insulation, mica aluminum orthophosphate bentonite.
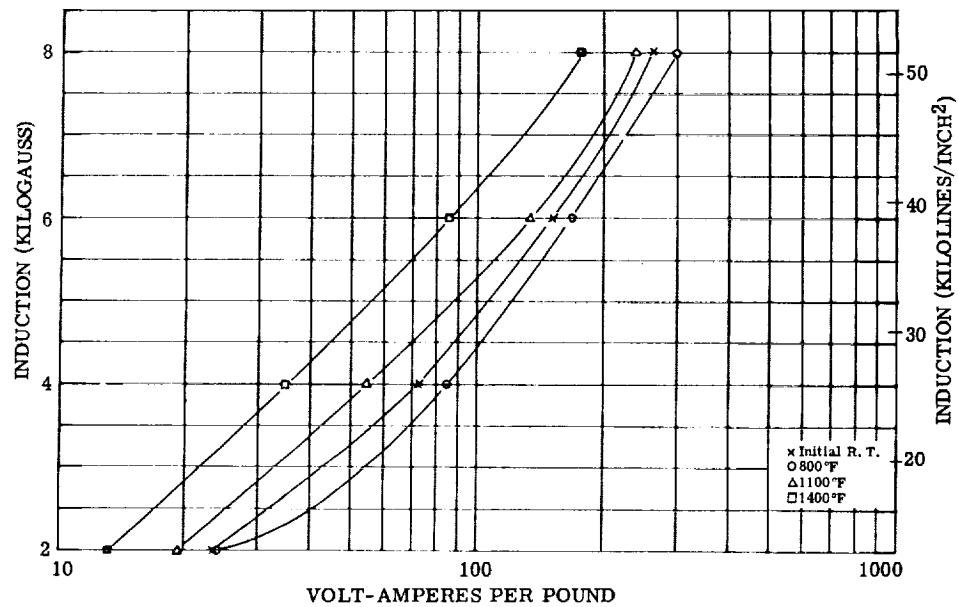
Figure 208. - Exciting volt-amperes per pound at 3200 cps for Hiperco 27 alloy 0.008-inch laminations, sample 4. Test atmosphere, argon; interlaminar insulation, mica aluminum orthophosphate bentonite.
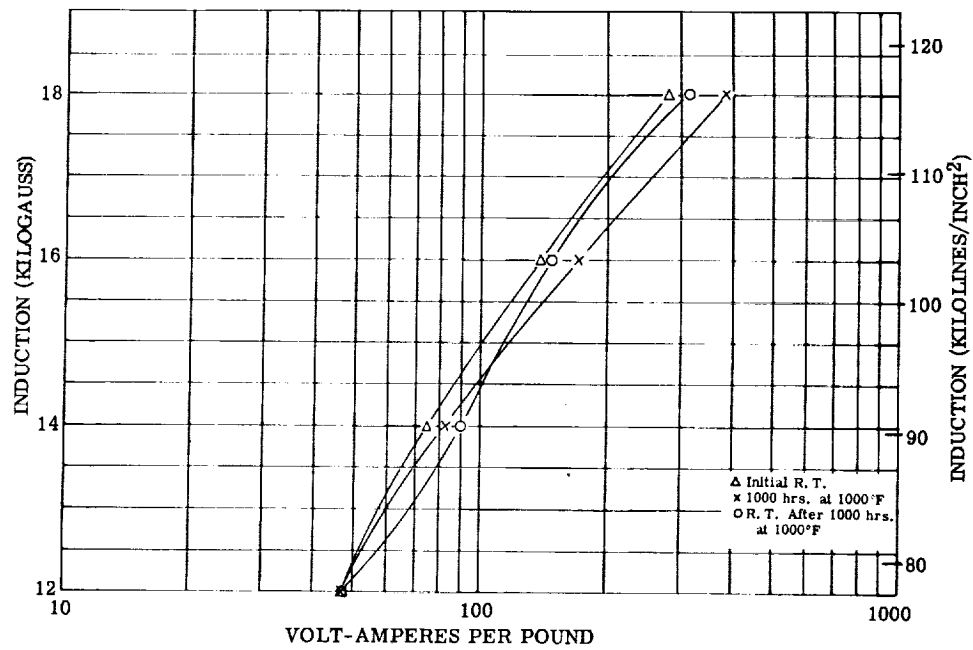
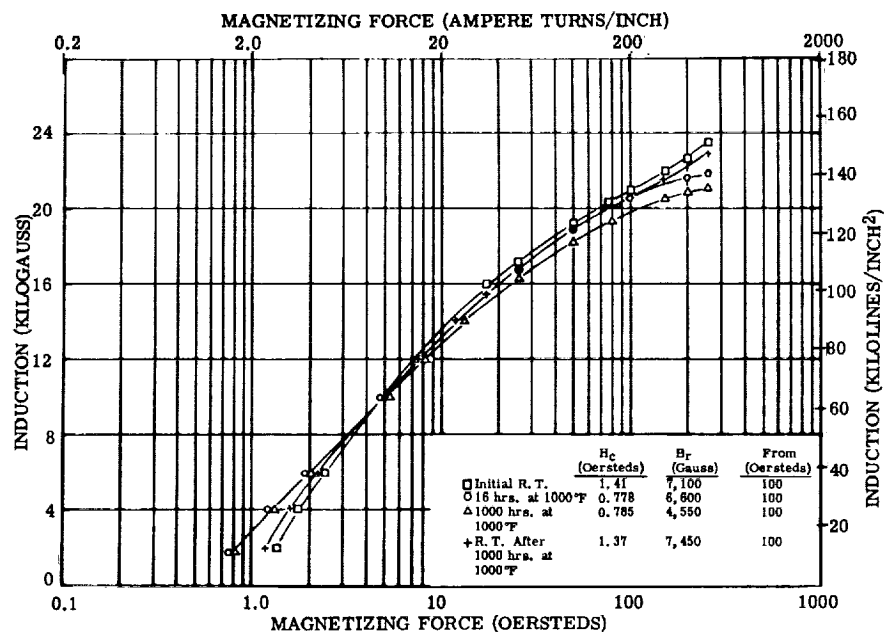Figure 209. - Exciting volt-amperes per pound at 400 cps for Hiperco 27 alloy 0.008-inch laminations, aging test, sample 5. Test atmosphere, argon; interlaminar insulation, mica aluminum orthophosphate bentonite.
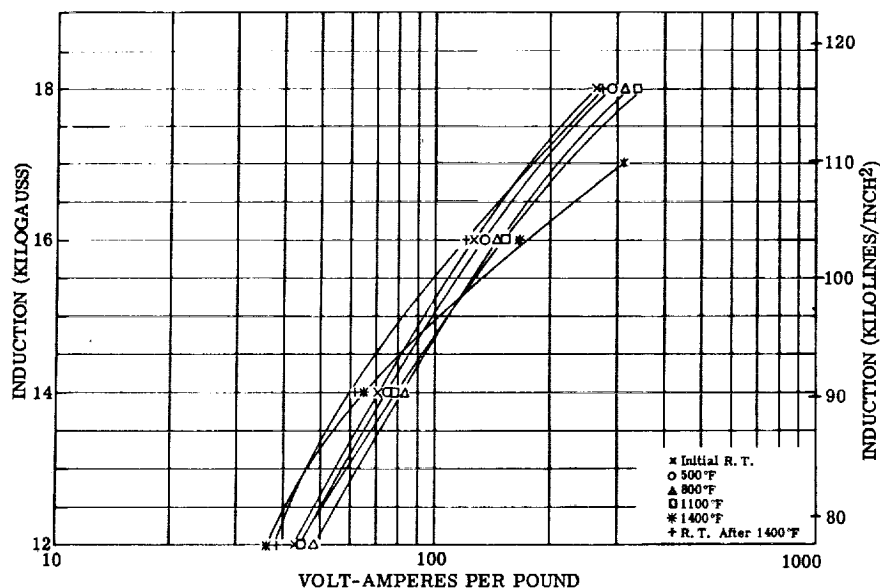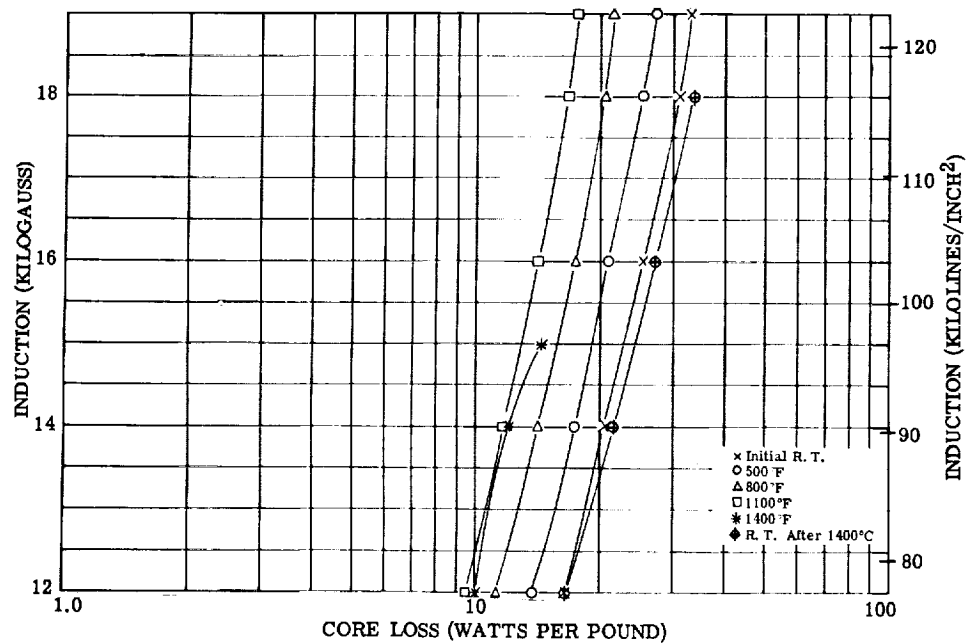
Figure 210. - Core loss at 400 cps for Hiperco 27 alloy 0.008-inch laminations, sample 3. Test atmosphere, air to 800° F and argon above 800° F; interlaminar insulation, aluminum orthophosphate.
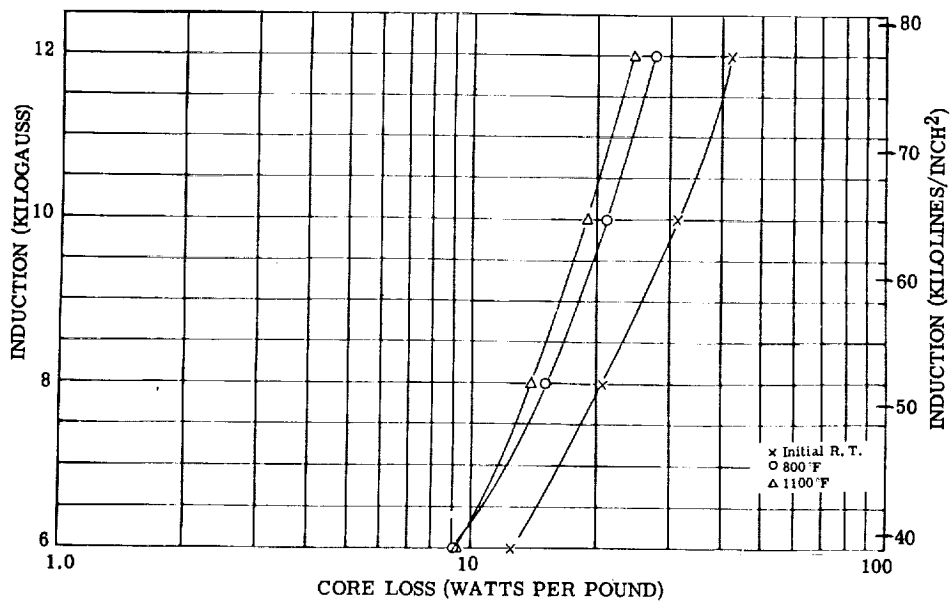
Figure 211. - Core loss at 800 cps for Hiperco 27 alloy 0.008-inch laminations, sample 3. Test atmosphere, air to 800° F and argon above 800° F; interlaminar insulation, aluminum orthophosphate.
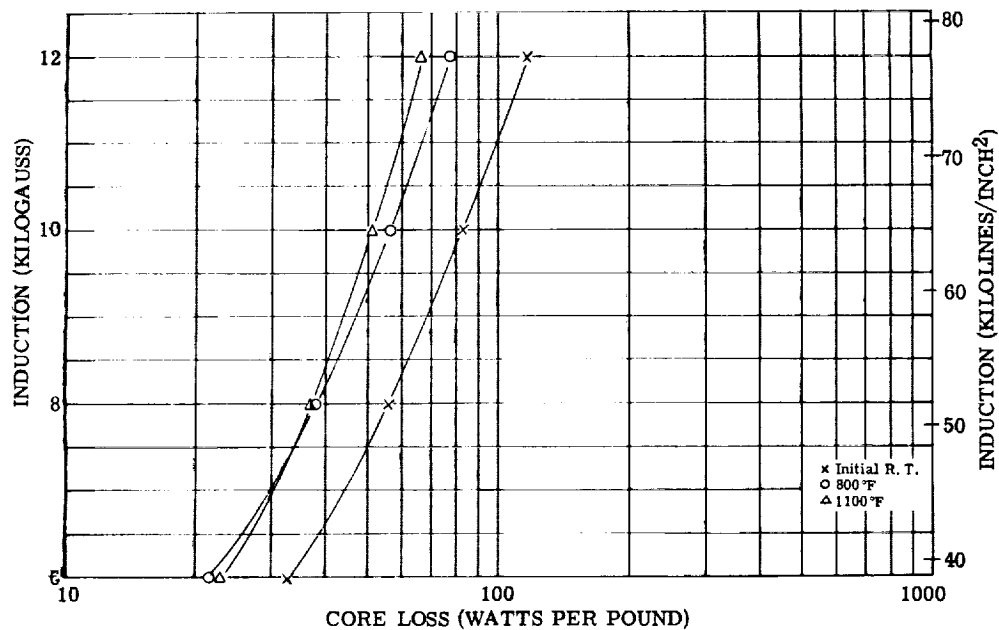
Figure 212. - Core loss at 1600 cps for Hiperco 27 alloy 0.008-inch laminations, sample 3. Test atmosphere, air to 800° F and argon above 800° F; interlaminar insulation, aluminum orthophosphate.
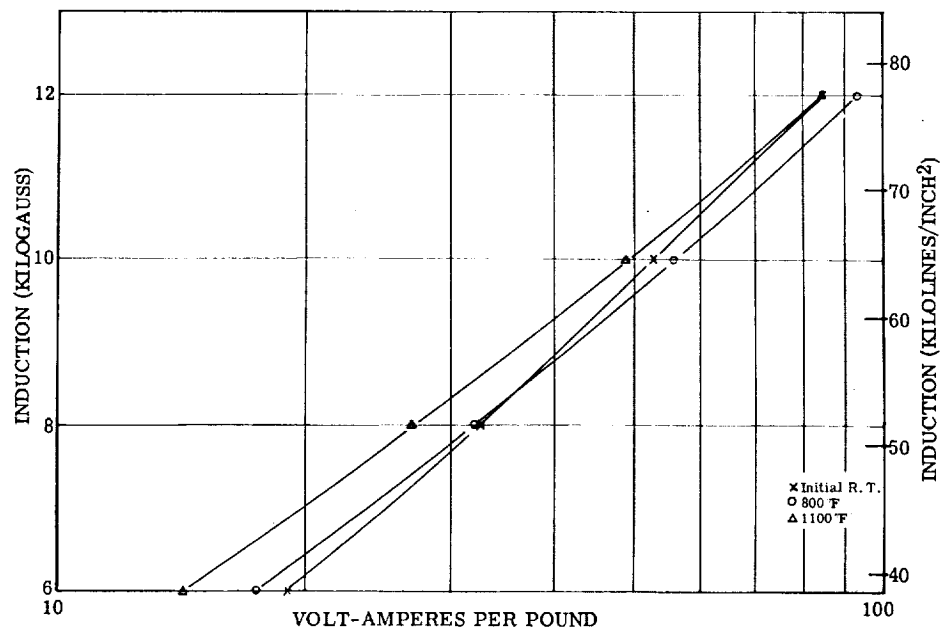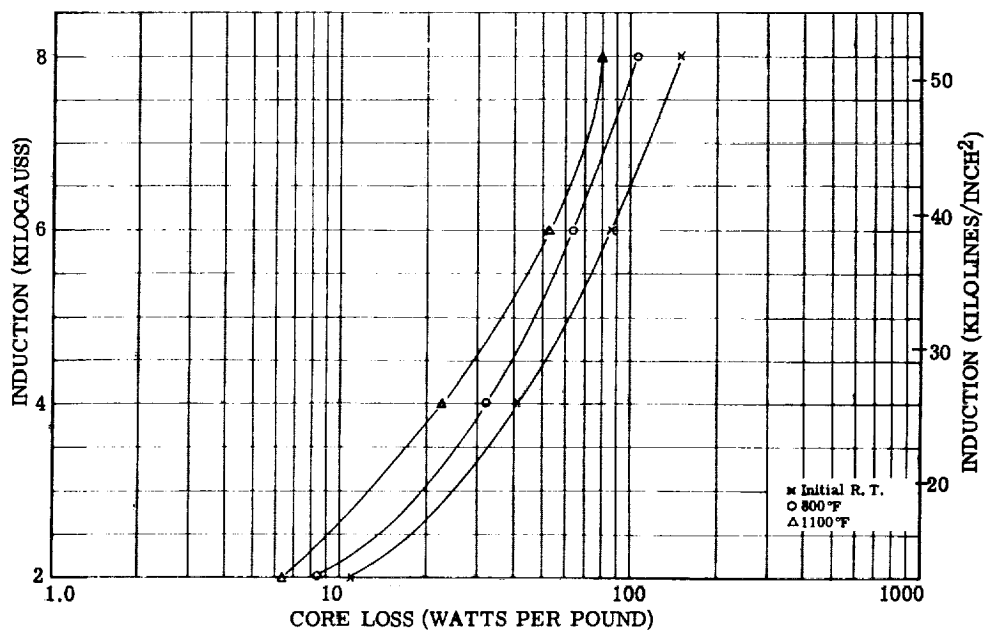

Figure 213. - Core loss at 3200 cps for Hiperco 27 alloy 0.008-inch laminations, sample 3. Test atmosphere, air to 800° F and argon above 800° F; interlaminar insulation, aluminum orthophosphate.

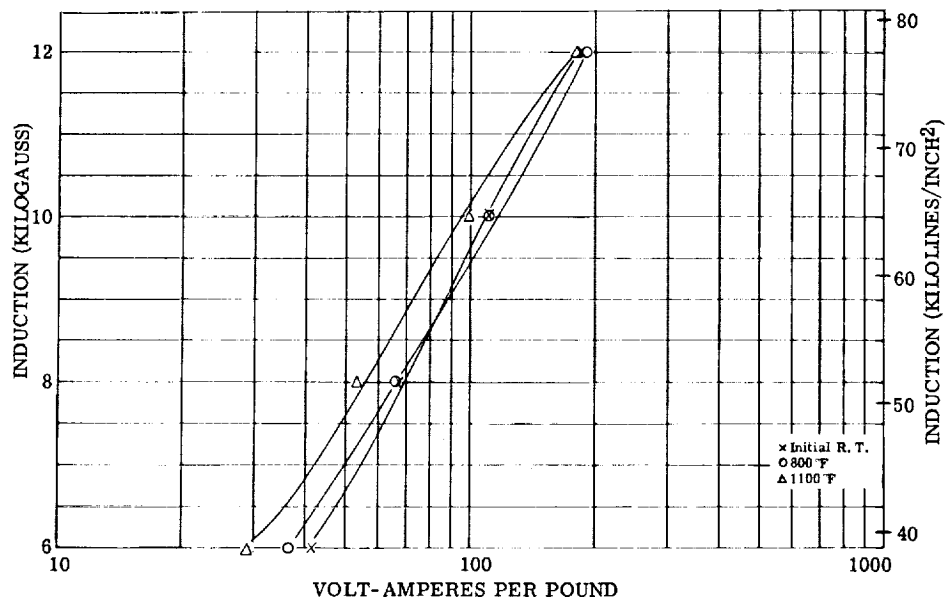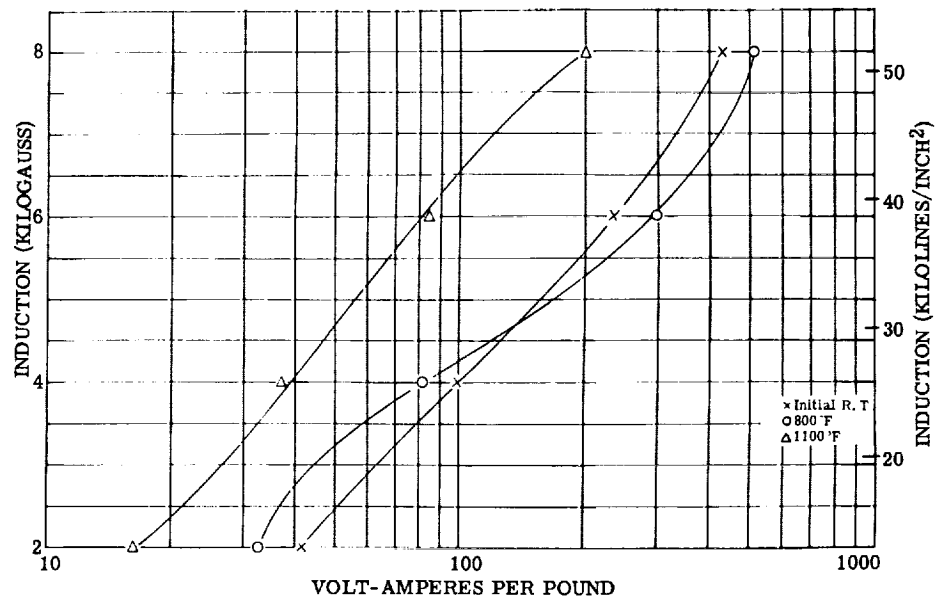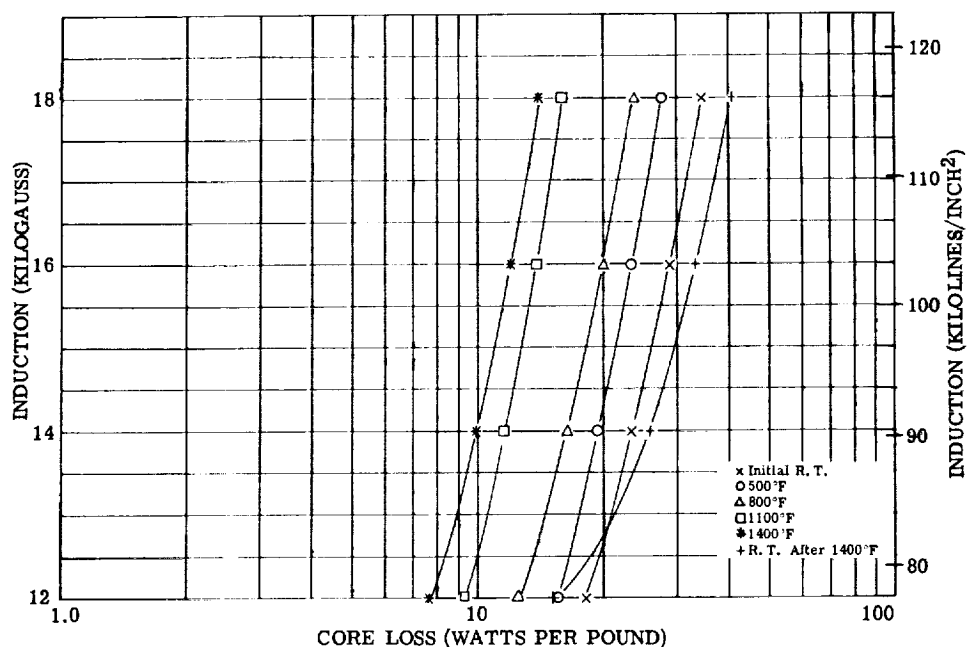Figure 214. - Core loss at 400 cps for Hiperco 27 alloy 0.008-inch laminations, sample 4. Test atmosphere, argon; interlaminar insulation, mica aluminum orthophosphate bentonite.
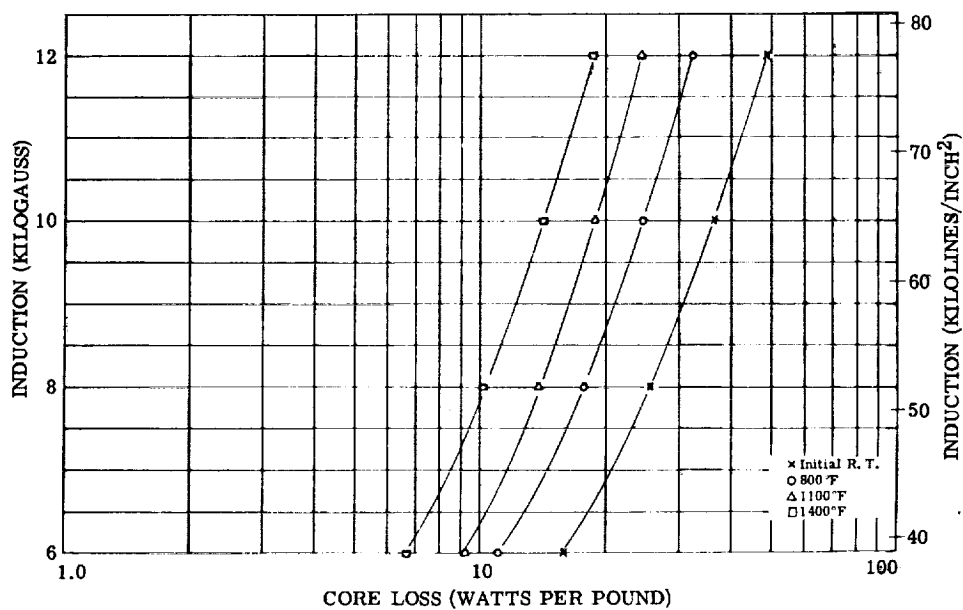
Figure 215. - Core loss at 800 cps for Hiperco 27 alloy 0.008-inch laminations, sample 4. Test atmosphere, argon; interlaminar insulation, mica aluminum orthophosphate bentonite.
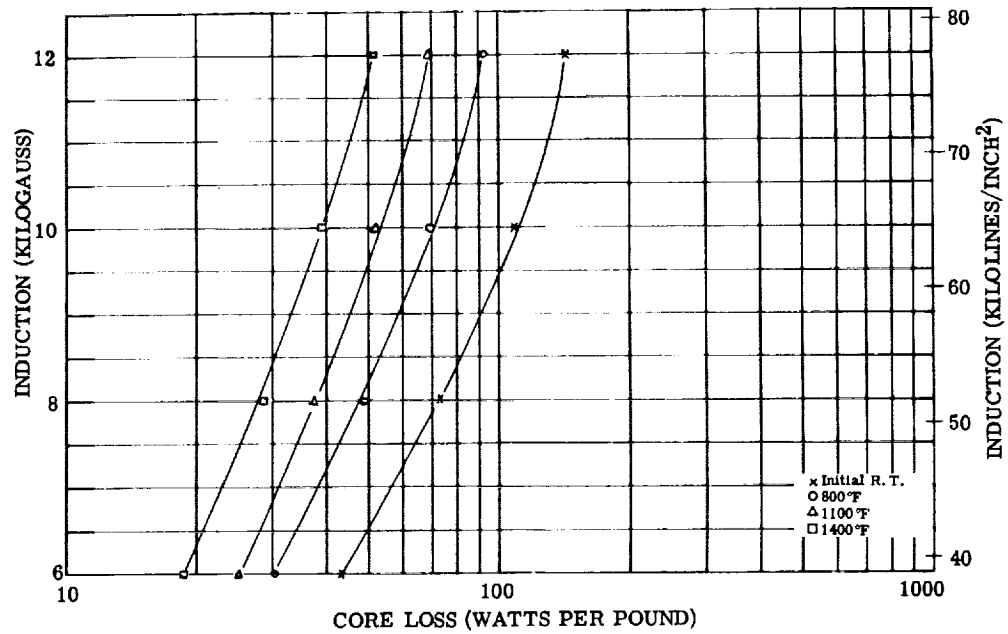
Figure 216. - Core loss at 1600 cps for Hiperco 27 alloy 0.008-inch laminations, sample 4. Test atmosphere, argon; interlaminar insulation, mica aluminum orthophosphate bentonite.
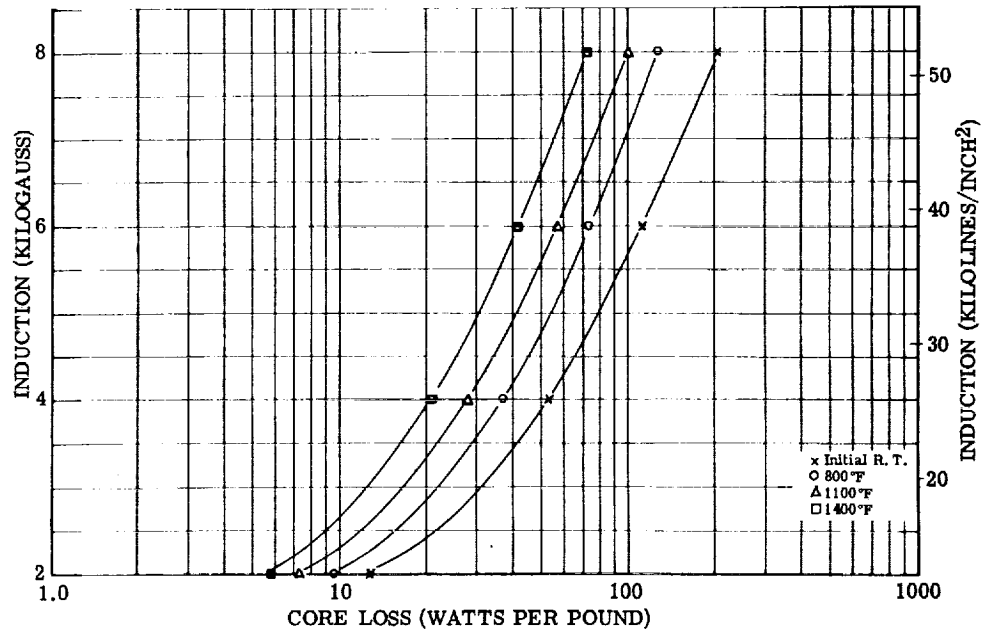
Figure 217. - Core loss at 3200 cps for Hiperco 27 alloy 0.008-inch-laminations, sample 4. Test atmosphere, argon; interlaminar insulation, mica aluminum orthophosphate bentonite.
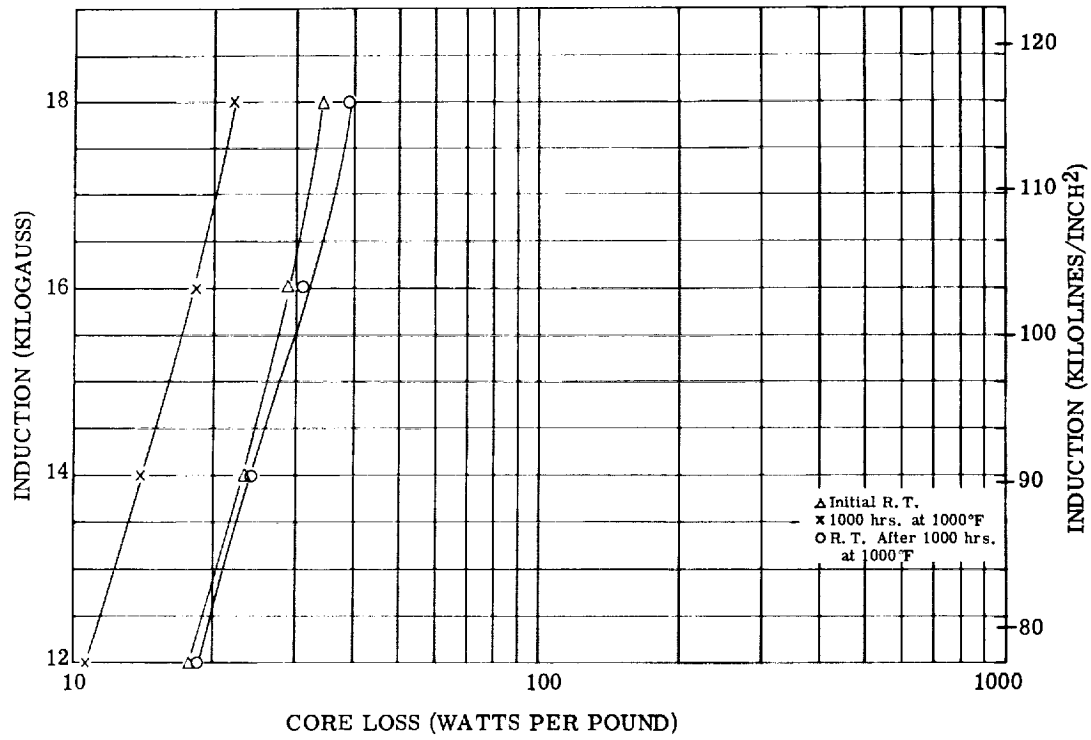
Figure 218. - Core loss at 400 cps for Hiperco 27 alloy 0.008-inch laminations, aging test, sample 5. Test atmosphere, argon; interlaminar insulation, mica aluminum orthophosphate bentonite.

TABLE 23. - POISSON'S RATIO FOR HIPERCO 27

ALLOY AT ROOM TEMPERATURE

[Width, 0.749 in.; thickness, 0.124 in.]

Specimen	Run	Poisson's ratio (a)	Average Poisson's ratio
1	1	0.305	
	2	.327	0.320
	3	.329	
2	1	0.330	
	2	.348	0.335
	3	.328	

[a]These data obtained from stress strain plots in
figs. 219 to 224 where Poisson's ratio μ is equal
to ratio of unit lateral strain to unit axial strain
below elastic limit e/e_1.
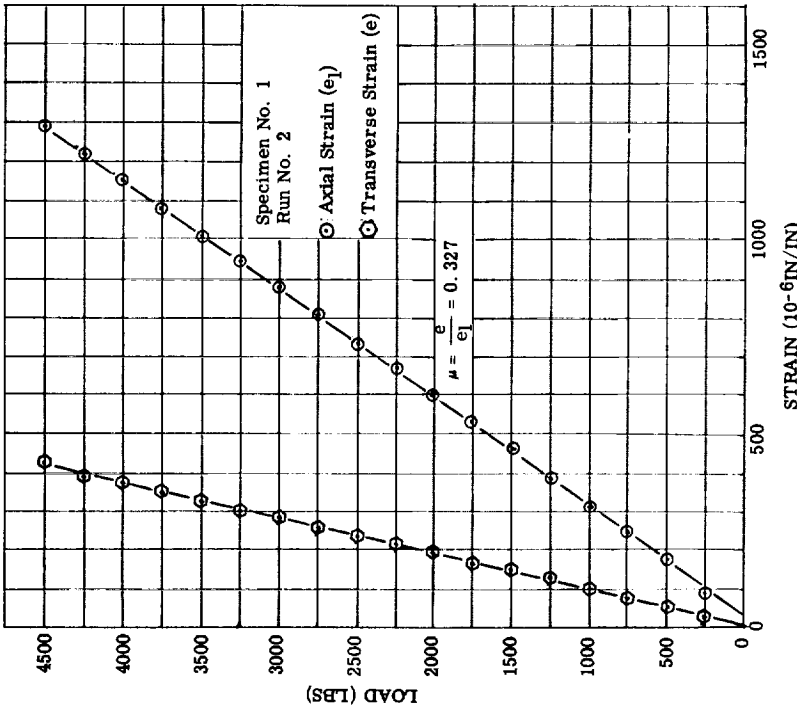
Figure 220. – Variation of elastic strain with load for Hiperco 27 alloy; room-temperature test for specimen 1, run 2.
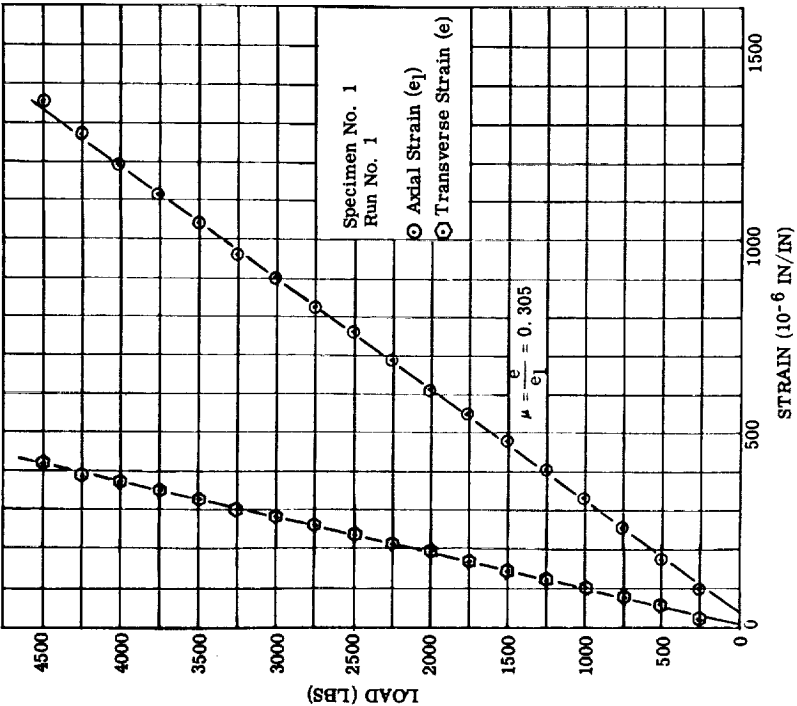
Figure 219. – Variation of elastic strain with load for Hiperco 27 alloy; room-temperature test for specimen 1, run 1.
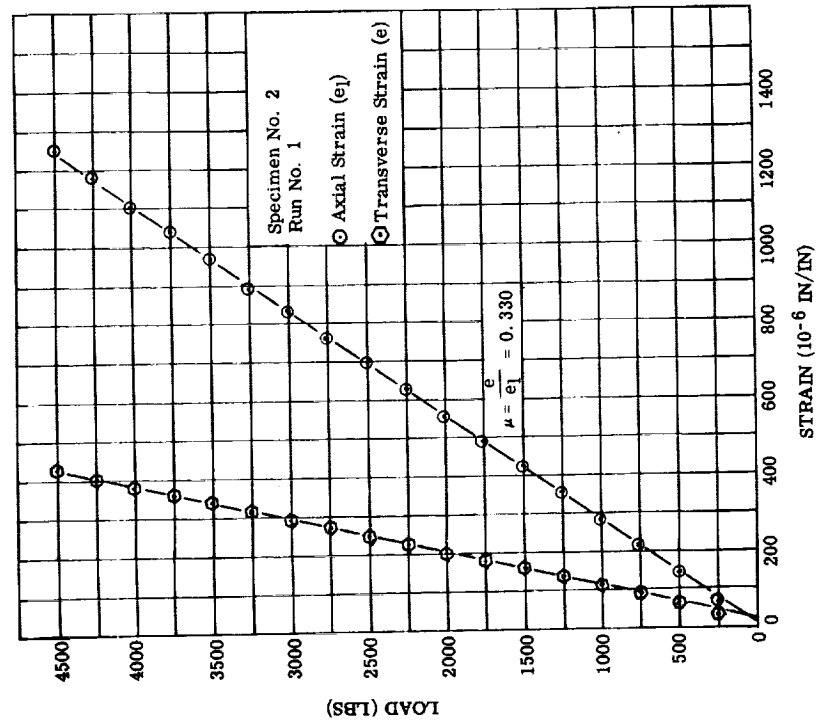
Figure 222. - Variation of elastic strain with load for Hiperco 27 alloy; room-temperature test for specimen 2, run 1.
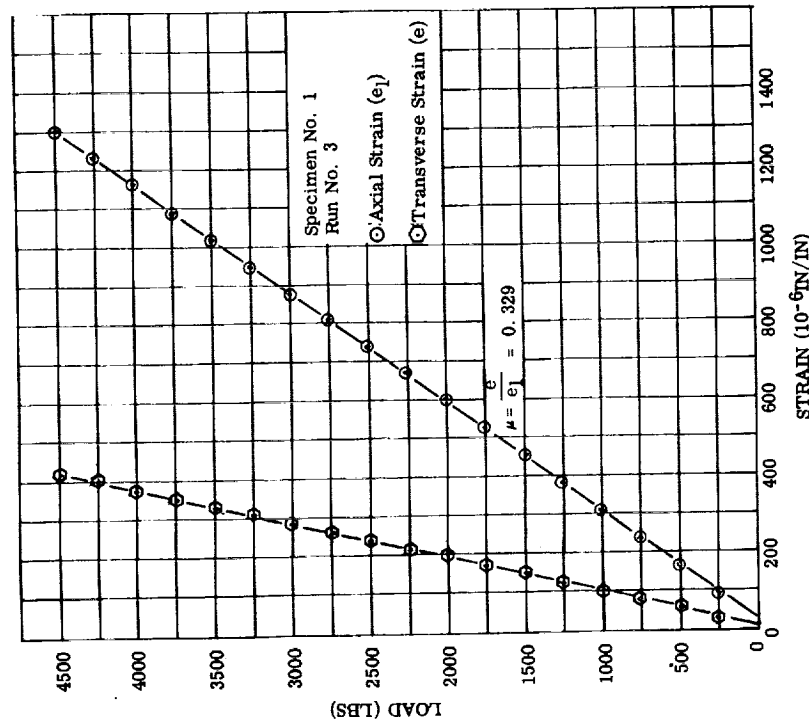
Figure 221. - Variation of elastic strain with load for Hiperco 27 alloy; room-temperature test for specimen 1, run 3.
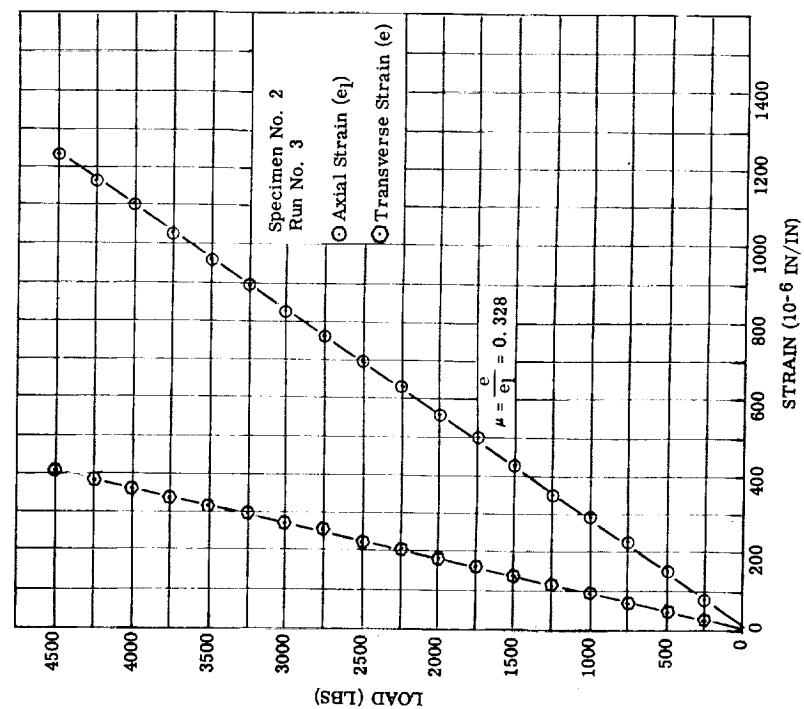
Figure 224. – Variation of elastic load with strain for Hiperco 27 alloy; room-temperature test for specimen 2, run 3.
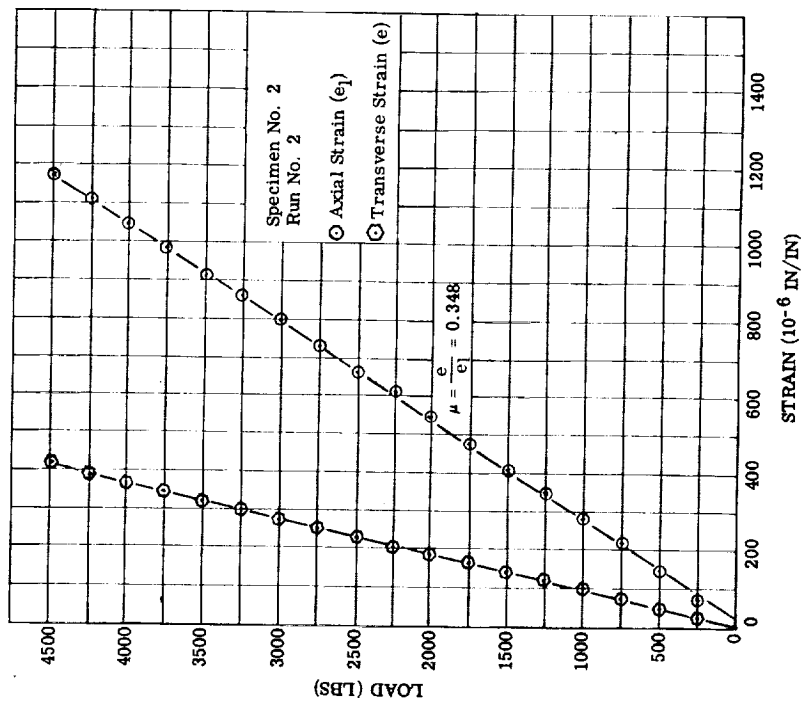
Figure 223. – Variation of elastic strain with load for Hiperco 27 alloy; room-temperature test for specimen 2, run 2.

TABLE 24. - TENSILE TEST DATA FOR VACUUM-MELTED FORGED HIPERCO 27 ALLOY

[Test, ASTM E21; strain rate, 0.005 in./(in.)(min) to yield and 0.050 in./(in.)(min) to failure.]

Specimen	Diameter, in.	Hardness, Rockwell B	Test temperature, °F	0.02 Percent offset yield strength, psi	0.2 Percent offset yield strength, psi	Ultimate strength, psi	Elongation in 2 in., percent	Reduction of area, percent	Modulus of elasticity, psi	Heat
1	0.506	97/99	72	80 750	82 450	94 700	26.5	73.0	33.9×10^6	8067
2	.505	95/96	72	68 600	a68 760	95 350	29.8	78.0	33.8	8027
3	.506	95/95	500	62 550	72 500	84 550	24.1	76.4	(b)	c8067
4	.506	96/96	500	74 850	81 300	89 000	19.9	74.1	(b)	c8067
5	.505	96/97	700	49 550	52 200	85 950	25.1	75.5	27.5	8027
6	.504	96/97	700	48 900	54 850	86 900	25.2	75.4	26.1	8027
7	.505	96/97	1000	43 500	50 150	67 100	13.1	43.1	24.0	8027
8	.505	96/97	1000	39 950	49 950	62 100	11.6	39.4	23.3	c8027
9	.506	96/96	1400	7 950	10 850	13 050	d71.5	89.1	(b)	c8067
10	.506	96/96	1400	6 850	9 300	13 200	d76.5	90.6	(b)	c8067

a Yield point exhibited by specimen.
b Properties not required.
c Tested in flowing argon.
d Quarter break.

Figure 226. – Tensile elongation and reduction of area for vacuum-melted forged Hiperco 27 alloy (data taken from two heats of material). (See table 24.)

▽ = Elongation
◻ = Reduction of Area

REDUCTION OF AREA AND ELONGATION (PERCENT)
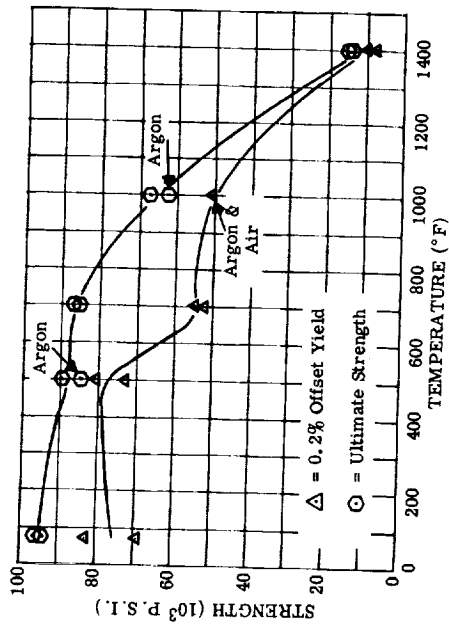
Figure 225. – Tensile strength of vacuum-melted forged Hiperco 27 alloy tested in air and argon (data taken from two heats of material). (See table 24.)

△ = 0.2% Offset Yield
◯ = Ultimate Strength

STRENGTH (10³ P.S.I.)
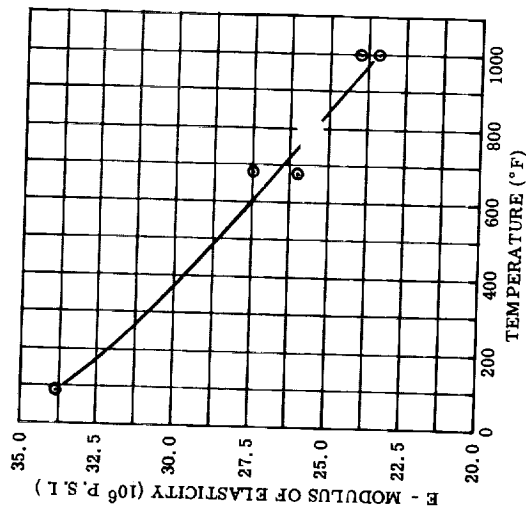
Figure 227. – Modulus of elasticity of vacuum-melted forged Hiperco 27 alloy as function of temperature. (See table 24.)

E - MODULUS OF ELASTICITY (10⁶ P.S.I.)

TABLE 25. - TENSILE TEST DATA FOR HIPERCO 27 ALLOY (INVESTMENT CAST AND ANNEALED)

[Test, ASTM E21; strain rate, 0.005 in./(in.)(min) to yield and 0.050 in./(in.)(min) to failure.]

Specimen	Diameter, in.	Hardness, BHN (a)	Test temperature, °F	0.02 Percent offset yield strength, psi	0.2 Percent offset yield strength, psi	Ultimate strength, psi	Elongation in 1.4 in., percent	Reduction of area, percent
1	0.250	149	72	33 800	43 200	65 800	[b]2.4	1.6
2	.250	166	72	37 800	44 600	62 750	[b]1.5	0
4	.249	153	500	26 500	35 300	73 300	27.0	59.1
5	.250	153	500	27 900	31 550	71 900	[b]29.2	48.7
6	.250	153	700	31 250	34 100	67 400	[b]14.4	28.1
7	.251	156	700	32 850	40 000	72 200	[b]21.5	39.5
8	.250	166	1000	31 050	36 450	66 700	[b]8.8	21.8
9	.251	159	1000	26 450	31 300	55 950	[b]9.3	21.8
10	.251	159	1400	9 700	11 700	12 100	[b]35.6	60.4
11	.250	163	1400	8 850	10 850	[c]12 300	[b]48.8	79.6

[a]Converted from Rockwell B hardness readings. Load, 300 kg.
[b]Quarter break.
[c]Tested in argon atmosphere. All others tested in air.

$$\frac{0.02\% \ \text{Offset Yield}}{(72 \leq T \leq 1100^\circ \text{ F})} \quad \text{Tensile Stress} = 1000 \left[0.12858\text{x}10^{-9}\text{T}^4 - 0.44428\text{x}10^{-6}\text{T}^3 + 0.48385\text{x}10^{-3}\text{T}^2 - 0.18262\text{T} + 46.865 \right] \text{(psi)}$$

$$\frac{0.2\% \ \text{Offset Yield}}{72 \leq T \leq 1400^\circ \text{ F}} \quad \text{Tensile Stress} = 1000 \left[0.73484\text{x}10^{-10}\text{T}^4 - 0.28273\text{x}10^{-6}\text{T}^3 + 0.331\text{x}10^{-3}\text{T}^2 - 0.1403 \ \text{T} + 52.389 \right] \text{(psi)}$$

$$\frac{\text{Ultimate Strength}}{(72 \leq T \leq 1400^\circ \text{ F})} \quad \text{Tensile Strength} = 1000 \left[-0.10933\text{x}10^{-9}\text{T}^4 + 0.27513\text{x}10^{-6}\text{T}^3 - 0.2741\text{x}10^{-3}\text{T}^2 + 0.1121 \ \text{T} + 57.527 \right] \text{(psi)}$$

◻ 0.02 Percent Offset Yield
⊙ 0.2 Percent Yield
◌ Ultimate Strength

Figure 228. - Tensile strength of investment case and annealed Hiperco 27 alloy tested in air. (See table 25.)

⊡ Reduction of Area
⊙ Elongation
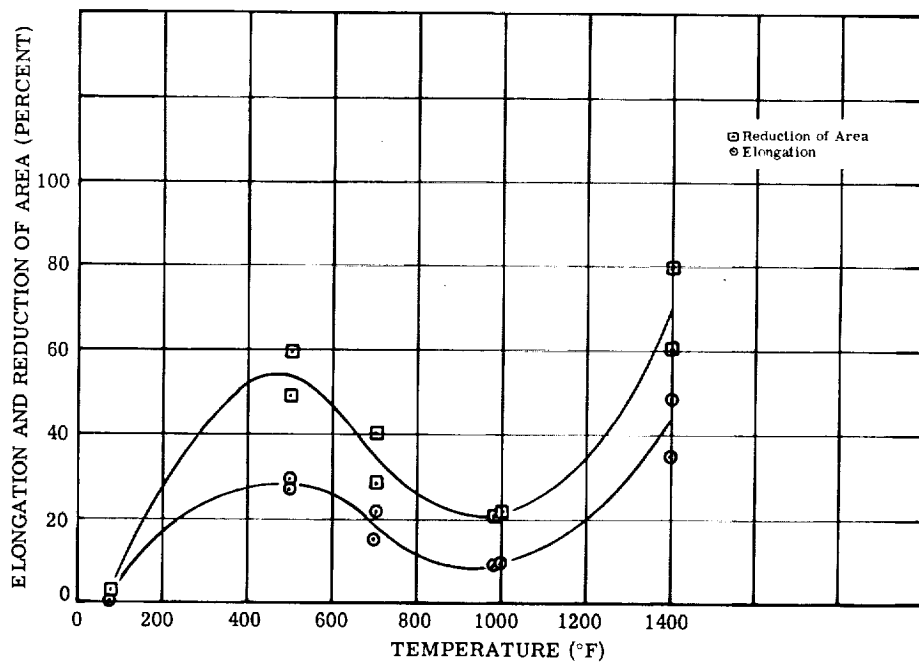
Figure 229. - Tensile elongation and reduction of area for investment cast and annealed Hiperco 27 alloy tested in air. (See table 25.)

TABLE 26. - COMPRESSION TEST DATA IN AIR FOR HIPERCO 27

VACUUM-MELTED FORGED BAR STOCK

[Test, ASTM E9; strain rate, 0.05 in./(in.)(min).]

Specimen	Diameter, in.	Test temperature, ^oF	0.02 Percent offset yield strength, psi	0.2 Percent offset yield strength, psi	Modulus of elasticity, psi
1	0.500	70	90 650	97 750	30.5×10^6
2	.499	70	81 800	97 400	32.3
3	.499	500	77 200	84 050	27.4
4	.499	500	78 550	83 550	27.2
5	.500	800	71 800	81 450	27.3
6	.500	800	70 000	80 450	27.2
7	.500	1100	47 350	58 300	26.0
8	.500	1100	61 100	66 200	24.0
9	.500	1400	10 500	15 500	18.6
10	.500	1400	9 150	14 600	20.7
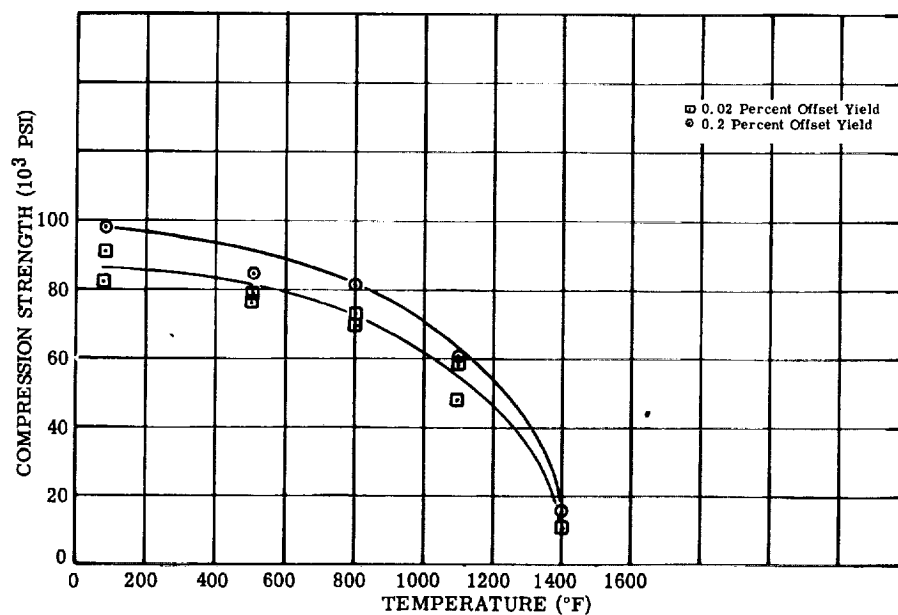
Figure 230. - Compression strength for 0.50-inch-diameter Hiperco 27 alloy vacuum-melted forged bar stock tested in air. Strain rate, 0.05 inch per inch per minute. (See table 26.)
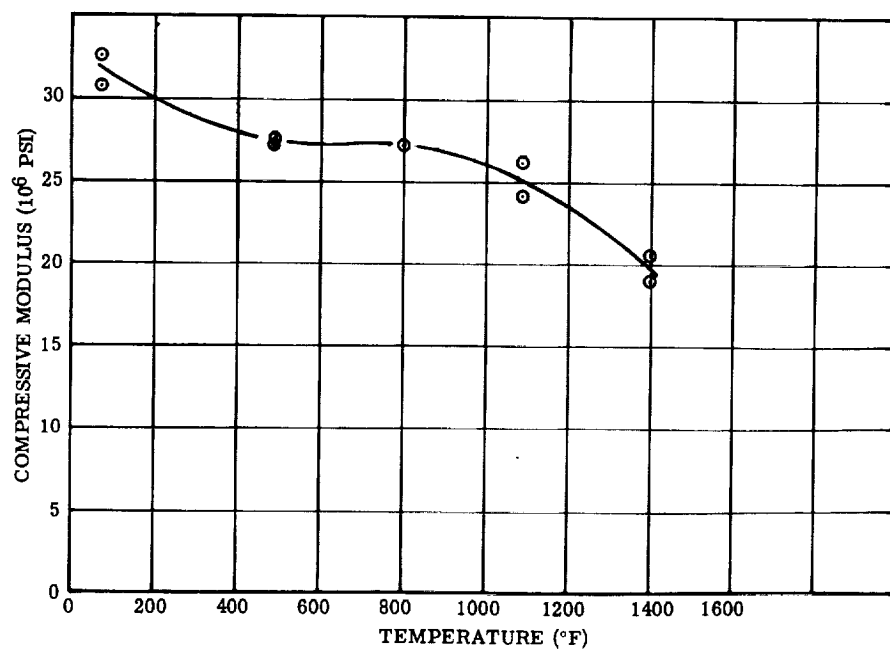
Figure 231. - Compressive modulus of elasticity for 0.50-inch-diameter Hiperco 27 alloy vacuum-melted forged bar stock tested in air. Strain rate, 0.05 inch per inch per minute. (See table 26.)
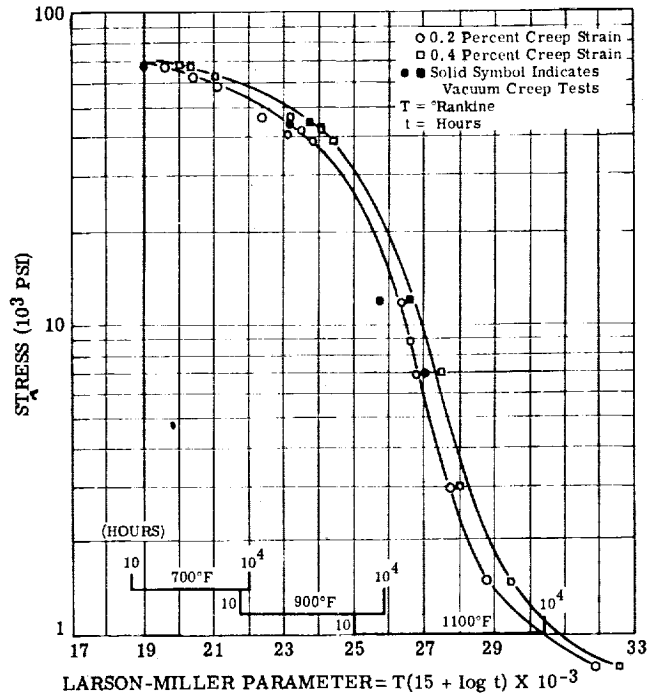
Figure 232. - Larson-Miller plot of vacuum-melted forged Hiperco 27 alloy creep data tested in air, argon, and vacuum, based on maximum of 2000-hour data.
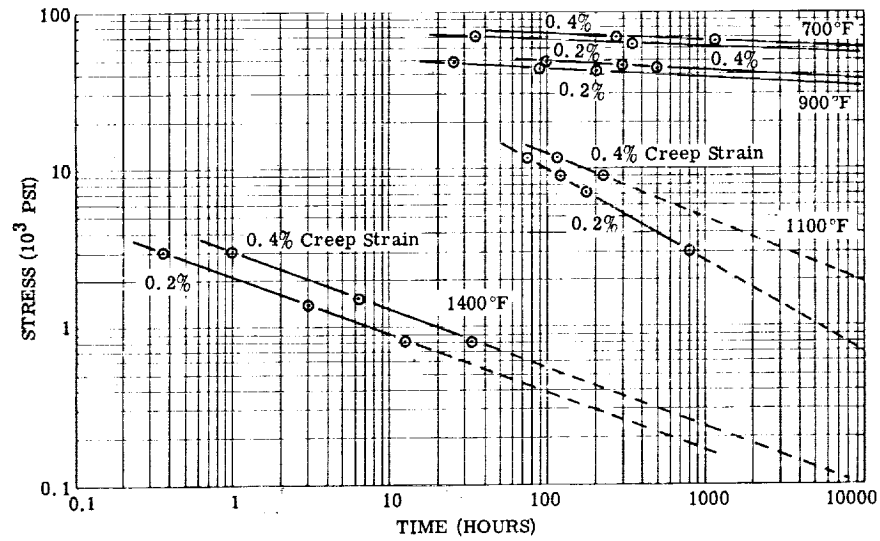
Figure 233. - Variation of stress with time to reach indicated creep strains for vacuum-melted forged Hiperco 27 alloy.
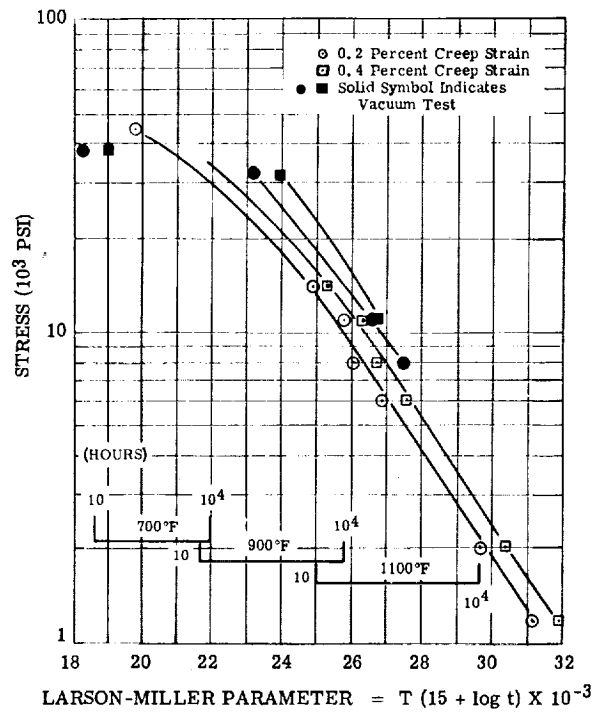
Figure 234. - Larson-Miller plot of investment cast Hiperco
27 alloy creep data tested in air and vacuum, based on
maximum of 2000-hour data.
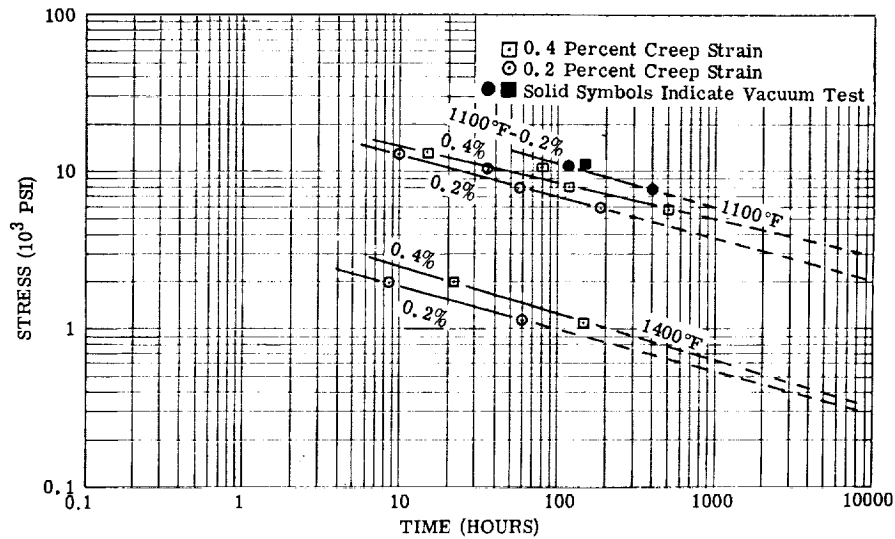
Figure 235. - Variation of stress with time to reach indicated creep strains for investment cast
and annealed Hiperco 27 alloy.

TABLE 27. - CREEP DATA FOR VACUUM-MELTED FORGED HIPERCO 27 ALLOY

TESTED IN AIR - FIRST TESTS

[Test, ASTM E139.]

Temperature, °F	700	a700	a700	a700	700	a700	a700	700	900	a900	1100
Stress, psi	31 000	40 000	50 000	55 000	35 000	46 000	60 000	75 000	18 000	40 000	3000
Duration of test, hr	474	212	184	506	215	355	1485	141	501	1003	1024
Total creep strain, percent	0.029	0.0167	0.0075	0.029	0.0291	0.0341	0.165	0.575	0.0412	0.489	0.235
Time to cause 0.2-percent creep strain, hr	(b)	(b)	(b)	(b)	(b)	(b)	(b)	0	(b)	520	818
Time to cause 0.4-percent creep strain, hr	(b)	(b)	(b)	(b)	(b)	(b)	(b)	(b)	(b)	890	(b)
Plastic strain obtained on loading specimen, percent	0	0	0	0	0	0	0	0.271	0	0	0
Strain-time plot given in fig.	236	236	236	236	237	237	237	238	239	239	241

a Stress raised on previous specimen.
b Did not reach required strain.
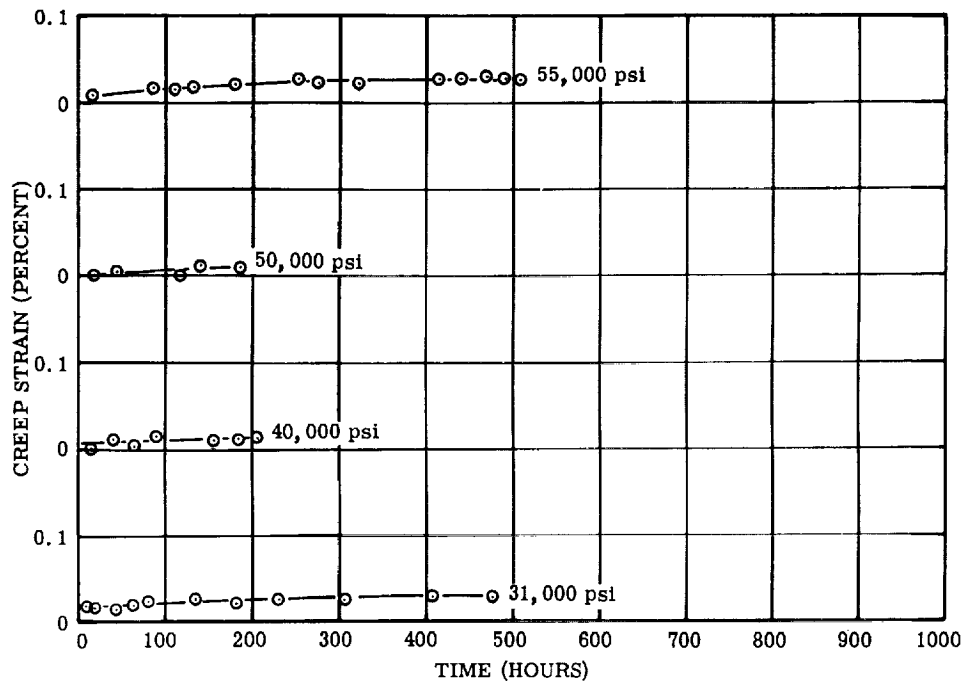
Figure 236. - Creep data for vacuum-melted forged Hiperco 27 alloy tested in air at 700° F and 31 000,
40 000, 50 000, and 55 000 psi (data obtained by increasing stress on single specimen). (See table 27.)
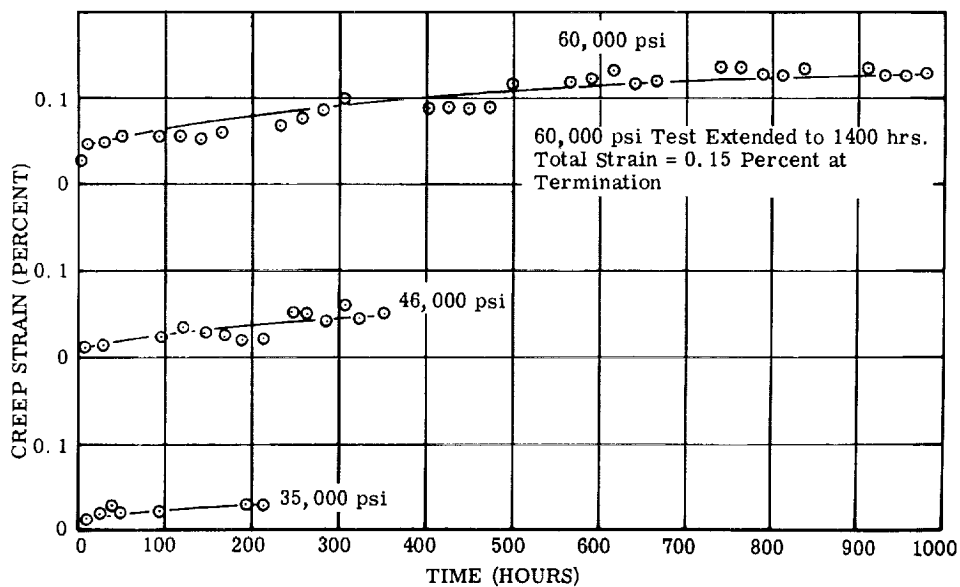
Figure 237. - Creep data for vacuum-melted forged Hiperco 27 alloy tested in air at 700° F and 35 000,
46 000, and 60 000 psi (data obtained by increasing stress on single specimen). (See table 27.)
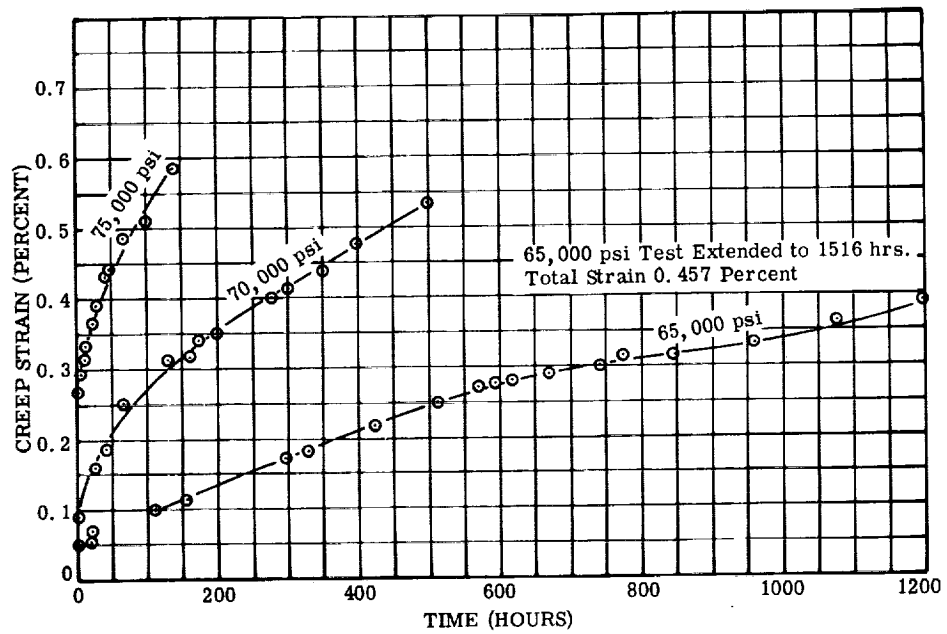
Figure 238. - Creep data for vacuum-melted forged Hiperco 27 alloy tested in air at 700° F and 65 000, 70 000, and 75 000 psi. (See tables 27 and 28.)
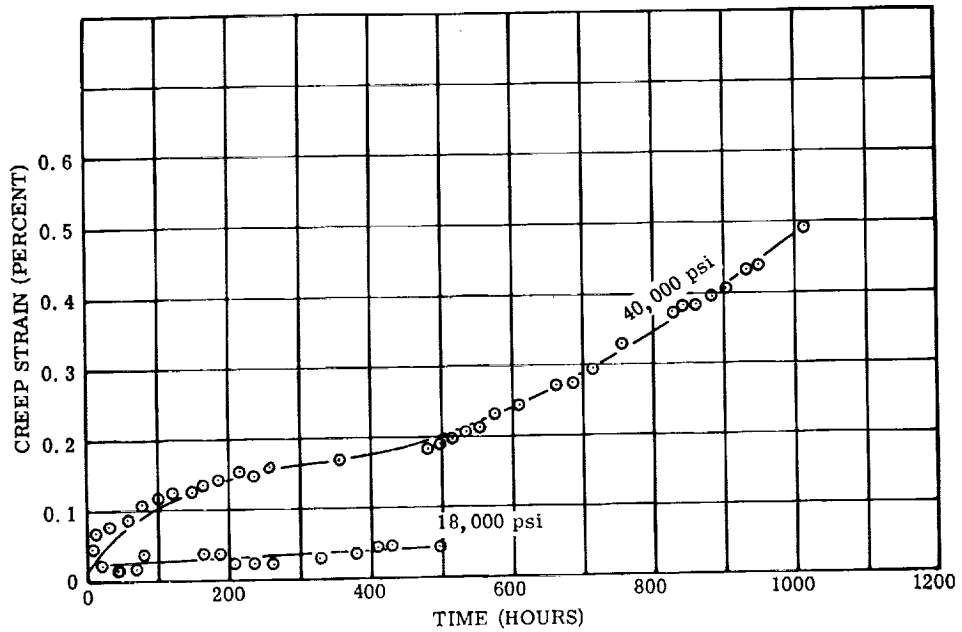
Figure 239. - Creep data for vacuum-melted forged Hiperco 27 alloy tested in air at 900° F and 18 000 and 40 000 psi (data obtained by increasing stress on one specimen). (See table 27.)

TABLE 28. - CREEP DATA FOR VACUUM-MELTED FORGED

HIPERCO 27 ALLOY TESTED IN AIR - SECOND TESTS

[Test, ASTM E139.]

Temperature, $^{\circ}$F	900	900	900	700	700
Stress, psi	46 000	44 000	48 000	70 000	65 000
Duration of test, hr	447	622	143	548	1516
Total creep strain, percent	0.5190	0.4848	0.4525	0.4489	0.457
Time to cause 0.2-percent creep strain, hr	94	202	28.0	36.0	372
Time to cause 0.4-percent creep strain, hr	303	511	118.0	276.0	1230
Plastic strain obtained on loading specimen, percent	0.0050	0.0201	0.0187	0.092	0.029
Strain-time plot given in fig. -	240	240	240	238	238
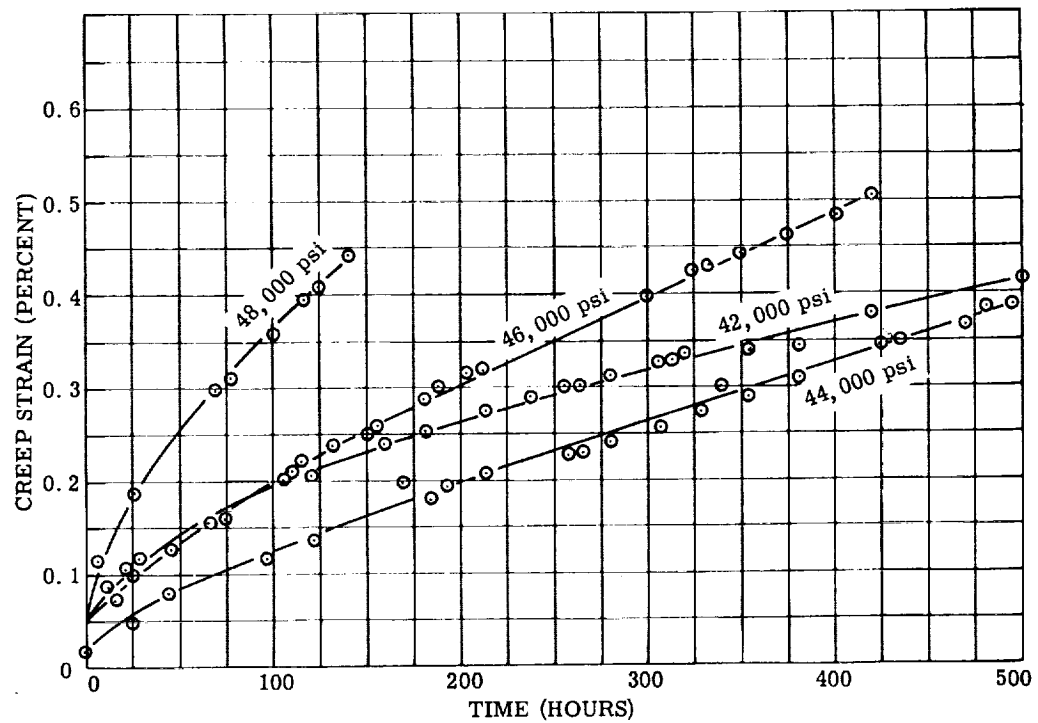
Figure 240. - Creep data for vacuum-melted forged Hiperco 27 alloy tested in air at 900° F and 42 000, 44 000, 46 000, and 48 000 psi. (See tables 28 and 29.)

TABLE 29. - CREEP DATA FOR VACUUM-MELTED FORGED

HIPERCO 27 ALLOY

[Test, ASTM E139; plastic strain obtained on loading specimen, O.]

Temperature, $^{\circ}$F	900	1100	1100	1100	1100	1400
Stress, psi	42 000	12 000	9000	7000	3000	800
Duration of test, hr	617	186.6	257.4	332	1024	56
Total creep strain, percent	0.494	0.84	0.52	0.337	0.236	0.587
Time to cause 0.2-percent creep strain, hr	108	76	127	182	755	14.7
Time to cause 0.4-percent creep strain, hr	482	122	213	-----	-----	34.8
Test atmosphere	Air	Argon	Argon	Argon	Air	Argon
Strain-time plot given in fig. -	240	241	241	241	241	242
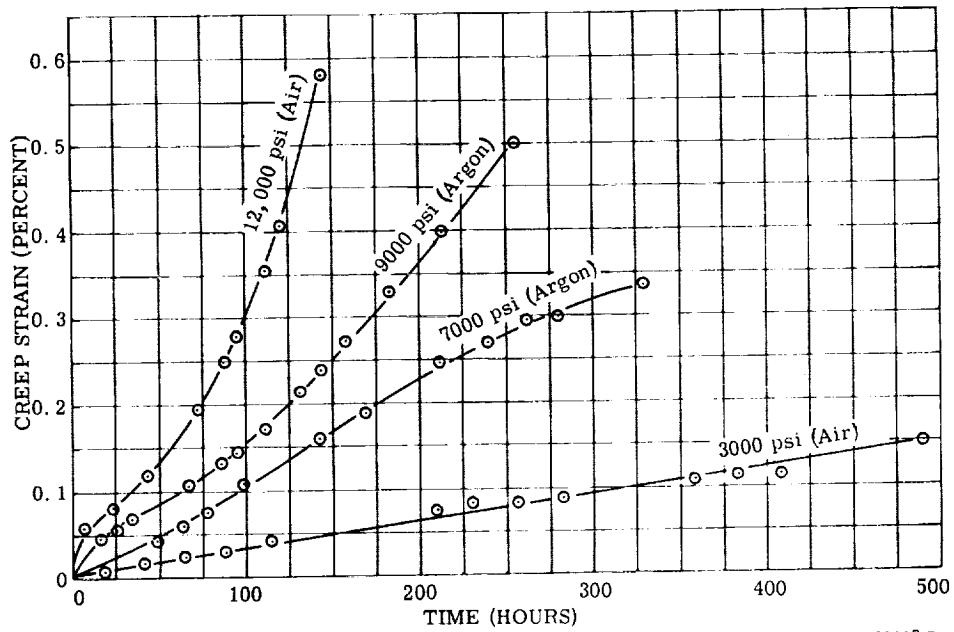
Figure 241. - Creep data for vacuum-melted forged Hiperco 27 alloy tested in air and argon at 1100° F
(3000-psi test terminated after 1030 hr at 0.23-percent creep strain). (See tables 27 and 29.)
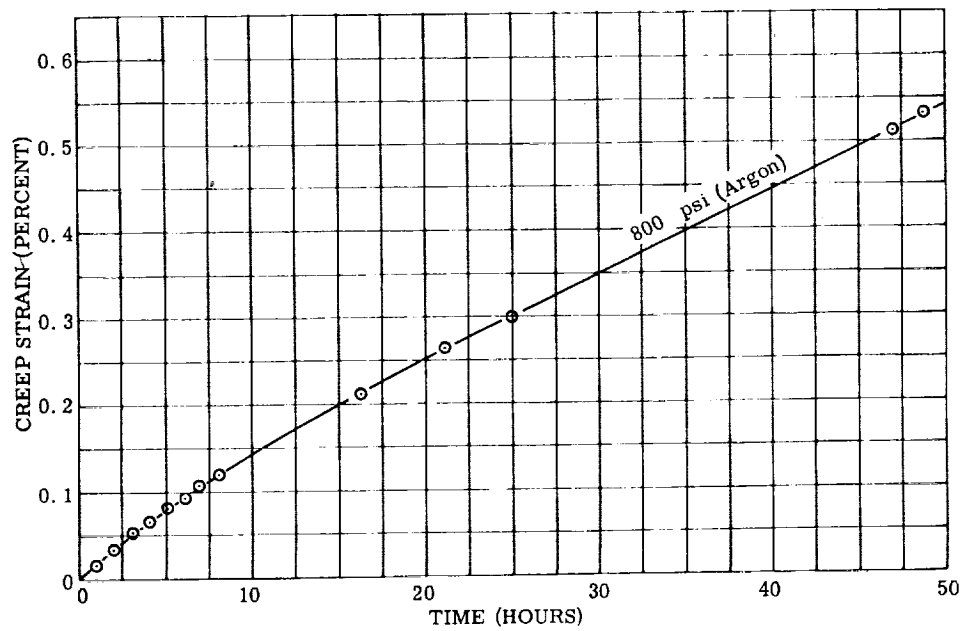
Figure 242. - Creep data for vacuum-melted forged Hiperco 27 alloy tested in argon at 1400° F. (See
table 29.)

TABLE 30. - CREEP DATA FOR VACUUM-MELTED

FORGED HIPERCO 27 BAR TESTED IN VACUUM

[Test, ASTM E139; see fig. 234 for Larson-Miller plot.]

Temperature, °F	700	900	1100	1100
Stress, psi	70 000	46 000	12 000	7000
Duration of test, hr	498	350	187	211
Total creep strain, percent	0.73	0.60	0.80	0.19
Time to cause 0.2-percent creep strain, hr	35	130	32	220
Time to cause 0.4-percent creep strain, hr	165	240	105	(a)
Plastic strain obtained on loading specimen, percent	-----	0	0	0
Larson-Miller parameter for 0.2-percent plastic strain	19.2	23.25	25.7	27.1
Larson-Miller parameter for 0.4-percent plastic strain	20.0	23.70	26.6	----

[a]Did not reach required strain.

TABLE 31. – CREEP DATA FOR INVESTMENT CAST AND ANNEALED HIPERCO 27 ALLOY TESTED IN AIR

[Test, ASTM E139.]

Temperature, °F	900	900	700	700	700	700	700	1100	1100	1100	1100	1100	1400	1400
Stress, psi	30 000	25 000	30 000	35 000	38 000	45 000	40 000	14 000	11 000	8000	3000	6000	2000	1200
Duration of test, hr	1102	1225	1200	1389	1686	1176	1578	74.1	138.8	646	1199	695	96.5	359
Total creep strain, percent	0.127	0.132	0.2061	0.1482	0.14	0.306	0.106	5.845	1.876	1.9416	0.132	0.525	1.9384	0.855
Time to cause 0.2-percent creep strain, hr	(a)	(a)	(b)	(a)	(a)	122	(a)	9.8	36	55	-----	190	8.5	60
Time to cause 0.4-percent creep strain, hr	(a)	(a)	-----	(a)	(a)	(a)	(a)	16	73	138	-----	505	22.5	166
Plastic strain obtained on loading specimen, percent	(c)	(c)	(c)	(c)	(c)	(c)	(c)	(c)	0.050	0	0	0	(c)	(c)
Strain-time plot given in fig. –	245	245	(b)	243	243	244	244	246	246	246	246	246	247	247

[a]Did not reach required strain.
[b]Not plotted; extensometer difficulties.
[c]Plastic strain not included in these data.
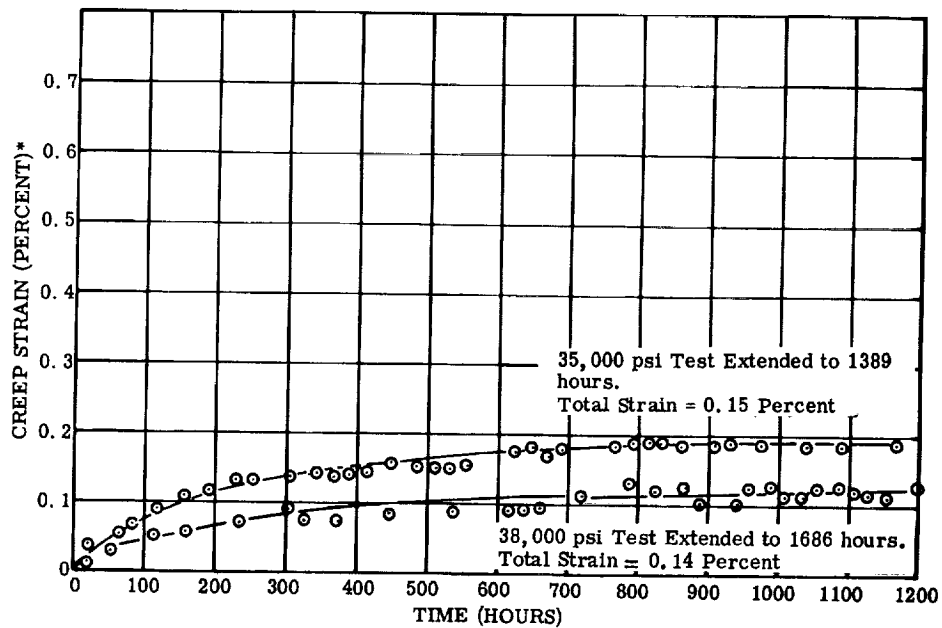
Figure 243. - Creep data for investment cast and annealed Hiperco 27 alloy tested in air at 700° F and
35 000 and 38 000 psi (plastic strain on load not included). (See table 31.)
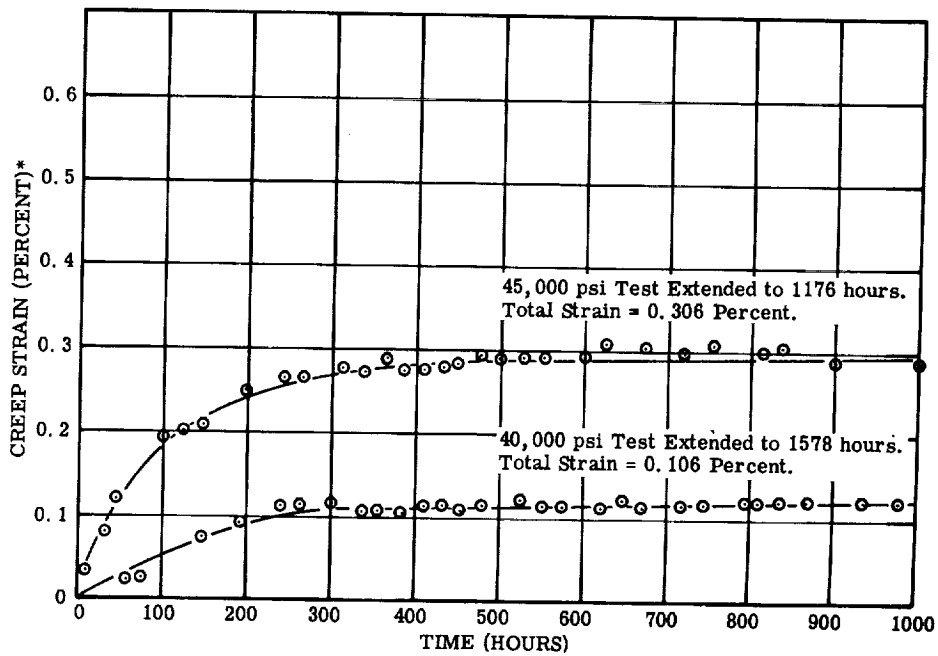
Figure 244. - Creep data for investment cast and annealed Hiperco 27 alloy tested in air at 700° F and
40 000 and 45 000 psi (plastic strain on load not included). (See table 31.)
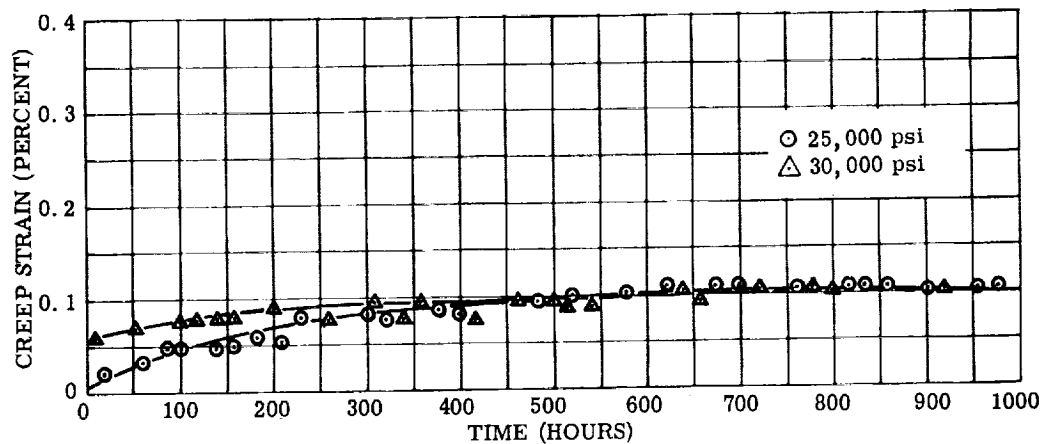
Figure 245. - Creep data for investment cast and annealed Hiperco 27 alloy tested in air at 900° F (plastic strain on load not included).   (See table 31.)
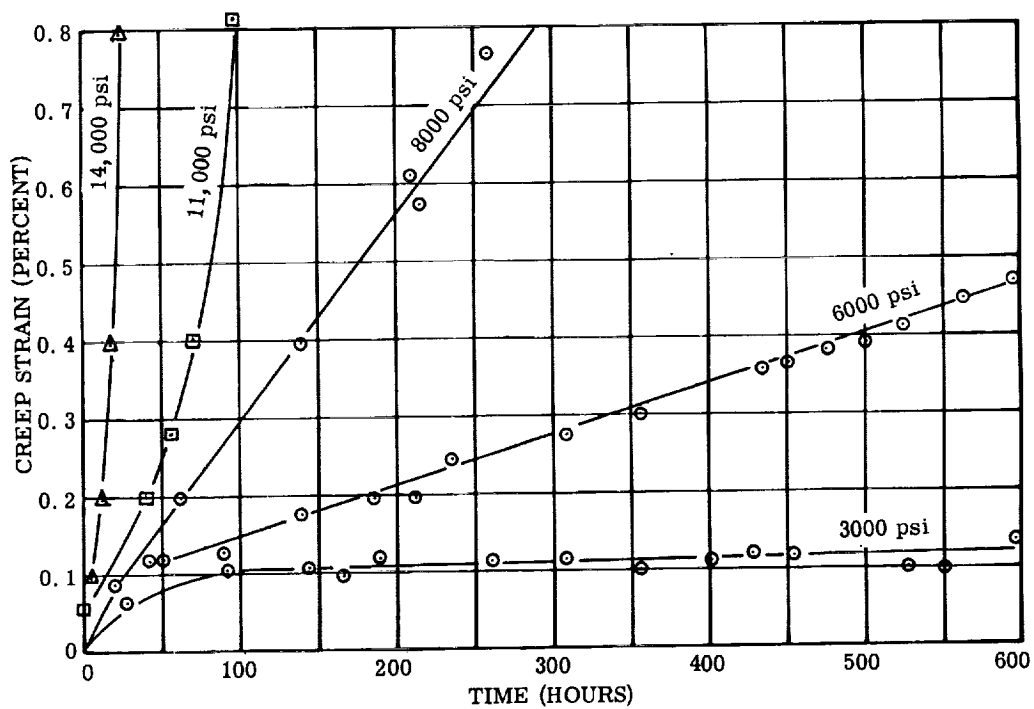
Figure 246. - Creep data for investment cast and annealed Hiperco 27 alloy tested in air at 1100° F.   (See table 31.)
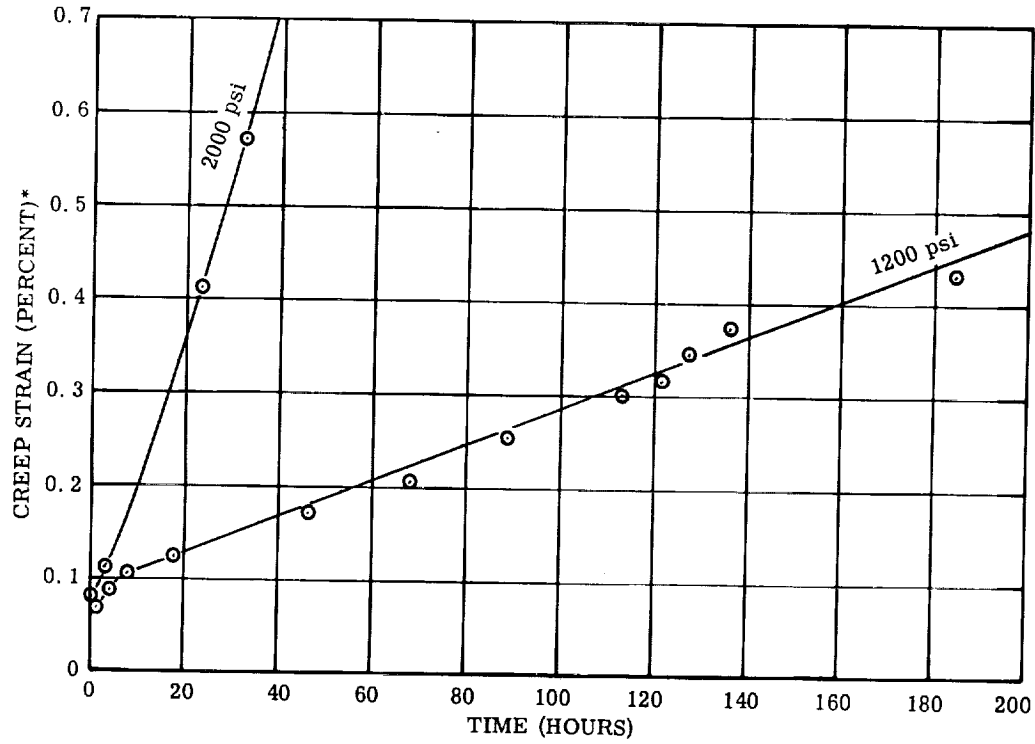
Figure 247. - Creep data for investment cast and annealed Hiperco 27 alloy tested in air at 1400° F (strain on load not included). (See table 31.)

TABLE 32. - CREEP DATA FOR INVESTMENT CAST AND

ANNEALED HIPERCO 27 ALLOY TESTED IN VACUUM

[Test, ASTM E139; see fig. 234 for Larson-Miller plot.]

Temperature, ^{O}F	700	900	1100	1100
Stress, psi	36 800	32 000	8000	11 000
Duration of test, hr	212	308	405	168
Total creep strain, percent	0.64	0.34	0.20	0.54
Time to cause 0.2-percent creep strain, hr	1.0	115	405	120
Time to cause 0.4-percent creep strain, hr	20.0	400	(a)	148
Plastic strain obtained on loading specimen, percent	0.13	0.10	0	0

[a]Did not reach required strain.

Iron 1-Percent Silicon Investment Casting (AMS 5210)

Iron 1-percent silicon investment casting (AMS 5210) is commercially available in the nominal composition of 1 percent silicon-iron. It was purchased and certified to conform to Aeronautical Materials Specification 5210. The actual chemical composition was not tested. When used as a magnetic material, it should be purchased to a performance requirement rather than chemical analysis.

Thermophysical properties.

Density, lb/cu in. (g/cu cm) 0.28 (7.75)

Solidus temperature, ^{O}F 2210

Curie temperature, ^{O}F 1380

Thermal conductivity, (Btu)(ft)/(sq ft)(hr)(^{O}F), at -

72° F 23.6

500° F 22.0

700° F 20.8

Coefficient of thermal expansion (from 72° to 932° F) (ref. 17),

in./(in.)(^{O}F) . . . . 8.0×10^{-6}

Specific heat (at 72° and 500° F), Btu/(lb)(^{O}F) 0.10

Electrical resistivity (ref. 9), ohm-cm, at -

72° F . . . . 21.0×10^{-6}

500° F . . . . 40.5×10^{-6}

700° F . . . . 51.0×10^{-6}

Magnetic properties. - All magnetic materials are stress relief annealed (SRA) unless otherwise specified. Investment-cast materials are not suitable for ac application; losses are very high. Constant current flux reset (CCFR) properties were not applicable to this material; they were measured only on materials used in magnetic amplifiers.

Direct current properties (solid ring) (H = 300 Oe):

Temperature, ^{O}F	Induction, B_{tip}, kG
72	21.0
800	19.8
1100	17.2

Mechanical properties. - Creep was not determined since the material is not used in highly stressed applications. Fatigue was not determined since the material is not used in cyclic stressed applications. The normal heat treatment was in accordance with AMS 5210.

Tensile properties:

Temper- ature, $^{\circ}F$	0.20-Percent offset yield strength, psi	Tensile strength, psi	Elongation in 1 in., percent	Reduction of area, percent	Modulus of elasticity (estimated), psi
72	28 950	54 200	37.2	60.6	28×10^6
800	22 900	41 000	36.7	67.8	------

TEMPERATURE (°F)

$(300°C < T \leq 500°C)$, $C_v = 0.18682 \times 10^{-5}T^2 - 0.12382 \times 10^{-2}T + 0.30489$ (Cal/Gram-°C)

$(0°C \leq T \leq 300°C)$, $C_v = 0.10$

SPECIFIC HEAT (CALORIES/GRAM - °C) OR (BTU/LB - °F)
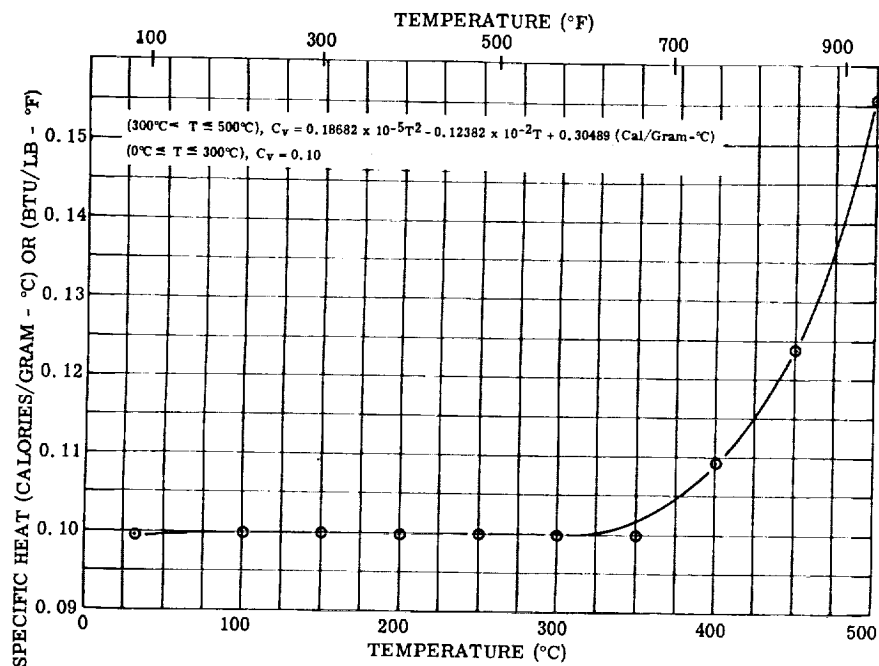
TEMPERATURE (°C)

Figure 248. - Specific heat of 1 percent silicon-iron in vacuum (10^{-5} Torr).

MAGNETIZING FORCE (AMPERE TURNS/INCH)

INDUCTION (KILOGAUSS)

INDUCTION (KILOLINES/INCH^2)

	H_c (Oersteds)	B_r (Gauss)	From Oersteds)
x Initial RT	1.05	10,400	250
⊕ 800°F	0.97	6,700	250
△ 1100°F	0.58	4,900	250

MAGNETIZING FORCE (OERSTEDS)
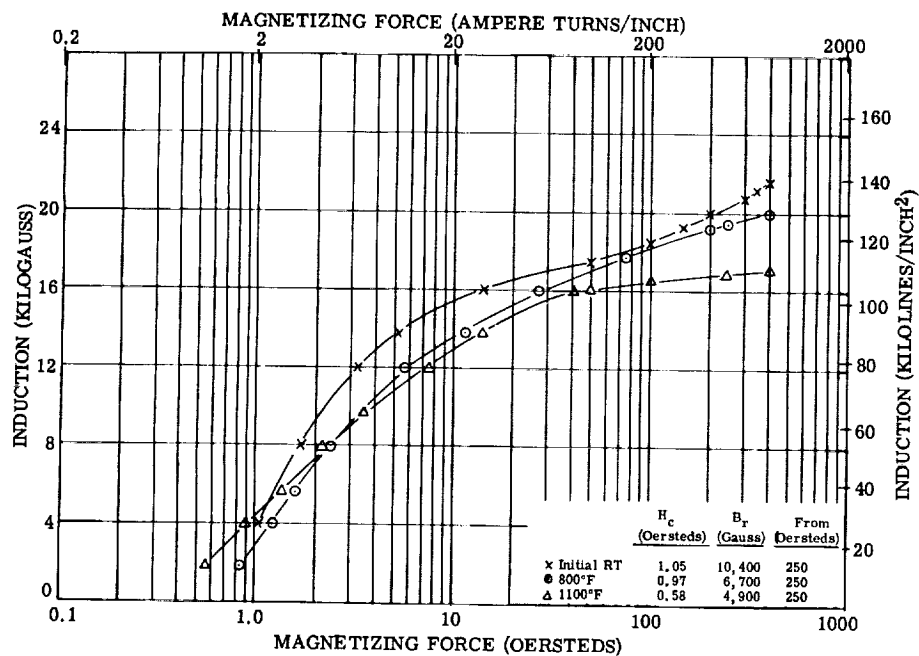
Figure 249. - Direct-current magnetization curves for AMS 5210 (1% Si-Fe) casting at initial room temperature, 800°, and 1100° F. Test atmosphere, air to 800° F and argon above 800° F.
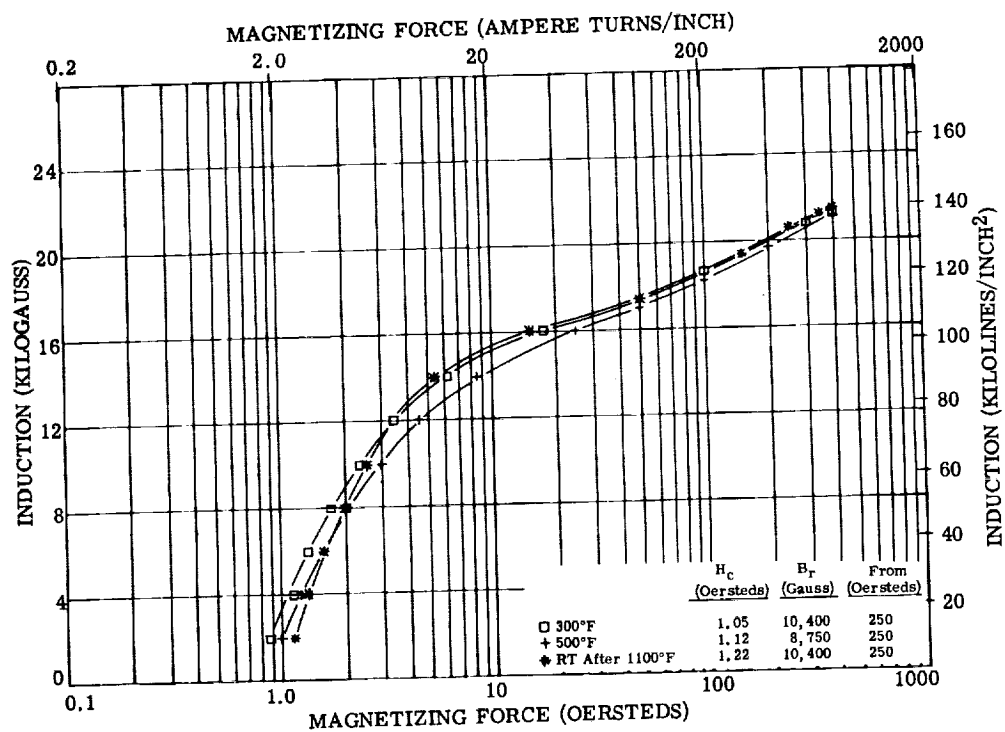
Figure 250. - Direct-current magnetization curves for AMS 5210 (1% Si-Fe) casting at 300°, 500° F, and room temperature after 1100° F. Test atmosphere, air to 800° F and argon above 800° F.

TABLE 33. - ROOM AND ELEVATED TEMPERATURE PROPERTIES OF AMS 5210 (1% Si-Fe)

[See figs. 251 and 252; strain rate, 0.005 in./(in.)(min) to yield and 0.050 in./(in.)(min) to failure.]

Specimen	Diameter, in.	Test temperature, °F	Hardness, Rockwell B	0.02 Percent offset yield strength, psi	0.2 Percent offset yield strength, psi	Ultimate strength, psi	Elongation in 1 in., percent	Reduction of area, percent
1	0.252	Room	64, 65, 66	25 450	28 450	55 200	36.1	56.1
2	.249	Room	65, 66, 66	25 850	29 450	53 200	38.3	65.1
3	.250	500	62, 63, 65	19 250	25 250	60 700	21.5	(a)
4	.248	500	65, 66, 67	22 750	26 200	62 100	22.6	44.3
5	.251	800	64, 64, 66	20 350	23 150	41 050	36.7	61.0
6	.251	800	62, 63, 64	19 550	22 700	41 000	36.7	74.5
7	.248	1000	62, 63, 64	13 150	15 100	20 800	53.6	80.7
8	.249	1000	62, 63, 63	14 100	15 950	20 400	63.0	85.2

[a]Nonuniform fracture area; percent reduction not calculated.
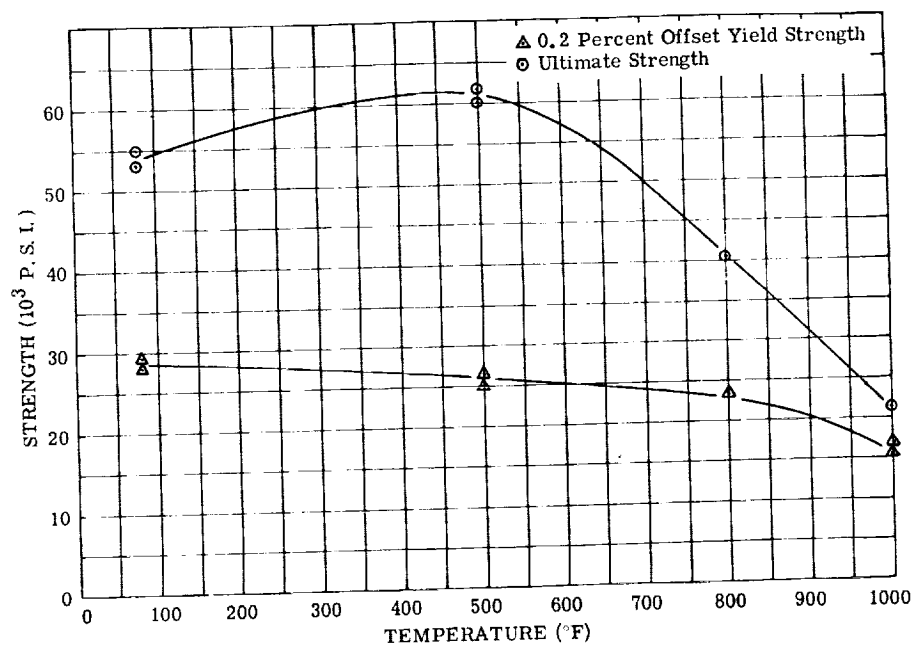
Figure 251. - Room- and elevated-temperature tensile strength properties in air of AMS 5210 (1% Si-Fe). (See table 33.)
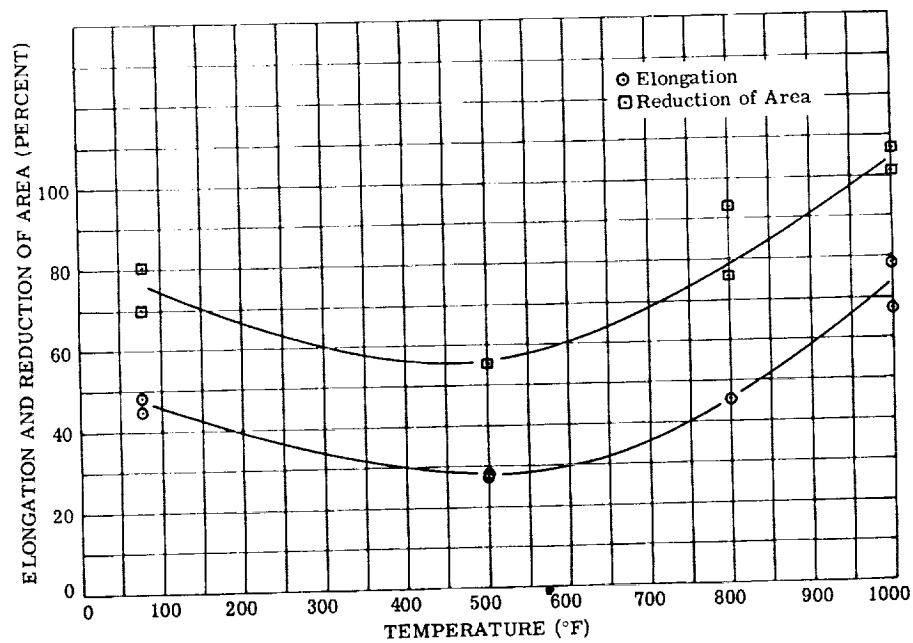
Figure 252. - Room- and elevated-temperature tensile ductilities of AMS 5210 (1% Si-Fe). (See table 33.)

15-Percent-Nickel Maraging Steel

The 15-percent-nickel maraging steel is an ultra-high-strength martensitic age-hardenable steel, possessing high strength and increased resistance to softening at elevated temperatures. It is available commercially in the nominal composition of 9 percent cobalt, 5 percent molybdenum, 0.70 percent titanium, 0.70 percent aluminum, 15 percent nickel, and the remainder, iron. Its tested composition agreed with the nominal composition.

Thermophysical properties. -

Density, lb/cu in. (g/cu cm) 0.289 (8.00)

Solidus temperature, ^oF . . . . approx. 2600

Curie temperature . . . . In maraging steel, time-temperature dependent (not fixed point, as in Cubex or H-11 alloys)

Coefficient of thermal expansion (from 72° to 900° F), in./(in.)(^oF) . . . 5.6×10^{-6}

Electrical resistivity at 72° F, ohm-cm . . . . 38×10^{-6}

Magnetic properties. - All magnetic materials were at a hardness of Rockwell C54.5 unless otherwise specified. Constant current flux reset properties are not applicable for maraging steel and were measured only for materials used in magnetic amplifiers.

Direct current:

Temperature, ^oF	H, Oe	Solid ring	0.016-in.-thick laminations
		Induction, B_{tip}, kG	
72	250	18.0	19.0
300	250	----	18.2
500	250	----	17.7
700	250	16.3	----
800	250	----	16.3
900	250	15.6	----
1100	200	13.0	----

Alternating current (400 cps; 0.016-in.-thick laminations; B = 10 kG):

Temperature, °F	Exciting volt-amperes per pound	Core loss, W/lb
72	177	108
300	180	106
500	177	104
800	181	102

Mechanical properties. - Poisson's ratio at 72° F is 0.31. This alloy possesses little potential for stressed applications at temperatures above 800° to 850° F, and the fatigue properties were therefore not determined. The normal heat treatment for this material is the same as for the 18-percent-nickel maraging steel.

Tensile properties:

Temperature, °F	0.20-Percent offset yield strength, psi	Tensile strength, psi	Elongation in 2 in., percent	Reduction of area, percent	Modulus of elasticity, psi
72	291 000	299 000	15	44	27.5×10^6
400	255 000	265 000	8	52	--------
600	250 000	264 000	8	52	--------
800	226 000	246 000	9	52	--------

Creep for bar stock tested in air:

Temperature, °F	Time, hr	Stress, psi, to produce creep of -	
		0.20 Percent	0.40 Percent
700	1 000	214 000 to 219 000	243 000
700	10 000	204 000 to 205 000	230 000
900	1 000	14 500 to 27 000	40 500 to 42 700
900	10 000	2 800 to 7 240	12 000 to 18 500

18-Percent-Nickel Maraging Steel

The 18-percent-nickel maraging steel is an ultra-high-strength martensitic age-hardenable steel, available commercially in the nominal composition of 8 percent cobalt, 4 percent molybdenum, 0.15 to 0.80 percent titanium, 18 percent nickel, and the balance, iron. It was not analyzed for exact composition. When used as a magnetic material, this steel should be purchased to a performance requirement rather than to a chemical analysis.

Thermophysical properties. -

Density, lb/cu in. (g/cu cm) 0.289 (7.93)
Solidus temperature, ^{O}F . . . . approx. 2600
Curie temperature . . . . In maraging steel, time-temperature
          dependent (not fixed point, as in Cubex or H-11 alloys)
Thermal conductivity (unpublished information from International Nickel Co.),
(Btu)(ft)/(sq ft)(hr)(^{O}F), at -
    72° F 8.4
    800° F. 11.4
Coefficient of thermal expansion (from 72° to 900° F), in./(in.)(^{O}F) . . . 5.6×10^{-6}
Specific heat (at 32° to 212° F) (unpublished information from International
    Nickel Co.), Btu/(lb)(^{O}F). 0.12
Electrical resistivity (at 72° F; full hard material), ohm-cm . . . . . . .38.0×10^{-6}

Magnetic properties (250 grade material). - All magnetic materials were at a hardness of Rockwell C51 to C53 unless otherwise specified. Constant current flux reset properties are not applicable for maraging steel and were measured only for materials used in magnetic amplifiers.

Direct current (H = 250 Oe):

Temperature, ^{O}F	Solid ring	0.014-in.-thick laminations
		Induction, B_{tip}, kG
72	17.6	18.1
300	----	17.6
500	----	16.8
800	15.0	15.1

Alternating current (400 cps; 0.01-in.-thick laminations; B = 10 kG):

Temperature, °F	Exciting volt-amperes per pound	Core loss, W/lb
72	285	116
300	294	118
500	308	119
800	336	118

Mechanical properties. - Poisson's ratio at 72° F (ref. 11) is 0.30. The normal heat treatment for this material is to heat to 1500°±25° F, hold at uniform temperature for 1 hour, cool at any convenient rate to produce the martensitic structure at room temperature, then age-harden for 3 hours at 875° to 925° F, and cool.

Tensile properties (all data except modulus of elasticity from ref. 11):

Temperature, °F	0.20-Percent offset yield strength, psi	Tensile strength, psi	Elongation, percent, in -		Reduction of area, percent	Modulus of elasticity, psi
			1 in.	2 in.		
72	250 000	257 000	12	--	55	27×10^6
700	220 600	240 000	--	15	55	------
900	185 000	197 000	--	15	63	------

Creep for bar stock tested in air (creep data taken and calculated from Larson-Miller plot in fig. 266, p. 234):

Temperature, °F	Time, hr	Stress, psi, to produce creep of -	
		0.20 Percent	0.50 Percent
700	1 000	133 000	164 000
700	10 000	110 000	128 000
900	1 000	51 400	59 000

Fatigue strength at 72° F for 10^7 cycles (ref. 11):

Material	Strength, psi
Notched bar, air melted	45 000
Smooth bar, vacuum melted	115 000
Smooth bar, air melted	97 000
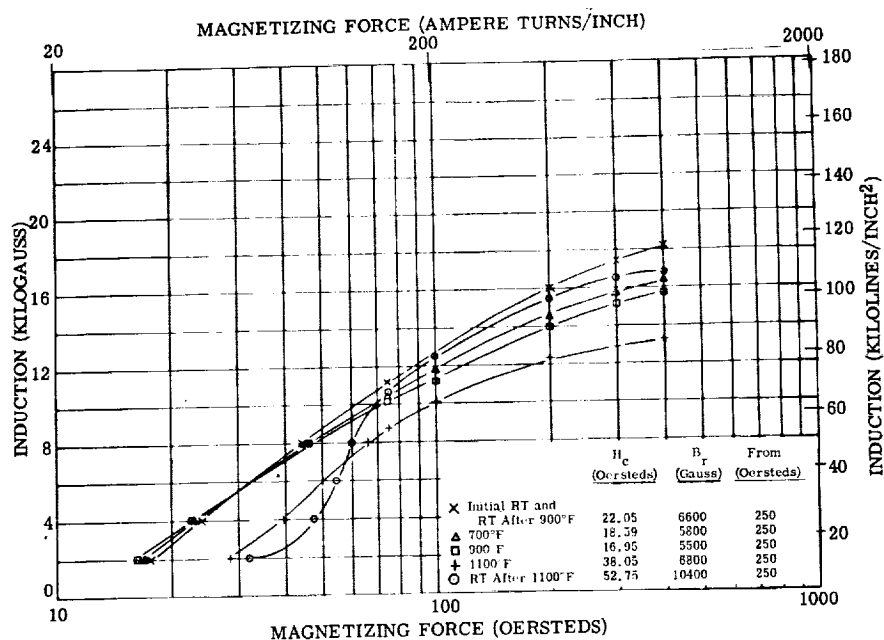
Figure 253. - Direct-current magnetization curves for 15-percent-nickel maraging steel forging.
Test atmosphere, air; data from work performed by Westinghouse under Contract AF33(615)-1551.
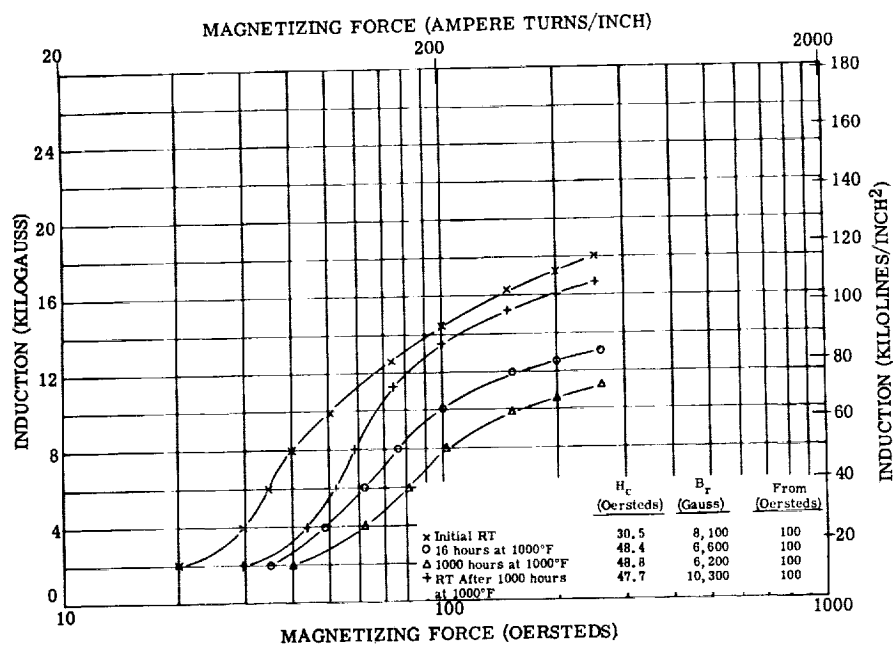
Figure 254. - Direct-current magnetization curves for 15-percent-nickel maraging steel
forging, aging test. Test atmosphere, argon.

MAGNETIZING FORCE (AMPERE TURNS/INCH)

	H$_c$ (Oersteds)	B$_r$ (Gauss)	From (Oersteds)
X Initial RT	22.6	11,300	100
O 300°F	22.2	10,850	100
△ 500°F	21.2	10,600	100
□ 800°F	19.6	9,700	100
✳ RT After 800°F	22.5	11,300	100

MAGNETIZING FORCE (OERSTEDS)
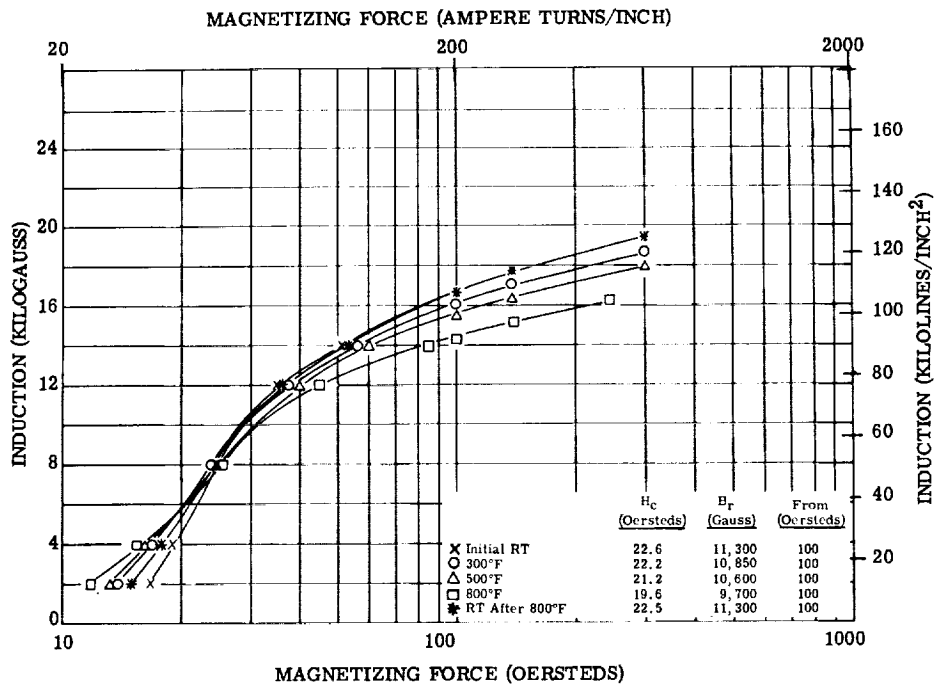
Figure 255. - Direct-current magnetization curves for 15-percent-nickel maraging steel 0.016-inch laminations. Test atmosphere, air; interlaminar insulation, aluminum orthophosphate.

x Initial RT
O 300°F
△ 500°F
□ 800°F
✳ RT After 800°F

VOLT-AMPERES PER POUND
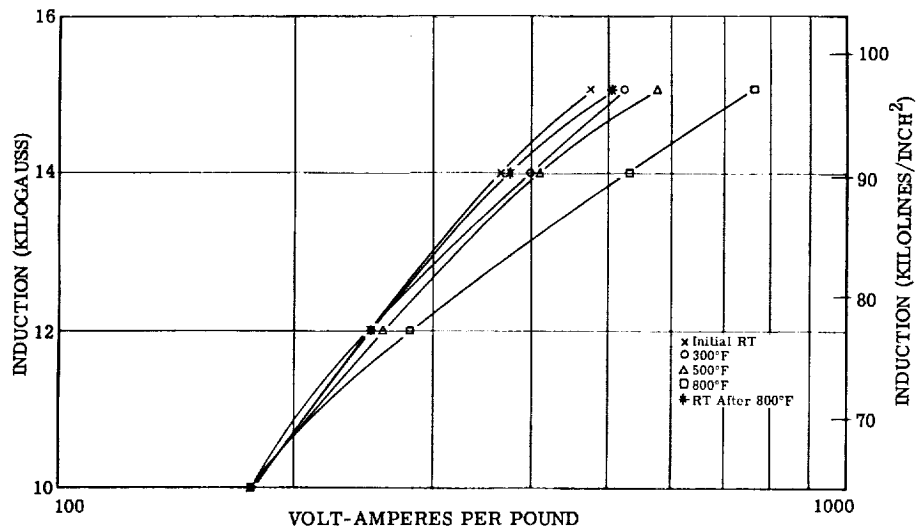
Figure 256. - Exciting volt-amperes per pound at 400 cps for 15-percent-nickel maraging steel 0.016-inch laminations. Test atmosphere, air; interlaminar insulation, aluminum orthophosphate.
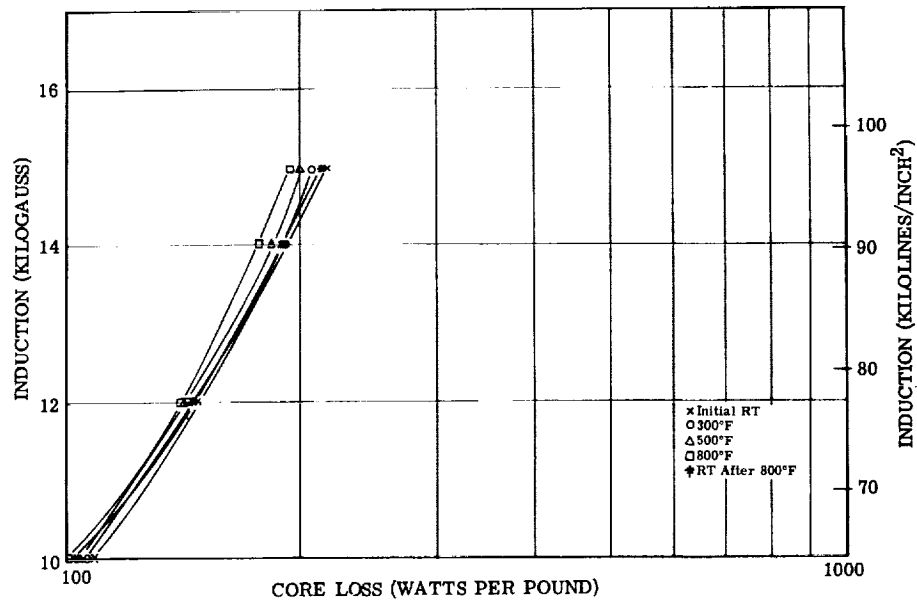
Figure 257. - Core loss at 400 cps for 15-percent-nickel maraging steel 0.016-inch laminations. Test atmosphere, air; interlaminar insulation, aluminum orthophosphate.
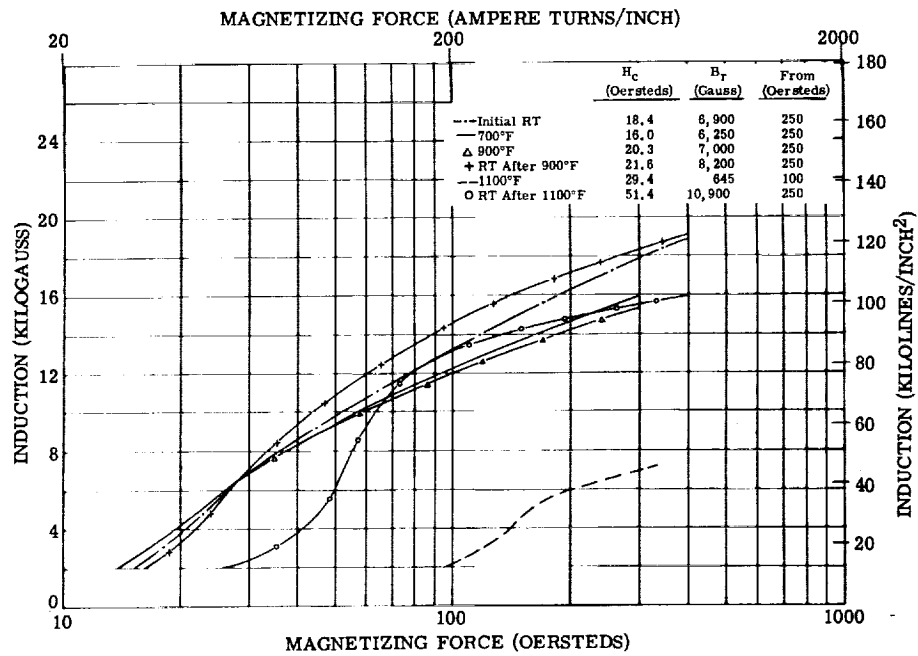
Figure 258. - Direct-current magnetization curves for 18-percent-nickel maraging steel forging. Test atmosphere, air; data from work performed by Westinghouse under Contract AF33(615)-1551.

MAGNETIZING FORCE (AMPERE TURNS/INCH)

	H$_c$ (Oersteds)	B$_r$ (Gauss)	From (Oersteds)
x Initial RT	27.19	8,150	200
o 300°F	26.33	7,800	200
Δ 500°F	26.33	7,500	200
□ 800°F	29.27	7,100	200
+ RT After 800°F	30.62	7,200	200

INDUCTION (KILOGAUSS)

INDUCTION (KILOLINES/INCH^2)

MAGNETIZING FORCE (OERSTEDS)
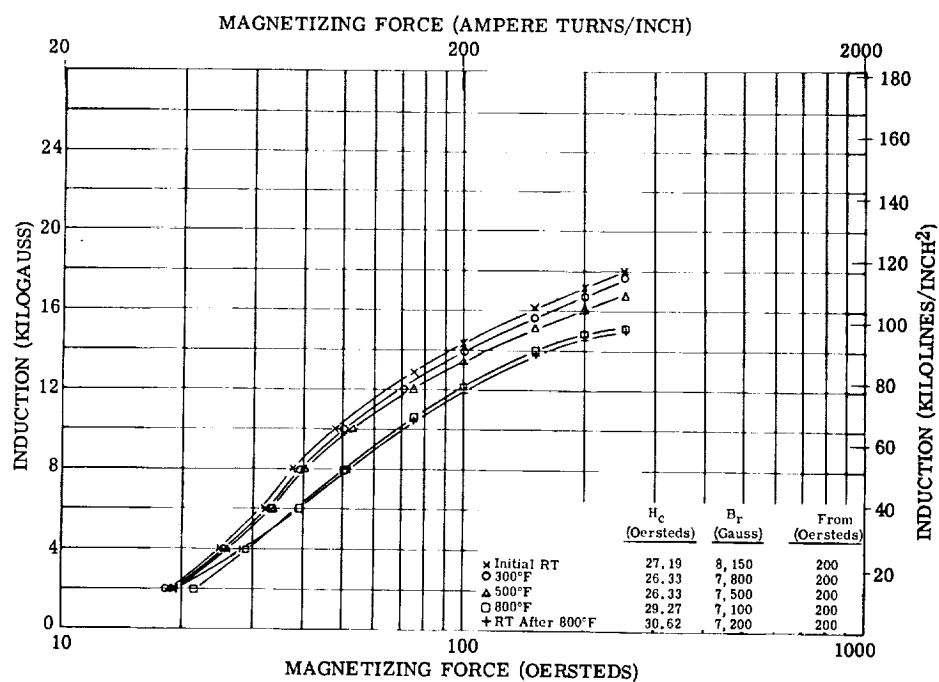
Figure 259. - Direct-current magnetization curves for 18-percent-nickel maraging steel 0.014-inch laminations. Test atmosphere, air; interlaminar insulation, aluminum orthophosphate.

INDUCTION (KILOGAUSS)

INDUCTION (KILOLINES/INCH^2)

X Initial RT
O 300°F
Δ 500°F
□ 800°F

VOLT-AMPERES PER POUND
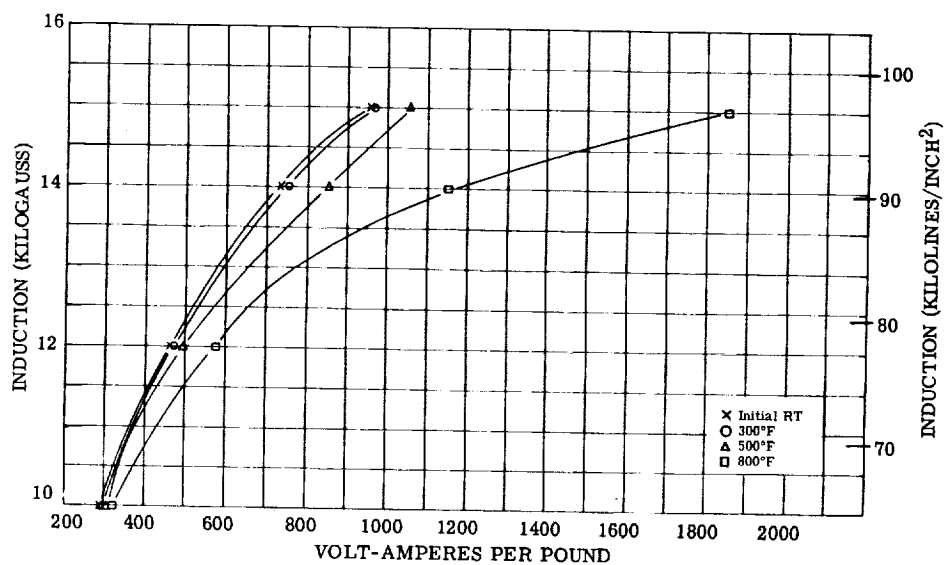
Figure 260. - Exciting volt-amperes per pound at 400 cps for 18-percent-nickel maraging steel 0.014-inch laminations. Test atmosphere, air; interlaminar insulation, aluminum orthophosphate.
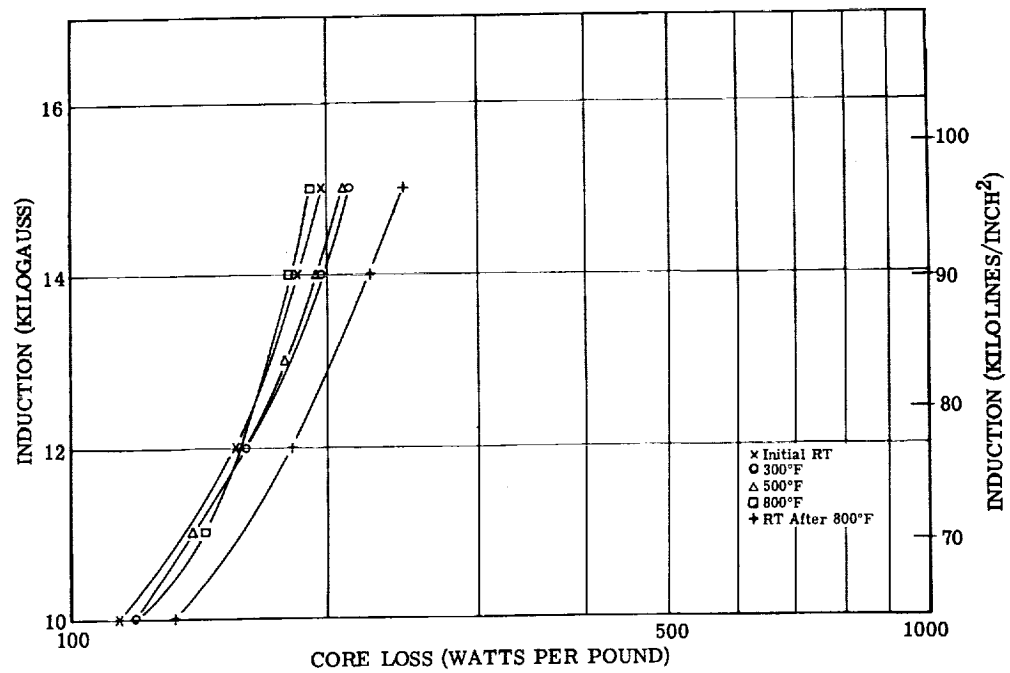
Figure 261. - Core loss at 400 cps for 18-percent-nickel maraging steel 0.014-inch laminations. Test atmosphere, air; interlaminar insulation, aluminum ortnophosphate.

TABLE 34. - TENSILE PROPERTIES OF 15-PERCENT-NICKEL MARAGING STEEL

TESTED IN AIR WITH TWO DIFFERENT HEAT TREATMENTS

[Ref. 13; see fig. 262; samples held at test temperature 1 hr before test.]

Heat treatment	Test temper- ature, °F	0.2 Percent offset yield strength, psi	Ultimate tensile strength, psi	Elongation, percent	Reduction of area, percent	Hardness after testing, Rockwell C
Material held at 1500° F for 1 hr, water quenched, and aged 3 hr at 900° F	70	291 000	299 000	15	44	----
	200	271 000	281 000	8	46	54.0
	400	255 000	265 000	8	52	54.1
	600	240 000	264 000	8	51	54.6
	800	226 000	246 000	9	52	55.3
	1000	177 000	192 000	15	48	55.5
Material held at 1800° F for 1 hr, water quenched, and aged 3 hr at 900° F	70	262 000	281 000	13	50	----
	200	250 000	268 000	10	52	----
	400	235 000	255 000	9	55	----
	600	225 000	241 000	12	53	----
	800	206 000	230 000	10	54	----
	1000	210 000	230 000	9	53	----

TABLE 35. - TENSILE PROPERTIES OF 18-PERCENT-

NICKEL MARAGING STEEL TESTED IN AIR

[Ref. 13; see fig. 262.]

Test temper- ature, °F	0.20 Percent offset yield strength, psi	Ultimate tensile strength, psi	Elongation, percent	Reduction of area, percent
12	250 000	257 000	6	57
200	238 000	250 000	12	59
400	228 000	240 000	11	58
600	216 000	228 000	10	57
800	196 000	210 000	12	60
1000	138 000	158 000	22	80
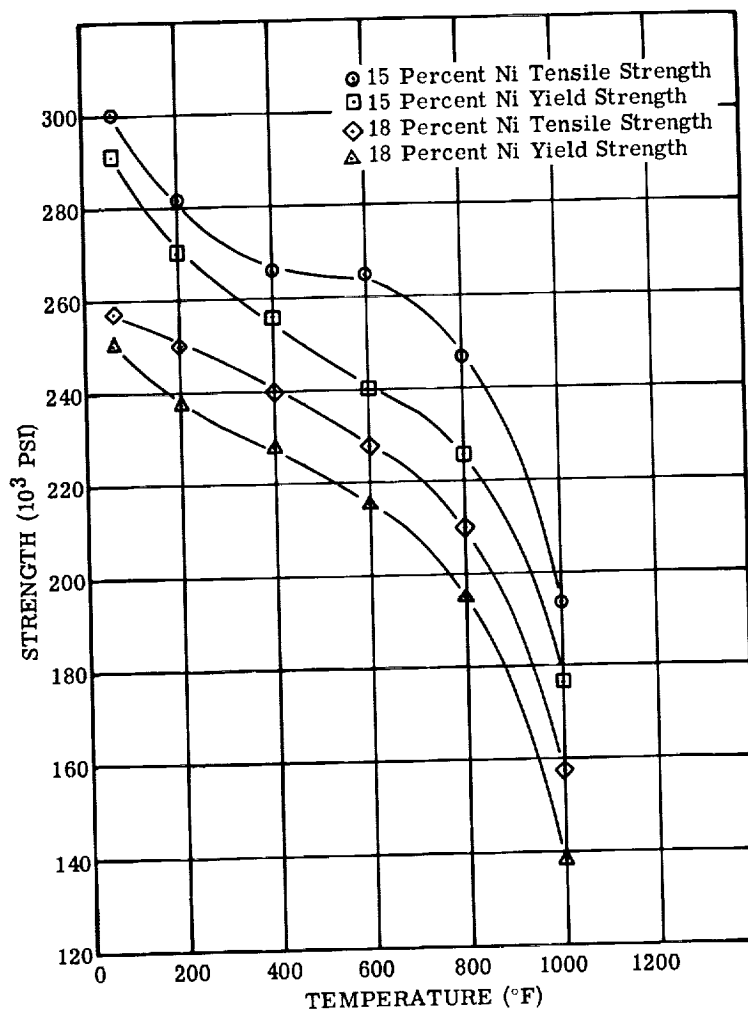
Figure 262. – Tensile strength of 15- and 18-percent-nickel maraging steels tested in air. (See tables 34 and 35, ref. 11.)
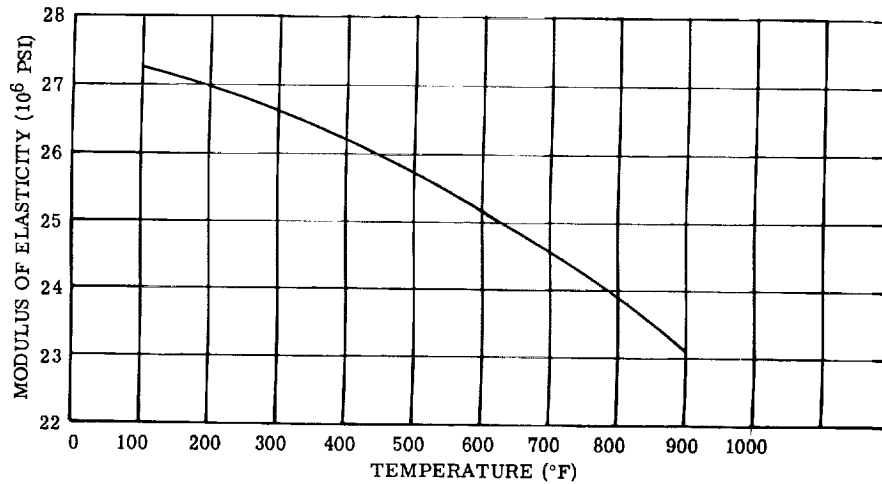
Figure 263. - Dynamic modulus of elasticity for 18-percent-nickel maraging steel, 250 000-psi grade (ref. 11).
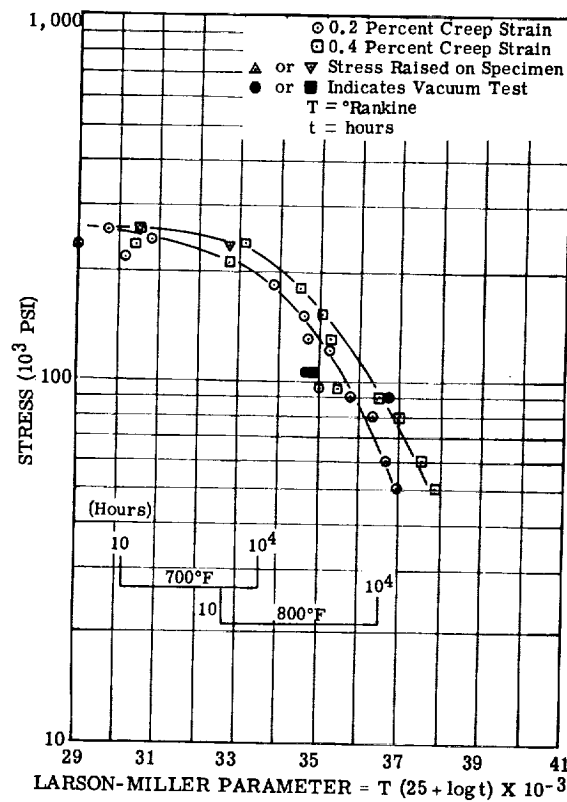
Figure 264. - Larson-Miller plot of 15-percent-nickel maraging steel creep data, based on maximum of 2000-hour data.
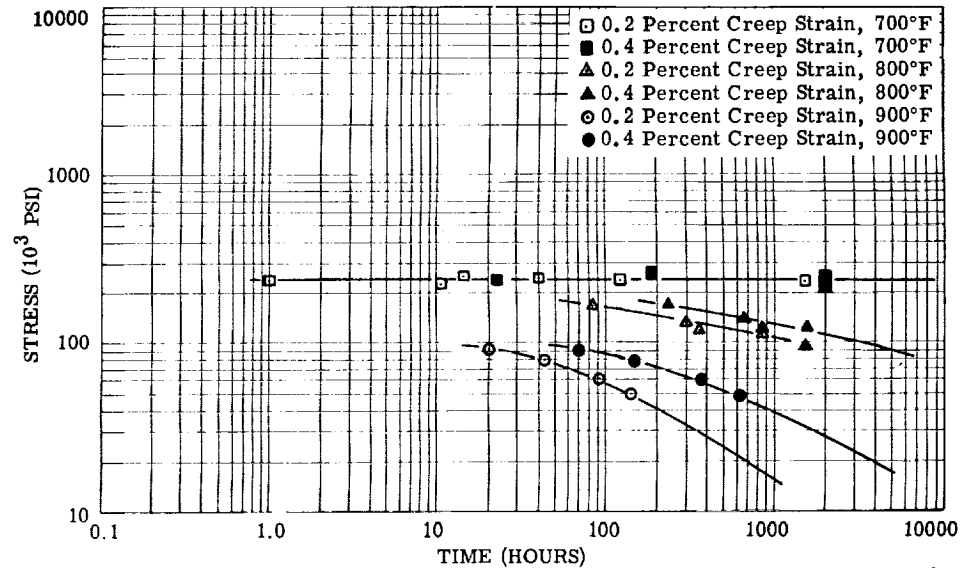
Figure 265. - Variation of time with 0.20 and 0.40 percent creep strain for 15-percent-nickel maraging steel tested in air.
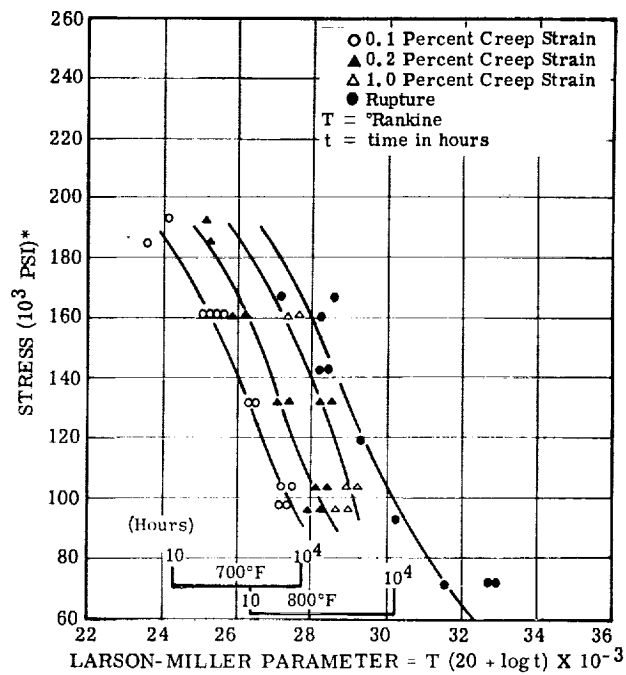
Figure 266. - Larson-Miller plot of creep and rupture strengths for 18-percent-nickel maraging steel aged at 900° F for 3 hours, based on maximum of 2000-hour data (ref. 12). (For purposes of comparison, ultimate strength is taken at 257 000 psi.)

TABLE 36. - CREEP DATA FOR 15-PERCENT-NICKEL MARAGING STEEL TESTED IN AIR

[Test, ASTM E139; see figs. 267 to 270.]

Temperature, ^{O}F	700	[a]700	700	700	800	800	800	800
Stress, psi	150 000	230 000	240 000	216 000	120 000	130 000	150 000	180 000
Duration of test, hr	811	[b]1685	[b]1385	[b]665	[b]1920	1028	[b]1150	314
Total creep strain, percent	0.115	0.195	0.40	0.343	0.425	0.463	0.706	0.525
Time to cause 0.2-percent creep strain, hr	(c)	1670	40	11	840	345	290	82
Time to cause 0.4-percent creep strain, hr	(c)	(c)	[d]1985	[d]1920	1765	870	652	231
Plastic strain obtained on loading specimen, percent	0	0	0.0362	0.1111	0	0	0	0
Strain-time plot given in figure -	267	267	268	268	269	269	270	270

[a]Data obtained by increasing stress.
[b]Test not completed at publishing date.
[c]Did not reach required strain.
[d]Extrapolated.

TABLE 37. - CREEP DATA FOR 15-PERCENT-NICKEL MARAGING STEEL TESTED IN AIR

[Test, ASTM E139; see figs. 271 to 275.]

Temperature, °F	900	900	700	700	700	800	900	900
Stress, psi	80 000	90 000	235 000	180 000	a259 000	95 000	50 000	60 000
Duration of test, hr	261	140	356	332	461	1513	838	522
Total creep strain, percent	0.521	0.643	0.525	0.048	0.589	0.375	0.447	0.482
Time to cause 0.2-percent creep strain, hr	42.0	14.5	1	----	17	460	138	92.0
Time to cause 0.4-percent creep strain, hr	155	68.5	23	----	183	1620	610	358
Plastic strain obtained on loading specimen, percent	0	0	0.1722	0	0.048	0	0	0
Strain-time plot given in fig.	275	275	271	271	271	272	273	274

aData for this test obtained by increasing stress on 180 000-psi specimen.

TABLE 38. - CREEP DATA FOR 15-PERCENT-NICKEL

MARAGING STEEL TESTED IN VACUUM

[Test, ASTM E139; see fig. 264 for Larson-Miller plot;
plastic strain obtained on loading specimen, 0.]

Test temperature, ^{O}F	800	900	900
Stress, psi	107 500	60 000	90 000
Duration of test, hr	283	502	192
Total creep strain, percent	0.07	0.07	0.26
Time to cause 0.2-percent creep strain, hr	[a]325	(b)	120
Time to cause 0.4-percent creep strain, hr	[a]395	(b)	(b)

[a]Extrapolated data.
[b]Did not reach required strain.
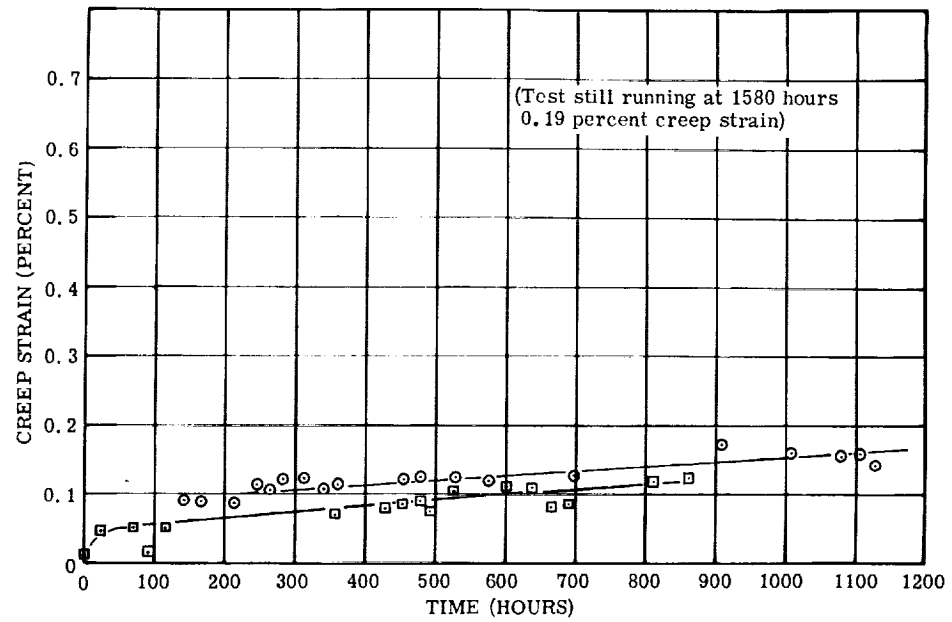
Figure 267. - Creep data for 15-percent-nickel maraging steel tested in air at 700° F (data obtained by increasing stress on single specimen). (See table 36.)
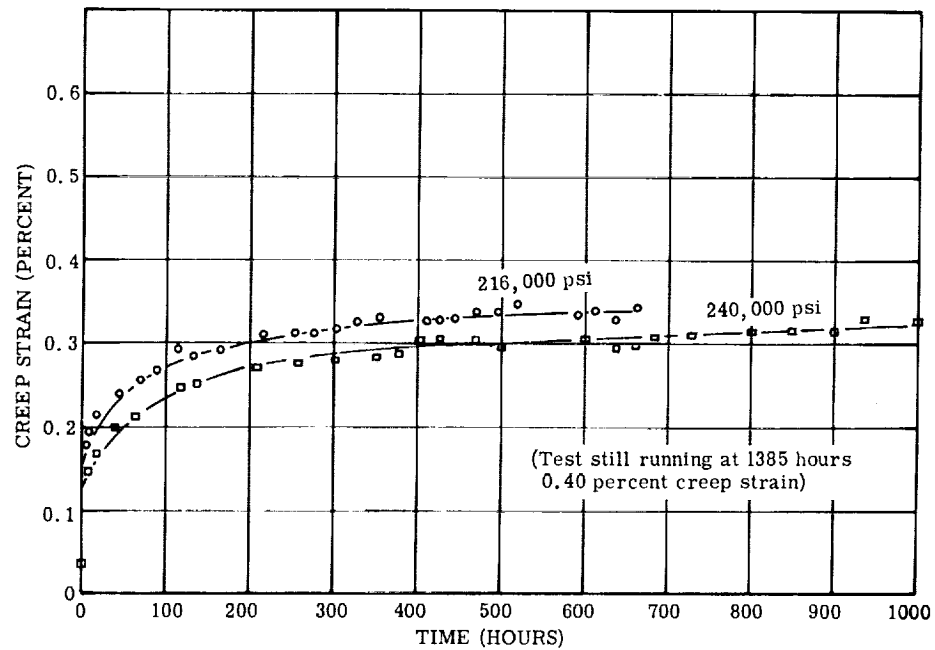
Figure 268. - Creep data for 15-percent-nickel maraging steel tested in air at 700° F and 216 000 and 240 000 psi. (See table 36.)
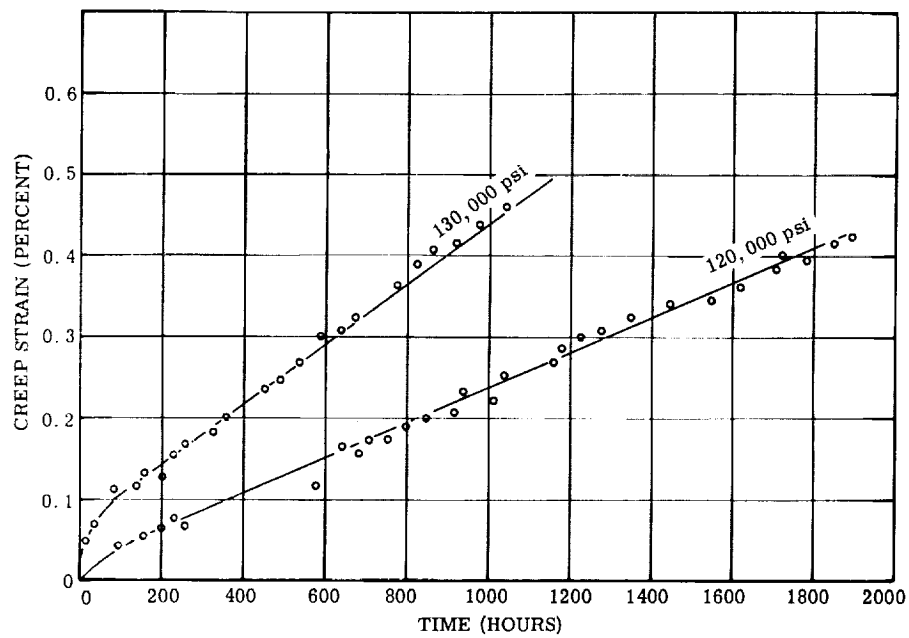
Figure 269. - Creep data for 15-percent-nickel maraging steel tested in air at 800° F and 120 000 and 130 000 psi. (See table 36.)
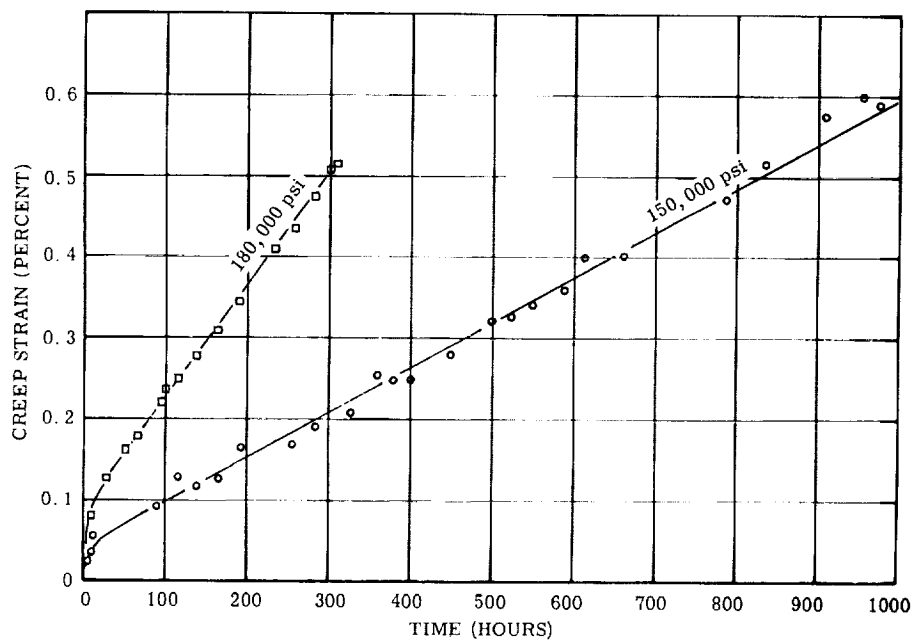
Figure 270. - Creep data for 15-percent-nickel maraging steel tested in air at 800° F and 150 000 and 180 000 psi. (See table 36.)
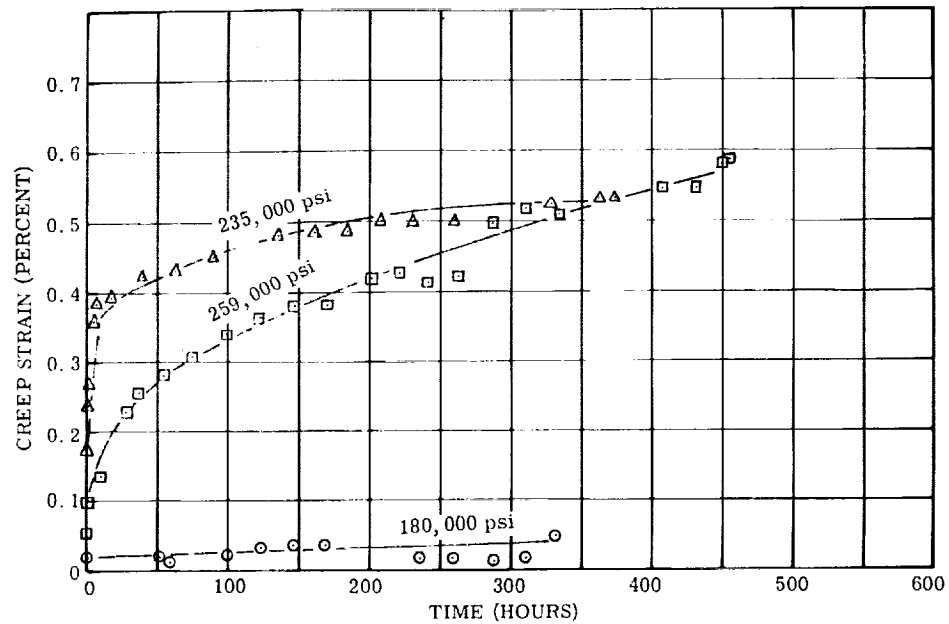
Figure 271. - Creep data for 15-percent-nickel maraging steel tested in air at 700° F and 180 000, 235 000, and 259 000 psi (data for 259 000 psi curve obtained by increasing stress on 180 000-psi specimen after 332 hr of testing). (See table 37.)
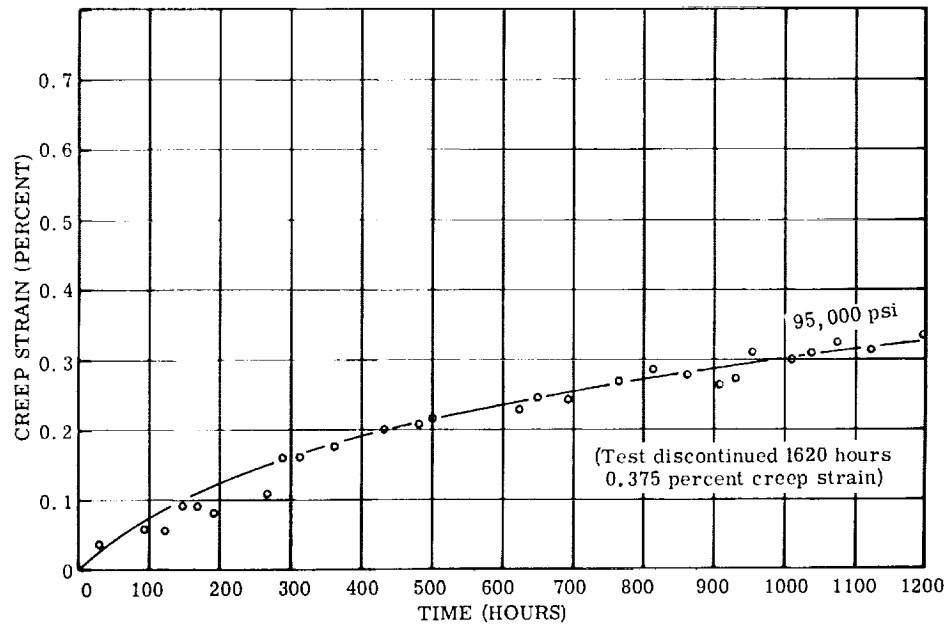
Figure 272. - Creep data for 15-percent-nickel maraging steel tested in air at 800° F and 95 000 psi. (See table 37.)
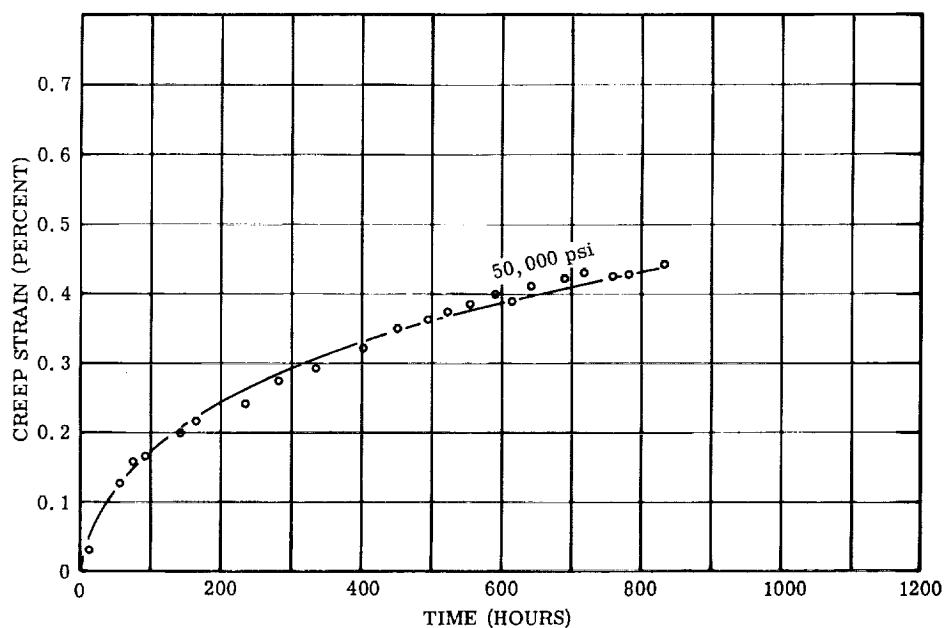
Figure 273. - Creep data for 15-percent-nickel maraging steel tested in air at 900° F and 50 000 psi. (See table 37.)
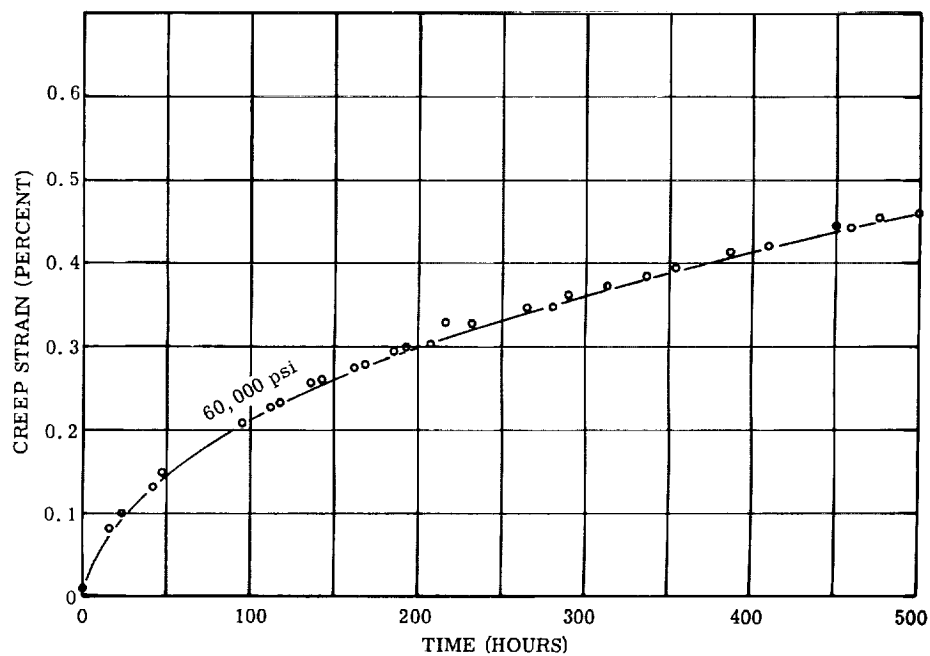
Figure 274. - Creep data for 15-percent-nickel maraging steel tested in air at 900° F and 60 000 psi. (See table 37.)
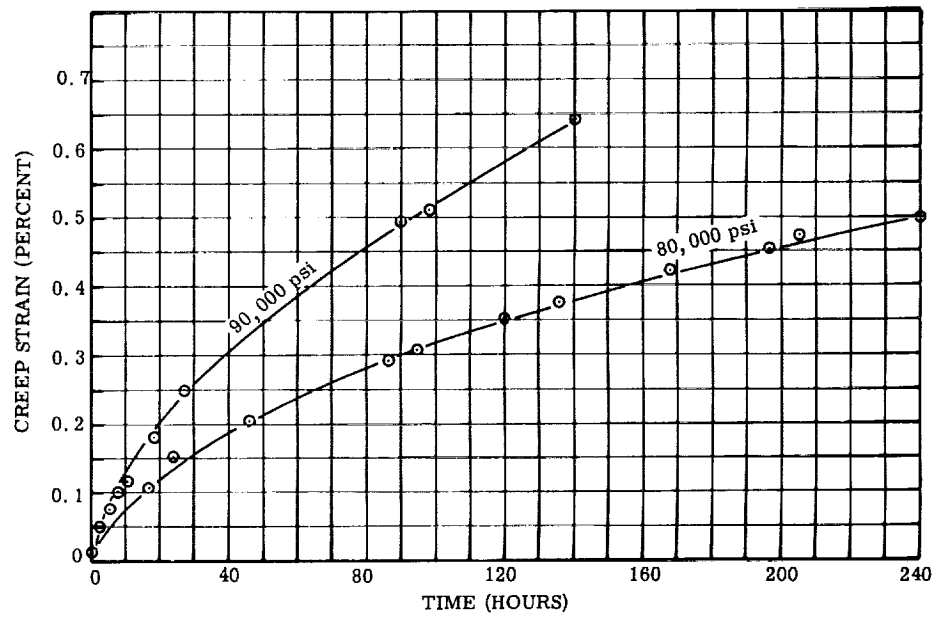
Figure 275. - Creep data for 15-percent-nickel maraging steel tested in air at 900° F and 80 000 and 90 000 psi. (See table 37.)
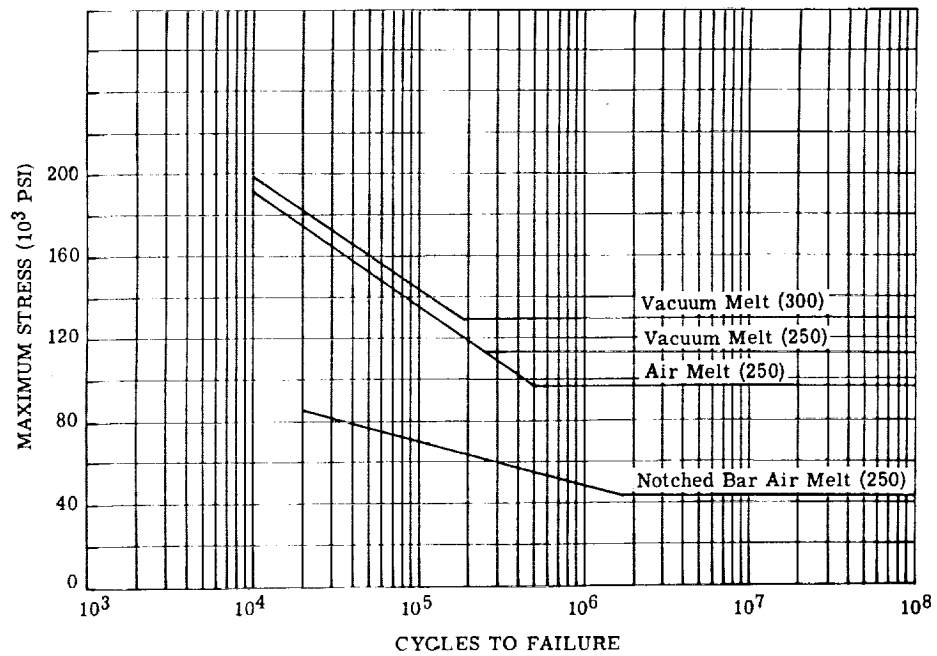
Figure 276. - Fatigue curve for 18-percent-nickel maraging steel from room temperature data in air (ref. 11)

AISI Grade H-11 Steel, Premium Quality (AMS 6487 and 6437)

AISI Grade H-11 steel, premium quality (AMS 6487 and 6437) is a commercially available steel with a nominal composition of 5 percent chromium, 1.3 percent molybdenum, 0.5 percent vanadium, 0.40 percent carbon, and the remainder, iron. Its tested composition was as follows:

	C	Si	Mn	S	P	Cr	U	Mo
	Composition, percent							
Bar	0.40	0.87	0.20	0.006	0.010	4.89	0.53	1.30
Sheet	.40	.91	.21	.006	.008	4.98	.42	1.31

Thermophysical properties. -

Density, lb/cu in. (g/cu cm) 0.281 (7.77)
Solidus temperature, ^{O}F . . . . 2750±25
Curie temperature, ^{O}F 1505
Thermal conductivity, (Btu)(ft)/(sq ft)(hr)(^{O}F), at -
    72° F 17.0
    800° F. 16.0
Coefficient of thermal expansion (from 72° to 900° F), in./(in.)(^{O}F) . . . 6.85×10^{-6}
Specific heat (at 72° F), Btu/(lb)(^{O}F). 0.11
Electrical resistivity of annealed AMS 6487, ohm-cm, at -
    72° F . . . . 46.5×10^{-6}
    500° F. . . . . 59.0×10^{-6}
    700° F. . . . . 68.0×10^{-6}
    800° F. . . . . 71.0×10^{-6}
    900° F. . . . . 76.5×10^{-6}

Magnetic properties. - All magnetic materials were at a hardness of Rockwell C 45 unless otherwise specified. Constant current flux reset properties are not applicable for H-11 steel and were measured only for materials used in magnetic amplifiers.

Direct current (solid ring) (H = 300 Oe):

Temperature, $^\circ$F	Induction, B_{tip}, kG
72	17.9
800	15.9
1100	13.8

Alternating current (400 cps; B = 10 kG; hardness, Rockwell C 45):

Temperature $^\circ$F	Lamination thickness, in.			
	0.014	0.025	0.014	0.025
	Exciting volt-amperes per pound		Core loss, W/lb	
72	172	179	105	115
800	157	157	90	87
1100	171	185	75	74

Mechanical properties. - Poisson's ratio at 72° F is 0.281 for H-11 steel.

Tensile properties:

Temperature, $^\circ$F	0.20-Percent offset yield strength, psi	Tensile strength, psi	Elongation in 1.4 in. percent	Reduction of area, percent	Modulus of elasticity, psi
72	180 000	215 000	15.2	29.0	30.5×10^6
800	144 000	174 000	15.0	40.0	27.3×10^6

Creep for bar stock tested in air or vacuum at 800° F (the creep strength of properly fabricated and heat-treated H-11 sheet (AMS 6437) is only slightly lower than that of the bar material):

Time, hr	Stress, psi, to produce creep of -	
	0.20 Percent	0.40 Percent
1 000	92 000	107 000
10 000	80 000	90 000

Fatigue strength of bar stock tested in air for 10^7 cycles (stress concentration factor K_t, 3):

Temperature, $^\circ$F	A	Smooth bar	Notched bar
		Fatigue strength, psi	
800	∞	72 000	45 000
	0.25	170 000	125 000
	2.00	98 000	48 000
1000	∞	70 000	33 000
	0.25	130 000	105 000
	2.00	100 000	40 000

The normal heat treatment for use as inductor rotor material is to preheat in a reducing atmosphere to 1200° to 1300° F, heat to $1850^\circ\pm25^\circ$ F in a neutral or slightly reducing (carbon potential 0.40, ref. 13) atmosphere and hold for 1 hour, and air-blast-quench to room temperature; then temper three times at 1075° to 1150° F to achieve a hardness of Rockwell C 44 to 45.5.

MAGNETIZING FORCE (AMPERE TURNS/INCH)

H_c (Oersteds)	B_r (Gauss)	From (Oersteds)
*Initial RT	24.65	11,500	100
Ο 500°F	21.40	10,550	100
▲ 800°F	20.11	9,800	100
⊟ 1100°F	16.43	8,400	100
+ RT After 1100°F	23.60	12,000	100

MAGNETIZING FORCE (OERSTEDS)
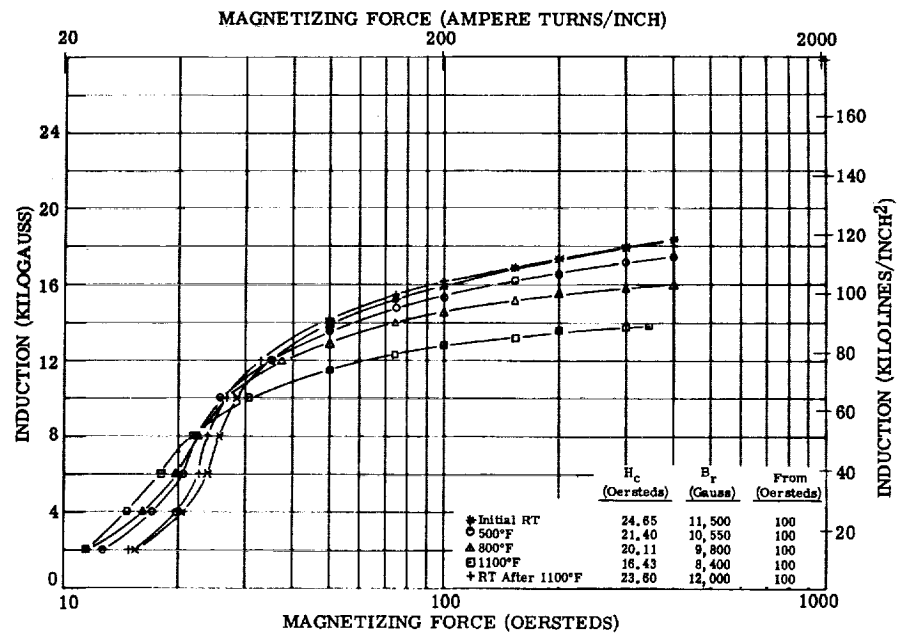
Figure 277. - Direct-current magnetization curves for H-11 steel forging. Test atmosphere, air to 500° F and argon above 500° F.

MAGNETIZING FORCE (AMPERE TURNS/INCH)

	H_c (Oersteds)	B_r (Gauss)	From (Oersteds)
x Initial RT	22.3	11,600	100
Ο 16 hours at 1000°F	15.2	7,900	100
△ 160 hours at 1000°F	13.5	8,250	100
☐ 328 hours at 1000°F	12.4	8,350	100
✳ 592 hours at 1000°F	10.6	8,900	100
● 760 hours at 1000°F	9.77	9,000	100
▲ 1000 hours at 1000°F	9.08	9,600	100
+ RT After 1000 hours at 1000°F	18.2	13,950	100

MAGNETIZING FORCE (OERSTEDS)
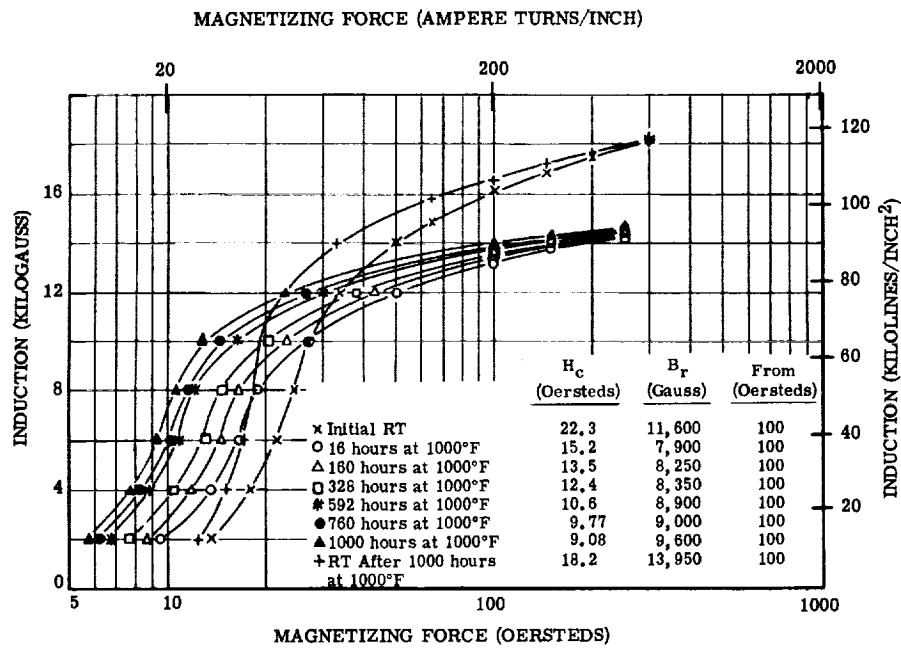
Figure 278. - Direct-current magnetization curves for H-11 steel forging, stability test. Test atmosphere, argon.

MAGNETIZING FORCE (AMPERE TURNS/INCH)

	H_c (Oersteds)	B_r (Gauss)	From (Oersteds)
X Initial RT	23.87	11,700	100
O 300°F	21.778	11,000	100
△ 500°F	20.395	10,300	100
□ 800°F	18.427	10,000	100
+ 1100°F	14.24	8,800	100
✳ RT After 1100°F	21.57	15,540	100

MAGNETIZING FORCE (OERSTEDS)
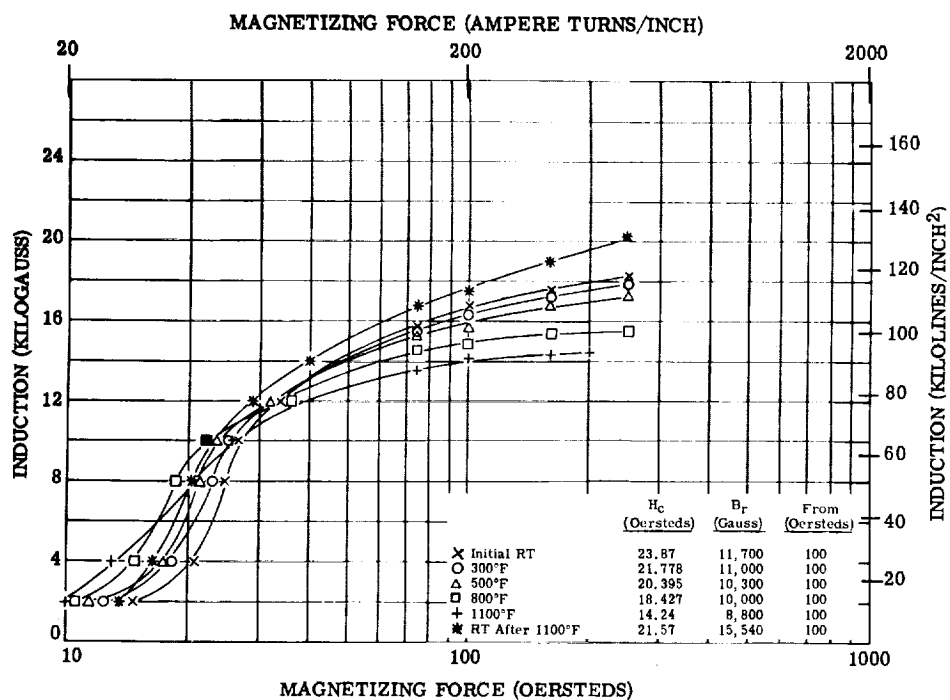
Figure 279. - Direct-current magnetization curves for H-11 steel 0.014-inch laminations. Test atmosphere, air to 800° F and argon above 800° F; interlaminar insulation, aluminum orthophosphate.

MAGNETIZING FORCE (AMPERE TURNS/INCH)

	H_c (Oersteds)	B_r (Gauss)	From (Oersteds)
X Initial RT	23.08	11,750	100
O 300°F	21.15	11,100	100
△ 500°F	20.94	9,900	100
□ 800°F	18.01	9,000	100
+ 1100°F	14.14	7,350	100
✳ RT After 1100°F	21.99	12,300	100

MAGNETIZING FORCE (OERSTEDS)
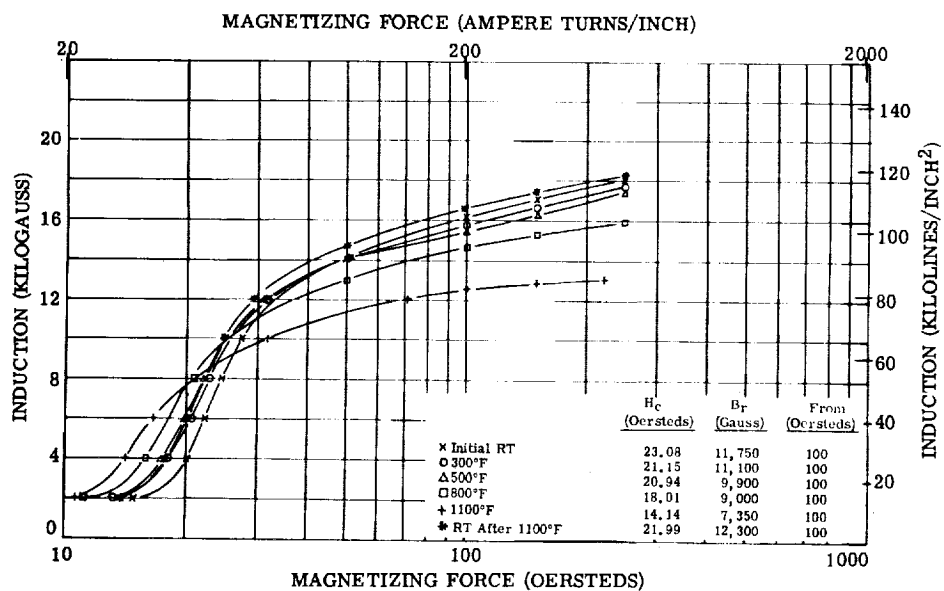
Figure 280. - Direct-current magnetization curves for H-11 steel 0.025-inch laminations. Test atmosphere, air to 800° F and argon above 800° F; interlaminar insulation, aluminum orthophosphate.
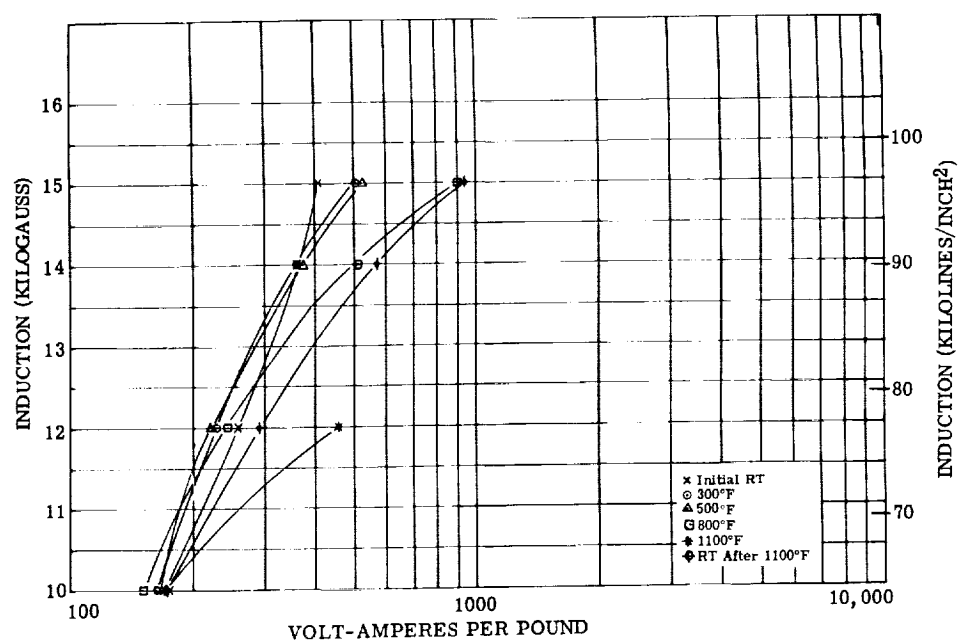
Figure 281. - Exciting volt-amperes per pound at 400 cps for H-11 steel 0.014-inch laminations. Test atmosphere, air to 800° F and argon above 800° F; interlaminar insulation, aluminum orthophosphate.
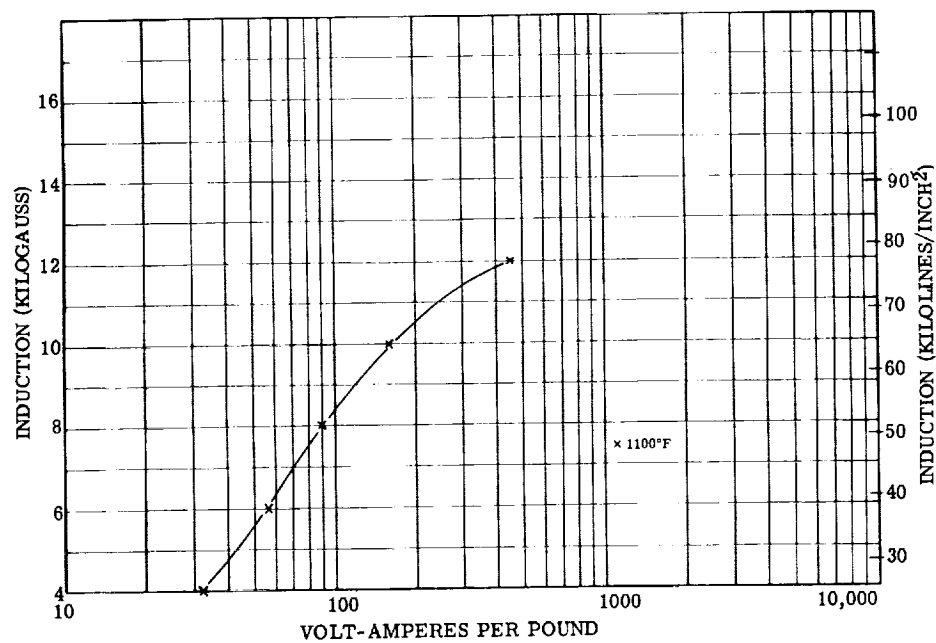
Figure 282. - Exciting volt-amperes per pound at 400 cps for H-11 steel 0.014-inch laminations at 1100° F. Test atmosphere, air to 800° F and argon above 800° F; interlaminar insulation, aluminum orthophosphate.
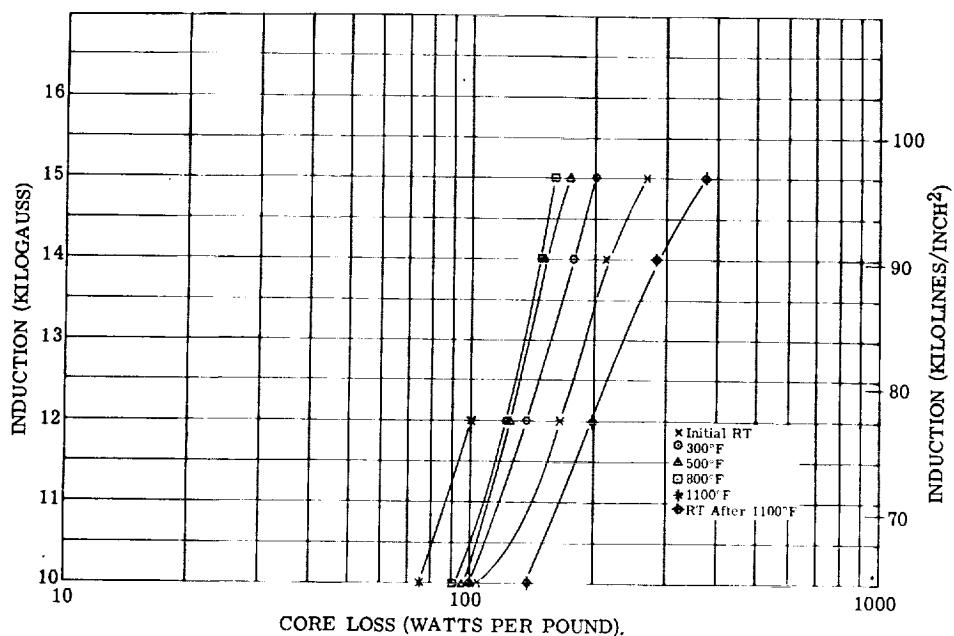
Figure 283. - Core loss at 400 cps for H-11 steel 0.014-inch laminations. Test atmosphere, air to 800° F; interlaminar insulation, aluminum orthophosphate.
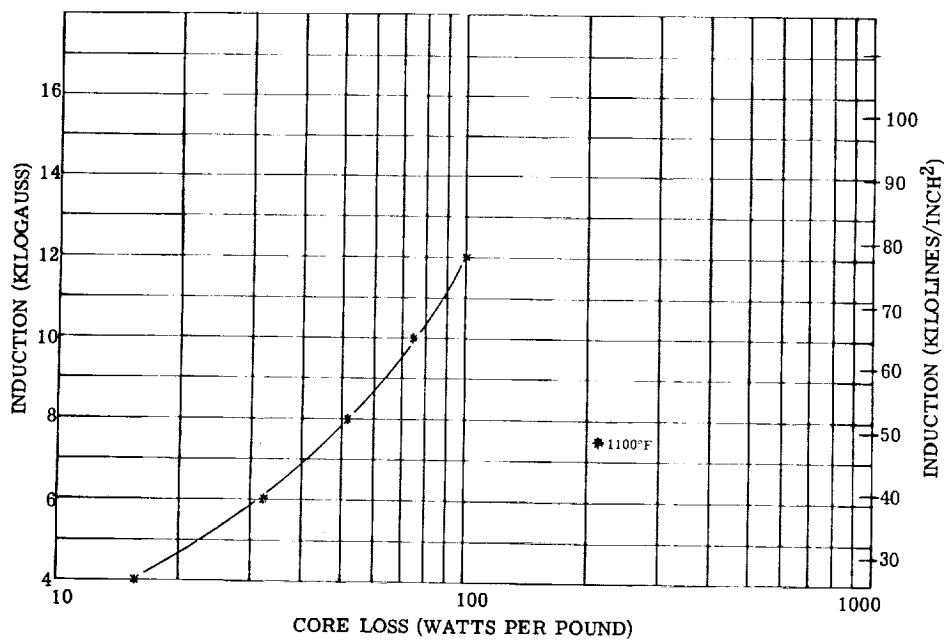
Figure 284. - Core loss at 400 cps for H-11 steel 0.014-inch laminations at 1100° F. Test atmosphere, air to 800° F and argon above 800° F; interlaminar insulation, aluminum orthophosphate.
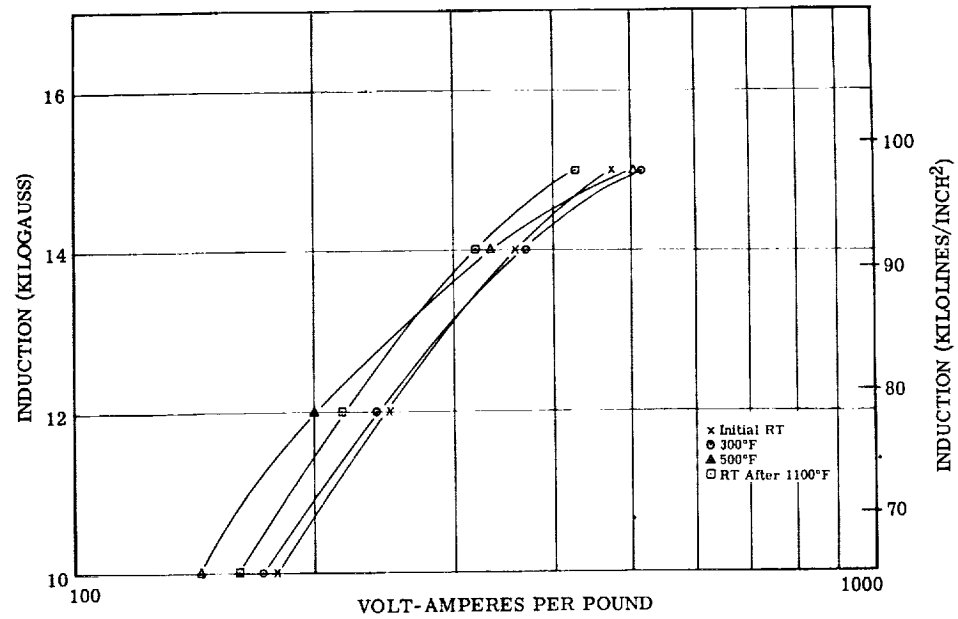
Figure 285. - Exciting volt-amperes per pound at 400 cps for H-11 steel 0.025-inch laminations at room temperature, 300°, and 500° F. Test atmosphere, air to 800° F and argon above 800° F; interlaminar insulation, aluminum orthophosphate.
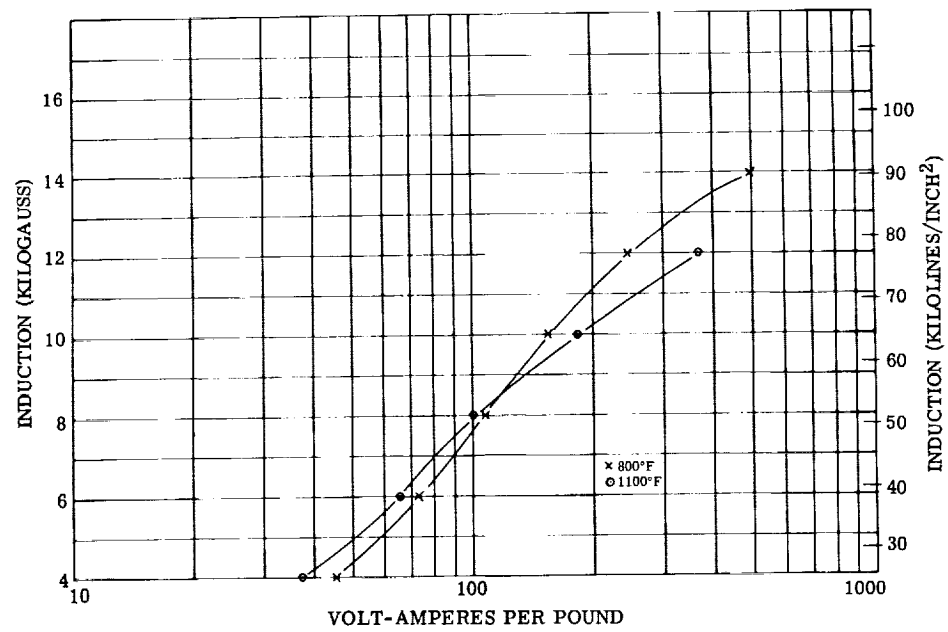
Figure 286. - Exciting volt-amperes per pound at 400 cps for H-11 steel 0.025-inch laminations at 800° and 1100° F. Test atmosphere, air to 800° F and argon above 800° F; interlaminar insulation, aluminum orthophosphate.
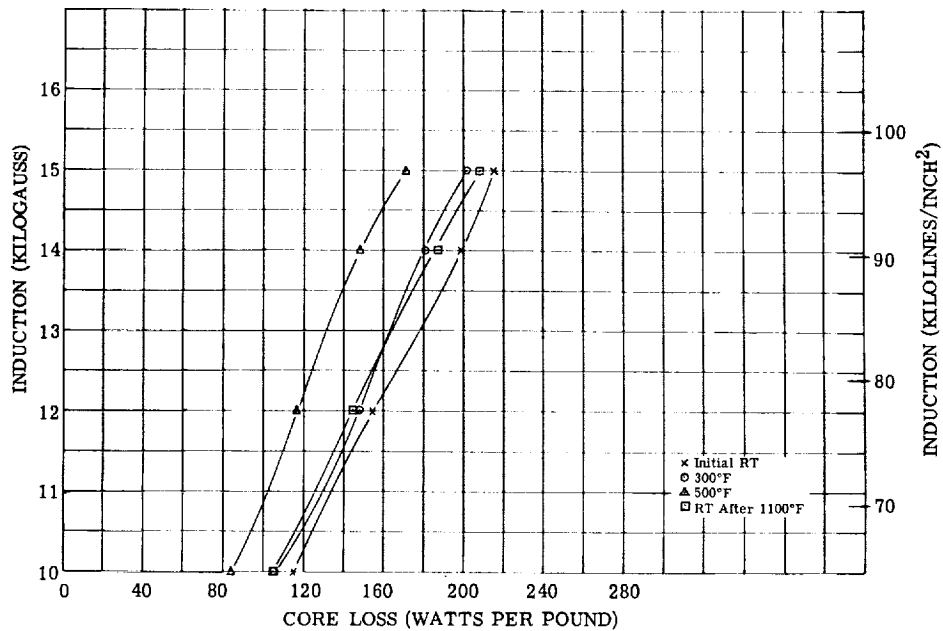
Figure 287. - Core loss at 400 cps for H-11 steel 0.025-inch laminations at room temperature, 300°, and 500° F. Test atmosphere, air to 800° F and argon above 800° F; interlaminar insulation, aluminum orthophosphate.
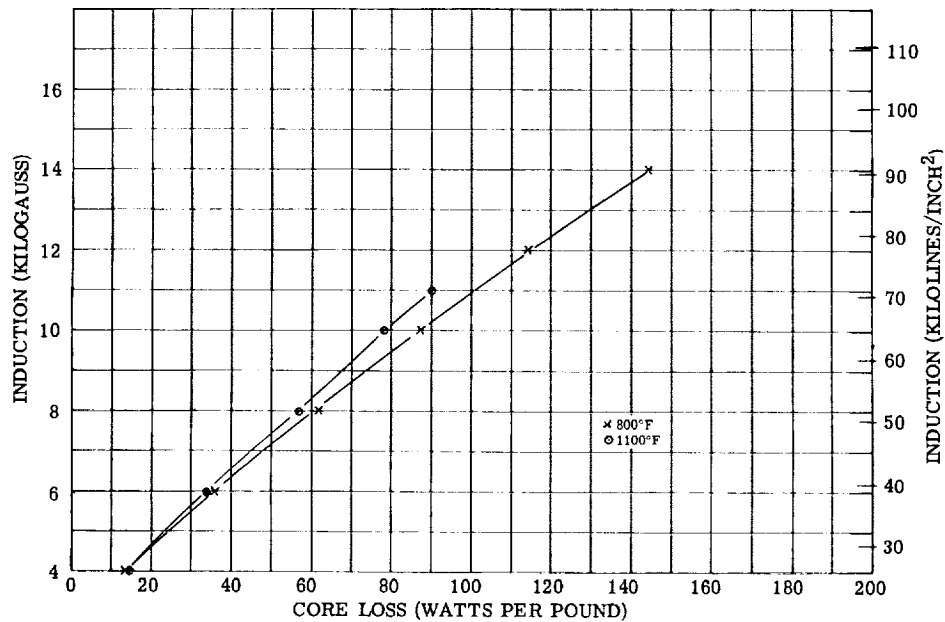
Figure 288. - Core loss at 400 cps for H-11 steel 0.025-inch laminations at 800° and 1100° F. Test atmosphere, air to 800° F and argon above 800° F; interlaminar insulation, aluminum orthophosphate.

TABLE 39. - TENSILE PROPERTIES OF

AMS 6487 (H-11) BAR TESTED IN AIR

[Data from work performed by Westinghouse on
Contract AF33(615)-1551; see fig. 289.]

Test temperature, °F	0.2-Percent offset yield strength, psi	Tensile strength, psi	Elongation in 1.4 in., percent	Reduction of area, percent
72	175 000	212 000	15.5	(a)
	185 000	217 000	17.5	34
	183 000	211 750	16.0	31
	174 000	213 280	18.5	34
	183 670	218 980	8.5	14.3
800	154 080	178 572	16.0	30.3
	150 000	180 000	17.0	40
	127 246	163 672	13.6	50.4
900	118 181	154 645	(a)	53.1
	117 352	152 450	15.6	67.5
	131 048	168 061	13.6	60.5
1000	92 778	128 385	27.6	72.5
	102 862	137 003	20.1	65.5

[a]Broken at gage mark.
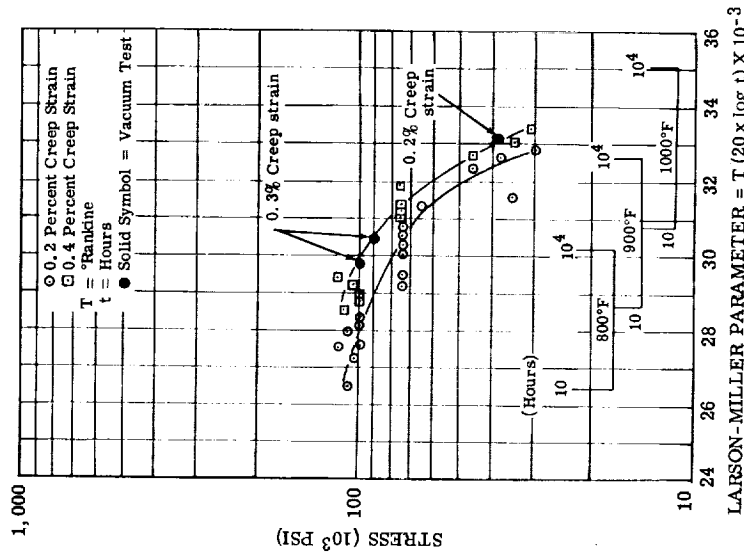
Figure 290. - Larson-Miller plots of AMS 6487 (H-11) bar creep data tested in air and vacuum, based on maximum of 2000-hour data (data partly from work performed by Westinghouse under Contract AF 33(615)1551). (See tables 41 to 43.)
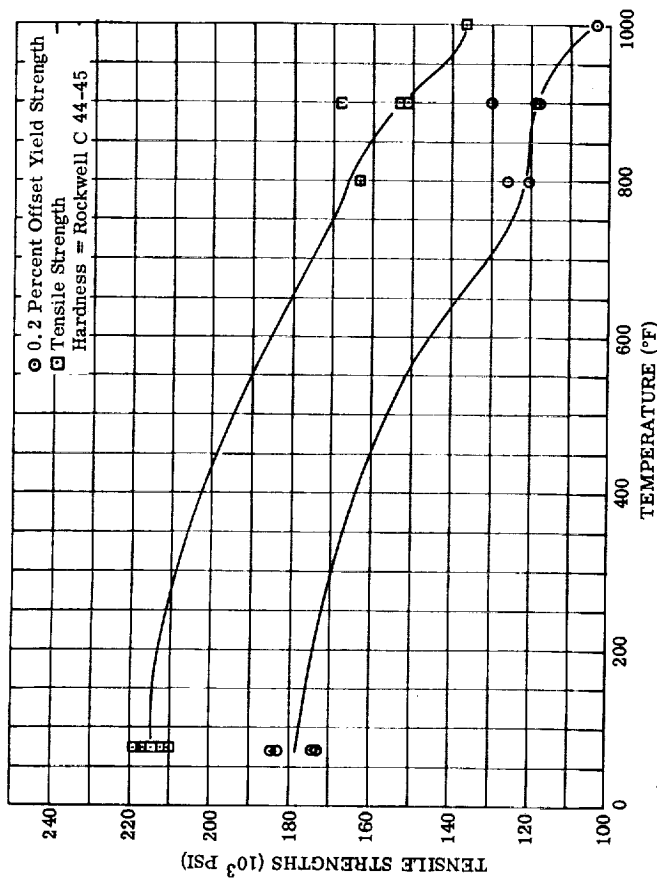
Figure 289. - Tensile strength for AMS 6487 (H-11) bar samples tested in air (data from work performed by Westinghouse under Contract AF33(615)-1551). (See table 39.)
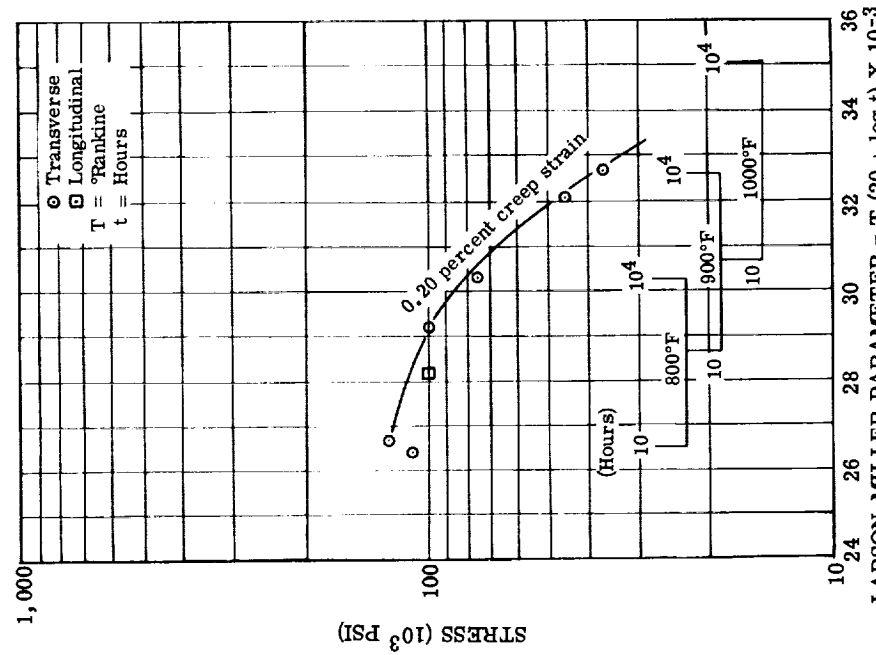
Figure 292. - Larson-Miller plot of 0.025-inch H-11 sheet creep data tested in air for 0.20 percent creep strain, based on maximum of 2000-hour data. (See table 41.)
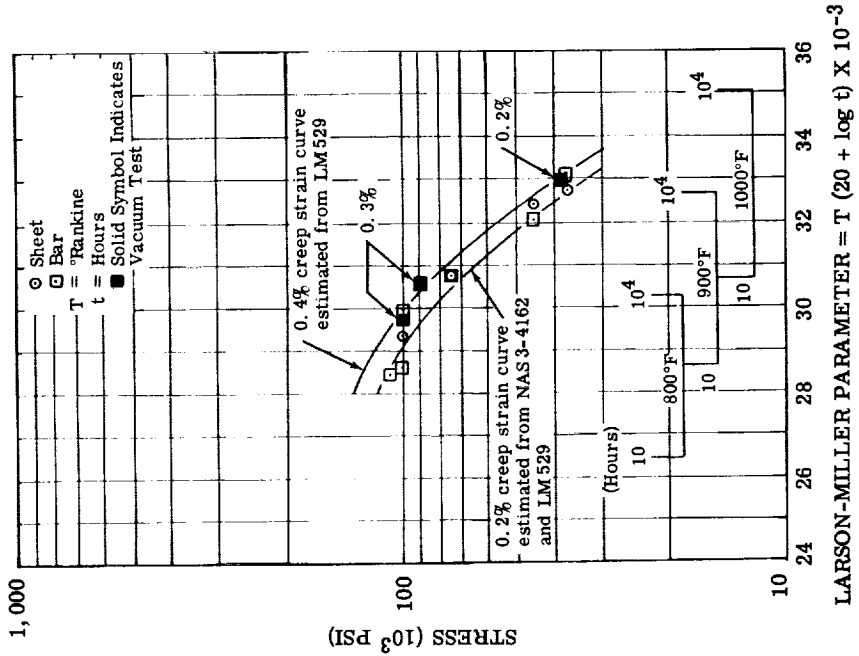
Figure 291. - Comparative Larson-Miller plot of 0.25- to 0.35-percent strain on sheet and bar H-11 creep data tested in air and vacuum, based on maximum of 2000-hour data (data from work performed by Westinghouse under Contract AF 33(615)-1551). (See tables 40, 41, and 43.)
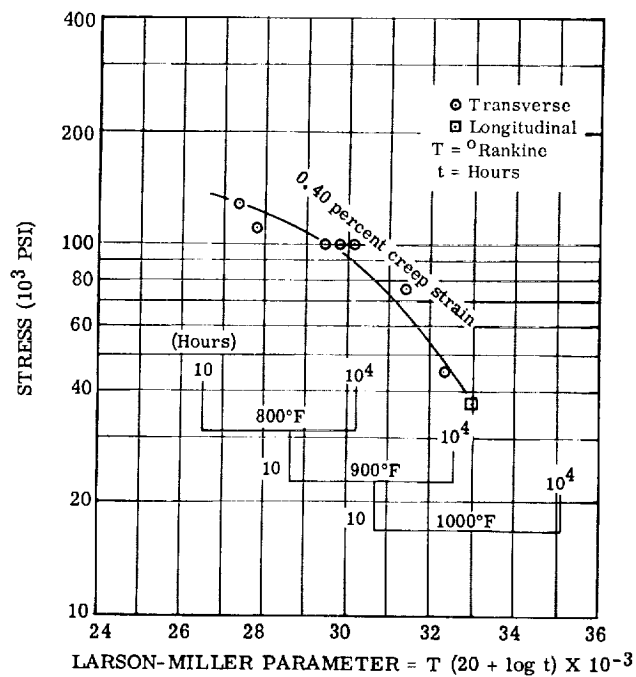
Figure 293. - Larson-Miller plot of 0.025-inch H-11 sheet
creep data tested in air for 0.40 percent creep strain,
based on maximum of 2000-hour data. (See table 41.)
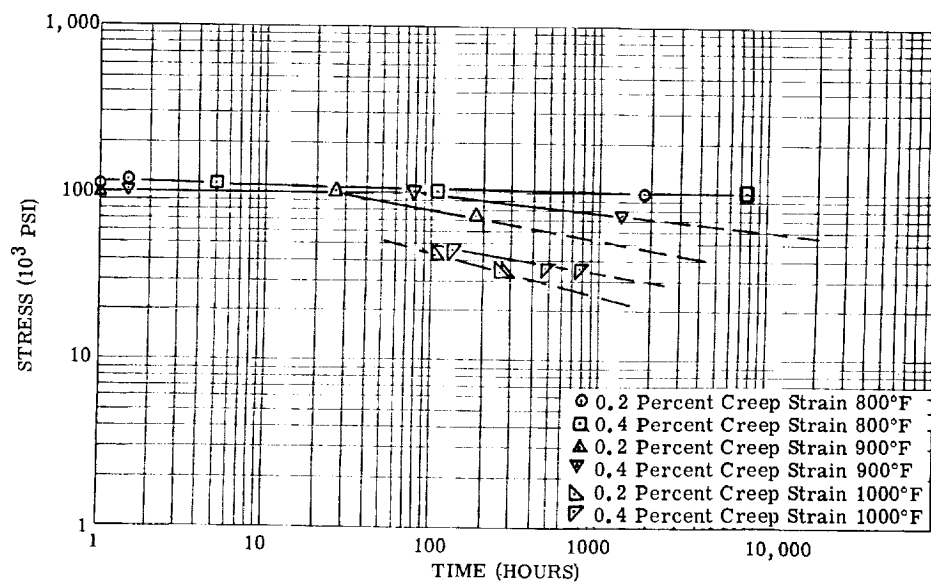
Figure 294. - Creep stress-time data for AMS 6437 (H-11) 0.025-inch-thick sheet longitudinal and
transverse specimens, heat treated to Rockwell C45 and tested in air. (See tables 40 to 42.)

TABLE 40. - COMPARISON OF CREEP DATA FOR AMS 6487 (BAR H-11) WITH

CREEP DATA FOR AMS 6437 (SHEET H-11)

[Test, ASTM E139; bar data from studies performed by Westinghouse under
Contract AF33(615)-1551; nominal hardness, Rockwell C 45; see figs.
295 to 299.]

Identification	Test temperature, °F	Stress, psi	Test time, hr	Creep strain, percent
Sheet (transverse)	1000	45 000	160	0.327
Forged (40)		45 000	100	.300
Sheet (transverse)		37 000	330	.363
Sheet (longitudinal)		37 000	329	.298
Forged (86)		37 000	500	.225
Sheet (transverse)	900	100 000	171	.681 (100 hr, 0.462)
Sheet (longitudinal)		100 000	140	.909 (100 hr, 0.705)
Forged (63)		100 000	100	.340
Sheet (transverse)		75 000	520	.315
Forged (82)			500	.280
Forged (83)				.325
Forged (95)				.370
Forged (94)				.340
Forged (99)				.375
Sheet (transverse)	800	128 000	289	.912 (100 hr, 0.861)
Forged (90)		128 000	250	.25
Sheet (transverse)		110 000	260	.54
Forged (39)			250	.38
Forged (68)				.331
Forged (73)				.256
Forged (74)				.244
Forged (71)				.203
Forged (72)				.344
Forged (79)				.286
Forged (80)				.316
Sheet (transverse)		100 000	2058	.210
Forged (36)			500	.250
Forged (88)			500	.246
Forged (89)			1000	.462
Forged (92)			500	.229
Forged (93)			500	.360

TABLE 41. - CREEP DATA FOR 0.025-INCH AMS 6437 (H-11) SHEET TESTED IN AIR

[Test, ASTM E139; plastic strain obtained on loading specimen, 0.]

Temperature, °F	800	800	800	900	900	1000	1000	a900	a1000	800	900
Stress, psi	128 000	110 000	100 000	100 000	75 000	45 000	37 000	100 000	37 000	128 000	75 000
Duration of test, hr	289	260	2058	171	520	160	330	140	329	b811	b1149
Total creep strain, percent	0.907	0.541	0.210	0.682	0.315	0.325	0.349	0.908	0.304	-------	-------
Time to cause 0.2-percent creep strain, hr	16	9.7	1757	29	194	106	247	1	266	-------	-------
Time to cause 0.4-percent creep strain, hr	52	109	c7780	79	c1359	138	359	16	388	-------	-------
Strain-time plot given in fig. -	295	295	295	296	296	297	298	296	299	-------	-------

a Longitudinal specimens.
b Did not reach 0.20-percent strain.
c Extrapolated value.
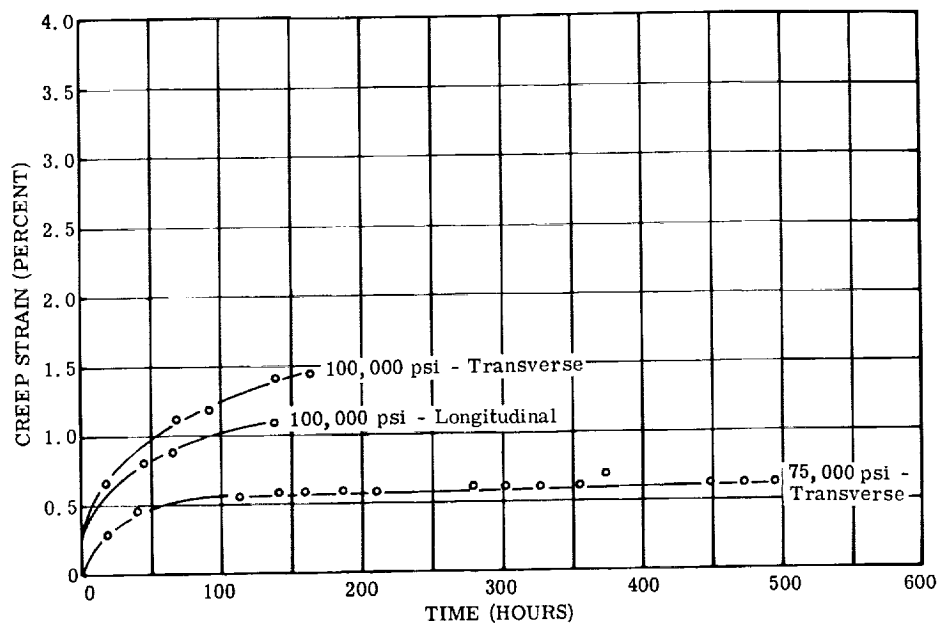
Figure 295. - Creep data for AMS 6437 (H-11) 0.025-inch-thick sheet transverse specimens tested in air at 800° F. (See table 41.)
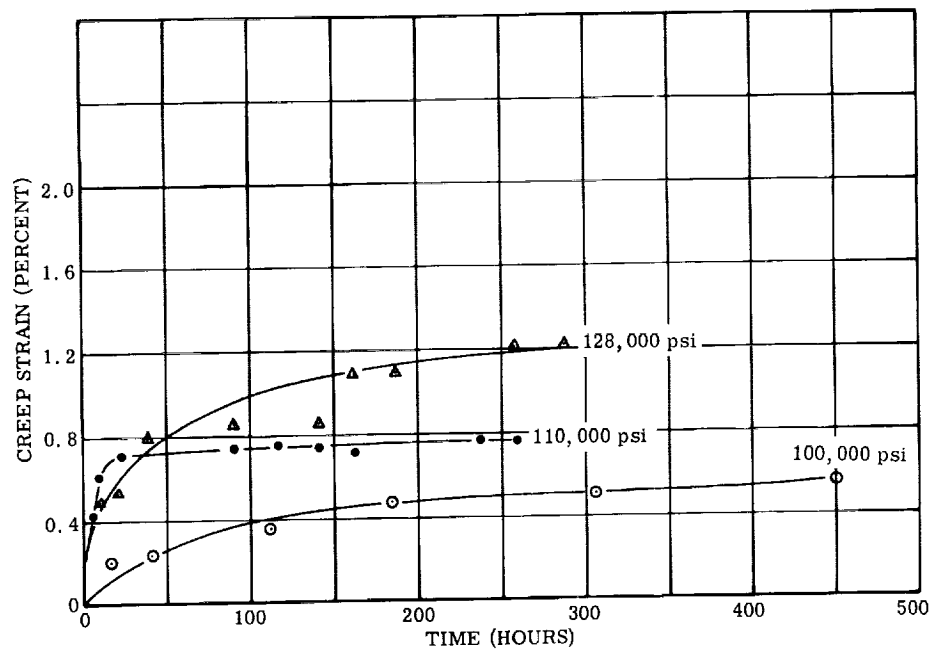
Figure 296. - Creep data for AMS 6437 (H-11) 0.025-inch-thick sheet transverse and longitudinal specimens tested in air at 900° F. (See table 41.)
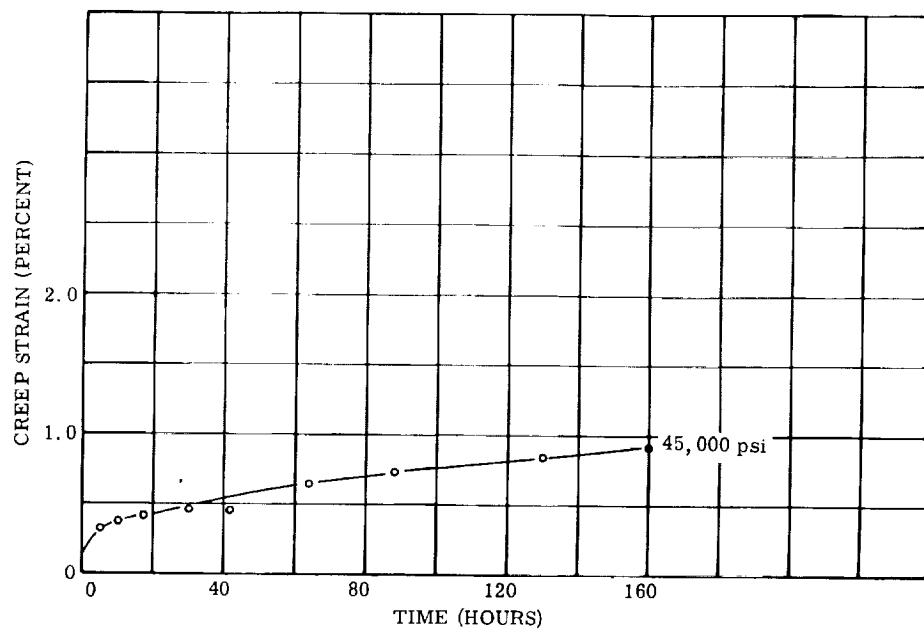
Figure 297. - Creep data for AMS 6437 (H-11) 0.025-inch-thick sheet transverse specimen tested in air at 1000° F and 45 000 psi. (See table 41.)
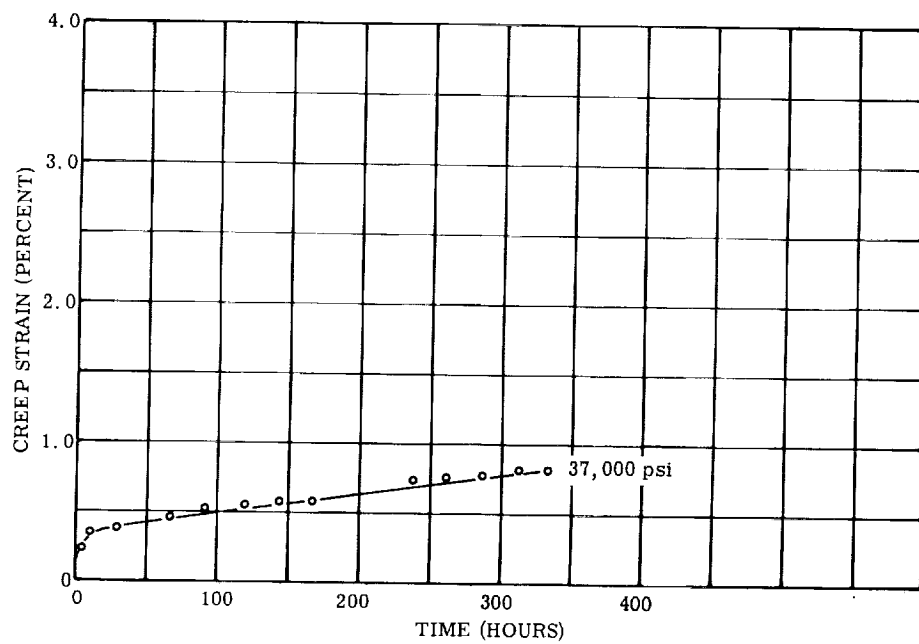
Figure 298. - Creep data for AMS 6437 (H-11) 0.025-inch-thick sheet longitudinal specimen tested in air at 1000° F and 37 000 psi. (See table 41.)
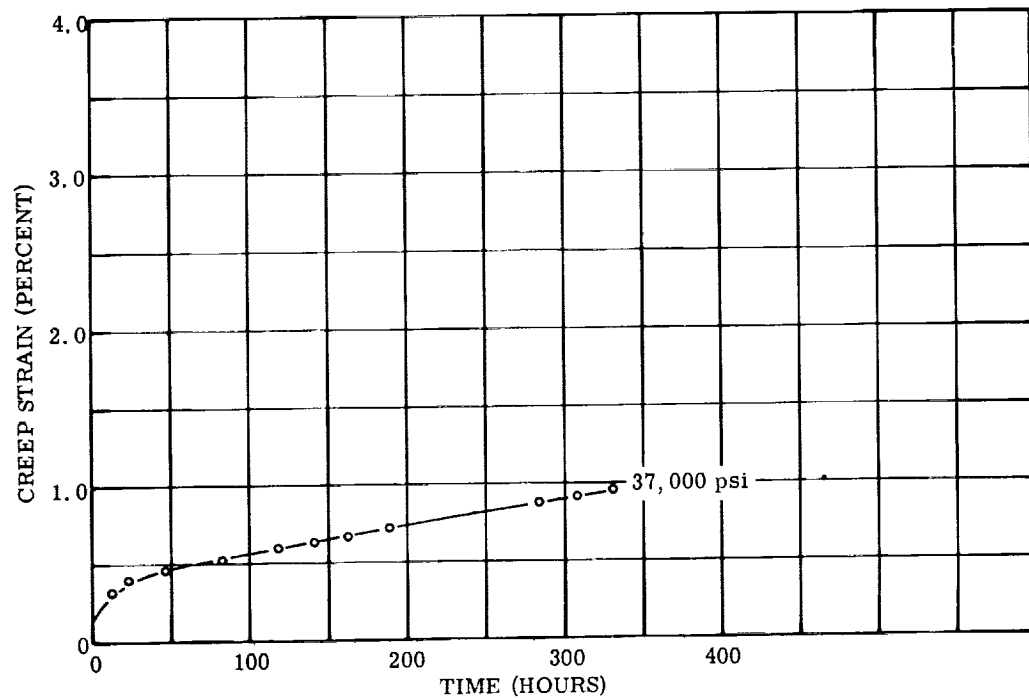
Figure 299. – Creep data for AMS 6437 (H-11) 0.025-inch-thick sheet transverse specimen tested in air at 1000° F and 37 000 psi. (See table 41.)

TABLE 42. – CREEP DATA FOR AMS 6487 (H-11) BAR TESTED IN AIR

[Test, ASTM E139; bar data from studies performed by Westinghouse under Contract AF33(615)1551; plastic strain obtained on loading specimen, 0.]

Temperature, °F	800	800	800	800	800	900	900	1000	900	900	900	1000	1000	800	900	900
Stress, psi	100 000	100 000	100 000	110 000	110 000	75 000	75 000	35 000	75 000	75 000	75 000	35 000	38 000	110 000	75 000	65 000
Duration of test, hr	501	1000	500	249	249	500	500	500	505	501	500	500	500	1002	1005	2500
Total creep strain, percent	0.256	0.462	0.229	0.256	0.245	0.279	0.324	0.438	0.372	0.291	0.220	0.333	0.419	0.364	0.324	0.349
Time to cause 0.2-percent creep strain, hr	282	100	393	124	166	253	208	45	135	34	231	41	212	13	475	1165
Time to cause 0.4-percent creep strain, hr	a1234	684	1133	a572	a536	a878	a673	419	565	a1059	2921	749	475	a1749	a1296	a2958
Specimen	88	89	92	73	74	82	83	85	99	100	101	102	124	120	122	123

a Extrapolated.

TABLE 43. - CREEP DATA FOR AMS 6487 (H-11)

BAR TESTED IN VACUUM

[Test, ASTM E139; plastic strain obtained on loading specimen, 0; see figs. 290 and 291 for Larson-Miller plots.]

Temperature, °F	850	900	1000
Stress, psi	100 000	90 000	37 000
Duration of test, hr	502	170	650
Total creep strain, percent	0.30	0.30	0.20
Time to cause 0.2-percent creep strain, hr	260	136	650
Time to cause 0.4-percent creep strain, hr	(a)	(a)	(a)

[a]Did not reach required strain.

TABLE 44. - FATIGUE DATA FOR H-11 ALLOY FOR USE IN

PLOTTING GOODMAN-TYPE DIAGRAMS

Temperature, °F	Fatigue specimen	Stress ratio, A (a)	Stress, psi		
			For 10^7 cycles	Alternating	Mean
800	Smooth bar	∞	83 000	------	-------
	Notched bar	∞	48 000	------	-------
	Smooth bar	0.25	170 000	34 000	136 000
	Notched bar	.25	128 000	25 600	102 400
	Smooth bar	2.0	100 000	66 000	34 000
	Notched bar	2.0	50 000	33 000	17 000
1000	Smooth bar	∞	76 000	------	-------
	Notched bar	∞	32 000	------	-------
	Smooth bar	0.25	137 000	27 400	109 600
	Notched bar	.25	111 000	22 200	88 800
	Smooth bar	2.0	113 000	75 333	37 667
	Notched bar	2.0	33 000	22 000	11 000

[a]Where A is ratio of alternating stress to mean stress.

Figure 301. - Modified Goodman-type diagram for AMS 6487 (H-11) alloy tested in air at 1000° F for 10⁷ cycles. Test sample hardness, Rockwell C 44.5 to 45.5. (See table 44.)
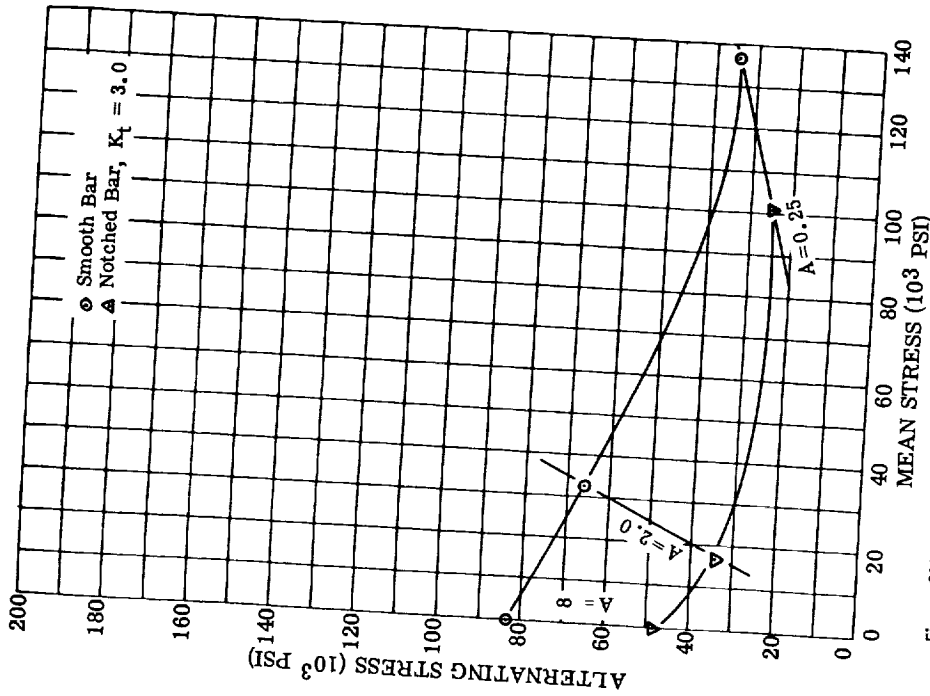
Figure 300. - Modified Goodman-type diagram for AMS 6487 (H-11) alloy tested in air at 800° F for 10⁷ cycles. Test sample hardness, Rockwell C 44.5 to 45.5. (See table 44.)

TABLE 45. - FATIGUE DATA FOR AMS 6487 H-11 ALLOY SMOOTH-BAR SAMPLES

[Test, ASTM STP 91; see figs. 302 to 305.]

Specimen	Test temperature, °F	Stress ratio, A (a)	Maximum stress, psi	Number of cycles to failure, N	Specimen	Test temperature, °F	Stress ratio, A (a)	Maximum stress, psi	Number of cycles to failure, N
246	800	∞	72 000	9 891 000	248	1000	∞	70 000	6 241 000
245			74 000	5 032 000	128			80 000	1 566 000
242			78 000	2 736 000	118			82 000	663 000
111			82 000	1 332 000	110			90 000	783 000
103			84 000	4 680 000	116			100 000	33 000
100			89 000	1 130 000	114			110 000	3 000
104			94 000	138 000	129		0.25	130 000	5 634 000
102			100 000	60 000	241			134 210	7 974 000
101			110 000	19 000	126			140 000	58 000
109		0.25	169 600	12 047 000	127			152 000	29 000
115			171 350	922 000	134			160 750	15 000
113			172 450	186 000	125			170 000	2 000
112			175 150	4 000	247		2.00	96 400	3 094 000
107			175 150	2 000	244			102 000	941 000
130		2.00	97 995	b10 000 000	138			108 000	3 424 000
123			108 866	628 000	135			114 000	1 600 000
124			108 866	1 155 000	137			120 000	826 000
108			112 250	1 213 000	136			129 000	394 000
122			115 015	1 386 000	243			135 000	5 000
117			120 050	572 000					
119			124 932	190 000					
133			135 000	166 000					

a Where A is ratio of alternating stress to mean stress.

b No failure.

TABLE 46. - FATIGUE DATA FOR AMS 6487 H-11 ALLOY

NOTCHED-BAR SAMPLES

[Test, ASTM STP 91; see figs. 302 to 305; stress concentration factor K_t, 3.0.]

Specimen	Test temperature, °F	Stress ratio, A (a)	Maximum stress, psi	Number of cycles to failure, N
203	800	∞	40 000	7 761 000
208			44 000	b14 000 000
202			46 000	12 245 000
206			50 000	35 000
215			50 000	b24 000 000
222			55 800	15 000
207			60 000	7 000
211			65 000	4 000
221		0.25	125 250	9 656 000
256			130 000	1 000 000
223			131 250	5 100 000
225			135 750	396 000
227			140 400	92 000
231			147 000	75 000
237		2.00	44 000	7 873 000
252			45 900	b13 086 000
240			47 000	b10 000 000
255			48 250	1 601 000
257			49 950	b14 885 000
220			52 500	50 000
228			65 000	13 000
226	1000	∞	32 000	5 272 000
218			33 600	14 995 000
239			33 000	b10 000 000
219			34 600	127 000
217			37 000	30 000
224			41 000	8 000
235		.25	103 950	b13 733 000
258			105 000	1 108 000
232			110 000	1 145 000
229			120 300	570 000
233			126 500	914 000
254			128 000	2 181 000
234			129 950	1 040 000
236			140 000	958 000
263			140 000	109 000
230		2.00	35 100	b10 221 000
251			40 200	b19 533 000
249			46 200	1 559 000
238			50 100	1 380 000
250			60 000	21 000
253			54 895	77 000

aWhere A is ratio of alternating stress to mean stress.
bNo failure.

For Smooth Bar
$(19 \leq N \leq 4680)$, Fatigue Stress $= 1000 [0.26155 \times 10^{-10} N^4 - 0.18126 \times 10^{-6} N^3$
$+ 0.31239 \times 10^{-3} N^2 - 0.17897 N + 112.032] (Psi)]$

For Notched Bar
$(4 \leq N \leq 24,000)$, Fatigue Stress $= 1000 [-0.10078 \times 10^{-10} N^3 + 0.43579 \times 10^{-6} N^2$
$- 0.004980 N + 57.7698] (Psi)$
(Where N = Cycles to Failure $\times 10^{-3}$)]

⊙ Smooth Bar Rockwell C45 This Study
▲ Notched Bar Rockwell C 45
● Literature Data, Hardness = Rockwell C 52
  Smooth Bar
▲ Literature Data, Hardness = Rockwell C 52
  Notched Bar
K_t = 3 All Samples

Figure 302. - Fatigue diagram for notched and smooth bar AMS 6487 (H-11) at Rockwell C 45 tested in air at 800° F with ratio of alternating stress to mean stress A of infinity. (See tables 45 and 46; plotted data partly from ref. 14.)

For Smooth Bar
$A = 0.25$, $(2 \leq N \leq 12047)$, Fatigue Stress $= 1000 [-0.119924 \times 10^{-3} N^3 + 0.159662 \times 10^{-4} N^2$
$- 0.017885 N + 175.21] (Psi)$

$A = 2.00$ $(166 \leq N \leq 10000)$, Fatigue Stress $= 1000 [-0.34421 \times 10^{-8} N^3 + 0.40941 \times 10^{-4} N^2$
$- 0.0695515 N + 141.54] (Psi)$

For Notched Bar
$A = 0.25$, $(75 \leq N \leq 9656)$, Fatigue Stress $= 1000 [0.107685 \times 10^{-6} N^2 - 0.002727 N$
$+ 141.713] (Psi)$

$A = 2.00$, $(13 \leq N \leq 10000)$, Fatigue Stress $= 1000 [-0.427427 \times 10^{-8} N^3 + 0.76859 \times 10^{-4} N^2$
$- 0.3434 N + 69.465] (Psi)$
(Where N = Cycles to Failure $\times 10^{-3}$)

⊙ Smooth Bar
▲ Notched Bar
K_t = 3.0

Figure 303. - Fatigue diagram for notched and smooth bar AMS 6487 (H-11) at Rockwell C 45 tested in air at 800° F with ratio of alternating stress to mean stress A or 0.25 and 2.00. (See tables 45 and 46.)

For Notched Bar

A = 0.25, (2 ≤ N ≤ 5634), Fatigue Stress = $1000[0.934106 \times 10^{-4} N^2 - 0.53328\ N$
$+ 169.45](Psi)$

A = ∞, (3 ≤ N ≤ 5171), Fatigue Stress = $1000[0.183059 \times 10^{-8} N^3 - 0.60283 \times 10^{-5} N^2$
$- 0.02365\ N + 105.36](Psi)$

For Smooth Bar

A = 0.25, (570 ≤ N ≤ 13700), Fatigue Stress = $1000[0.172079 \times 10^{-7} N^3 - 0.26503 \times 10^{-3} N^2$
$+ 0.40382\ N - 26.7029](Psi)$

A = ∞, (8 ≤ N ≤ 15000), Fatigue Stress = $1000[-0.106691 \times 10^{-10} N^3 + 0.30319 \times 10^{-6} N^2$
$- 0.0024242\ N + 37.706](Psi)$

(Where N = Cycles to Failure x 10^{-3})

Figure 304. - Fatigue diagram for notched and smooth bar AMS 6487 (H-11) at Rockwell C 45 tested In air at 1000° F with ratio of alternating stress to mean stress A of 0.25 and infinity. (See tables 45 and 46.)

For Smooth Bar

(5 ≤ N ≤ 1600), Fatigue Stress = $1000[-0.67368 \times 10^{-8} N^3 + 0.29845 \times 10^{-4} N^2 - 0.04941 N + 144.25]$ (Psi)

For Notched Bar

(1380 ≤ N ≤ 10200), Fatigue Stress = $1000[-0.0016966\ N + 52.4414]$ (Psi)
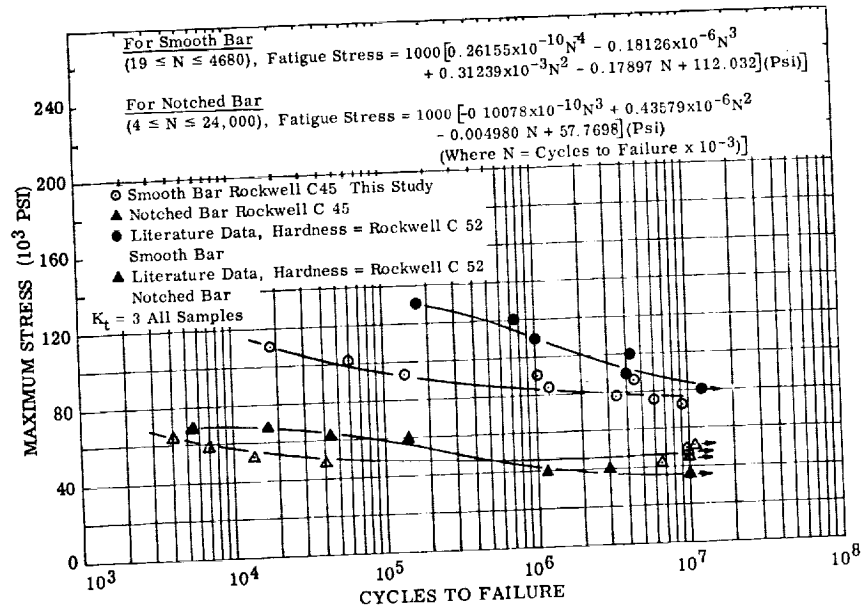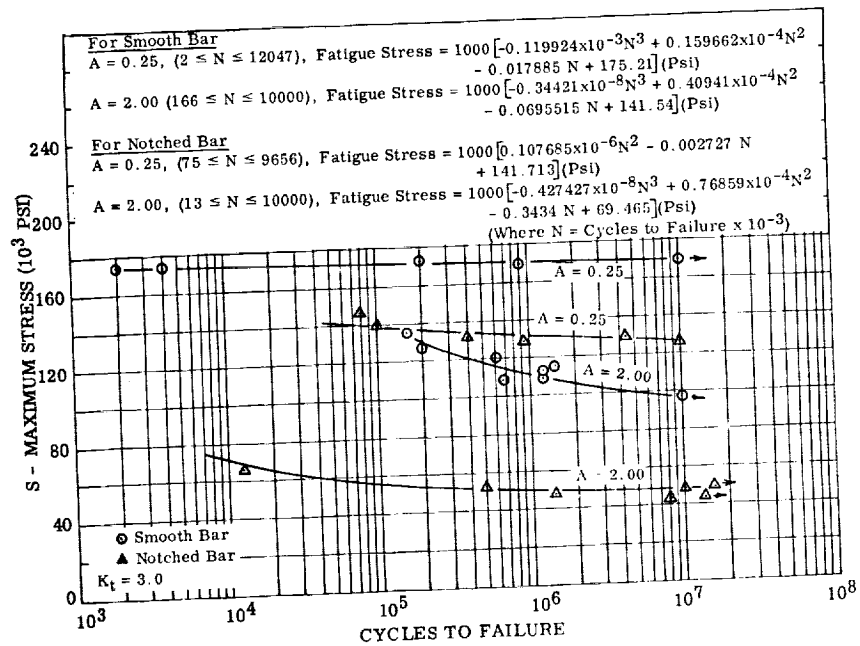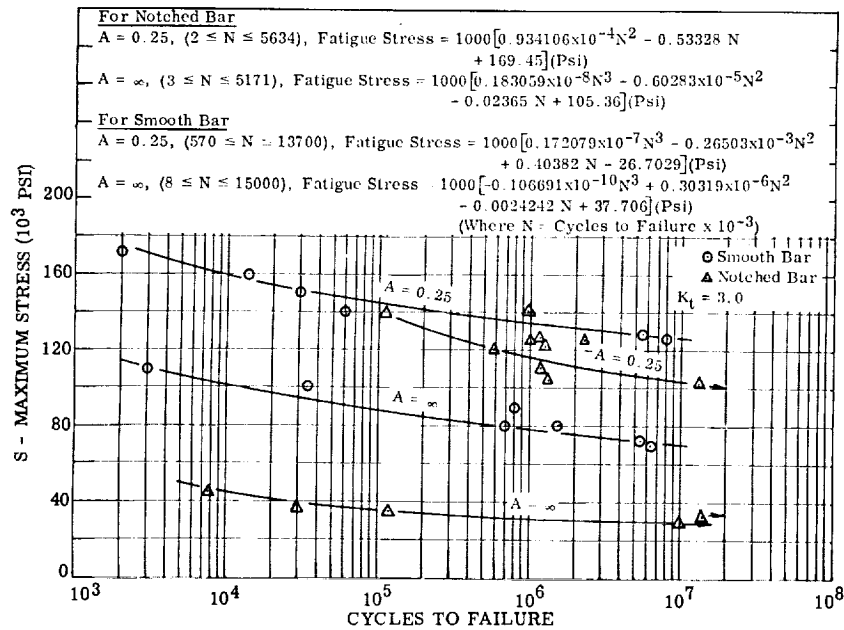
(Where N = Cycles to Failure x 10^{-3})
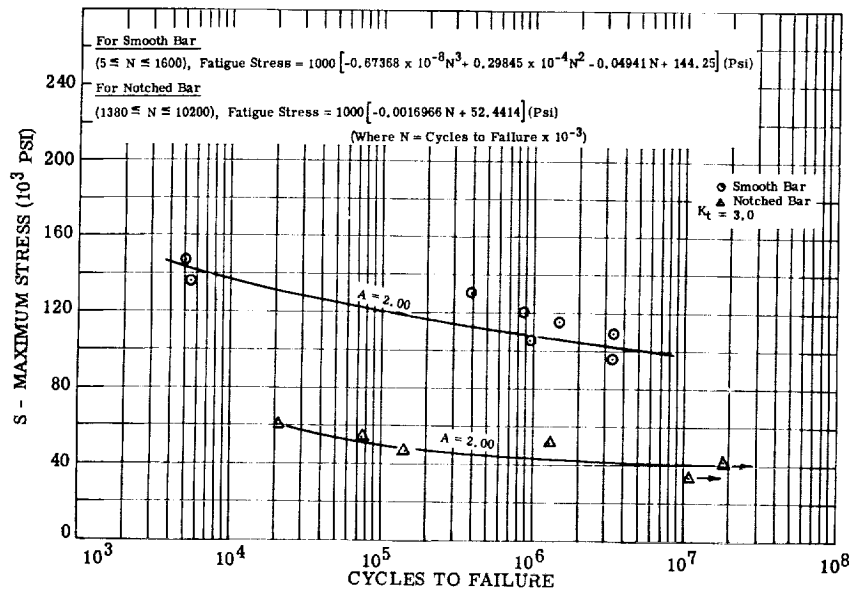
Figure 305. - Fatigue diagram for notched and smooth bar AMS 6487 (H-11) at Rockwell C 45 tested in air at 1000° F with ratio of alternating stress to mean stress A of 2.00. (See tables 45 and 46.)

Nivco Alloy

Nivco alloy, a high-temperature steam-turbine blading alloy, is a commercial single-source product manufactured by the Westinghouse Electric Corporation, Blairsville, Pennsylvania. Its nominal composition is 23 percent nickel, 2 percent titanium, 1 percent zirconium, and the balance, cobalt. Its tested composition was as follows

	Ni	Zr	Al	Ti	Co
	Composition, percent				
Bar	23.5	1.03	0.25	2.04	Bal.
Sheet	23.9	~1.00	.33	1.96	Bal.

Thermophysical properties.

Density, lb/cu in. (g/cu cm) 0.312 (8.61)
Curie temperature, ^{O}F 1800
Thermal conductivity, (Btu)(ft)/(sq ft)(hr)(^{O}F), at -
   72° F 25.5
   900° F 18.7
   1100° F 17.8
Coefficient of thermal expansion (from 72° to 1200° F), in./(in.)(^{O}F) . . $7.4C \times 10^{-6}$
Specific heat, Btu/(lb)(^{O}F), at -
   72° F 0.102
   900° F 0.111
   1100° F 0.124
Electrical resistivity, ohm-cm, at -
   72° F . . . . 27.98×10^{-6}
   900° F . . . . 52.27×10^{-6}
   1100° F . . . . 60.73×10^{-6}

Magnetic properties. - All magnetic materials were at a hardness of Rockwell C 38 to 42 unless otherwise specified. Constant current flux reset properties are not applicable for Nivco alloy and were measured only for materials used in magnetic amplifiers.

Direct current (solid ring):

Temperature, $^{\circ}$F	H, Oe	Induction, B_{tip}, kG
72	300	12.6
800	300	12.0
1100	300	11.6
1400	230	9.9

Alternating current (400 cps; B = 6 kG):

Temperature, $^{\circ}$F	Lamination thickness, in.			
	0.014	0.025	0.014	0.025
	Exciting volt-amperes per pound		Core loss, W/lb	
72	183.0	149.0	96.0	80.0
800	113.0	-----	63.0	----
900	-----	94.8	----	51.6
1100	98.0	77.0	54.5	41.3
1400	27.3	42.0	51.0	27.0

Mechanical properties. - Poisson's ratio at 72° F is 0.320.

Tensile properties for bar stock tested in air:

Temperature, $^{\circ}$F	0.20-Percent offset yield strength, psi	Tensile strength, psi	Elongation in 1.4 in., percent	Reduction of area, percent	Modulus of elasticity, psi
72	112 400	165 400	30.7	43.6	29.1×10^{6}
900	89 200	133 800	21.0	43.7	25.7
1100	89 900	124 600	24.3	47.0	18.6
1400	-------	-------	----	----	9.7
1600	-------	-------	----	----	4.2

Creep (for creep in argon or vacuum, this information applies; for temperatures above 1100° F, actual test data should be consulted):

Temperature, °F	Time, hr	Stress, psi, to produce creep of -	
		0.20 Percent	0.40 Percent
Bar stock			
900	1 000	92 000	100 000
	10 000	90 000	95 000
1100	1 000	68 000	75 800
	10 000	58 000	63 000
0.025-in.-thick sheet[a]			
900	1 000	29 300	-------
1100	10 000	16 200	-------

[a]The creep for sheet represents a very limited number of tests. Initial creep data for material which had been solution-annealed, quenched, cold-finished, and aged was unexpectedly poor and is not worth presenting. These sheet creep data were obtained with completely reheat-treated test bars. While the sheet creep properties do not approach those of forged bar stock, a considerable reduction in creep rate is measured. Complete discussions of Nivco alloy sheet and creep data are found in earlier sections.

Fatigue strength of bar stock tested in air or argon for 10^7 cycles (stress concentration factor K_t, 3):

Temperature, $^\circ$F	A	Smooth bar	Notched bar
		Fatigue strength, psi	
900	∞	60 000	35 000
	0.25	135 000	135 000
1000	∞	60 000	35 000
	0.25	128 000	120 000
1100	∞	60 000	30 000
	0.25	108 000	95 000

Heat treatment: The normal heat treatment for use as solid inductor rotor material in solid form and resultant hardness is to heat to $1725^\circ \pm 25^\circ$ F, hold at temperature for 1 hour, water-quench, and age 25 hours at $1225^\circ \pm 5^\circ$ F. (The hardness is approximately Rockwell C 38 to 42.) Special heat treatment for use as laminated rotor or stator materials is to heat to $1900^\circ \pm 25^\circ$ F, hold at temperature for 1 hour, water-quench, and age 25 hours at $1225^\circ \pm 5^\circ$ F. (The aged hardness is approximately Rockwell C 38 to 42.)
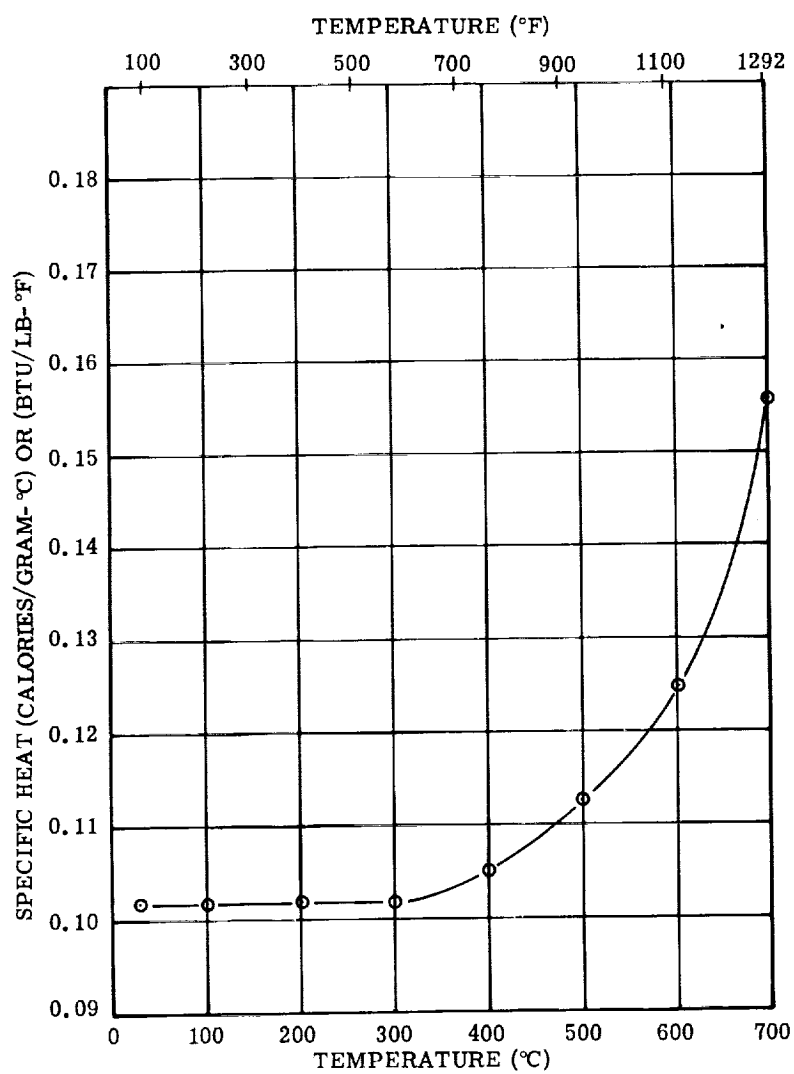
Figure 306. - Specific heat of Nivco forging in vacuum.

TABLE 47. - ELECTRICAL RESISTIVITY OF

NIVCO RIBBON IN VACUUM - FIRST TEST

[Specimen 1 with continuous heating; width,
0.247 in.; thickness, 0.0255 in.;
length, 11.54 in.; see fig. 307.]

| Temperature, °F	Resistance, ohms	Resistivity, michrohm-cm
78	0.01313	18.20
200	.01471	20.39
300	.01666	23.10
400	.01863	25.83
500	.02116	29.33
603	.02373	32.89
700	.02642	36.63
800	.02920	40.48
900	.03231	44.79
1004	.03610	50.04
1100	.03942	54.65
1200	.04305	59.68
1300	.04693	65.06
1400	.04993	69.22
1500	.05410	75.00
1600	.05751	79.73
1450	.05368	74.42
1250	.04912	68.10
1044	.04221	58.51
850	.03660	50.74
635	.03100	42.97
450	.02655	36.81
250	.02302	31.91
150	.02130	29.53
79	.02017	27.96
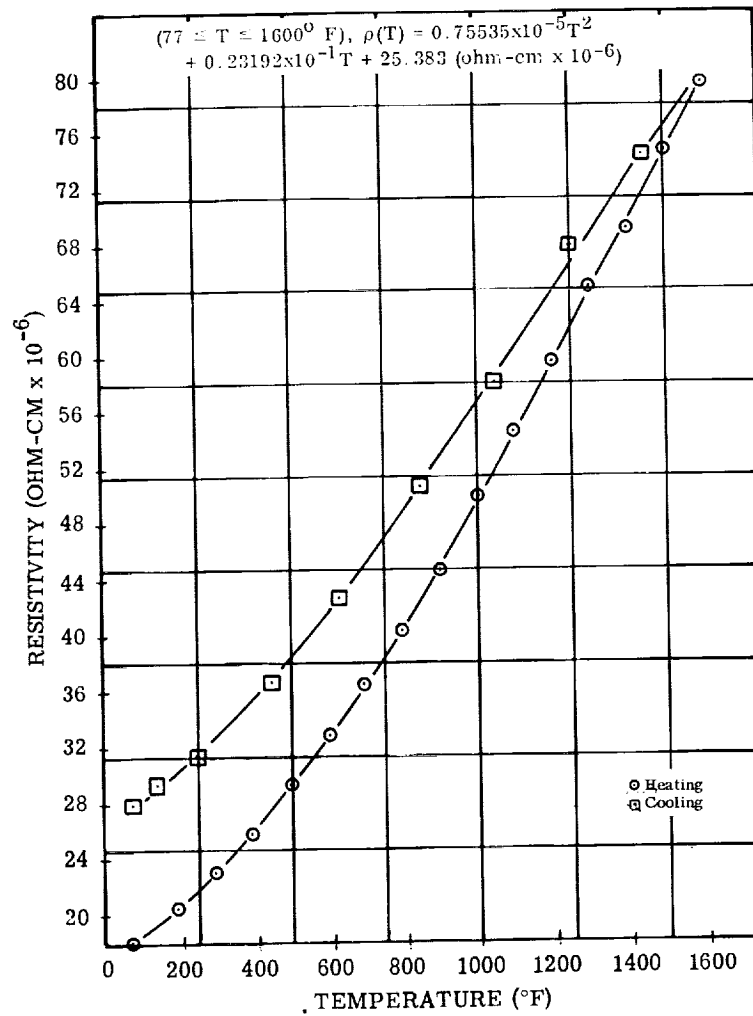
Figure 307. – Electrical resistivity of Nivco ribbon tested in vacuum, specimen 1, first test. (See table 47.)

TABLE 48. - ELECTRICAL RESISTIVITY OF

NIVCO RIBBON IN VACUUM - SECOND TEST

[Specimen 1 with continuous heating; width,
0.247 in.; thickness, 0.0255 in.;
length, 11.54 in.; see fig. 308.]

Temperature, °F	Resistance, ohms	Resistivity, michrohm-cm
77	0.02025	28.07
200	.02184	30.28
300	.02370	32.86
406	.02565	35.56
500	.02771	38.41
600	.02989	41.44
700	.03246	45.00
821	.03566	49.43
900	.03792	52.57
1000	.04080	56.56
1100	.04381	60.73
1200	.04660	64.60
1300	.04895	67.86
1400	.05293	73.38
1500	.05575	77.29
1600	.05832	80.85
1450	.05360	74.31
1234	.04900	67.93
1050	.04262	59.09
850	.03681	51.03
650	.03155	43.74
450	.02704	37.49
250	.02319	32.15
150	.02141	29.68
75	.02031	28.16
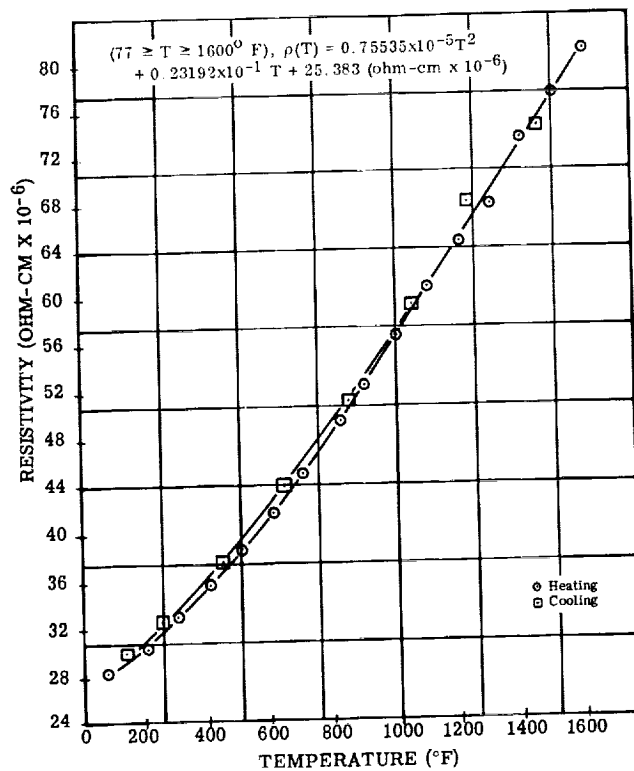
Figure 308. - Electrical resistivity of Nivco ribbon tested in vacuum; specimen 1, second test. (See table 48.)
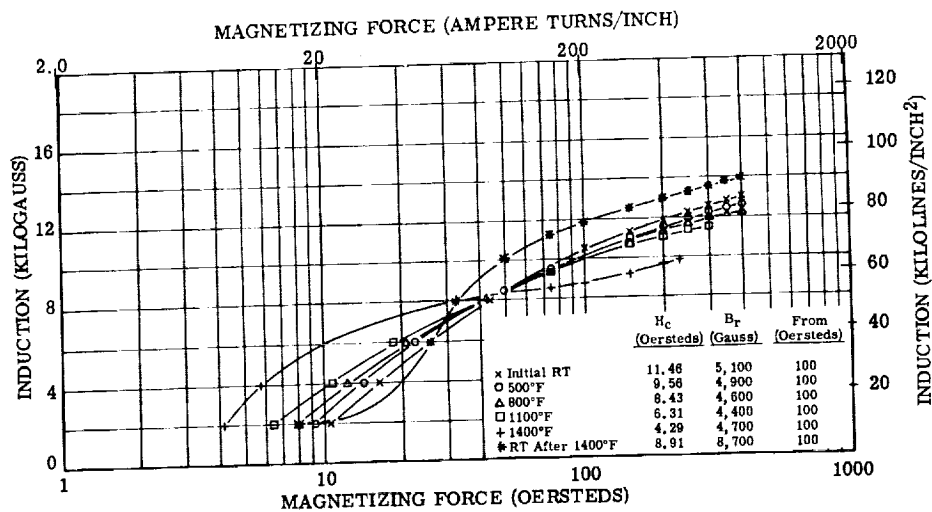
Figure 309. - Direct-current magnetization curves for Nivco forging, test atmosphere, air to 800° F and argon above 800° F.

Figure 310. - Direct-current magnetization curves for Nivco forging, aging test. Test atmosphere, argon.

Figure 311. - Direct-current magnetization curves for Nivco alloy 0.014-inch laminations. Test atmosphere, air to 800° F and argon above 800° F; interlaminar insulation, aluminum orthophosphate.

MAGNETIZING FORCE (AMPERE TURNS/INCH)

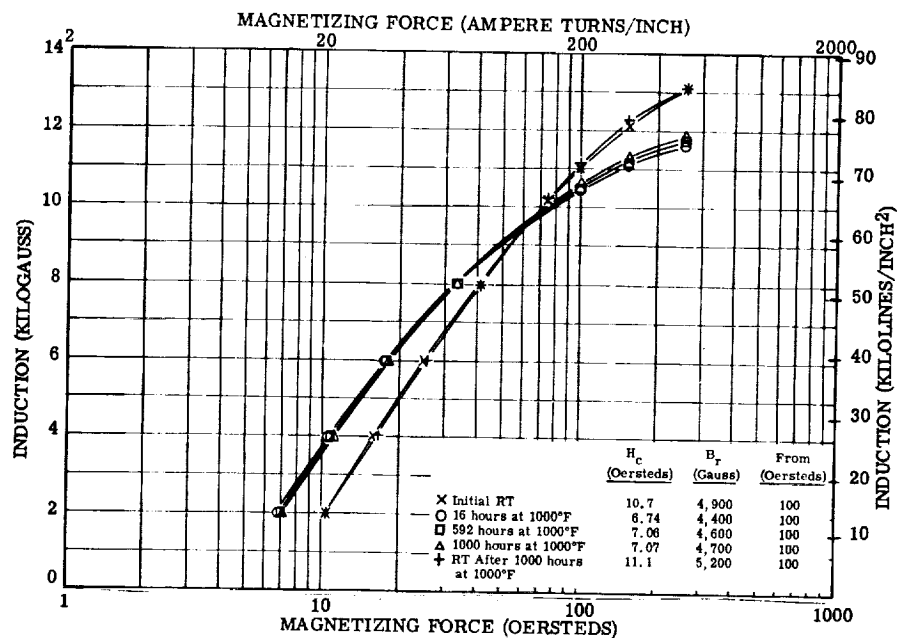| H$_c$ (Oersteds)	B$_r$ (Gauss)	From (Oersteds)
x Initial RT	35.48	8,000	100
O 500°F	30.19	8,250	100
△ 800°F	26.17	8,150	100
□ 1100°F	20.88	7,800	100
✱ 1400°F	8.86	5,750	100
+ RT After 1400°F	23.15	10,100	100

MAGNETIZING FORCE (OERSTEDS)

Figure 312. - Direct-current magnetization curves for Nivco alloy 0.025-inch-laminations. Test atmosphere, air to 800° F and argon above 800° F; interlaminar insulation, aluminum orthophosphate.

x Initial RT
O 500°F
△ 800°F
□ 1100°F
+ 1400°F
✱ RT After 1400°F

VOLT-AMPERES PER POUND
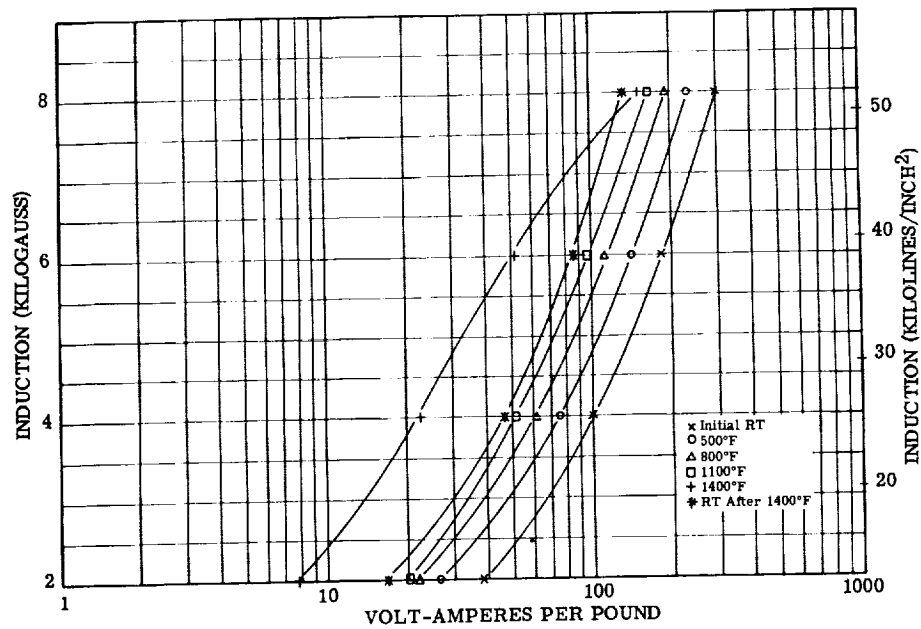
Figure 313. - Exciting volt-amperes per pound at 400 cps for Nivco alloy 0.014-inch laminations. Test atmosphere, air to 800° F and argon above 800° F; interlaminar insulation, aluminum orthophosphate.
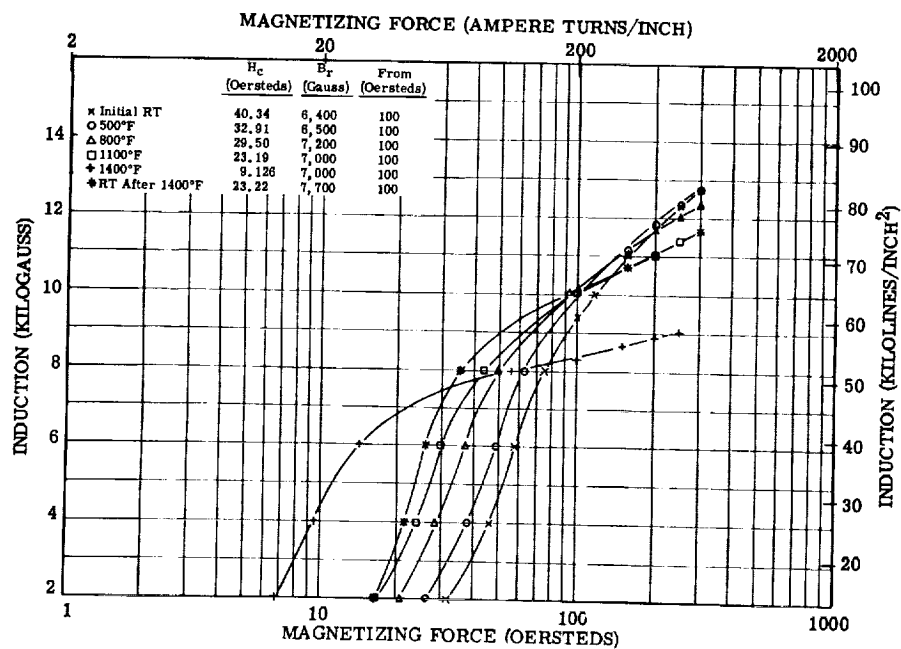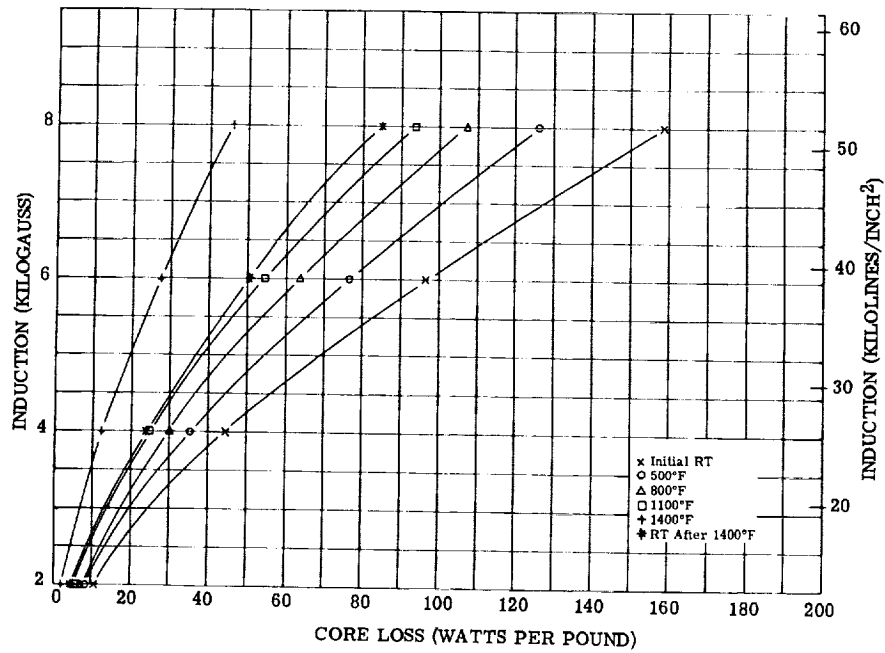
Figure 314. - Core loss at 400 cps for Nivco alloy 0.014-inch laminations. Test atmosphere, air to 800° F and argon above 800° F; interlaminar insulation, aluminum orthophosphate.
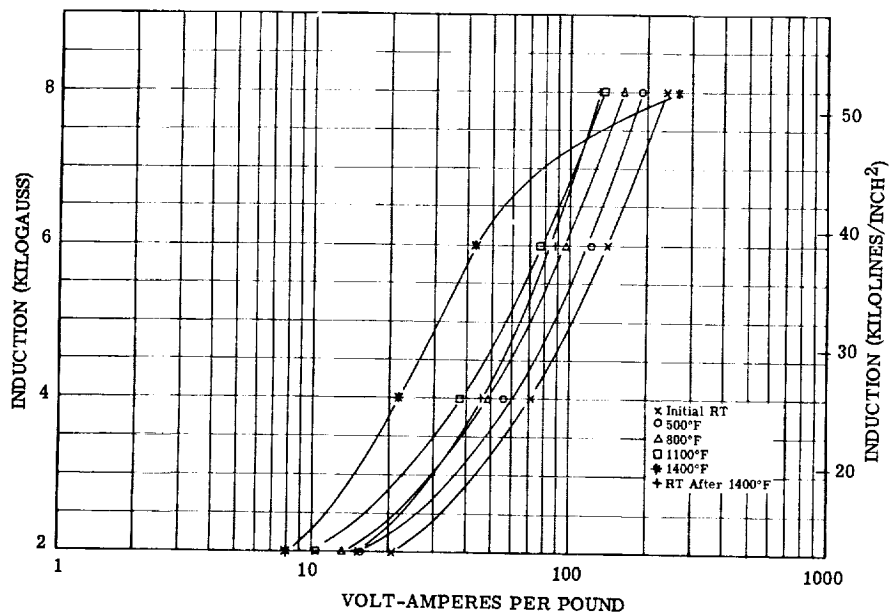
Figure 315. - Exciting volt-amperes per pound at 400 cps for Nivco alloy 0.025-inch laminations. Test atmosphere, air to 800° F and argon above 800° F; interlaminar insulation, aluminum orthophosphate.
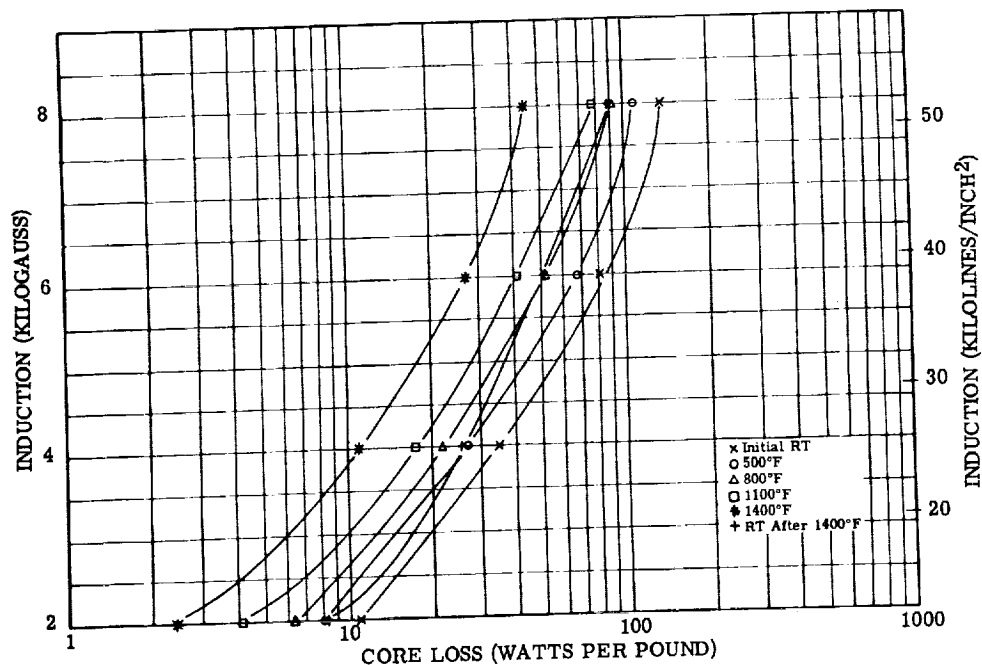
Figure 316. - Core loss at 400 cps for Nivco alloy 0.025-Inch laminations. Test atmosphere, air to 800° F and argon above 800° F; interlaminar insulation, aluminum orthophosphate.

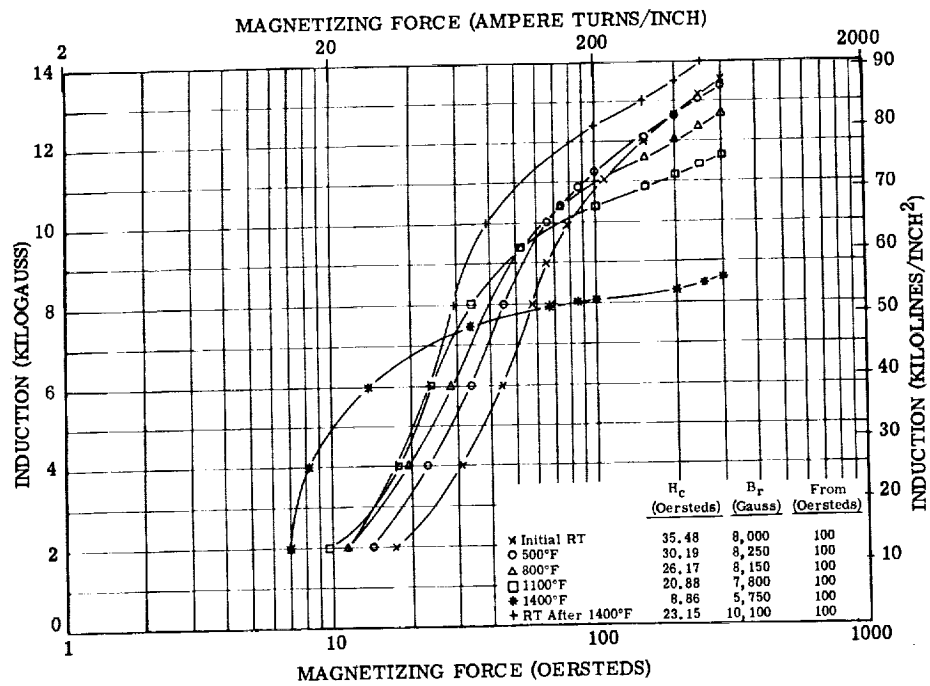$$0.02\% \text{ Yield Stress} = 1000\left[0.59018 \times 10^{-9} T^4 - 0.2324 \times 10^{-5} T^3 + 0.2992 \times 10^{-2} T^2 - 1.3639 T + 185.84\right] (\text{Psi})$$

$$0.20\% \text{ Yield Stress} = 1000\left[0.68097 \times 10^{-4} T^4 - 0.26624 \times 10^{-5} T^3 + 0.3396 \times 10^{-2} T^2 - 1.5258 T + 205.63\right] (\text{Psi})$$

$$\text{Ultimate Strength} = 1000\left[0.79956 \times 10^{-9} T^4 - 0.308 \times 10^{-5} T^3 + 0.38482 \times 10^{-2} T^2 - 1.7017 T + 269.05\right] (\text{Psi})$$

Figure 317. - Effect of temperature on strength of Nivco forging tested in air. (See table 49.)

TABLE 49. - TENSILE TEST DATA FOR NIVCO FORGING TESTED IN AIR

[Test, ASTM E21; strain rate, 0.005 in./(in.)(min) to yield and 0.050 in./(in.)(min) to failure.]

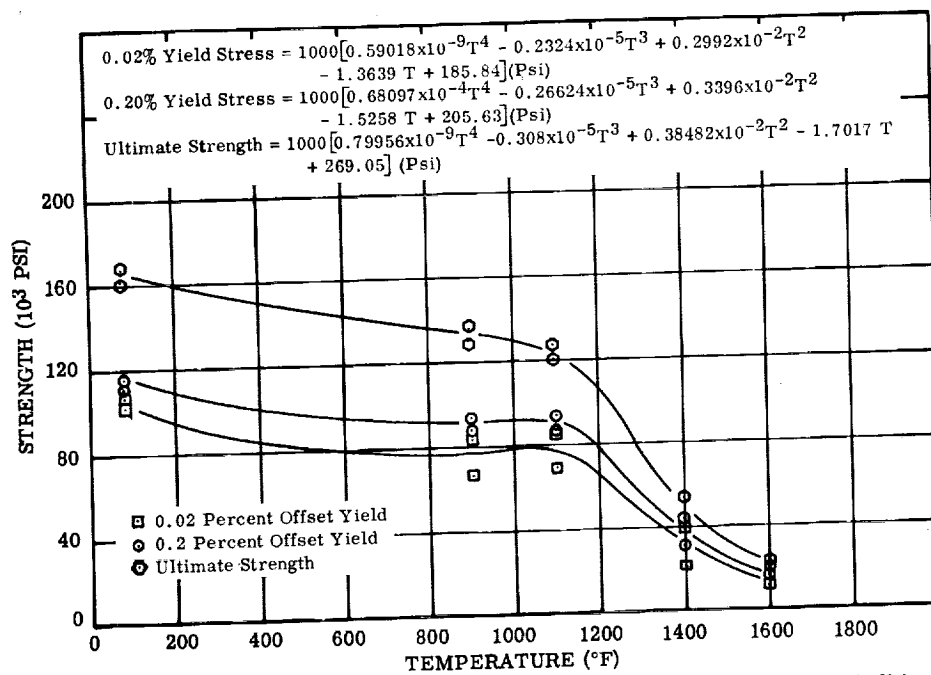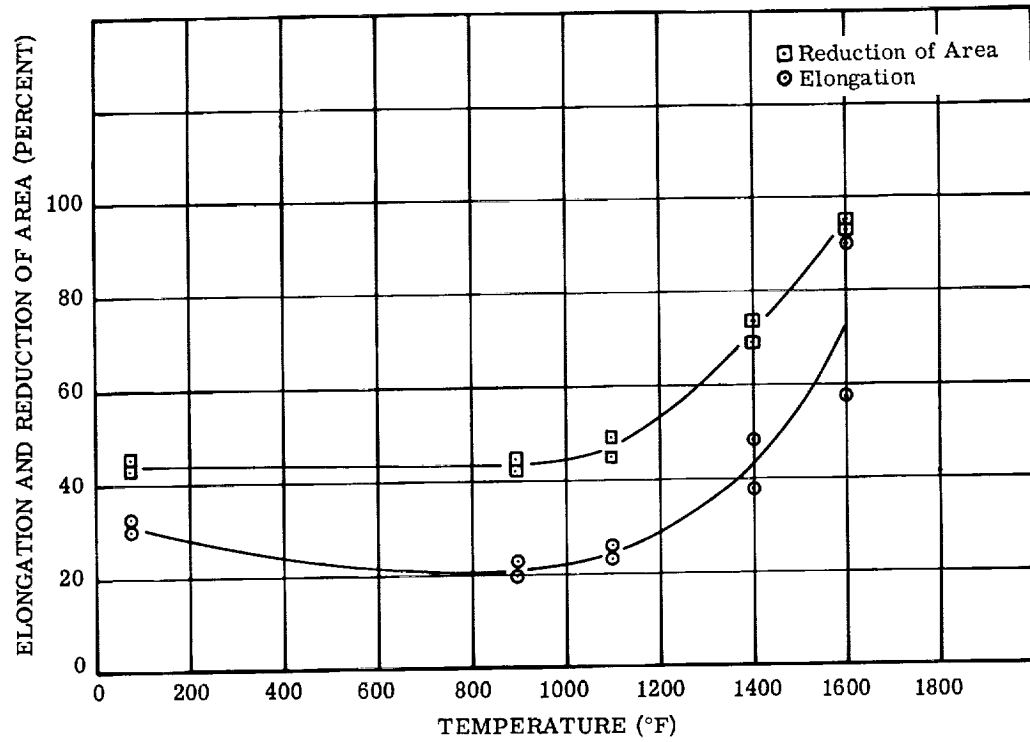| Specimen	Diameter, in.	Hardness, BHN (a)	Test temperature, °F	0.02-Percent offset yield stress, psi	0.2-Percent offset yield stress, psi	Ultimate strength, psi	Elongation in 1.4 in., percent	Reduction of area, percent
5	0.357	316	Room	104 700	112 400	166 350	31.3	44.9
6	.357	316	Room	99 900	112 400	164 350	30.1	42.4
1	.358	336	900	83 150	91 750	136 300	21.4	43.6
7	.357	302	900	66 950	86 600	131 350	20.7	43.7
2	.358	331	1100	84 500	94 150	127 850	24.6	45.2
8	.358	316	1100	69 500	85 650	121 400	24.0	48.9
3	.358	321	1400	22 600	29 000	43 700	b47.9	73.9
9	.357	321	1400	40 350	43 550	54 650	37.4	68.9
4	.358	326	1600	12 950	15 750	20 800	57.6	94.3
10	.357	321	1600	12 400	16 200	23 150	90.2	93.9

aLoad, 3000 kg.
bQuarter break.

Figure 318. – Effect of temperature on elongation and reduction of area of Nivco forging tested in air. (See table 49.)

TABLE 50. - TENSILE TEST DATA FOR NIVCO 0.025-INCH

TRANSVERSE SHEET MATERIAL TESTED IN AIR

[Test, ASTM E21; strain rate, 0.005 in./(in.)(min) to yield
and 0.050 in./(in.)(min) to failure.]

Mark	Test temperature, °F	0.02-Percent offset yield stress, psi	0.2-Percent offset yield stress, psi	Ultimate strength, psi	Elongation in 2 in., percent
26 T	80	103 200	151 900	(a)	(a)
4 T	80	155 300	171 900	180 950	2.7
30 T	900	73 700	109 750	126 450	12.2
31 T	900	71 900	105 950	125 300	[b]9.8
32 T	1100	54 100	79 100	101 200	10.1
33 T	1100	(c)	(c)	107 550	13.2
27 T	1400	23 250	34 950	44 150	[b]25.0
34 T	1400	25 400	35 350	43 550	35.0
35 T	1600	10 000	13 950	20 000	52.4
36 T	1600	9 450	14 100	19 950	64.1

[a]Broke in grips.
[b]Quarter break.
[c]Curve unreliable; extensometer slipped on specimen.

0.02% Yield Stress $= 1000 \left[0.88774 \times 10^{-9} T^4 - 0.3085 \times 10^{-5} T^3 + 0.3574 \times 10^{-2} T^2 - 1.541 T + 231.2 \right]$ (Psi)

0.20% Yield Stress $= 1000 \left[0.7312 \times 10^{-7} T^3 - 0.2343 \times 10^{-3} T^2 + 0.09928 T + 155.41 \right]$ (Psi)

Ultimate Strength $= 1000 \left[0.412 \times 10^{-9} T^4 - 0.1549 \times 10^{-5} T^3 + 0.1875 \times 10^{-2} T^2 - 0.8578 T + 238.36 \right]$ (Psi)

□ 0.02 Percent Offset Yield
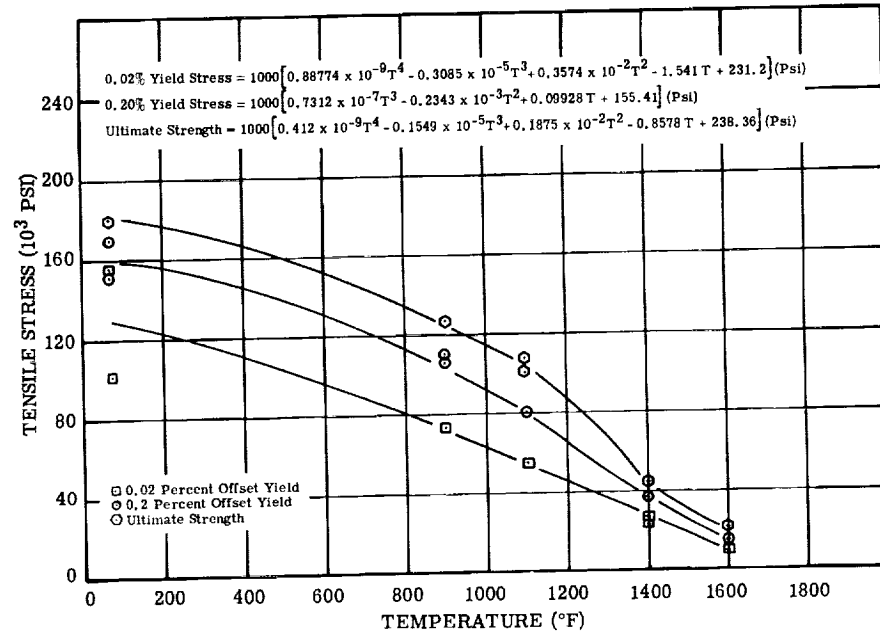◎ 0.2 Percent Offset Yield
◯ Ultimate Strength

Figure 319. – Effect of temperature on tensile stress of 0.025-inch Nivco transverse sheet tested in air. (See table 50.)

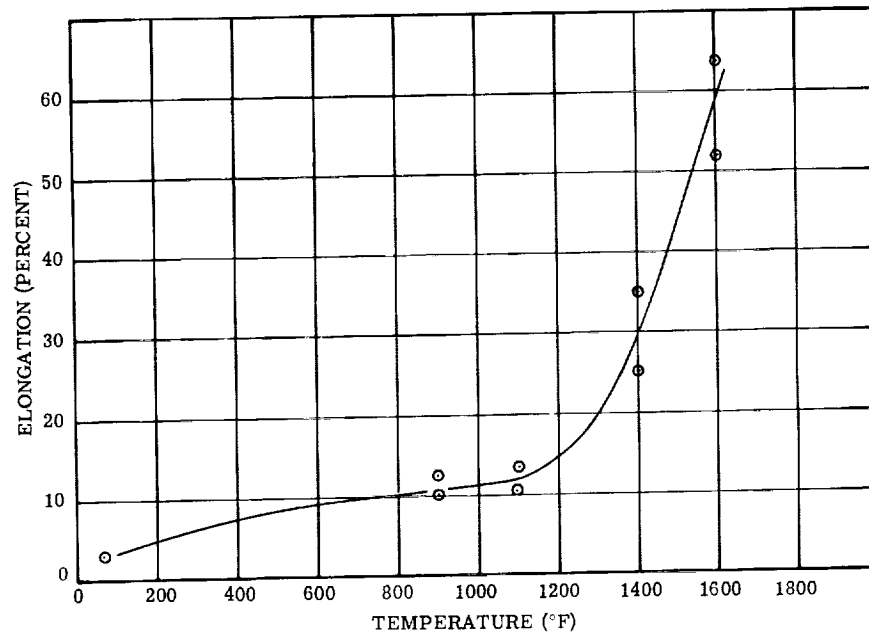Figure 320. – Effect of temperature on elongation of 0.025-inch Nivco transverse sheet tested in air. (See table 50.)
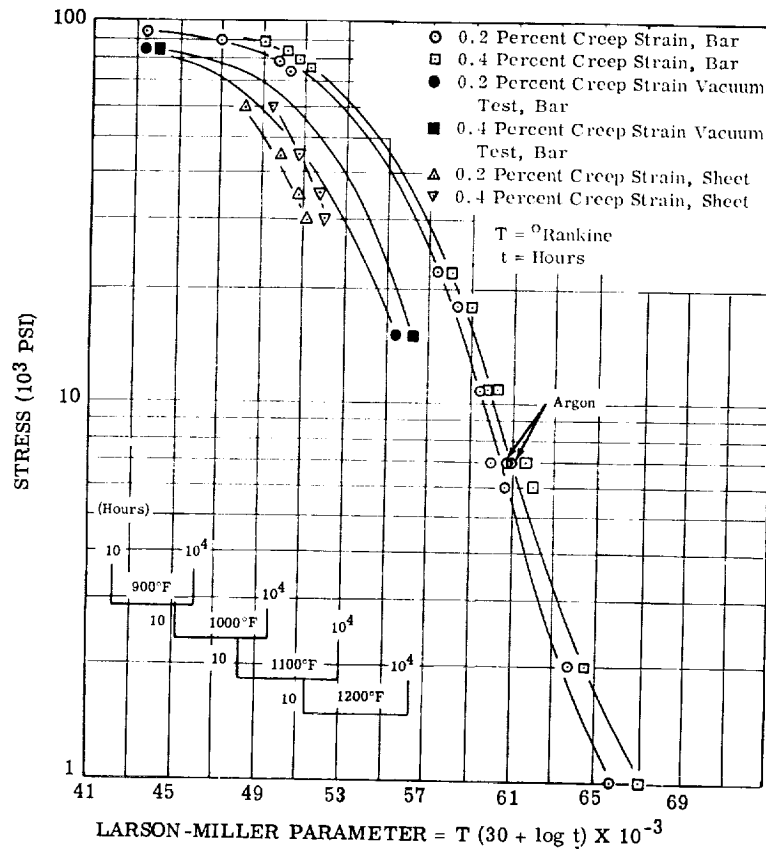
Figure 321. - Larson-Miller plot of forged Nivco bar and Nivco sheet creep data tested in air, argon, and vacuum, based on maximum of 2000-hour data.
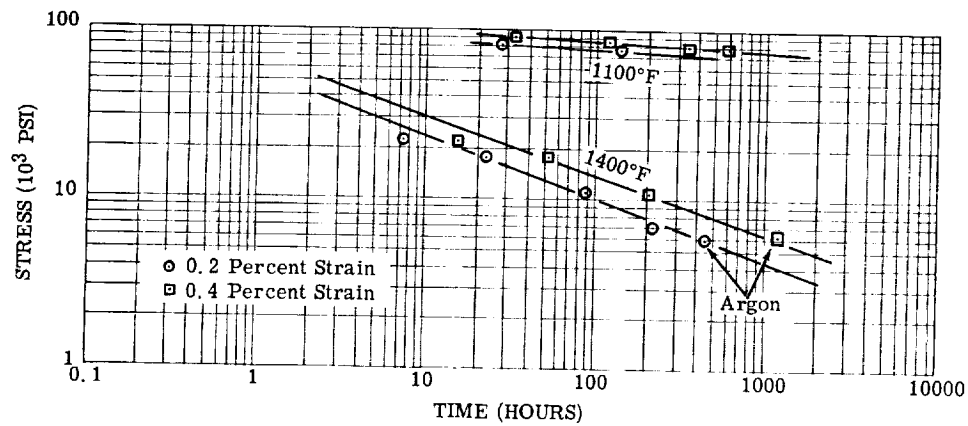
Figure 322. - Variation of stress with time to reach indicated creep strain for forged Nivco bar tested in air and argon at 1100° and 1400° F.

Figure 323. - Variation of stress with time to reach indicated creep strain for forged Nivco bar tested in air and argon at 1600° F.

Figure 324. - Variation of stress with time to reach indicated creep strain for Nivco sheet tested in air at 1100° F.

TABLE 51. - CREEP DATA FOR FORGED NIVCO BAR TESTED IN AIR AT 900° AND 1100° F

[Test, ASTM E139; see figs. 325 to 330.]

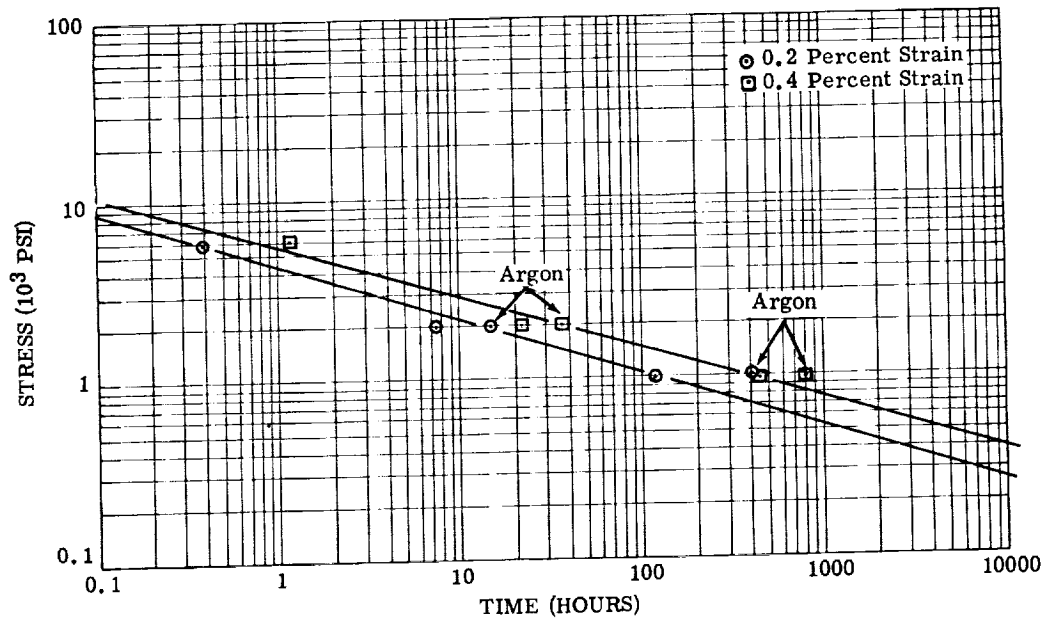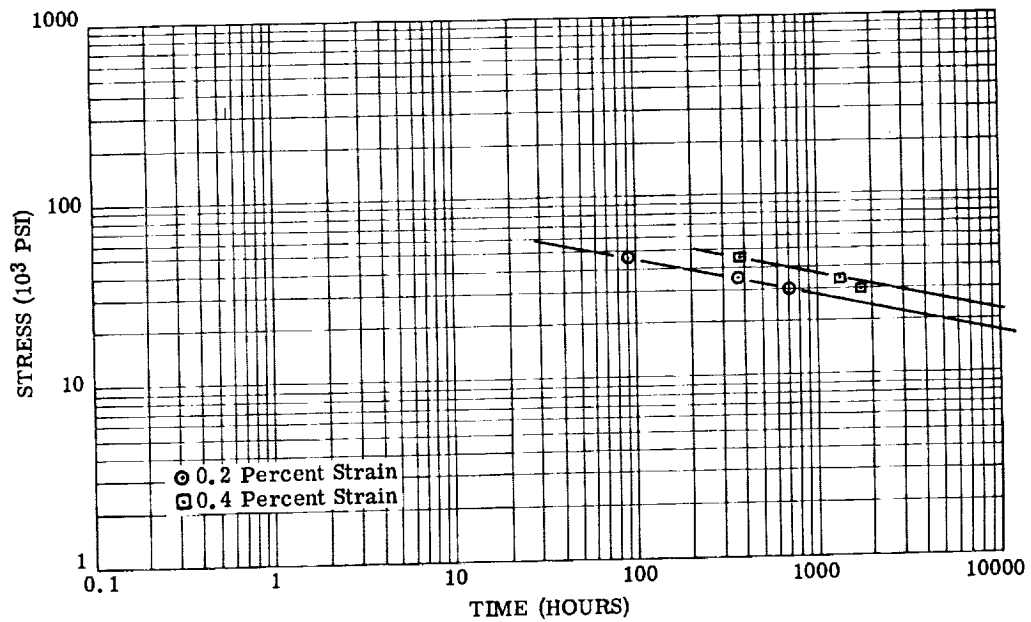| Temperature, °F	900	900	900[a]	900	900[a]	1100	1100[a]	1100	1000	1100	1100
Stress, psi	95 000	80 000	100 000	90 000	104 500	65 000	88 000	78 000	85 000	80 000	90 000
Duration of test, hr	1204	692	1202	789	1149	674	305	713	773.7	526	70.9[b]
Total creep strain, percent	0.263	0.013	0.209	0.111	0.502	0.108	0.667	0.459	2.710	0.518	0.9756
Time to cause 0.2-percent creep strain, hr	96	(c)	325	(c)	0	(c)	39	149	27	69	1.3
Time to cause 0.4-percent creep strain, hr	(c)	(c)	(c)	(c)	4	(c)	162	594	120	350	32.2
Plastic strain obtained on loading specimen, percent	0.118	0	0	0.0368	0.333	0	0.0436	0	0.0102	0	0.0588
Strain-time plot given in fig.	325	326	326	327	327	328	328	329	329	329	330

[a] Stress raised on previous specimen.
[b] Notch failure.
[c] Did not reach required strain.

Figure 325. - Creep data for forged Nivco bar tested in air at 900° F and 95 000 psi. (See table 51.)

Figure 326. - Creep data for forged Nivco bar tested in air at 900° F and 80 000 and 100 000 psi. (See table 51.)

Figure 327. - Creep data for forged Nivco bar tested in air at 900° F and 90 000 and 104 500 psi (data obtained by increasing stress on one specimen). (See table 51.)
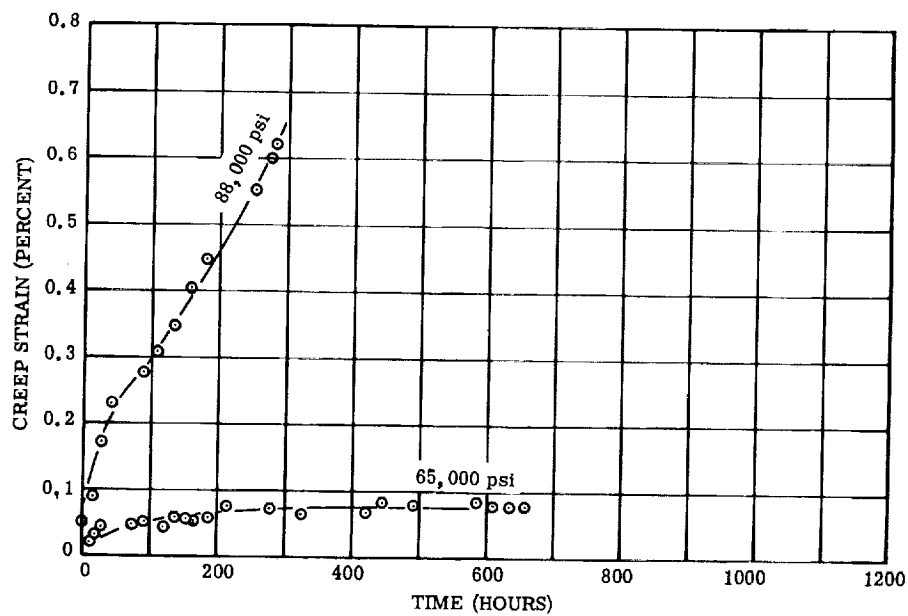
Figure 328. - Creep data for forged Nivco bar tested in air at 1100° F and 65 000 and 88 000 psi (data obtained by increasing stress on one specimen). (See table 51.)

Figure 329. - Creep data for forged Nivco bar tested in air at 1100° F and 78 000, 80 000, and 85 000 psi. (See table 51.)
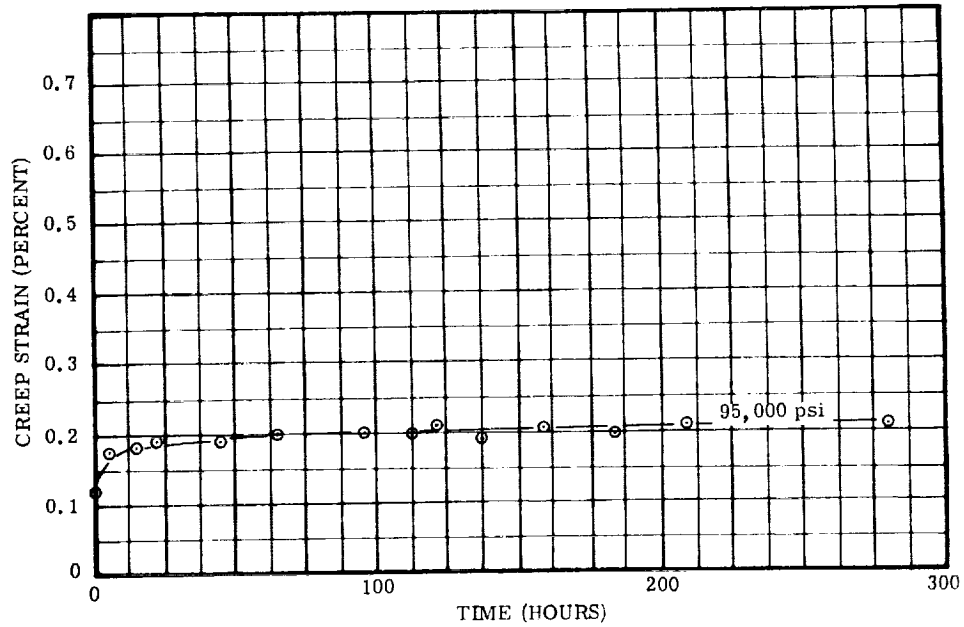

Figure 330. - Creep data for forged Nivco bar tested in air at 1100° F and 90 000 psi. (See table 51.)

TABLE 52. - CREEP DATA FOR FORGED NIVCO BAR

TESTED IN AIR AT 1400° AND 1600° F

[Test, ASTM E139; see figs. 331 and 332; plastic strain obtained on loading specimen, 0.]

Temperature, °F	1400	1400	1400	1400	1600	1600	1600
Stress, psi	22 000	18 000	11 000	7000	11 000	6000	2000
Duration of test, hr	48	120	240	214	1.75	20.7	119
Total creep strain, percent	2.35	1.18	0.47	0.1920	7.37	5.91	1.43
Time to cause 0.2-percent creep strain, hr	7.2	23	87.5	[a]217.0	0.05	0.4	7.6
Time to cause 0.4-percent creep strain, hr	16	51	202	------	0.09	1.25	21.6
Strain-time plot given in fig.	331	331	331	331	(b)	332	332

[a]Extrapolated.

[b]Data not plotted; test duration too short to obtain valid stress-time data.
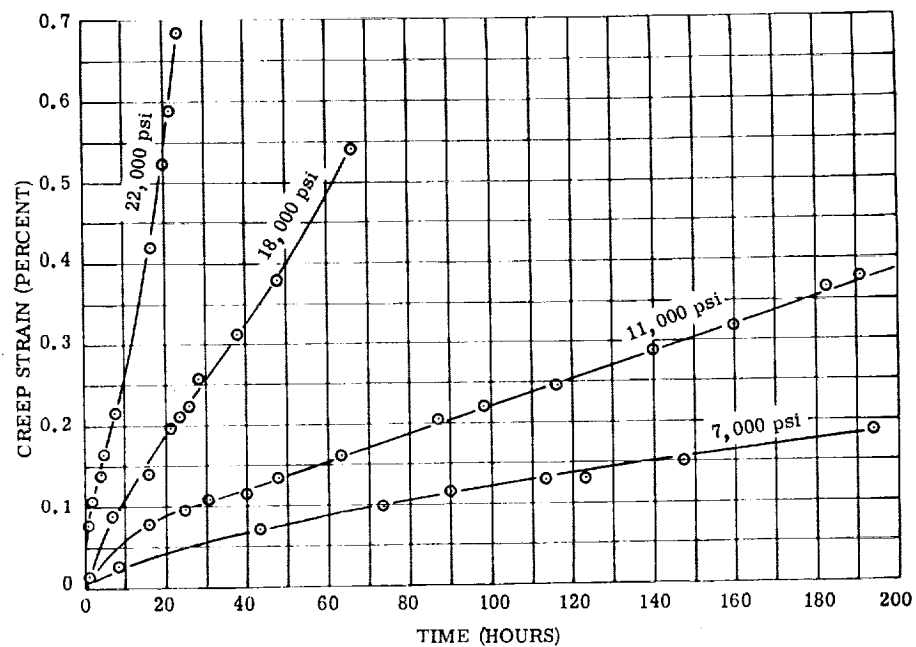
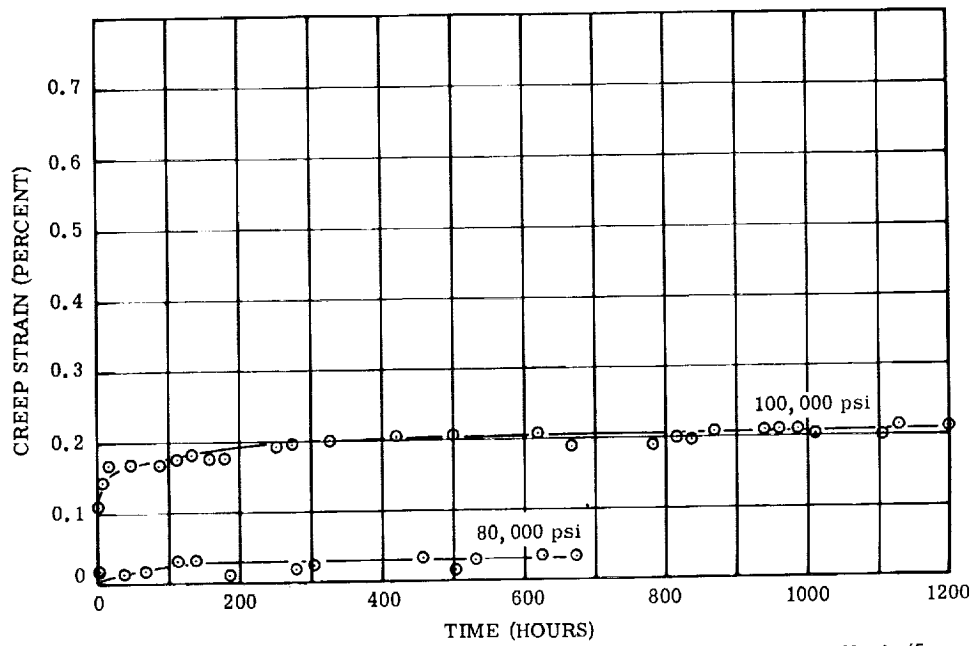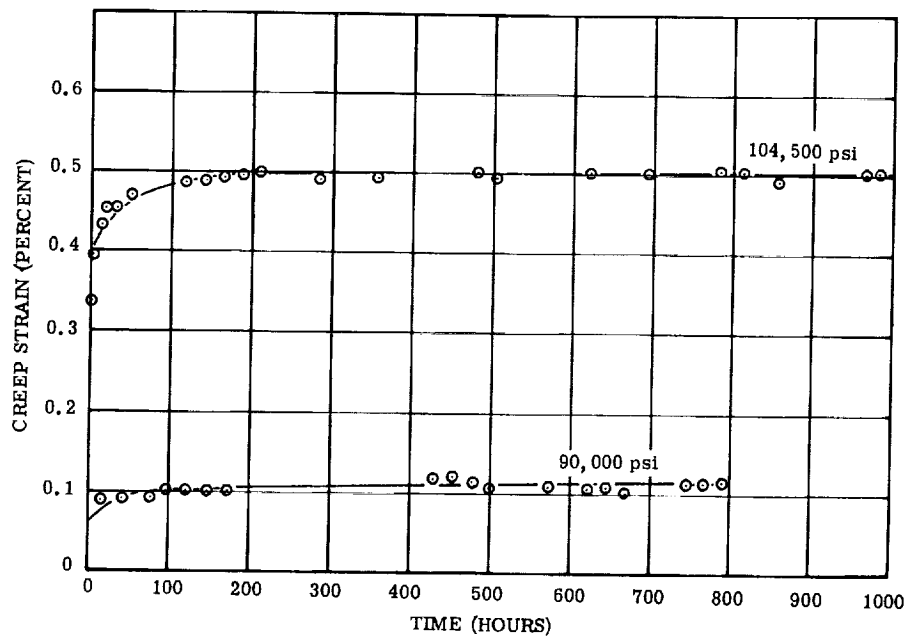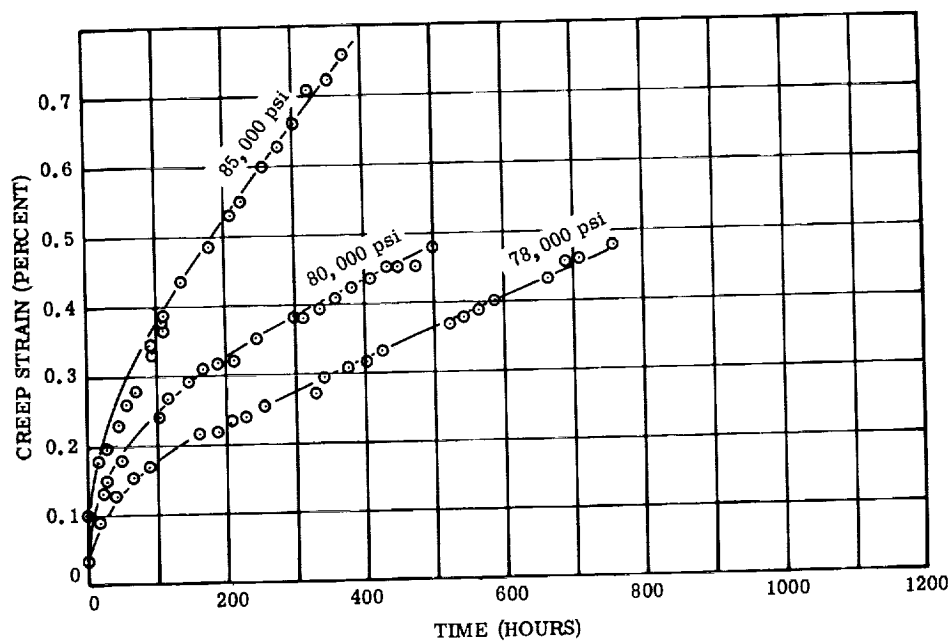Figure 331. - Creep data for forged Nivco bar tested in air at 1400° F. (See table 52.)

Figure 332. - Creep data for forged Nivco bar tested in air at 1600° F and 2000 and 6000 psi. (See table 52.)

TABLE 53. - CREEP DATA FOR FORGED NIVCO BAR TESTED IN AIR AND ARGON

[Test, ASTM E139; see figs. 333 to 338.]

Temperature, °F	1600	1600	1600	1400	1400	900	900	900
Stress, psi	1000	1000	2000	3000	6000	98 000	98 000	96 000
Duration of test, hr	497	1267	169	1031	1512	1031	910	719
Total creep strain, percent	0.431	0.437	1.92	0.0911	0.448	0.272	0.993	0.500
Time to cause 0.2-percent creep strain, hr	115	410	15.7	-----	460	0	0	0
Time to cause 0.4-percent creep strain, hr	437	1215	36.2	-----	1189	-----	0	0
Plastic strain obtained on loading specimen, percent	0	0	0	0	0	0.200	0.928	0.4303
Test atmosphere	Air	Argon	Argon	Argon	Argon	Air	Air	Air
Strain-time plot given in fig.	333	333	334	335	336	337	337	338

Figure 333. – Creep data for forged Nivco bar tested in air and argon at 1600° F and 1000 psi. (See table 53.)
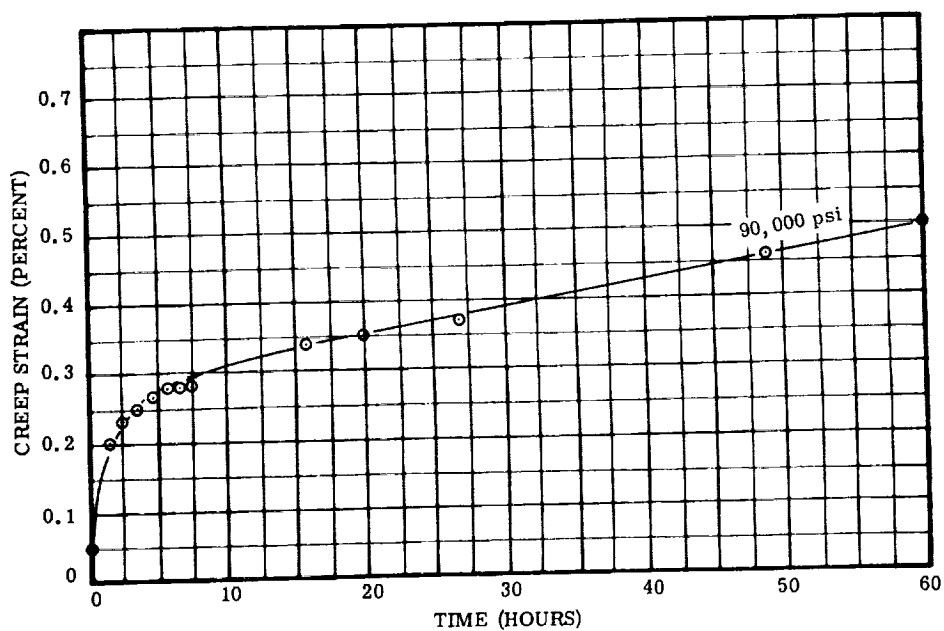

Figure 334. – Creep data for forged Nivco bar tested in argon at 1600° F and 2000 psi. (See table 53.)
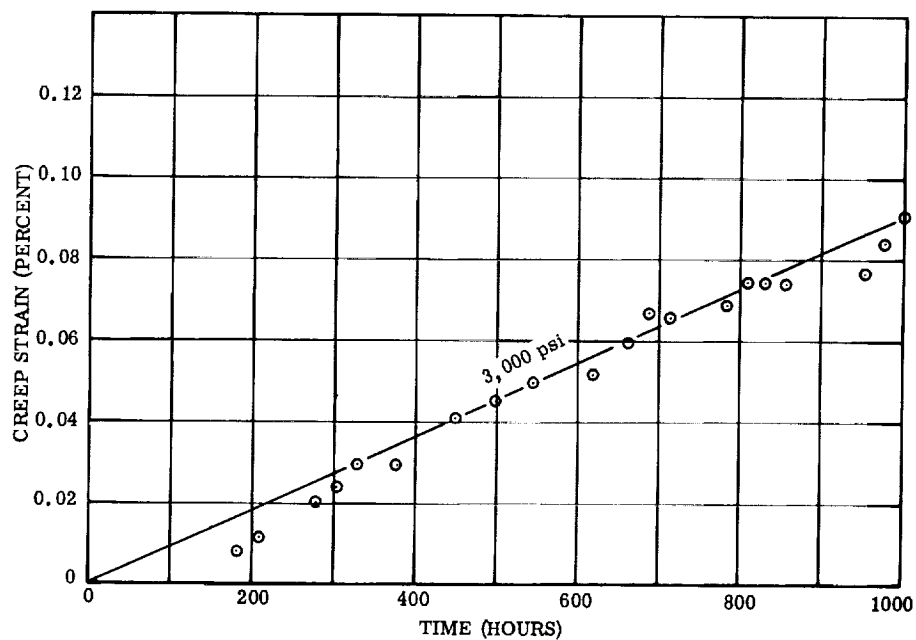
Figure 335. – Creep data for forged Nivco bar tested in argon at 1400° F and 3000 psi. (See table 53.)
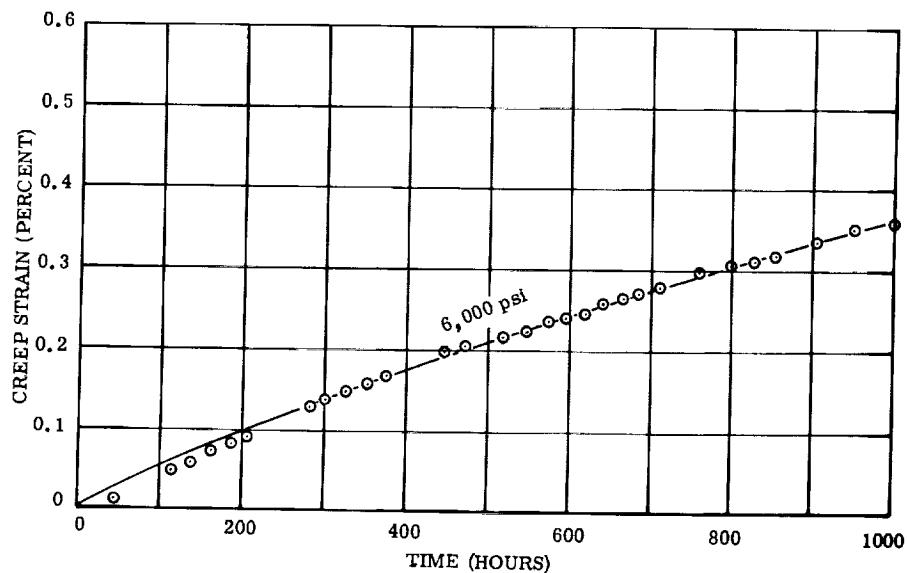
Figure 336. – Creep data for forged Nivco bar tested in argon at 1400° F and 6000 psi. Test concluded at 1512 hours at 0.448 percent creep strain. (See table 53.)
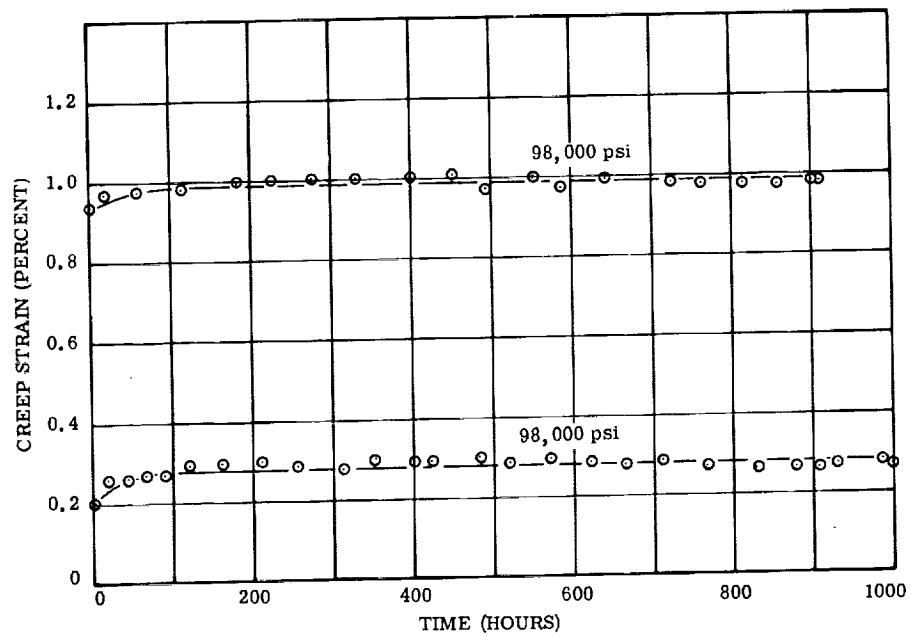
Figure 337. - Creep data for forged Nivco bar tested in air at 900° F and 98 000 psi. (See table 53; see section Detailed Discussion of Materials for discussion of scatter.)
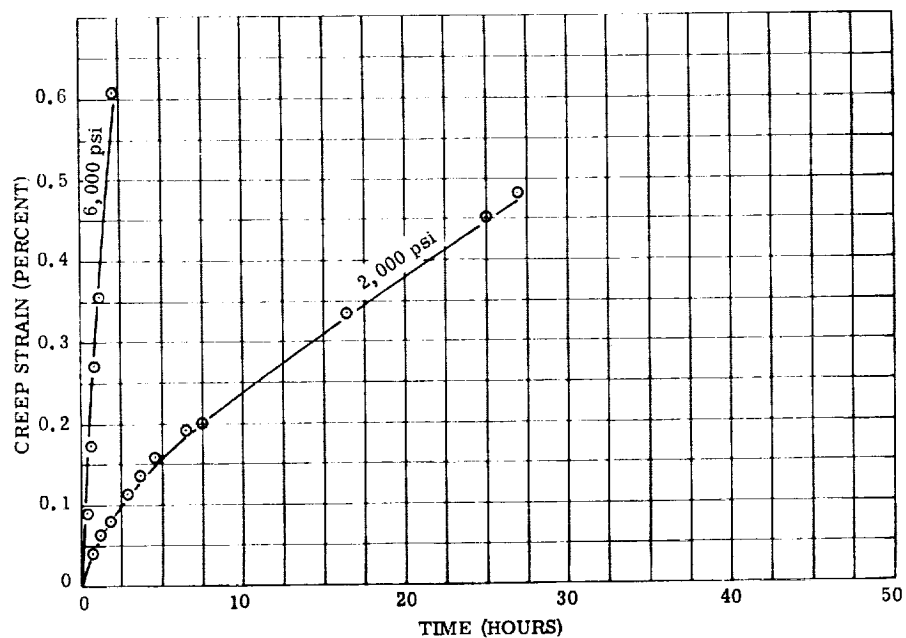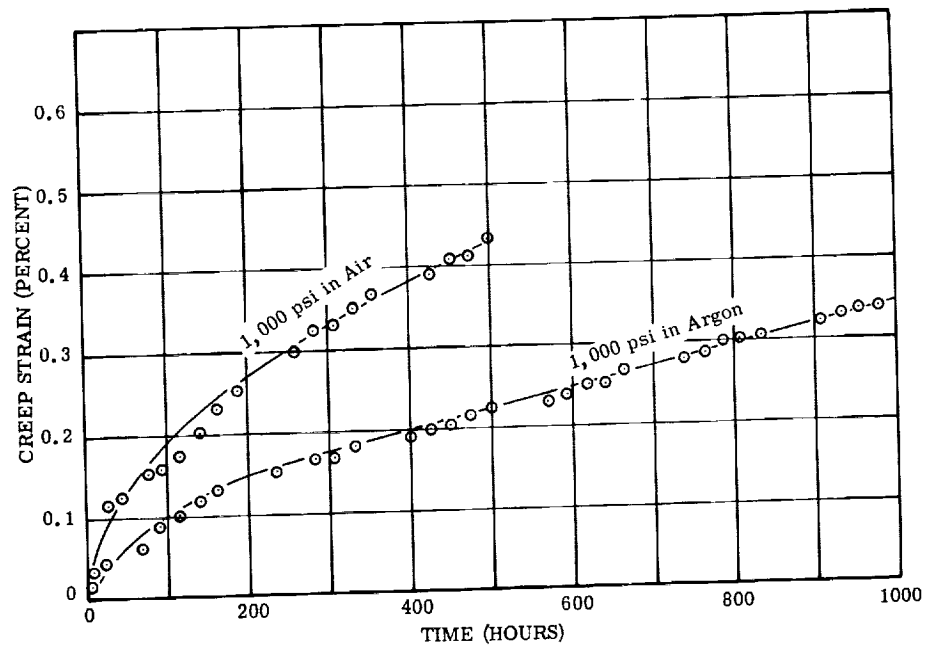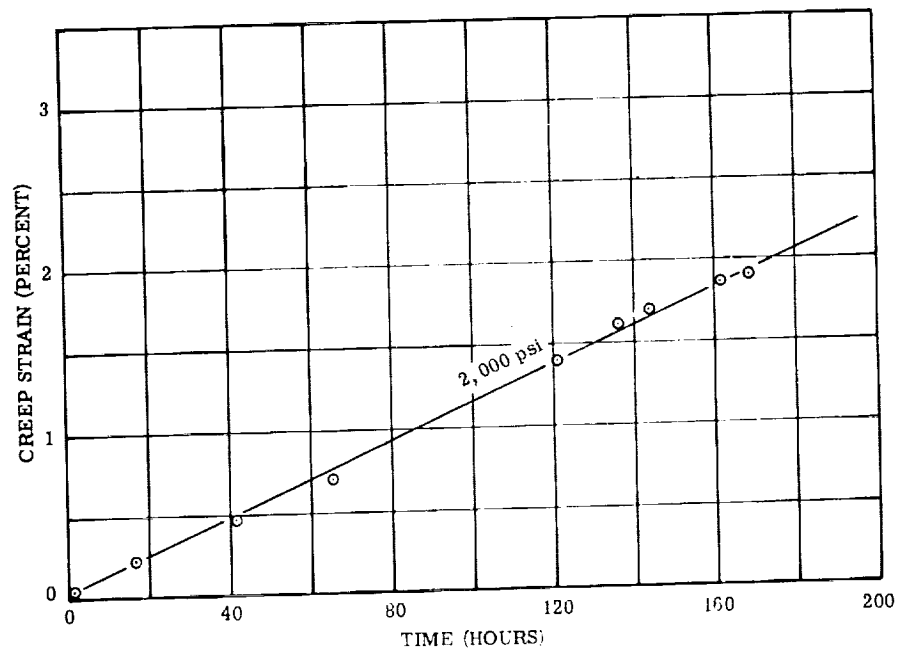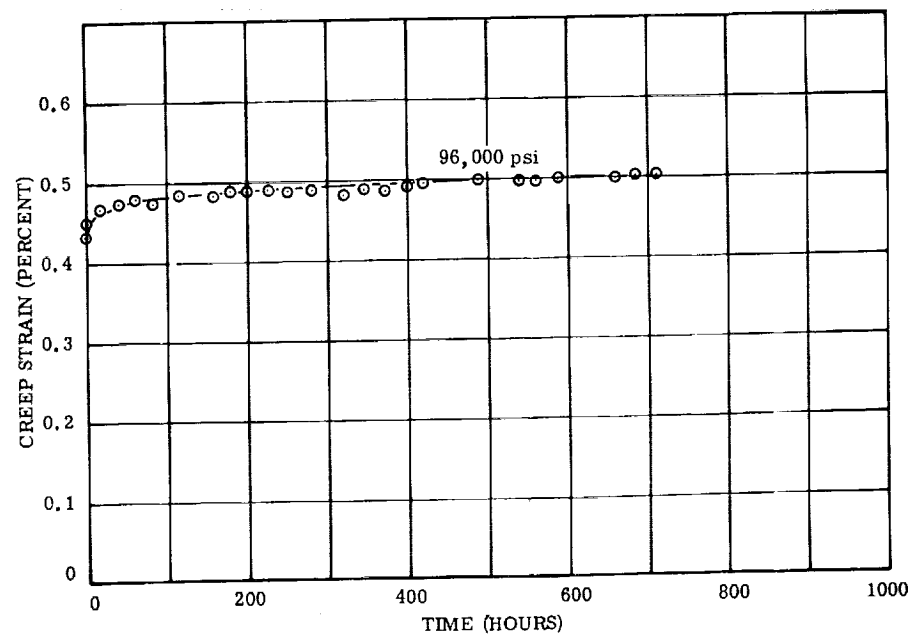

Figure 338. - Creep data for forged Nivco bar tested in air at 900° F and 96 000 psi. (See table 53.)

TABLE 54. - CREEP DATA FOR FORGED NIVCO BAR

TESTED IN VACUUM

[Test, ASTM E139; plastic strain obtained on loading
specimen, 0; see fig. 321 for Larson-Miller plot.]

Temperature, °F	900	1100	1400	1400
Stress, psi	85 000	80 000	8000	16 000
Duration of test, hr	496	356	163	5
Total creep strain, percent	0.66	0.07	0.10	0.52
Time to cause 0.2-percent creep strain, hr	65	(a)	(a)	0.65
Time to cause 0.4-percent creep strain, hr	225	(a)	(a)	1.95
Larson-Miller parameter[b] for 0.2-percent plastic strain	43.3	(a)	(a)	55.5
Larson-Miller parameter[b] for 0.4-percent plastic strain	44.0	(a)	(a)	56.4

[a]Did not reach required strain.
[b]Larson-Miller constant, 30.

TABLE 55. - CREEP DATA FOR NIVCO SHEET TESTED IN AIR

[Test, ASTM E139; see figs. 339 to 341; plastic strain obtained on
loading specimen, 0.]

Temperature, °F	900	1100	1100	1100	[a]1100
Stress, psi	45 000	30 000	35 000	45 000	60 000
Duration of test, hr	[b]1410	1123	[b]1172	[b]668	163
Total creep strain, percent	0.124	0.2790	0.372	0.589	0.6460
Time to cause 0.2-percent creep strain, hr	(c)	690	360	91	8
Time to cause 0.4-percent creep strain, hr	(c)	[d]1770	[d]1387	389	111
Strain-time plot given in fig.	339	340	340	340	341

[a]Longitudinal specimen.
[b]Test incomplete.
[c]Did not reach required strain.
[d]Extrapolated.
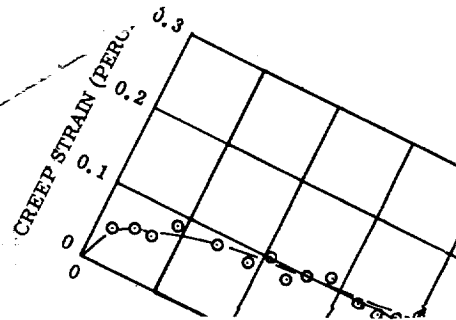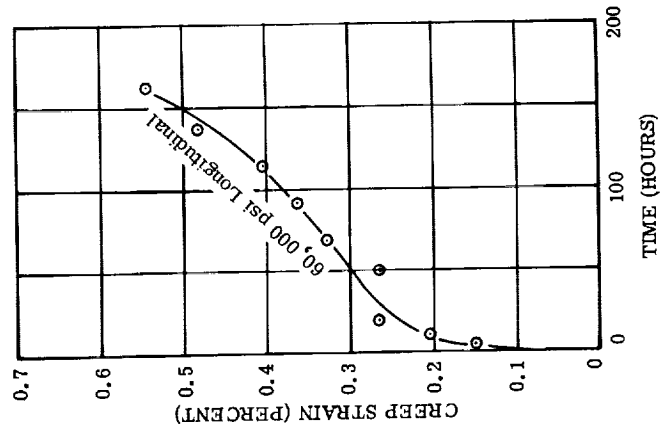
Figure 341. – Creep data for Nivco sheet (longitudinal) tested in air at 1100° F. (See table 55.)
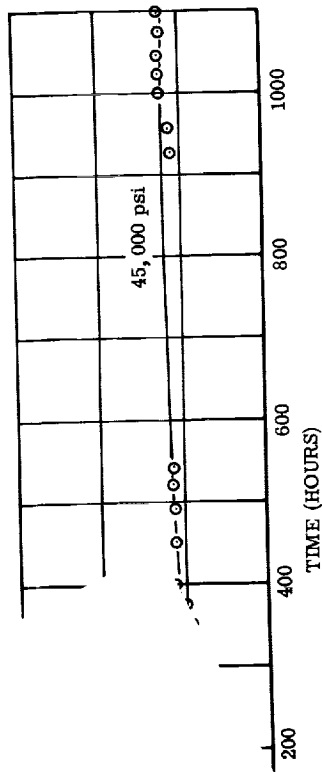
Figure 339. – Creep data for Nivco sheet tested in air at 900° F. (See table 55.)
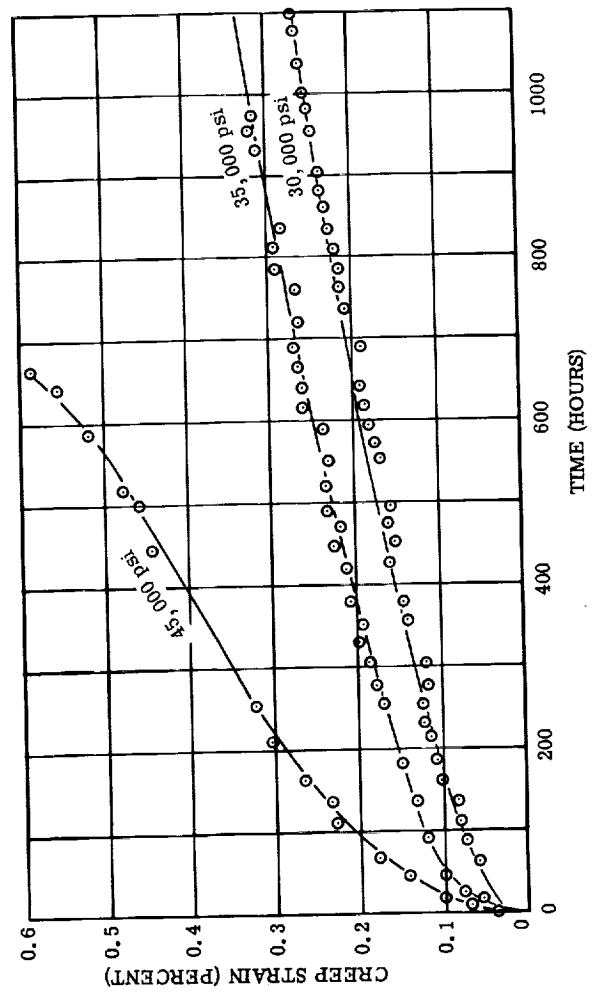
Figure 340. – Creep data for Nivco sheet tested in air at 1100° F. (See table 55.)

TABLE 56. - FATIGUE TEST DATA FOR 10^7 CYCLES ON SMOOTH-

AND NOTCHED-BAR FORGED NIVCO SPECIMENS

Test temperature, °F	Fatigue specimen	Stress ratio, A (a)	Stress, psi		
			For 10^7 cycles	Alternating	Mean
900	Smooth bar	∞	63 000	------	-------
	Notched bar	∞	40 000	------	-------
	Smooth bar	0.25	133 000	26 600	106 400
	Notched bar	.25	133 000	26 600	106 400
1000	Smooth bar	∞	67 000	------	-------
	Notched bar	∞	33 000	------	-------
	Smooth bar	0.25	129 000	25 800	103 200
	Notched bar	.25	129 000	25 800	103 200
1100	Smooth bar	∞	62 000	------	-------
	Notched bar	∞	32 000	------	-------
	Smooth bar	0.25	108 000	21 600	86 400
	Notched bar	.25	95 000	19 000	76 000

[a]Where A is ratio of alternating stress to mean stress.
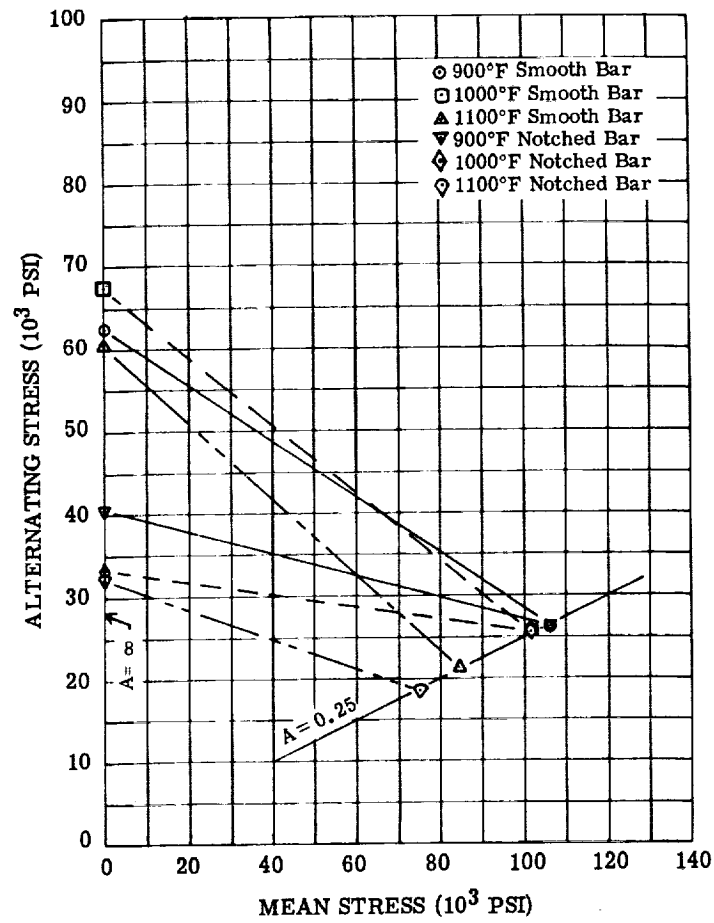
Figure 342. - Modified Goodman-type diagram for forged Nivco alloy tested at 900°, 1000°, and 1100° F for 10[7] cycles. (See table 56.)

TABLE 57. - FATIGUE TEST DATA FOR NIVCO SMOOTH-BAR SPECIMENS TESTED IN AIR

[Test, ASTM STP 91.]

Specimen	Test temperature, °F	Stress ratio, A (a)	Maximum stress, psi	Number of cycles to failure, N	Specimen	Test temperature, °F	Stress ratio, A (a)	Maximum stress, psi	Number of cycles to failure, N
300	900	∞	100 000	1 500	320	1000	0.25	150 000	6 000
304			80 000	84 000	322			146 250	8 000
305			70 000	662 000	318			143 750	553 000
325			65 000	3 194 000	302			135 900	828 000
327			60 000	2 415 000	332			129 950	4 488 000
335			55 000	b10 000 000	321			128 000	12 474 000
307		0.25	150 000	23 000	317	1100	∞	82 000	31 000
316			146 250	10 000	314			74 000	200 000
314			143 750	204 000	319			70 000	722 000
312			142 000	4 532 000	341			68 000	c3 299 000
333			138 650	9 000	323			66 000	4 500 000
334			136 700	263 000	343			64 000	c4 885 000
310		∞	135 000	b18 000 000	303			62 000	8 690 000
308	1000		90 000	7 000	324		.25	134 750	28 000
309			80 000	96 000	330			129 950	159 000
313			74 000	563 000	329			125 800	299 000
306			69 750	3 639 000	342			120 000	103 000
311			66 000	7 250 000	326			120 000	716 000
337			62 000	1 665 000	331			115 500	637 000
340			62 000	11 360 000	336			113 000	3 657 000
					338			112 000	1 605 000
					328			110 000	b9 830 000

a Where A is ratio of alternating stress to mean stress.
b No failure.
c Argon atmosphere.

TABLE 58.-- FATIGUE TEST DATA FOR NIVCO NOTCHED-BAR SPECIMENS TESTED IN AIR

[Test, ASTM STP 91.]

Specimen	Test temperature, °F	Stress ratio, A (a)	Maximum stress, psi	Number of cycles to failure, N
400	900	∞	55 000	18 000
402			50 000	23 000
406			45 000	62 000
404			42 500	108 000
409			40 000	b10 330 000
428			36 000	55 000
418			33 000	b12 000 000
438		0.25	165 000	17 000
413			150 000	121 000
416			145 000	148 000
405			142 000	78 000
420			139 750	8 790 000
410			135 000	b10 000 000
435	1000	∞	49 750	12 000
425			40 000	56 000
412			37 500	b10 045 000
408			35 000	9 791 000
411			35 000	b15 000 000
403			30 000	b9 729 000
427		.25	152 000	33 000
439			145 000	240 000
422			134 000	955 000
419			125 000	7 490 000
417			122 000	8 004 000
441			118 000	b10 000 000

Specimen	Test temperature, °F	Stress ratio, A (a)	Maximum stress, psi	Number of cycles to failure, N
437	1100	∞	45 000	16 000
424			40 000	36 000
434			37 000	12 250 000
414			35 000	2 419 000
426			35 000	2 849 000
433			30 000	b10 000 000
436		0.25	144 000	4 000
423			134 000	120 000
440			128 000	65 000
415			120 000	980 000
421			114 000	805 000
429			106 000	705 000
432			106 000	822 000
407			100 000	1 450 000
430			90 000	2 825 000
401			80 000	b15 000 000

a Where A is ratio of alternating stress to mean stress.

b No failure.

For Smooth Bar
$(1.5 \leq N \leq 3194)$, Fatigue Strength = $1000[0.43471 \times 10^{-10} N^4 - 0.2763 \times 10^{-6} N^3$
$+ 0.524810^{-3} N^2 \ 0.2849 \ N + 100.41](Psi)$

For Notched Bar
$(18 \leq N \leq 10330)$, Fatigue Strength = $1000[0.122623 \times 10^{-4} N^2 - 0.12809 \ N + 54.707](Psi)$
(Where N = Cycles to Failure x 10^{-3})

⊙ Smooth Bar
△ Notched Bar
$K_t = 3.0$

Figure 343. - Fatigue diagram for smooth and notched Nivco bar tested in air at 900° F with stress ratio of infinity. (See tables 57 and 58.)

For Smooth Bar
$(7 \leq N \leq 7250)$, Fatigue Strength = $1000[-0.763567 \times 10^{-9} N^3 + 0.95815 \times 10^{-5} N^2 - 0.02945 \ N + 86.87](Psi)$

For Notched Bar
$(12 \leq N \leq 10,000)$, Fatigue Strength = $1000[-0.209113 \times 10^{-8} N^3 + 0.43549 \times 10^{-4} N^2 - 0.22791 N + 52.55](Psi)$
(Where N = Cycles to Failure x 10^{-3})

⊙ Smooth Bar
△ Notched Bar
$K_t = 3.0$

Figure 344. - Fatigue diagram for smooth and notched Nivco bar tested in air at 1000° F with stress ratio of infinity. (See tables 57 and 58.)

For Smooth Bar
$(31 \leq N \leq 8690)$, Fatigue Strength $= 1000 \left[-0.384755 \times 10^{-4} N^3 + 0.53354 \times 10^{-5} N^2 - 0.019945 N + 80.551 \right]$ (Psi)

For Notched Bar
$(16 \leq N \leq 12250)$, Fatigue Strength $= 1000 \left[0.30846 \times 10^{-6} N^2 - 0.42939 \times 10^{-2} N + 42.84 \right]$ (Psi)

(Where N = Cycles to Failure x 10^{-3})

⊙ Smooth Bar
△ Notched Bar
$K_t = 3.0$

Figure 345. - Fatigue diagram for smooth and notched Nivco bar tested in air at 1100° F with stress ratio of infinity. (See tables 57 and 58.)

For Smooth Bar
$(10 \leq N \leq 18,000)$, Fatigue Strength $= 1000 \left[0.65295 \times 10^{-3} N + 146.37 \right]$ (Psi)

For Notched Bar
$(17 \leq N \leq 10,000)$, Fatigue Strength $= 1000 \left[-0.173792 \times 10^{-8} N^3 + 0.32582 \times 10^{-4} N^2 - 0.1553 N + 167.74 \right]$ (Psi)

(Where N = Cycles to Failure x 10^{-3})
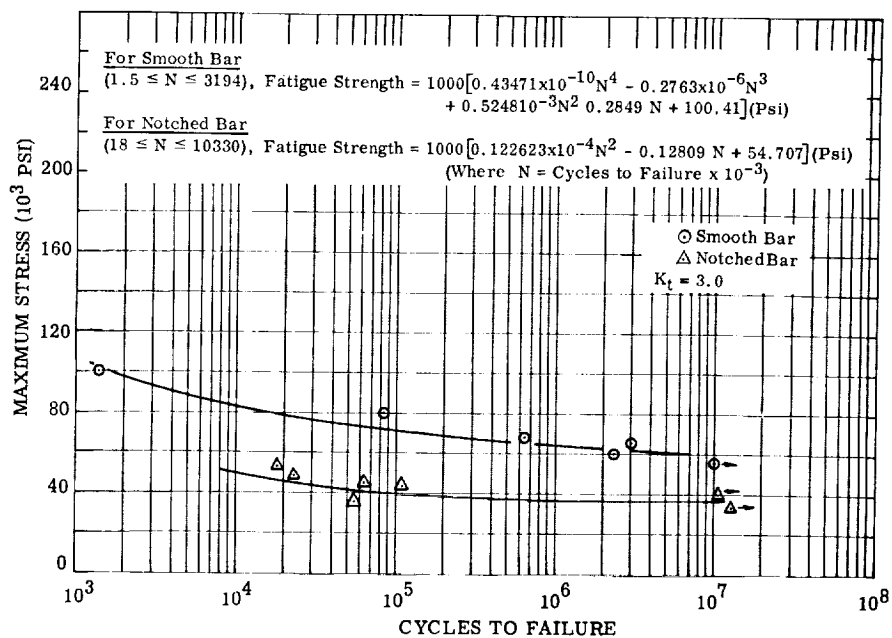
⊙ Smooth Bar
△ Notched Bar
$K_t = 3.0$

Figure 346. - Fatigue diagram for smooth and notched Nivco bar tested in air at 900° F with stress ratio of 0.25. (See tables 57 and 58.)
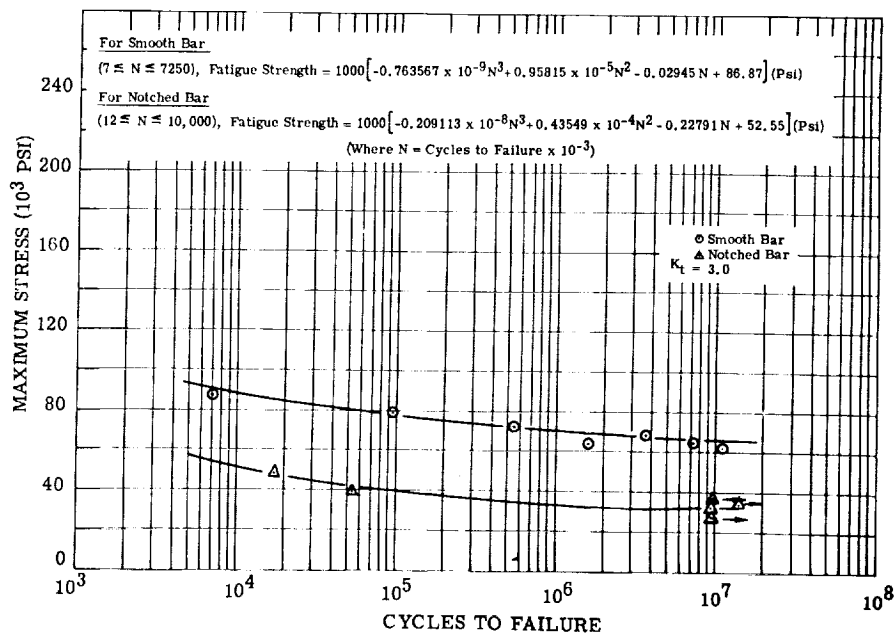
Figure 347. - Fatigue diagram for smooth and notched Nivco bar tested in air at 1000° F with stress ratio of 0.25. (See tables 57 and 58.)
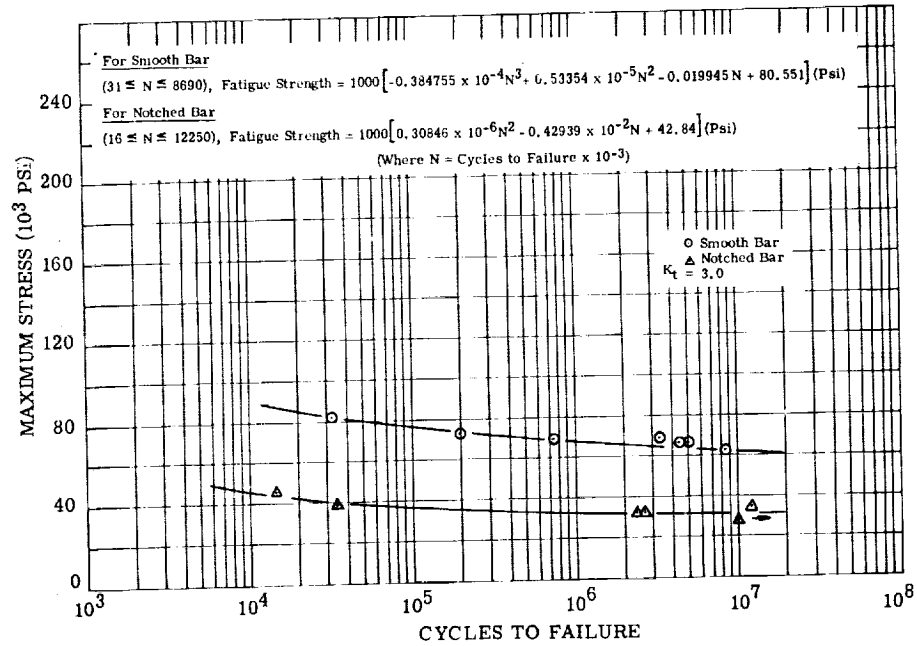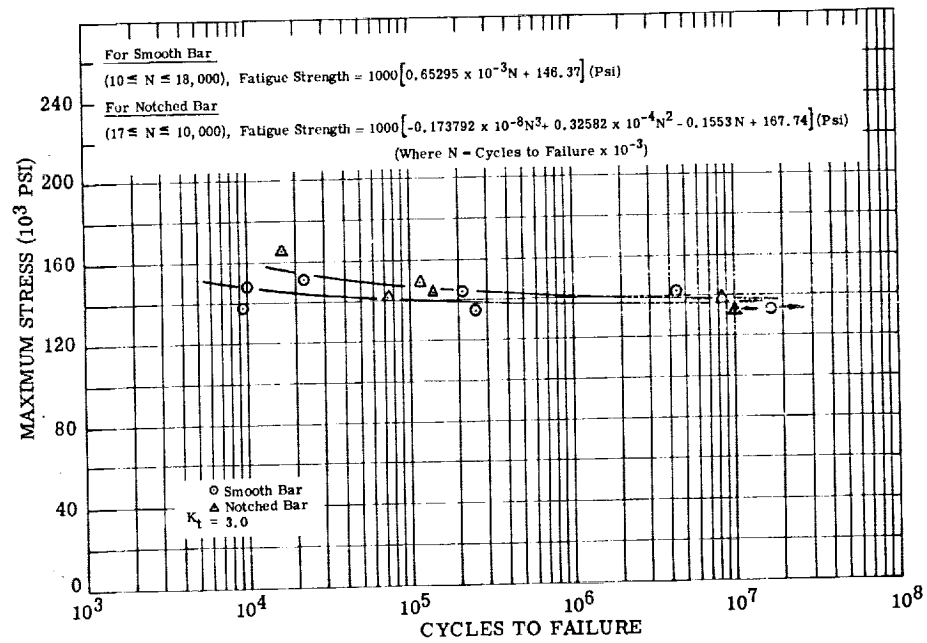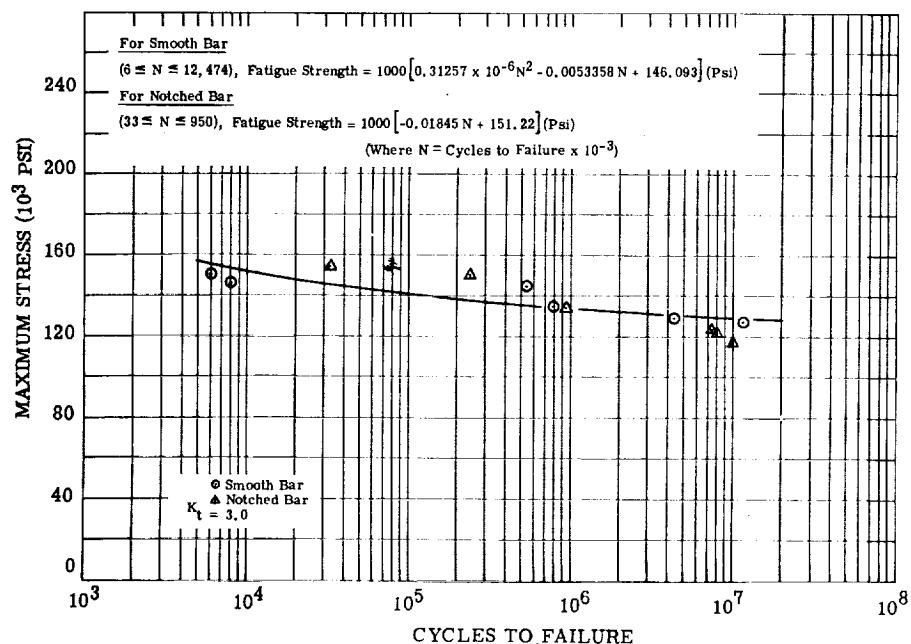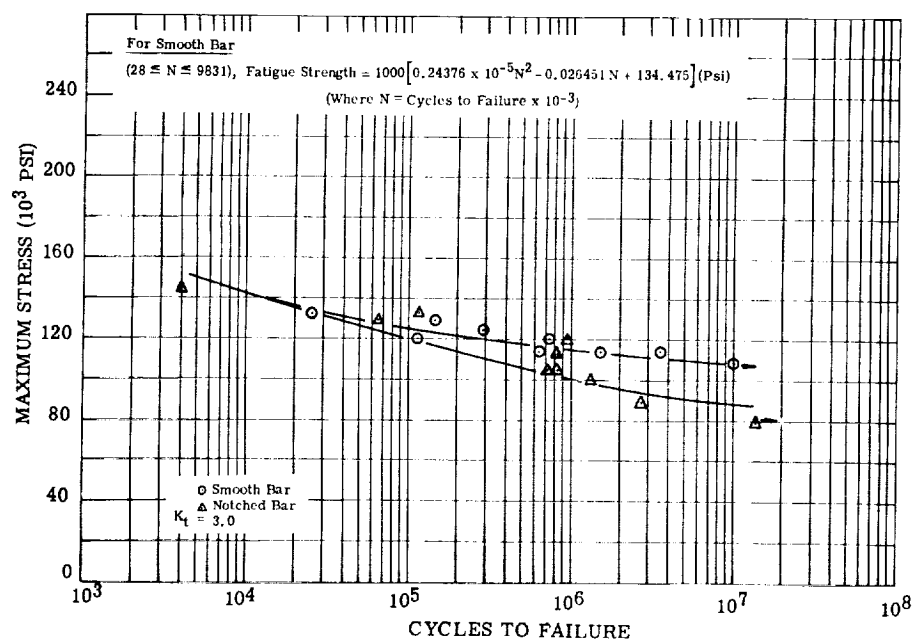

Figure 348. - Fatigue diagram for smooth and notched Nivco bar tested in air at 1100° F with stress ratio of 0.25. (See tables 57 and 58.)

APPENDIX - NOMENCLATURE

Symbols

A	stress ratio (see Definitions)
AT	H_1
B	magnetic induction, kG
B_d	remanent induction (see Definitions)
BHN	brinell hardness number
B_m	maximum induction, measures at H_m
B_r	residual magnetic induction, or (from saturation) the retentivity (see Definitions)
B_r/B_m	loop squareness ratio
B_s	saturation magnetic induction
B_{tip}	maximum induction reached during magnetization
CCFR	constant current flux reset
C_v	specific heat at constant volume (for solids)
DAT	$H_1 - H_2$
e	transverse strain (see definition of μ)
e_1	axial strain (see definition of μ)
H	magnetic coercive force, Oe
H_c	coercive force (see Definitions)
H_m	peak field intensity
H_0	reset magnetic field intensity (see Definitions)
H_1, H_2	see Definitions
K_t	stress concentration factor (see Definitions)
$\Delta L/L$	change in length divided by original length in thermal expansion measurements
MFA	magnetic field annealed
N	number of cycles in fatigue test

S	stress
SAT	B_m
SRA	stress relief annealed
T	temperature
t	time
α	coefficient of thermal expansion
κ	thermal conductivity
μ	Poisson's ratio (see Definitions)
ρ	electrical resistivity

Definitions

A	stress ratio; ratio of alternating stress to mean stress in biased fatigue test
B_d	remanent induction; magnetic induction that remains in magnetic circuit after removal of applied magnetomotive force
B_r	residual magnetic induction; magnetic induction remaining when the magnetizing force is reduced to zero
$B_m - B_r$	flux density change measured at zero reset magnetic field intensity; a measure of squareness that is utilized to determine squareness ratio
creep strain	total nonrecoverable plastic deformation corrected for thermal expansion and elastic strain
fatigue strength	maximum stress that can be sustained for a specified number of cycles without failure, the alternating stress being completely reversed within each cycle; fatigue strength was determined for 10^7 cycles
gain	measure, in terms of permeability, of loop steepness, $(\Delta B_2 - \Delta B_1)/(H_2 - H_1)$
H_0	reset magnetic field intensity required to produce cyclic change of induction ΔB_0 equal to one-half maximum flux density change

H_1 reset magnetic field intensity required to produce cyclic change of induction ΔB_1 equal to one-third maximum flux density change

H_2 reset magnetic field intensity required to produce cyclic change of induction ΔB_2 equal to two-thirds maximum flux density change

H_c magnetization force at which magnetic induction is zero

R_c hardness value in Rockwell "C" scale units when a 150 kg load and diamond Braille indenter are used

Stress concentration factor K_t ratio of greatest stress in region of notch or stress riser, as determined by advanced theory, photoelasticity, or direct measurement of elastic strain, to corresponding nominal stress; stress concentration factor was calculated by the theory of elasticity

Poisson's ratio, absolute value of ratio of transverse strain to corresponding axial strain in a body subjected to uniaxial stress in elastic portion of stress-strain curve, e/e_1

REFERENCES

1. Jennings, Burgess H.; and Rogers, Willard, L.: Gas Turbine Analysis and Practice. McGraw-Hill Book Co., Inc., 1953, p. 393.

2. Doughman, C. L.: Space Electric Power Systems Study. Vol. 2. Westinghouse Electric Corp. (NASA CR-50862), 1963.

3. Verkamp, J. P.: Electromagnetic Alkali Metal Pump Research Program. General Electric Co. (NASA CR-54036), May 22, 1964.

4. Gordon, D. I.: Environmental Evaluation of Magnetic Materials. Electro-Technology, vol. 67, no. 1, Jan. 1961, pp. 118-125.

5. Pasnak, Michael; and Lundsten, Richard: Effects of Ultrahigh Temperature on Magnetic Properties of Core Materials. AIEE Trans., Pt. I - Communications and Electronics, vol. 78, 1959, pp. 1033-1039.

6. Gordon, D. I.: Magnetic Cores and Permanent Magnets in Hyper-Environments. Proceedings of the Institute of Environmental Sciences, Los Angeles, Apr. 6-8, 1960, pp. 205-228.

7. Reid, B. J.; and Greenwood, J. N.: Intergranular Cavitation in Stressed Copper-Nickel Alloys. AIME Trans., vol. 212, no. 4, Aug. 1958, pp. 503-507.

8. Anon.: Preliminary Product Data Sheet PD5-963, Allegheny-Ludlum Steel Corp.

9. Anon.: Electric Steel Sheets Engineering Manual. Fourth ed., United States Steel Corp., 1954.

10. Anon.: Hiperco 27: Product Literature. Westinghouse Electric Corp.

11. Anon.: ALMAR 18-250: Product Literature. Allegheny-Ludlum Steel Corp.

12. Campbell, J. E.; Barone, F. J.; and Moon, D. P.: The Mechanical Properties of the 18 Percent Nickel Maraging Steels. Rep. No. 198 (DDC No. AD-600427), Defense Metals Information Center, Feb. 24, 1964.

13. Lyman, Taylor, ed.: Heat Treating, Cleaning and Finishing. Vol. 2 of Metals Handbook. 8th ed. American Society for Metals, 1964, pp. 89-91.

14. Brodrick, R. F.: Fatigue and Dynamic Creep of High-Strength Steels. Lessells and Associates, Inc. (AFASD-TDR-62-480), Aug. 1962.

15. Anon.: SNAP 50/SPUR Power System. Rep. No. APS-5090-R1, AiResearch
    Mfg. Co., May 18, 1964. (Available from DDC as AD-440789.)

16. Dannan, J. H.: SNAP 50/SPUR Power System. Rep. No. APS-5071-R,
    Airesearch Mfg. Co., Jan. 31, 1964. (Available from DDC as AD-439687.)

17. Lyman, Taylor, ed.: Properties and Selection of Metals. Vol. 1 of Metals
    Handbook. 8th ed. American Society for Metals, 1961, p. 1207.

BIBLIOGRAPHY

General

Anon.: Cobalt Monograph. Centre d'Information du Cobalt, Brussels, and Battelle Memorial Institute, 1960.

Anon.: Proceedings of the IEE/APS Conference on Magnetism and Magnetic Materials. J. Appl. Phys., Supplements, 1956-1963.

Bozorth, Richard M.: Ferromagnetism. D. Van Nostrand Co., Inc., 1951.

Gerlach, Walther: The Temperature Dependence of Ferromagnetic Properties as a Basis for Research on the Physical Properties of Metals. Metallforschung, vol. 2, no. 9, 1947, pp. 275-280.

Heddle, T. A.: On The Temperature Sensitivity of Special Magnetic Materials. Brit. J. Appl. Phys., vol. 4, June 1953, pp. 161-166.

Köster, Werner: Die Temperaturabhängigkeit des Elastizitätsmoduls Reiner Metalle. Z. Metallkunde, vol. 39, Jan. 1948, pp. 1-9.

Lyman, Taylor, ed.: Properties and Selection of Metals. Vol. 1 of Metals Handbook. 8th ed. American Society for Metals, 1961.

Smithells, Colin J., ed.: Metals Reference Book. Second ed. Interscience Publishers, 1955.

Teviotdale, A.: Zener's Treatment of Ferromagnetism. Phys. Soc. Proc., Ser. A, vol. 65, no. 11, Nov. 1952, pp. 957-958.

Vonsovskiy, S. V.: Metal Physics and Its Contribution to the Material and Technical Basis of Communism. Phys. Metals Metallography, vol. 14, no. 3, 1962, pp. 1-4.

Zaikova, V. A.; Shur, Ya. S.; and Falaleyev, G. A.: Dependence of Magnetic Properties on the Thickness of Ferromagnetic Sheets. Phys. Metals Metallography, vol. 13, no. 4, 1962, pp. 38-44.

H-11 Steel

Anon.: Air Hardening Dynaflex. Tech. Bul., Latrobe Steel Co.

Anon.: Carpenter Pyromet 882. Tech. Data Sheet P6, Carpenter Steel Corp., Sept. 1961.

Anon.: Firth Sterling HWD2. Tech. Data Sheet, Firth Sterling Steel Co., Sept. 1958.

Anon.: Potomac: A High Strength Steel. Tech. Bul., Allegheny-Ludlum Steel Corp., 1959.

Anon.: SNAP 50/SPUR Power System. Rep. No. APS-5090-R2, AiResearch Mfg. Co., Aug. 18, 1964. (Available from DDC as AD-444826.)

Anon.: Unimach No. 1. Tech. Bul. P29, Universal Cyclops Steel Corp.

Brodrick, R. F.: Fatigue and Dynamic Creep of High-Strength Steels. (AFASD-TDR-62-480), Lessells and Associates, Inc., Boston, Aug. 1962.

Favor, R. J.; and Achbach, W. P.: Design Information on 5 Cr-Mo-V Alloy Sheets (H-11 and 5 Cr-Mo-V Aircraft Steel) for Aircraft and Missiles. Rep. No. 116 Rev., Defense Metals Information Center, Sept. 30, 1960.

Hill, W. H.; and Shimmin, K. D.: Elevated Temperature Dynamic Elastic Moduli of Various Metallic Materials. (WADD TR 60-438, AD-264825), Metals and Ceramics Lab., Wright-Patterson AFB, Mar. 1961.

Jones, R. L.: Evaluation of 18 Ni-Co-Mo (300), 9 Ni-4Co and SAE 4340 Steel Forgings. Third Maraging Steel Project Review. Rep. No. RTD-TDR-63-4048 (AD-430647), Air Force Systems Command, Nov. 1963, pp. 438-501.

Kovacs, André; and Laurent, Pierre: Influence de la Fatigue sur les Proprietes Magnétiques des Aciers. Acad. Sci. Paris, Compt. Rend., vol. 235, no. 20, Nov. 17, 1952, pp. 1224-1226.

Morral, F. R.; and Achbach, W. P.: 5Cr Alloy Steels for Aircraft and Missiles. Rep. No. 116, Defense Metals Information Center, Aug. 28, 1959.

Sliney, Joseph L.; and Schmid, Fred: The Notch Properties and Shear Transitional Behavior of H11 Steel. Rep. No. WAL-TR-766.5/2, Watertown Arsenal Labs., Feb. 1963. (Available from DDC as AD-2993222.)

Cubex Alloy

Ganz, Dieter: Effect of Direction of Magnetic Properties of Fe-Si Sheets, Containing 3% Si, with Goss and Cube Texture. Z. Angew. Phys., vol. 14, May 1962, pp. 313-322.

Koksharova, I. K.; Lyasko, M. V.; and Mironov, L. V.: Formation of the Cubic Texture of Transformer Steel. Phys. Metals Metallography, vol. 14, no. 3, 1962, p. 125.

Krivonosova, Ye. G.; and Livshits, B. G.: Hysteresis Anisotropy of Deformed Silicon-Iron Crystals. Phys. Metals Metallography, vol. 14, no. 6, 1962, pp. 115-116.

Kunakov, Ya. N.; and Livshits, B. G.: Role of Surface Energy in the Formation of a Cubic Texture in Silicon Iron. Phys. Metals Metallography, vol. 14, no. 5, 1962, pp. 76-80.

Kunakov, Ya. N.; and Livshits, B. G.: Magnetic Properties of Transformer Steel with Cubic Texture. Phys. Metals Metallography, vol. 15, no. 1, 1963, pp. 52-55.

Markuszewicz, M. J.: Effect of Some Impurities on Grain Growth and Magnetic Anisotropy of 3.25% Silicon-Iron Strips. Iron Steel Inst. J., vol. 200, pt. 3, Mar. 1962, pp. 223-228.

Cobalt

Anon.: Cobalt and Cobalt-Base Superalloys - Wrought. Materials Design Eng., vol. 56, no. 5, Mid-Oct. 1962, p. 114.

Anon.: Cobalt Monograph. Centre d'Information du Cobalt, Brussels, and Battelle Memorial Institute, 1960.

Anon.: Metallic Elements and Alloys. Vol. 1 of Thermophysical Properties Data Book, Purdue University Research Center, 1963.

Bozorth, Richard M.: Ferromagnetism. D. Van Nostrand Co., Inc., 1951, pp. 261-267.

Campbell, J. E.; Goodwin, H. B.; and Wagner, H. J.: Introduction to Metals for Elevated-Temperature Use. Rep. No. 160, Defense Metals Information Center, Oct. 27, 1961.

Fine, M. E.; and Greener, E. H.: Internal Friction and Young's Modulus of Hexagonal and Cubic Cobalt. AIME Trans., vol. 212, no. 4, Aug. 1958, pp. 476-478.

Freche, John C.; Ashbrook, Richard L.; and Klima, Stanley J.: Cobalt-Base Alloys for Space-Power Systems. J. Metals, vol. 15, no. 12, Dec. 1963, pp. 928-934.

Graham, C. D., Jr.: Magnetic Annealing of Cobalt. Phys. Soc. Japan J., vol. 16, no. 7, July 1961, pp. 1481-1482.

Hampel, Clifford A., ed.: Rare Metals Handbook. Reinhold Publ. Corp., 1954, p. 117.

Hampel, Clifford A., ed.: Rare Metals Handbook. Second ed., Reinhold Publ. Corp., 1961, p. 126.

Mantell, Charles L.: Engineering Materials Handbook. McGraw-Hill Book Co., Inc., 1958, p. 13.

Peters, Robert L.: Nomograph: Thermal Conductivity at Any Temperature. Materials Design Eng., vol. 55, no. 2, Feb. 1962, pp. 90-91.

Sambongi, Takashi; and Mitui, Tadayasu: Magnetic Annealing Effect in Cobalt. Phys. Soc. Japan J., vol. 16, no. 7, July 1961, p. 1478.

Sambongi, Takashi; and Mitui, Tadayasu: Stress Annealing Effect in Cobalt. Phys. Soc. Japan J., vol. 16, no. 10, Oct. 1961, p. 2066.

Savitskii, Evgenii M. (D. Sherby, trans.): The Influence of Temperature on the Mechanical Properties of Metals and Alloys. Stanford University Press, 1961, pp. 134-136.

Seagle, S. R.; Martin, R. L.; and Bertea, O.: Electron-Beam Melting - Does it Improve the Properties of Metals and Compounds? J. Metals, vol. 14, no. 11, Nov. 1962, pp. 812-820.

Young, Roland S.: Cobalt: Its Chemistry, Metallurgy, and Uses. Reinhold Publ. Corp., 1960, pp. 64-71.

Iron-Cobalt

Baer, Günter; and Thomas, Hans: Characteristics and Structures of Cobalt-Iron Alloys Containing 50% Cobalt and Small Additions (up to 4%) of Vanadium. Z. Metallkunde, vol. 45, no. 11, 1954, pp. 651-655.

Hall, R. C.: Solid State Research for the Advancement of Electronic Materials. QPR 3, Sept. 1-Nov. 30, 1958, Westinghouse Electric Corp., 1958. (Available from DDC as AD-209618.)

Hall, R. C.: Solid State Research for the Advancement of Electronic Materials. QPR 4, Dec. 1, 1958 - Feb. 28, 1959, Westinghouse Electric Corp., 1959. (Available from DDC as AD-216073.)

Keller, Heinz; and Hillmann, Hans: Iron-Cobalt Alloys with Low Coercive Field Strengths. Z. Angew. Phys., vol. 14, Apr. 1962, pp. 243-245.

Pshechenkova, G. V.; and Skokov, A. D.: Temperature Dependence of the Magnetic Saturation Induction of Alloys of the Iron-Cobalt System. Phys. Metals Metallography, vol. 14, no. 5, 1962, pp. 145-147.

Maraging Steels

Anon.: ALMAR Maraging Steels. Allegheny-Ludlum Steel Corp., 1962.

Anon.: ALMAR 15 (280HT). Allegheny-Ludlum Steel Corp., 1963.

Anon.: Austenitic Stainless Steels and Maraging Steels. Materials in Design Eng., vol. 57, no. 3, Mar. 1963, p. 127.

Anon.: Maraging Steels. Tech. Data Sheet, International Nickel Co., June 1962.

Anon.: Materials. Space/Aeronautics R & D Tech. Handbook, vol. 40, no. 2, July 1963, p. 219.

Anon.: Nominal 200KSI Yield Strength 18 Percent Nickel Maraging Steel. Publ. No. TL-12 Pl-3, International Nickel Co., Nov. 2, 1962.

Anon.: Tentative Data on 18 Percent Nickel Maraging Steel. Maraging Steel Data Book. International Nickel Co., Nov. 1962.

Anon.: The 18 Percent Nickel Maraging Steels. Tech. Bul., Latrobe Steel Co.,
    Dec. 1962.

Anon.: Ultra High Strength Steels - Wrought. Materials Design Eng., vol. 56,
    no. 5, Mid-Oct. 1962, p. 71.

Anon.: 18 Percent Nickel Maraging Steel. Interim Data Sheet, International
    Nickel Co., Nov. 26, 1962.

Arnold, S. V.: Aging Response of 18% Ni-Co-Mo Steel. Rep. No. WAL-TR-
    320.1/11, Watertown Arsenal Lab., Feb. 1963.

Campbell, J. E.; Barone, F. J.; and Moon, D. P.: The Mechanical Properties
    of the 18 Percent Nickel Maraging Steels. Rep. No. 198 (AD-600427), Defense
    Metals Information Center, Feb. 24, 1964.

Decker, R. F.; Eash, J. T.; and Goldman, A. J.; 18% Nickel Maraging Steel.
    ASM Trans., vol. 55, no. 1, Mar. 1962, pp. 58-76.

Decker, R. F.; Yeo, R. B. G.; Eash, J. T.; and Bieber, C. G.: The Maraging
    Steels. Materials Design Eng., vol. 55, no. 5, May 1962, pp. 106-111.

Drennen, D. C.; and Roach, D. B.: Properties of Maraging Steels. Memo No.
    156, Defense Metals Information Center, July 2, 1962.

Field, Joseph: Discussion of 18% Nickel Maraging Steel. ASM Trans., vol. 55,
    1962, pp. 1010-1011.

Floreen, S.; and Decker, R. F.: Maraging Steel for 1000 F Service. ASM Trans.,
    vol. 56, no. 3, Sept. 1963, pp. 403-411.

Hall, A. M.: Report on Meeting to Review Maraging Steel Products. Memo No.
    162, Defense Metals Information Center, Dec. 28, 1962.

Jones, R. L.: Evaluation of 18Ni-Co-Mo (300), 9Ni-4Co and SAE 4340 Steel Forg-
    ings. Third Maraging Steel Project Review. Rep. No. RTD-TDR-63-4048
    (AD-430647), Air Force Systems Command, Nov. 1963, pp. 438-501.

May, J. A.: Maraging Steel in Elevated Temperature Airframe Design. Rep. No.
    TFD-63-552, North American Aviation, Inc., July 19, 1963.

Novak, C. J.; and Diran, L. M.: What are the Effects of Residual Elements in
    Maraging Steels? J. Metals, vol. 15, no. 3, Mar. 1963, pp. 200-204.

Puzak, P. P.; and Loyd, K. B.: Fundamental Study of Weld Joint Behavior.
    Report of NRL Progress, Sept. 1963, pp. 31-36.

Sparks, Robert B.: Working with Maraging Steels. Metal Progress, vol. 84, no. 1, July 1963, pp. 74-77.

Stefanides, E. J.: Wrought Steels. Design News, vol. 18, no. 20, Oct. 1963, pp. s1-s80.

Supermendur

Anon.: Bulletin TC-113. Arnold Engineering Co., Nov. 18, 1957.

Gordon, D. I.: Environmental Evaluation of Magnetic Materials. Electro-Technology, vol. 67, no. 1, Jan. 1961, pp. 118-125.

Gould, H. L. B.; and Wenny, D. H.: Supermendur - New Rectangular Loop Magnetic Material. Conference on Magnetism and Magnetic Materials, Boston, Oct. 16-18, 1956. Publ. T-91, AIEE, Feb. 1957, pp. 675-681.

Lauriente, M.; and Lynn, G. E.: Characteristics of Supermendur at 500° C. J. Appl. Phys., vol. 31, no. 5, suppl., May 1960, pp. 237s-238s.

Pasnak, Michael; and Lundsten, Richard: Effects of Ultrahigh Temperature on Magnetic Properties of Core Materials. AIEE Trans., pt. I - Communications and Electronics, vol. 78, 1959, pp. 1033-1039.

Shull, Daniel S., Jr.: Improved Magnetic Properties of High-Purity Iron-Cobalt Alloys Containing 27-43% Cobalt. J. Appl. Phys., vol. 32, no. 3, suppl., Mar. 1961, pp. 356s-357s.

Trapp, R. H.; Robenold, D. G.; and Facaros, G.: Soft Magnetic Materials for 930 F Plus. Materials Design Eng., vol. 55, no. 5, May 1962, pp. 113-115.

Hiperco 27 and Hiperco 50

Bozorth, Richard M.: Ferromagnetism. D. Van Nostrand Co., Inc., 1951, pp. 190-205.

Hall, R. C.; Conrad, G. P.; and Libsch, J. F.: Ordering and Magnetic Heat Treatment of the 50 Pct Fe-50 Pct Co Alloy. J. Metals, vol. 7, no. 9, Sept. 1955, pp. 985-989.

Pavlik, Norman: High-Temperature Stability of Magnetic Materials. J. Appl. Phys., vol. 32, no. 3, supple., Mar. 1961, pp. 372s-373s.

Trapp, R. H.; Robenold, D. G.; and Facaros, G.: Soft Magnetic Materials for 930 F Plus. Materials Design Eng., vol. 55, no. 5, May 1962, pp. 113-115.

Witherell, C. E.; Corrigan, D. A.; and Petersen, W. A.: Working with Maraging Steels - Welding. Metal Progress, vol. 84, no. 1, July 1963, pp. 81-83.

Witherell, C. E.; and Fragetta, W. A.: Weldability of 18% Nickel Steel. Welding Res. Suppl., vol. 41, no. 11, Nov. 1962, pp. 481-s to 487-s.

Nivco Alloy

Anon.: Cobalt-Base Superalloys - Cast, Wrought. Materials Design Eng., vol. 56, no. 5, Mid-Oct. 1962, p. 115.

Silicon Steel

Nefedov, A. A.; and Borzova, P. I.: Cold Rolled Nonoriented Electrical Steel. Electric Tech. USSR, vol. 1, 1961, pp. 79-84.

Ni-Co-Fe Alloys

Schafer, E.: Resistivity and Magnetic Data of Various Materials. Data Sheet, Electronic Properties Information Center, Dec. 1963.